

Titre: De la caractérisation des matériaux et simulation du procédé à l'optimisation de la fabrication des composites par injection sur renfort
Title:

Auteur: Eduardo Ruiz
Author:

Date: 2004

Type: Mémoire ou thèse / Dissertation or Thesis

Référence: Ruiz, E. (2004). De la caractérisation des matériaux et simulation du procédé à l'optimisation de la fabrication des composites par injection sur renfort [Ph.D. thesis, École Polytechnique de Montréal]. PolyPublie.
Citation: <https://publications.polymtl.ca/7270/>

 **Document en libre accès dans PolyPublie**
Open Access document in PolyPublie

URL de PolyPublie: <https://publications.polymtl.ca/7270/>
PolyPublie URL:

Directeurs de recherche:
Advisors:

Programme: Unspecified
Program:

UNIVERSITÉ DE MONTRÉAL

DE LA CARACTÉRISATION DES MATÉRIAUX ET SIMULATION DU PROCÉDÉ
À L'OPTIMISATION DE LA FABRICATION DES COMPOSITES
PAR INJECTION SUR RENFORT

EDUARDO RUIZ

DÉPARTEMENT DE GÉNIE MÉCANIQUE
ÉCOLE POLYTECHNIQUE DE MONTRÉAL

THÈSE PRÉSENTÉE EN VUE DE L'OBTENTION
DU DIPLÔME DE PHILOSOPHIAE DOCTOR

(GÉNIE MÉCANIQUE)

JANVIER 2004



National Library
of Canada

Bibliothèque nationale
du Canada

Acquisitions and
Bibliographic Services

Acquisitions et
services bibliographiques

395 Wellington Street
Ottawa ON K1A 0N4
Canada

395, rue Wellington
Ottawa ON K1A 0N4
Canada

Your file Votre référence

ISBN: 0-612-89235-2

Our file Notre référence

ISBN: 0-612-89235-2

The author has granted a non-exclusive licence allowing the National Library of Canada to reproduce, loan, distribute or sell copies of this thesis in microform, paper or electronic formats.

L'auteur a accordé une licence non exclusive permettant à la Bibliothèque nationale du Canada de reproduire, prêter, distribuer ou vendre des copies de cette thèse sous la forme de microfiche/film, de reproduction sur papier ou sur format électronique.

The author retains ownership of the copyright in this thesis. Neither the thesis nor substantial extracts from it may be printed or otherwise reproduced without the author's permission.

L'auteur conserve la propriété du droit d'auteur qui protège cette thèse. Ni la thèse ni des extraits substantiels de celle-ci ne doivent être imprimés ou autrement reproduits sans son autorisation.

In compliance with the Canadian Privacy Act some supporting forms may have been removed from this dissertation.

Conformément à la loi canadienne sur la protection de la vie privée, quelques formulaires secondaires ont été enlevés de ce manuscrit.

While these forms may be included in the document page count, their removal does not represent any loss of content from the dissertation.

Bien que ces formulaires aient inclus dans la pagination, il n'y aura aucun contenu manquant.

Canada

UNIVERSITÉ DE MONTRÉAL
ÉCOLE POLYTECHNIQUE DE MONTRÉAL

Cette thèse intitulée :

DE LA CARACTÉRISATION DES MATÉRIAUX ET SIMULATION DU PROCÉDÉ
À L'OPTIMISATION DE LA FABRICATION DES COMPOSITES
PAR INJECTION SUR RENFORT

présentée par : RUIZ Eduardo

en vue de l'obtention du diplôme de : Philosophiae Doctor

a été dûment acceptée par le jury d'examen constitué de :

M. SANSCHAGRIN Bernard, D. Ing., président

M. TROCHU François, Ph. D., membre et directeur de recherche

M. HUBERT Pascal, Ph. D., membre

M. VADEAN Aurelian, Doct., membre

*A mis amigos, a mis hermanos,
a los que están aquí y a los que viven en mí.*

A mi madre, que me despertó

a la aventura de crecer y creer.

De la raíz al fruto, somos alegoría de adulto.

REMERCIEMENTS

Je tiens à remercier mon directeur de recherche M. François Trochu, qui m'a accueilli depuis le début au sein du CRASP, son enthousiasme m'a embarqué dans la navette du défi scientifique. Ses conseils judicieux dans mon travail et son soutien personnel ainsi que ses encouragements sont une partie intégrante de ce travail.

La bonne conduite de la recherche nécessite un travail d'équipe. A tous les membres de l'équipe CCHP (Chaire sur les composites à haute performance), pour leurs qualités humaines et leur agréable compagnie durant ces quatre années, reçoivent ma profonde reconnaissance.

Je tiens également à remercier les techniciens du CRASP, M. Jacques Beausoleil et M. Christian C. Martel, pour leurs conseils opportuns et leur disponibilité pour résoudre les nombreux problèmes qui se sont présentés au cours de mes travaux expérimentaux.

J'adresse mes remerciements au professeur Raymond Gauvin pour les discussions fructueuses, ses conseils scientifiques et son constant bonheur.

Je souhaite aussi remercier les professeurs Bernard Sanschagrin, Pascal Hubert et Aurelian Vadean pour avoir accepté de juger cette thèse.

RÉSUMÉ

Les applications des matériaux composites renforcés par des fibres continues ont connu une croissance importante dans de nombreux secteurs industriels. Les techniques de moulage par transfert de résine LCM (« Liquid Composite Molding ») sont devenues des méthodes de fabrication de plus en plus utilisées ces dernières années. Les objectifs de cette thèse consistent à développer des équations caractéristiques du comportement thermomécanique et du changement de phase des matériaux composites thermodurcissables, mettre au point des modèles numériques pour la simulation de la mise en forme et, finalement, établir une méthodologie d'optimisation du cycle de cuisson et de refroidissement des pièces. Dans ces procédés, le renfort fibreux est progressivement saturé par la résine liquide. Une fois la cavité du moule remplie, la résine thermodurcissable polymérise et se solidifie. Du point de vue de la simulation numérique, le procédé peut être divisé en trois étapes principales: (1) remplissage, (2) cuisson et (3) refroidissement et démoulage. La caractérisation, la simulation et l'optimisation de ces trois étapes font partie des développements présentés dans cette thèse.

Les composites à matrice polymère sont souvent appelés « laminés » parce qu'ils sont constitués par la superposition d'un certain nombre de couches de renforts fibreux imprégnés par une matrice polymère. Des phénomènes physiques importants se produisent à travers l'épaisseur de ces matériaux lors de leur fabrication. En particulier, lorsqu'ils sont fabriqués par injection, l'écoulement de la résine et les transferts de chaleur qui lui sont associés quand la résine ou le moule sont chauffés, sont des phénomènes tridimensionnels. Cependant comme l'épaisseur des pièces composites est généralement faible par rapport à leur taille, l'analyse numérique de l'écoulement et des transferts thermiques pendant leur fabrication par injection et pendant la cuisson lors de la polymérisation peut avantageusement en tenir compte en découplant l'approximation

à travers l'épaisseur par rapport aux autres approximations. Cette thèse porte sur l'analyse de l'écoulement et de la cuisson d'un composite en tenant compte de l'importance physique des phénomènes qui se produisent à travers l'épaisseur du matériau. La thèse est divisée en 7 articles qui commencent par une synthèse faisant le point sur la bibliographie des procédés suivi par la modélisation des procédés d'injection sur renfort.

La première partie de l'étude fait le point sur la caractérisation de la cinétique de polymérisation et du comportement viscoélastique d'un composite verre/polyester. Un modèle semi-empirique a été développé pour tenir compte des effets de l'inhibiteur et de la transition vitreuse du matériau sur la cinétique de polymérisation. Deux modèles différents ont été proposés pour décrire l'influence des effets thermiques et chimiques sur les propriétés élastiques du matériau. Le premier est un modèle thermochimique élastique non linéaire qui considère la relaxation totale du matériau à l'état caoutchoutique au-dessus de la température de transition vitreuse. Le deuxième est un modèle viscoélastique complexe fondé sur la mesure de la relaxation des contraintes et le principe de superposition temps/température.

Une solution numérique de l'équation de l'énergie couplée à une analyse de contraintes unidimensionnelle a été développée pour simuler les effets thermiques, chimiques et mécaniques pendant la cuisson. Le calcul numérique des contraintes résiduelles et la modélisation des propriétés élastiques ont été vérifiés expérimentalement en moulant des plaques minces. Une étude a porté sur l'évaluation des contraintes internes pendant les cycles de cuisson et refroidissement des plaques épaisses. À partir de la comparaison de différents profils de température typiquement utilisés dans l'industrie, d'importantes conclusions ont été tirées sur l'évolution du degré de polymérisation à travers l'épaisseur. Cette étude a apporté une conclusion sur la relation qui existe entre le gradient thermique à travers l'épaisseur d'un composite et l'évaluation du degré de cuisson et des contraintes internes.

Pour la simulation numérique de l'étape de remplissage non isotherme et la cuisson des pièces minces, une méthode d'extrapolation de maillage a été mise au point et un nouvel élément fini tridimensionnel non conforme développé. Une formulation hybride d'éléments finis et différences finies a été proposée pour la solution de l'équation de l'énergie. L'algorithme présenté permet de prendre en compte plusieurs niveaux de couplage entre l'écoulement de la résine et les échanges thermiques. La méthodologie proposée dans ce travail permet à l'utilisateur du code de définir, à partir du même maillage 2D initial, le niveau de complexité devant être utilisé par le modèle numérique.

L'optimisation des cycles de chauffage, cuisson et refroidissement dans la fabrication des pièces composites par LCM a finalement été traitée. L'approche développée porte sur la minimisation du temps du cycle, l'amélioration des propriétés mécaniques et la réduction des contraintes résiduelles dans le composite. Un algorithme d'évolution fondé sur les algorithmes génétiques et appelé LeCoq (« Logical Evolutionary Curing Optimization and Quenching ») a été développé pour optimiser les profils de température du moule. Enfin, la cuisson d'une pièce composite épaisse a été optimisée avec cet algorithme.

ABSTRACT

During the last years, applications of composite materials reinforced with continuous fibers have increased in many industrial fields. Composite materials being lightweight and corrosion free, their scope of application covers the aerospace, automobile, marine and sport sectors. The Liquid Composite Molding techniques (LCM) have become widely used composite manufacturing methods for medium to small production volumes. The objectives of this thesis consist of developing characteristic equations that describe the thermo-mechanical behaviour and phase changes of thermosetting matrix composites, create and implement new numerical models for process simulation and finally, propose a new and comprehensive optimization methodology based on genetic algorithms for the curing and cooling of LCM parts. In these processes, the fibrous reinforcement is progressively saturated by the liquid resin. Once the mold cavity is filled, the thermosetting resin polymerizes and solidifies. From the point of view of the numerical simulation, the process can be divided into three principal stages: (1) filling, (2) curing and (3) cooling and demolding. The material characterisation, numerical simulation and optimization of these three stages are included in the scope of works of this thesis.

Polymer composites are often called *laminates* because they are made of stacked layers of fibrous reinforcements impregnated by a polymer matrix. During manufacturing, important physical phenomena take place through the thickness of these composite materials. When they are fabricated by liquid resin injection, resin flow and heat transfer are strongly coupled if the mold is heated. This three-dimensional effect may be neglected in thin parts (i.e., when the thickness is small compared to the other dimensions). However, although in this case decoupling of the in-plane flow and transverse heat flow may be propitious for fast analysis of the three-dimensional effects. This thesis has focused on the analysis of the filling and curing of composite parts when

through-thickness physical phenomena (i.e., heat and flow transfer through the thickness of the laminate) must be taken into account. This work is divided into 7 publications beginning with a bibliographic review followed by one article on material characterization, two articles on process modeling, two articles on numerical simulation and one final article on process optimization.

The first part of this study concerns the characterization of the cure kinetics and the viscoelastic behaviour of a glass/polyester composite. A semi-empirical model was developed to take into account the effects of inhibitor decomposition and glass transition on cure kinetics. Two models are proposed to describe the chemical and thermal effects on the mechanical properties of the composite. The first one is a thermo-chemical elastic non-linear model that considers total matrix relaxation in the rubbery state above the glass transition temperature. The second one is a viscoelastic model based on the stress relaxation and the time/temperature superposition principle.

A one-dimensional solution of the heat equation coupled with stress analysis has been developed to simulate thermal, chemical and mechanical effects during cure. The calculation of residual stresses and the elastic model have been experimentally verified by molding thin composite plates. A study has been carried out on the evolution of internal stresses during the curing and cooling of thick parts. The comparison of different mold temperature profiles typically used in industry has showed important conclusions on the evolution of the curing front through the thickness of the laminate. This work discusses finally important conclusions on the relationship between through-thickness thermal gradients, the cure front and internal stresses.

To analyze the non isothermal filling and curing stages, a mesh extrapolation method has been developed, and a new three-dimensional non-conforming finite element proposed. A finite element formulation coupled with finite differences has been proposed to solve the energy equation in three dimensions. The algorithm presented

allows the introduction of various levels of coupling between the fluid and heat flows. The methodology developed on this work allows the program user to define, from the same initial 2D mesh, the level of complexity to be used by the numerical model.

The optimization of the pre-heating, curing and cooling stages in the manufacturing of composite parts by LCM is finally treated. This comprehensive approach incorporates several objectives in the same optimization procedure: minimization of cycle time, improvement of mechanical properties and reduction of laminate residual stresses. An evolutionary algorithm based on genetic algorithms, the code called LeCoq (Logical Evolutionary Curing Optimization and Quenching), has been developed to optimize the mold temperature transient profile. Finally, the curing of a thick composite part has been optimized with this algorithm.

TABLE DES MATIÈRES

DÉDICACE.....	iv
REMERCIEMENTS.....	v
RÉSUMÉ.....	vi
ABSTRACT.....	ix
TABLE DES MATIÈRES.....	xii
LISTE DES FIGURES.....	xviii
LISTE DES TABLEAUX.....	xxxix
LISTE DES ANNEXES.....	xxxvi
INTRODUCTION	1
0.1 Les matériaux composites.....	1
0.2 Moulage liquide des composites.....	1
0.3 Simulation numérique des procédés LCM.....	4
0.4 Objectifs de la recherche.....	5
0.4.1 Caractérisation thermique et mécanique des matériaux.....	5
0.4.2 Analyse unidimensionnelle de la cuisson et contraintes résiduelles.....	6
0.4.3 Simulation numérique d'un écoulement stratifié et cuisson	6
0.4.4 Optimisation du chauffage du moule et de la cuisson du composite.....	7
0.5 Organisation de la thèse	8
CHAPITRE 1. STATE OF THE ART REVIEW OF NUMERICAL SIMULATION OF LIQUID COMPOSITE MOLDING PROCESSES	12
1.1 Abstract.....	13
1.2 Introduction.....	14
1.3 Model of fiber impregnation.....	16
1.4 Heat transfer analysis.....	24
1.5 Resin kinetics	30
1.6 Resin mechanical properties	40
1.7 Part quality and process residual stresses	43

1.8 RTM process optimization.....	47
1.9 References.....	55
CHAPITRE 2. THERMO-MECHANICAL PROPERTIES DURING CURE OF GLASS-POLYESTER RTM COMPOSITES: ELASTIC AND VISCOELASTIC MODELING	61
2.1 Abstract.....	63
2.2 Introduction.....	65
2.3 Kinetic modeling.....	67
2.3.1 Identification of the Arrhenius factor $K_1(T)$	72
2.3.2 Identification of functions $K_2(\alpha)$ and $K_3(T, \alpha)$	73
2.3.3 Inhibitor decomposition	74
2.4 Thermo-mechanical modeling	75
2.4.1 Physical analysis	75
2.4.2 Normalized parameters	77
2.4.3 General semi-empirical model.....	79
2.4.4 Shear modulus.....	81
2.4.5 Composite effective properties	81
2.5 Viscoelastic modeling.....	83
2.5.1 Modeling of stress relaxation.....	84
2.5.2 Cure dependent relaxation modulus.....	86
2.6 Volume changes during cure	87
2.7 Longitudinal and transverse CTE	88
2.8 Summary	90
2.9 Acknowledgements.....	92
2.10 References.....	92
CHAPITRE 3. INTERNAL STRESSES AND WARPAGE OF THIN COMPOSITE PARTS MANUFACTURED BY RTM.....	117
3.1 Abstract.....	118
3.2 Introduction.....	119
3.3 Thermo-mechanical modeling	120
3.3.1 Thermo-mechanical model	121

3.3.2 Model of volume changes.....	124
3.3.3 Coefficients of thermal expansion	125
3.3.4 Strain-stress modeling.....	126
3.4 Analysis of thin composite plates during cooling.....	126
3.5 Conclusion	128
CHAPITRE 4. NUMERICAL ANALYSIS OF CURE TEMPERATURE AND INTERNAL STRESSES IN THIN AND THICK RTM PARTS.....	126
4.1 Abstract.....	137
4.2 Introduction.....	138
4.3 Thermo-mechanical analysis	142
4.3.1 Heat transfer equation.....	143
4.3.2 Chemical reaction	144
4.3.3 Induction time	145
4.3.4 Thermo-chemical dependencies of mechanical properties.....	146
4.3.5 Composite effective mechanical properties.....	149
4.3.6 Volume changes.....	150
4.3.7 Longitudinal and transverse coefficient of thermal expansions (CTE) ..	151
4.3.8 Strain-stress modeling.....	152
4.4 Analysis of thin composite plate cooling.....	153
4.5 Analysis and optimization of thick plate processing	155
4.5.1 <i>Outside-to-Inside</i> cure.....	156
4.5.2 <i>Inside-to-Outside</i> cure.....	157
4.5.3 <i>One-side</i> cure	157
4.5.4 Optimization of cure cycle.....	158
4.6 Summary	159
4.7 Acknowledgements.....	160
4.8 References.....	161
CHAPITRE 5. COUPLED NON-CONFORMING FINITE ELEMENT AND FINITE DIFFERENCE APPROXIMATION BASED ON LAMINATE EXTRAPOLATION TO SIMULATE LIQUID COMPOSITE MOLDING PROCESSES. PART I: ISOTHERMAL FLOW.....	180
5.1 Abstract.....	182

5.2 Introduction.....	183
5.3 Governing equations	185
5.4 Potential formulation	187
5.5 Finite elements discretization	188
5.5.1 Mass conservation and div-conform approximation.....	189
5.5.2 Finite elements for LCM simulation.....	190
5.6 Flow front advancement	193
5.7 Application to 3-dimensional flows in LCM	193
5.8 Mesh generation for through-thickness flow analysis	195
5.8.1 Structure of the laminate.....	198
5.9 Experimental validation – Case I.....	199
5.10 Experimental validation – Case II.....	202
5.11 Case study – Truck fender	204
5.12 Summary.....	208
5.13 Acknowledgements.....	209
5.14 References.....	209
CHAPITRE 6. COUPLED NON-CONFORMING FINITE ELEMENT AND FINITE DIFFERENCE APPROXIMATION BASED ON LAMINATE EXTRAPOLATION TO SIMULATE LIQUID COMPOSITE MOLDING PROCESSES. PART II: NON-ISOTHERMAL FLOW	234
6.1 Abstract.....	236
6.2 Introduction.....	237
6.3 Governing equations	243
6.3.1 Momentum equation	243
6.3.2 Energy and chemical species	245
6.4 Finite elements formulation	248
6.5 Solution of shell-like geometries	251
6.6 Finite difference formulation	253
6.7 Numerical implementation of the hybrid FE/FD model.....	258
6.8 Analytical validations	260
6.8.1 Case I: 3D heat conduction - steady-state.....	260

6.8.2 Case II: 3D heat diffusion - un-steady-state	262
6.8.3 Case III: heat diffusion with source term - curing analysis	264
6.8.4 Case IV: heat convection test.....	266
6.9 Case study – Automotive front hood	268
6.10 Summary	270
6.11 Acknowledgements.....	271
6.12 References	271
CHAPITRE 7. COMPREHENSIVE THERMAL OPTIMIZATION OF LIQUID COMPOSITE MOLDING TO REDUCE CYCLE TIME AND PROCESSING STRESSES.....	296
7.1 Abstract.....	298
7.2 Introduction.....	299
7.3 Governing equations	304
7.3.1 Energy balance equation	305
7.3.2 Strain-stress modeling.....	306
7.4 Evolutionary algorithms.....	307
7.4.1 Problem identification.....	308
7.4.2 Final extent of cure	309
7.4.3 Maximum exothermic temperature.....	310
7.4.4 Cross-over at After Gel Point objective.....	311
7.4.5 Cure gradients after AGP.....	313
7.4.6 Curing stresses	315
7.4.7 Cooling stresses	316
7.4.8 Processing time	317
7.4.9 Design parameters.....	317
7.5 Fitness function.....	319
7.6 Results and discussion	320
7.6.1 Two ramps curing-cycle	321
7.6.2 Thin part optimization.....	325
7.6.3 Thick part optimization.....	327
7.7 Summary	332

7.8 Acknowledgements.....	334
7.9 References.....	334
CHAPITRE 8. DISCUSSION GÉNÉRALE ET PERSPECTIVES	351
8.1 Discussion générale	351
8.2 Perspectives.....	358
8.3 Importance des travaux pour l'industrie canadienne	362
8.4 Matériaux utilisés.....	362
8.4.1 Résine.....	363
8.4.2 Renforts.....	363
8.5 Instruments de caractérisation.....	364
8.6 Statistiques du travail.....	367
CONCLUSION.....	371
BIBLIOGRAPHIE.....	373
ANNEXES.....	381

LISTE DES FIGURES

Figure 0.1. Le procédé RTM.....	3
Figure 1.1. Resin transfer molding process for manufacturing of composite materials.....	15
Figure 1.2. Filling algorithms to analyze the flow development depicted in a): b) Lagrangian solution, c) MAC, d) Control Volume methods.	19
Figure 1.3. Part and mold design by using numerical simulations [1], a) designed part, b) filling numerical simulation, c) tool design and, c) mold deflection analysis from filling pressures	21
Figure 1.4. Re-meshing algorithms applied to RTM injection [34]	23
Figure 1.5. Coupling of phenomena present in the LCM process.	26
Figure 1.6. Comparison of degrees of polymerization from DSC with predictions of three kinetic models for a constant heating ramp of 7 °C/min. Autocatalytic equation diverges at the end of curing. Kamal-Sourour equation approaches the measured data although some differences are noticed at the end of curing. The Ruiz equation (named proposed model) is the most accurate.	40
Figure 1.7. Resin modulus development during cure	41
Figure 1.8. Linear variations of the resin mechanical properties with cure degree.	43
Figure 1.9. Shrinkage defects in a fiber-reinforced composite part.....	44
Figure 1.10. Two examples of matrix cracking and delamination during processing of thick composite plates. Defects appear commonly in thick composites processed at high mold temperature.	45
Figure 1.11. a) typical processing stresses within a composite laminate, b) macro and micro levels of internal stresses	45
Figure 1.12. Process design parameters and issues to optimize	48

Figure 1.13. RTM optimization methods, a) optimization curve of filling time versus mold temperature, and b) parametric Kriging surfaces intersection to optimize cure temperature, by Ruiz [77]	52
Figure 2.1. DSC measurements of heat flows during dynamic cure of T580-63 polyester resin. Raw data have been processed using a second scan as base line and a linear interpolation of the specific heat.....	95
Figure 2.2. Thermographs obtained from DSC data during dynamic cure for several heating rates.....	95
Figure 2.3. Reaction rate at peak and time to peak obtained from DSC measurements. Logarithmic functions relate both parameters with peak temperature...	96
Figure 2.4. Temperature dependence of factor K_1 and parameter n of the power function K_3 for the kinetic modeling of equation (2.5). While n seems to be constant, K_1 exhibits an Arrhenius type of temperature dependence.....	96
Figure 2.5. Kinetic factor K_2 as a function of polymerization degree fitted by a 6 th degree polynomial curve.....	97
Figure 2.6. Maximum degree of polymerization and induction times as a function of curing temperature. Experimental data comes from DSC measurements. Fitting curves are polynomial for the degree of cure and an integral equation (2.13) for induction times.....	97
Figure 2.7. Comparisons of the degree of polymerization from DSC with predictions of three kinetic models for a constant heating ramp of 10 °C/min. Autocatalytic equation diverges at the end of curing. Kamal-Sourour equation approaches the measured data although some differences are noticed. The proposed model of equation (2.8a-d) is the most accurate.	98
Figure 2.8. DSC measurements of the degree of polymerization and predictions of the proposed kinetic model of equation (2.8a-d). A good agreement between the model and experimental data is observed for all heating ramps measured.....	98

Figure 2.9. DMTA measurements of fully cured resin elastic modulus as a function of temperature and curve fitting of the experimental data. Isothermal values are reported for each temperature.	99
Figure 2.10. Measured degree of polymerization and elastic modulus versus time during isothermal curing cycle. DSC and DMTA runs were carried out at 75 °C. While DSC measures are reproducible, DMTA data show important variations.	99
Figure 2.11. Evolution of elastic modulus during resin cure for runs at constant heating ramp. Initial temperature was set to 75 °C and the heating ramp to 3 °C/min. Elastic modulus increases with the polymerization reaction, but decreases afterwards with temperature.	100
Figure 2.12. Description of the methodology used to determine the normalized elastic modulus during cure. DMTA measures of partially cured samples are stabilized at 70 °C and then heated at 3 °C/min. The normalized elastic modulus is calculated as the difference between measured value (3) and modulus at AGP (2) in percent of the fully cured modulus (1), see equation (2.14).	101
Figure 2.13. Comparison between degrees of polymerization and normalized elastic modulus \hat{E}' during a specified curing cycle. Thermal (DSC) and mechanical (DMTA) measures differ.	102
Figure 2.14. Quasi-linear relation between the logarithms of \hat{E}' and of the normalized degree of cure.	102
Figure 2.15. Logarithmic approximation and extended model of \hat{E}' as a function of the degree of polymerization. Extended model of equation (2.19b) is in good agreement with DMTA/DSC measures.	103
Figure 2.16. Temperature shift factor as a function of temperature for various degrees of polymerization. Also glass transition temperature T_g is plotted as a function of degree of cure.	103
Figure 2.17. DMTA measurements of E' for partially and fully cured samples of T580-63 polyester resin. Lines represent predictions of the elastic model of	

equation (2.18). For all tested degrees of cure, the model predicts with reasonable accuracy the resin elastic modulus.....	104
Figure 2.18. Measured and predicted E' in both directions for a NCS-82620 composite with $V_f = 42\%$. Fully and partially cured composite samples were tested in principal directions (i.e., E_1 , E_2). Predictions of elastic model of equation (2.21) are in good agreement with measured values.	104
Figure 2.19. Measured and predicted E' for different fiber volume fractions. Fully cured composite samples of NCS-82620 fabric and U101 mat were tested in the DMTA. Lines are fitting the elastic model of equation (2.21).	105
Figure 2.20. Rule of mixture for E' as a function of fiber volume fraction. Intervals A and B represent the validity range of V_f for U101 and NCS-82620 materials respectively.	105
Figure 2.21. Measured E' in DMTA relaxation test. Fully cured sample of T580-63 polyester resin.	106
Figure 2.22. Stress relaxation profiles for the fully cured resin samples at various isothermal temperatures, from 30 to 170 °C.	106
Figure 2.23. Relaxation modulus master curve for the fully cured resin samples. Relaxation spectrum is also shown as a function of reduced time.	107
Figure 2.24. Shift function used for the time-temperature superposition to construct the master curve.	107
Figure 2.25. Curve fitting of relaxation modulus by the proposed viscoelastic model for the fully cured samples of T580-63 polyester resin.	108
Figure 2.26. Model fit of stress relaxation profiles for the fully cured resin samples at various isothermal temperatures after applying TTS shift function a_T	108
Figure 2.27. Measured E' in DMTA relaxation test at some polymerization degrees for the T580-63 polyester resin.....	109
Figure 2.28. Linear interpolation of Ω_1 and Ω_3 parameters used in equation (2.17) for viscoelastic modeling as a function of polymerization degree. Also unrelaxed modulus are presented as a function of cure.....	109

Figure 2.29. Model fit of the relaxation modulus for some polymerization degrees for the T580-63 polyester resin.....	110
Figure 2.30. Shift functions data and linear modeling for some resin polymerization degrees.	110
Figure 2.31. Viscoelastic modeling of stress relaxation profiles for the resin sample cured at 93%, for various isothermal temperatures.	111
Figure 2.32. Viscoelastic modeling of stress relaxation profiles for the resin sample cured at 45%, for various isothermal temperatures.	111
Figure 2.33. Viscoelastic modeling of stress relaxation profiles as a function of time for the glass/resin composite sample (direction 1 at $V_f=45\%$).....	112
Figure 2.34. Viscoelastic modeling of stress relaxation profiles as a function of time for the glass/resin composite sample (direction 2 at $V_f=40\%$).....	112
Figure 2.35. Linearization of chemical shrinkage induced by resin polymerization (TMA versus DSC measures).	113
Figure 2.36. Coefficient of thermal expansion for partially and fully cured resin samples (from TMA measures).	113
Figure 2.37. Coefficients of thermal expansion for fully cured composite samples of NCS-82620 fabric. Symbols d1 and d2 indicate the principal planar directions of the fabric, while T refers to the transverse direction.	114
Figure 3.1. Comparison of polymerization degree and E' during specified curing cycle.	130
Figure 3.2. DTMA measures of E' for partially and fully cured resin samples (lines presents model predictions).	130
Figure 3.3. Measured and predicted E' in both directions for composite with $V_f=42\%$ of NCS-82620 (fully and partially cured samples).	131
Figure 3.4. Measured and predicted E' for different V_f . Fully cured composite samples of NCS-82620 fabric and U101 mat.	131
Figure 3.5. Rule of mixtures for E' as function of V_f . A and B represent validity range of V_f for U101 and NCS materials respectively.	132

Figure 3.6. Coefficients of thermal expansion for fully cured composite samples of NCS-82620 fabric. d1 and d2 indicate principal planar directions of the fabric, while T refers to transverse direction.....	132
Figure 3.7. A) Stacking sequence for thin plates. The number of NCS plies was changed while mold thickness was maintained constant and 2 plies of U101 were used in every cases. B) Warpage appearing in thin composite plates after manufacture. Total deflection at the center is the sum of longitudinal and transverse deflections.....	133
Figure 3.8. Measure of typical plate deflection during cooling from above the glass transition temperature. The sample has 2 plies of NCS-82620 fabric and 2 plies of U101 mat.....	133
Figure 3.9. Comparison of measured plates deflections with numerical predictions of the thermo-mechanical model.	134
Figure 4.1. Scope of works related to part quality in RTM manufacturing. The global problems need to be defined, requirements of material characterization stated and appropriate objective functions derived for processing optimization.	163
Figure 4.2. Comparison of DSC measurements of the resin degree of polymerization with predictions of the resin cure kinetics model. Heating ramps from 5 to 35°C/min are compared and shown a good agreement with model predictions.....	164
Figure 4.3. Curves of resin maximum degree of polymerization and induction time as a function of curing temperature. These results were obtained from DSC measurements data after applying the isoconversion methodology.	164
Figure 4.4. Comparison of the resin Young's modulus (E') and degree of polymerization during a specified curing cycle: E' is measured with a DMA while the degree of polymerization comes from DSC measurements.....	165
Figure 4.5. A non-linear correlation between E' and the degree of polymerization was found for the polyester resin tested. Here DMA measurements of E' are plotted as a function of degree of polymerization obtained from DSC results.....	165

Figure 4.6. Temperature shift factor as a function of temperature for various degrees of polymerization. The glass transition temperature T_g is also drawn as a function of the degree of polymerization.	166
Figure 4.7. Comparison of the model predictions and DMA measures of Young's moduli E' for partially and fully cured resin samples (the lines present model predictions).	166
Figure 4.8. Measured and predicted Young's modulus E' in both directions for a composite with volume fraction $V_f=42\%$ of NCS-82620 (fully and partially cured samples).	167
Figure 4.9. Measured and predicted E' for different fiber volume fractions V_f of fully cured composite samples made of NCS-82620 fabric and U101 mat.	167
Figure 4.10. Rule of mixtures for E' as a function of fiber volume fraction V_f . Regions A and B represent the experimental domain of validity of V_f for U101 and NCS materials respectively.	168
Figure 4.11. Linearization of chemical shrinkage induced by resin polymerization (TMA versus DSC measures).	168
Figure 4.12. Coefficients of thermal expansion for partially and fully cured resin samples (from TMA measurements).	169
Figure 4.13. Coefficients of thermal expansion for fully cured composite samples of NCS-82620 fabric: d1 and d2 indicate the principal planar directions of the fabric, while T refers to the transverse direction.	169
Figure 4.14. Stacking sequence for thin plates: the number of NCS plies was changed while mold thickness remained constant; two plies of U101 were used for all the test samples.	170
Figure 4.15. Warpage appearing in thin composite plates after manufacture due to unbalanced layup. Total deflection at the plate center is the sum of longitudinal and transverse deflections.	170
Figure 4.16. Measure of typical plate deflection during cooling from above the glass transition temperature. The sample has 2 plies of NCS-82620 fabric and 2 plies of	

U101 mat. While temperature decreases from 140°C to room temperature, plate deflection increases from 5 to 17 mm.	171
Figure 4.17. The measured plate deflection during cooling is compared with the numerical prediction of the thermo-mechanical model. Three measures were performed for each plate. The two samples show a good agreement with predicted values.	172
Figure 4.18. Two examples of matrix cracking and delamination during processing of thick composite plates. Defects appear commonly in thick composites processed at high mold temperature.	173
Figure 4.19. Schematics of the evolution of the curing front through the thickness of a thick part: <i>Outside-to-Inside</i> , <i>Inside-to-Outside</i> and <i>One-Inside</i> cure scenarios are considered.	173
Figure 4.20. Numerical calculation of temperature and Young's modulus E' for a 15 mm thick composite cured at a mold temperature of 120 °C: high exothermic temperature peaks are observed.	174
Figure 4.21. Through-thickness calculation of polymerization degrees during <i>outside-to-inside</i> cure of a 15 mm thick composite. A and B denote the AGP level at the surface and middle thickness respectively.	174
Figure 4.22. Calculated stresses developed during <i>outside-to-inside</i> cure. Internal stresses rapidly develop during cure after 10 min., due to resin shrinkage in the core.	175
Figure 4.23. Through-thickness chemical strains induced by resin polymerization shrinkage for an <i>outside-to-inside</i> cure. At about 10.7 minutes, fast curing of the core generates high chemical strains.	175
Figure 4.24. Numerical calculation of temperature and through-thickness degree of polymerization for an <i>inside-to-outside</i> cure. The thick plate is processed at a temperature of 70 °C.	176
Figure 4.25. Computed internal stresses during <i>inside-to-outside</i> cure (plate processed at 70 °C). While no stresses are developed during the cure phase, contraction stresses appear in the core due to thermal variations.	176

Figure 4.26. Calculated temperature and degree of polymerization during <i>one-side</i> cure. Resin polymerization evolves from the hot to cold surface, resulting in a high exothermic peak in the regions close to the cold surface.....	177
Figure 4.27. Numerical internal stresses during <i>one-side</i> cure. Internal stresses grow up in the regions close to the cold surface during resin polymerization (after around 24 minutes).....	177
Figure 4.28. Numerical calculation of temperature and degree of cure for an optimized curing cycle. Initial mold overheating and appropriate heating ramps result in a quasi-constant through-thickness progression of polymerization and minimization of temperature gradients.	178
Figure 4.29. Calculation of through-thickness internal stresses during optimized curing cycle. Low residual stresses are found after processing while final polymerization degree is maximized.	178
Figure 5.1. Schematic representation of the domain Ω representing the mold cavity. The boundary is defined by $\partial\Omega = \Gamma_q \cup \Gamma_p \cup \Gamma_d$. (Note that Γ_d was deliberately removed for clarity.)	212
Figure 5.2. Triangular finite element: (a) incoming and out-coming flows in the FE; (b) conforming shape function at node N_1 ; (c) non-conforming shape function associated to edge E_1	213
Figure 5.3. Triangular and prismatic (6 nodes) non-conforming finite elements. The degrees of freedom are assigned at the middle edges; ζ , η and τ denote the local coordinates in the reference element.....	213
Figure 5.4. Extrusion of a midplane mesh through the thickness of the composite. From 2D finite elements, a solid mesh consisting of N_l layers may be constructed to calculate 3D flows.....	214
Figure 5.5. Procedure for mesh extrusion: (a) the nodes normal are computed from the normals in adjacent elements, (b) new nodes are created along the calculated normal, (c) finally adjacent elements are extruded.....	215

- Figure 5.6. Selection of the extrusion direction using the χ and γ coefficients of equation (21). (a) the position of the new nodes can be computed from the midplane position; (b) from the half thickness; (c) or in the opposite normal direction; (d) ply thickness can also be set as a spatial function.....216
- Figure 5.7. (a) In composite manufacturing, layers of fibrous materials are stacked to form a compact preform. (b) The plies of the laminate can have a different thickness and fiber orientation.....216
- Figure 5.8. Data structure used to relate zones of PamRTM [11] with the structure of the laminate. Each ply of the laminate is related to a fabric material. Multiple zones can be connected to the same laminate and different plies can point to the same material.....217
- Figure 5.9. Typical applications of the extrusion algorithm. Examples of three-dimensional meshes for various stacked materials may be constructed from the midsurface mesh and structure of the laminate. The first example shows an irregular surface of revolution. The second example is a ribbed part. The third example shows that an impermeable foam core can also be considered as part of the laminate structure.....218
- Figure 5.10. Schematic diagram of the through-thickness flow front shape measurement system used by Diallo et al. [14].219
- Figure 5.11. Three-dimensional model used to simulate the experiments of Diallo et al. [14]. In each layer of the laminate, the mesh contains 4 *prism6* finite elements in the through-thickness direction.....219
- Figure 5.12. Flow front progression in the top and bottom mold surfaces. Numerical results are compared to experimental values. The flow front distortion is stabilized after 20 sec. The numerical through-thickness front at 88 seconds is shown in the bottom right caption and is very close to the experimental profile.....220
- Figure 5.13. Progression of the flow front in the midplane for different anisotropy ratios. Compared to the two-dimensional (triangles) solution, the tetrahedron and *prism6* solutions predict well the filling at the interface.....221

- Figure 5.14. Comparison of mass loss for simulations with triangles, tetrahedrons and *prism6* elements. In all cases, the mass loss is less than 3%. The *prism6* solution is systematically more conservative than tetrahedrons and never worse than the triangle solution.....222
- Figure 5.15. The distortion of the through-thickness flow front profile for *prism6* and tetrahedrons is compared to a 2D reference simulation (triangles). Tetrahedrons are able to represent correctly the front geometry for high anisotropy ratios. When the size of the *prism6* mesh is increased to a half of the elements of the tetrahedron mesh, the flow front error is even improved compared to the tetrahedron solution.....223
- Figure 5.16. Schematic drawing of a spherical central injection. The experiment of Bréard et al. [15] was carried out in a thick rectangular mold. The fibrous preform had an anisotropy ratio of 4.25 between the planar and transverse permeabilities. X-Ray radioscopy was implemented to detect the progression of the three-dimensional fluid flow.....224
- Figure 5.17. Comparison of predicted and measured flow fronts in the spherical injection. Numerical results are in good agreement with experimental values. At the beginning of the injection (before 2 *sec*), preform compaction may be the cause of the observed divergence with the numerical predictions.....224
- Figure 5.18. Comparison of flow front positions calculated for different mesh sizes with the theoretical solution of an elliptic flow through an isotropic material.....225
- Figure 5.19. Convergence of mesh refinement for the elliptic flow through an isotropic material. For the same number of elements on radius, the *prism6* solution yields better results than the tetrahedron one.....225
- Figure 5.20. a Typical LCM part used to demonstrate the capabilities of the model. The mesh contains 17,000 triangles and 8,500 nodes. The injection strategy consists of four inlet gates at the upper part corners, at the stiffener ends, and in the laminated zone. An impermeable foam core is wrapped by fabric skins in zone 10. Draping effects are represented as regions with high or low permeabilities.226

Figure 5.21. Injection strategy used for the truck fender. Four injection gates are set in the mold. Open channels are used for a better distribution of the resin flow. To ensure filling of the stiffener, an open channel is created at the extremity of the rib...	227
Figure 5.22. Three-dimensional model obtained after mesh extrusion. The mesh contains 60,000 <i>prism6</i> elements and 40,000 nodes.....	228
Figure 5.23. Predicted filling times with the triangular mesh for through-thickness averaged permeabilities. A total filling time of 24.6 <i>sec</i> was calculated. “D” indicates possible dry spots.....	229
Figure 5.24. Predicted flow front locations with the prismatic mesh with multi-layer extrapolation. A total filling time of 30.6 <i>sec</i> was calculated. An air bubble was trapped in the upper foam skin.....	230
Figure 5.25. Predicted flow front positions with the triangular mesh with the <i>bottom</i> foam skin permeability. A filling time of 23.5 <i>sec</i> was obtained.	231
Figure 5.26. Predicted flow front positions with the triangular mesh with the <i>top</i> foam skin permeability. A filling time of 27.2 <i>sec</i> was calculated.....	231
Figure 6.1. Coupling of physical phenomena in Liquid Composite Molding (LCM)..	274
Figure 6.2. Cross-section of the mold cavity showing the three-dimensional heat and fluid flows. The trough-thickness temperature profile results in variable resin viscosity and transverse fluid flow.	274
Figure 6.3. Because conforming finite elements are used in the heat transfer formulation, the coupling between 2D in-plane and 1D gapwise solutions is done via the control volume of the FD nodes defined by the centroids and mid-edges of connected elements.	275
Figure 6.4. Control volume of the one-dimensional finite difference approximation.	275
Figure 6.5. One-dimensional finite difference grid through the part thickness. The mold walls are heated or cooled by duct pipes maintained at a known reference temperature T_{ref}	276
Figure 6.6. Different levels of inter-layer coupling with the mesh extrapolation algorithm and the 1D finite difference grid.	276

Figure 6.7. Schematic representation showing increasingly complex integration of flow, conduction and transport solutions. Different levels degrees of coupling are obtained by combining FE meshes and FD grids.	277
Figure 6.8. Flow chart of the numerical algorithm for the non-isothermal analysis. ...	278
Figure 6.9. Domain used for the validation test I.	279
Figure 6.10. Two meshes used for test case I: extrapolated parallel layers coincide with the midplanes of each connected layer.	279
Figure 6.11. Comparison of pure FE and hybrid FE/FD solutions with theoretical values for test case I.	280
Figure 6.12. Maximum error of both formulations obtained for different mesh and grid sizes in test case I.	280
Figure 6.13. Rectangular domain used for validation test II and display of the 3D and parallel layers meshes.	281
Figure 6.14. Comparison with analytical values of adimensional temperature at point $X=Y=1$ for pure FE and hybrid FE/FD solutions (test case II.).	281
Figure 6.15. Convergence for 3D mesh refinement and parallel layers increment. The rate of convergence increases more with the number of layers (FE/FD solution) than with the number of nodes (FE solution). Note that the number of finite difference nodes is twice the number of layers.	282
Figure 6.16. Evolution of temperature and cure profiles at the cavity centre is depicted for pure finite elements and hybrid FE/FD solutions. The 2D FE solution is used as reference.	283
Figure 6.17. Comparison of error in the estimation of curing time for different mesh sizes. The hybrid formulation gives a better approximation than pure finite elements for the same number of through-thickness layers.	284
Figure 6.18. The performance of diver solutions is compared for various meshes with increased number of through-thickness layers of finite differences nodes. The hybrid formulations seem to give a better performance for curing analyses.	285

Figure 6.19. Rectangular cavity used for the 2D convection test with different top and bottom mold wall temperatures.....	286
Figure 6.20. Temperature evolution at the control point for the six solutions tested. ...	286
Figure 6.21. Temperature distribution at the end of filling along the cavity midplane for the six solutions tested.....	287
Figure 6.22. Midplane geometry and finite element discretization of the automotive hood used for the case study.	287
Figure 6.23. Flow front position in time for the non-isothermal mold filling of an automotive front hood. The solutions of four solution tested are depicted.	288
Figure 6.24. Degree of conversion at the end of filling in the automotive front hood. The two dimensional solutions seems to better account for cure transport at flow front.....	289
Figure 6.25. Evolution of the degree of conversion after filling for a curing time of 1500 sec. A curing front from the part perimeter to the center is induced by the non-isothermal filling.....	290
Figure 6.26. Comparison of computer times required for each model tested. While previous 3D solutions with tetrahedrons required more than 44 hours, the new <i>prism6</i> runs in 1 hour 40 min and the hybrid FE/FD solutions in 5 minutes.....	291
Figure 7.1. Process parameters and issues in LCM optimization.....	336
Figure 7.2. Square error versus sigmoid function for the final extent of cure sub-objective function. The sigmoid permits to increase the learning speed of the evolutionary algorithm (EA) near the desired optimization space.	336
Figure 7.3. Schematic of the through-thickness curing front in a typical thick composite laminate. The cross-over point $\alpha_{cross-over}$ must approach the α_{AGP} level to decrease the initiation delay.....	337
Figure 7.4. Comparison between the square error of g_{AGP} and the sigmoid objective J_{AGP} of equation (7.7).....	337

Figure 7.5. Schematic representation of the cure differentials between the part surface and the core. The sum of differentials is used to construct the objective sigmoid J_{cure} .	338
Figure 7.6. Comparison between the square error of ε_c and the sigmoid objective J_{cure} of equation (7.11).	338
Figure 7.7. Discretization of the temperature profile into a series of dwell times and heating/cooling ramps.	339
Figure 7.8. Two step curing cycle used for the evaluation of the fitness function.	339
Figure 7.9. Contour plot of the fitness function F_f for the curing cycle with two heating ramps (without considering internal stresses).	340
Figure 7.10. Contour plot of the fitness function F_f for the curing cycle with two heating ramps (considering the effects of internal stresses).	341
Figure 7.11. Cure cycle of the optimized temperature profile (with stress analysis) for the two heating ramps: $Q_1 = 0.82 \text{ } ^\circ\text{C}/\text{min}$ and $dt_2 = 46 \text{ min}$.	342
Figure 7.12. Convergence of the fitness function for LeCoq optimization for the two heating ramps with and without curing stresses.	342
Figure 7.13. Typically temperature profile used for the curing optimization of thin composite laminates.	343
Figure 7.14. Optimized temperature and cure profiles for the elastic and viscoelastic modeling of mechanical properties.	343
Figure 7.15. Temperature profile used for the curing optimization of thick composite laminates.	344
Figure 7.16. Optimized temperature and cure profiles for the 25 mm thick laminate with cure gradients minimization (i.e., no stress analysis).	344
Figure 7.17. Optimized temperature and cure profiles for the 25 mm thick laminate with elastic modeling of mechanical properties.	345
Figure 7.18. Optimized temperature and cure profiles for the 25 mm thick laminate with viscoelastic modeling of mechanical properties.	345

Figure 7.19. Processing stresses for the 25 <i>mm</i> thick laminate applying the optimized temperature profile with minimization of cure gradients (i.e., no stress analysis). The viscoelastic modeling was used for the stress calculation.....	346
Figure 7.20. Processing stresses for the 25 <i>mm</i> thick laminate with the optimized temperature profile and elastic modeling of mechanical properties.	346
Figure 7.21. Processing stresses for the 25 <i>mm</i> thick laminate with the optimized temperature profile and viscoelastic modeling of mechanical properties.....	347
Figure 8.1. Couplage possible des optimisations unidimensionnelles.....	360
Figure 8.2. Algorithme d'optimisation globale des procédés d'injection sur renfort....	361
Figure 8.3. Calorimètre DSC 910 et ordinateur de traitement des données.	364
Figure 8.4. Instrument d'essais mécaniques dynamiques : a) DMTA 2980 de TA Instrument, b) montage typique d'un échantillon en flexion double cantilever.	365
Figure 8.5. Instrument d'essais thermomécaniques : a) TMA 2940 de TA Instrument, b) montage d'expansion thermique.	366
Figure 8.6. Echancier des travaux réalisés.....	369
Figure 8.7. Statistiques des codes développés	370

LISTE DES TABLEAUX

Table 1.1. Mathematical models for phenomena present in the LCM process.....	26
Table 2.1. Values obtained for the kinetic parameters used in the cure modeling of T580-63 polyester resin.	115
Table 2.2. Parameters of the model of thermo-mechanical properties of T580-63 resin.....	115
Table 2.3. Values obtained for the modeling of the mechanical properties of T580-63 resin, NCS-82620 fabric and U101 mat composite.	116
Table 2.4. Parameters obtained for equations (26) to (28) to fit viscoelastic data of T580-63 resin.	116
Table 3.1. Plates dimensions and curvatures after manufacture for eight thin plates samples. Reported thicknesses are the average of 10 measures along the plates.	135
Table 3.2. Ultimate plate deflection when cooling after re-heating at 150°C. Both, numerical and measured deflections are at room temperature.....	135
Table 4.1. Summary of dimensions and curvatures of eight thin plate samples after demolding. Reported thicknesses are the average of 10 measures along the plates. Curvatures in the X-axis are calculated from 10 measures along this axis.	179
Table 4.2. Comparison of ultimate plate deflection during cooling after re-heating at 150 °C. Numerical and measured deflections are taken at room temperature.	179
Table 5.1. Series of test carried out to quantify the resin mass loss when using <i>prism6</i> finite elements.....	232
Table 5.3. Permeability and porosity for each zone of the truck fender model.....	233
Table 6.2. Kinetic model and thermal properties used in test case III.....	292
Table 6.3. Combination of different formulations and elements used for test case IV.	293
Table 6.4. Computer times required to calculate for each solution of test case IV (times are in seconds).....	293

Table 6.6. Description of the five models used to compute the non-isothermal filling and curing of the automotive front hood.....	294
Table 6.7. Comparison of results obtained with the five models tested for the non-isothermal filling and curing of the automotive front hood.....	295
Table 7.1. Characterized material properties to evaluate the energy and species balances during processing. Models are described in [A2].	348
Table 7.2. Characterized mechanical properties for the analysis of internal processing stresses. Models are described in [A2].	348
Table 7.4. Comparison of standard cure cycles with optimized cycles for the thin composite laminate.	349
Table 7.5. Summary of the optimized cure cycles for a 25 <i>mm</i> thick composite laminate.....	350

LISTE DES ANNEXES

ANNEXE I. CODES C++	381
ANNEXE II. ALGORITHME UNDIMENSIONNEL DE CONTRAINTES RESIDUELLES	393
ANNEXE III. COURBES DE CARACTÉRISATION DE LA CINÉTIQUE DE CUISSON	395
ANNEXE IV. DIAPOSITIVES DE LA PRÉSENTATION DE SOUTENANCE	399
ANNEXE V. FICHES TECHNIQUES DES MATÉRIAUX	421

INTRODUCTION

0.1 Les matériaux composites

Les matériaux composites à renfort fibreux sont de plus en plus utilisés dans les industries aéronautique et automobile. Beaucoup de ces matériaux présentent une combinaison de rigidité et de résistance comparable à celle des matériaux métalliques traditionnels. Comme leur densité est plus faible que celle des matériaux métalliques, les pièces composites sont plus légères. Ceci représente un des principaux avantages de leur utilisation dans l'industrie aéronautique. La résistance à la corrosion est une autre propriété importante des composites, notamment dans les applications marines.

Les matériaux composites à matrice polymère thermodurcissable les plus communs utilisent des renforts en fibres de verre, carbone, kevlar ou des fibres naturelles. La matrice polymère est généralement polyester, vinylester ou époxy. Le rôle des renforts est de supporter la charge mécanique appliquée à la pièce, tandis que celui de la matrice est de maintenir les renforts selon l'orientation désirée, de transférer les charges mécaniques entre les fibres et de les protéger contre les atteintes de l'environnement.

0.2 Moulage liquide des composites

Il existe plusieurs procédés pour fabriquer ces pièces comme le laminage manuel, l'utilisation de renforts préimprégnés en effectuant la cuisson de la matrice sous pression, l'infusion ou l'injection de résine liquide sur renfort, etc. Les procédés d'imprégnation de résine par infiltration dans un moule fermé ou dans une cavité sous vide ont été regroupés sous le terme générique de moulage liquide des composites ou

LCM (« Liquid Composite Molding »). Une des méthodes les plus développées dans l'industrie pendant les dernières années est le moulage par transfert de résine ou RTM (« Resin Transfer Molding »). Les bateaux, bains, douches, pièces de construction et cabines de camions constituent autant d'exemples de pièces fabriquées par RTM. On considère aussi que l'industrie automobile représente un potentiel d'applications important pour la mise en forme de pièces composites pour des moyennes et grandes séries. Le procédé RTM permet de fabriquer des pièces complexes par injection de la résine sur les renforts fibreux secs. Le renfort sec, ou préforme fibreuse, est placé dans un moule en deux parties, qui est ensuite fermé (voir Figure 0.1). Une résine thermodurcissable liquide est injectée sous pression pour imprégner le renfort fibreux. La réaction chimique de polymérisation est initiée par un catalyseur mélangé à la résine avant l'injection. Quand la polymérisation est terminée, le moule est ouvert et la pièce est éjectée.

Une des caractéristiques principales de la mise en forme des composites à matrice thermodurcissable est l'utilisation de la chaleur pour accélérer la réticulation de la résine. Ceci confère au procédé RTM la possibilité de réaliser un grand volume de production en assurant une bonne répétabilité dans les qualités mécaniques des pièces. Ce procédé nécessite des investissements relativement bas comparativement aux autres procédés comme le SMC (« Sheet Molding Compound »). De plus, comme la fabrication est réalisée en moule fermé, on réduit considérablement les émanations de styrène qui sont considérées comme un gaz hautement toxique. Ainsi, l'utilisation de ce procédé s'est étendue à plusieurs domaines pour lesquels les volumes de production sont raisonnables (au maximum de 20,000 pièces par année). De la fabrication des pièces structurales pour l'industrie aéronautique aux pièces de carrosserie d'automobile, le procédé RTM s'est révélé l'une des technologies les plus prometteuses pour la fabrication des matériaux composites à matrice thermodurcissable.

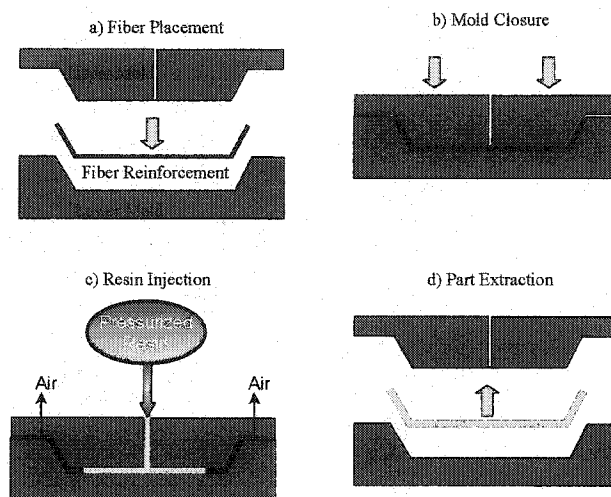


Figure 0.1. Le procédé RTM

Les résines thermodurcissables possèdent deux caractéristiques importantes: la réaction chimique de polymérisation est exothermique et un retrait est causé par l'établissement des liaisons chimiques pendant la polymérisation. La nature exothermique de la résine lors de la cuisson peut influencer énormément la température développée dans le composite en raison des effets combinés de la chaleur de réaction et de la conduction de chaleur à l'intérieur du composite. Le retrait qui résulte de la réticulation de la résine peut, sous certaines conditions, influencer de manière importante l'état des contraintes internes du composite et à l'extrême, induire des fissures. Ces caractéristiques sont généralement faibles pour les composites de petite épaisseur, mais deviennent déterminantes pour les plus grandes épaisseurs. Il est donc important de déterminer les paramètres thermiques du procédé qui influencent principalement la cristallisation et les variations volumétriques dans le composite.

Un intérêt grandissant est actuellement porté vers l'utilisation d'équipements permettant de chauffer le moule et la résine avant l'injection. La diminution de viscosité de la résine ainsi obtenue permet d'augmenter le débit de résine tout en

maintenant la pression d'injection au minimum. La diminution de l'écart entre la température de la résine injectée et celle du moule chauffé minimise les variations de volume produites par l'expansion thermique et améliore la cuisson de la pièce.

0.3 Simulation numérique des procédés LCM

Le procédé d'injection sur renfort RTM est délicat à mettre en œuvre. Dans le cas de pièces complexes, la position des points d'injection et des évents est cruciale pour que la pièce soit remplie correctement et que la polymérisation soit uniforme. Choisir expérimentalement la position optimale de ces points serait très coûteux car, pour chaque essai, il faudrait soit fabriquer un nouveau moule, soit modifier un moule existant. Il est donc préférable de procéder à une simulation numérique de la mise en forme afin de vérifier et d'améliorer la conception du moule.

Pour optimiser le procédé RTM, plusieurs facteurs doivent être pris en compte comme la pression d'injection, les conditions thermiques de la mise en forme et la formulation de la résine, c'est-à-dire le mélange des différents constituants ajoutés à la matrice polymère comme le styrène, les additifs mouillants, anti-bulles ou accélérateurs, le catalyseur et la charge. Un des aspects importants du procédé est le facteur thermique. La simulation thermique aide à mieux comprendre l'influence des changements de viscosité sur le remplissage de la pièce. Elle permet en outre de prendre en compte dans le bilan thermique la chaleur dégagée par la réaction chimique de polymérisation. La simulation thermique apporte des informations importantes pour choisir correctement le catalyseur, assurer une bonne régulation thermique du moule et contrôler la réaction chimique. On peut modifier numériquement les paramètres afin de trouver une séquence de remplissage correct du moule, amorcer la réaction de polymérisation au bon moment et refroidir la pièce lorsque la cuisson est terminée. Le temps de cycle peut également être réduit en accélérant les phases de remplissage, de polymérisation et de

refroidissement. On peut aussi choisir d'optimiser le procédé pour obtenir des pièces avec une meilleure qualité de surface ou des propriétés mécaniques améliorées. Enfin, il est possible aussi de préchauffer le moule ou la résine et donc de diminuer encore le temps d'injection et de polymérisation. La température constitue ainsi une variable importante dans ce genre de procédé, car elle régularise le temps de fabrication et possède une grande influence sur la qualité de la pièce finie. Il est donc indispensable de bien contrôler la température dans le moule et de tenir compte des effets thermiques dans la simulation numérique du procédé.

0.4 Objectifs de la recherche

Les objectifs généraux des recherches menées dans le cadre de cette thèse s'articulent en quatre volets principaux, qu'on peut énumérer comme suit :

- I. Caractérisation thermique et mécanique des matériaux.
- II. Analyse unidimensionnelle de la cuisson et des contraintes résiduelles.
- III. Simulation numérique d'un écoulement stratifié dans un composite et cuisson.
- IV. Optimisation du chauffage du moule et de la cuisson du composite.

Ces quatre volets de notre étude sont motivés par la nécessité d'étudier les phénomènes thermiques à travers l'épaisseur du composite afin d'optimiser le cycle de fabrication et les propriétés mécaniques des pièces. Ces différents aspects, dont les objectifs sont décrits brièvement plus bas, doivent être pris en compte dans une démarche globale d'optimisation du procédé.

0.4.1 Caractérisation thermique et mécanique des matériaux

Lors de la mise en forme des matrices thermodurcissables, les flux de chaleur entrant et sortant du matériau constituent la clé qui permet de démarrer et de contrôler la

polymérisation de la résine. Les propriétés mécaniques du composite sont directement reliées au degré de polymérisation atteint à la fin de la cuisson. Donc, la qualité mécanique de la pièce dépend de l'histoire thermique du procédé. Pour étudier les effets des paramètres de moulage sur la qualité de la pièce, différentes propriétés de la résine et du composite doivent être définies. La recherche présentée débute par la caractérisation thermomécanique de ces propriétés. La finalité de cette première partie du travail est la création de modèles semi-empiriques de la cinétique de polymérisation et de l'évolution des propriétés mécaniques.

0.4.2 Analyse unidimensionnelle de la cuisson et contraintes résiduelles

Une fois la caractérisation thermomécanique des matériaux complétée, une analyse unidimensionnelle de la cuisson va permettre de comprendre les différents phénomènes physiques qui ont lieu au sein du matériau. La haute réaction exothermique de la résine conjuguée à la basse conductivité thermique du composite peut générer un processus auto-accélééré qui aboutira à des températures très élevées et à une possible dégradation de la matrice polymère. Les effets combinés de l'expansion/contraction du composite et du retrait de polymérisation de la résine sont la source du développement des contraintes internes dans la pièce. Ainsi, la simulation numérique de la cuisson couplée à une analyse mécanique des contraintes permet d'étudier l'influence de la formulation de la résine et de la régulation thermique du moule sur la qualité finale de la pièce.

0.4.3 Simulation numérique d'un écoulement stratifié et cuisson

Pour optimiser la fabrication et les propriétés mécaniques des composites, il est nécessaire d'injecter la résine à une température plus élevée que la température ambiante. Comme la température possède une influence non négligeable sur la viscosité de la résine et donc sur le remplissage de la pièce, un gradient thermique à travers

l'épaisseur génère un écoulement stratifié au lieu du front de résine habituellement droit qui caractérise les injections isothermes en milieux poreux.

D'autres facteurs contribuent également à perturber l'écoulement à travers l'épaisseur, quand le renfort est constitué par exemple, comme c'est souvent le cas, de plusieurs couches de tissus ou bien quand la pièce contient une âme de mousse compressible ou des inserts susceptibles de se déplacer sous l'effet de la pression. Tous ces phénomènes ayant un effet sur la réponse thermique du composite, ils devront faire l'objet d'une étude approfondie et leur influence doit être prise en compte dans une démarche globale d'optimisation du procédé. La simulation non isotherme de la phase de remplissage permet d'étudier les effets d'une distribution de température dans la cavité du moule sur la saturation de la préforme et la cuisson non uniforme de la pièce. Les perturbations de l'écoulement de la résine à travers l'épaisseur d'une pièce composite vont donc constituer le troisième aspect de cette étude.

0.4.4 Optimisation du chauffage du moule et de la cuisson du composite

Dans la fabrication à haute température des composites (habituellement 80 °C ou plus sont utilisés), après le remplissage de la cavité, le moule est chauffé à la température de cuisson désirée. Une fois que la réaction de polymérisation de la résine est terminée, le moule est refroidi et la pièce démoulée. Le temps du cycle de cuisson peut être réduit en accélérant les phases de préchauffage, de polymérisation et de refroidissement. La qualité des pièces produites (que ce soit du point de vue de leurs propriétés mécanique ou de leur aspect de surface), peut être optimisée si la séquence de chauffage est bien choisie. Un des objectifs principaux de cette thèse est d'optimiser la cuisson à travers l'épaisseur des composites renforcés par des fibres de verre ou de carbone. Même si la méthodologie proposée s'applique à la fois aux pièces minces ou épaisses, c'est surtout dans le cas des pièces structurales épaisses ou contenant une âme de mousse que les effets analysés seront les plus importants. La matrice polymère utilisée pour la

validation est un polyester insaturée typique des applications automobiles, mais il est clair que l'essentiel du travail de modélisation est applicable aussi aux résines époxy utilisées dans le domaine aérospatial. On s'intéressera donc principalement dans cette étude à déterminer les conditions optimales de chauffage et de refroidissement du moule.

0.5 Organisation de la thèse

Cette thèse est présentée sur la forme d'une thèse par articles. Dans un premier temps, un compte rendu détaillé de la recherche bibliographique sur les procédés LCM (spécialement sur le RTM) est présenté dans le **chapitre 1**. Cette étude bibliographique est réalisée sous la forme d'un article de revue intitulé « *State of the Art Review of Numerical Simulation of Liquid Composite Molding Processes* ». L'objectif de cette étude est de répertorier les phénomènes physiques importants ayant lieu dans la fabrication de pièces composites par LCM. Pour chacun des phénomènes décrits, l'état d'avancement de la recherche sur le plan mondial est établi.

Dans le **chapitre 2**, un article intitulé « *Thermo-Mechanical Properties during Cure of Glass-Polyester RTM Composites: Elastic and Viscoelastic Modeling* » a pour objet la caractérisation des propriétés thermomécaniques du composite et de la cinétique de polymérisation de la résine. Cette étude expérimentale est consacrée initialement à la modélisation semi-empirique de la cinétique de polymérisation d'une résine polyester insaturée commerciale. Les effets de la décomposition de l'inhibiteur et de la température de transition vitreuse sont aussi soulignés. Par la suite, les propriétés mécaniques dynamiques sont caractérisées et modélisées avec deux approches différentes. La première est un modèle simplifié qui considère la relaxation totale du matériau à l'état caoutchoutique. Le deuxième est un modèle viscoélastique complexe reposant sur le principe de superposition temps/température. Finalement, les

coefficients d'expansion thermique de la résine et du composite sont caractérisés et le retrait de polymérisation de la résine est exprimé en fonction du degré de polymérisation.

L'objectif des **chapitres 3 et 4** est de modéliser la cuisson unidimensionnelle et d'étudier le développement des contraintes résiduelles pendant la mise en forme de pièces composites minces et épaisses respectivement. Les paramètres qui gouvernent l'évolution des contraintes internes sont la température de moulage, l'épaisseur du composite et les propriétés thermiques et mécaniques des matériaux. L'article présenté dans le chapitre 3 est intitulé « *Internal Stresses and Warpage of Thin Composite Parts Manufactured by RTM* », et celui du chapitre 4 est « *Numerical Analysis of Cure Temperature and Internal Stresses in Thin and Thick RTM parts* ». L'analyse du premier article (chapitre 3) porte uniquement sur la post-cuisson de pièces minces, tandis que le second (chapitre 4) considère aussi les pièces épaisses. Dans les deux articles, différents profils de température sont étudiés et une analyse détaillée de la réaction de polymérisation est effectuée. Les variations volumétriques résultant de la cuisson sont examinées, ainsi que leur influence sur les contraintes résiduelles.

Les **chapitres 5 et 6** présentent une formulation mixte sur l'analyse numérique du remplissage tridimensionnel de pièces composites. Les travaux sont présentés dans un article en deux parties. La première partie intitulée « *Coupled Non-Conforming Finite Element and Finite Difference Approximation Based on Laminate Extrapolation to Simulate Liquid Composite Molding Processes – Part I. Isothermal Flow* » traite le cas d'une injection isotherme et prend en compte les interactions entre les différentes couches de renfort. Partant d'un maillage bidimensionnel, une méthode d'extrapolation du maillage est proposée pour générer des éléments finis tridimensionnels dans la cavité du moule. Un nouvel élément fini discontinu est proposé pour mieux tenir compte des variations de pression à travers l'épaisseur pendant le remplissage. La deuxième partie de l'article intitulé « *Coupled Non-Conforming Finite Element and*

Finite Difference Approximation Based on Laminate Extrapolation to Simulate Liquid Composite Molding Processes – Part II. Non-isothermal Flow » est consacrée à l'analyse numérique du remplissage non isotherme et à la cuisson de pièces composites tridimensionnelles. Pour augmenter la vitesse des calculs de remplissage et améliorer les résultats sur la cuisson, une formulation mixte couplant éléments finis et différences finies est présentée pour calculer une solution approchée du problème thermique. Un certain nombre de comparaisons avec des solutions analytiques est exposé pour étudier la qualité des solutions numériques proposées. Une étude de convergence pour divers cas est réalisée pour démontrer les avantages de cette approche par rapport aux méthodes traditionnelles.

À partir des résultats des chapitres précédents, le **chapitre 7** présente une méthode pour faire l'optimisation numérique du procédé. L'article de ce chapitre est intitulé « *Comprehensive Thermal Optimization of Liquid Composite Molding to Reduce Cycle Time and Processing Stresses* ». L'optimisation thermique de la cuisson et du refroidissement en une dimension d'espace (à travers l'épaisseur de la pièce) permet d'obtenir les profils temporels optimaux de température qui réduisent le temps de cuisson et maximisent les propriétés mécaniques de la pièce. La méthode d'optimisation développée est donc fondée sur la minimisation du temps du cycle, la réduction des contraintes résiduelles et la maximisation de degré de polymérisation final de la pièce. Un algorithme d'évolution (EA) fondé sur les Algorithmes Génétiques (GA) est utilisé pour minimiser une fonction objectif à plusieurs paramètres de design. La simulation unidimensionnelle de la cuisson et des contraintes résiduelles permet d'évaluer cette fonction objective. Une étude de l'optimisation de la cuisson et du refroidissement de pièces minces et épaisses est finalement présentée pour illustrer le potentiel de la méthode proposée.

Pour terminer, une discussion générale est présentée sur l'ensemble des développements de la thèse et les perspectives futures de cette recherche. Un échéancier

des travaux réalisés et un résumé des matériaux et équipement utilisées pour amener cet recherche sont aussi décrits. Enfin, dans l'annexe I, sont imprimés les codes écrits pour calculer chacune des solutions analytiques présentées dans les articles. Dans l'annexe II pourra être trouvé l'algorithme unidimensionnel d'analyse thermique et contraintes résiduelles. L'annexe III contient une description plus détaillée de la caractérisation cynégétique de la résine, les résultats de la méthode d'isoconversion de temps/température et les courbes obtenues après la modélisation.

CHAPITRE 1

STATE OF THE ART REVIEW OF NUMERICAL SIMULATION OF LIQUID COMPOSITE MOLDING PROCESSES

Présentation du chapitre

Cette étude bibliographique sous la forme d'un article de synthèse soumis à la demande de la revue « *Recent Research Developments in Material Science & Engineering* » est destinée à donner une vision des connaissances générales sur la modélisation numérique des procédés LCM, spécialement le RTM. L'étude démarre avec une exposition globale afin d'introduire les concepts basiques des phénomènes que interviennent dans les différents étapes du procédé. Ensuite, une discussion est amenée sur les travaux publiés dans le domaine de la modélisation des écoulements dans milieux poreux et l'imprégnation des renforts. Par la suite, le modèle typique utilisé pour l'analyse des transferts thermiques est présenté, et les influences de la température sur les paramètres de moulage sont décrites. Après, la cinétique de polymérisation d'une résine thermodurcissable est expliquée, et les différents modèles présentés. À la fin, les propriétés mécaniques des composites et les effets des contraintes résiduelles sur la qualité des pièces sont décrites.

State of the Art Review of Numerical Simulation of Liquid Composite Molding Processes

Edu Ruiz and François Trochu

Centre de Recherches Appliquées Sur les Polymères (CRASP)

Département de Génie Mécanique,

École Polytechnique de l'Université de Montréal,

H3C 3A7, Canada

e-mails: eduardo.ruiz@polymtl.ca, francois.trochu@polymtl.ca

Article soumis à la revue

Recent Research Developments in Material Science & Engineering

Décembre 2003

1.1 Abstract

The present review aims at summing up the most recent developments on material characterization and numerical simulation of Liquid Composite Molding (LCM). This family of related composite manufacturing processes regroups different ways of injecting a liquid resin through a fibrous reinforcement. As lightweight materials that resist corrosion, polymer composites are increasingly used in many industrial applications. New manufacturing techniques have appeared in recent years and bring important reduction of production costs. Process simulation and virtual prototyping are key technologies that will allow mastering of the complex issues connected with

material selection, mold design, cycle time, part quality and production cost. In order to perform accurate simulations, rapid and reliable material characterization techniques need to be developed. This study concerns the rheological, thermal, chemical and viscoelastic phenomena that occur during processing of a composite part manufactured by LCM. Numerical optimization procedures are also reported for different composite manufacturing processes such as Structural Reaction Injection Molding (SRIM), Sheet Molding Compound (SMC), Bulk Molding Compound (BMC) or autoclave curing. Although the present work mainly addresses thermosetting matrix materials (i.e., polyester or epoxy based resins), information on thermoplastic resins is also reported from the literature.

1.2 Introduction

Liquid Composite Molding (LCM) regroups a number of widely used manufacturing techniques for fibre reinforced composite parts such as the well known Resin Transfer Molding (RTM) process. LCM techniques are well recognized for their versatility in part dimension and low cost production. The basic process consists in the pressurized injection of a pre-catalyzed thermoset resin into the mold cavity containing a fibrous preform (see figure below). Once the cavity is filled up, and the preform is completely saturated, the liquid resin system reacts following an exothermic process. The polymerization reaction results in a three-dimensional cross-linked polymer network that gives the solid shape of the part.

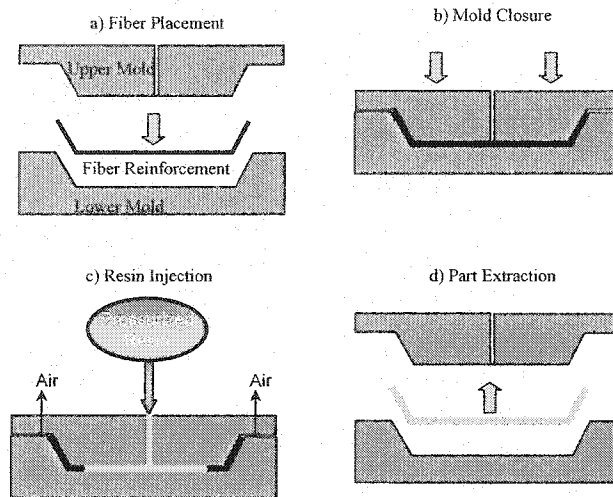


Figure 1.1. Resin transfer molding process for manufacturing of composite materials

The prediction of mold filling or impregnation phase in LCM has been studied by many investigators [1-20]. Several authors have considered this problem in the isothermal case only [1-10]. The cure of thermosets is a recognized problem and several researchers have considered the prediction of resin cure degree for other fabrication processes such as Reaction Injection Molding (RIM), Structural Reaction Injection Molding (SRIM), pultrusion, etc. For some composite manufacturing processes, mathematical models have been developed to predict resin cure [11-20]. The typical approach considers transient heat conduction problem coupled with the internal heat generated by the resin polymerization reaction [21-23]. By combining the impregnation model with such a cure model, a prediction can be made for the temperature history of the entire cycle. Although the impregnation phase plays an important role, experimental work [10,14] has shown that the time required to heat and cure the resin system is a major factor inhibiting further reduction in cycle time.

1.3 Model of fiber impregnation

The typical filling process involves the injection of a liquid resin into the mold cavity. The central issue in the analysis of a filling process is the tracking of the free surface between the filling material (i.e., liquid resin) and the escaping gas (usually air), which is present in the cavity of the mold before the injection. The flow of fluid through a fibrous network has been analyzed either at the microscopic or macroscopic levels. In the microscopic approach, the flow through the fibrous mat is studied by solving Navier-Stokes equation. However, this method may be misleading and difficult to resolve because the fiber architecture is complex and the needed boundary conditions are not easy to find. In macroscopic studies, the flow of resin through a fiber preform is usually assumed to be equivalent to that of an incompressible fluid through a porous medium. Therefore the filling phase in liquid composite molding is based on incompressible fluid mass conservation and uses Darcy's law to evaluate the pressure drop of the flow.

A porous medium may be defined as a solid containing holes or voids, connected or not, dispersed either regularly or in a random way. The porosity of a porous material is the fraction of the bulk volume of the material occupied by voids. Permeability is that property of a porous media which characterizes the ease of a fluid flow to permeate through the medium when a pressure field is applied. Many attempts have been made to construct a theory that relates the pore structure with permeability. The theory of Carman-Kozeny [25] treats the porous medium as a bundle of capillary tubes of equal length. Kozeny has shown that the permeability K for such structure may be approximated by the following equation:

$$K = \frac{d_b^2}{4k} \frac{\phi^3}{(1-\phi)^2} \quad (1-1)$$

where d_b is the averaged bundle diameter, k is an experimental value (called Kozeny constant) and ϕ the medium porosity. This equation was originally developed for granular beds consisting of ellipsoids and it was shown to be also valid for porous media consisting of fibers.

In order to simulate the filling process, several assumptions must be made to simplify the problem. In general, the fabric reinforcement placed in the mold cavity is assumed to be rigid during mold filling. Inertia effects are neglected because of the low Reynolds number of the resin flow. Furthermore, at the pressure usually created in the cavity to drive the flow, surface tension is considered negligible compared with the dominant viscous force. The equation of mass conservation for the fluid phase can be written as:

$$\nabla(\rho \bar{u}) = 0 \quad (1-2)$$

where ρ is the density of the injected resin and \bar{u} is the superficial fluid velocity, i.e., the velocity at which the fluid actually travels, rather than the observed macroscopic velocity. Darcy's law is usually written as [26]:

$$\bar{u} = -\frac{1}{\mu} [K] \cdot \nabla P \quad (1-3)$$

in which $[K]$ is the permeability tensor, taking the form of a 3x3 matrix, μ and ∇P are the resin viscosity and the pressure gradient respectively. Equation (1-3) relates the three components of the superficial fluid velocity vector to the associated pressure gradient. This relationship is valid for Newtonian fluids and ignores gravity effects, although some authors have also developed a more elaborated equation taking into account these effects [13]. Flow experiments used to measure reinforcement permeability have demonstrated that Darcy's law can be applied to a wide range of injection pressures or flow rates, larger than the usual values used in LCM technology.

Owen, Kendall et al. [3] presented three analytical solutions for Darcy's flow in liquid composite molding. The document was illustrated with examples for rectangular molds and convergent and divergent flows in a circular mold. Based on Kendall's work, they illustrate the approximate relationships for the pressure distribution, fluid velocity, filling time and total force on the mold wall for the above-described geometries. A comparison with experimental results showed that a proper model must include non-isothermal filling effects. For three simple geometries, they found a good agreement with the experimental results for the pressure and temperature fields. These analytical solutions represented a good test to validate numerical algorithms developed to resolve Darcy's flow in complex shapes. Boccard et al. [4] developed a geometrical model to describe the mold filling of thin two-dimensional parts. The method was able to include several injection points and can be modified to model a variable injection pressure. Based on this geometrical approach, combining radial and channel-like flows, the time required to fill the mold was obtained without using of a filling algorithm. Experimental results corroborated the analytically calculated time. With this technique only isothermal injections can be modeled and only thin parts with relatively simple geometries will provide accurate results.

In general, the simulation of the filling stage in LCM processing requires the coupled solution of the flow equations (i.e., Navier-Stokes or Darcy equations) with some means of tracking the free surface. Three alternative tracking approaches have been identified in the literature [2]:

- Lagrangian: In this approach, the computational grid deforms as the flow calculation proceeds and a line of nodal points (or grid cell boundaries) always coincides with the free surface (see Figure 1.2.b) [7,8,10]. An alternative, but equivalent approach, consists of using a domain transformation to perform calculations in a fixed domain with a simple geometry [9].

Coulter et al. [10] carried out an experimental investigation on resin impregnation in the manufacturing of composite materials to corroborate the numerical result of the simulation software. The code is based on the assumption of two-dimensional quasi-steady isothermal flow of a viscous fluid through a porous medium, using boundary-fitted finite differences with a numerical grid generation along with a stream function formulation. They considered constant velocity at the mold inlet, zero velocity along all walls, and zero shear stress on the resin front as boundary conditions. The numerical result yielded a resin front more elongated than the experiment. The second notable difference is connected with the no-slip boundary condition which delayed the flow along the mold walls.

Other workers have improved this approach in order to reproduce experimental data [7-9]. Although the final results show a good agreement with experiments, the most important problem with this methodology remains the expensive computational time required to solve the flow in complex parts (see Trochu and Gauvin [31]). Numerical instabilities were also observed by Trochu and Gauvin [31] when obstacles are present in the mold cavity (as inserts) or multiple fluid fronts merge to completely fill the part. According to this discussion, the finite element method was considered as a more appropriate alternative for modeling purposes.

The necessity to redefine the geometry of the domain in which the governing equations are solved, makes imperative the generation of a new mesh after each successive calculation steps. Mesh generation could represent the most tedious part of the simulation. In this context, finite element control volume (FE/CV) is an attractive technique, as it is not needed to remesh and it is possible to simulate the filling of thin cavities with very complex geometries. A key feature of the FE/CV approach is rough approximation of the domain shape combined with a thorough accounting of resin mass conservation. The most recent advances have been made using this technique [1-8]. Experimental validations and simulations for complex industrial shapes show the

benefits of this approach in terms of computer time, mesh generation and numerical simulation. Models and simulations are already proving to accurately resolve the non-isothermal filling phase in liquid injection technology. As illustrated by Ruiz and Demaria [1], the numerical simulation has the potential to be a useful guide in the design of parts, tooling and process. Figure 1.3 shows how the design and manufacturing process can be integrated. Figure 1.3.a display images of and automotive part, while the filling simulation of the mold cavity is presented in Figure 1.3.b. The two mold halves used to manufacture the part as well as an analysis of the mold deflection during resin injection are illustrated in Figure 1.3.c and d respectively.

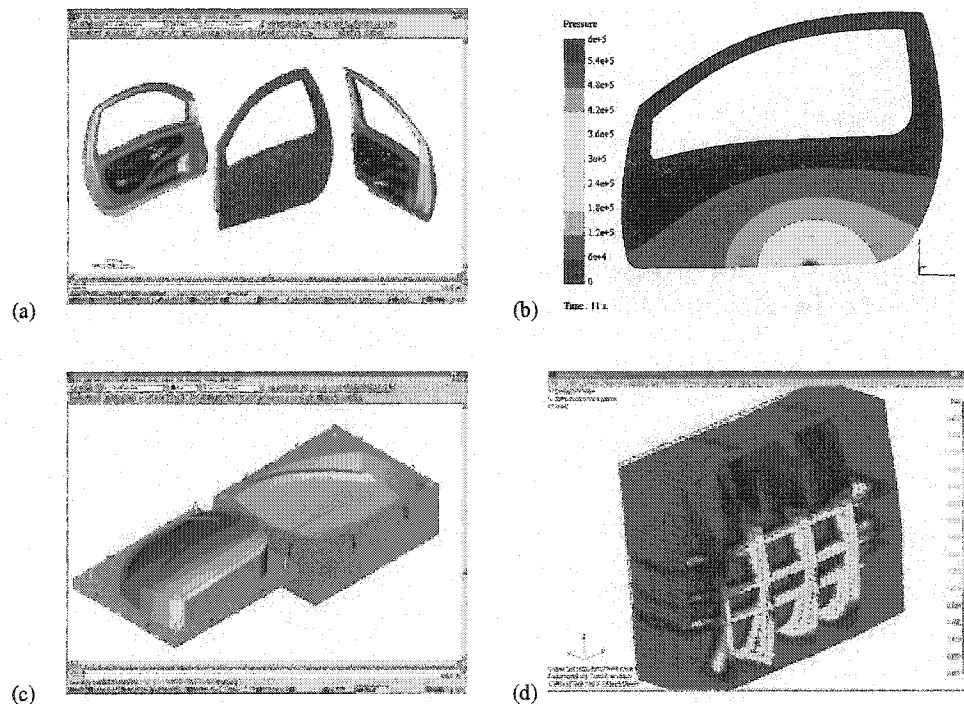


Figure 1.3. Part and mold design by using numerical simulations [1], a) designed part, b) filling numerical simulation, c) tool design and, c) mold deflection analysis from filling pressures

Gauvin and Trochu [32] presented a different approach based on finite elements, in which the elements of the mesh are used to track the resin flow instead of control volumes associated to the nodes. In their program, called RTMFlot (after updated to LCMFlot), nonconforming finite elements are used with a fixed triangular mesh to numerically solve the equations. This technique allows a better local fluid mass conservation than FE/CV. In the FE/CV method, the conservation of mass is imposed for all control volume associated to the nodes of the fixed mesh. In RTMFlot, each element is at the same time its own control volume. With this technique it is no longer necessary to generate a control volume around each node. Nonconforming finite elements present several advantages over the more conventional FE/CV for the numerical simulation of RTM and SRIM processes. The two main advantages are an exact local conservation of resin mass and no requirement to refine the mesh near internal boundaries where the permeability varies significantly. Remacle, Trochu et al. [33] introduced discontinuous finite elements on tetrahedrons to simulate liquid composite molding process on three-dimensional parts. The pressure interpolated with discontinuous elements allows to obtain perfectly conservative results. The conservation of resin mass is crucial to simulate injection molding processes. The authors compared the pressure distribution and the flow rates across the flow front and at the injection gate for both continuous and discontinuous finite element solutions. They concluded that a classical finite element interpolation i.e., using conforming finite elements with pressure approximation at the nodes of triangles or tetrahedrons, does not gives accurate results and no conclusion can be drawn. With the non-conforming approach, the mass conservation was insured even for coarse meshes.

In common LCM industrial applications the resin is injected at room temperature into a heated mold cavity. In this case, the resin that comes in contact with the heated mold walls, i.e., the resin on the flow front, reaches progressively a higher temperature. Because several properties of the polymer resin depend on temperature, significant

variations of the material parameters occurs on the flow front. It is difficult to resolve accurately this problem with a fixed finite element mesh. A highly refined mesh results in an expensive computer time, and process optimization cannot be contemplated. Bechet et al. [34] presented a new approach consisting of automatic remeshing in the vicinity of the flow front. The solution implements the remeshing algorithm combined with a method of velocity extrapolation to account for the flow movement in time. The procedure allows the user to define the refinement level at the resin front, injection and vent gates (see figure below). This interesting approach provides the accurate solution of strong properties variations in the neighborhood of the flow front.

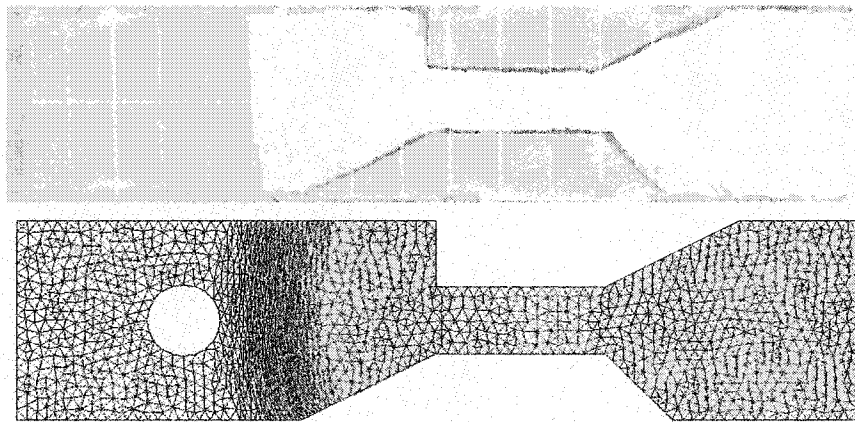


Figure 1.4. Re-meshing algorithms applied to RTM injection [34]

For complex three-dimensional parts with ribs, Darcy's boundary value problem can be approximated on a solid finite element mesh [13-15,19-20]. This approach appears to be the most consistent with thermal and flow phenomena through the thickness of the cavity, while giving also the possibility to include the thermal effects of the mold as has been demonstrated by Guyonvach et al. [20]. Although the three dimensional solution of the filling stage is well recognized for its robustness and accuracy, the principal problem is related to the computer time required to perform a simulation. Because the thickness of the cavity is very small compared to the length or surface of the part, it is

necessary to use a minimum number of finite elements through the thickness of the part to ensure a good accuracy of the thermal solution. Moreover, the elements can't be too degenerated to avoid numerical inconsistency. Finally, the number of three dimensional finite elements needed to resolve the coupled problem of heat transfer and mold filling can be extremely high. The large number of degrees of freedoms needed to model the complex three dimensional differential equations results in an expensive computer time and makes process optimization extremely difficult, if not impossible.

1.4 Heat transfer analysis

Because of the resin exotherm and the energy transferred by conduction from the mold walls and convected by the resin flow, heat transfer phenomena cannot be neglected during the filling stage in liquid composite molding processes. Moreover, the viscosity of the thermoset resin changes in function of temperature and of the polymerization degree. In order to model the effects of heat transfer on the temperature of the resin, of the mold and of the fiber reinforcement, it is necessary to carry out an energy balance between each of the constituents. In general, two approaches may be followed to find the temperature field [12-15]. In the first one, the resin and the fibers are considered as separate constituents (two phase model). Their temperatures may differ at any point of the mold. In the second approach, the resin and fibers are assumed to be at the same temperature (the so-called "lumped" system). In general, the equilibrium model i.e., the second approach, is considered reasonably accurate for LCM [12,14], where flow is a relatively slow process.

Considering the lumped system, an energy balance for the resin-fiber mix leads to a transient absolute temperature T at time t and positions x, y and z , $0 \leq z \leq h$, where h is the total cavity thickness of the composite, given by the following equation:

$$\rho C_p \frac{\partial T}{\partial t} + \phi \rho_r C_{p_r} \nabla(\bar{u} \cdot T) = k \nabla^2 T + Q \quad (1-4)$$

where the effective density, heat capacity and conductivity of the composite are defined by

$$C_p = C_{p_r} w_r + C_{p_f} w_f \quad \text{and} \quad \rho = \frac{\rho_r \rho_f}{\rho_r w_r + \rho_f w_f} \quad (1-5)$$

$$k = \frac{k_r k_f}{k_r w_r + k_f w_f} \quad \text{and} \quad w_r = \frac{\phi / \rho_f}{\left(\phi / \rho_f + 1 - \phi / \rho_r \right)}$$

$$w_f = 1 - w_r$$

In the above equations ϕ is the porosity and w_r, w_f denote the weight fractions of resin and fibers, respectively. The subscript “f” stands for the fibers and “r” for the resin. The internal heat source term Q accounts for the heat generated by the exothermic chemical reaction of thermoset resin systems.

The control of heat transfer and chemical reaction in liquid composite molding is complex because so many factors interact. These interactions are indicated schematically in Figure 1.5 and described in Table 1.1. The resin flowing across the mold cavity absorbs heat by conduction from the mold walls and from the heated preform; temperature is also transported by convective forces. The rheological phenomena depend on the temperature and degree of conversion of the resin via the resin viscosity. In turn, the velocity field characterizing the fluid flow transports the chemical species and influences the thermal field. It also determines how the mold is going to be filled up by the resin and the quantity of heat that will be generated by viscous dissipation.

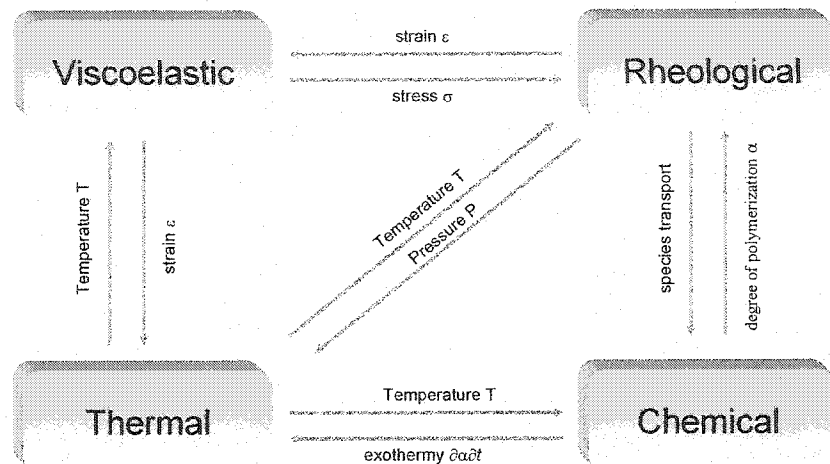


Figure 1.5. Coupling of phenomena present in the LCM process.

Table 1.1. Mathematical models for phenomena present in the LCM process.

Category	Phenomena	Mathematic Models
Rheology	Flow porous media Capillary forces Variations of viscosity	Darcy's Law Constituent Law
Thermal	<u>Mold</u> : conduction, surface losses <u>Part</u> : conduction, diffusion, convection, heat generation	Heat equation, coefficient of heat transfer (conduction-convection) Convection-diffusion equation with source term, modeling one or two temperatures
Chemical	Chemical species transport, diffusion and chemical dispersion. Polymerization	Convection-diffusion equation with source term; resin kinetics model
Viscoelastic	Fluid flow stress, viscoelastic forces	Linear strain-stress relationship with relaxation term

On one hand, the chemical reactivity of the resin increases with temperature, on the other hand the exothermy of the polymerization reaction is usually sufficient to increase the temperature notably. Resin thermal and mechanical properties such as specific heat,

thermal conductivity or elastic modulus depend on temperature and resin degree of conversion. The strain-stress relationship depends on temperature through the thermal expansion/contraction of the resin; it is also related to the degree of cure via the chemical shrinkage produced during the cross-linking polymerization. Finally, viscoelastic behaviour of the polymer depends on temperature, degree of cure and time (stress relaxation is observed during cure). The multiple interactions between these phenomena make the numerical modeling of the full process a complex, and sometimes unfeasible task.

Researchers have resolved this complexity by building mathematical models and computer simulations of flow, heat transfer, chemical reaction and strain-stress relationship. Finite element software has been developed to implement some of these mathematical models for complex three-dimensional parts [16-20]. The energy equation was resolved by finite elements and finite differences. Guyonvach et al. [20] presented a heat transfer analysis integrated with a non-isothermal 3D filling model. They used a Taylor-Galerkin method in a finite element model that permits to guarantee a reasonable stability and precision of the temperature calculation even when convection terms become dominant. However, the numerical scheme is not unconditionally stable, which created difficulties to make it user friendly. The simulation calculates the three-dimensional temperature distribution in the cavity and in the heating mold, but the computational cost is high. The calculated transient temperature response in a preheated mold showed a good agreement with experiment. The temperature calculated during mold filling simulations permits to reproduce the high temperature gradients observed experimentally during fiber impregnation across the thickness of the part and mold.

Lebrun et al. [27] conducted an experimental investigation of heat transfer during the filling stage in a RTM cavity by measuring temperatures through the thickness of the part at four different locations in the flow direction. The authors presented a finite

difference program used to evaluate the temperature distribution through the thickness of the steel wall. They showed that it is possible to evaluate the effective thermal conductivity of a resin saturated fiber preform by recording the temperatures inside the mold wall and in the mold cavity during the filling stage. Such an evaluation was also shown to be useful in gaining confidence in the thermal properties obtained with the rule of mixtures and used to evaluate the Nusselt number. Large discrepancies were obtained between the Nusselt numbers referred in the literature and experimental results. In fact, all models underestimate the heat transfer at the surface of the mold, except the model taking the thermal dispersion into account, which overestimates the heat transfer. The experimental Nusselt numbers have been shown to be dependent on the molding conditions. An increase of the injection pressure increased the experimental Nusselt number, consistently with an augmentation in resin velocity under these conditions. However, an increase of the mold temperature induced a drop in the Nusselt number. This was caused by the competing effect between the temperature gradient at the mold surface and the difference between the surface temperature and the inlet resin temperature. Finally, the authors presented a model for the Nusselt number, taking into account the effects of the thermal dispersion, of the variable resin viscosity and of the influences induced by the fiber volume content and the mold temperature. This model gave better results than the models documented previously in the literature.

Tucker [29] presented a comprehensive analysis of issues in the modeling of heat transfer and chemical reaction in resin transfer molding and structural reaction injection molding. The discussion was organized around four steps of modeling: incorporating the physical phenomena into a model, gathering material data, analyzing the model to provide physical understanding, and solving the model for relevant cases. A rigorous derivation of the governing equations by the local volume averaging method has cleared up ambiguities about how some terms should be handled, and has introduced the need of adding dispersion terms in the energy and cure equations. This part of the model seems to be well in hand. Equally rigorous equations for the two-temperature

model have been derived, but the few two-temperature treatments presented in the literature up to now ignored many terms in these equations. He explains that two-temperature models are important. Indeed, further theoretical and experimental work is needed to sort out the best governing equations. Tucker points out also the effect of pressure drop by binder dissolution in the resin flow. Binders are thermoplastic coatings on the fiber preform. They help to maintain the shape of the reinforcement after preforming. Some binders will dissolve in the resin during mold filling. Since the binders consist of long-chain molecules, even small amounts of dissolved binder can significantly increase the viscosity of the resin, and thus affect the subsequent pressure drop and filling of the cavity. The author has presented a useful set of dimensionless parameters for the flow, heat transfer and cure models, and analytical solutions for a few special cases.

Another important observation was made by Lebrun et al. [28] about the through-thickness temperature profiles in the mold cavity during the filling phase. The reported temperatures were recorded by using wire thermocouples placed between the reinforcement layers and steel-sheathed thermocouples in a flat steel RTM mold. The need for reliable temperature and pressure recordings to validate numerical models was highlighted by showing that a thermal boundary layer is developed during the impregnation phase. Through-thickness temperature variations were shown to have an influence on the formation of mid-thickness in-plane defects in thick parts. These defects were generated by the racetracking of less viscous resin flowing close to the mold surface. Gauvin and Trochu [32] presented a discussion on flow in multilayers preforms. Experimental results showing the influence of the mold temperature on the resin temperature have been presented. They showed that non-isothermal filling simulations need to consider a variable resin temperature through the part thickness. Since resin viscosity is highly sensitive to temperature, a reliable simulation should take this dependence into account.

1.5 Resin kinetics

Thermosetting polymers play an essential role in many industrial applications, because of their great flexibility to tailor the required ultimate properties of composite systems. Knowledge of the degree of cure and thermal history of the resin material is necessary in order to interpret the structural and physical property changes. A knowledge of the heat of reaction and the rate of heat generated in function of time and temperature is requested to quantify the heat transfer in the molding process. Process optimization of composite manufacturing requires a good understanding of the effects of various factors (fillers, additives, chemical composition, etc.) on the curing process. Therefore the analysis of resin kinetics is important.

The chemical reactions of thermoset resins usually involve either a step growth polymerization, a chain growth polymerization, or a combination of both [15]. An ideal kinetic model should be simple enough to be combined with a process simulation model to predict mold filling and curing. Yet, the model should be able to describe both the kinetic changes of the reacting material and physical phenomena such as gelation and vitrification effects. Furthermore, the effect of major chemical ingredients on reaction kinetics, and consequently, the physical properties or defects of the molded product, needs to be addressed for material design. Obviously, it would be difficult to develop a single model that could fulfill all the above requirements. An alternate approach consists of considering several levels of models.

Resin kinetics measurement during the reactive processing is difficult. Resin solidification due to chemical cross-linking, domain formation or crystallization represent obstacles for most experimental techniques [15]. High polymerization temperatures and pressures, fast reaction rates further complicate this task. Various methods have been employed to monitor the progress of the cure reaction in polymer

processing. These methods fall into two categories: (1) determination of the absolute conversion by monitoring the disappearance of reactive groups or the appearance of particular species; (2) determination of changes in the physical and mechanical properties of the sample resulting from the cross-linking polymerization. Some of these techniques are differential scanning calorimetry (DSC), FTIR (Fourier Transform Infrared) spectroscopy analysis, dielectrometry, rheological measurements, torsional and flexural braid analysis, and a variety of other techniques [13-15,23]. These techniques serve three main functions:

- The evaluation of resin formulations during material selection.
- The measurement of residual reactivity for resin samples during process development.
- The provision of data for the simulation of heating and curing processes.

Since most liquid molding polymerizations are fast and highly exothermic, one of the simplest ways to follow the overall resin conversion is to monitor the heat generated during polymerization. In this way, DSC [13-15,23] is the most widely used technique and involves the analysis of heat flow into a small specimen of the test material within a calibrated control cell. By controlling the heating rate and the sample temperature, a number of important thermal and chemical reaction constants can be deduced from either isothermal or ramped heating tests. It is potentially useful for making time-temperature predictions and for optimizing process variables as well as performing quality control for the molding composite. In the bulk of works done by DSC analysis for studying cure kinetics, the rate of heat generation is assumed to be proportional to the rate of the cure reaction [25]. This method has the advantage of simplicity, with less limitation and the capacity to yield simultaneously information regarding resin kinetics and thermal properties. However, the method only measures the overall heat released

and cannot differentiate between multiple reactions and physical changes such as crystallization.

The development of FTIR spectroscopy has enabled to perform an accurate monitoring of fast and complex polymerizations. Several researchers [15,22,35,37] have successfully used an FTIR to follow fast bulk polymerization. Huang and Su [35] compared results from both DSC and FTIR during the curing of an unsaturated polyester resin with low profile additives (a thermoplastic additive). They found a notable difference in the polymerization degree that shows the advantage of FTIR in the analysis of coupled phenomena for thermosetting and thermoplastic resins. The disadvantages of spectroscopic methods are that the equipment is more expensive. Sample preparation and data analysis are also more time-consuming than DSC.

A large number of studies have been conducted on the resin kinetics of thermosetting systems, and a number of different kinetic models have been proposed in the literature. Generally, researchers have studied the connection of the chemical reaction with the other independent variables, namely time and temperature [23]. In general, the kinetic models can be phenomenological or mechanistic. A phenomenological model captures the main features of the reaction kinetics ignoring the details of how individual species react with one another. On the other hand, mechanistic models are obtained from balances of species involved in the reaction. Hence, they are better for prediction and interpretation. However, because thermosetting reactions are rather complex, mechanistic models require more kinetic parameters than phenomenological models. Therefore phenomenological models are more popular for thermosetting systems.

Although several simultaneous reactions occur during the curing process, simple models have been developed based on the assumption that only one reaction can represent the whole cure process. The simplest model corresponds to a n^{th} -order kinetic expression [13-15,23]:

$$\frac{d\alpha}{dt} = k_A \cdot (1 - \alpha)^n \quad (1-6)$$

where n is the reaction order and k_A is the rate constant given by an Arrhenius temperature dependence:

$$k_A = k_0 \exp\left(\frac{-E_A}{R \cdot T}\right) \quad (1-7)$$

The efficiency of this model for most polymerizations has been postulated by some authors [15,21,23]. However, an n^{th} -order equation cannot realistically describe the progress of the entire reaction because the material undergoes different transitions (gelation, vitrification) during cure. For an isothermal reaction, equation (1-6) predicts a maximum of reaction rate at time zero. So this equation cannot be used for autocatalytic reactions. Kamal and Sourour [21] have shown that the following model describes adequately the cure kinetics of both epoxy and unsaturated polyester resin systems:

$$\frac{d\alpha}{dt} = (k_1 + k_2 \cdot \alpha^m) \cdot (1 - \alpha)^n \quad (1-8)$$

where k_1 and k_2 are rate constants which follow an Arrhenius relationship with the absolute temperature, m_1 and n_1 are catalytic constants. The relative degree of cure, α , is defined by

$$\alpha = \frac{Q}{Q_u} \quad (1-9)$$

where Q is the total amount of heat generated isothermally from the beginning of the reaction until time t_r , and Q_u is the ultimate heat of cure obtained from the total area under the scanned exotherm curve. For non-isothermal curves, a numerical procedure is

proposed in order to calculate α and $d\alpha/dt$ during a linear temperature scan [21]. According to equation (1-8) the initial rate of autocatalytic reaction is not necessarily zero, since there is a possibility that reactants be converted into products through alternative paths. The reaction rate achieves a maximum value at some intermediate conversion, where the position of the peak will depend on the values of m and n . Since $d\alpha/dt$ equals zero, the fractional conversion at peak is given by

$$\alpha_p = \frac{m}{(m + n)} \quad (1-10)$$

An autocatalyzed thermoset usually has its maximum heat evolution around 30-40% of the total conversion [23]. Equation (1-8), the so-called Kamal-Sourour kinetic equation, has been widely used as an effective cure model for thermosetting resins. In general, thermosetting materials exhibit the vitrification phenomenon which stops the reaction before complete conversion is achieved. As the cure progresses and the resin cross-links, the glass transition temperature, T_g , of the system rises. When it approaches the curing temperature, the resin passes from a rubbery to a glassy state. At this time, the mobility of the reacting groups is hindered and the rate of conversion is controlled by diffusion rather than by the chemical reaction. This accounts for the fact that the experimental conversion and reaction rates, at diffusion controlled step, are lower than those predicted by Kamal-Sourour equation.

Salla and Ramis [38] have studied different cure kinetics for an unsaturated polyester resin system by DSC and compared different dynamic and isothermal procedures. They compared four methods used to evaluate the degrees of conversion and the reaction rates of resin systems from isothermal and dynamical temperatures. The authors present also a comparison of different resin kinetics analyses: autocatalytic analysis,

isoconversional adjustments, Ozawa's method and Kissinger's method. The following conclusion is reached:

- For isothermal cures below T_g , the material does not cure thoroughly, since it is possible to detect a residual heat flow when a dynamic post-cure is performed. The sum of the isothermal heat plus the residual heat is always lower than the heat flow obtained dynamically because part of the heat cannot be detected isothermally. Taking into account these considerations, the real degree of cure and reaction rate can be obtained.
- The advantage of the autocatalytic adjustment is that it can provide many kinetic parameters, such as the rate constant at different temperatures, the reaction orders, the activation energy and the frequency factor. A disadvantage is that such a complex process as the curing is associated with a single reactive process with a single activation energy, so the physicochemical interpretation of the kinetic parameters is difficult.
- Improved results were found by using a simple method called isoconversional adjustment.

A number of important and new issues concerning the kinetic behavior of polyester and vinylester systems have become apparent during the manufacture of thick parts by LCM. The novel behavior is primarily due to the lower processing temperatures required to produce thick parts of quality. At these lower temperatures, the thermoset resin cure is diffusion controlled and the cure reaction can reach a steady plateau before full conversion is achieved. The final conversion of the resin or maximum extent of cure is therefore temperature dependent up to a temperature that is high enough to provide sufficient molecular mobility to make all species react within the system. The

situation is further complicated by the possibility that the ultimate conversion of a multi-component resin depends on its temperature history. Depending on the respective reaction rates for the polymerization of each component and the copolymerization between two different components, the final cross-linked structure can change dramatically in function of temperature.

Kamal and Sourour [21] accounted for an incomplete cure of a resin by using a temperature dependent reduction parameter. Michaud et al. [40] analyzed these effects in the kinetic parameters of a Dow Derakane 411 vinylester resin. They denoted that the kinetic behavior below 85 °C was significantly different than previously reported by other researchers. At the lower curing temperatures, a significant portion of the resin remains uncured. The activation energy of the resin also appeared to be smaller. Michaud and co workers used a straightforward method to account for the incomplete cure. Instead of subtracting the extent of cure from unity in equation (1-8), they replayed the unity term which a temperature dependent variable, α_{max} , by assuming an overall reaction order equal to 2 (i.e., $m+n = 2$). The following equation was presented:

$$\frac{d\alpha}{dt} = k_A \cdot \alpha^m (\alpha_{max} - \alpha)^{2-m} \quad (1-11)$$

The maximum extent of cure of the resin system was found by DSC analysis to be much less than unity at temperatures typical of thick part curing. The authors used an empirical linear relationship to fit the experimental data to approximate the resin's maximum extent of cure, as expressed in the equation below:

$$\alpha_{max} = \alpha_0 + B \cdot T \quad (1-12)$$

where B represents the slop of the curve and T the curing temperature.

Yousefi [23] realized a complex description of the cure kinetics for promoted polyester and vinylester resin systems. In this work, low temperature cures were compared to high temperature cures, and fiber filled specimens were also analyzed. In spite that non-promoted polyester resins showed constant kinetic parameters, in the case of promoted polyester resin kinetics parameters were considered temperature dependent to account for the complexity of cure mechanism in the presence of the promoter. This complexity was caused by the promoter which chemically induced the cure reactions at low temperatures. The primary effect of the glass fiber filler was a decrease in the overall reaction rate at low cure temperatures. Acting as heat sinks, glass fibers absorbed the heat of reaction, and yielded a different cure behavior in the isothermal cure. The document presents new procedures to correct the unrecorded extent of cure during isothermal DSC measurements. This procedure attempts to estimate the kinetic parameters in a certain temperature dependent function. A polynomial and an Arrhenius temperature dependence of the reaction exponents m and n was reported. On the basis of estimated kinetic parameters, two temperature regions with different cure characteristics were observed. The sum of reaction exponents was not found to be constant due to the changes caused by the promoter in the cure characteristics of the polyester system. Moreover, the total isothermal heat of reaction was almost identical for both filled and unfilled promoted systems. Finally, the author reports a quite good agreement in the evolution of the cure degree between experimental results and the proposed models. In this work a correlation between kinetic models for isothermal cures was found for polyester and vinylester resins in the presence of glass fibers and promoter.

Another interesting work by Atarsia and Boukhili [39] proposed a methodology based on DSC data discretization to go from dynamic to isothermal data, and vice versa. This method can be generalized to non-uniform temperature heating profiles. This is particularly important in composite processing where the temperature profiles are not

uniform. It allows a fast and secure data processing to simulate numerically the best process window of the cure cycle.

In polyester and vinylester systems, inhibitors are placed within the resin to increase shelf-life by combining with the free-radicals that initiate polymerization of the resin. Inhibition agents generally increase significantly the processing time of thick parts. While these inhibitors disappear quickly at the normal processing temperatures of thin composites, the kinetics of inhibitor deactivation can be very slow at the lower temperature required to successfully cure thick parts. Michaud et al. [40] reported that a significant effect in resin kinetics at low temperature cures is related to the slow deactivation of the inhibitors in the resin system. If the inhibitor concentration Z is scaled by its original concentration Z_0 , the change in the relative inhibitor concentration Z/Z_0 is given by:

$$\frac{d\frac{Z}{Z_0}}{dt} = -k_{inh} \quad (1-13)$$

The rate constant, k_{inh} , was assumed to follow an Arrhenius relationship. The time lag observed during a DSC run before heat is detected by the cell, known as induction time t_{ind} , can be measured at each temperature. The researchers assumed that the polymerization can begin once the inhibitor concentration reaches zero, so the rate constant is related to the inhibition time by:

$$k_{inh} = \frac{1}{t_{ind}} \quad (1-14)$$

and the Arrhenius relationship of the inhibitor concentration for a time step $(t+1)$ was evaluated from:

$$\left(\frac{Z}{Z_0}\right)^{i+1} = \left(\frac{Z}{Z_0}\right)^i - A_{inh} \cdot \exp\left(\frac{E_{inh}}{T}\right) \cdot dt \quad (1-15)$$

Michaud et al. [40] concluded that while most of resin kinetics and inhibitor deactivation parameters can be experimentally determined from the neat resin using DSC, the scaling parameter for the maximum extent of cure relationship and the initial inhibitor concentration need to be evaluated from actual RTM experiments. The presence of fibers within the composite can dramatically affect the curing behavior of the resin and current analysis techniques have not been able to adequately describe this behavior.

Ruiz et al. [84] recently studied the kinetics of an unsaturated polyester resin T580-63 from AOC Canada Inc. with 1.5 % of Norox Pulcat A catalyzer. A comparison was carried out for the autocatalytic, Kamal-Sourou and a new kinetic model. It was finally concluded that new model better represents the experimental data. The model has the advantage to take into account the effect of the glass transition temperature with ease to understand parameters of quick determination. Ruiz and Trochu also tested these models with a Dual Kriging [43] surface that directly represents the data obtained in DSC analysis. This kinetic surface shows the advantage to be fast implemented due to the no necessity to determine any kinetic parameter. However, the DSC analysis must be done at similar thermal conditions of those used in the industrial process. Figure 1.6 shows a comparison of the three kinetic models.

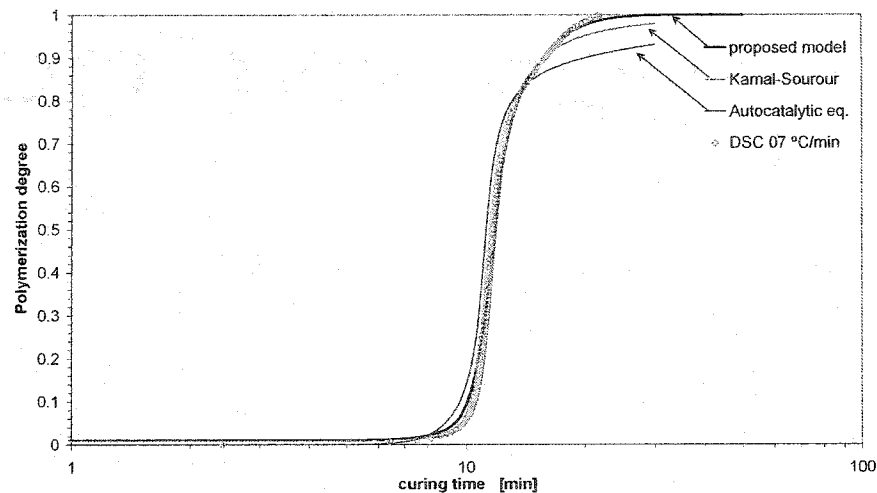


Figure 1.6. Comparison of degrees of polymerization from DSC with predictions of three kinetic models for a constant heating ramp of $7\text{ }^{\circ}\text{C}/\text{min}$. Autocatalytic equation diverges at the end of curing. Kamal-Sourour equation approaches the measured data although some differences are noticed at the end of curing. The Ruiz equation (named proposed model) is the most accurate.

1.6 Resin mechanical properties

During the process cycle the cure degree and, consequently, the microstructure of the material changes. As a thermosetting resin cures its material characteristics change dramatically, transitioning from the behavior of a viscous liquid (low shear stiffness), in its uncured state, to a viscoelastic or elastic solid (high shear stiffness), in its cured state. The cross-link polymerization developed within the resin directly influences the effective mechanical properties. Thus, for accurate representation of the mechanical response of a polymeric composite material during processing, the change in mechanical properties during cure must be ascertained. The curing process of a thermosetting resin may be separated into three regions, as described in Figure 1.7 [47].

In region I, the resin is fully uncured and assumed to behave as a viscous liquid (negligible stiffness). Region II denotes the cure process, where a significant increase in stiffness (chemical hardening) begins to occur. Resin modulus development is generally assumed to begin at the gel point (α_{gel}), and grows until conversion is controlled by diffusion. At this point, marked as α_{diff} , it can be considered a quite constant value. Region III remarks the end of the curing process, where the resin exhibits traditional Viscoelastic behavior at elevated temperatures and approaches elastic behavior at lower temperatures.

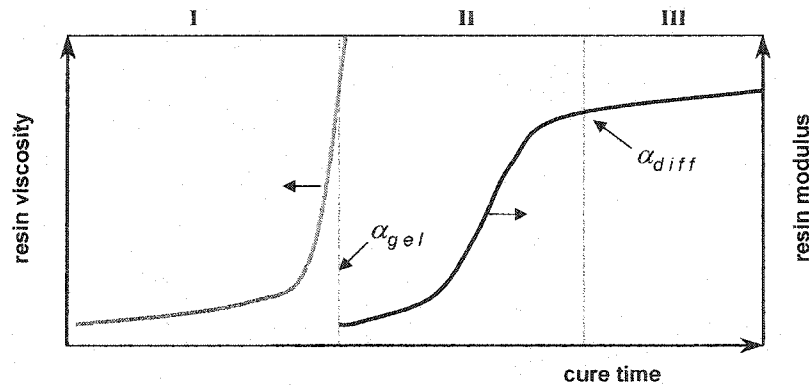


Figure 1.7. Resin modulus development during cure

The growing mechanical properties of the resin system during polymerization were studied and modeled for several authors [14,41,44-**Erreur ! Source du renvoi introuvable.**]. The resin modulus is strongly cure dependent, influenced by the kinetic-viscoelastic interactions successfully modeled by Dillman and Seferis [44]. While their model was rigorous, independent evaluation of the kinetic and viscoelastic parameters required extensive data reduction procedures. In addition, model predictions outside the temperature range characterized by the authors were not reliable. In general, for simplification motives, it is assumed that the resin modulus and Poisson's ratio vary approximately as a linear function of the polymerization degree [45-**Erreur ! Source du renvoi introuvable.**]. This model was first proposed by Osswald [45,54]. It

oversimplifies the relation between degree of cure and elastic constant and neglects time relaxation of Young's moduli and Poisson's ratio during polymerization. An improved linear model was used by Bogetti and Gillespie [47], to represent the resin mechanical properties as function of cure degree for unsaturated polyester and epoxy resin systems. The authors used a convenient α -mixing rule model to describe the kinetic-viscoelastic behavior of the resin modulus during cure. The instantaneous isotropic resin moduli, denoted E_r^α , was expressed explicitly in terms of degree of cure by:

$$E_r^\alpha = (1 - \alpha_{\text{mod}}) \cdot E_r^o + \alpha_{\text{mod}} \cdot E_r^\infty + \gamma \cdot \alpha_{\text{mod}} \cdot (1 - \alpha_{\text{mod}}) \cdot (E_r^\infty - E_r^o) \quad (1-16)$$

where

$$\alpha_{\text{mod}} = \frac{\alpha - \alpha_{\text{gel}}}{\alpha_{\text{diff}} - \alpha_{\text{gel}}} \quad \text{and} \quad (-1 < \gamma < 1) \quad (1-17)$$

The parameters E_r^o and E_r^∞ denote the fully uncured and fully cured resin modulus, respectively. The terms α_{gel} and α_{diff} represent the bounds on the degree of cure, between which the resin modulus is assumed to develop (see Figure 1.8). The term γ was introduced to quantify the competing mechanism between stress relaxation and chemical hardening. Increasing γ physically corresponds to a more rapid increase in modulus at lower degree of cure before asymptotically approaching the fully cured modulus. The authors assumed in that work, that the terms E_r^o and E_r^∞ are constant. Also, they assumed that $\alpha_{\text{gel}} = 0$ and $\alpha_{\text{diff}} = 1$ and $\gamma = 0$. Golestanian and El-Gizawy [46], proposed a similar linear dependence of the material properties with cure degree for an epoxy resin. This model assumes that material properties begins develop from a small cure degrees (5%) until reach its maximum at 85% of the total cure. Millischer [41], assumed also the Young's modulus as linearly dependent of the polymerization degree for a polyester low-profile resin for SMC propose.

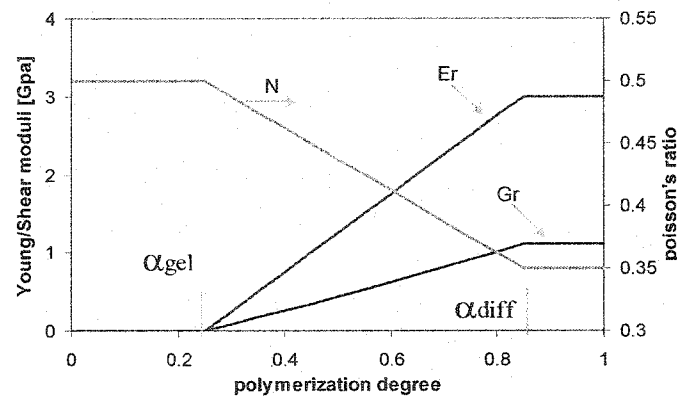


Figure 1.8. Linear variations of the resin mechanical properties with cure degree.

The mechanical properties of the resin also vary as the temperature changes. It is well reported this thermal dependence of elastic and shear moduli and Poisson's ratio [36,41,50-53].

1.7 Part quality and process residual stresses

The tendency of polymers to expand or contract during processing is a problem that has been widely recognized. When thermoset systems are processed, the shrinkage that occurs due to the polymerization reaction further complicates the situation. If the material contains fibers for reinforcement, the net result of the volume change may be a poor surface appearance and high thermal stresses. As pictured in Figure 1.9 poor composite part design conduces to excessive matrix shrinkage in the rib position. This rib should be thinner than the wall to avoid sinks and voids generation. Thus, understanding the volumetric changes during the processing of thermoset polymers can save time and expenses associated with trial and error testing and can improve the part

quality. A wide range of studies have been conducted to gain insight into the volumetric changes that occur during thermoset polymer processing [13-15,41,55-57].

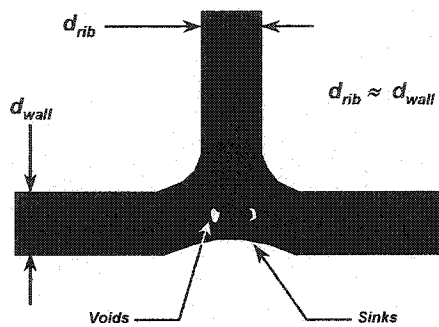


Figure 1.9. Shrinkage defects in a fiber-reinforced composite part

The properties and durability of parts manufactured with polymeric materials are strongly affected by internal stresses, which may lead to defects in the part both during processing, in the form of voids and microcracks, or after manufacture, as warpage, spring-in, premature delamination or debonding (see Figure 1.10). The geometry of a part can restrict the effects of internal stresses. Dimensional stability concerns a dimensional change of the part dependent of time in response to internal or external forces. An example of a lack of dimensional stability is the warpage of a molded part as it is removed from mold after manufacture, as depicted in Figure 1.11.a. Internal stresses in polymeric composite laminate may be generated from the intrinsic heterogeneity and anisotropy of the composite and the thermochemical dependence nature of the constituent mechanical properties. This implies that internal stress fields may act simultaneously on both macro (Figure 1.10.a) and microscopic (Figure 1.10.b) levels and may be driven by both the thermodynamic and kinetic nature of the material and processes. These different degrees of scale are schematically shown in Figure 1.11.b. At each level the stresses are self-equilibrating and the overall stress state can be found by the summation of all of them.

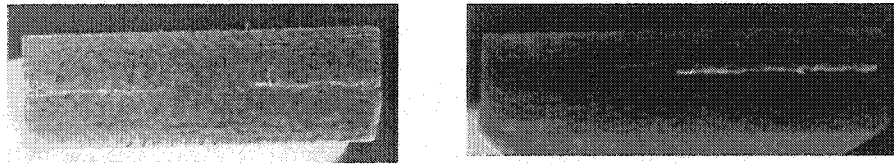


Figure 1.10. Two examples of matrix cracking and delamination during processing of thick composite plates. Defects appear commonly in thick composites processed at high mold temperature.

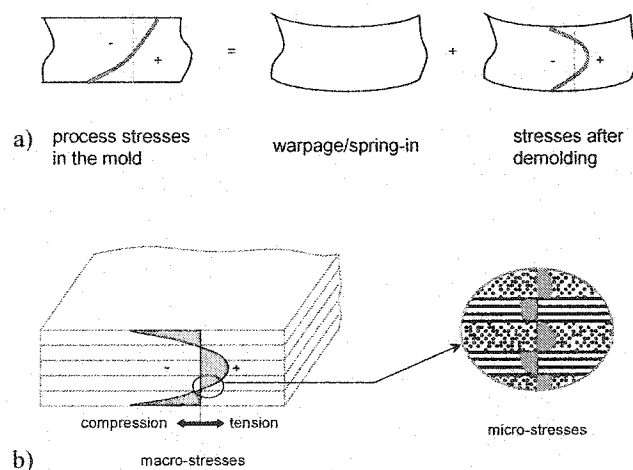


Figure 1.11. a) typical processing stresses within a composite laminate, b) macro and micro levels of internal stresses

The study of residual stresses generated during processing of composite materials has been widely attacked by researchers [15,46-53,58-68]. The mayor quantity of studies is concerned to thermoplastic [59-61,66] and epoxy matrices [46,47,50-53,62-65]. The principal difference in the analysis of thermoplastic or thermosetting matrix is related to their mechanical properties. While thermoplastic materials crystallize during cool-down from high temperatures, and mechanical properties are generated in this period,

thermosetting materials exotherm during cure at the same rate that mechanical properties are developed. In general terms, time, temperature and pressure conditions between typical processing of these materials are strongly different. Although exist these particular differences in the processing conditions and mechanical properties, the nature of the residual stresses generated has the same origin. In thermosetting matrices, the study has been directed to epoxy resins and some authors reported studies in polyesters [40,41,47,58] and other materials [48,67,68].

In calculating the thermal residual stresses in composites, a stress-free state at highest temperature in the curing cycle is commonly assumed. Thus the attention is focused on the optimization of the cooling path so as to minimize the residual stresses within the part. As described by Stringer et al. [50,51], when focused only on thermal stresses during cool-down from the elevated temperature the stress model predicted a low through-thickness tensile stress than measured. This level of predicted stress was not sufficient to cause delamination in a fully cured composite. A fundamental consideration of the mechanisms involved during cure process of composite component led to the hypothesis [52] that stresses arising in the cure cycle prior to cool-down may be responsible for delamination. Before the cool-down begins, the matrix undergoes significant volume changes that also produce residual stress in composites. This residual stress is relieved by several mechanisms such as fiber waviness, warping, delamination, and microcracking. It is then important to consider both kinetic and thermodynamic sources of the internal stress generation to ensure that suitable analytical techniques are used in their evaluation.

In many works it is assumed that the composite is under stress-free state by the end of cross-linking of the polymer resin. Due to the viscous behavior of the resin through the polymerization process, the residual stress developed within the material can be negligible. Bogetti and Gillespie [47] studied the process-induced stresses in thick-sectioned composite laminates. In this work, the results indicate that the assumption of

a stress-free temperature for residual stress predictions is not appropriate for thick-sectioned parts. They denoted in the study of graphite/epoxy laminates that the curvature and transverse modulus both increase sharply immediately after the gel point, possibly indicating that the development of residual stress can be significantly affected by the mechanical properties of the resin before full cure has been reached. Although it is important to remark that the authors did not consider the thermal variations of the mechanical properties of the resin during cure, and either, the effect of stress relaxation above the glass transition temperature.

1.8 RTM process optimization

In the LCM process, there are a large number of design variables which impact the process performance (see Figure 1.12). The mold temperature and inlet pressure must be well selected so that the resin will not gel during filling allowing a proper fill up of the mold. The determination of the process parameters is the key to have successful molding conditions. In addition, proper choices of the process conditions can reduce cycle time, heating sources, resin injection apparatus, mold deformation and clamping systems. Minimization of the mold filling and curing times is equivalent to reduce energy consumption during molding cycle. Finally, and may be the most important in the processing of thick composites, the optimum choice of process variables will result in minimum part defects, such as micro cracks, delamination, warpage, spring-in, etc., it means that the optimized process will result in a high part quality. As shows Figure 1.12, exist a sophisticated relation between design parameters and measurable process issues. Due to this complexity in the interactions, many LCM process designers depend more often on their experience or knowledge rather than a systematic optimization search engine. However, recent advances in LCM simulation and optimization tools have created new applications in process design.

It is comprehensible that final mechanical properties of the composite will be affected by the processing of the part. Several developers have understood this relationship and presented experimental investigation on the sensibility of mechanical properties to the process parameters [14,69-71]. In general words, it is accorded that preheating of the mold help the wet-out of the preform and consequently aids product quality. Preheating of the resin at the injection gate has also showed to improve the results of mechanical analyses in the full cured part [14,71]. It is also reasonable that injection pressure and fiber/mold temperature during filling will have a decisive role in process where the gel time is close to the filling time.

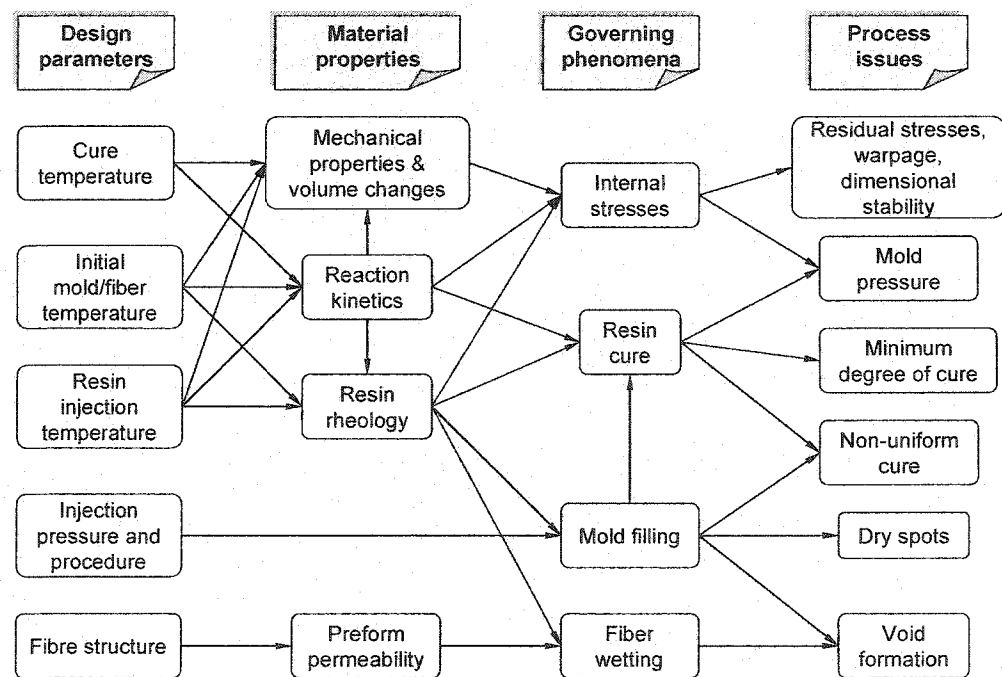


Figure 1.12. Process design parameters and issues to optimize

Despite the fact that many authors have published works in the field of LCM simulation and the fact that process parameters influence critically on product quality, few research works have been done on the area of process optimization [71-83]. At the early beginning, investigators adapted to the LCM process design tools used for traditional aerospace composite fabrication methods, such as autoclave. But quickly it was found that these techniques don't support the optimization of design and manufacture under LCM conditions. Several fundamental aspects differentiate these processes. It is a matter of fact that the principal discrepancy comes from the mold concept. In autoclave curing, one mold surface is used to geometrically support a pre-impregnated preform. So that autoclave temperature and pressure are directly applied to one surface of the part. These conditions generates a principal resin flow through the thickness of the part, at the same time that composite compacts increasing fiber volume content. In the other hand, LCM process uses two mold surfaces, implicating that part compaction during exotherm period will be constrained by the mold. In this case, the principal resin flow will be developed on the plane of the part, and through-thickness conduction and in-plane convection will be the dominant thermal effects. It implicates, that the resin that first touches the mold walls will be the first in react, or in other words, the resin closer to the vent gate will cure prior to the resin close to the injection gate. These differences show that special and careful analysis should be done to be able to accurately optimized the LCM process.

Historically, autoclave cure cycles have been developed using trial-and-error methods. But this procedure is evidently inefficient and depends on the acquired knowledge. So many others approaches have been developed to obtain the optimal cure cycles. The result of these trial-and-error methods have led to the development of various rule-based heuristic expert systems to guide process development. Xiao et al. [72] developed an expert heuristic system for LCM, comparing mechanical properties after curing with different curing conditions. Two variables, injection pressure and mold temperature were studied. Johnson et al. [71] used an expert heuristic system for the optimization of

the heating injection temperature of the resin with microwave in a LCM process. However, the applicability of heuristic approaches is often limited by the specific material, geometry and practical restrictions. These approaches cannot obtain an optimal design, especially where there are large numbers of design parameters and constraints involved that cannot always be measurable.

Spoerre et al. [73] proposed the use of Genetic Algorithms (GA), in conjunction with the cascade correlation neural networks architecture (CCA-NN), to establish a model that predicts and optimize performance and quality of LCM parts. In this method, the authors did not use numerical simulations to construct the objective function to be optimized, but used a database of experimental results. They conclude that although the process optimization showed good convergence to the estimates optimum values, the use of this technique is restrained to the development of a resin transfer molding database. Chen et al. [83] analyzed the effects of moisture upon the optimal cooling temperature path after post cure of a symmetric composite laminate. They constructed a based gradient algorithm to found the optimum cooldown temperature path that minimizes thickness-averaged residual stresses after post cure. The used technique was well adapted to the simple number of parameters used within the one-dimensional simulation, but it may be hard to resolve in a complex combination of design parameters and evaluation functions.

Recently, Li, Trucker et al. [76] proposed the method of design sensitivity analysis to optimize the autoclave temperatures in a graphite/epoxy composite. Design sensitivity information is extracted based on an analytical, direct differentiation approach. The sensitivities are then used with a gradient-based optimization technique to systematically improve the curing process. In this work, the cure cycle is constrained to a maximum temperature within the composite and a minimum degree of cure. To obtain the minimum cure cycle, one, two and three dwell temperatures were proposed. Finally, the optimization algorithm finds a smoothed cure and temperature profiles

through the thickness. The authors conclude that the method is most useful for improving designs that are generated by less precise methods, such as design rules, expert system, and heuristics. Starting from the estimates of these less precise methods, the approach should produce optimal cure cycles.

Ruiz [77] analyzed the one-dimensional optimization of the non-isothermal filling process and the optimization of the temperature ramp and dwell cure temperature for RTM parts. By using resin chemical changes at mold wall temperature as constraint, he found the proper mold temperature to obtain a minimum filling time. In this simple case, the interpolation between the result of numerical simulations was done by a Kriging curve [43], as shows Figure 1.13.a. Intersections between Kriging curves were used to obtain the adequate result. For the optimization of the one-dimensional, through-thickness, thermokinetic analysis he selected as objective functions the minimum curing time, a maximum acceptable exothermic temperature and certain constrains in the through-thickness cure profile. Finally, the heating ramp and dwell temperature were found by intersecting parametric Kriging surfaces, as depicted in Figure 1.13.b. Although the method showed an excellent and quick convergence to correct values, it can be applicable when only a couple of parameters are required for the optimization.

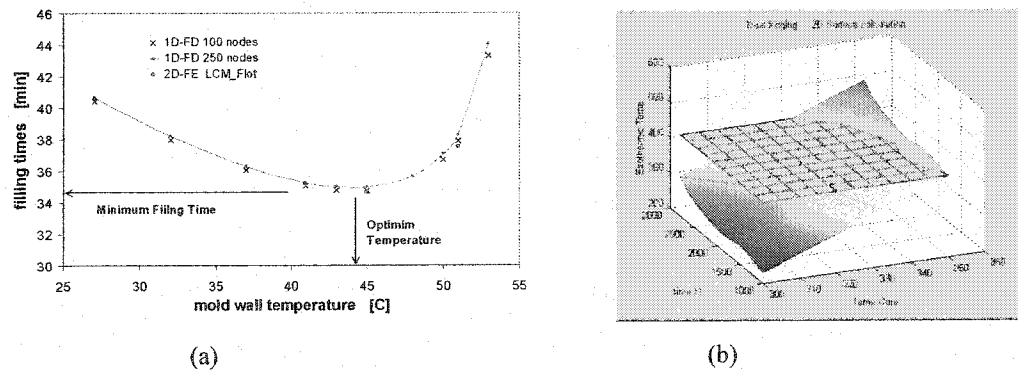


Figure 1.13. RTM optimization methods, a) optimization curve of filling time versus mold temperature, and b) parametric Kriging surfaces intersection to optimize cure temperature, by Ruiz [77]

Young [74] used a GA algorithm to search for the optimal gate locations and constant injection pressure that minimize the filling time. The GA code converged to near optimal global solutions in large searching space with many local maximums, but a poor rate of convergence was found. A comparison with random search and hill climbing shows that hill climb is the faster in converge, but because there are many local solutions in the searching space, this method usually converges to the local hill. In the other hand, random search showed to have less rate of convergence of GA. In the last year, Lin and co workers [75] presented a RTM filling process optimization with an interesting discussion over two different search methodologies to found optimum values. They tested and compared the convergence of gradient-based algorithms and genetic algorithms. Objective functions were based in the injection gates locations and a simple design variable, the filling time, was used to determine the optimization. The conclusion of this work indicates that GA are strong enough to found a near optimal solution, although are not recommended because of their poor rate of convergence. If only one or two design parameters are involved, a brute force search method might be the most efficient. If the number of design parameters is large, a gradient-based method

such as the quasi-Newton method is recommended. It may be remarked that the authors used GA along without any other method to accelerate convergence. They also found an important convergence error due to the refinement of the FE mesh. The size of the mesh must be small enough so that gate locations can be varied for small distances. As an scope of future work, the authors propose the use of remeshing algorithms to accelerate convergence of the solutions and avoid excessive numerical error due to the forced change in the gate positions, because the use of a fixed FE mesh.

Shead et al. [80] developed an optimization algorithm to search the optimum autoclave processing conditions. An objective function based on minimum degree of cure, part temperature, processing time and warpage was used to evaluate the cure cycle. In this work, the authors developed an optimizer based on the GA method. The GA shows to be more appropriate because the strong convergence without expert knowledge upon the minimum scope of initial parameters and therefore are less case specific. Yu and Young [81] presented a RTM filling optimization based on GA. They used the GA to search for a suitable mold temperature that minimizes the filling time. After the first optimization, a new mold temperature was searched to the cure stage, with the constraint of maximum allowable exotherm temperature. Although the convergence of GA shows that are quite stable under different conditions, the number of generations required is high. In this study, for a constant resin injection temperature, around forty iterations are needed to assure the convergence of the results. For a complex three-dimensional part hundred of non-isothermal simulations is not recommended for an optimization procedure. Luo et al. [82] have optimized the RTM filling stage by changing the position of the injection gates and evaluating the filling times. This approach was built upon an RTM simulation engine coupled with a neural-network (NN) genetic algorithm optimization procedure. The NN-based process model proved to be a quick and accurate tool for RTM process performance prediction, better than the use of GA along (because relatively large number of iterations are required).

From the above studied, the optimizations already investigated in the composite processing, especially suitable for RTM process, can be divided into two windows:

- a) The selection of the objective functions and design variables. Optimizations have been done for the filling stage or cure process alone. The filling optimizations are based in the selection of mold temperature or gate position for an optimum filling. Cure optimizations are based in assure a minimum cure degree, maximum exotherm temperature and minimum deformation (during cool-down). The appropriate selection of the objective functions and design variables will lead to a proper and quick optimization. Even a sensibility analysis has shown to be proper development tool to improve the adequate selection of the parameters.
- b) The selection of the optimization schema. A proper choice of the optimization schema is imperative to an effective and reliable operation of the process optimizer. Several algorithms have been seeing to successfully satisfy the optimizations in RTM process, including: 1) expert based systems, 2) heuristic approach, 3) gradient-based methods (as Newton-Raphson), and 4) genetic algorithms (including variants to accelerate convergence).

1.9 References

1. Ruiz, E., and Demaria, C., 1998, Diseño, Análisis y Procesos de Fabricación de la puerta de un vehículo eléctrico ciudadano en RTM, Eng. thesis, Instituto Universitario Aeronáutico, Universidad Católica de Córdoba, Argentine.
2. Voller, V., and Peng, S., 1995, Polymer Eng. and Sci., 35, 1758.
3. Owen, M., Rudd, C., and Kendall, K., 1991, Modelling the Resin Transfer Molding (RTM) Process, Advanced Composite Materials Conf., Detroit, Michigan USA, Sept. 30–Oct. 3, 187.
4. Boccard, A., Lee, and W., Springer, G., 1995, J. of Composite Materials, 29, 306.
5. Trochu, F., Gauvin, R., and Gao, D., 1993, Advances in Polymer Technology, 12, 329.
6. UM, M.-K., and Lee, W.-I., 1991, Polymer Eng. and Sci., 31, 765.
7. Alexandrou, A., and Ahmed, A., 1993, Polymer Eng. and Sci., 33, 1055.
8. Papathanasiou, T., and Kamal, M., 1991, The Use of Boundary Fitted Curvilinear Coordinates to Model the Filling Stage of Injection Molding in Complex Cavities, 49th Annual Technical Conference ANTEC'91.
9. Coulter, J., and Guceri, S., 1988, J. of Reinforced Plastics and Composites, 7, 201.
10. Coulter, J., and Guceri, S., 1989, Composites Sci. and Technology, 35, 317.
11. Guyonvarch, G., Audet, M., Qian, Y., Trochu, F., and Delaunay, D., 1996, Validation of Non Isothermal Resin Transfer Molding Simulations, Joint European Conference JEC, Paris, France.
12. Lin, R., Lee, L., and Llou, M., 1991, Mold Filling and Curing Modeling of RTM and SRIM Processes”, Advanced Composite Materials Conf., Detroit, Michigan USA, 165.
13. Advani, S. G. (Ed.), 1994, Flow and Rheology in Polymer Composites Manufacturing, Elseiver Sci.
14. Rudd, C., Long, A., Kendall, K., and Mangin, C., 1997, Liquid Moulding Technologies, SAE International book.

15. Gutowski, T. (Ed.), 1997, Advanced Composites Manufacturing, John Wiley & Sons, Inc.
16. Ferland, P., Trochu, F., Gauvin, R., Guittard, D., and Boime, B., 1995, Rate of Conversion, Temperature Variation and Flow Simulation of Reactive Liquid during RTM and SRIM Mold Filling, ENERCOMP'95 conf., Montreal, Canada.
17. Chang, A., and Hwang, S., 1992, Polymer Eng. and Sci., 32, 310.
18. Chen, B., and Liu, W., 1989, Polymer Eng. and Sci., 29, 1039.
19. Boime, B., Guittard, D., Ferland, P., Trochu, F., and Gauvin, R., 1995, Mold Filling Simulation of the Resin Transfer Molding Process for Complex Three Dimensional Ribbed Parts, SAMPE 40th conf., Anaheim, CA USA.
20. Guyonvach, G., Audet, M., Qian, Y., Trochu, F., and Delaunay, D., 1996, Validation of Non Isothermal Resin Transfer Molding Simulations, Joint European Conference JEC'96, Paris, France.
21. Kamal, M., and Sourour, S., 1973, Polymer Eng. & Sci., 13, 59.
22. Han, C., and Lem, K., 1983, J. of Applied Polymer Sci., 28, 3155.
23. Yousefi-Moshirabad, A., 1996, Cure Analysis of Promoted Polyester and Vinylester Reinforced Composites and Heat Transfer in RTM Molds, PhD. Thesis, École Polytechnique de Montreal.
24. Lebrun, G., Rudd, C., and Gauvin, R., 1995, J. of Reinforced Plastics and Composites, 14, 1069.
25. Carman, P., 1937, Trans. Int. Chem. Eng., 15, 150.
26. Darcy, H., 1856, Les Fontaines Publiques de la Ville de Dijon, Paris, Dalmont.
27. Lebrun, G., and Gauvin, R., 1995, J. of Material Processing and Manufacturing Sci. 4, 81.
28. Lebrun, G., Gauvin, R., and Kendall, K., 1996, Composites Part A, 27, 347.
29. Tucker, C., 1996, Polymer Composites, 17, 60.
30. Erhun, M., and Advani, S., 1992, Int. J. for Numerical Methods in Eng., 35, 351.
31. Trochu, F., and Gauvin, R., 1992, J. of Reinforced Plastics and Composites, 11, 772.

32. Gauvin, R., and Trochu, F., 1998, *Polymer Composites*, 19, 233.
33. Remacle, J.-F., Breard, J., and Trochu, F., 1999, Numerical Simulation of mould Filling for Three-Dimensional Composites Parts, *Flow Processes in Composite Materials EPCM-5 Conf.*, 81.
34. Bechet, E., Ruiz, E., Trochu, F., and Cuilliere, J.-C., 2001, Re-Meshing Algorithms Applied to Resin Transfer Molding Simulations, *Int. Canada Composites Conference CANCOM'01*, Montreal, Canada.
35. Huang, Y.-J., and Su, C.-C., 1995, *J. of Applied Polymer Sci.*, 55, 305.
36. Han, C., and Lem, K.-W., 1984, *J. of Applied Polymer Sci.*, 29, 1879.
37. Han, C., and Lee, D., 1987, *J. of Applied Polymer Sci.*, 336, 2859.
38. Salla, J., and Ramis, X., 1996, *Polymer Eng. Sci.*, 36, 835.
39. Atarsia, A., and Boukhili, R., 2000, *Polymer Eng. Sci.*, 40, 607.
40. Michaud, D., Beris, A., and Dhurjati, P., 1998, *J. of Composite Materials*, 32, 1273.
41. Millischer, A., 2000, *Transferts Thermiques dans le Procède d'Injection BMC*, PhD. Thesis, École Polytechnique de l'Université de Nantes, France.
42. Sobotka, V., 2001, *Détermination des Paramètres Thermophysiques et Cinétiques d'une Résine Polyester Insaturée*, Rapport de Stage, École Polytechnique de Montreal (CRASP).
43. Trochu, F., 1999, Krigeage en CAO et FAO, MEC6310 course, École Polytechnique de Montreal.
44. Dillman, S., and Seferis, J., 1987, *J. of Macromolecular Sci.-Chemistry*, 24, 110.
45. Osswald, T., 1991, *J. of Thermoplastic Composite Materials*, 4, 173.
46. Golestanian, H., and El-Gizawy, S., 1997, *J. of Composite Materials*, 31, 2402.
47. Bogetti, T., and Gillespie, J., 1992, *J. of Composite Materials*, 26, 626.
48. White, S., and Hahn, H., 1992, *J. of Composite Materials*, 26, 2402.
49. Johnston, A., Vaziri, R., and Poursartip, A., 2001, *J. of Composite Materials*, 35, 1435.

50. Wisnom, M., Stringer, L., Hayman, R., Hinton, M., Badcock, R. and Wisnom, M., 1999, Curing Stresses in Thick Polymer Composite Components, Part I, ICCM-12 Conf., Paris, France.
51. Stringer, L., Hayman, R., Hinton, M., Badcock, R. and Wisnom, M., 1999, Curing Stresses in Thick Polymer Composite Components, Part II, ICCM-12 Conf., Paris, France.
52. Corden T.J., Jones I. A., Jones D.T., and Middleton V., 1998, Composites Part A, 29, 455.
53. Klisch, A., Fiedler, B. and Schulte, K., 1999, Influence of the Thermal Dependent Matrix Properties on the Residual Stress Distribution in a Model Composite, ICCM-12 Conf., Paris, France.
54. Stevenson, J., 1996, Innovation in Polymer Processing: Molding, Carl Hanser (Ed.), USA.
55. Kinkelaar, M., and Lee, L., 1992, J. of Applied Polymer Sci., 45, 37.
56. Kinkelaar, M., Muzumdar, S., and Lee, L., 1995, Polymer Eng. and Sci., 35, 823.
57. Liu, C., Kiasat, M., Nijhof, A., Blokland, H., and Marissen, R., 1999, Polymer Eng. and Sci., 39, 18.
58. Riopel, S., 1999, Étude Expérimentale de la Cuisson d'un Composite Unidirectionnel Verre/Polyester de Grande Épaisseur, Mémoire de Maîtrise, École Polytechnique de Montreal.
59. Sunderland, P., 1997, Measurement and Prediction of Techniques for Internal Stresses in Polymers and Composites, PhD. Thesis, École Polytechnique Fédérale de Lausanne.
60. Manson J.-A., and Seferis, J., 1992, J. of Composite Materials, 26, 405.
61. Sunderland, P., Yu, W., and Manson, J.-A., 1995, A Technique for the Measurement of Process-Induced Internal Stresses in Polymers and Polymer Composites, ICCM-10 Conf., Whistler, Canada, 125.
62. Eom, Y., Boogh, L., Michaud, V., Sunderland, P., and Manson, J., 2000, Polymer Eng. and Sci., 40, 1281.

63. Kim, Y., and White, S., 1997, Secondary Structure Effects on the Process-Induced Residual Stress Development of Cylinder Structure, ICCM-11 Conf., Gold Coast, Australia.
64. Albert, C., Fernlund, G., and Poursartip, A., 2001, The Effect of Part Design and Process Parameters on Spring-In of Angled Composite Parts, Int. Canada Composites Conference CANCOM'01, Montreal, Canada.
65. Jayaraman, K., and Reifsnider, K., 1992, J. of Composite Materials, 26, 770.
66. Oosthuizen, J., and Groenewald, W., 1997, Curing Strains Developed During the Manufacture of GRP Tubes, ICCM-11 Conf., Gold Coast, Australia.
67. White, S., and Hahn, H., 1993, Journal of Composite Materials, 27, 1353.
68. Davidoff, A., Jacque, F., Bung, H., and Chen, S., 1992, Post Filling Simulation, Mold Cooling, and Part Warpage, ANTEC'92 Conf., 1882.
69. Pearce, N., Guild, F., and Summerscales, J., 1998, Composites Part A, 29, 141.
70. Patel, N., Perry, M., and Lee, J., 1991, Influence of RTM and SRIM processing Parameters on Molding and Mechanical Properties, Advanced Composite Materials Conference, Detroit, USA.
71. Johnson, M., Rudd, C., and Hill, D., 1997, Effects of Microwave Resin Preheating on the Quality of RTM Laminates, ICCM-11 Conf., Gold Coast, Australia.
72. Xiao, X., Astakhov, V., and Su, T., 1999, A Study of Resin Transfer Molding Process Using Experimental Design Method, ICCM-12 Conf., Paris, France.
73. Spoerre, J., Zhang, C., Wang, B., and Parnas, R., 1998, J. of Composite Materials, 32, 1244.
74. Young, W.-B., 1994, J. of Composite Materials, 28, 12.
75. Lin, M., Murphy, M., and Hahn, H., 2000, Composites Part A, 31, 361.
76. Li, M., Zhu, Q., Geubelle, H., and Trucker, C., 2001, Polymer Composites, 2, 118.
77. Ruiz, E., 2000, Thermal Optimization of RTM process, internal report, Ecole Polytechnique de Montreal.
78. Binetruy, C., Krawczak, P., and Cauchois, J., 2001, Application of Numerical Simulation to the Cost Effective Improvement of Resin Transfer Molding for

Engineered Composite Parts, Int. Canada Composites Conference CANCOM'01, Montreal, Canada.

79. Kang, M., Jung, J., and Lee, W., 2000, Composites Part A, 31, 407.

80. Shead, M., Hudek, M., Raghavan, J., Cole, R., and Hendrickson, L., 2001, Modelling and Optimization of Autoclave Processing Polymer Composites, Int. Canada Composites Conference CANCOM'01, Montreal, Canada.

81. Yu, H.-W., and Young, W.-B., 1997, J. of Composite Materials, 31, 1113.

82. Luo, J., Liang, Z., Zhang, C., and Wang, B., 2001, Composites Part A, 32, 877.

83. Chen, R., Tu, C., and Tsai, H., 1993, J. of Composite Materials, 27, 1578.

84. Ruiz, E., Trochu, F., and Gauvin, R., 2003, Thermal Optimization of Thick Composite Parts Manufactured by Resin Transfer Molding, Advancing with composites COMP'03, Int. Meeting on Composite Materials, Corfu, Greece.

CHAPITRE 2

THERMO-MECHANICAL PROPERTIES DURING CURE OF GLASS-POLYESTER RTM COMPOSITES: ELASTIC AND VISCOELASTIC MODELING

Présentation du chapitre

L'article présenté dans le chapitre 2 porte sur l'étude expérimentale et la caractérisation des propriétés thermomécaniques les plus importantes dans les composites fabriqués par les procédés de moulage par injection sur renfort (LCM). Initialement, la cinétique de polymérisation d'une résine polyester insaturée commerciale est étudiée dans un calorimètre différentiel DSC (« Differential Scanning Calorimeter »). Un modèle semi-empirique de la cinétique de cuisson est développé pour tenir compte des effets de l'inhibiteur et de la transition vitreuse du matériau. Le modèle permet aussi de calculer le degré de polymérisation maximum à une température de cuisson donnée.

Ensuite, l'évolution des propriétés mécaniques de deux composites verre/polyester est déterminée par une analyse mécanique dynamique dans un appareil DMTA (« Dynamical Mechanical Thermal Analyzer »). Deux modélisations différentes des propriétés mécaniques sont présentées. La première est un modèle thermochimique élastique non linéaire qui considère la relaxation totale du matériau à l'état caoutchoutique. Ce modèle tient compte des variations du degré de polymérisation et de la transition vitreuse sur la relaxation totale du composite. La deuxième est un modèle viscoélastique complexe fondé sur une mesure de la relaxation des contraintes et le principe de superposition temps/température.

Finalement, les coefficients d'expansion thermique de la résine et du composite sont caractérisés au moyen d'un analyseur thermomécanique TMA (« Thermo-Mechanical Analyzer »). Le retrait de polymérisation de la résine est mesuré et exprimé comme une fonction linéaire du degré de polymérisation.

Thermo-Mechanical Properties during Cure of
Glass-Polyester RTM Composites:
Elastic and Viscoelastic Modeling

Edu Ruiz and François Trochu

Centre de Recherches Appliquées Sur les Polymères (CRASP)

Département de Génie Mécanique,

École Polytechnique de l'Université de Montréal,

H3C 3A7, Canada

e-mails: eduardo.ruiz@polymtl.ca, francois.trochu@polymtl.ca

Keywords: RTM, resin cure, elastic model, viscoelastic model.

Article soumis à la revue *Journal of Composite Materials*

November 2003

2.1 Abstract

Resin transfer molding (RTM) is a widely used manufacturing technique of composite parts. A proper selection of process parameters is the key to yield successful molding results and obtain a good part. During composite consolidation, resin cure, also called chemical conversion, plays a decisive role on the final mechanical properties of the part. The modeling of resin kinetics and the evolution of composite properties during cure are crucial for process optimization. In this paper, the curing of a thermosetting polyester resin was studied by differential scanning calorimetry (DSC). A semi-

empirical autocatalytic model was implemented to describe the kinetics of the chemical reaction. The model accounts for the maximum degree of polymerization as a function of cure temperature and induction time, i.e., the time required to attain total inhibitor degradation.

The evolution of mechanical properties during resin cure for two glass/polyester composites was also studied with a dynamical mechanical thermal analyzer (DMTA) and thermo-mechanical analyzer (TMA). Given that for a low chemical conversion the elastic properties of the resin remain small, an initial degree of polymerization called *after gel point* (AGP) was introduced in the analysis of mechanical properties during cure. A normalized elastic modulus was defined from the value at AGP taken as a reference. The normalized elastic modulus was then compared to the polymerization degree. The logarithm of chemical conversion was found to be almost-linearly related to the logarithm of the elastic modulus. Based on this comparison, a thermo-chemical model is proposed to describe the evolution of mechanical properties during the cure of composite samples with different fiber volume fractions.

The viscoelastic behavior was also determined by performing stress relaxation tests with the DMTA. Resin specimens were tested for different cure states below the glass transition temperature, and master curves of stress relaxation during cure were constructed by applying the time-temperature superposition principle. The measurements depict the relaxation modulus of polyester resins as sharply affected by the degree of polymerization. Based on the experimental data, a relaxation modulus was modeled in a thermorheologically simple manner using exponential and power laws. Finally, a linear volume change model was constructed based on TMA measurements of thermal expansion and resin shrinkage. The volume changes resulting of composite expansion/contraction and resin polymerization shrinkage are modeled as a function of temperature and degree of polymerization.

The purpose of this work is to develop appropriate models of resin kinetics, elastic and viscoelastic behaviors and volume changes that occur during the cure of glass/polyester composites. These models will be used in future investigations for thermal and curing optimization of composites processed by resin transfer molding.

2.2 Introduction

As the composite industry grows, thick parts and pieces of complex shape have become more common. The composite components for structural applications require larger cross-sections than for non-structural applications. The curing of thick parts is challenging because of the low thermal conductivity of the composite and the large heat of reaction generated during the cross-linking polymerization. This combination of low thermal conductivity and large heat source in the part during cure can lead to significant thermal gradients and temperature peaks. This generates residual stresses, which may result in polymer degradation. In order to improve the quality of thick composites, the processing temperature needs to be controlled so that thermal gradients remain small. Moreover, the chemorheology and cure kinetics may be considerably different from what is observed at higher temperatures [2]. The reinforcing fibers are not really affected during the process cycle, but the polymer matrix can shrink during cross-linking by as much as 9% [1]. During processing, these different thermal behaviors induce internal stresses in composite parts. When curing fiber-reinforced composites, residual stresses have a significant effect on the part quality and mechanical properties, generating warpage or initiating matrix cracks and delamination [2].

It is common to observe different surface and structural defects in composite parts manufactured by RTM. Non-appropriate processing parameters result in typical problems such as bad surface appearance, waviness of flat geometries, part warpage, spring-in, matrix degradation and composite delamination [24]. Based on a knowledge of material

behavior during resin cure [1, 5-13], a computational analysis of processing stresses can be carried out. The results of numerical simulations depend directly on the quality of experimental investigations, i.e., on the repeatability of the experiments carried out to characterize a desired material property.

Appropriate modeling of reaction kinetics is essential in the processing of thermosetting materials. The reaction kinetics of epoxy and polyester resins has been widely studied in the past by several authors [2, 4, 14-19]. The kinetic models derived from calorimetric investigations are based primarily on the autocatalytic assumption. Yousefi-Moshirabad [18] has determined the dependence of kinetic parameters on temperature and has studied the influence of low curing temperature on gel time and final degree of polymerization. Recently a methodology was established to determine the parameters of several kinetic models using genetic algorithms [15].

Many investigators in the past have assumed that the mechanical properties of composite are elastic and vary linearly with the degree of polymerization of the matrix [20-22]. Although this approach represents the simplest way to compute internal processing stresses, viscoelastic effects and glass transition of the resin limit the accuracy of such analysis. Viscoelastic modeling is well suited for material characterization of stress relaxation and glass transition effects [5, 8-13, 23]. Nevertheless, the requirement of time integrals and close loop iterations make these models hard to implement in numerical optimization schemes because of the large number of iterative calculations required.

Generally, below the glass transition temperature (T_g), the material behavior is predominantly elastic, while above that temperature it becomes more viscous or rubber-like. This paper presents a new approach to describe the mechanical behavior of polymer composites without excessive computational times. The model is based on the mechanical properties of the resin in the elastic unrelaxed and fully relaxed phases. To do so, a function of the glass transition temperature is introduced to model phase transformation.

This relaxed/unrelaxed model is also compared with a simple linear viscoelastic model that describes stress relaxation in polyester glass composites.

The article begins by presenting the physical phenomena that govern resin cure and the basic thermal equation associated. A semi-empirical autocatalytic kinetic equation is proposed to describe free-radical polymerization. Then, a new methodology is outlined to model the dependence of composite mechanical properties on temperature, degree of polymerization and glass transition temperature. This thermo-chemical analysis is carried out for one polyester resin and two different fiberglass reinforcements. Next, the experimental procedure followed to measure the stress relaxation modulus of these composites is presented. A simple rheological model is used to describe the linear viscoelastic behavior as a function of degree of polymerization. Then models of volume change and evolution of material behavior during composite processing are introduced. Both models depend on fiber volume fraction, temperature and degree of polymerization.

2.3 Kinetic modeling

If an instantaneous equilibrium temperature between the resin and fibers is assumed at each time [3], the transient absolute temperature $T(z,t)$ at position z and time t through the total part thickness (Z_T) is given by the one-dimensional Fourier's heat conduction equation :

$$\tilde{\rho}\tilde{C}_p \frac{\partial T}{\partial t} = \tilde{k} \frac{\partial^2 T}{\partial z^2} + \Phi \rho_r \dot{H} \quad 0 \leq z \leq Z_T \quad (2.1)$$

where the density $\tilde{\rho}$, heat capacity \tilde{C}_p and conductivity \tilde{k} of the composite are defined as the effective properties obtained by the rule of mixture [3]:

$$\begin{aligned}\tilde{C}_p &= C p_r w_r + C p_f w_f, & \tilde{\rho} &= \frac{\rho_r \rho_f}{\rho_r w_r + \rho_f w_f} \\ \tilde{k} &= \frac{k_r k_f}{k_r w_r + k_f w_f}, & w_r &= \frac{\phi / \rho_f}{\left(\phi / \rho_f + 1 - \phi / \rho_r \right)} \\ w_f &= 1 - w_r\end{aligned}\quad (2.2)$$

In the above equations ϕ is the porosity, and w_r, w_f denote the weight fractions of resin and fibers, respectively. The subscript f stands for the fibers, and r for the resin. The last term on the right hand side of equation (2.1) represents a heat source produced by the exothermic chemical reaction of the resin. The instantaneous heat \dot{H} generated by the cross-linking polymerization of the resin. This source term is assumed to be proportional to the reaction rate:

$$\dot{H} = \frac{dH}{dt} = \frac{d\alpha}{dt} \cdot H_T \quad (2.3)$$

where $d\alpha/dt$ is the reaction rate or rate of conversion, and H_T is the total or ultimate heat of reaction during cure.

During the thermal cure of polyester resins, although the polymerization reaction always involves the breaking of double $C=C$ links to form single $C-C$ links, different reaction mechanisms may take place simultaneously depending on the resin additives. Thus the proportionality assumption between the polymerization reaction and the heat released may not be expected to hold in all cases. This means that, when measuring calorimetric conversion by Differential Scanning Calorimetry (DSC), the amount of heat released by the sample may not proportionally coincide with the chemical conversion. Nevertheless, thermal measurements during cure remain a good and reliable methodology to characterize the polymerization reaction of thermosetting

resins. If the diffusion of chemical species is neglected, the degree of cure α (or resin conversion) may be defined as:

$$\alpha = \int_0^t \frac{d\alpha}{dt} \cdot dt \quad \text{or} \quad \frac{d\alpha}{dt} = f(T, \alpha) \quad (2.4)$$

In order to resolve the energy equation (2.1), the dependence of the reaction rate must be modeled in function of temperature and degree of polymerization. For the unsaturated polyester resin T580-63 from AOC Inc. used in this work, kinetic measurements were performed with a DSC 910 Du Pont Instruments. An ultimate heat of reaction (H_T) of 365 J/g was found when adding 1.5 *phr* of Andonox Pulcat-A peroxide. Dynamic DSC measurements were carried out for constant heating ramps from 30° to 190 °C. The weight of the sample ranged from 3 to 4 *mg* in order to ensure small thermal gradients. Reaction rates were computed from dynamic DSC data using a second scan as base line. The whole analysis is based on a linear interpolation between the cured and uncured specific heat [16].

Results of dynamic cure experiments are summarized in Figures 2.1 and 2.2. In Figure 2.1, DSC measurements processed from raw data are presented for a wide range of heating ramps, i.e., between 5 °C/*min* to 35 °C/*min*. Figure 2.2 shows the DSC thermographs of the dynamic cure for various heating ramps. As attained, the analysis of the heating rate peaks shows that the cure kinetics may be defined by exponential laws of the reaction rate as a function of temperature. To determine the validity of the DSC measurements, the heating rate peaks may be separated into the analysis of the reaction rate at peak $\dot{\alpha}_p$ (or peak curing temperature T_p) and the peak time t_p , both as a function of the curing temperature. The reaction rates and times to peak drawn in Figure 2.3 as a function of temperature reveal a good exponential correlation between DSC measurements performed for different heating rates.

A large number of studies have been conducted on the resin kinetics of thermosetting polymer systems, and a number of different kinetic models have been proposed in the literature. Generally, researchers have studied the connection of the chemical reaction with the other independent variables, such as time and temperature. In general, kinetic models can be of phenomenological or mechanistic origin. A phenomenological model captures the main features of reaction kinetics, but ignores the details of how individual species react with one another. On the other hand, mechanistic models are obtained from the balance of chemical species involved in the reaction. Hence, they provide better prediction and interpretation. However, because thermosetting reactions are rather complex, mechanistic models require more kinetic parameters than phenomenological models. Therefore phenomenological models are more popular for thermosetting polymer systems. Although several simultaneous reactions occur during the curing process, simple models have been developed based on the assumption that only one reaction can represent the whole cure process. The simplest model corresponds to an n^{th} -order kinetic expression:

$$\frac{d\alpha}{dt} = K_A \cdot (1 - \alpha)^n \quad (2.5)$$

where α is the degree of polymerization, n is the reaction order and K_A is the rate constant given by an Arrhenius temperature dependence:

$$K_A = K_0 \exp\left(\frac{-E_A}{R \cdot T}\right) \quad (2.6)$$

with K_0 , E_A and R being respectively the Arrhenius constant, the activation energy and the ideal gas constant. This model is well suited for most polymer systems as widely demonstrated in the past. However, a n^{th} -order equation cannot realistically describe the progress of the entire reaction because the material undergoes different transitions (gelation, vitrification) during cure. For an isothermal reaction, equation (2.5) predicts a maximum reaction rate at time zero. So this equation cannot be used for autocatalytic

reactions. Kamal and Sourour [17] have shown that the following model describes adequately the cure kinetics of both epoxy and unsaturated polyester resin systems:

$$\frac{d\alpha}{dt} = (K_1 + K_2 \cdot \alpha^m) \cdot (1 - \alpha)^n \quad (2.7)$$

where K_1 and K_2 are rate constants with an Arrhenius type of dependence with temperature, and m and n are catalytic constants.

Although the model of Kamal and Sourour [17] contains several interesting features, it is limited to two simple rate constants. When multiple autocatalytic reactions take place, a more detailed description is required. In this investigation, resin cure was modeled by an empirical autocatalytic kinetic equation that describes free-radical polymerization through a combination of Arrhenius and polynomial functions. The model of Bailleul [16] has been extended to consider the effects of glass transition temperature on the reaction rate. In this approach, the rate of conversion $d\alpha/dt$ is defined by the following equations:

$$\frac{d\alpha}{dt} = K_1(T) \cdot K_2(\alpha) \cdot K_3(T, \alpha) \cdot K_4(I_d) \quad (2.8a)$$

$$K_1(T) = k_{ref} \cdot \exp \left[-A \cdot \left(\frac{T_{ref}}{T} - 1 \right) \right] \quad (2.8b)$$

$$K_2(\alpha) = \sum_{i=0}^s a_i \cdot \alpha^i \quad (2.8c)$$

$$K_3(T, \alpha) = (\alpha_{max} - \alpha)^n; \quad n = f(T) \quad (2.8d)$$

The rate of conversion is the product of four terms:

- 1) $K_1(T)$ is an Arrhenius factor that depends on temperature and is expressed by equation (2.8b) with the usual Arrhenius constant k_{ref} , activation energy A and reference temperature T_{ref} .
- 2) $K_2(\alpha)$ is a function of the rate of conversion obtained like in Ballieul's approach by fitting a polynomial of degree s .
- 3) $K_3(T, \alpha)$ accounts for the termination of the kinetic reaction at a maximum rate of conversion, which is a function of glass transition temperature (i.e., α_{max} depends on T_g). Note that the power exponent n may also depend on temperature.
- 4) $K_4(I_d)$ is a weight function of the induction time I_d that accounts for the effect of the inhibitor decomposition.

To resolve the proposed kinetic model a procedure in three stages was devised:

2.3.1 Identification of the Arrhenius factor $K_1(T)$

A given polymerization degree is assumed to exist such that

$$K_2(\alpha) \cdot K_3(T, \alpha) \cdot K_4(I_d) = 1 \quad (2.9)$$

For this given polymerization degree set to, say $\alpha = 0.5$, equation (2.8a) reduces to

$$\left(\frac{d\alpha}{dt} \right)_{\alpha=0.5} = K_1(T) \quad (2.10)$$

Dynamic DSC data is used to solve equation (2.10) and derive the constant factors of equation (2.8b).

2.3.2 Identification of functions $K_2(\alpha)$ and $K_3(T, \alpha)$

The second stage requires to consider that $K_4(I_d) = 1$, (i.e., resin inhibitors have totally disappeared). Then functions K_2 and K_3 are defined by the following relation:

$$\left(\frac{d\alpha}{dt} \right) / K_1(T) = K_2(\alpha) \cdot K_3(T, \alpha) \quad (2.11)$$

The coefficients of K_2 and K_3 in equations (2.8c) and (2.8d) were obtained by a genetic algorithm [15]. To better account for the isothermal curing, the isoconversion methodology of Atarsia and Boukhili [4] was applied to dynamic DSC cures. This approach permits to translate dynamic DSC measurements to equivalent isothermal results, and vice versa. The kinetic model was constructed from the isoconversion curves. Figures 2.4 and 2.5 compare experimental data against the model for functions K_1 , K_2 and parameter n of function K_3 . While n seems to remain constant for the temperatures tested, K_1 appears as a well defined Arrhenius function. Averaged values of K_2 for all DSC curves are used to construct the α -dependent polynomial function. The result is then fitted by a polynomial of degree 6. The final resin conversion or maximum extent of cure α_{max} is temperature dependent up to a temperature high enough that provides sufficient molecular mobility to allow all species to react within the system [2]. The final polymerization degree is usually less than one for the curing temperatures typically used to process thick parts. In fact, the potential polymerization links cannot all be activated at low temperature. Therefore a temperature dependent parameter α_{max} is introduced in the kinetic equation to account for the incomplete resin chemical reaction. By using the isoconversion methodology proposed by Atarsia and Boukhili [4], a maximum degree of cure was derived from dynamic DSC data and modeled as follows:

$$\alpha_{\max} = \sum_{i=0}^N f_i \cdot T^i \quad \text{with } T \text{ in } ^\circ\text{C} \quad (2.12)$$

where N is the degree of the polynomial fitting. Figure 2.6 shows the calculated maximum polymerization degrees after isoconversion and the model fitting. Note that above 70 °C, a nearly linear dependence on temperature is found. For temperatures below this value, the maximum polymerization degree strongly decreases. This is because the initiator and inhibitor of the resin system are respectively activated and deactivated at around 70 °C.

2.3.3 Inhibitor decomposition

In polyester-based formulations, inhibitors are placed in resin systems to increase shelf life. They combine with the free radicals that initiate polyester-styrene cross-linking. Inhibition agents in the resin system increase significantly the curing time. While these inhibitors disappear quickly at high temperature, the kinetics of the inhibitor deactivation can be very slow at lower temperature, such as the one required to successfully cure thick composite parts. Assuming that the polyester-styrene linkage begins only when the concentration of inhibitor reaches zero, the induction time $I_d(t, T)$ prior to the initiation of the chemical reaction can be represented by a time integral of the thermal history [15]:

$$I_d(T, t) = t_{ref} - \int_0^t \exp\left(-C_{ind} \cdot \left(\frac{T_{ind}}{T} - 1\right)\right) \cdot dt, \quad K_4(I_d) = \begin{cases} = 0 & \text{if } I_d > 0 \\ = 1 & \text{if } I_d \leq 0 \end{cases} \quad (2.13)$$

Here t_{ref} , C_{ind} and T_{ind} are fitting coefficients called respectively reference time, induction constant and induction reference temperature. The weight function $K_4(I_d)$ of equation (2.8a) is then set to 1 when the induction time is zero.

Measured versus predicted induction times are also compared in Figure 2.6 for a wide range of curing temperatures. Note that for low processing temperatures (i.e., less than 60 °C) larger induction periods (around 20 minutes) are required before the polymerization reaction begins. In that case the ultimate polymerization degree may not be greater than 40%. As recommended by the resin manufacturer, composite parts made with this resin system should be processed in a range of temperature between 90 °C and 120 °C to decrease processing time and reach an appropriate level of polymerization. Table 2.1 presents the parameters of the kinetic model developed in this study. As a result of the proposed kinetic model, Figure 2.7 shows the evolution of the degree of polymerization obtained by dynamic DSC measurements compared with the solution of the kinetic equation for a constant heating rate of 10 °C/min. The proposed model was also compared to standard kinetics models, the classical autocatalytic equation and Kamal-Sourour model. The proposed model predicts more accurately the cross-linking polymerization reaction for the polyester resin tested in this investigation. In Figure 2.8, comparisons of model predictions with DSC measurements illustrate the accuracy of the model in predicting the degree of polymerization for all the measured heating ramps.

2.4 Thermo-mechanical modeling

2.4.1 Physical analysis

The need to predict accurately the intrinsic behavior of the material and the properties of the final part is vital to assess part quality and achieve process control. Much like thermo-kinetic behavior, the mechanical properties of the resin vary as the part cures. Some authors [5-7] have reported a linear correlation between the mechanical properties and the degree of polymerization of the resin for different thermosetting polymers. In this work,

mechanical properties were measured with a dynamic mechanical thermal analyzer (DMTA 2980 TA Instruments) as a function of temperature and degree of polymerization. At the beginning, fully cured resin samples (60.0 mm x 12 mm x 2.8 mm) were manufactured and tested in deflection with the DMTA apparatus. The beam specimens were clamped on the DMTA fixture and maintained at 30 °C during 10 minutes. The specimens were then isothermally deformed with three point bending clamps, and elastic modulus data was recorded. Temperature was then progressively increased of 10 °C, and when thermal equilibrium is attained, a new elastic modulus is measured. This procedure is repeated by increasing the temperature until 190 °C. Figure 2.9 presents elastic modulus data acquired with the DMTA apparatus as a function of temperature. A curve fit of the measured values is also drawn.

To account for the cure dependent mechanical properties, partially cured resin samples were tested under similar conditions with the DMTA and DSC equipments. It was found that long after the gel point, for a polymerization degree less than 40%, the resin elastic modulus is still very low (below 10 MPa). This polymerization degree, that we call here After Gel Point (AGP), was taken as reference point line to analyze the evolution of mechanical properties at higher polymerization levels. Resin samples cured at the AGP stage were mechanically tested on the DMTA for a specified curing cycle. Mechanical testing of resin samples cured at AGP showed that the evolution of material properties is very sensitive to the glass transition temperature. If the DMTA is set to isothermally measure the evolution of the elastic modulus at temperatures just above the glass transition temperature of the partially cured sample, the acquired data strongly varies between samples (see Figure 2.10). The order of magnitude of modulus variation does not permit to estimate the evolution of material properties during cure. Likewise, longer curing times are required to achieve a certain polymerization degree, and the ultimate extent of cure reached may not be high enough for reliable prediction.

As shown in Figure 2.11, this inconvenient was solved by maintaining the partially cured resin samples at their glass transition temperature until the polymerization reaction resumes. Then specimens were uniformly heated at $3\text{ }^{\circ}\text{C}/\text{min}$ until $180\text{ }^{\circ}\text{C}$ to increase the cross-linking reaction and achieve appropriate ultimate extents of cure. Under these thermal conditions, two phenomena compete in the development of the measured elastic modulus: the growth of mechanical properties as a result of resin cure and the diminution of those properties due to temperature increments. To understand the competition between these phenomena, the evolution of the resin elastic modulus during dynamic cure may be drawn together with the fully cured resin modulus and the elastic modulus at the AGP level (see Figure 2.12). A pure resin sample cured at AGP is initially heated in the DMTA to a temperature above the glass transition temperature (in this case around $70\text{ }^{\circ}\text{C}$). The sample is then maintained isothermal until the polymerization reaction begins (detected by small increments of the elastic modulus). At this time (around 13 minutes for the samples of Figure 2.12), the temperature is incremented at a constant rate of $3\text{ }^{\circ}\text{C}/\text{min}$. Due to the temperature increment, the reference elastic moduli of the fully cured and partially cured resin samples (points 1 and 2) undergo a decrement. The elastic modulus of the measured specimens (point 3) increases because of resin cure, but decreases proportionally to the temperature increment. As a result, the elastic modulus of the specimen can be evaluated using the base lines of the fully cured and partially cured resin (i.e., point 3 is considered as a percent of the difference between points 1 and 2).

2.4.2 Normalized parameters

In order to construct a semi-empirical model that will correspond to the physical phenomena that come into play during resin cure, it is important to normalize the main parameters that describe the state of the material: Young's modulus, degree of polymerization and temperature. Young's modulus in equation (2.14) is normalized with respect to the value at AGP, because below that value this parameter cannot be measured with the DMTA. As a matter of fact, before AGP and at temperatures above the glass

transition, the material is in a rubbery state in which any imposed constraint is quickly relaxed (i.e., comparing with processing times usually observed in LCM). Therefore, a normalized elastic modulus (\hat{E}') during resin cure can then be considered in the following form:

$$\hat{E}' = \frac{E'_m - E'_{agp}}{E'_c - E'_{agp}} \quad (2.14)$$

where E'_m is the measured elastic modulus during cure, E'_c the fully cured resin modulus, and E'_{agp} the resin modulus at AGP.

The degree of polymerization α will also be normalized in a similar way as Young's modulus by setting

$$\hat{\alpha} = \frac{\alpha - \alpha_{agp}}{\alpha_{ult} - \alpha_{agp}} \quad (2.15)$$

The normalized degree of polymerization $\hat{\alpha}$ will be used to approximate the variations of material properties between the AGP (α_{agp}) and the ultimate degree of polymerization (α_{ult}), for which E' reaches its maximum value.

Finally, a normalized temperature \hat{T} can be obtained as follows:

$$\hat{T} = \frac{T_g(\alpha) - T}{T_g(\alpha) - T_{ref}} \quad (2.16)$$

where $T_g(\alpha)$ is the glass transition temperature that depends on the degree of polymerization α , and T_{ref} is a reference temperature (in our case $T_{ref} = 120$ °C).

2.4.3 General semi-empirical model

Figure 2.13 shows the evolutions in time of the normalized Young's modulus \hat{E}' in-time measured with the DMTA, and of the resin degree of polymerization α measured with the DSC under similar thermal conditions. \hat{E}' increases from its value at the AGP level (i.e., $\hat{E}' \approx 0$) until it reaches a maximum in the fully cured state for 97% of total resin polymerization (i.e., $\alpha_{ult} = 97\%$). Figure 2.13 does not show any direct correlation between the evolutions of \hat{E}' and α in time. However, an almost linear relationship was found in Figure 2.14 when comparing the logarithms of \hat{E}' and α . A non-linear relationship was also recently reported by Ramis et al. [23] for polyester based powder coatings. Hence, Figure 2.14 suggests to approximate the logarithms of \hat{E}' and $\hat{\alpha}$ related by the following linear relationship:

$$\frac{\text{Log}(\hat{E}')}{\text{Log}(\hat{\alpha})} = C_{C-M} \quad \text{or} \quad \hat{E}' = \hat{\alpha}^{C_{C-M}} \quad (2.17)$$

In most cases when a linear correlation between \hat{E}' and $\hat{\alpha}$ is observed, the constant C_{C-M} is equal to one (where the sub-index C-M states for chemo-mechanical dependences). In other cases, such as for the polyester resin tested in this study, the constant may vary above or below one. The main disadvantage of this *double-logarithmic* model is that it does not account for the changes in the glass transition temperature during cure unless C_{C-M} is considered as a function of glass transition temperature. Therefore a semi-empirical model is proposed to estimate more accurately the evolution of mechanical properties during cure. This approach combines a hyperbolic cosine law that properly

describes the temperature dependence of the elastic modulus (see equations below) with two functions: $F_r(\alpha)$ accounts for the degree of polymerization and $W_r(T_g)$ models the dependence on glass transition temperature:

$$E_r(T, \alpha) = E_{agp}(T) + [E_c(T) - E_{agp}(T)] \cdot F_r(\alpha) \cdot W_r(T_g) \quad (2.18)$$

$$E_c(T) = \frac{E'_c}{\cosh(a_1 \cdot T)^{b_1}} \quad E_{agp}(T) = \frac{E'_{agp}}{\cosh(a_2 \cdot T)^{b_2}} \quad (2.19a)$$

$$F_r(\alpha) = c \cdot \exp(d \cdot \hat{\alpha}) + e \cdot \hat{\alpha} \quad (2.19b)$$

$$W_r(T_g) = h \cdot \exp(\hat{T}) \quad T_g(\alpha) = a_g \cdot \exp\left(\frac{-b_g}{1 - \hat{\alpha}}\right)^{-1} \quad (2.19c)$$

Subscripts r , c , g and agp of these constants denote resin, composite, glass transition and after gel point. Function $F_r(\alpha)$ is the sum of a linear plus an exponential function of the normalized degree of polymerization. The coefficients of equation (2.19b) can be estimated from the curve of Figure 2.15. The model of equation (2.18) accounts for the glass transition temperature dependence of the resin elastic modulus by a temperature shift factor $W_r(T_g)$. This factor considers the transition to complete viscoelastic relaxation at vitrification (or when the material is in the rubbery state, i.e., for $T \geq T_g^a$). As presented in Figure 2.16, the temperature shift factor shows fully relaxed coefficients for some polymerization degrees above AGP. Glass transition temperatures are also depicted in the same graphic, showing that the initial glass transition T_g^0 is around 55 °C, and the fully cured transition T_g^∞ around 110 °C (T_g^∞ was practically taken as the glass transition temperature at 95% of total resin polymerization). Constants a , b , c , d and e in equations (2.18) and (2.19a-c) were obtained by a genetic algorithm that provided a proper fit to the measured data. Figure 2.17 shows DMTA measurements of several resin specimens cured for different polymerization degrees

between the α_{agp} and α_{ult} levels. The predictions of the proposed thermo-chemical model exhibit relatively good agreement with experimental data for all tested samples. The parameters of equations (2.18) and (2.19a-c) that model the mechanical properties of T-580-63 resin are listed in Table 2.2.

2.4.4 Shear modulus

In the case of shear properties, two possible approaches may be used. On one hand, Levitsky and Shaffer [8] assumed that the plain strain bulk modulus remains constant during cure so that elastic moduli and Poisson's ratio vary as the part cures. On the other hand, Bogetti and Gillespie [5] considered that Poisson's ratio is constant during processing. They found that differences in Poisson's ratio of the resin during cure do not play a significant role on the properties of the macroscopic composite, nor on process-induced strains or residual stresses. Both models predicted nearly identical values of elastic and shear moduli. Poisson's ratio is also expected to relax to ~ 0.5 as the thermosetting polymer approaches the rubbery state. Nevertheless it was found by O'Brien et al. [9] that the effect on the shear modulus is relatively minor. According to these researchers, the variation of Poisson's ratio has no real influence. For that reason, in this work a constant value of $\nu_r = 0.35$ was used, which was measured at room temperature on a fully cured sample. The instantaneous resin shear modulus during cure is based on the following isotropic material relation:

$$G_r(T, \alpha) = \frac{E_r(T, \alpha)}{2 \cdot (1 + \nu_r)} \quad (2.20)$$

2.4.5 Composite effective properties

The effective homogeneous mechanical properties of the composite laminate are highly dependent on the matrix, reinforcement and fiber volume fraction. Thermal and

mechanical properties of the reinforcement may be considered constant and independent of temperature and of the polymerization degree, while matrix properties vary during processing according to the models previously presented. Although a self-consistent micro-mechanical model [10] was initially used to determine reinforcement properties, over-predictions were obtained for temperatures close to the matrix glass transition. Empirical models were then implemented to estimate the composite elastic moduli $E_{comp}^{1,2}$ as a function of temperature T and fiber volume fractions V_f in the two principal fiber directions:

$$E_{comp}^i = \left(\frac{V_f \cdot (E_f^i - E_r(T, \alpha))}{1 + A_i \cdot \exp(B_i \cdot T)} + E_r(T, AGP) \right) \cdot \left(\frac{E_r(T, \alpha)}{E_r(T, 1)} \right) \text{ with } i = 1, 2; \quad (2.21)$$

where A_i and B_i are fitting constants for each material direction ($i=1,2$). Subindexes r, f and $comp$ stand for resin, fiber and composite respectively.

Two reinforcing materials have been used in this study to analyze thermal effects on processing stresses, a continuous glass random mat U101 from Vetrotex and a bi-directional balanced non-crimp glass fabric NCS 82620 from J.B. Martin. Figure 2.18 presents results of Young's modulus measurements in both directions (E_{comp}^1, E_{comp}^2) for a composite plate made with NCS-82620 bidirectional fabric ($V_f = 42\%$). For the partially and fully cured samples, the mechanical model approaches the experimental curves at temperatures close to T_g . Composite specimens of these materials were measured and fitted by equation (2.18). As depicted in Figure 2.19, between two and three fiber volume contents were tested for each material. Note that the rule of mixture used in this work may be accurate only around measured values of fiber volume content. The range of validity considered for the tested materials is presented in Figure 2.20. Symbols "A" and "B" denote the accepted range of fiber volume fractions for

U101 mat and NCS-82620 fabric respectively. Table 2.4 contains the parameters of the mechanical model of equation (2.21) for both materials tested.

2.5 Viscoelastic modeling

The previous thermo-mechanical model must be extended in order to take into account the time dependence of mechanical properties is taken into account. In fact, it has been widely recognized that viscoelastic effects in thermosetting resin systems play a significant role on the evolution of mechanical properties during cure [5, 8-13]. These effects are particularly important for an appropriate description of process-induced residual stresses, mainly when the manufacturing process is long enough to allow the material to relax. For the polyester resin used in this work, the viscoelastic behavior was determined by performing stress relaxation tests in the DMTA equipment. Rectangular beam specimens $60.0\text{ mm} \times 12\text{ mm}$ of thickness 2.8 mm were manufactured for stress relaxation tests. The beams were clamped on the DMTA fixture and the temperature maintained at $30\text{ }^{\circ}\text{C}$ during 10 minutes. The specimens were then isothermally deformed to an initial displacement of 0.2 mm , and stress relaxation data was recorded during 20 minutes. Temperature was then progressively increased and relaxation data, delay and recovery times acquired for each temperature increment until $170\text{ }^{\circ}\text{C}$. Figure 2.21 shows raw data of relaxation tests for fully cured samples of T580-63 polyester resin. The measured relaxation data may be scaled by the adimensional ratio $E(t,T) / E_u$, where E_u is the unrelaxed modulus ($t = 0$) at $30\text{ }^{\circ}\text{C}$. The adimensional relaxation stress profiles for the fully cured resin sample are plotted in Figure 2.22. Subsequently, each isothermal measurement may be shifted to obtain a master curve based on the principle of time-temperature superposition (TTS). Applying a shift factor, a reduced time ξ can be obtained as follows [12]:

$$\xi = \int_0^t \frac{1}{a_T} dt \quad (2.22)$$

where a_T is the temperature dependent shift function. Figure 2.23 shows the master curve for the fully cured resin after TTS has been applied, and Figure 2.24 presents the shift factor a_T used to obtain the master curve. The approximated relaxation spectra $H(t)$ are calculated by the Alfrey approximation [12] as follows:

$$H(t) = \left| \frac{d(E')}{d(\log(\xi))} \right|_{(\xi = t)} \quad (2.23)$$

The relaxation spectrum is plotted in Figure 2.23, in addition to the relaxation modulus.

2.5.1 Modeling of stress relaxation

The stress relaxation curve for a thermorheologically simple material is usually modeled either by a power law:

$$E(\xi) = E_u \cdot \exp \left[- \left(\frac{\xi}{\tau_p} \right)^b \right] \quad (2.24)$$

where b is a material constant and τ_p is the spectrum peak shown in Figure 2.23, or by a discrete exponential series :

$$E(\xi) = E_\infty + (E_u - E_\infty) \cdot \sum_{\omega=1}^N W_\omega \cdot \exp \left[- \frac{\xi}{\tau_\omega} \right] \quad (2.25)$$

In the above expression, E_∞ is the fully relaxed modulus, E_u is the unrelaxed modulus, W_ω are weight factors, τ_ω are discrete stress relaxation times, and ξ is the reduced time. Generally, first step derivations of stress relaxation modulus and least-square techniques as Levenberg-Marquardt method are used to fit the viscoelastic modulus [9,

12, 13]. As reported by Kim and White [12], it was found that a single value of b is not sufficient to describe the stress relaxation of the epoxy resin tested over a wide range of temperatures. On the other hand, discrete exponential series (such as Prony series) provide a good accuracy through the use of recursive techniques for the integral calculations required by time-temperature superposition [9, 12, 13]. Although exponential series are interesting in terms of accuracy, they require a long time of analysis and are often hard to implement in numerical simulations (~20 series coefficients are common). In this work, a thermo-rheologically simple material was considered and the power law model was extended in the following way:

$$E(\xi) = E_u \cdot \exp\left[-\Omega_1 \cdot (\xi + \tau_o)^{\Omega_2}\right] \cdot (\xi + \tau_o)^{-\Omega_3} \quad (2.26)$$

where Ω_1 , Ω_2 , Ω_3 and τ_o are material constants and E_u is the unrelaxed material modulus.

In this investigation, the implementation of a genetic algorithm was preferred to standard least-square techniques to fit the relaxation modulus. Figure 2.25 compares relaxation data and viscoelastic predictions of equation (2.26) for the fully cured resin sample. The relaxation modulus may be related to time using the shift factors a_T to transform the reduced times ξ of equation (2.26) in delay times t . As can be noted in Figure 2.24, shift functions may be linearly fitted with respect to temperature by the following relation:

$$\log(a_T) = a_o + a_1 \cdot T \quad (2.27)$$

where a_o and a_1 are material constants. In Figure 2.26, DMTA relaxation data in function of the delay time are compared to model predictions after applying TTS to the fully cured resin sample at various isothermal temperatures.

2.5.2 Cure dependent relaxation modulus

Transforming relaxation data to master curves, viscoelastic material behavior can be analyzed over a wide range of resin conversion values. Master curves of measured relaxation modulus for the T580-63 resin are displayed in Figure 2.27 for different degrees of resin polymerization. It is well understood that when uncured resin samples are exposed to temperatures just above their glass transition temperature, they continue to cure. So, when testing uncured resin samples with a DMTA, temperature cannot exceed the glass transition temperature determined for the polymerization degree of the sample being tested. Relaxation DMTA data were collected between room temperature and appropriate temperatures below the glass transition temperature in each case. Coefficients of equation (2.26) were again solved for each polymerization degree using the Genetic Algorithm Search engine. Comparing coefficients between master curves, it was found that while Ω_2 and τ_o seem to be independent of the resin degree of polymerization, Ω_1 and Ω_3 were linearly dependent. The unrelaxed modulus E_u is also cure dependent and was modeled by a power law as follows:

$$E_u = U_o \cdot \alpha^{U_1} \quad (2.28)$$

$$\Omega_k = \Omega_k^0 + \Omega_k^1 \cdot \alpha \quad \text{with } k = 1, 3$$

where coefficients Ω_k^0 , Ω_k^1 , U_o and U_1 are constants of the model for each parameter. The resulted fitting curves given by equation (2.28) for Ω_1 , Ω_3 and the unrelaxed modulus E_u are drawn in Figure 2.28 as a function of cure for the T-580-63 resin tested. Resolving equation (2.26) with coefficient variations computed by equation (2.28), relaxation moduli were compared with experimental data for partially and fully cured resin samples as a function of reduced time (ξ). As can be seen in Figure 2.29, the response of the model seems to correctly predict the viscoelastic behavior of the polyester resin for all the degrees of polymerization tested. Table 2.4

regroups the coefficients of equations (2.26) to (2.28) found via the Genetic Algorithms to adjust these equations to the data collected for the polyester resin used in this investigation.

The implementation of equation (2.26) in order to describe the viscoelastic behavior of the resin during cure requires that the shift factors used in the time-temperature superposition principle be analytically determined. Some authors have reported non-linear dependences of the shift functions with respect to the degree of cure for epoxy resins. Although it was seen on these resin systems that the slope of the shift factors versus temperature is affected by resin cure, in the case of the polyester resin tested in this investigation, it was found that variations in the slope of the shift factors are relatively minor. Figure 2.30 displays shift factor data for different degrees of polymerization with the linear model of equation (2.27) used for the fully cured resin sample.

Finally, the proposed viscoelastic model permits to describe the stress relaxation behavior for any degree of polymerization reached by the resin. Figures 2.31 and 2.32 depict experimental data of relaxation moduli as a function of time for partially cured resin samples (45% and 93% cured). DMTA experimental data are overlaid on the relaxation moduli predicted with the viscoelastic model of equations (2.26) to (2.28). The viscoelastic behavior of glass/polyester composites was also tested by combining T580-63 resin with NCS 82620 fabric. Relaxation experiments were performed in the principal layup directions for fiber volume fractions of 40% and 45%. Experimental modulus collected for the two fiber volume fractions are presented in Figures 2.33 and 2.34 after the TTS principle has been applied. A self-consistent micro-mechanical model [10] was then used to determine reinforcement properties from fabric and matrix properties. Regarding the comparison of the viscoelastic model with DMTA data, it can be noticed that although shift factors of the TTS seem to vary between resin and

composite, the proposed model of relaxation modulus is still reliable. Relatively accurate results were found for the two fiber volume fractions tested experimentally.

2.6 Volume changes during cure

Some experimental studies have also been conducted to gain insight on the volumetric changes that occur during thermoset polymer processing. Hill et al. [14] measured the volume changes during curing as a function of temperature and degree of polymerization for unsaturated polyester resins. Hill proposed that the overall volumetric changes of a thermoset resin during cure can be considered as a combination of thermal expansion or contraction and polymerization shrinkage. Therefore it can be written as follows:

$$\left(\frac{1}{V_o} \frac{dV}{dt} \right)_{\text{Overall}} = \left(\frac{1}{V_o} \frac{dV}{dt} \right)_{\text{Thermal Contribution}} - \left(\frac{1}{V_o} \frac{dV}{dt} \right)_{\text{Polymerization Shrinkage}} \quad (2.29)$$

The first term on the right hand side represents the bulk thermal expansion/contraction contribution, which can be expressed by

$$\left(\frac{1}{V_o} \frac{dV}{dt} \right)_{\text{Thermal Contribution}} = \beta_{\text{gel}} \cdot \frac{dT}{dt} + [(\beta_{\text{cured}} - \beta_{\text{gel}})] \cdot \alpha \cdot \frac{dT}{dt} \quad \beta_{\text{cured}}, \beta_{\text{gel}} = a_0 + b_0 \cdot T \quad (2.30)$$

where β_{gel} and β_{cured} are the coefficients of thermal expansion (CTE) of the gelled and fully cured resin respectively. Here a_0 and b_0 are the constants of the linear fit with temperature. Note that the CTE is assumed to vary monotonically with the polymerization degree α . The second term on the right hand side of equation (2.29) represents the contribution of chemical shrinkage (i.e., volume shrinkage induced by the resin cross-linking during polymerization). Resin shrinkage was measured with a thermomechanical analyzer (TMA 2940 from TA Instruments) as a function of the

degree of polymerization. As can be seen in Figure 2.35, the linear relationship of equation (2.31) was obtained experimentally for the polyester resin tested. The total polymerization shrinkage λ_{chem} for the fully cured sample was about 7%:

$$\left(\frac{1}{V_o} \frac{dV}{dt} \right)_{\text{Polymerization Shrinkage}} = \lambda_{chem} \frac{d\alpha}{dt} \quad (2.31)$$

2.7 Longitudinal and transverse CTE

The coefficient of thermal expansion (CTE) of pure resin samples and composite plates were also measured with the thermo-mechanical analyzer. The thermal expansion of uncured resin samples (i.e., for $\alpha = 0$), partially cured (i.e., for $\alpha = 0.45$ and 0.80) and fully cured samples has been determined and is reported in Figure 2.36. Experimental data were fitted by bilinear functions and a CTE model can be written as a function of temperature and polymerization degree as follows:

$$CTE_r(T, \alpha) = CTE_{agg}(T) \cdot (1 - \hat{\alpha}) + CTE_{cured}(T) \cdot \hat{\alpha} \quad (2.31)$$

where $\hat{\alpha}$ is the normalized degree of cure given by equation (2.15).

The CTE of composite samples of NCS 82620 and U101 reinforcements were also measured (see Figure 2.37) in the three principal directions (Longitudinal, Transverse and Through-Thickness). The model stands as follows:

$$CTE_{comp}^d = CTE_r \cdot (1 - V_f) + CTE_{fibre}^d \cdot V_f \quad \text{where } d = L, T, \text{ and T-Thickness} \quad (2.32)$$

2.8 Summary

In this paper, models are proposed to describe chemical and rheological changes in polyester matrix composites as a function of fiber volume content, temperature and polymerization degree. These models were applied to two fiber glass reinforcing materials, a NCS-82620 fabric and a U101 random mat embedded in a polyester resin T580-63 from AOC Inc. A semi-empirical autocatalytic model was implemented to describe the resin kinetics of the chemical reaction. The model accounts for the maximum degree of polymerization as a function of cure temperature as well as for induction times induced by inhibitor decomposition.

The evolution of mechanical properties during resin cure and for two other glass/polyester composites was also studied with a dynamic mechanical thermal analyzer (DMTA) and thermo-mechanical analyzer (TMA). Given that at low chemical conversion the elastic properties of the resin remain small, an initial degree of polymerization called *after gel point* (AGP) was introduced as a reference point to study the evolution of mechanical properties during cure. A normalized elastic modulus was defined as reference from the value at AGP and compared with the evolution of the degree of polymerization. Based on this comparison, the logarithm of the chemical conversion was found to be directly related to the logarithm of the elastic modulus. A thermo-mechanical model was proposed to describe the evolution of mechanical properties during the cure of composite samples for different fiber volume fractions.

The viscoelastic behavior was also determined by performing stress relaxation tests with the DMTA equipment. Resin specimens were tested for different cure states below their glass transition temperature, and master curves of stress relaxation behavior during cure were then constructed by applying the time-temperature superposition principle. The measurements show that the relaxation modulus of polyester resin is sharply affected by the degree of polymerization. Based on the experimental data, the

relaxation modulus was modeled in a thermorheologically simple manner using exponential and power laws.

Finally, a linear model of volume change was constructed using TMA measurements of thermal expansion and resin chemical shrinkage. This model accounts for the composite expansion/contraction and resin polymerization shrinkage as a function of temperature and degree of polymerization. This thermo-mechanical model of polyester resin can be used during numerical simulation of the curing phase in RTM to describe the elastic or viscoelastic behaviors of the composite. To compute internal stresses generated during and after resin cure, the evolution of mechanical properties must be taken into account in the strain-stress model. Both the elastic and viscoelastic models can be implemented in the numerical scheme to find the processing strain and stresses.

It is well known that discrepancies usually appear between stresses predicted by elastic models and experimental measurements, mainly when long relaxation times appear during processing. However, if an elastic model is used instead of a viscoelastic one, the internal stresses predicted during processing can still give a good idea of the experimental behavior on a qualitative, but not quantitative basis. Despite this disadvantage in terms of accuracy, the use of an elastic model involves much shorter computer times. On the other hand, the time dependence of viscoelastic models requires time integration and close loop iterations to converge to suitable values. This may create difficulties when optimization algorithms are used to improve composite processing. The computer time required to run optimization algorithms under the same constraints, but with the two different mechanical models, can differ in terms of hours. Future work is needed to compare the performance of the two proposed mechanical models in the prediction of internal stresses. The difference between the elastic and viscoelastic models remains to be evaluated thoroughly for the numerical optimization of composite processing.

2.9 Acknowledgements

The authors are grateful to the *National Science and Engineering Research Council of Canada* (NSERC) and *Fonds Québécois de Recherche sur la Nature et la Technologie* (FQRNT) for their financial support. The contribution of *Auto 21* and *Ford Motor Co.* for the development of characterization molds is also gratefully acknowledged as well as the support of the *Bourses d'Excellence du Ministère de l'Éducation du Québec*. The authors would like to thank *Vetrotex* for the reinforcement samples and Nicolas Juillard from *J. B. Martin* for his constant support over the last fifteen years.

2.10 References

- [1] White, S. R. and Hahn, H. T. (1992). Process Modeling of Composite Materials: Residual Stress Development during Cure, *J. of Composite Materials*, 26(16):2402-2453.
- [2] Michaud, D. and Beris A, Dhurjati P. (1998). Curing Behavior of Thick-Sectioned RTM Composites, *J. of Composite Materials*, 32(14):1273-1295.
- [3] Lin, R. J., Lee, L. J. and Liou, M. L. (1991). Mold Filling and Curing Molding of RTM Process, *Advanced Composite Materials*, Conference Proceedings, Detroit, Michigan USA, Sept. 30, pgs 165-174.
- [4] Atarsia, A. and Boukhili, R. (2000). Relationship Between Isothermal and Dynamic Cure of Thermosets Via the Isoconversion Representation, *Polymer Eng. Sci.*, 40(3):607-620.
- [5] Bogetti, T. and Gillespie, J. (1992). Process-Induced Stress and Deformation in Thick-Sectioned Thermoset Composite Laminates, *J. of Composite Materials*, 26(5):626-660.

- [6] Golestanian, H. and El-Gizawy, S. (1997). Cure Dependent Lamina Stiffness Matrices of Resin Transfer Molded Composite Parts with Woven Fiber Mats, *J. of Composite Materials*, 31(23):2402-2423.
- [7] Osswald, T. A., Sun, E. M. and Tseng, S.-C. (1994). Experimental Verification on Simulating Shrinkage and Warpage of Thin Compression Moulded SMC Parts, *Polymers & Polymer Composites*, 2(3):187A-198A.
- [8] Levitsky, M. and Shaffer, B. M. (1974). Thermal Stresses in Chemical Hardening Elastic Media with Application to the Molding Process, *J. of Applied Mechanics*, 41:647-651.
- [9] O'Brien, D. J., Mather, P. and White, S. R. (2001). Viscoelastic Properties of an Epoxy Resin during Cure, *J. of Composite Materials*, 35(10):883-904.
- [10] Whitney, J. M. (1967). Elastic Moduli of Unidirectional Composites with Anisotropic Filaments, *J. of Composite Materials*, 1:188.
- [11] Ferry, J. D. (1994). Chapter 2, *Viscoelastic Properties of Polymers*, 3rd Edition, John Wiley & Sons Inc. 641 p. ISBN: 0471048941.
- [12] Kim, Y. K. and White, S. R. (1996). Stress Relaxation Behavior of 3501-6 Epoxy Resin During Cure, *Polymer Eng. & Sci.*, 36(23):2852-2862.
- [13] Kim, Y. K. and White, S. R. (1996). Process-Induced Stress Relaxation Analysis of AS4/3501-6 Laminate, *J. of Reinforced Plastics and Composites*, 16(1):2-16.
- [14] Hill, R., Muzumar, S. and Lee, L. (1995). Analysis of Volumetric Changes of Unsaturated Polyester Resin During Curing, *Polymer Eng. & Sci.* 35(10):852-859.
- [15] Louchard, S. (2002). *Guide de mesures DSC et de calcul des modèles cinétiques de cuisson de résines thermodurcissables*, rapport de stage présenté au CRASP, Ecole Polytechnique de Montréal 09-2002, 73 pgs.
- [16] Bailleul, J.-L., Sobotka, V., Delaunay, D. and Jarny, Y. (2003). Inverse Algorithm for Optimal Processing of Composite Materials, *Composites Part A*, 34(8):695-708.
- [17] Ryan, M. E. and Dutta, A. (1979). Kinetics of epoxy cure: a rapid technique for kinetic parameter estimation, *Polymer*, 20:203-206.

- [18] Yousefi-Moshirabad, A. (1996). *Cure Analysis of Promoted Polyester and Vinylester Reinforced Composites and Heat Transfer in RTM Molds*, PhD. Thesis, Dep. of Chemical Eng. École Polytechnique de Montréal.
- [19] Han, C. D. and Lem, K.-W. (1983). Chemorheology of Thermosetting Resins. I. Chemorheology and Cure Kinetics of Unsaturated Polyester Resin, *J. of Applied Polymer Sci.*, 28:3155-3183.
- [20] Stevenson, J. F. (1996). *Innovation in Polymer Processing: Molding*, S.L.:l'auteur, 600 p. ISBN 3-446-17433-8.
- [21] Yi, S. and Hilton, H. H. (1998). Effects of Thermo-Mechanical Properties of Composites on Viscosity, Temperature and Degree of Cure, *J. of Composite Materials*, 32(7):600-622.
- [22] Bogetti, T. A. and Gillespie, J. W. (1992). Process-Induced Stress and deformation in Thick-Section Thermoset Composite Laminate, *J. of Composite Materials*, 26(5):626-660.
- [23] Ramis, X., Cadenato, A., Morancho, J. M. and Salla, J. M. (2003). Curing of a thermosetting powder coating by means of DMTA, TMA and DSC, *Polymer*, article in press, 10/2/2003 DOI:10.1016/S0032-3861(03)00059-4.
- [24] Ruiz, E. and Trochu, F. (October 2003). Numerical Analysis of Cure Temperature and Internal Stresses in Thin and Thick RTM parts, Submitted to *Composites Part A*, 38 pgs.

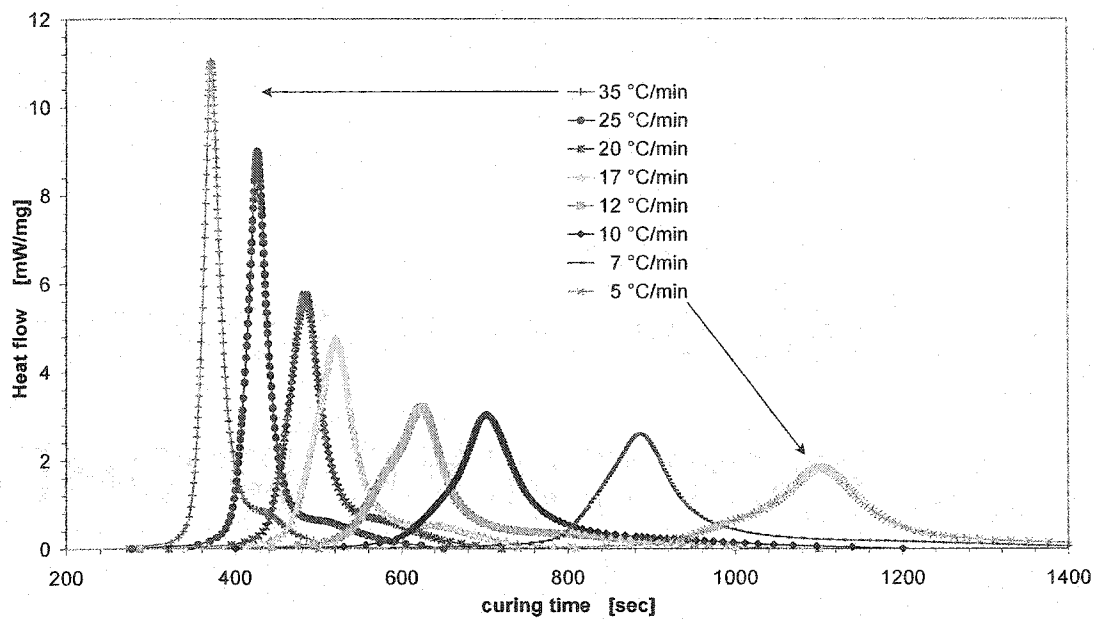


Figure 2.1. DSC measurements of heat flows during dynamic cure of T580-63 polyester resin. Raw data have been processed using a second scan as base line and a linear interpolation of the specific heat.

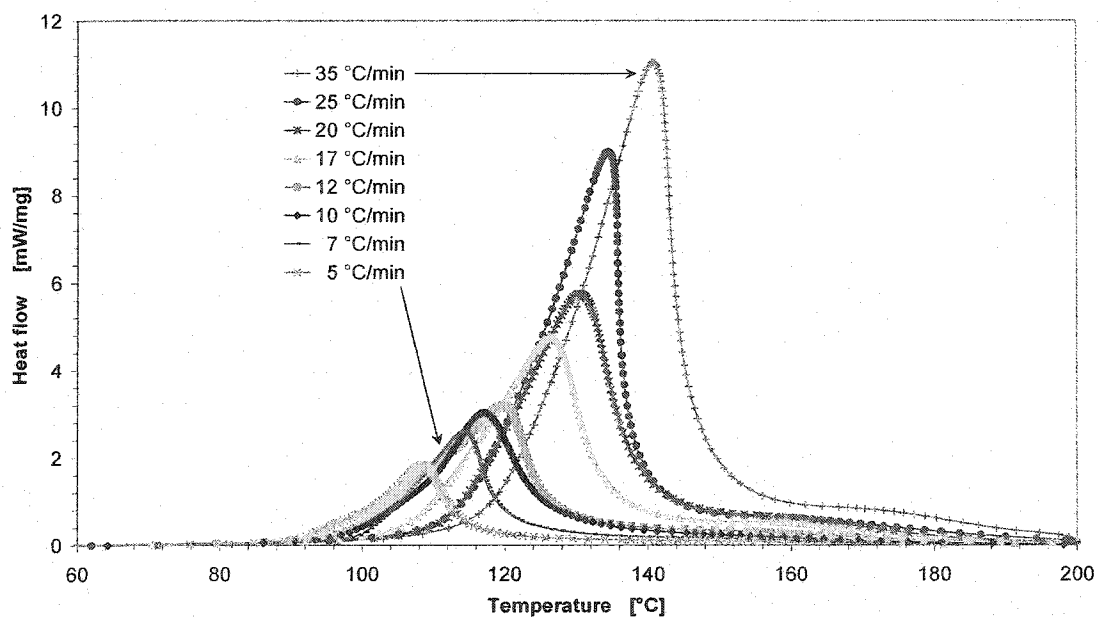


Figure 2.2. Thermographs obtained from DSC data during dynamic cure for several heating rates.

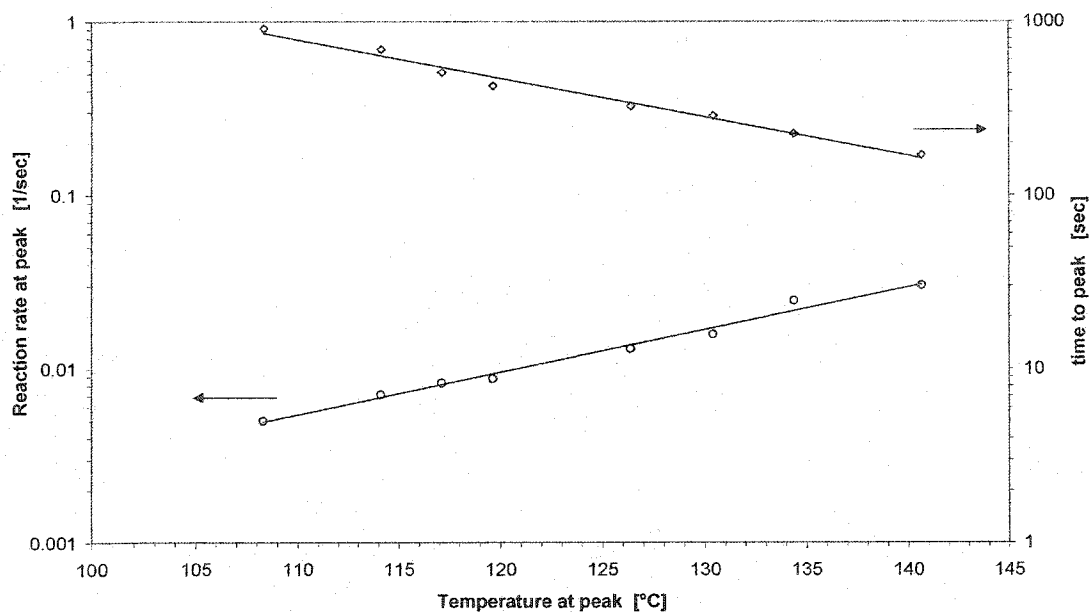


Figure 2.3. Reaction rate at peak and time to peak obtained from DSC measurements. Logarithmic functions relate both parameters with peak temperature.

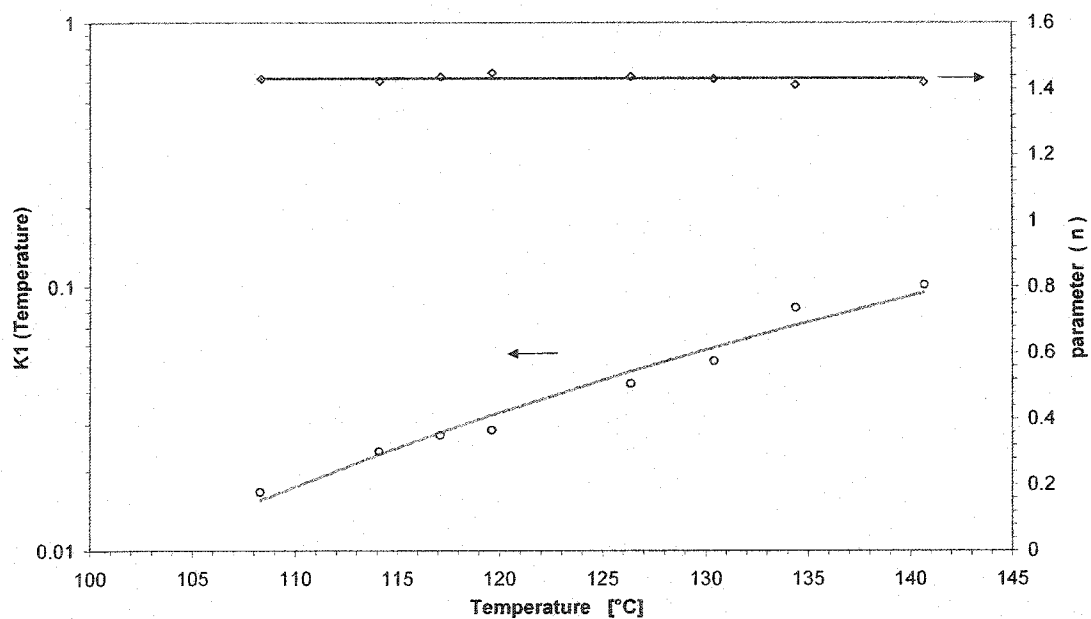


Figure 2.4. Temperature dependence of factor K_1 and parameter n of the power function K_3 for the kinetic modeling of equation (2.5). While n seems to be constant, K_1 exhibits an Arrhenius type of temperature dependence.

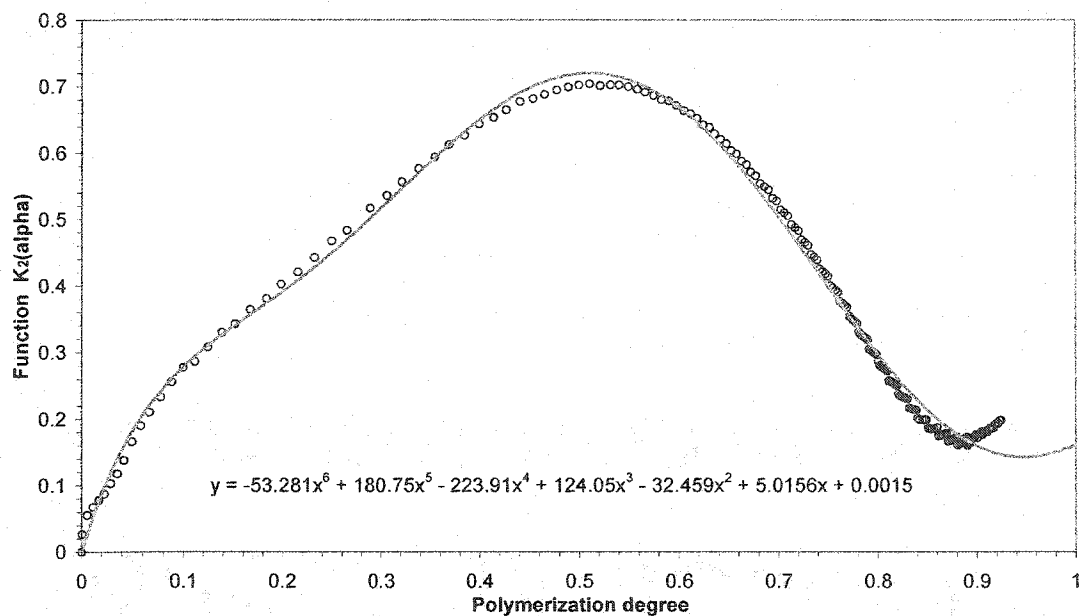


Figure 2.5. Kinetic factor K_2 as a function of polymerization degree fitted by a 6th degree polynomial curve.

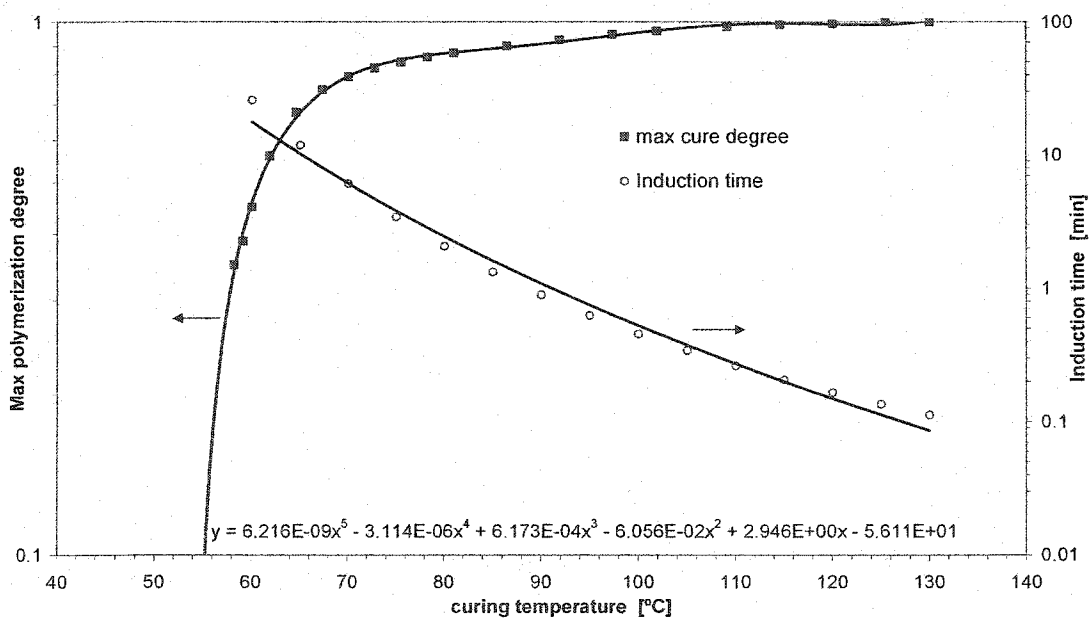


Figure 2.6. Maximum degree of polymerization and induction times as a function of curing temperature. Experimental data comes from DSC measurements. Fitting curves are polynomial for the degree of cure and an integral equation (2.13) for induction times.

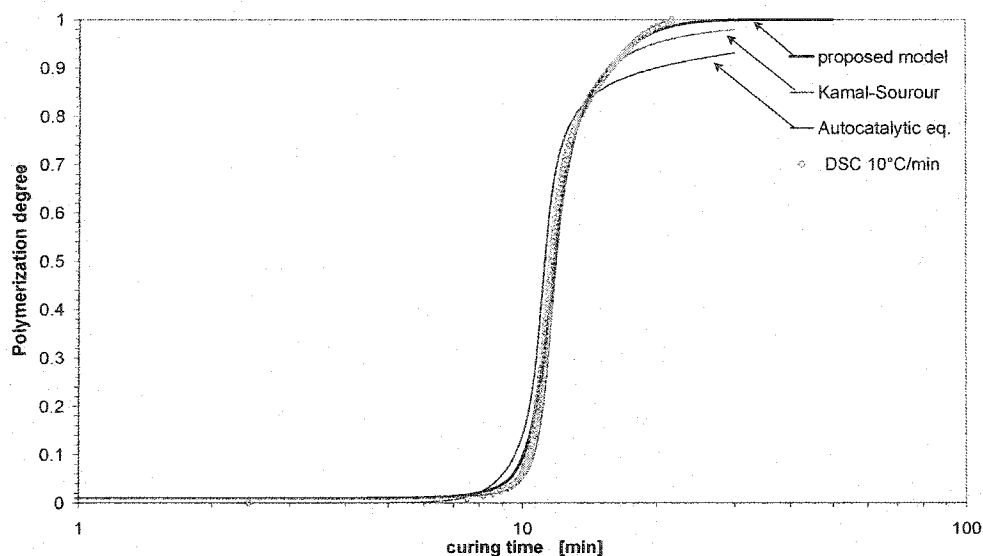


Figure 2.7. Comparisons of the degree of polymerization from DSC with predictions of three kinetic models for a constant heating ramp of $10\text{ }^{\circ}\text{C}/\text{min}$. Autocatalytic equation diverges at the end of curing. Kamal-Sourour equation approaches the measured data although some differences are noticed. The proposed model of equation (2.8a-d) is the most accurate.

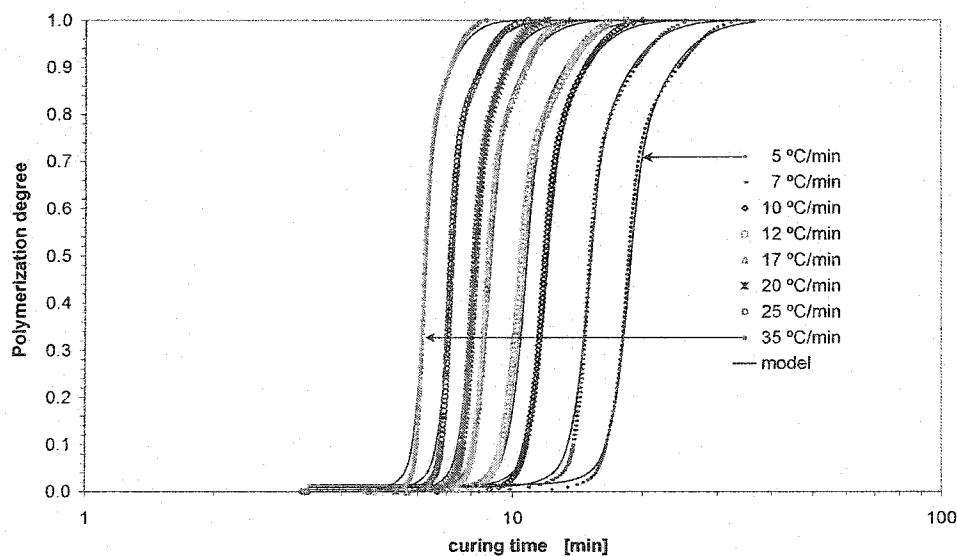


Figure 2.8. DSC measurements of the degree of polymerization and predictions of the proposed kinetic model of equation (2.8a-d). A good agreement between the model and experimental data is observed for all heating ramps measured.

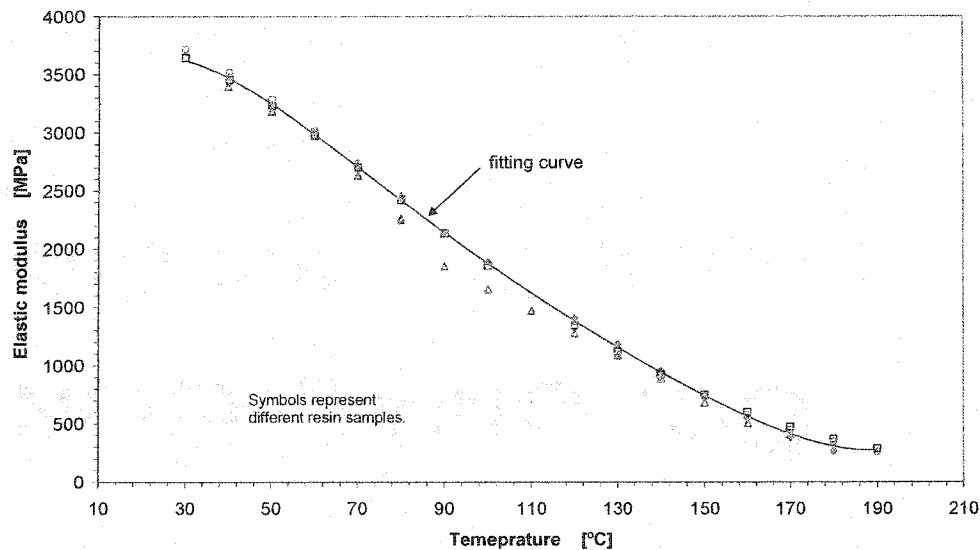


Figure 2.9. DMTA measurements of fully cured resin elastic modulus as a function of temperature and curve fitting of the experimental data. Isothermal values are reported for each temperature.

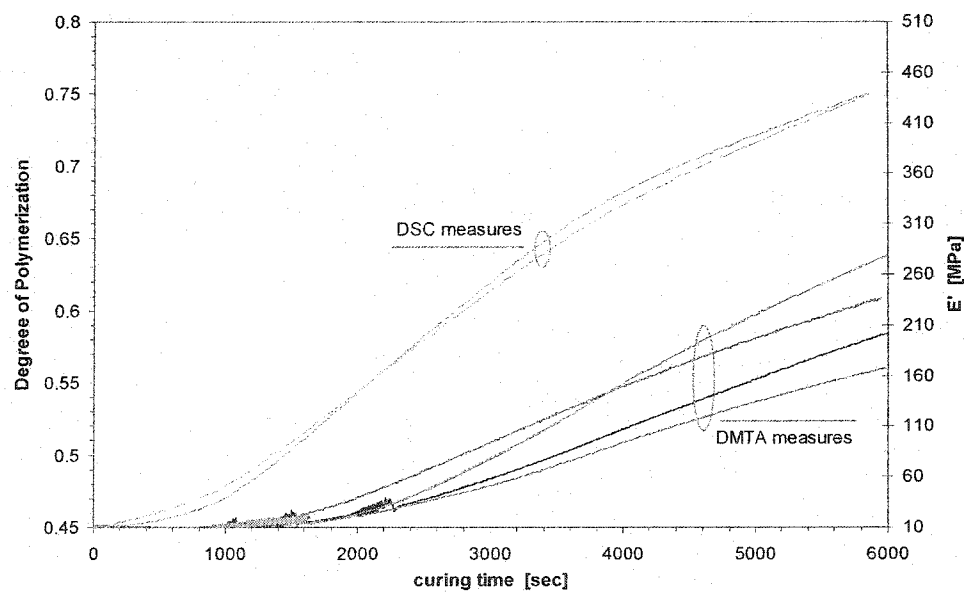


Figure 2.10. Measured degree of polymerization and elastic modulus versus time during isothermal curing cycle. DSC and DMTA runs were carried out at 75 °C. While DSC measures are reproducible, DMTA data show important variations.

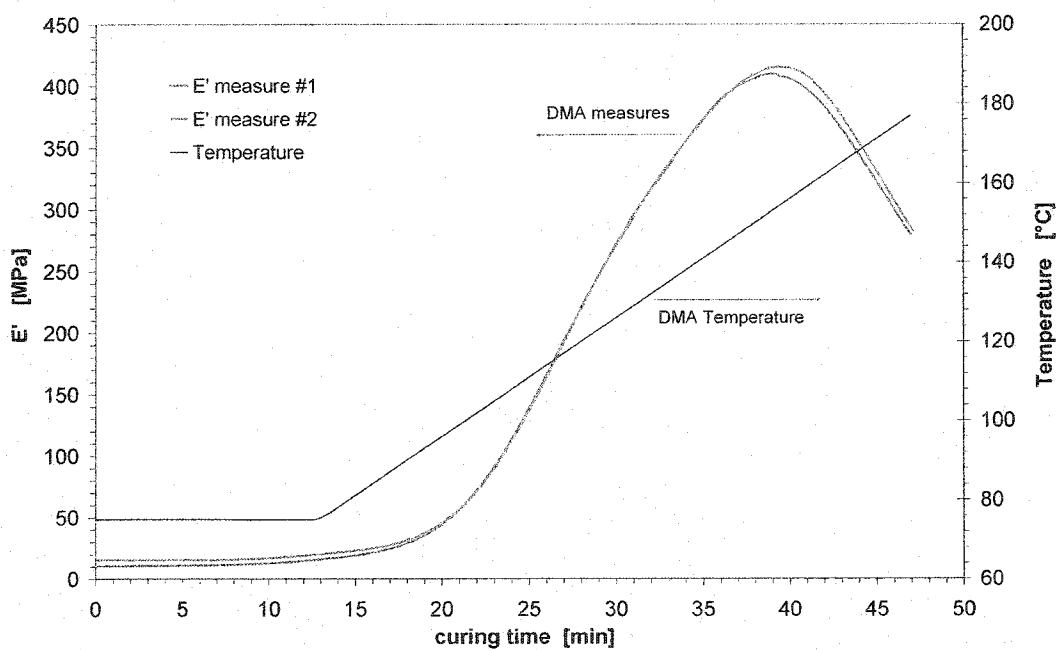


Figure 2.11. Evolution of elastic modulus during resin cure for runs at constant heating ramp. Initial temperature was set to 75 $^{\circ}\text{C}$ and the heating ramp to 3 $^{\circ}\text{C}/\text{min}$. Elastic modulus increases with the polymerization reaction, but decreases afterwards with temperature.

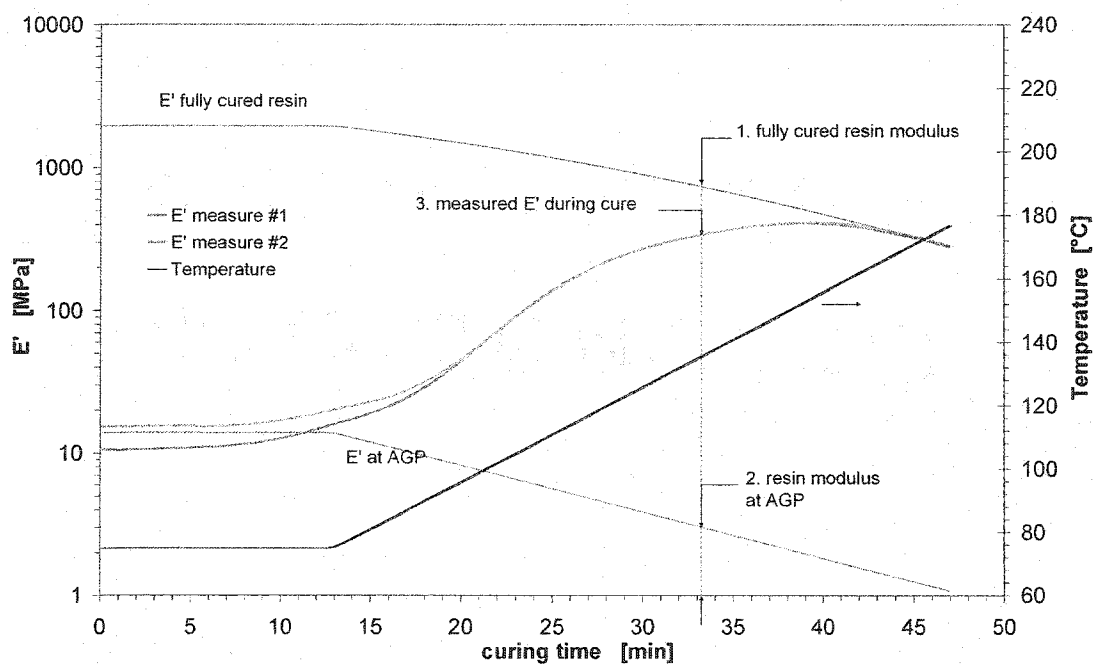


Figure 2.12. Description of the methodology used to determine the normalized elastic modulus during cure. DMTA measures of partially cured samples are stabilized at 70 °C and then heated at 3 °C/min. The normalized elastic modulus is calculated as the difference between measured value (3) and modulus at AGP (2) in percent of the fully cured modulus (1), see equation (2.14).

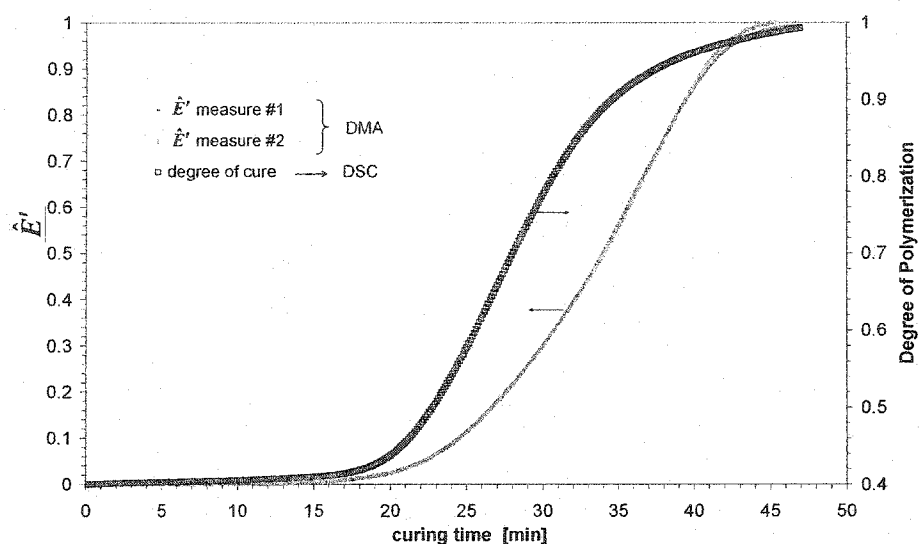


Figure 2.13. Comparison between degrees of polymerization and normalized elastic modulus \hat{E}' during a specified curing cycle. Thermal (DSC) and mechanical (DMTA) measures differ.

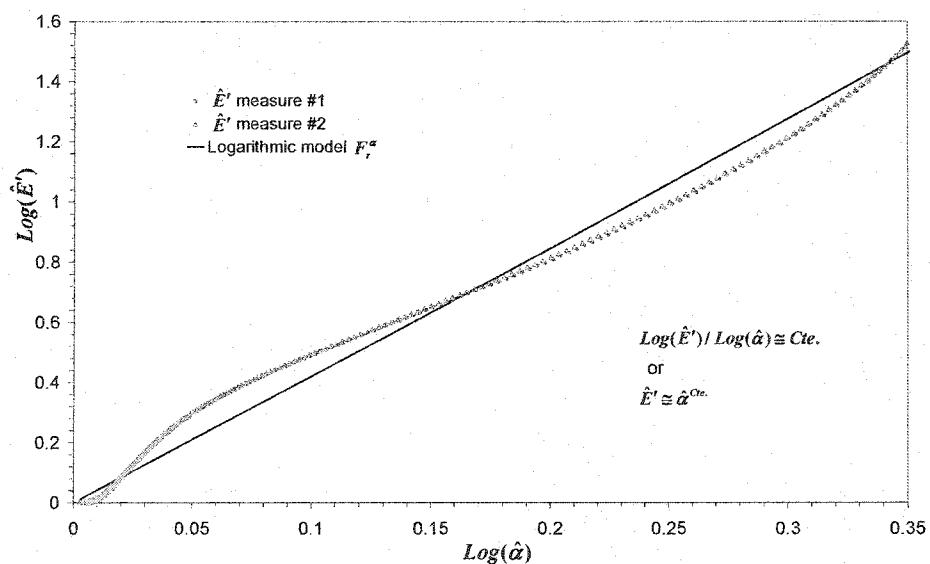


Figure 2.14. Quasi-linear relation between the logarithms of \hat{E}' and of the normalized degree of cure.

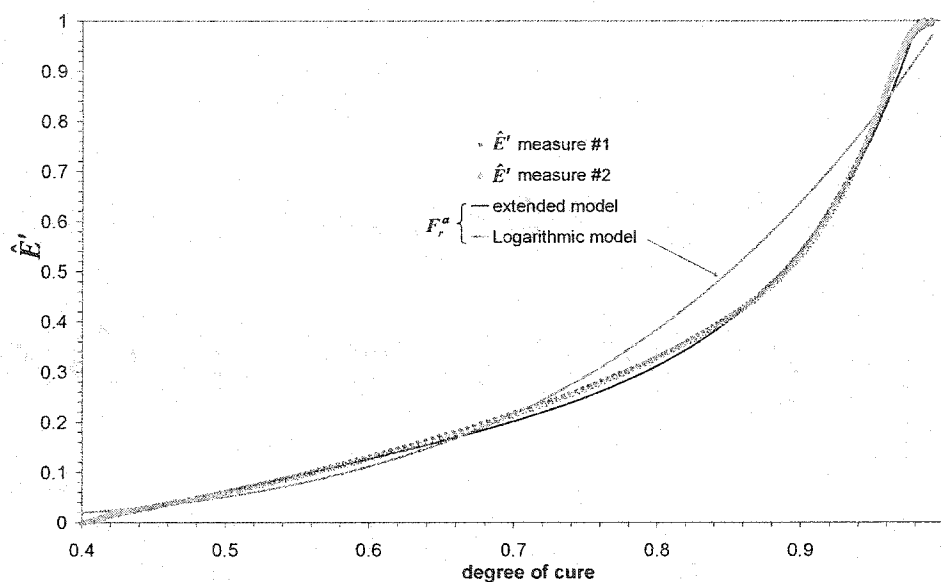


Figure 2.15. Logarithmic approximation and extended model of \hat{E}' as a function of the degree of polymerization. Extended model of equation (2.19b) is in good agreement with DMTA/DSC measures.

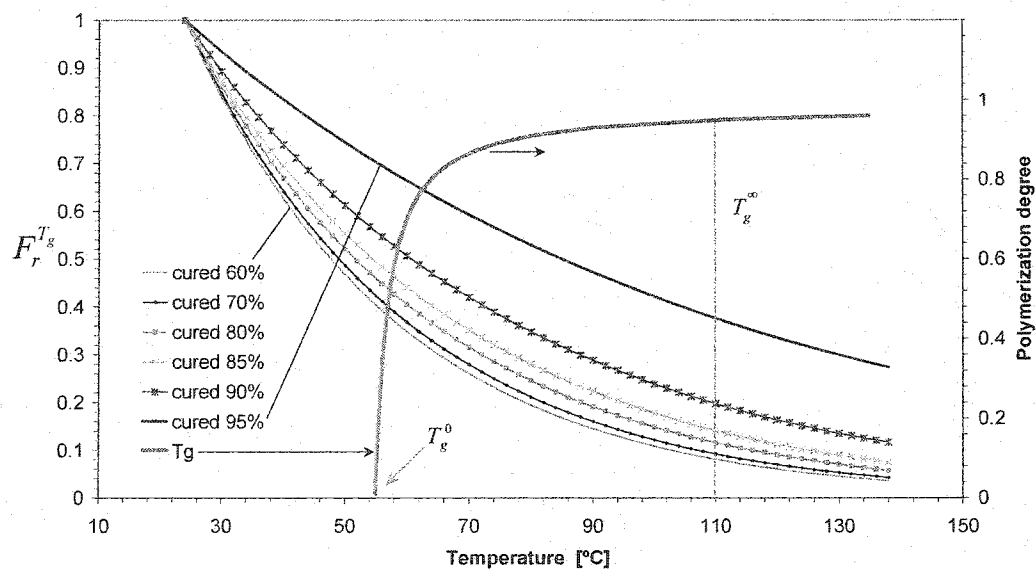


Figure 2.16. Temperature shift factor as a function of temperature for various degrees of polymerization. Also glass transition temperature T_g is plotted as a function of degree of cure.

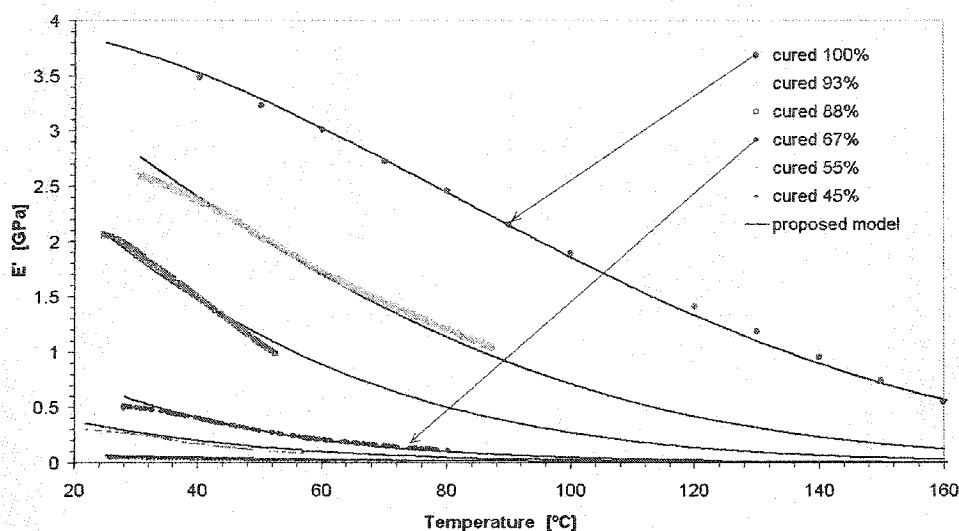


Figure 2.17. DMTA measurements of E' for partially and fully cured samples of T580-63 polyester resin. Lines represent predictions of the elastic model of equation (2.18). For all tested degrees of cure, the model predicts with reasonable accuracy the resin elastic modulus.

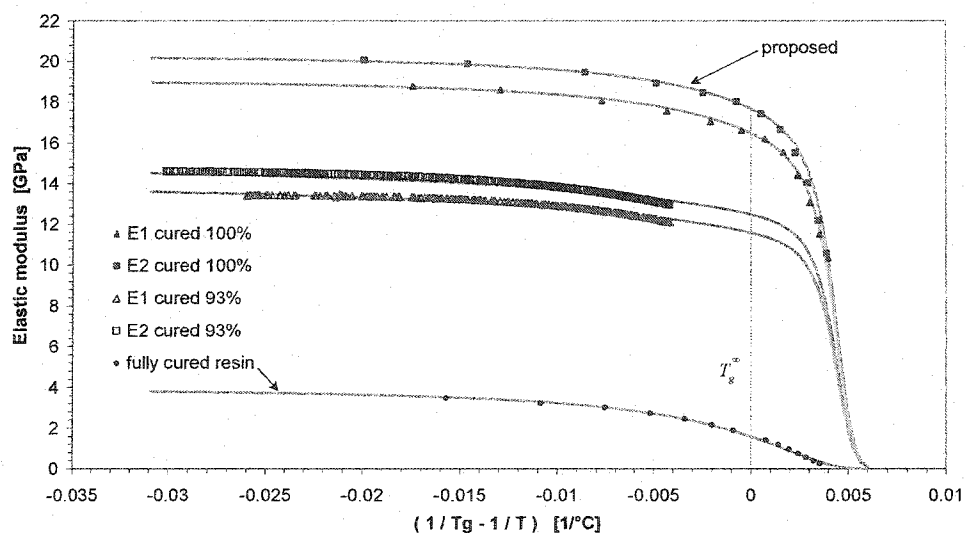


Figure 2.18. Measured and predicted E' in both directions for a NCS-82620 composite with $V_f = 42\%$. Fully and partially cured composite samples were tested in principal directions (i.e., E_1 , E_2). Predictions of elastic model of equation (2.21) are in good agreement with measured values.

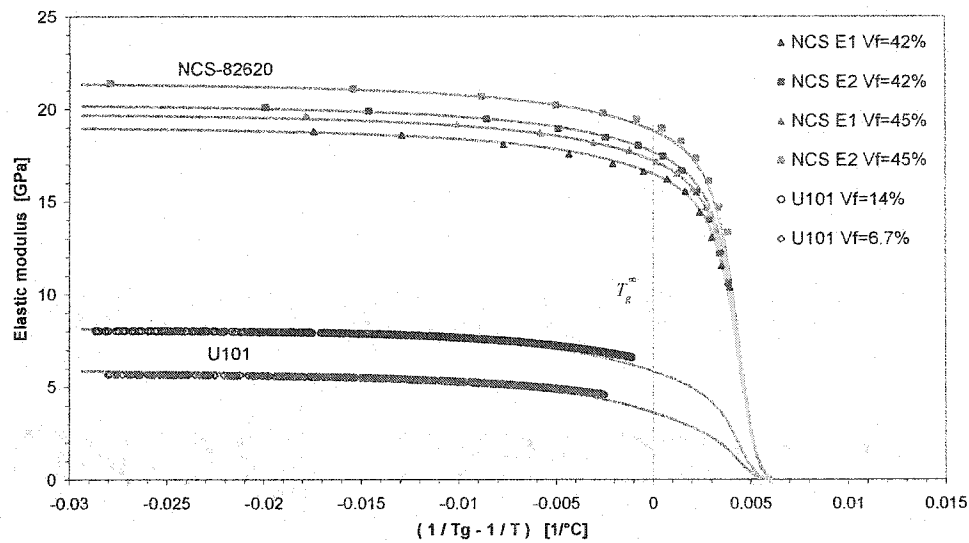


Figure 2.19. Measured and predicted E' for different fiber volume fractions. Fully cured composite samples of NCS-82620 fabric and U101 mat were tested in the DMTA. Lines are fitting the elastic model of equation (2.21).

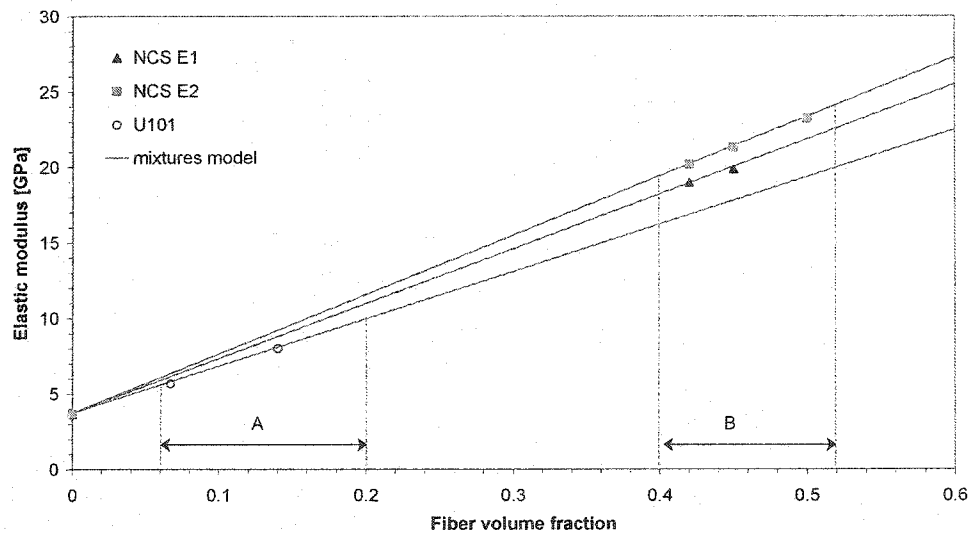


Figure 2.20. Rule of mixture for E' as a function of fiber volume fraction. Intervals A and B represent the validity range of V_f for U101 and NCS-82620 materials respectively.

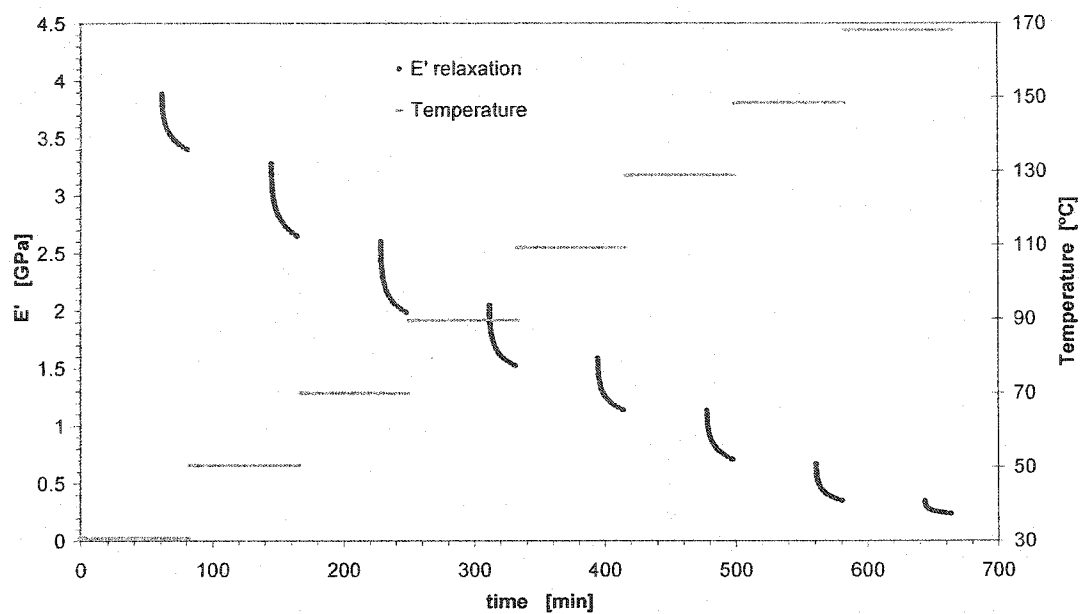


Figure 2.21. Measured E' in DMTA relaxation test. Fully cured sample of T580-63 polyester resin.

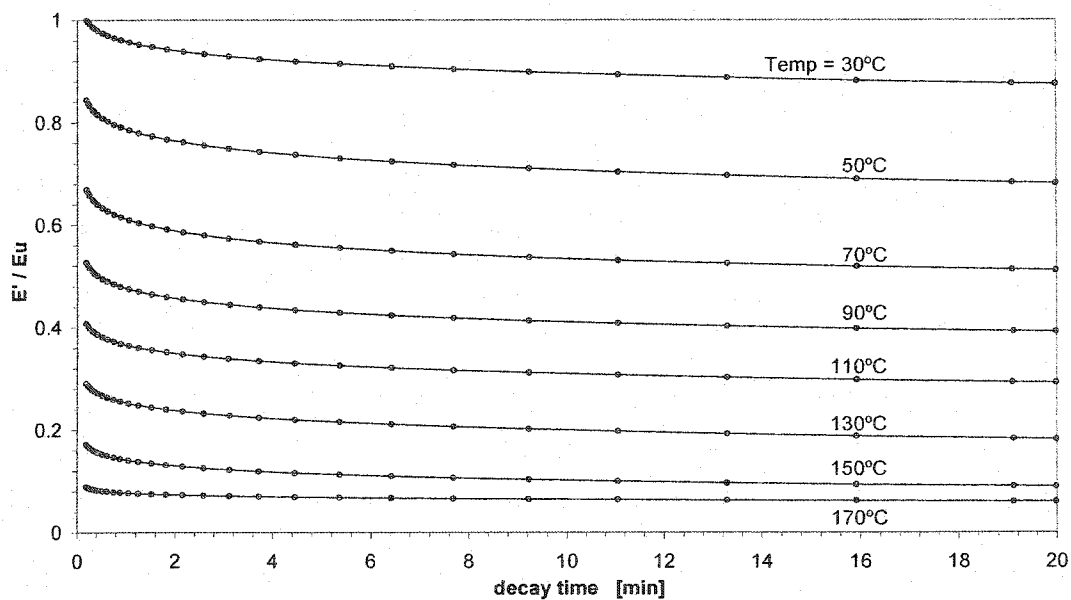


Figure 2.22. Stress relaxation profiles for the fully cured resin samples at various isothermal temperatures, from 30 to 170 °C.

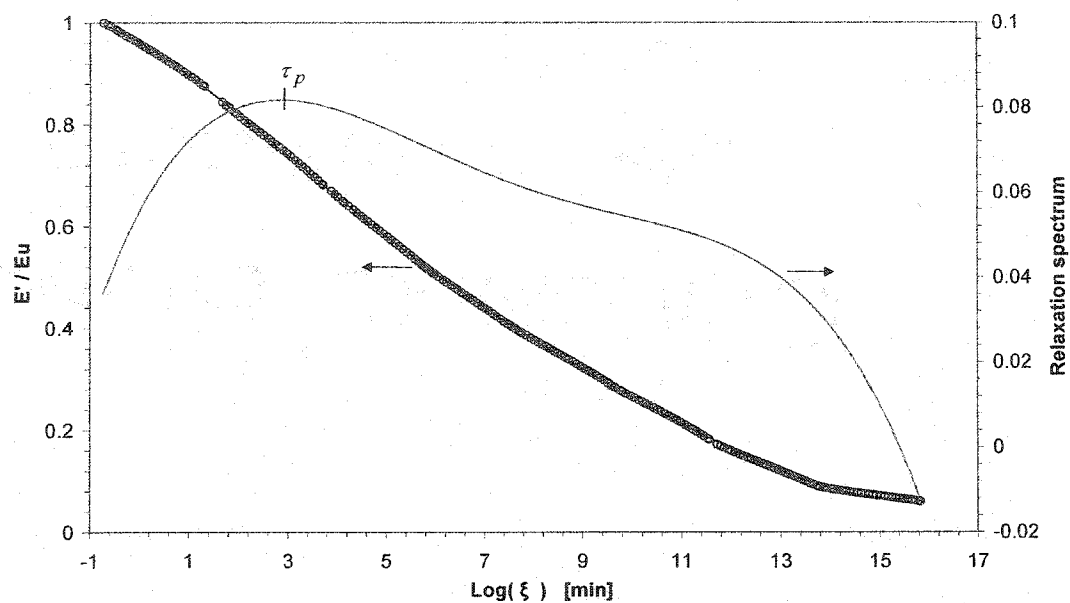


Figure 2.23. Relaxation modulus master curve for the fully cured resin samples. Relaxation spectrum is also shown as a function of reduced time.

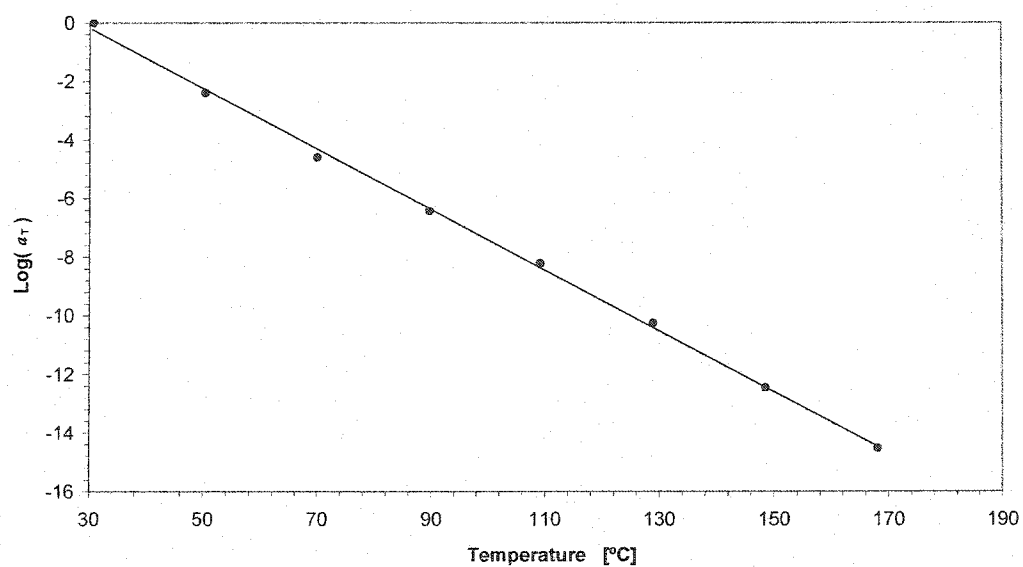


Figure 2.24. Shift function used for the time-temperature superposition to construct the master curve.

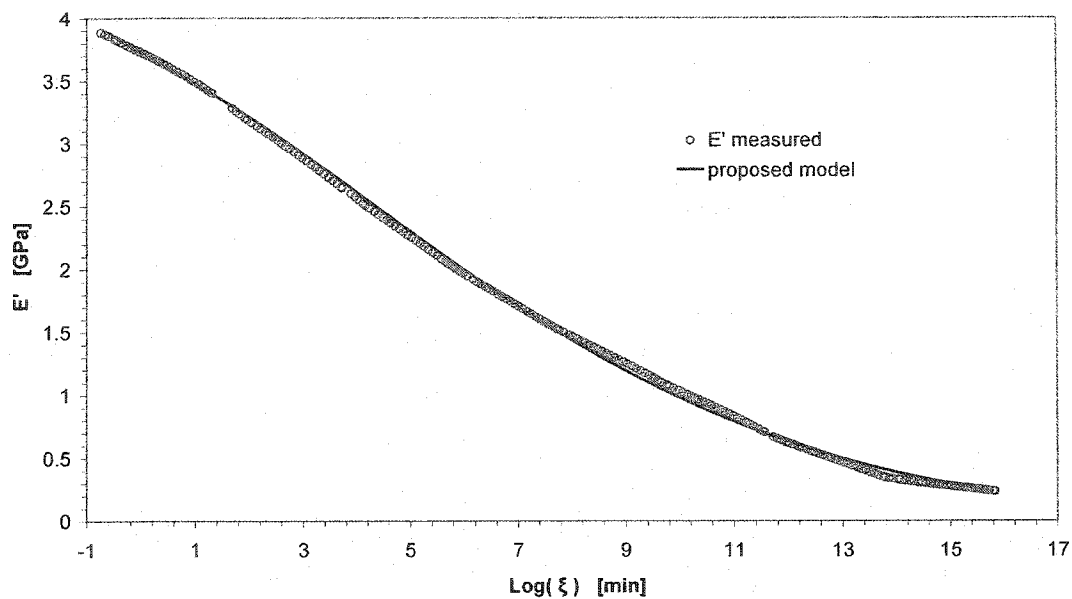


Figure 2.25. Curve fitting of relaxation modulus by the proposed viscoelastic model for the fully cured samples of T580-63 polyester resin.

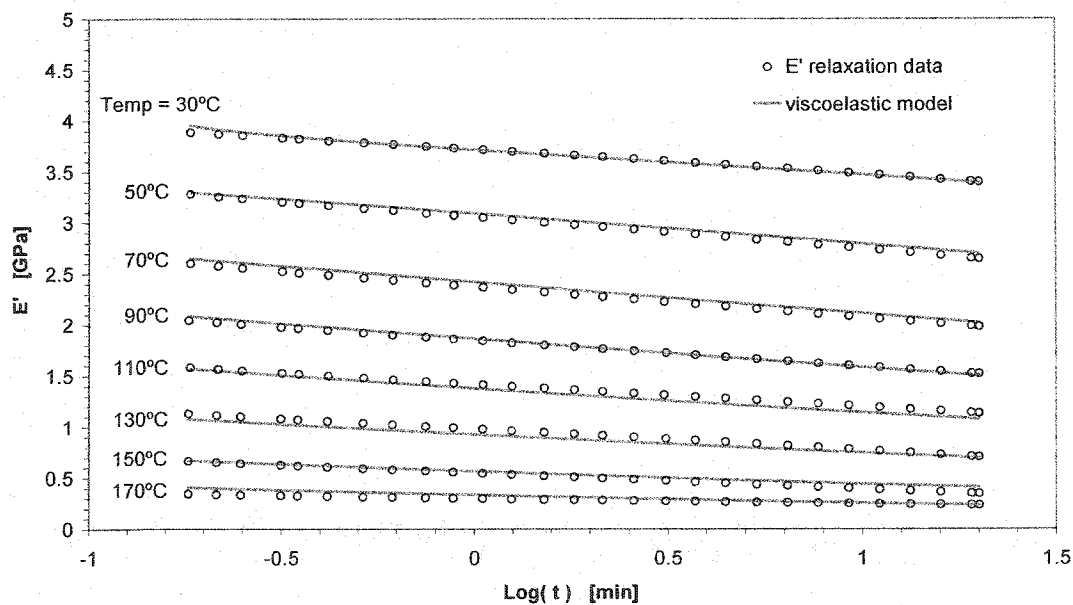


Figure 2.26. Model fit of stress relaxation profiles for the fully cured resin samples at various isothermal temperatures after applying TTS shift function a_T .

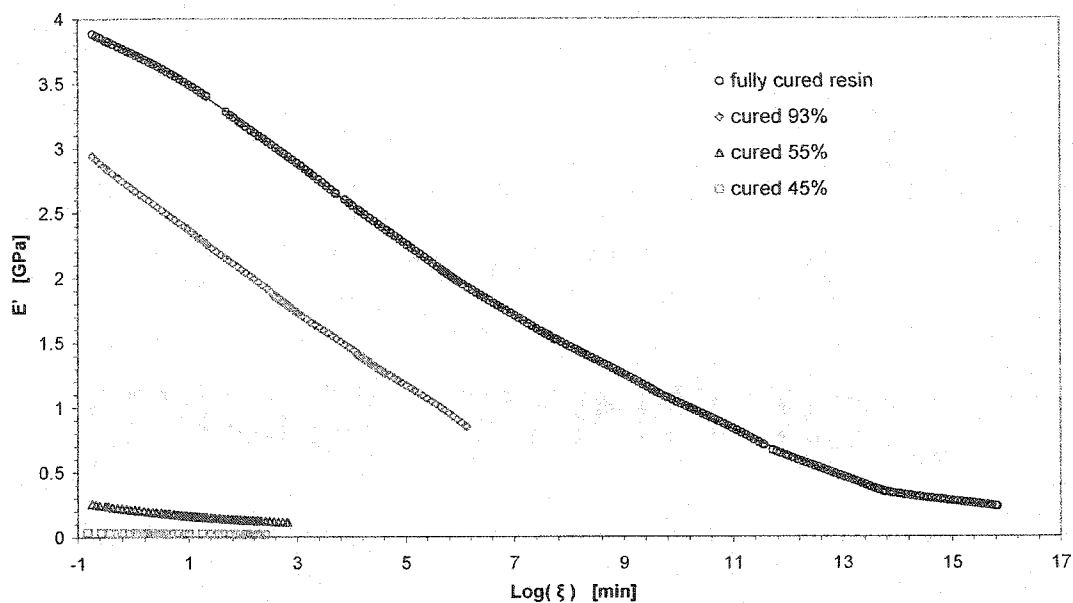


Figure 2.27. Measured E' in DMTA relaxation test at some polymerization degrees for the T580-63 polyester resin.

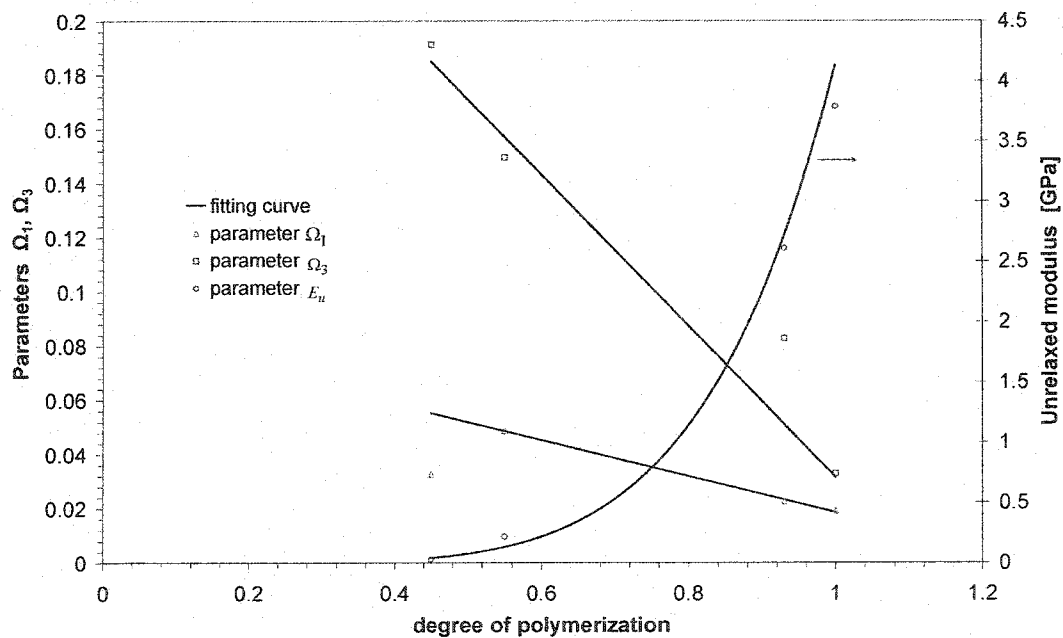


Figure 2.28. Linear interpolation of Ω_1 and Ω_3 parameters used in equation (2.17) for viscoelastic modeling as a function of polymerization degree. Also unrelaxed modulus are presented as a function of cure.

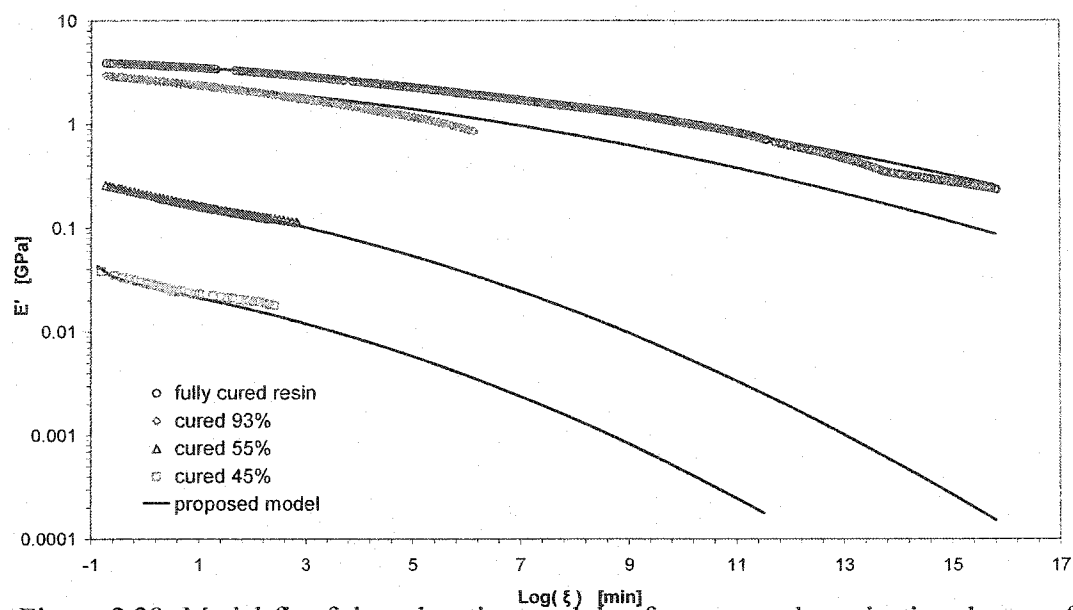


Figure 2.29. Model fit of the relaxation modulus for some polymerization degrees for the T580-63 polyester resin.

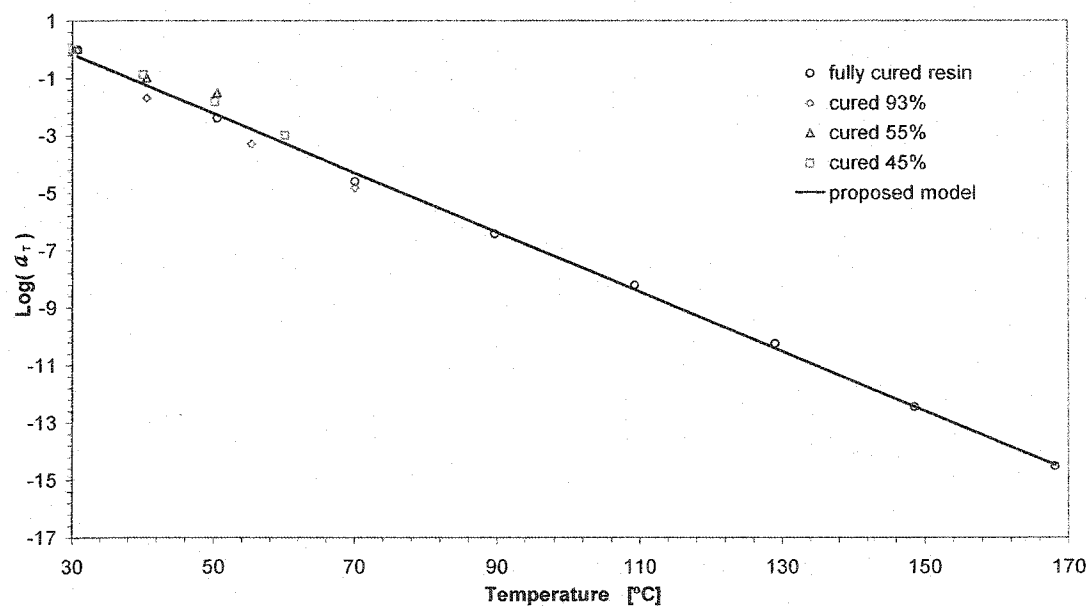


Figure 2.30. Shift functions data and linear modeling for some resin polymerization degrees.

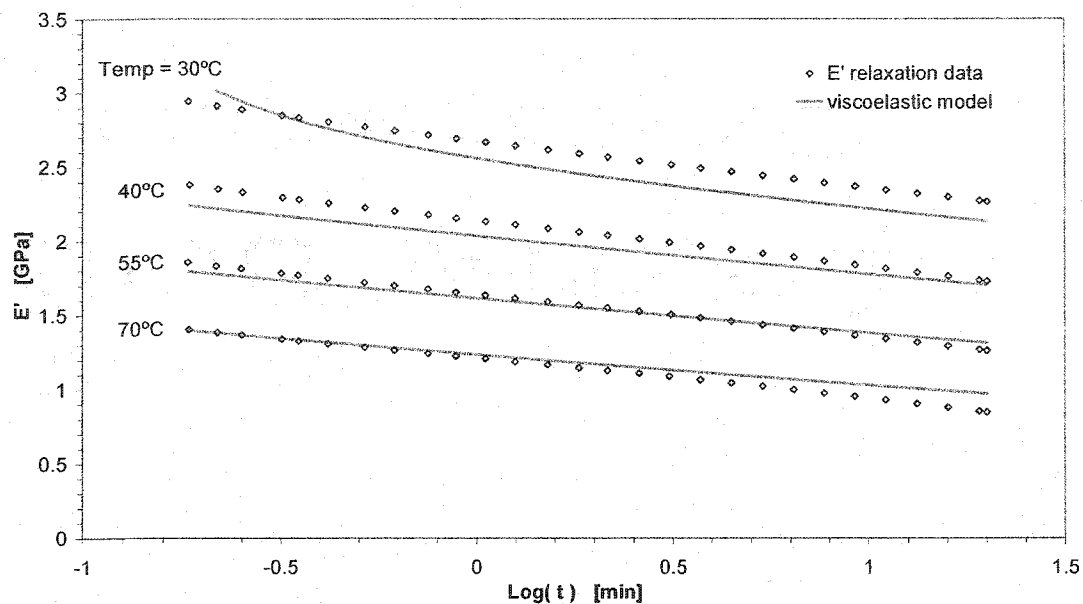


Figure 2.31. Viscoelastic modeling of stress relaxation profiles for the resin sample cured at 93%, for various isothermal temperatures.

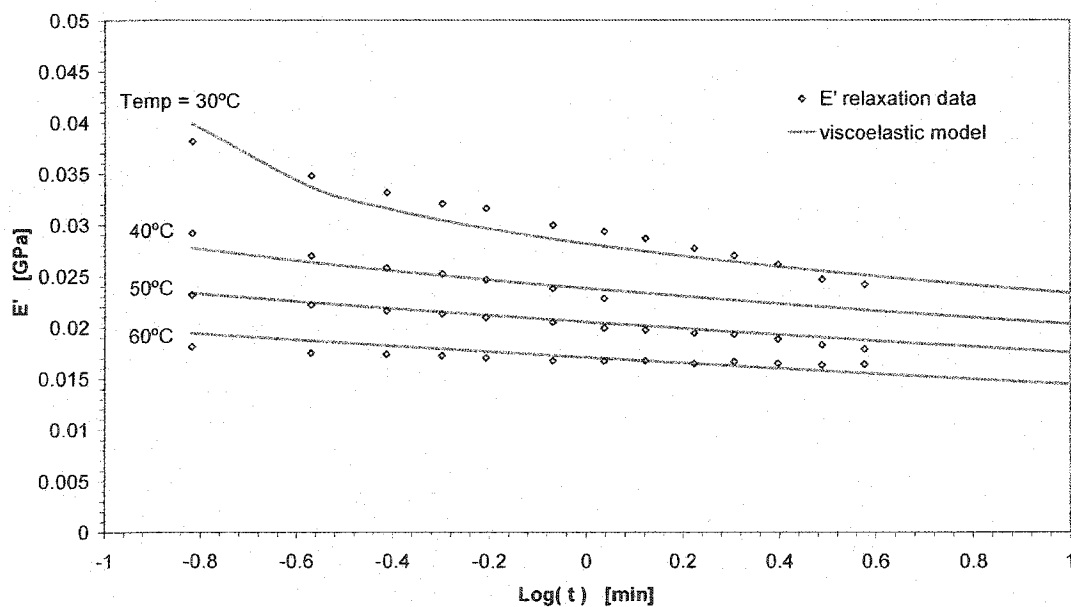


Figure 2.32. Viscoelastic modeling of stress relaxation profiles for the resin sample cured at 45%, for various isothermal temperatures.

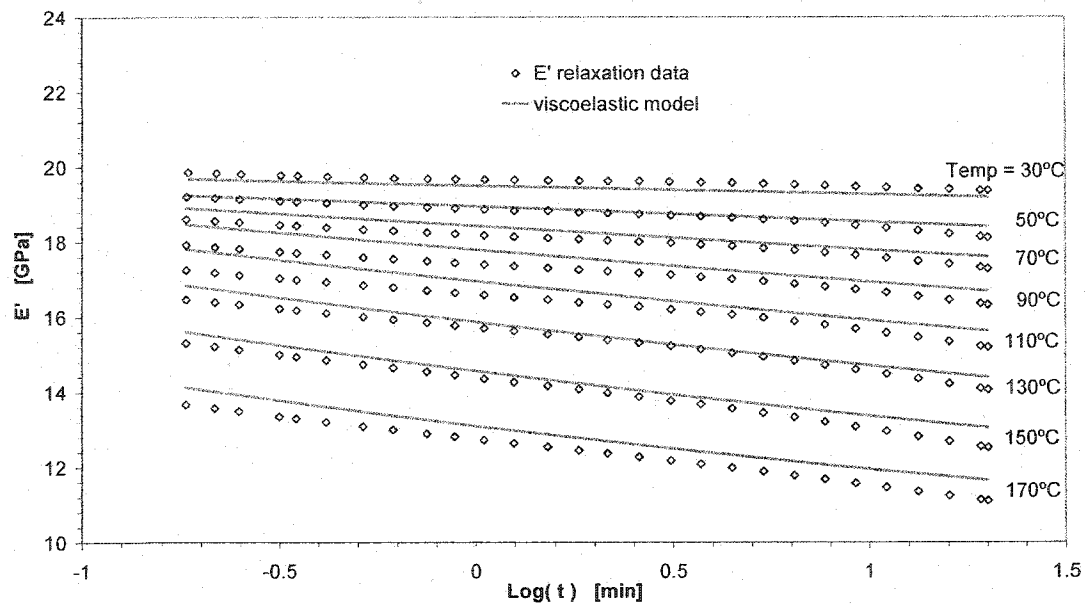


Figure 2.33. Viscoelastic modeling of stress relaxation profiles as a function of time for the glass/resin composite sample (direction 1 at $V_f=45\%$).

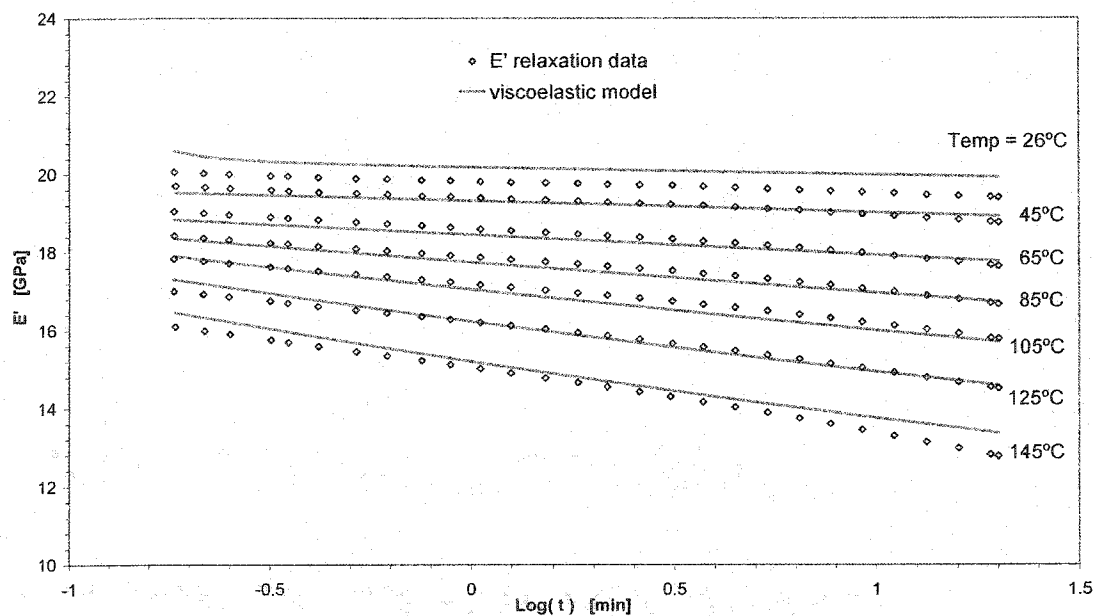


Figure 2.34. Viscoelastic modeling of stress relaxation profiles as a function of time for the glass/resin composite sample (direction 2 at $V_f=40\%$).

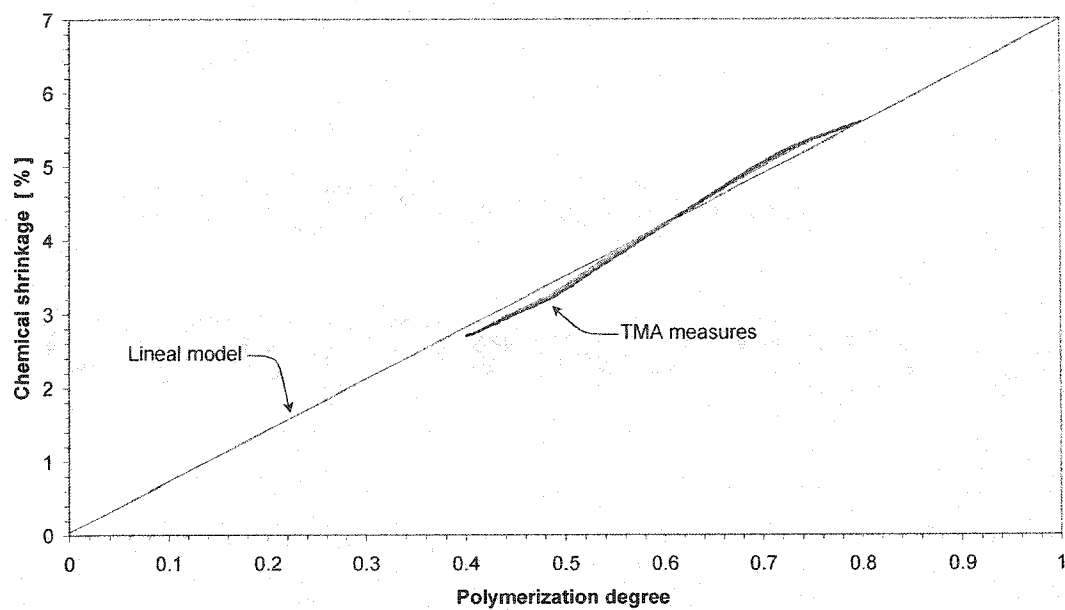


Figure 2.35. Linearization of chemical shrinkage induced by resin polymerization (TMA versus DSC measures).

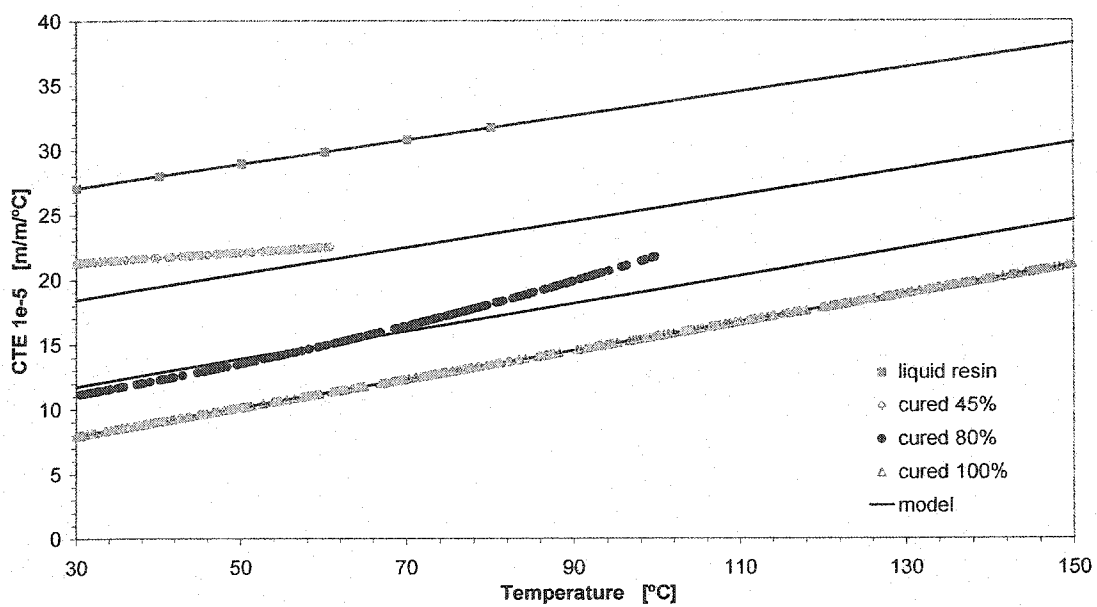


Figure 2.36. Coefficient of thermal expansion for partially and fully cured resin samples (from TMA measures).

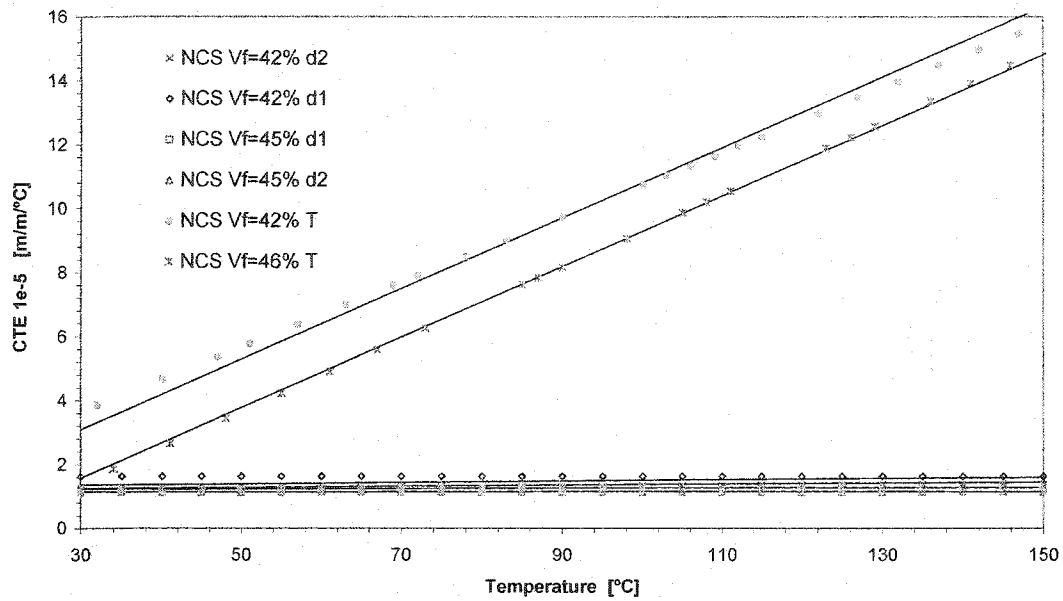


Figure 2.37. Coefficients of thermal expansion for fully cured composite samples of NCS-82620 fabric. Symbols d1 and d2 indicate the principal planar directions of the fabric, while T refers to the transverse direction.

Table 2.1. Values obtained for the kinetic parameters used in the cure modeling of T580-63 polyester resin.

K_1	$K_{ref} [1/sec]$	$T_{ref} [^{\circ}C]$	A
	3.707644	120	852.7575
K_2	See figure (5)		
K_3	A	$B [1/^{\circ}C]$	
	1.427792	3.20E-05	
α_{max}	See figure (6)		
Id	$t_{ref} [sec]$	$T_{ref} [^{\circ}C]$	C
	9.9175	120	5.050475

Table 2.2. Parameters of the model of thermo-mechanical properties of T580-63 resin.

$E_c(T)$	E'_c	a_1	b_1
	3985.365	0.001782	48.4
$E_{agp}(T)$	E'_{agp}	a_2	b_2
	87.31002	0.055178	0.453156
$F_r(\alpha)$	c	d	e
	0.000574	7.236569	0.35987
$F_r(T)$	T_{ref}	h	
	24	0.36788	
$T_g(\alpha)$	a_g	b_g	
	52.9857	0.067918	
$\hat{\alpha}$	α_{agp}	α_{ult}	
	0.45	0.97	

Table 2.3. Values obtained for the modeling of the mechanical properties of T580-63 resin, NCS-82620 fabric and U101 mat composite.

NCS-82620	E^1_{comp}	A_1	B_1	E^1_f
		0.0001839	0.0417394	40100
	E^2_{comp}	A_2	B_2	E^2_f
		0.0001839	0.0417394	43000
U101	E^1_{comp}	A_1	B_1	E^1_f
		0.0001839	0.0417394	35000

Table 2.4. Parameters obtained for equations (26) to (28) to fit viscoelastic data of T580-63 resin.

Parameters of the viscoelastic model									
τ_o (min)	U_o (GPa)	U_1	Ω_1^0	Ω_1^1	Ω_2	Ω_3^0	Ω_3^1	a_o (min)	a_1 (min/ °C)
1	4.132981	5.759529	0.085304	-0.066726	1.752134	0.310671	-0.279135	2.93251	-0.10353

CHAPITRE 3

INTERNAL STRESSES AND WARPAGE OF THIN COMPOSITE PARTS MANUFACTURED BY RTM

Présentation du chapitre

Dans l'article précédent, les propriétés thermomécaniques d'un composite verre/polyester et la cinétique de polymérisation de la résine ont été caractérisées. Dans le chapitre 3, ces modèles sont utilisés pour étudier les changements thermiques et rhéologiques qui se produisent lors de la cuisson des pièces minces. Ce travail a été initialement présenté à la conférence « 5th *International Symposium on Advanced Composites COMP'03* » ayant lieu à Corfu, Grèce. En raison de l'intérêt suscité par cette recherche, la revue *Advanced Composites Letters* a offert de publier le compte-rendu de cette conférence sous la forme d'un article. L'étude est consacrée à la modélisation numérique des contraintes internes dans un laminé mince causées par un refroidissement au-delà de la température de transition vitreuse. L'équation de l'énergie unidimensionnelle (à travers l'épaisseur) est solutionnée par une formulation de différences finies de type Crank-Nicolson. La théorie classique des laminés est utilisée pour calculer les contraintes internes dans un composite stratifié. Pour valider les caractérisations physiques effectuées et les modèles numériques implémentés dans cette recherche, une série d'échantillons de verre/polyester sont fabriqués par injection et testés. Une extension de ce travail pour des pièces épaisses est présentée au chapitre suivant.

Internal Stresses and Warpage of Thin Composite Parts
Manufactured by RTM

Edu Ruiz, François Trochu and Raymond Gauvin

Centre de Recherches Appliquées Sur les Polymères (CRASP)

Département de Génie Mécanique,

École Polytechnique de l'Université de Montréal,

e-mails: eduardo.ruiz@polymtl.ca, francois.trochu@polymtl.ca,
raymond.gauvin@polymtl.ca

Keywords: RTM, resin cure, processing stresses, residual stresses, warpage.

Article accepté dans la revue *Advanced Composites Letters*

September 2003

3.1 Abstract

Resin transfer molding (RTM) is a widely used manufacturing technique of composite parts. A proper selection of process parameters is the key to yield successful molding results and obtain a good part. Among other things, when thermoset resins are processed, the shrinkage that occurs due to the polymerization reaction further complicates the situation. In this paper, a finite difference analysis is proposed to simulate the effect of thermal and rheological changes during thin plates cooling after processing. Classical Laminate Theory is here implemented to compute composite internal stresses resulting from these thermo-rheological conditions. Laminate stresses

are then computed and warpage obtained with the proposed numerical algorithm. Samples of thin plates were molded combining two glass reinforcement materials. During cooling, after processing plates warpage was recorded and results compared to model predictions. This analysis presents the basis of a further numerical optimization for thick composite parts.

3.2 Introduction

As the composite industry grows, thick parts and pieces of complex shape have become more common. The composite components for structural applications require larger cross-sections than for non-structural applications. The curing of thick parts is challenging because of the low thermal conductivity of the composite and the high heat of reaction generated during the cross-linking polymerization. This combination of low thermal conductivity and large heat source in the part during cure can lead to significant thermal gradients and temperature peaks. This generates residual stresses and may result in polymer degradation. In order to improve the quality of thick composites, the processing temperature needs to be controlled so that thermal gradients remain small. This typically means that for thick parts, the mold temperature needs to be lower than for thin parts. Also, the chemorheology and cure kinetics may be considerably different from what is observed at higher temperatures.

The reinforcing fibers are not really affected during the process cycle, but the polymer matrix can shrink during cross-linking by as much as 9% [1]. As well as chemically induced shrinkage, there are also thermally induced deformations during processing. The fibers show a small thermal expansion coefficient along their longitudinal axis that produces little deformation at the curing phase. The polymer matrix has a much higher thermal expansion coefficient and is more affected by temperature changes. During part processing, these different thermal behaviors induce residual stresses. When curing fiber-

reinforced composites, the induced residual stresses can have a significant effect on the part quality and mechanical properties promoting warpage or initiating matrix cracks and delamination [2].

The purpose of this paper is the study of chemo-mechanical properties of the composite, and validates a numerical model of heat transfer and stress calculation through the thickness of a composite. The intention of the numerical model is to assist in the future finding optimal temperature cycles to avoid highly induced stresses in thick parts. Firstly the thermal phenomenon in composite parts is presented and energy equation stated. Then models of volume changes as well as material behavior during composite processing are presented. Both models are depending on fiber volume fractions, temperature and degree of polymerization. A methodology for predicting residual stresses during and after processing of composite laminates was developed. Classical Laminated Plate Theory (CLT) was used to compute internal stresses. Thin composite plates were molded combining two fiber reinforcements to induce warpage after processing. For each specimen, plate deflection (warpage) was recorded during cooling. The numerical methodology was implemented to predict cooling stresses and induced warpage of the plates. Experimental results are finally compared to numerical values and concluding remarks detailed.

3.3 Thermo-mechanical modeling

In the present work the simulation of heat transfer is analyzed through the thickness of the composite part. An instantaneous equilibrium temperature is assumed to be reached between the resin and the fibers at each instant of the thermal analysis. This corresponds to the lumped approach of Lin et al. [3]. The transient absolute temperature $T^{t,z}$ at time t and position z , through the total part thickness H is given by the one-dimensional Fourier's heat conduction equation :

$$\bar{\rho} \bar{C}_p \frac{\partial T}{\partial t} = \bar{k} \frac{\partial^2 T}{\partial z^2} \quad 0 \leq z \leq H \quad (3.1)$$

where the thermal properties are those effective properties of the composite (resin + fibers) obtained with a rule of mixture.

3.3.1 Thermo-mechanical model

The need to predict accurately the intrinsic behavior of the material and the properties of the resulting part is vital to determine part quality and achieve process control. As thermo-kinetic properties do, mechanical properties of the resin vary as the part cures. Some authors [4-6] have considered a linear correlation between the mechanical properties and the resin degree of polymerization for different thermosetting polymers. For the unsaturated polyester resin used on this work (T580-63 from AOC), mechanical properties were measured with a dynamic mechanical analyzer (DMTA 2980 TA Instruments) as a function of temperature and polymerization degree. It was found that long after the gel point, for a polymerization degree less than 40%, the resin elastic modulus is still very low (below 10 MPa). This polymerization degree, that we call here the After Gel Point (AGP), was then taken as base line to analyze the properties evolution at higher polymerization levels. Resin samples cured at the AGP stage were mechanically tested on the DMTA during a specified curing cycle. As showed on figure 3.1, elastic modulus increases from its value at the AGP (E'_{agp}) until it reaches a maximum considered as the fully cured modulus (E'_c) for 97% of the total resin polymerization. Measured values depict a non-linear correlation between DMTA mechanical properties and polymerization degree from calorimetric measures. This relationship was model by combining a hyperbolic cosines law that properly describe the temperature dependence of the elastic modulus (see equations below) with two functions to account for the polymerization degree (F_r^α) and glass transition temperatures (F_r^{Tg}) dependences.

$$E_r^{T,\alpha} = E_{agp}^T + (E_c^T - E_{agp}^T) \cdot F_r^\alpha \cdot F_r^{T_g} \quad (3.2)$$

$$E_c^T = \frac{E_c'}{\cosh(a_c \cdot T)^{b_1}} \quad E_{agp}^T = \frac{E_{agp}'}{\cosh(a_{agp} \cdot T)^{b_2}} \quad (3.3)$$

$$F_r^\alpha = c_r \cdot \exp(d \cdot \alpha_m) + e_r \cdot \alpha_m \quad \alpha_m = \frac{\alpha - \alpha_{agp}}{\alpha_{ult} - \alpha_{agp}} \quad (3.4)$$

$$F_r^{T_g} = h \cdot \exp\left(\frac{T_g^\alpha - T}{T_g^\alpha - T_{ref}}\right) \quad T_g^\alpha = a_g \cdot \exp\left(\frac{-b_g}{1 - \alpha_m}\right)^{-1} \quad (3.5)$$

A convenient α -mixing rule is used here in order to approximate the variations of material properties between the AGP level (α_{agp}) and the cure degree where E' reaches its ultimate value ($\alpha_{ult} \approx 97\%$). Furthermore, the presented model accounts for the glass transition temperature dependence of the resin elastic modulus by a temperature shift factor ($F_r^{T_g}$). This factor considers the transition to complete viscoelastic relaxation at vitrification (or when material is at the rubbery state, i.e. $T \geq T_g^\alpha$). Constants a , b , c , d and e of equations (3.2 to 3.5) were obtained by implementing a Genetic Algorithms Search Engine that properly fit the models to the measured data. Subscripts r , c , g and agp of these constants denote resin, composite, glass transition and after gel point. Figure 3.2 shows DMTA measurements of several resin specimens cured at different polymerization degrees between the α_{agp} and α_{ult} levels. The predictions of the proposed thermo-chemical model exhibit relatively good agreement with experimental data for all tested samples. In the case of shear properties, two possible approaches may be used, Levitsky and Shaffer [7] assumed the plain strain bulk modulus to be constant during cure so that elastic moduli and Poisson's ratio vary as part cures. On the other hand, Bogetti and Gillespie [4] considered the Poisson's ratio constant over the processing. They found that differences on resin Poisson's ratio during cure have no significant influences on the macroscopic composite properties, process-induced strains and residual stresses. Both models predicted nearly identical values of elastic and shear

modulus. Poisson's ratio is also expected to relax to ~ 0.5 as the thermosetting polymer approaches the rubbery state, nevertheless it was found by O'Brien et al. [8] that the effect on shear moduli is relatively minor. According to these researchers, the variation of the Poisson's ratio has no significant effect. For that reason, in this work we have used a constant value ($\nu_r = 0.35$) which was measured at room temperature on a fully cured sample. The instantaneous resin shear modulus during cure is based on the isotropic material relation:

$$G_r^{T,a} = \frac{E_r^{T,a}}{2 \cdot (1 + \nu_r)} \quad (3.6)$$

The effective homogeneous mechanical properties of the composite laminate are highly dependent on the matrix and reinforcement constituent properties and its volume fractions. Thermal and mechanical properties of the reinforcement may be considered constant and independent of temperature and polymerization degree, while matrix properties vary during processing according to the models previously presented. Although a self-consistent micro-mechanical model [9] was initially used to determine reinforcement properties, over-predictions were found at temperatures close to the matrix glass transition. Empirical models were then implemented to estimate composite elastic modulus $E_c^{1,2}$ as function of temperature T and fiber volume fractions V_f for the two principal fiber directions.

$$E_c^i = \left(\frac{V_f \cdot (E_f^i - E_r^{T,a})}{1 + A_i \cdot \exp(B_i \cdot T)} + E_r^0 \right) \cdot \left(\frac{E_r^{T,a}}{E_r^{T,1}} \right) \quad \text{with } i = 1, 2; \quad (3.7)$$

where A and B are fitting constants for each material direction ($i=1,2$).

Two reinforcing materials have been used in this study to analyze thermal effects on processing stresses, a continuous glass random mat U101 from Vetrotex and one bi-

directional balanced non-crimp glass fabric NCS 82620 from J.B. Martin. Figure 3.3 presents results of Young's modulus measures in both directions (E_c^1, E_c^2) for a composite plate made with NCS-82620 bidirectional fabric ($V_f = 42\%$). For the partially and fully cured samples, the mechanical model approaches the experimental curves at temperatures close to T_g . Composites specimens of these materials were measured and fitted by equation (3.7), as depicted on figure 3.4 two to three fiber volume contents were tested for each material. It must be noticed that rule of mixture used in this work may be accurate only for values around measured values. It is presented on figure 3.5 the range of validity considered for tested materials.

3.3.2 Model of volume changes

Some experimental studies have been conducted to gain insight into the volumetric changes that occur during thermoset polymer processing, Hill et al. [10] measured the volume changes during curing due to temperature variation and degree of polymerization for unsaturated polyester resins. Hill proposed that the overall volumetric changes of a thermoset resin during curing can be considered as a combination of thermal expansion or contraction and polymerization shrinkage. Therefore it can be written as follows:

$$\left(\frac{1}{V_o} \frac{dV}{dt} \right)_{\text{Overall}} = \left(\frac{1}{V_o} \frac{dV}{dt} \right)_{\text{Thermal Contribution}} - \left(\frac{1}{V_o} \frac{dV}{dt} \right)_{\text{Polymerization Shrinkage}} \quad (3.8)$$

The first term on the right hand side represents the bulk thermal expansion/contraction contribution, which can be expressed by

$$\left(\frac{1}{V_o} \frac{dV}{dt} \right)_{\text{Thermal Contribution}} = \beta_{\text{gel}} \cdot \frac{dT}{dt} + [(\beta_{\text{cured}} - \beta_{\text{gel}})] \cdot \alpha \cdot \frac{dT}{dt} \quad \beta_{\text{cured}}, \beta_{\text{gel}} = a_0 + b_0 \cdot T \quad (3.9)$$

where β_{gel} and β_{cured} are the coefficients of thermal expansion (CTE) of the gelled and fully cured resin respectively. Note that the CTE is assumed to vary monotonically with the polymerization degree α . The second term on the right hand side of equation 8 represents the contribution of chemical shrinkage (i.e., volume shrinkage induced by the resin cross-linking during polymerization). Resin shrinkage was measured by using a thermomechanical analyzer (TMA 2940 from TA Instruments) as function of the degree of polymerization. An acceptable linear relationship expressed by equation 10 was experimentally obtained for the polyester resin tested. The total polymerization shrinkage λ_{chem} for the fully cured sample was about 7%.

$$\left(\frac{1}{V_o} \frac{dV}{dt} \right)_{\text{Polymerization Shrinkage}} = \lambda_{chem} \frac{d\alpha}{dt} \quad (3.10)$$

3.3.3 Coefficients of thermal expansion

CTE of pure resin samples and composites plates were also measured on the thermo mechanical analyzer. Thermal expansions of uncured resin samples (i.e. $\alpha = 0$), partially cured ($\alpha = 0.45$, and 0.80) and fully cured samples have been determined. Data were fitted by bilinear functions and resin CTE model as function of temperature and polymerization degree can be then written as:

$$CTE_r^{T,\alpha} = CTE_{agg}^T \cdot (1 - \alpha_m) + CTE_{cured}^T \cdot \alpha_m \quad (3.12)$$

Composite samples of NCS 82620 and U101 reinforcements were also measured (see figure 3.6) in the three principal directions (i.e. Longitudinal, Transverse and Through-Thickness) and model as follows.

$$CTE_{comp}^d = CTE_r^{T,\alpha} \cdot (1 - V_f) + CTE_{fibre}^d \cdot V_f \quad \text{where } d = L, T, \text{ and } T\text{-Thickness} \quad (3.13)$$

3.3.4 Strain-stress modeling

In the present analysis, it is assumed that the Classical Laminated plate Theory (CLT) is applicable to the infinitesimal regions of the composite unit cell. By introducing the expressions of the thermo-chemical dependent mechanical properties into the formulation of the CLT, for loading of thermal and chemical origins, it can be written:

$$\{\sigma_j\}_t = \int_{t(AGP)}^t [C_j]_t^{T,\alpha} \cdot \left\{ \frac{\partial \varepsilon_j}{\partial t} \right\} \cdot dt \quad j=1 \text{ to } N \text{ plies} \quad (3.14)$$

where the strain vector is defined as:

$$\varepsilon_j = \varepsilon_j^{Thermal} + \varepsilon_j^{chemical} \quad \varepsilon_j^{chemical} = \sqrt[3]{1 + (\lambda_{chem} \cdot \alpha)} - 1$$

In order to account for the potentially nonlinear behavior of the material, the stiffness matrix $[C_j]^{T,\alpha}$ should be calculated at each processing time. In this way, $[C_j]$ is the algebraic average of $[C_j]_t$ and $[C_j]_{t+dt}$. A step-by-step computational method has been used to predict laminate thermo-chemical response during processing. At each running step, planar stresses and out-of-plane curvatures are computed from the strains induced by thermal gradients and chemical changes of the composite.

3.4 Analysis of thin composite plates during cooling

The properties and durability of composite parts manufactured with thermosetting matrix materials are strongly affected by internal stresses. The source of internal stresses depend on material properties and on the processing conditions, they are most commonly created during manufacture as result of thermal and mechanical behavior differences between the phases the constitutive materials go through. Internal stresses

may lead to defects in the part both during processing, in the form of voids and microcracking, or after manufacture, as warpage and spring-in, premature delamination or debonding. In this work, to identify part defects caused by internal stresses after processing (during cooling), thin composite plates, 50 cm length by 10 cm width and 3 mm thick, were molded using several combinations of NCS-82620 fabric and U101 mat. As showed on figure 3.7a, NCS and U101 plies were asymmetrically layered. Differences on the linear CTE and mechanical properties at each reinforcement side obviously generate warpage phenomena on molded plates. Thermocouples were embedded between plies to measure through-thickness temperature profiles during processing. Plates cured at 120°C showed a warpage in the form of a curvature in the longitudinal as well as in the transverse direction, as depicted on figure 3.7b. The transverse curvature is important and is taken into account to correctly estimate the plate curvatures. For each material combination, plates dimensions and curvatures were measured with a Linear Variable Displacement Transducer (LVDT). Several plates were molded, and four are reported on table 3.1. It is appropriate to remark that special care must be taken on the specimen preparation, mainly due to the surface density variation of the U101 mat. Non-uniform surface densities of the mat result in variable plate thickness after curing, and the assumption of cylindrical deflection may not correctly predict the experiment values. After curing, three plates were re-heated and maintained during 20 minutes at 150°C which is above their glass transition temperature, allowing matrix to relax. Once residual stresses were relaxed, flat plates were cooled to room temperature while recording temperature profiles and deflection with time. A typical result of temperature and deflection recorded during cooling is presented in figure 3.8. On figure 3.9, experimental results of two specimens are compared with those predicted by the thermo-mechanical model. For the three specimens, the error between measured and calculated values was relatively small. As reported in table 3.2, an error of less than 2% was found for the tested plates. These tests on thin plates are used to experimentally corroborate the proposed thermo-

mechanical model, and suggest that the quality of the model predictions for internal stresses of thermal origin is excellent.

3.5 Conclusion

In this paper, models are proposed to describe changes in composite mechanical properties as a function of fiber volume content, temperature and polymerization degree of the resin. These models were used for two reinforcing materials (NCS-82620 fabric and U101 mat), embedded in a polyester resin (T580-63 from AOC). Energy equation was solved by finite differences through the thickness of the part. The analysis of process-induced stresses in composite parts was based on Classical Laminated plate Theory. Asymmetrically layered thin plates were processed to validate the thermo-mechanical model by comparing calculated and measured plates deflection during cooling. A good accuracy of the model predictions was shown with errors of less than 2%. This analysis shows that in the processing of thin composites by RTM, numerical simulation can be a useful tool to properly determine residual stresses and geometrical defects of the molded part. A thermal optimization can then be used to increase mechanical performances of the part while reducing residual stresses and processing times.

3.6 References

- [1] White, S. R. and Hahn, H. T., "Process Modeling of Composite Materials: Residual Stress Development during Cure", *J. of Composite Materials*, 26/16 (1992), 2402-2453.
- [2] Michaud, D., Beris, A. and Dhurjati, P., "Curing Behavior of Thick-Sectioned RTM Composites", *J. of Composite Materials*, 32/14 (1998), 1273-1295.
- [3] Lin, R. J., Lee, L. J. and Liou, M. L., "Mold Filling and Curing Molding of RTM Process", *Advanced Composite Materials, Conference Proceedings*, Detroit, Michigan USA, Sept. 30, 1991, pgs 165-174.
- [4] Bogetti. T. and Gillespie. J., "Process-Induced Stress and Deformation in Thick-Sectioned Thermoset Composite Laminates", *J. of Composite Materials*, 26/5 (1992), 626-660.
- [5] Golestanian. H. and El-Gizawy. S., "Cure Dependent Lamina Stiffness Matrices of Resin Transfer Molded Composite Parts with Woven Fiber Mats", *J. of Composite Materials*, 31/23 (1997), 2402-2423.
- [6] Osswald. T. A., Sun, E. M. and Tseng, S-C., "Experimental Verification on Simulating Shrinkage and Warpage of Thin Compression Moulded SMC Parts", *Polymers & Polymer Composites*, 2/3 (1994), 187A-198A.
- [7] Levitsky, M. and Shaffer, B. M., "Thermal Stresses in Chemical Hardening Elastic Media with Application to the Molding Process", *J. of Applied Mechanics*, 41 (1974), 647-651.
- [8] O'Brien, D. J., Mather, P. and White, S. R., "Viscoelastic Properties of an Epoxy Resin during Cure", *J. of Composite Materials*, 35/10 (2001), 883-904.
- [9] Whitney, J. M., "Elastic Moduli of Unidirectional Composites with Anisotropic Filaments", *J. of Composite Materials*, 1 (1967), 188.
- [10] Hill, R., Muzumar, S. and Lee, L., "Analysis of Volumetric Changes of Unsaturated Polyester Resin During Curing" *Polymer Eng. & Sci.*, 35/10 (1995), 852-859.

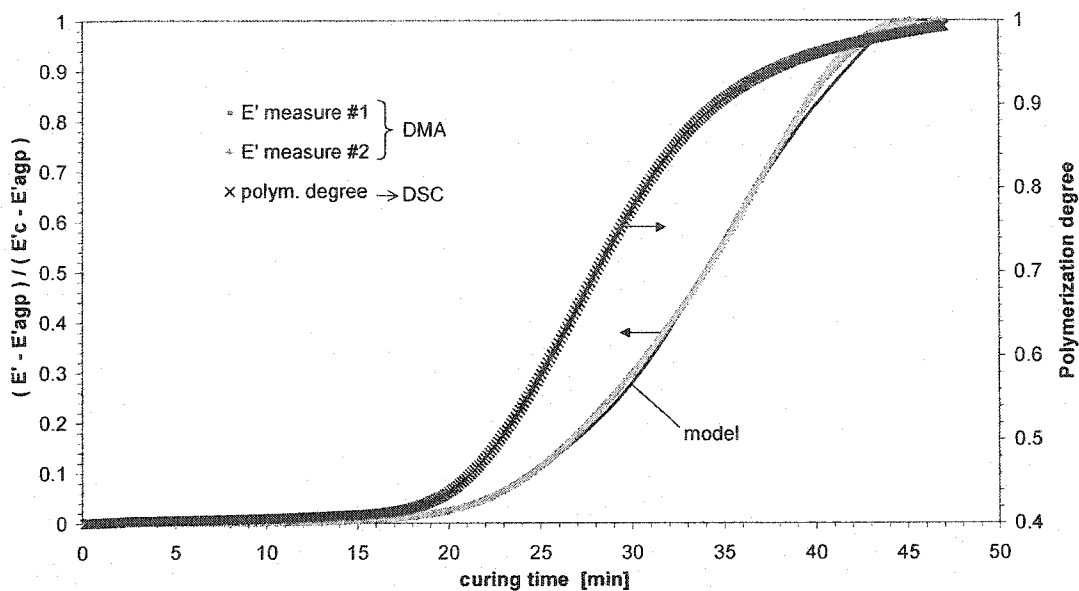


Figure 3.1. Comparison of polymerization degree and E' during specified curing cycle.

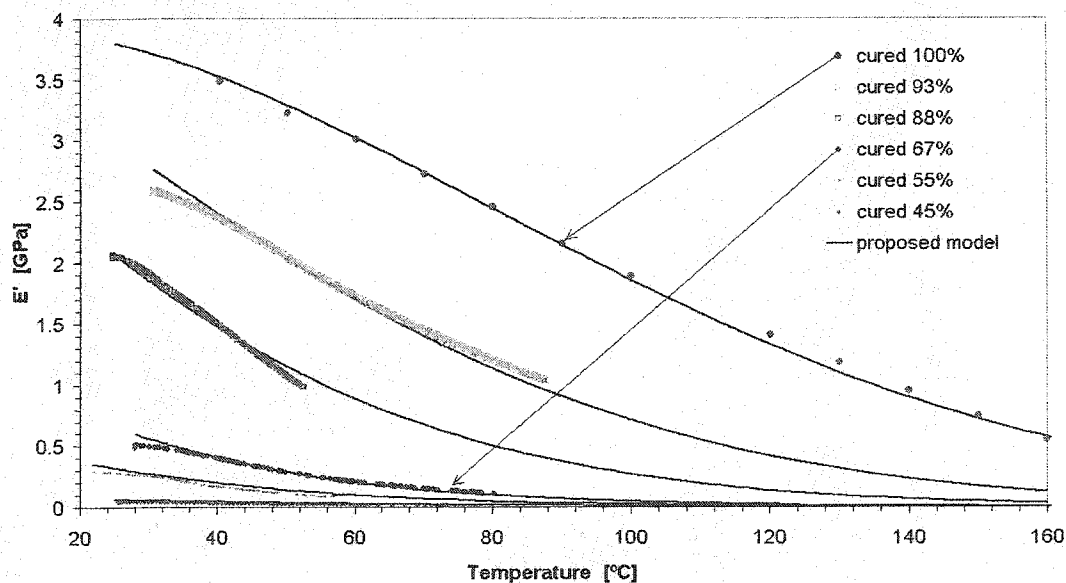


Figure 3.2. DTMA measures of E' for partially and fully cured resin samples (lines presents model predictions).

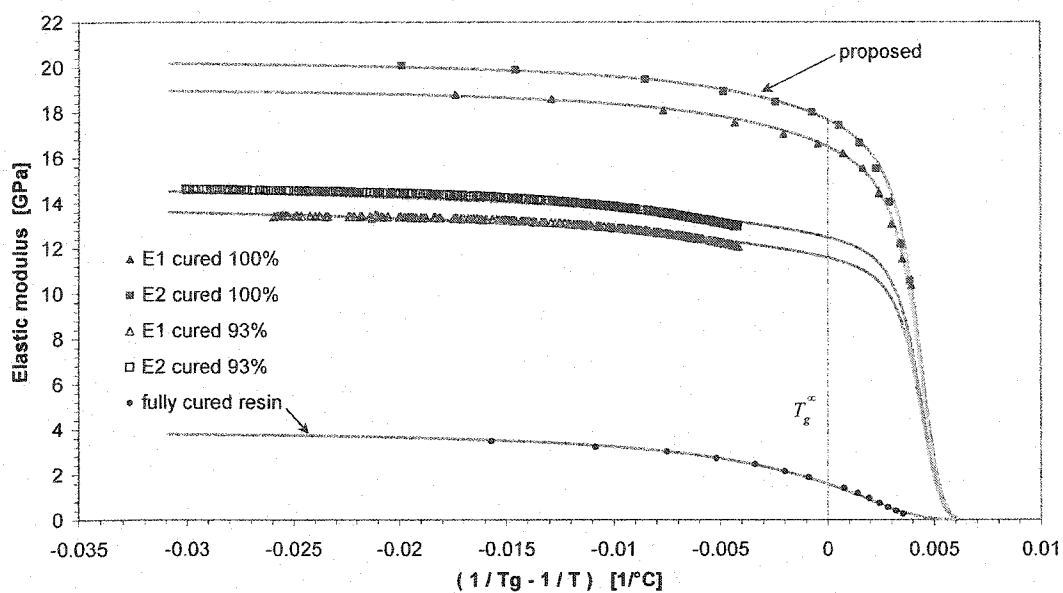


Figure 3.3. Measured and predicted E' in both directions for composite with $V_f=42\%$ of NCS-82620 (fully and partially cured samples).

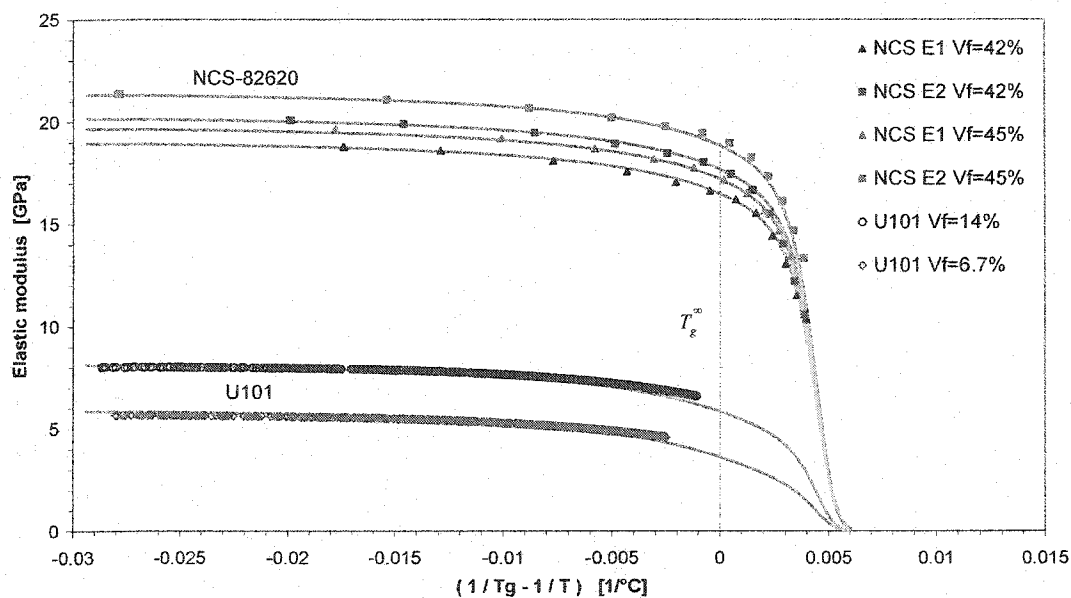


Figure 3.4. Measured and predicted E' for different V_f . Fully cured composite samples of NCS-82620 fabric and U101 mat.

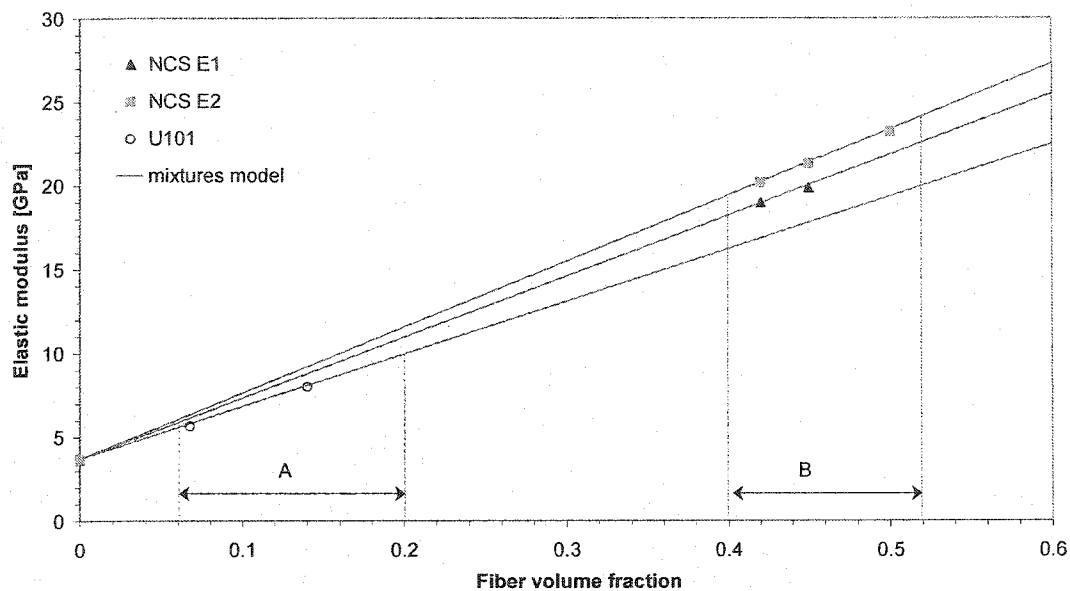


Figure 3.5. Rule of mixtures for E' as function of V_f . A and B represent validity range of V_f for U101 and NCS materials respectively.

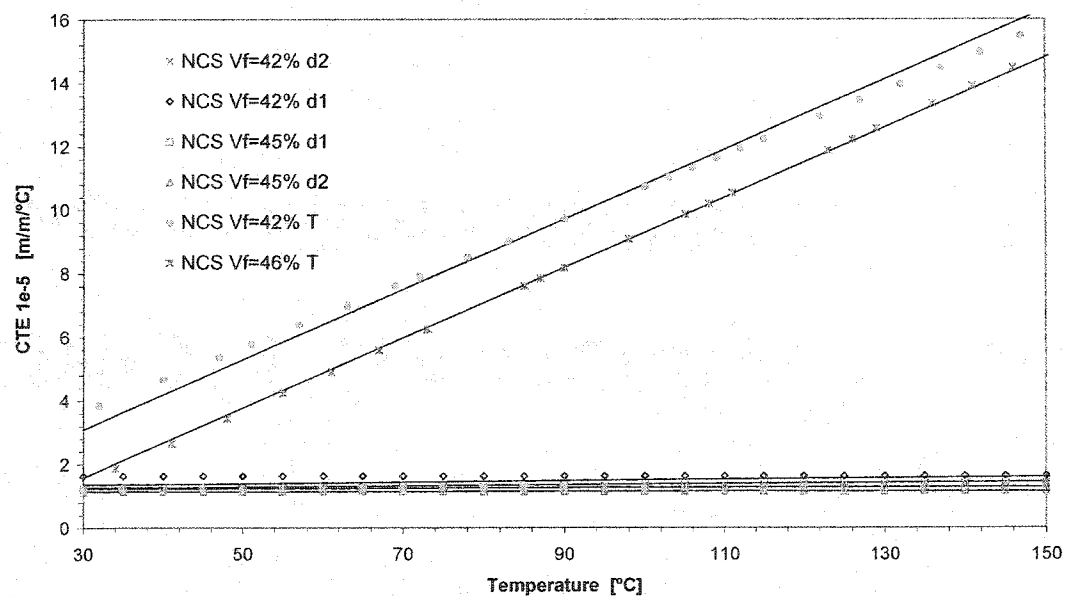


Figure 3.6. Coefficients of thermal expansion for fully cured composite samples of NCS-82620 fabric. d1 and d2 indicate principal planar directions of the fabric, while T refers to transverse direction.

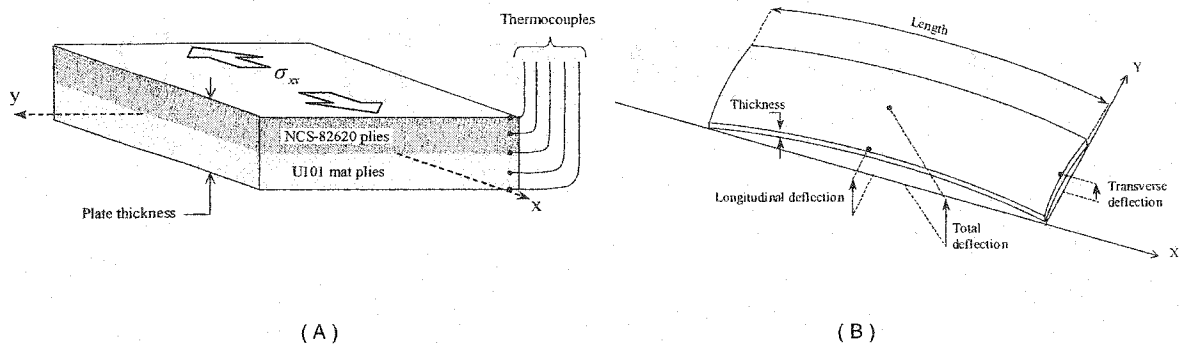


Figure 3.7. A) Stacking sequence for thin plates. The number of NCS plies was changed while mold thickness was maintained constant and 2 plies of U101 were used in every cases. B) Warpage appearing in thin composite plates after manufacture. Total deflection at the center is the sum of longitudinal and transverse deflections.

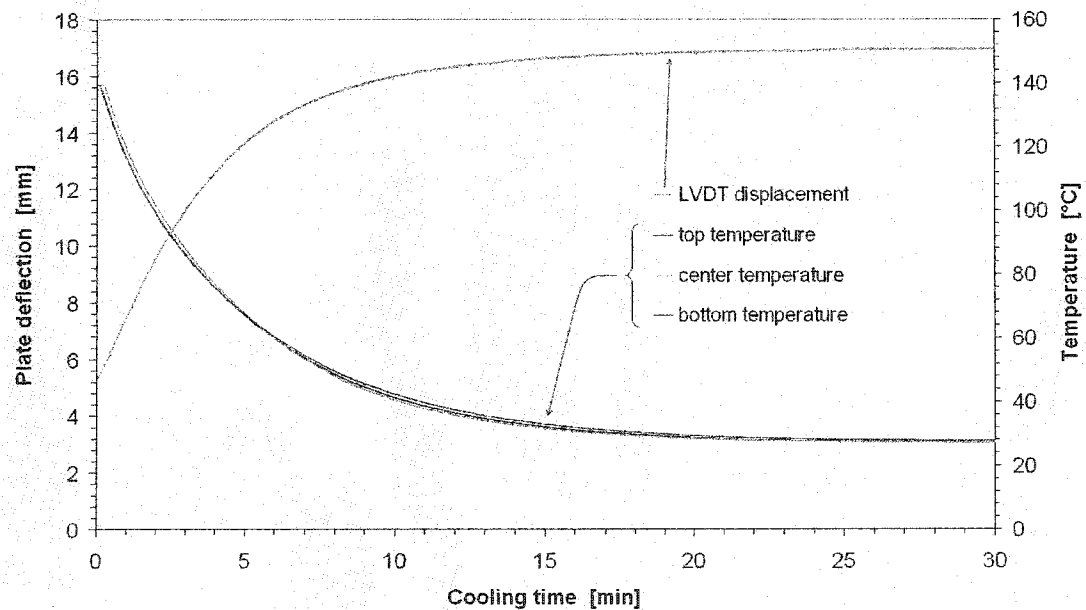


Figure 3.8. Measure of typical plate deflection during cooling from above the glass transition temperature. The sample has 2 plies of NCS-82620 fabric and 2 plies of U101 mat.

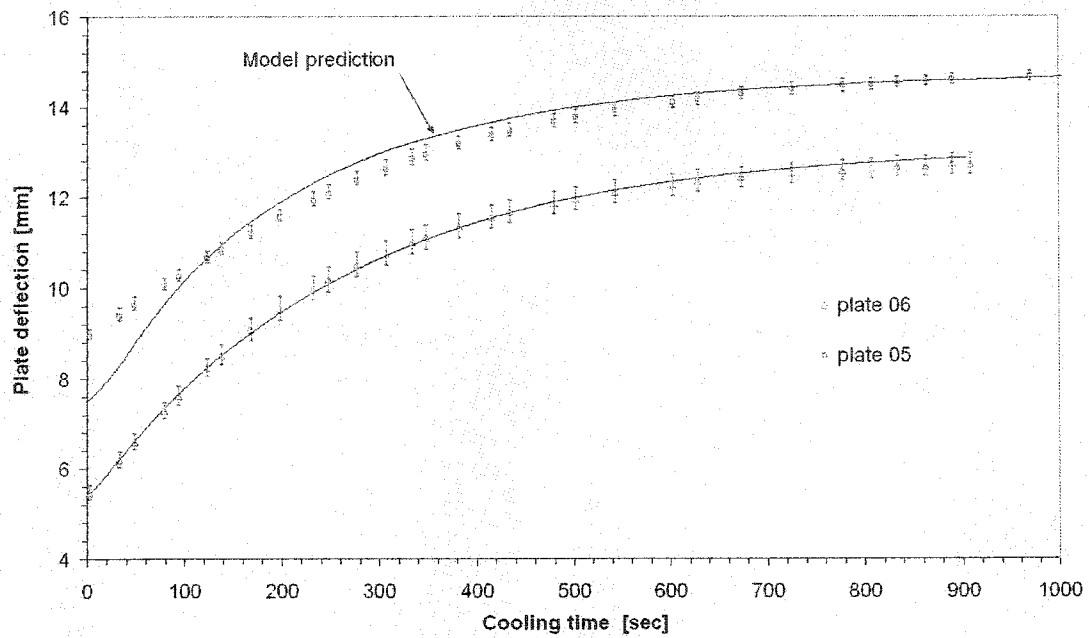


Figure 3.9. Comparison of measured plates deflections with numerical predictions of the thermo-mechanical model.

Table 3.1. Plates dimensions and curvatures after manufacture for eight thin plates samples. Reported thicknesses are the average of 10 measures along the plates.

Test number	NCS 82620 # of plies	U101 # of plies	Length [mm]	thickness [mm]	X curvature [1/m]
1	2	2	515	2,7	0,314
5	3	2	489	2,7	0,356
6	2	2	493	2,6	0,292
7	4	2	499	2,7	0,496

Table 3.2. Ultimate plate deflection when cooling after re-heating at 150°C. Both, numerical and measured deflections are at room temperature

Test number	measured deflection [mm]	numerical deflection [mm]	Error [%]
2	12,8	13,0	1,79
5	15,0	14,8	1,27
6	12,7	12,9	1,09

CHAPITRE 4

NUMERICAL ANALYSIS OF CURE TEMPERATURE AND INTERNAL STRESSES IN THIN AND THICK RTM PARTS

Présentation du chapitre

En complément au travail présenté dans le chapitre précédent, le chapitre 4 porte sur l'étude des changements thermiques et rhéologiques pendant et après la cuisson des pièces minces et épaisses. Cette recherche s'intéresse à la prédiction des contraintes résiduelles et de la déformation de pièces composites lors de la mise en forme. À cette fin, une analyse thermique unidimensionnelle par différences finies est couplée avec la théorie classique des laminés. Dans le cas des pièces minces, les prédictions sont comparées avec la mesure des déformations de plaques en verre/polyester. Pour les composites épais, l'étude vise à mettre en évidence les effets sur les contraintes internes du principal paramètre de moulage, la température. Différentes stratégies de cuisson sont comparées pour une pièce de 15 *mm* d'épaisseur. Dans chacun des cas, l'évolution des contraintes internes est calculée d'une manière détaillée.

L'objectif de ce travail est de proposer et de valider un modèle numérique pour calculer les variations thermiques et rhéologiques du matériau pendant la cuisson. L'étude des pièces épaisses amène une compréhension approfondie de la relation qui existe entre les contraintes internes et la progression du front de polymérisation de la résine à travers l'épaisseur du composite. L'analyse démontre l'importance d'utiliser des températures de moulage optimisées pour améliorer la qualité des pièces fabriquées par injection sur renfort.

Numerical Analysis of Cure Temperature and Internal Stresses in Thin and Thick RTM parts

Edu Ruiz and François Trochu

Centre de Recherches Appliquées Sur les Polymères (CRASP)

Département de Génie Mécanique,

École Polytechnique de l'Université de Montréal

e-mails: eduardo.ruiz@polymtl.ca, francois.trochu@polymtl.ca

Keywords: Transfer Molding (RTM), resin cure, thermal analysis, residual stress, weaving.

Article soumis à la revue *Composites Part A*

Novembre 2003

4.1 Abstract

Resin transfer molding (RTM) is a widely used manufacturing technique of composite parts. A proper selection of processing parameters is critical to yield successful molding results and obtain a good part. Among other things, when thermoset resins are processed, the shrinkage that results from resin polymerization increases the complexity of the problem. Numerical prediction of internal stresses during composite manufacturing has three objectives: improve knowledge on the process, analyze the influence of processing parameters on the mechanical integrity of the part and validate the principles of thermal optimization. The scope of this investigation is focused on the

prediction of residual stresses and part deformation (i.e., warpage) in thin and thick composites. Material characterization is essential in the numerical analysis of the phenomena that govern the appearance of processing stresses. For this purpose, a model of reaction kinetics of the resin is presented, together with a description of mechanical properties as a function of the degree of polymerization and glass transition temperature, and a linear model predicting volume changes in glass-polyester composites. A finite difference analysis is carried out to simulate the effect of thermal and rheological changes during the processing of sample plates. Classical laminate theory is implemented to compute the internal stresses resulting from processing conditions. The processing stresses are compared for different curing strategies in the case of thick composite parts. Finally, a thermal optimization algorithm is implemented to demonstrate the advantages of optimal transient heating and cooling temperature profiles to minimize processing stresses and avoid thermal degradation of the material or composite delamination.

4.2 Introduction

As the composite industry grows, thick parts and pieces of complex shape have become more common. Composite components for structural applications require larger cross-sections. The curing of thick parts remains a challenge because of the low thermal conductivity of the composite and the high heat of reaction generated during cross-linking polymerization. The combination of low thermal conductivity and large heat source in the part during cure can lead to significant thermal gradients and temperature peaks. This in turn generates residual stresses and may result in polymer degradation. In order to improve the quality of thick composites, processing temperatures need to be controlled so that thermal gradients remain small through the thickness of the part. This means that the mold temperature must be lower for thick parts than for thin ones. Moreover, the chemorheology and cure kinetics may be considerably different from what is observed at

higher temperatures. The reinforcing fibers are not really affected during the process cycle, but the polymer matrix can shrink during cross-linking, in some cases by as much as 9% [1].

In addition to chemically induced shrinkage, thermal deformations are generated during processing. The fibers possess a small thermal expansion coefficient along their longitudinal axis that produces little deformation during resin cure. The polymer matrix has a much higher thermal expansion coefficient and hence, is more affected by temperature changes. During processing, these different thermal behaviors induce residual stresses. During the cure of fiber-reinforced composites, the residual stresses generated can have a significant effect on the part quality and on its mechanical properties, promoting warpage or initiating matrix cracks and delamination [2]. Thick parts are usually too rigid to relieve internal stresses by distortion, so matrix damage is more likely to occur in this case. The processing of thick composites at a lower temperature should reduce thermally induced residual stresses. However, a minimum temperature must be reached to initiate the cross-linking chemical reaction. At low temperature, the cure reaction takes a longer time and the number of links created may not be high enough to obtain the required mechanical properties. In the processing of composite materials by RTM (Resin Transfer Molding), the three most relevant processing parameters are curing time, temperature and pressure. A judicious choice of these three parameters will produce a material which is fully cured, well compacted and of high quality.

As depicted in Figure 4.1, a number of surface and structural defects may appear in the processing of composite parts by RTM. Non-appropriate processing parameters result in typical problems such as bad surface appearance, waviness, warpage or spring-in, matrix degradation or delamination. The influence of processing parameters on these defects may be experimentally studied by rule-based heuristic expert systems or by numerical analysis of the physical phenomena involved during composite processing [1, 5-10]. Heuristic methods are interesting because they seem at first to be faster in terms of computer time

and do not require detailed material characterization. However, the results strongly depend on the knowledge of the expert and it is difficult to assess the level of optimization reached. Thanks to a better understanding of material behavior during processing, numerical analysis is increasingly used in process optimization. However, the implementation of computational methods is limited by the wide requirements in terms of material characterization. In addition, the results of numerical simulations depend on the quality of experimental data, i.e., on the repeatability of the experiments carried out to characterize a specific material property. The property investigated can only be studied on a given experimental domain, which restricts the space available for numerical analysis and optimization. Then, for process optimization the global problems to be studied need to be defined, the requirements of material characterization stated and finally, comprehensive objective functions must be developed to reflect the complexity of the composite processing.

In reference to material characterization, prediction of reaction kinetics is a key element in the processing of thermosetting materials. The reaction kinetics of epoxy and polyester resins has been widely investigated by several authors [2,4,11-17]. Calorimetric studies have been performed and kinetic models are based primarily on the autocatalytic assumption. Yousefi-Moshirabad [16] has determined the dependence of kinetic parameters on temperature, as well as the influence of low curing temperature on gel time and final degree of polymerization. Recently, a methodology was established by Ruiz and Trochu [14] to determine the parameters of several kinetic models using genetic algorithms.

The evolution of mechanical properties during resin cure is another issue that limits the scope of numerical predictions of processing stresses. Many investigators in the past have assumed that the mechanical properties of the composite are elastic and vary linearly with the degree of polymerization of the matrix [19-21]. Although this method is the simplest way to compute internal stresses during processing, viscoelastic effects and glass

transition of the resin limit the accuracy of calculations. Viscoelastic modeling [5,8-10,14] is well suited for material characterization of relaxation and glass transition effects. Nevertheless, the requirement of time integrals and close loop iterations make these models difficult to implement in numerical optimization schemes, which require a large number of iterative calculations. Another possibility, still accurate and without requiring excessive computational time, consists of modeling mechanical properties in their unrelaxed and fully relaxed stages [14], where a function of the glass transition temperature describes the phase transformation.

The purpose of this paper is to show how a numerical model of through-thickness heat transfer can assist in finding optimal temperature cycles. Firstly the physical phenomena that govern curing are presented together with the thermal equation that models the heat exchanged between the part and its surrounding. Then models of volume changes and of material behavior during composite processing are presented. Both models depend on fiber volume fractions, temperature and degree of polymerization. A methodology based on Classical Laminated Plate Theory (CLT) is developed to predict residual stresses during the cure of composite laminates. The thermo-chemical model predicts the temperature and degree of polymerization through the thickness of the part. The mechanical model based on CLT evaluates the through-thickness strain and stresses as a function of the thermo-chemical evolution of the material. On one hand, differential dilatation of the plies generates thermal stresses. On the other hand, differences in the polymerization degree result in a non-uniform shrinkage of the polymer matrix and create residual stresses of chemical origin.

Thanks to these thermo-chemical and mechanical models, processing stresses can be computed and compared for three different curing strategies through the thickness of the composite laminate: *outside-to-inside* cure, *inside-to-outside* cure and *one-side* cure. Firstly, the curing and cooling of *asymmetrical thin* laminates is investigated. Predictions of warpage for a series of thin plate samples have been validated experimentally. Then the

analysis of processing stresses is carried out for thick composite plates. The advantage and drawbacks of three possible curing scenarios are compared and the best heating strategy is identified. Finally, a thermal optimization algorithm illustrates the gains of optimized heating and cooling temperature profiles in time to minimize processing stresses and avoid material thermal degradation or composite delamination.

4.3 Thermo-mechanical analysis

In a non-isothermal RTM injection, the mold is typically at a higher temperature than the resin and fibers. The heat exchanged between the preform, the resin and the mold walls during resin injection produces temperature variations in the part. Sometimes, curing is affected by the heat transfer in the cavity during the filling stage. However, when thermal effects during filling have little influence on the initial polymerization degree of the resin, it is possible to decouple filling and curing as two distinct stages of the manufacturing process. In order to verify if the chemical reaction can be neglected during mold filling, an adimensional number called the gelling ratio (Ge) is used. This number relates the time required to fill up the mold (*injection time*) with the time needed to cure the part (*reaction time*). For a small gelling ratio, it is possible to decouple the curing process from the filling stage. In the case of polyester based resin systems, the free radicals generated are initially deactivated by reacting with an inhibitor, so the gelling number can be defined as the ratio of the filling time (t_f) over the inhibition time (t_{in}) at mold temperature. From this definition, a gelling ratio smaller than unity means that the curing process can be decoupled from mold filling, which is the case assumed in this investigation.

$$Ge = \frac{\text{injection time}}{\text{reaction time}} = \frac{\text{filling time}}{\text{inhibition time}} = \frac{t_f}{t_{in}} < 1 \quad (4.1)$$

4.3.1 Heat transfer equation

In the present work the resin cure is analyzed through the thickness of the composite. An instantaneous equilibrium temperature is assumed to exist between the resin and the fibers at each time. This corresponds to the lumped approach of Lin et al. [3]. The transient absolute temperature $T(z,t)$ at position z and time t , through the total part thickness H is given by the one-dimensional Fourier's heat conduction equation :

$$\tilde{\rho} \tilde{C}_p \frac{\partial T}{\partial t} = \tilde{k} \frac{\partial^2 T}{\partial z^2} + Q \quad 0 \leq z \leq H \quad (4.2)$$

where the density $\tilde{\rho}$, heat capacity \tilde{C}_p and conductivity \tilde{k} of the composite are defined as the effective properties obtained by the rule of mixture [3]:

$$\begin{aligned} \tilde{C}_p &= C_{p_r} w_r + C_{p_f} w_f, & \tilde{\rho} &= \frac{\rho_r \rho_f}{\rho_r w_r + \rho_f w_f} \\ \tilde{k} &= \frac{k_r k_f}{k_r w_r + k_f w_f}, & w_r &= \frac{\phi / \rho_f}{\left(\phi / \rho_f + 1 - \phi / \rho_r \right)} \\ & & w_f &= 1 - w_r \end{aligned}$$

In the above equations ϕ is the porosity and w_r, w_f denote the weight fractions of resin and fibers, respectively. The subscript f stands for the fibers and r for the resin. The source term Q represents the instantaneous heat generated by the cross-linking polymerization of the resin. This term is assumed to be proportional to the reaction rate.

4.3.2 Chemical reaction

Resin cure is modeled by an empirical autocatalytic kinetic equation that describes free-radical polymerization. Let α denote the degree of polymerization, i.e., the ratio of the instantaneous heat released by the reaction to the ultimate heat of reaction. The rate of conversion $d\alpha/dt$ is given by the following equations [12]:

$$\frac{d\alpha}{dt} = K_1(T) \cdot K_2(\alpha) \cdot K_3(T, \alpha) \cdot K_4(I_d) \quad (4.3)$$

$$K_1(T) = k_{ref} \cdot \exp \left[-A \cdot \left(\frac{T_{ref}}{T} - 1 \right) \right] \quad K_2(\alpha) = \sum_{i=0}^m a_i \cdot \alpha^i \quad (4.4)$$

$$K_3(T, \alpha) = (\alpha_{max} - \alpha)^n$$

The term $K_1(T)$ is an Arrhenius factor that depends on temperature. Function $K_2(\alpha)$ is a fit with a polynomial of degree m . Function $K_3(T, \alpha)$ accounts for the maximum degree of polymerization α_{max} that depends on temperature. Finally, $K_4(I_d)$ is a characteristic function that models the effect of the inhibitors: $K_4(I_d) = 1$, if induction time $I_d > 0$, and $K_4(I_d) = 0$ otherwise. For the unsaturated polyester resin used in this investigation (T580-63 from AOC), kinetic measurements were performed with a DSC 910 from DuPont Instruments. An ultimate heat of reaction of 365 J/g was found when 1.5 phr of Andonox Pulcat-A peroxide was added as catalyst. Figure 4.2 compares the degree of cure in time measured by dynamic DSC measurements for different heating rates with predictions derived from the kinetic equation (4.3). The autocatalytic model seems to predict accurately the cross-linking evolution in all the cases considered.

The final resin conversion, or maximum extent of cure, depends on temperature up to a temperature high enough to provide sufficient molecular mobility so as to allow all species to react within the system [2]. The final polymerization degree is commonly

less than one for the curing temperatures typically used to process thick parts (i.e., not all polymerization links can be developed at low temperature). Note that a temperature dependent parameter α_{max} is introduced in the kinetic equation to account for the incomplete chemical reaction. By using the isoconversion methodology proposed by Atarsia and Boukhili [4] to convert dynamic DSC tests for a series of constant heating ramps to isothermal results, the maximum cure degree can be derived from dynamic DSC data and modeled as a polynomial function of temperature of degree N :

$$\alpha_{max} = \sum_{i=0}^N f_i \cdot T^i \quad \text{with } T \text{ in } ^\circ\text{C} \quad (4.5)$$

Figure 4.3 shows the maximum degree of polymerization attained as a function of cure temperature for the AOC resin.

4.3.3 Induction time

In polyester-based formulations, inhibitors are placed in resin systems to increase shelf-life. They combine with the free radicals that initiate polyester-styrene cross-linking. Inhibition agents in the resin system increase significantly the curing time. While these inhibitors disappear quickly at high curing temperatures, the kinetics of the inhibitor deactivation can be very slow at the lower temperatures required to successfully cure thick parts. Assuming that the polyester-styrene linkage begins only when the inhibitor concentration reaches zero, the induction time $I_d(T, t)$ required to initiate the chemical reaction can be represented by a time integral of the thermal history [13].

$$I_d(T, t) = t_{ref} - \int_0^t \exp\left(-C_{ind} \cdot \left(\frac{T_{ind}}{T} - 1\right)\right) \cdot dt, \quad K_d(I_d) = \begin{cases} = 0 & \text{if } I_d > 0 \\ = 1 & \text{if } I_d \leq 0 \end{cases} \quad (4.6)$$

where t_{ref} , C_{ind} and T_{ind} are fitting coefficients called respectively reference time, induction constant and induction reference temperature. The weight function $K_4(I_d)$ of equation (4.3) is then set to 1 when the induction time is zero. Measured versus predicted induction times are compared in Figure 4.3 for a wide range of curing temperatures for the AOC resin T580-63. Note that for low processing temperatures (i.e., less than 60 °C), larger induction periods (around 20 minutes) are required before polymerization begins. The ultimate polymerization degree may not be greater than 40%. As recommended by the resin manufacturer, composite parts made with this resin system should be processed in the range of 90 to 120 °C in order to decrease the processing time and reach an adequate level of polymerization.

4.3.4 Thermo-chemical dependencies of mechanical properties

The need to predict accurately the intrinsic behavior of the material and the properties of the final part is crucial to assess quality and control the manufacturing process. In a similar way, much like thermo-kinetic properties, the mechanical properties of the resin vary as the part cures. Some authors [5-7] have reported a linear correlation between the mechanical properties and the degree of polymerization for different thermosetting polymers. In this work, mechanical properties were measured with a dynamic mechanical analyzer (DTMA 2980 from TA Instruments) as a function of temperature and degree of polymerization. It was found that long after the gel point, the resin elastic modulus is still very low (below 10 MPa) for a polymerization degree less than 40%. This polymerization degree, called *After Gel Point* (AGP) [14], was then taken as base line to analyze the evolution of mechanical properties for higher polymerization levels. Resin samples cured until the AGP stage were mechanically tested with the DMA during a specified curing cycle. As shown in Figure 4.4, the elastic modulus has an initial value defined at AGP (E'_{agp}) and then increases, until it reaches a maximum considered as the fully cured modulus (E'_c) for 97% of total resin polymerization.

Figure 4.5 depicts a non-linear correlation between Young's modulus and the polymerization degree. This relationship was modeled by introducing hyperbolic cosine laws that properly describe the temperature dependence of the elastic moduli of the AGP and fully cured resin (see equations below) and two functions to account for the dependency on the polymerization degree ($F_r(\alpha)$) and glass transition temperature ($W_r(T_g)$) [14]:

$$E_r(T, \alpha) = E_{agp}(T) + [E_c(T) - E_{agp}(T)] \cdot F_r(\alpha) \cdot W_r(T_g) \quad (4.7)$$

$$E_c(T) = \frac{E'_c}{\cosh(a_1 \cdot T)^{b_1}} \quad E_{agp}(T) = \frac{E'_{agp}}{\cosh(a_2 \cdot T)^{b_2}} \quad (4.8)$$

$$F_r(\alpha) = c \cdot \exp(d \cdot \hat{\alpha}) + e \cdot \hat{\alpha} \quad \hat{\alpha} = \frac{\alpha - \alpha_{agp}}{\alpha_{ult} - \alpha_{agp}} \quad (4.9)$$

$$W_r(T_g) = h \cdot \exp\left(\frac{T_g(\alpha) - T}{T_g(\alpha) - T_{ref}}\right) \quad T_g(\alpha) = a_g \cdot \exp\left(\frac{-b_g}{1 - \hat{\alpha}}\right)^{-1} \quad (4.10)$$

The expression $F_r(\alpha)$ is as the sum of a linear plus an exponential function of the polymerization degree that can be estimated from the curve of Figure 4.5. A convenient rule of mixtures ($\hat{\alpha}$) is used here in order to approximate the variations of material properties between the AGP level (α_{agp}) and the cure degree for which E' reaches its ultimate value (for $\alpha_{ult} \approx 97\%$). Furthermore, the model presented accounts for the glass transition temperature dependence of the resin elastic modulus by a temperature shift factor ($W_r(T_g)$). This factor considers the transition to complete viscoelastic relaxation at vitrification (or when the material is in a rubbery state, i.e., when $T \geq T_g$). Constants a , b , c , d and e of equations (4.7) to (4.10) were obtained by implementing a Genetic Algorithms Search Engine that properly fit the models to the measured data. Subscripts r , c , g and agp of these constants denote respectively resin, composite, glass transition

and after gel point. Figure 4.6 shows the temperature shift factor of fully relaxed coefficients for polymerization degrees above AGP. Glass transition temperatures are also depicted in the same graphic, showing that the initial glass transition T_g^0 stands around 55 degrees Celsius, while the fully cured transition T_g^∞ is at about 110 °C (T_g^∞ was practically taken as the glass transition temperature for 95% of total resin conversion). Figure 4.7 shows DMA measurements of the elastic modulus for several resin specimens cured at different polymerization degrees between α_{agg} and α_{ult} . The predictions of the proposed thermo-chemical model exhibit a relatively good agreement with experimental data for all tested samples.

In the case of shear properties, two possible approaches may be used. On one hand, Levitsky and Shaffer [8] assumed the plain strain bulk modulus to be constant during cure, so that the elastic moduli and Poisson's ratio vary as the part cures. On the other hand, Bogetti and Gillespie [5] considered that Poisson's ratio remains constant during processing. They found that differences in the resin Poisson's ratio during cure have no significant influence on the properties of the macroscopic composite, on process-induced strains and on residual stresses. Both models predicted nearly identical values of elastic and shear moduli. Poisson's ratio is also expected to relax to ~ 0.5 as the thermosetting polymer approaches the rubbery state, nevertheless it was found by O'Brien et al. [9] that the effect on the shear modulus is relatively minor. According to these researchers, variations of Poisson's ratio do not play an important role. For that reason, in this investigation a constant value $\nu_r = 0.35$ was used, as measured at room temperature for a fully cured sample. The instantaneous resin shear modulus during cure is based on the classical relationship for isotropic materials:

$$G_r(T, \alpha) = \frac{E_r(T, \alpha)}{2 \cdot (1 + \nu_r)} \quad (4.11)$$

4.3.5 Composite effective mechanical properties

The effective homogeneous mechanical properties of the composite laminate are highly dependent on that of the matrix and reinforcement and on the fiber volume fraction. The thermal and mechanical properties of the reinforcement may be considered constant and independent of temperature and of the polymerization degree, while matrix properties vary during processing according to the models previously presented. Although the self-consistent micro-mechanical model of Whitney [10] was initially used to determine reinforcement properties, over-predictions were found at temperatures close to the matrix glass transition. Empirical models were then implemented to estimate the composite elastic modulus $E_{comp}^{1,2}$ as a function of temperature T and fiber volume fractions V_f in the two principal fiber directions :

$$E_{comp}^i = \left(\frac{V_f \cdot (E_f^i - E_r(T, \alpha))}{1 + A_i \cdot \exp(B_i \cdot T)} + E_{agp}(T) \right) \cdot \left(\frac{E_r(T, \alpha)}{E_r(T, 1)} \right) \quad \text{with } i = 1, 2; \quad (4.12)$$

where A_i and B_i are fitting constants for each material direction ($i=1,2$). Subindexes r, f and $comp$ stand for resin, fiber and composite respectively.

Two reinforcing materials have been used in this study to analyze thermal effects on processing stresses: a continuous glass random mat U101 from Vetrotex and one bi-directional balanced non-crimp glass fabric NCS 82620 from J.B. Martin. Figure 4.8 shows measurement results of Young's modulus in both directions (E_{comp}^1, E_{comp}^2) for a composite plate made with NCS-82620 bidirectional fabric ($V_f = 42\%$). For the partially and fully cured samples, the mechanical model approaches the experimental curves at temperatures close to T_g . Young modulus of composite specimens with these materials were measured and fitted by equation (4.12). As depicted in Figure 4.9, between two

and three fiber volume contents were tested for each material. Note that the rule of mixture used here may be accurate only around measured values of fiber volume content. The range of validity considered for the materials tested is presented in Figure 4.10.

4.3.6 Volume changes

Some experimental studies have been conducted to gain insight on the volumetric changes that occur during thermoset polymer processing. Hill et al. [11] measured the volume changes of unsaturated polyesters during resin cure due to variations of temperature and degree of polymerization. Hill proposed that the overall volumetric changes of a thermoset resin during cure be considered as a combination of thermal expansion or contraction and polymerization shrinkage as follows:

$$\left(\frac{1}{V_o} \frac{dV}{dt} \right)_{\text{Overall}} = \left(\frac{1}{V_o} \frac{dV}{dt} \right)_{\text{Thermal Contribution}} - \left(\frac{1}{V_o} \frac{dV}{dt} \right)_{\text{Polymerization Shrinkage}} \quad (4.13)$$

The first term on the right hand side represents the bulk thermal expansion/contraction contribution, which can be expressed by

$$\left(\frac{1}{V_o} \frac{dV}{dt} \right)_{\text{Thermal Contribution}} = \beta_{\text{gel}} \cdot \frac{dT}{dt} + [(\beta_{\text{cured}} - \beta_{\text{gel}})] \cdot \alpha \cdot \frac{dT}{dt} \quad \beta_{\text{cured}} \cdot \beta_{\text{gel}} = a_0 + b_0 \cdot T \quad (4.14)$$

where β_{gel} and β_{cured} are the coefficients of thermal expansion (CTE) of the gelled and fully cured resin, respectively. These coefficients are assumed to vary linearly with temperature, and a_0 and b_0 are the constants of the linear fitting. Equation (4.14) means that the thermal expansion or contraction is assumed to vary monotonically with the polymerization degree α . The second term on the right hand side of equation (4.13)

represents the contribution of chemical shrinkage (i.e., the volume shrinkage induced by the resin cross-linking during polymerization). Resin shrinkage was measured with a thermomechanical analyzer (TMA 2940 from TA Instruments) as a function of the degree of polymerization. As observed in Figure 4.11, the linear relationship of equation (4.15) was derived experimentally for the polyester resin tested. The total polymerization shrinkage λ_{chem} for the fully cured sample was about 7%.

$$\left(\frac{1}{V_o} \frac{dV}{dt} \right)_{\substack{\text{Polymerization} \\ \text{Shrinkage}}} = \lambda_{chem} \frac{d\alpha}{dt} \quad (4.15)$$

4.3.7 Longitudinal and transverse coefficient of thermal expansions (CTE)

The CTE of pure resin samples and composite plates were also measured with the thermo-mechanical analyzer. As presented in Figure 4.12, thermal expansions of uncured resin samples (i.e., for $\alpha = 0$), partially cured (for $\alpha = 0.45$ and 0.80) and fully cured ones have been experimentally determined. During curing, the CTE of the resin decreases nearly in proportion with the degree of polymerization. Based on this assumption, experimental data can be fitted by a bilinear function of temperature and degree of polymerization. Then, the resin CTE can be written as a rule of mixture between the uncured (*After Gel Point*) and cured CTE:

$$CTE_r(T, \alpha) = CTE_{agp}(T) \cdot (1 - \hat{\alpha}) + CTE_{cured}(T) \cdot \hat{\alpha} \quad (4.16)$$

where $\hat{\alpha}$ is the normalized degree of cure given by equation (4.9).

Composite samples of NCS 82620 and U101 reinforcements were also measured (see Figure 4.13) in the three principal directions (i.e., Longitudinal, Transverse and Through-Thickness). The model follows the rule of mixture:

$$CTE_{comp}^d = CTE_r(T, \alpha) \cdot (1 - V_f) + CTE_{fibre}^d \cdot V_f \quad \text{where } d = L, T, \text{ and } T-T \quad (4.17)$$

4.3.8 Strain-stress modeling

The present analysis assumes that the Classical Laminated Theory (CLT) is applicable to the infinitesimal region of a composite unit cell. By introducing the expressions of thermo-chemically dependent mechanical properties into the CLT formulation, we get for thermal and chemical loadings:

$$\{\sigma_j\}_t = \int_{t(AGP)}^t [C_j]_t \cdot \left\{ \frac{\partial \varepsilon_j}{\partial t} \right\} \cdot dt, \quad \text{for } j=1 \text{ to } N \text{ plies} \quad (4.18)$$

where the strain vector is defined as:

$$\varepsilon_j = \varepsilon_j^{Thermal} + \varepsilon_j^{chem}, \quad \varepsilon_j^{chem} = \sqrt[3]{1 + (\lambda_{chem} \cdot \alpha)} - 1$$

Here ε_j^{chem} is the incremental isotropic shrinkage strain defined by Bogetti and Gillespie [5]. In order to account for the potentially nonlinear behavior of the material, the stiffness matrix $[C_j]$ (that depends of the composite temperature and resin degree of cure) must be calculated at each processing time. In this way, $[C_j]$ is the algebraic average of $[C_j]_t$ and $[C_j]_{t+dt}$. A step-by-step computational method has been used to predict the thermo-chemical response of the laminate during processing. For each calculation step, planar stresses and out-of-plane curvatures are computed from the strains induced by thermal gradients and chemical changes in the composite.

4.4 Analysis of thin composite plate cooling

The properties and durability of composite parts manufactured with thermoset polymers are strongly affected by internal stresses. The source of internal stresses depends on material properties and processing conditions. These processing stresses are most commonly created during composite manufacturing as a result of thermal and mechanical differences of behavior between the phases of the constitutive materials. Internal stresses may lead to defects in the part in the form of voids and micro-cracking during processing, or warpage, spring-in, premature delamination or debonding after manufacture.

In order to identify defects caused by internal stresses during cooling, a total of sixteen 3 mm thick composite plates of 50 cm by 10 cm were molded using several combinations of NCS-82620 fabric and U101 mat. As shown in Figure 4.14, NCS and U101 plies were asymmetrically layered. The samples contained between two and six plies of NCS 82620 fabric together with two plies of U101 mat. The thickness of the plates was measured at ten locations and averaged. The stacking sequence, length and thickness of eight samples are reported in Table 4.1. The thickness of the plates after manufacture varies between 2.6 and 2.8 mm with an average of 2.7 mm.

Differences in the linear CTE and mechanical properties of each ply obviously generate warpage in molded plates. Thermocouples were embedded between plies to measure through-thickness temperature profiles during processing. As depicted in Figure 4.15, the warpage of plates cured at 120 °C resulted in a curved shape along the longitudinal and transverse directions. Because of the existence of a transverse curvature, one single measurement in the centre is not enough to estimate the longitudinal curvature. For each material combination, the longitudinal deflections of the plate samples after manufacture were measured using a Linear Variable Displacement Transducer (LVDT)

at several locations on the middle axis of the samples. The longitudinal plate curvature was then estimated from these measures along the sample length. As presented in Table 4.1, the longitudinal curvature of the samples after demolding varied for the different material combinations tested. While for test #2 (2 plies of U101 and 2 of NCS 82620) a curvature of 0.292 m^{-1} was obtained, for test #5 (2 plies of U101 and 5 of NCS 82620) a curvature of 0.506 m^{-1} was measured.

Special care must be taken in the specimen preparation, mainly due to surface density variations of the U101 mat. Non-uniform surface density of the mat results in variable plate thickness after curing, so the assumption of cylindrical deflection may not correctly predict the experimental values. After demolding, a number of plates were reheated and maintained during 20 minutes at $150\text{ }^{\circ}\text{C}$, which is above their glass transition temperatures, so as to allow relaxation of the matrix. Once processing and demolding stresses have relaxed, the flat plates were cooled to room temperature. As illustrated in Figure 4.16, temperatures at different thickness and length positions were recorded during cooling. The bottom, mid-plane and top temperatures decreased uniformly enough to neglect transverse thermal effects. A Linear Variable Displacement Transducer (LVDT) was placed to measure the deflection of the plates at the gravity center. While sample temperature decreases, the deflection in the center increases from 5 to 17 mm.

The measured temperatures were then used as thermal boundary conditions for the thermo-mechanical model. The deflection of the specimens was calculated by solving iteratively equations (4.2), (4.12), (4.17) and (4.18). The results of the proposed model are compared to experimental values in Figure 4.17. A minimum of three measures were carried out for each plate to analyze the dispersion of the experiments. A comparison for two specimens is presented that shows a good agreement between predictions of the thermo-mechanical model and measured deflections. Based on the same procedure, the deflections of all plates were measured in time. The deflections

measured at the end of cooling are compared with calculated values in Table 4.2. A review of the results for the five plates tested shows an error of less than 2%. These tests on thin plates provide an experimental validation of the proposed thermo-mechanical model. Excellent predictions were obtained for residual stresses of thermal origin on non balanced plates.

4.5 Analysis and optimization of thick plate processing

The processing of thermosetting matrix composites creates internal stresses during resin cure due to the volume mismatch between composite plies. As well as thermally induced deformations, chemically induced shrinkage occurs also during composite processing. These deformations generate residual stresses in the composite. To study processing defects in thick composites, 15 mm thick plates were cured at different mold temperatures. As shown in Figure 4.18, processing thick plates at mold temperatures normally used for thin plates results in important residual stresses, which in some cases were high enough to cause matrix cracking and composite delamination. To avoid these defects, lower curing temperatures are required for thick composites.

The progression of the curing front through the thickness is another important issue connected with the development of internal stresses. Figure 4.19 illustrates three basic scenarios that commonly appear when curing thick parts [15]: *inside-to-outside*, *outside-to-inside* and *one-side* curing. To study these curing scenarios, numerical simulations were carried out for a 15 mm thick plate made of NCS-82620 fabric with 48% fiber volume fraction and AOC polyester resin matrix. Figures 4.20 to 4.29 present the computational values of temperature, degree of polymerization, Young's modulus E' and internal stresses for these three scenarios.

4.5.1 *Outside-to-Inside* cure

In the first case, when curing progresses from the outward surfaces towards the middle (*outside-to-inside* cure), the surfaces gel and vitrify before the core. When the gelled material at the core cures and shrinks, the already rigid surfaces resist the deformation, hence producing high internal stresses and promoting void formation or possible composite delamination in the center. This is the case when thick parts are cured at temperatures typically used for thin plates. Figure 4.20 displays numerical calculations of temperature and Young's modulus E' when processing the 15 mm thick composite plates at a mold temperature of 120 °C. Heating at this temperature results in an *outside-to-inside* cure. The evolution of the degree of polymerization at different locations through the thickness of the sample is plotted in Figure 4.21. Point A shows that the surface reaches the AGP polymerization level prior to the core. Point B shows a fast curing in the center occurring when the surfaces are already cured. Internal stresses calculated along the longitudinal X-axis are plotted in Figure 4.22 for this curing scenario. Stresses mainly developed during the curing phase, between 10 and 11 minutes. Although mechanical properties at that time just begin their evolution, resin polymerization shrinkage is important enough to create high stresses in the part. Figure 4.23 displays the strain calculated through the thickness of the part at different times around AGP. At about 10.7 minutes, fast curing of the core generates high chemical strain gradients that result in growing internal stresses, called curing stresses. At this stage, these stresses can become critical and cause matrix cracking and delamination, because of the low tensile strength of the partially cured resin.

The *outside-to-inside* cure generates high exothermic temperature peaks produced by the fast curing of the core, due to the high resin reactivity and low thermal conductivity of the composite. During cooling of the part from the exothermic peak to room temperature, internal stresses, also called cooling stresses, continue to develop due to through-thickness thermal gradients. Consequently, because of all the disadvantages of

outside-to-inside cure, high temperature processing of thick composite parts must absolutely be avoided.

4.5.2 *Inside-to-Outside* cure

In the second curing scenario, when the cure front progresses from the middle thickness towards the surfaces of the part (*inside-to-outside* cure), the core gels and vitrifies before the exterior surface. A solid core surrounded by a gelled material is created. As the rigid core continues to cure inside the gelled material, minimal internal stresses are generated at the interface. This progression of the cure front can be achieved by processing the 15 mm thick part at a lower temperature, as presented in the analysis of Figures 4.24 and 4.25. In Figure 4.24, numerical values of through-thickness temperatures and degrees of polymerization are depicted for a 70 °C processing temperature. Exothermic temperature peaks are much reduced in this case. The internal stresses calculated for this curing scenario are shown in Figure 4.25. In this case, processing stresses are inverted compared to the *outside-to-inside* cure. In the *inside-to-outside* cure strategy, compression stresses appear in the core and tensile stresses at the surface. The quarter thickness shows nearly no stress, but it is surrounded by two inverted states of stresses. So shear stresses will then appear at this position inside the composite. Although this cure scenario presents many interesting features concerning reduction of internal stresses, two main disadvantages must be noticed: longer processing times are required to successfully cure the composite and low mechanical properties result from an incomplete resin cure. Note that this latter disadvantage, however, can be overcome with a post cure.

4.5.3 *One-side* cure

For the above reasons, another processing strategy is worth considering: it consists of having the curing front move from one surface of the part to the opposite one. In such a

one-side cure strategy, the generation of processing stresses can be explained by simulating the displacement of the curing front through a gelled material. A *one-side* cure progression can be achieved when processing the 15 mm thick composite at different temperatures on the upper and lower mold surfaces. Simulation results are presented in Figures 4.26 and 4.27 for mold temperatures of 70 °C and 90 °C on the top and bottom surfaces respectively. The temperature profiles of Figure 4.26 show that curing temperature can be higher without increasing so much the exothermic peak. This results in a significant diminution of the curing time. The internal stresses calculated for this processing strategy are drawn in Figure 4.27. The major disadvantage of the *one-side* cure strategy is the unsymmetrical pattern of residual stresses generated that can lead to deformations and geometric distortion of the composite part.

4.5.4 Optimization of cure cycle

Based on the understanding of the different curing strategies previously studied and on their effect on part distortion and mechanical performance, an optimized processing cycle can now be determined. In order to minimize the internal stresses generated during resin cure, ideally the degree of polymerization through the thickness should remain constant at each instant. In fact, minimizing chemically induced strain gradients between plies will result in a net diminution of curing stresses. In the same way, if through-thickness thermal gradients are minimized during cure and subsequent cooling, residual stresses will be decreased and processing defects avoided.

In this work, an optimization methodology based on genetic algorithms is implemented to determine the appropriate mold temperatures that minimize residual stresses and processing time. Figures 4.28 and 4.29 present computational results for the same 15 mm thick composite plates processed this time with optimized mold temperatures. Figure 4.28 shows numerical results of internal temperature and degree of polymerization. Initial mold overheating helps to decrease processing time while

minimizing through-thickness thermal and curing gradients. A second heating ramp is necessary to successfully cure the part up to the desired final polymerization degree, while avoiding high exothermic temperature peaks. The internal stresses calculated during the optimized cure cycle are drawn in Figure 4.29 and illustrate how curing and cooling stresses are significantly reduced by this approach. These results demonstrate that numerical optimization of the thermal boundary condition can be a useful tool to minimize residual stresses, and especially in the case of thick composites increase mechanical performance of the cured part while minimizing processing time.

4.6 Summary

In this paper, models are proposed to describe changes of composite mechanical properties as a function of fiber volume content, temperature and degree of polymerization of the resin. These models were used for two reinforcing materials (NCS-82620 fabric and U101 mat) embedded in a polyester resin (T580-63 from AOC). A kinetic model, including inhibition times induced by inhibitor decomposition, is also proposed to describe the resin polymerization during processing. The energy equation was solved by finite differences through the thickness of the part. The analysis of process-induced stresses in the composite is based on *Classical Laminated Theory*. Asymmetrically layered thin plates were first processed to validate the thermo-mechanical model by comparing calculated and measured plate deflections during cooling. The predictions of the model were verified with an accuracy of less than 2%. To identify processing defects in thick composites, 15 mm plates were fabricated by RTM at different mold temperatures. Processing these plates in the range of molding temperatures normally used for thin plates resulted in important residual stresses, which in some cases were high enough to cause matrix cracking and composite delamination. It was shown analytically that the progression of the curing front through the thickness of the composite is critical for the development of internal stresses.

High processing temperature produces an *outside-to-inside* progression of the curing front that leads to important internal stresses. Low temperature processing generates an *inside-to-outside* cure that prevents matrix cracking. However, mechanical properties fall due to the lower degree of polymerization achieved after cure. Different temperatures on the upper and lower mold surfaces produce a *one-side* cure that decreases processing time and improves mechanical properties. However, unsymmetrical residual stresses lead to part deformation and distortion. Finally, an optimized curing cycle obtained with genetic algorithms was used for analysis. By applying the optimized thermal boundary condition on thick parts, curing and cooling stresses can be strongly decreased. The numerical results show that thermal optimization can be a useful tool to minimize residual stresses in the processing of thick composites by RTM. Not only mechanical performance of the part is increased, but processing time is also reduced. An instrumented mold is actually under construction to validate experimentally the thermal optimization method presented in this paper for composites processed by resin transfer molding.

4.7 Acknowledgements

The authors are grateful to the *National Science and Engineering Research Council of Canada* (NSERC) and *Fonds Québécois de Recherche sur la Nature et la Technologie* (FQRNT) for their financial support. The contribution of *Auto 21* and *Ford Motor Co.* for the development of characterization molds is also gratefully acknowledged as well as the support of the *Bourses d'Excellence du Ministère de l'Éducation du Québec*. The authors would like to thank *Vetrotex* for the reinforcement samples and Nicolas Juillard from *J. B. Martin* for his constant support over the last fifteen years.

4.8 References

- [1] White S R, Hahn H T. Process Modeling of Composite Materials: Residual Stress Development during Cure. *J. of Composite Materials* 1992; 26(16):2402-2453.
- [2] Michaud D, Beris A, Dhurjati P. Curing Behavior of Thick-Sectioned RTM Composites. *J. of Composite Materials* 1998; 32(14):1273-1295.
- [3] Lin R J, Lee L J, Liou M L. Mold Filling and Curing Molding of RTM Process. *Advanced Composite Materials, Conference Proceedings, Detroit, Michigan USA, Sept. 30, 1991; pgs 165-174.*
- [4] Atarsia A, Boukhili R. Relationship Between Isothermal and Dynamic Cure of Thermosets Via the Isoconversion Representation. *Polymer Eng. Sci.* 2000; 40(3):607-620.
- [5] Bogetti T, Gillespie J. Process-Induced Stress and Deformation in Thick-Sectioned Thermoset Composite Laminates. *J. of Composite Materials* 1992; 26(5):626-660.
- [6] Golestanian H, El-Gizawy S. Cure Dependent Lamina Stiffness Matrices of Resin Transfer Molded Composite Parts with Woven Fiber Mats. *J. of Composite Materials* 1997; 31(23):2402-2423.
- [7] Osswald T A, Sun E M. Tseng, S-C. Experimental Verification on Simulating Shrinkage and Warpage of Thin Compression Moulded SMC Parts. *Polymers & Polymer Composites* 1994; 2(3):187A-198A.
- [8] Levitsky M, Shaffer B M. Thermal Stresses in Chemical Hardening Elastic Media with Application to the Molding Process. *J. of Applied Mechanics* 1974; 41:647-651.
- [9] O'Brien D J, Mather P, White S R.. Viscoelastic Properties of an Epoxy Resin during Cure. *J. of Composite Materials* 2001; 35(10):883-904.
- [10] Whitney J M. Elastic Moduli of Unidirectional Composites with Anisotropic Filaments. *J. of Composite Materials* 1967; 1:188.
- [11] Hill R, Muzumar S, Lee L. Analysis of Volumetric Changes of Unsaturated Polyester Resin During Curing. *Polymer Eng. & Sci.* 1995; 35(10):852-859.

- [12] Louchard S. Guide de mesures DSC et de calcul des modèles cinétiques de cuisson de résines thermodurcissables. Rapport de stage présenté au CRASP, Ecole Polytechnique de Montréal Sept. 2002; 73 pgs.
- [13] Sobotka V. Détermination des paramètres thermophysiques et cinétiques d'une résine polyester insaturée. Rapport de stage présenté au CRASP, Ecole Polytechnique de Montréal Sept. 2001 ; 75 pgs.
- [14] Ruiz E, Trochu F. Thermal and Mechanical Properties during Cure of Glass-Polyester RTM Composites: Elastic vs. Viscoelastic Modeling. Submitted to J. of Composite Materials, March 2003; 38 pgs.
- [15] Tutorial on Polymer Composite Molding from Michigan State University. <http://islnotes.cps.msu.edu/trp/intro.html> (web page consulted 2002-05-12).
- [16] Yousefi-Moshirabad A. Cure Analysis of Promoted Polyester and Vinylester Reinforced Composites and Heat Transfer in RTM Molds. PhD. Thesis, Dep. of Chemical Eng. École Polytechnique de Montréal, April 1996.
- [17] Han C D, Lem K-W. Chemorheology of Thermosetting Resins. I. Chemorheology and Cure Kinetics of Unsaturated Polyester Resin. J. of Applied Polymer Sci. 1983; 28:3155-3183.
- [18] Ramis X, Cadenato A, Morancho J M, Salla J M. Curing of a thermosetting powder coating by means of DMTA, TMA and DSC. Polymer, article in press, 10/2/2003 DOI:10.1016/S0032-3861(03)00059-4.
- [19] Stevenson J F. Innovation in Polymer Processing: Molding, Compression Molding. S.L.:l'auteur, 1996; 600 p. ISBN 3-446-17433-8.
- [20] Yi S, Hilton H H. Effects of Thermo-Mechanical Properties of Composites on Viscosity, Temperature and Degree of Cure. J. of Composite Materials 1998; 32(7):600-622.
- [21] Bogetti T A, Gillespie J W. Process-Induced Stress and deformation in Thick-Section Thermoset Composite Laminate. J. of Composite Materials 1992; 26(5):626-660.

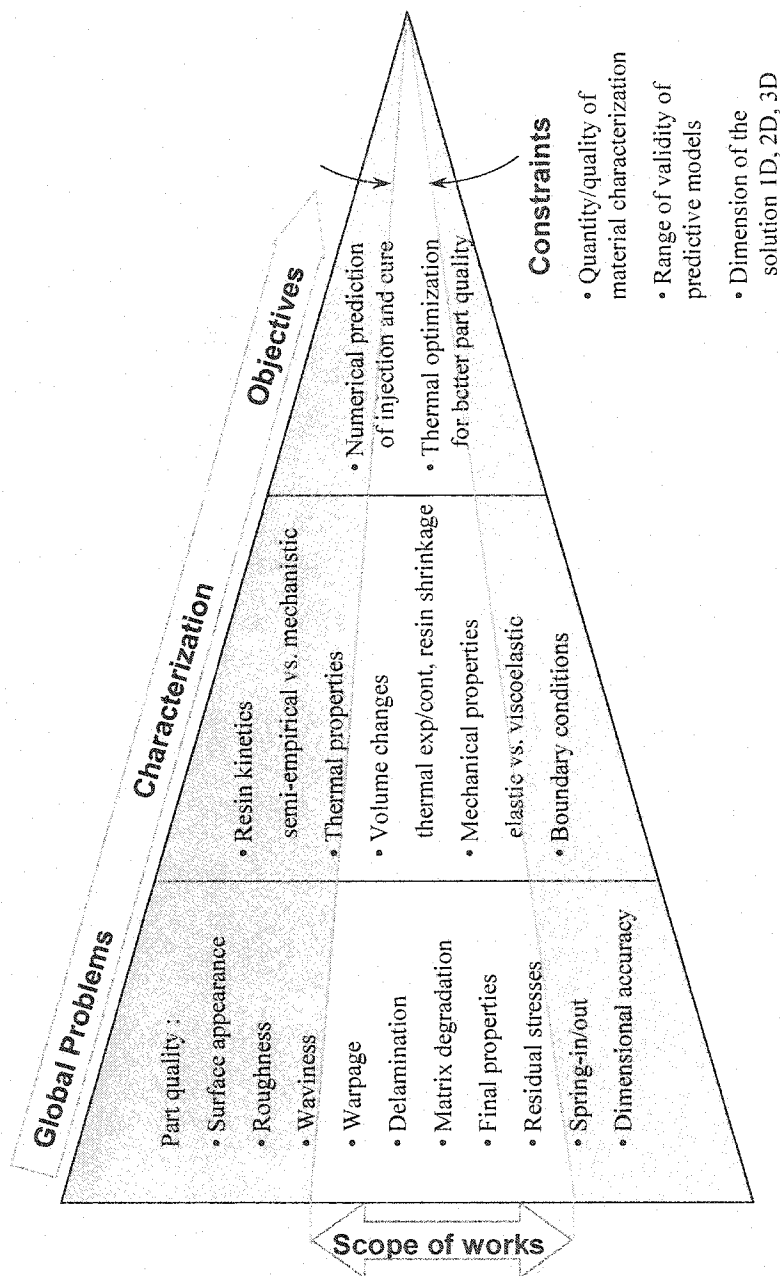


Figure 4.1. Scope of works related to part quality in RTM manufacturing. The global problems need to be defined, requirements of material characterization stated and appropriate objective functions derived for processing optimization.

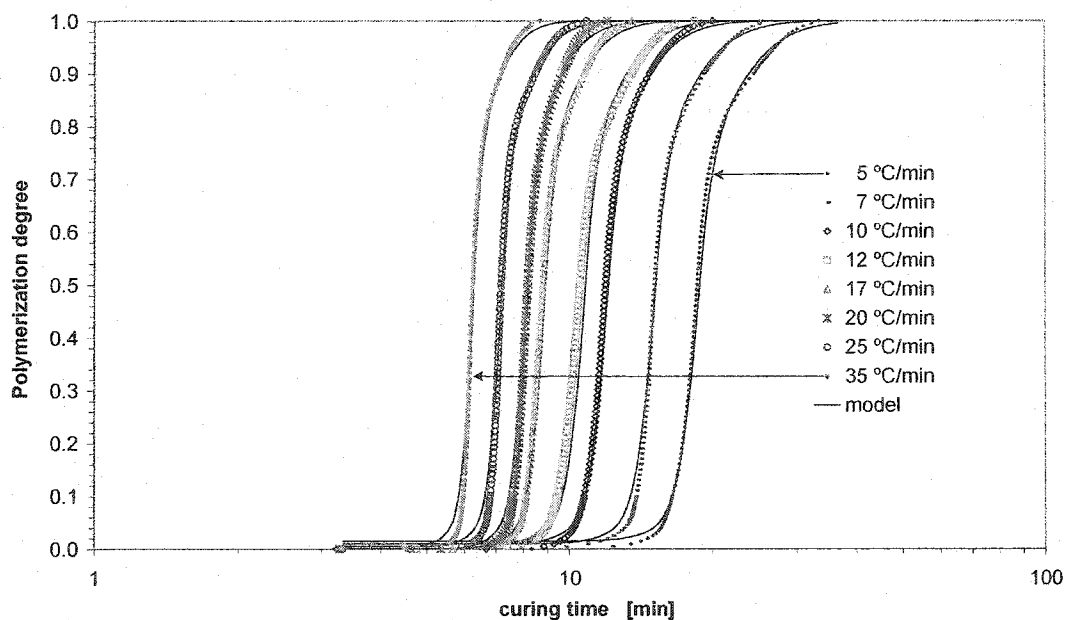


Figure 4.2. Comparison of DSC measurements of the resin degree of polymerization with predictions of the resin cure kinetics model. Heating ramps from 5 to 35°C/min are compared and shown a good agreement with model predictions.

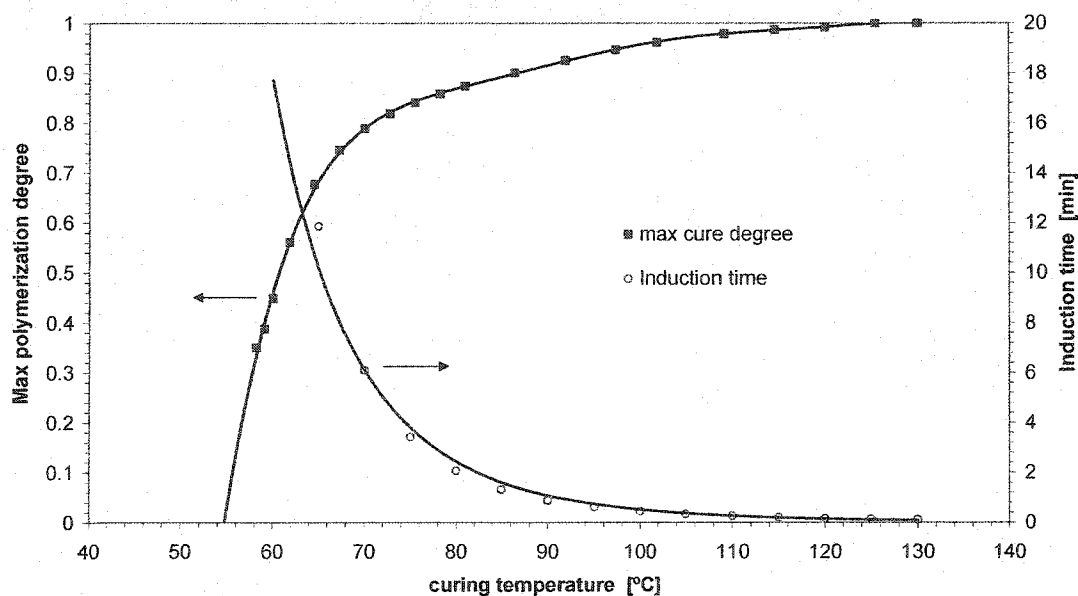


Figure 4.3. Curves of resin maximum degree of polymerization and induction time as a function of curing temperature. These results were obtained from DSC measurements data after applying the isoconversion methodology.

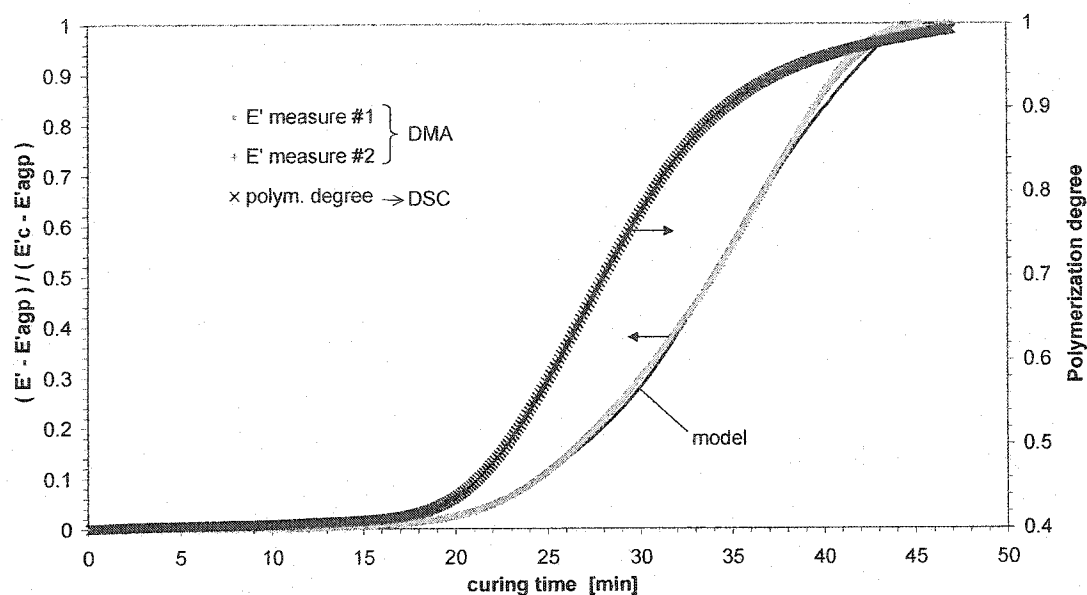


Figure 4.4. Comparison of the resin Young's modulus (E') and degree of polymerization during a specified curing cycle: E' is measured with a DMA while the degree of polymerization comes from DSC measurements.

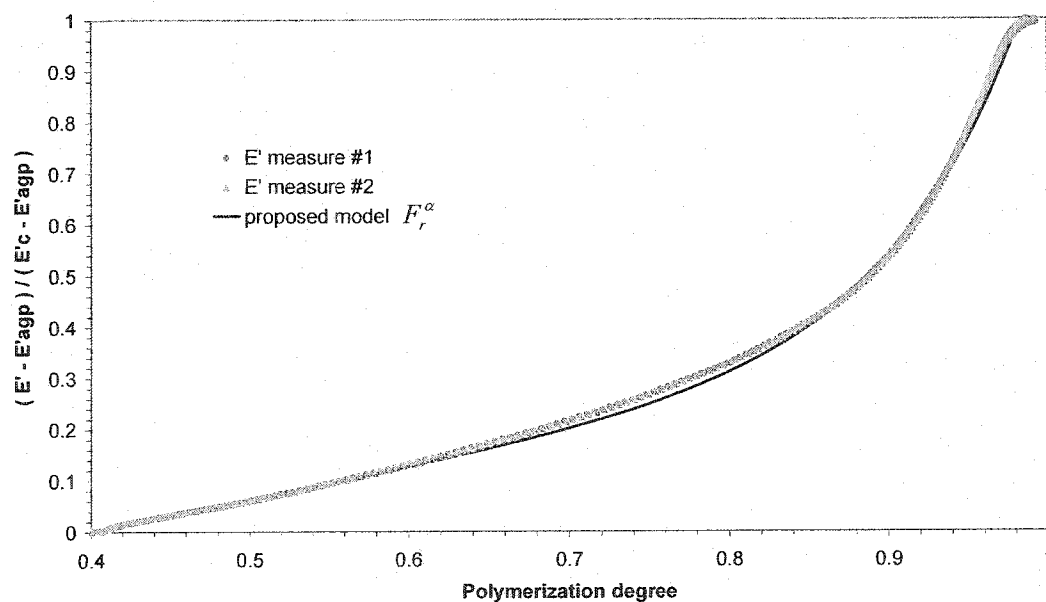


Figure 4.5. A non-linear correlation between E' and the degree of polymerization was found for the polyester resin tested. Here DMA measurements of E' are plotted as a function of degree of polymerization obtained from DSC results.

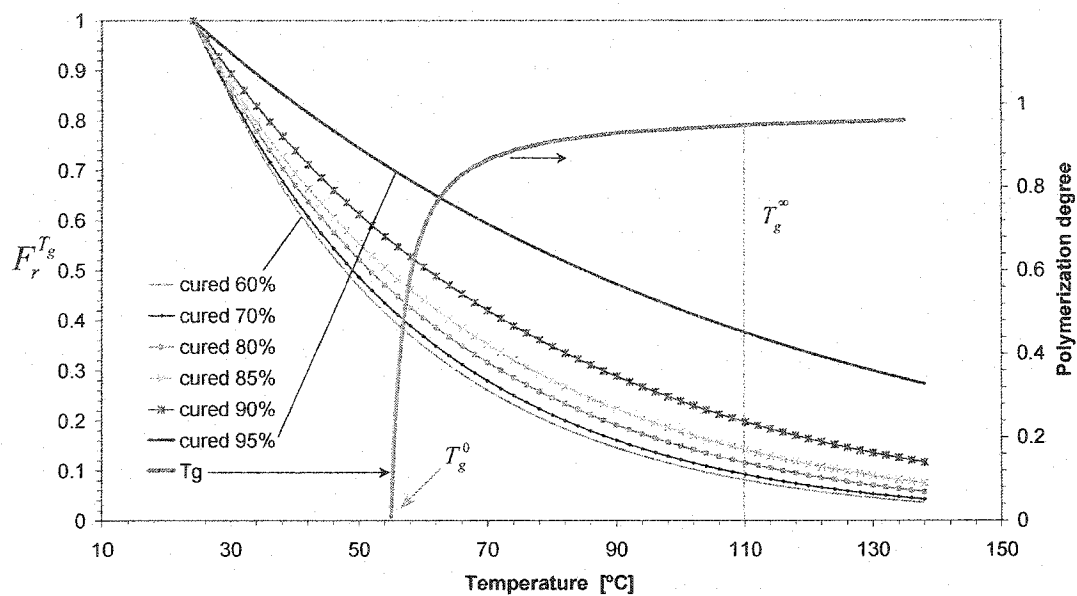


Figure 4.6. Temperature shift factor as a function of temperature for various degrees of polymerization. The glass transition temperature T_g is also drawn as a function of the degree of polymerization.

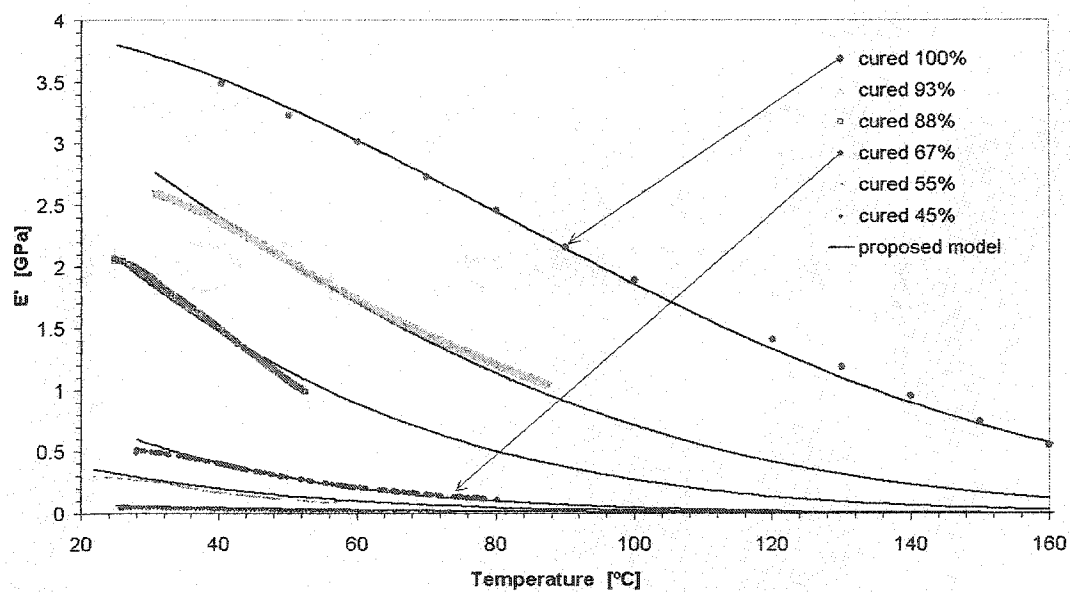


Figure 4.7. Comparison of the model predictions and DMA measures of Young's moduli E' for partially and fully cured resin samples (the lines present model predictions).

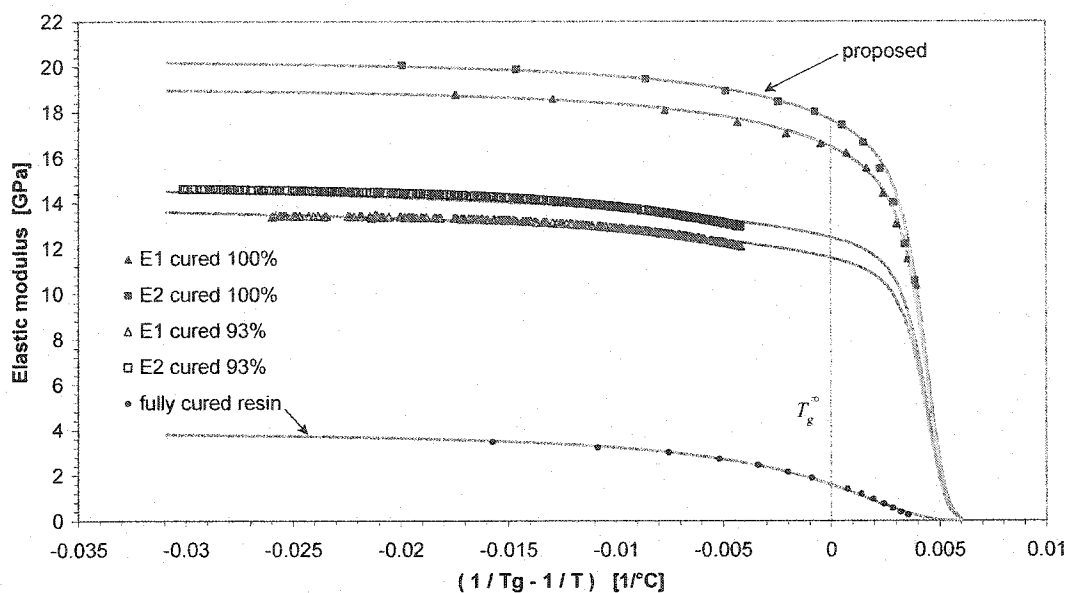


Figure 4.8. Measured and predicted Young's modulus E' in both directions for a composite with volume fraction $V_f=42\%$ of NCS-82620 (fully and partially cured samples).

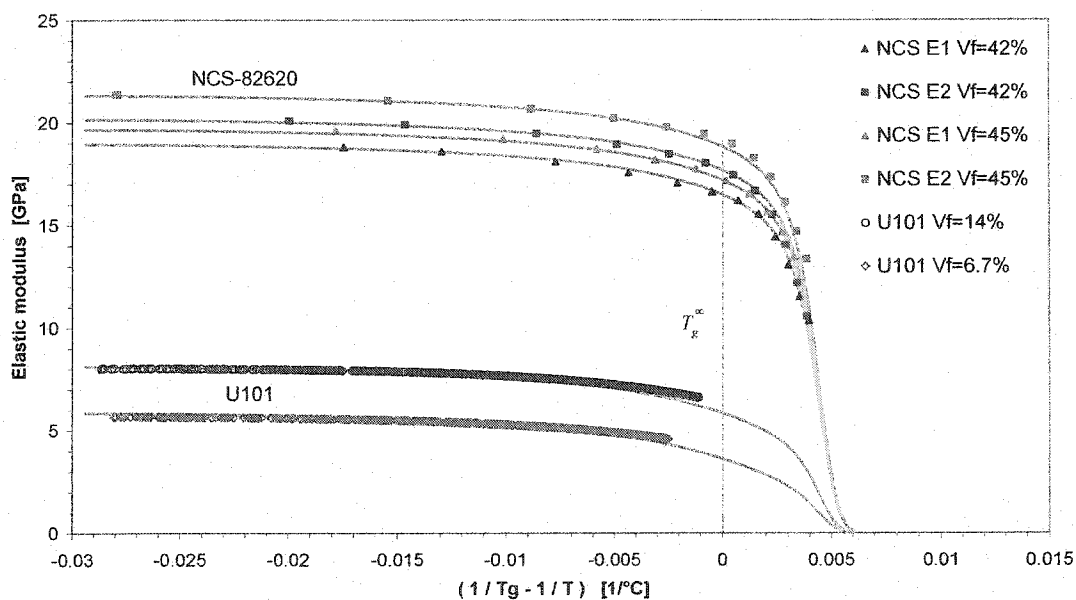


Figure 4.9. Measured and predicted E' for different fiber volume fractions V_f of fully cured composite samples made of NCS-82620 fabric and U101 mat.

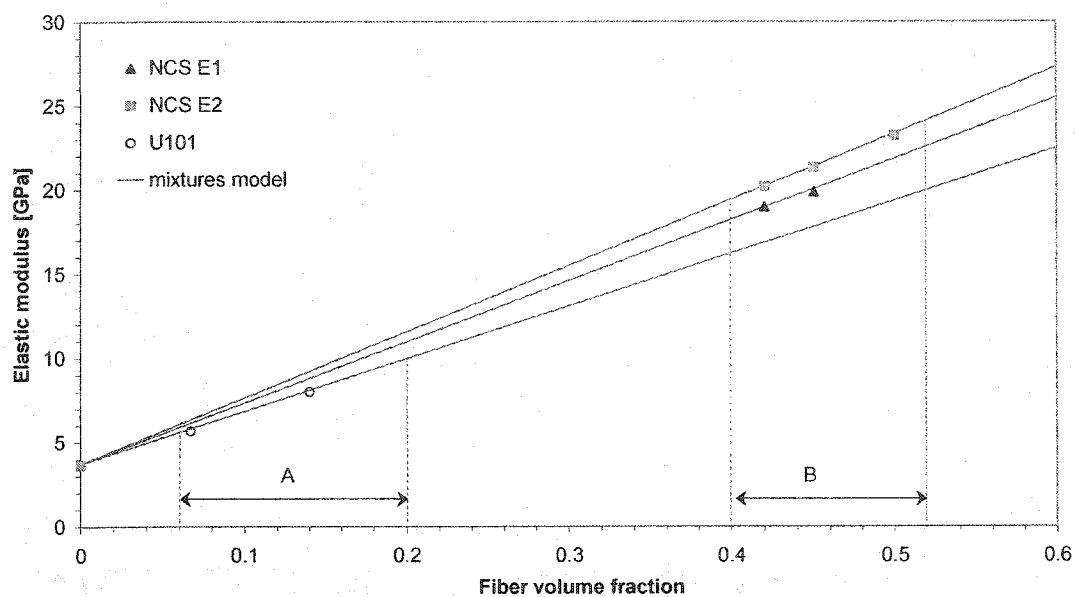


Figure 4.10. Rule of mixtures for E' as a function of fiber volume fraction V_f . Regions A and B represent the experimental domain of validity of V_f for U101 and NCS materials respectively.

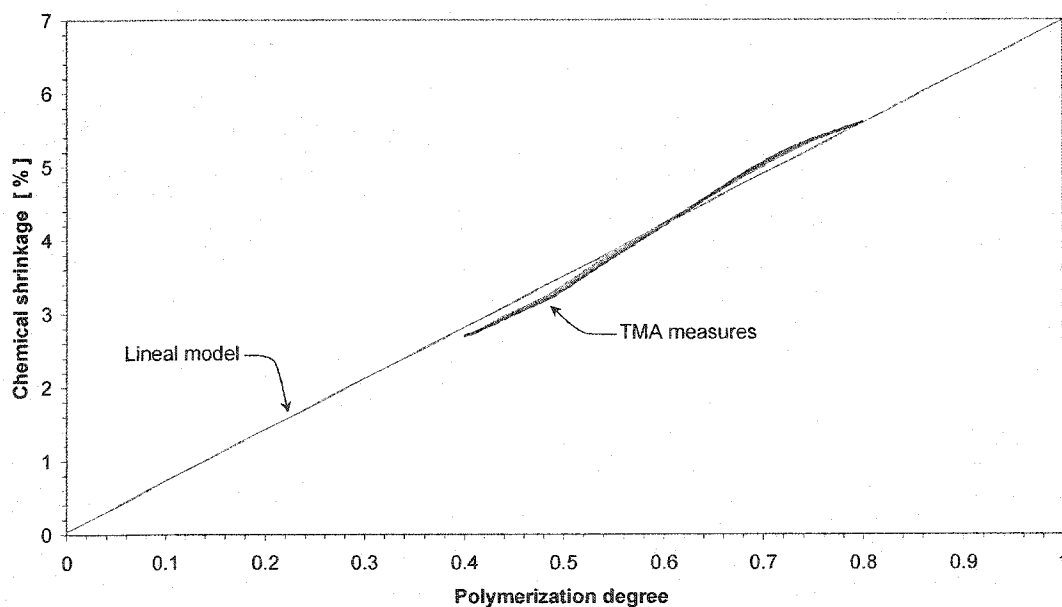


Figure 4.11. Linearization of chemical shrinkage induced by resin polymerization (TMA versus DSC measures).

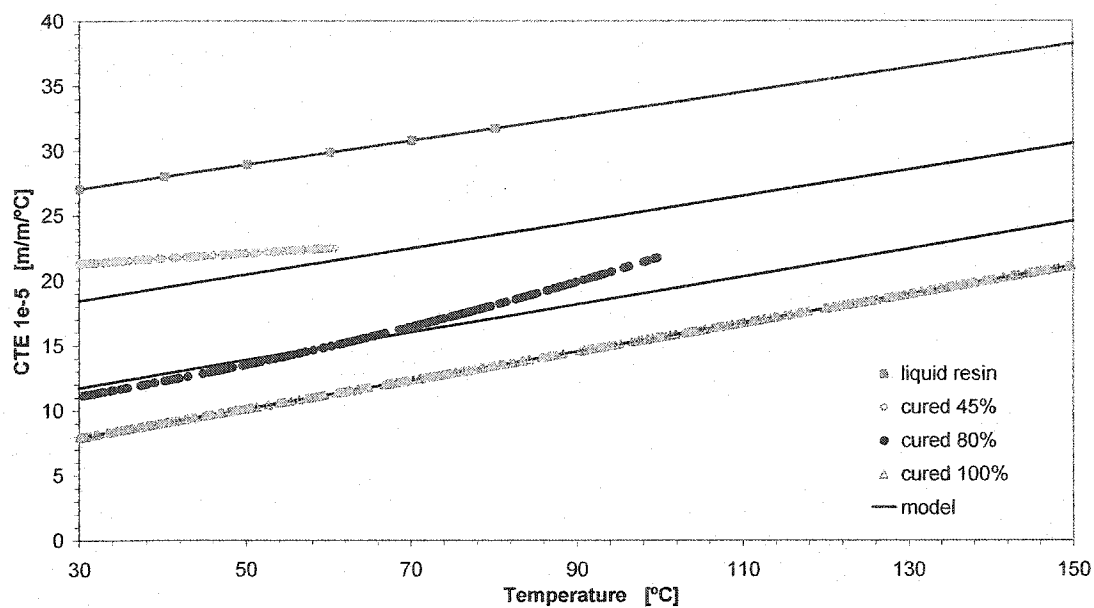


Figure 4.12. Coefficients of thermal expansion for partially and fully cured resin samples (from TMA measurements).

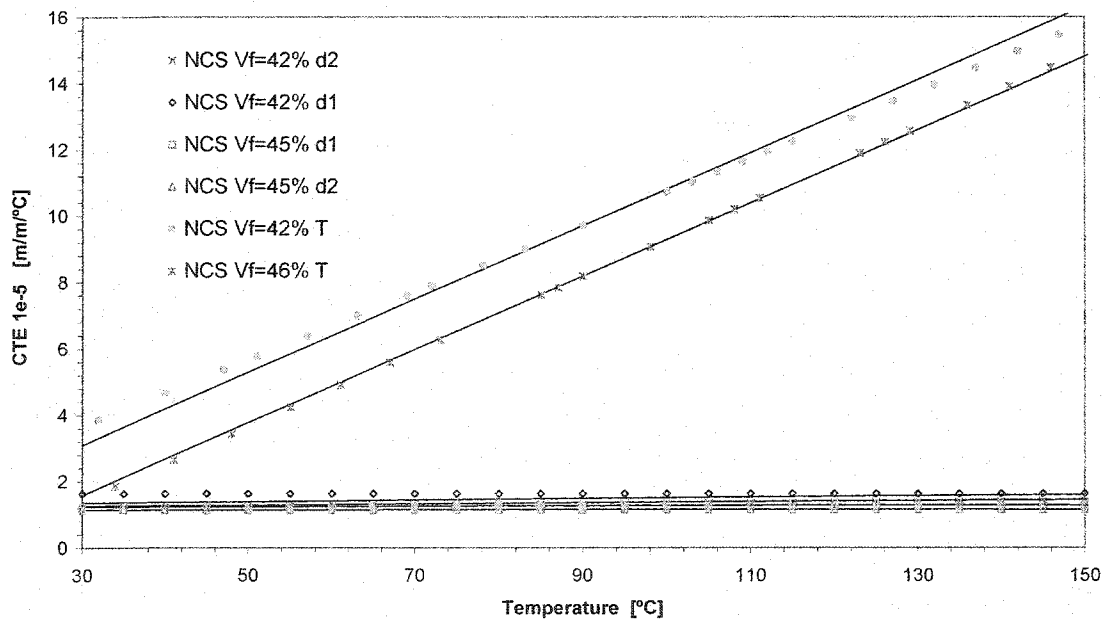


Figure 4.13. Coefficients of thermal expansion for fully cured composite samples of NCS-82620 fabric: d1 and d2 indicate the principal planar directions of the fabric, while T refers to the transverse direction.

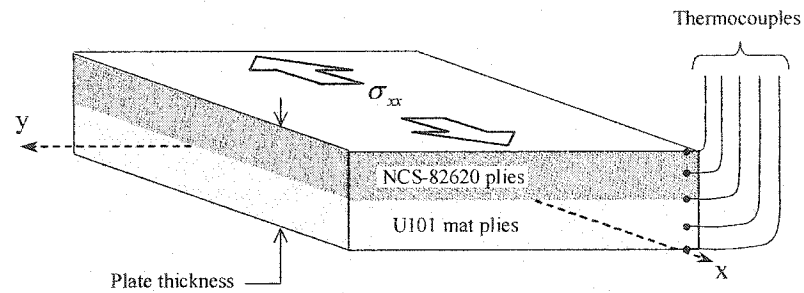


Figure 4.14. Stacking sequence for thin plates: the number of NCS plies was changed while mold thickness remained constant; two plies of U101 were used for all the test samples.

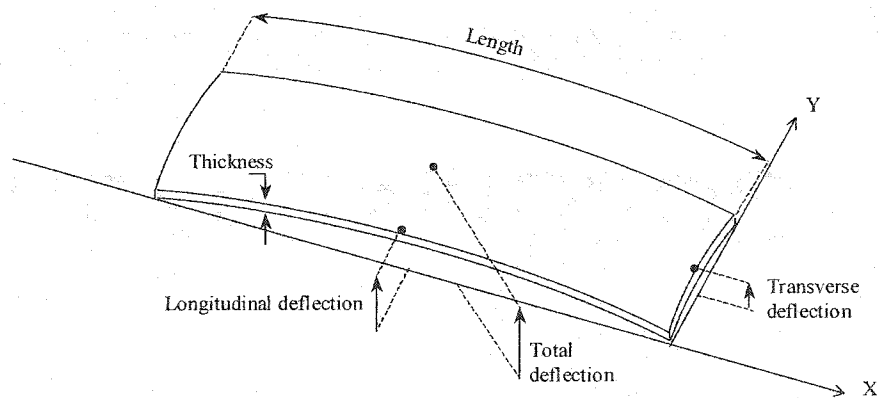


Figure 4.15. Warpage appearing in thin composite plates after manufacture due to unbalanced layup. Total deflection at the plate center is the sum of longitudinal and transverse deflections.

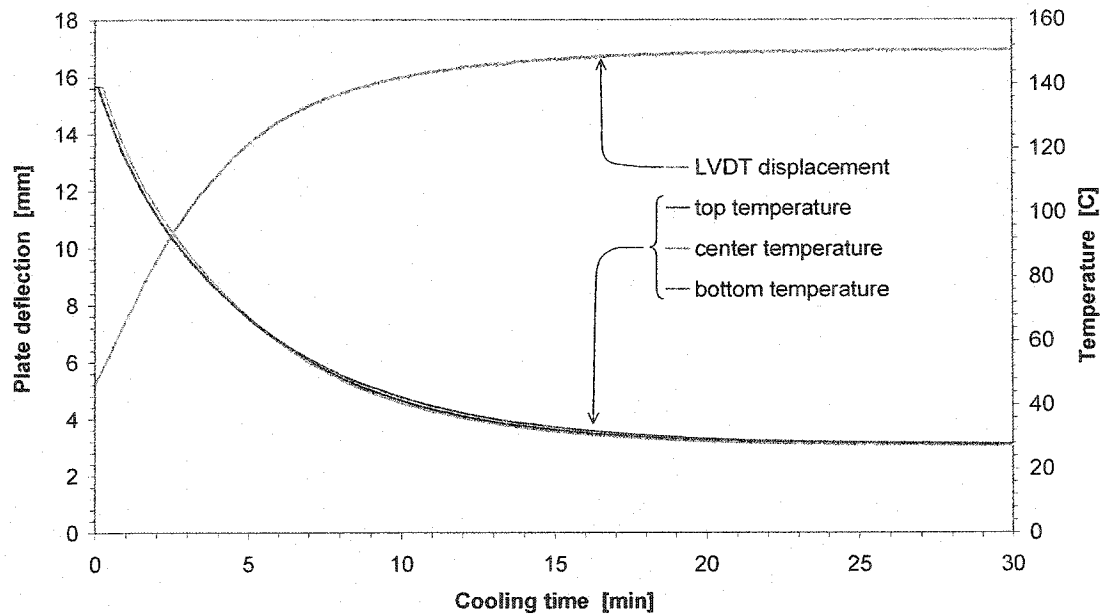


Figure 4.16. Measure of typical plate deflection during cooling from above the glass transition temperature. The sample has 2 plies of NCS-82620 fabric and 2 plies of U101 mat. While temperature decreases from 140°C to room temperature, plate deflection increases from 5 to 17 *mm*.

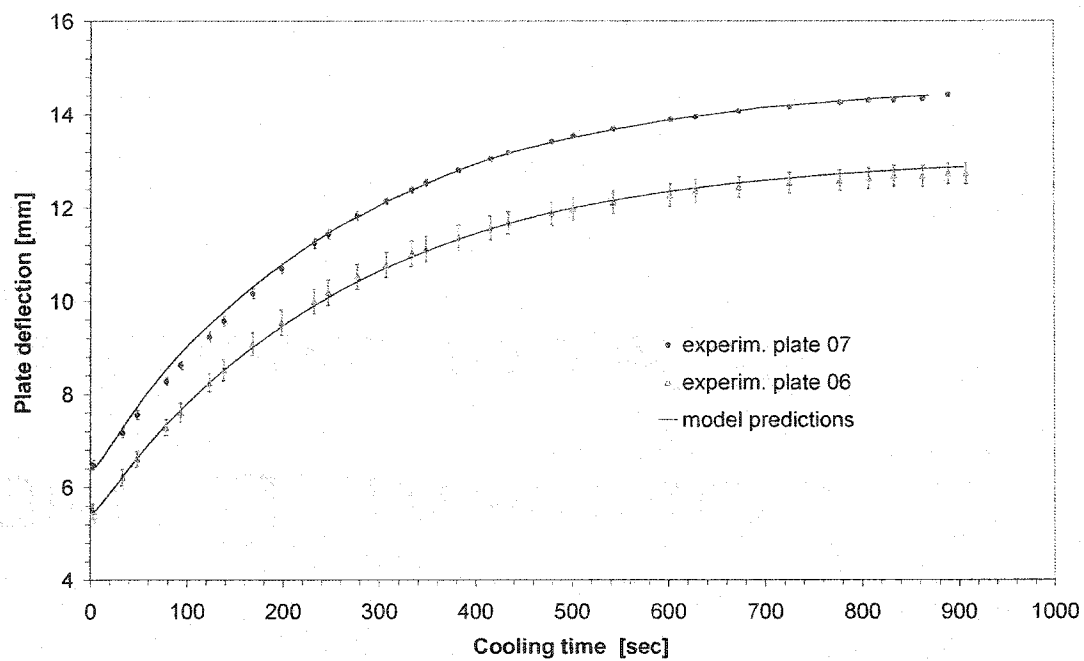


Figure 4.17. The measured plate deflection during cooling is compared with the numerical prediction of the thermo-mechanical model. Three measures were performed for each plate. The two samples show a good agreement with predicted values.

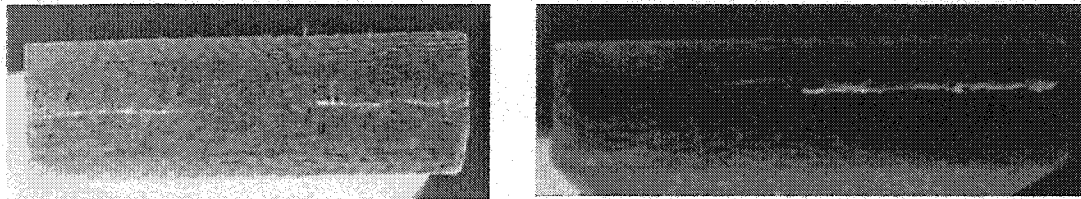


Figure 4.18. Two examples of matrix cracking and delamination during processing of thick composite plates. Defects appear commonly in thick composites processed at high mold temperature.

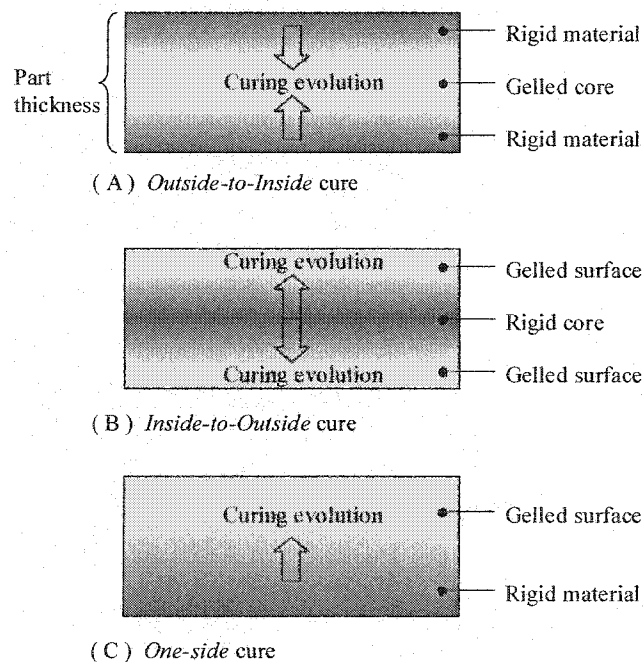


Figure 4.19. Schematics of the evolution of the curing front through the thickness of a thick part: *Outside-to-Inside*, *Inside-to-Outside* and *One-Inside* cure scenarios are considered.

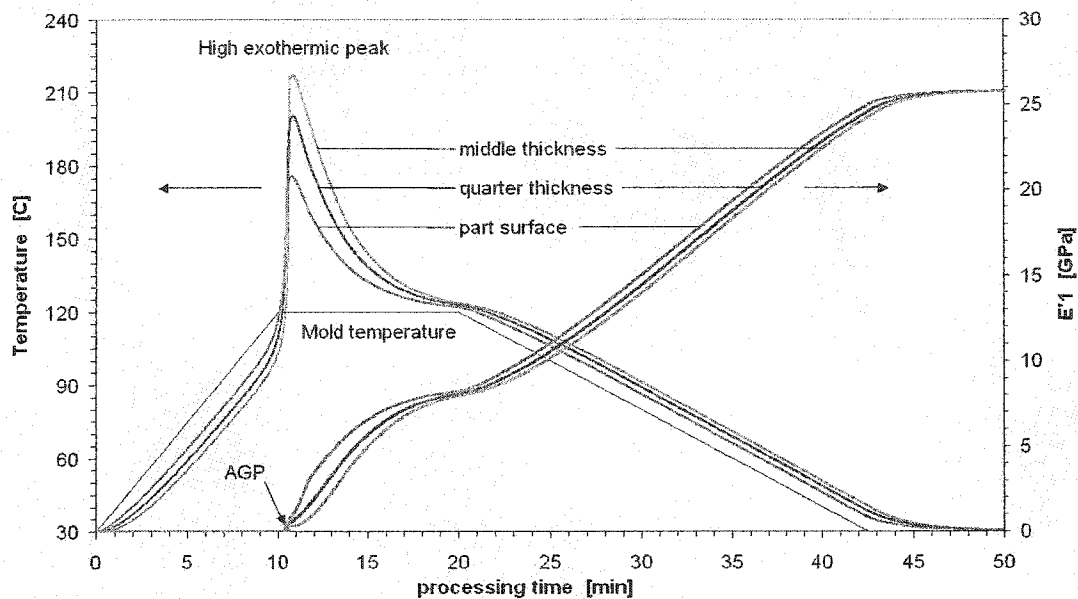


Figure 4.20. Numerical calculation of temperature and Young's modulus E' for a 15 mm thick composite cured at a mold temperature of 120 °C: high exothermic temperature peaks are observed.

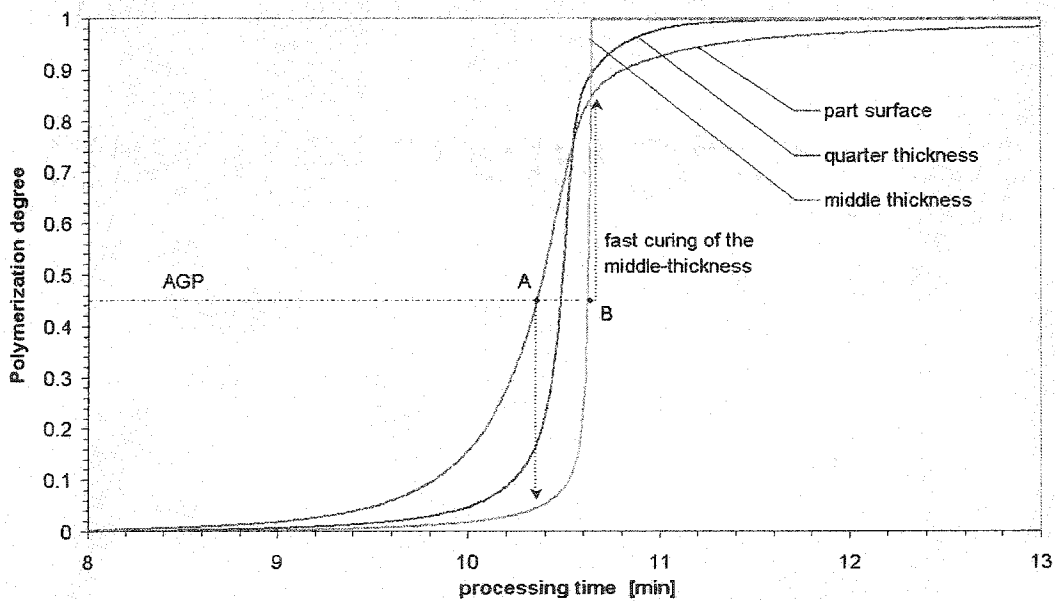


Figure 4.21. Through-thickness calculation of polymerization degrees during *outside-to-inside* cure of a 15 mm thick composite. A and B denote the AGP level at the surface and middle thickness respectively.

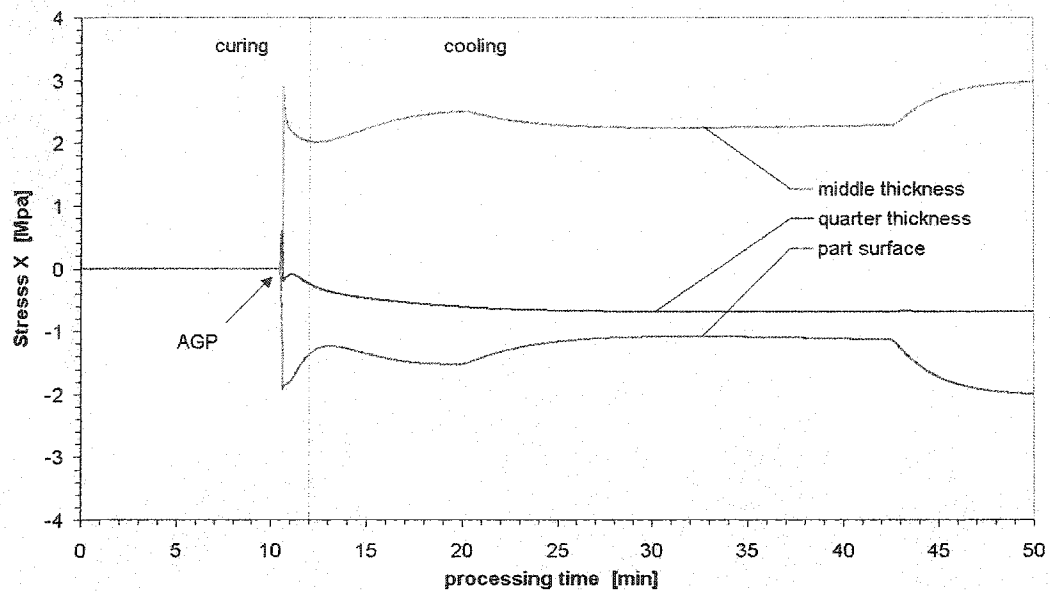


Figure 4.22. Calculated stresses developed during *outside-to-inside* cure. Internal stresses rapidly develop during cure after 10 min., due to resin shrinkage in the core.

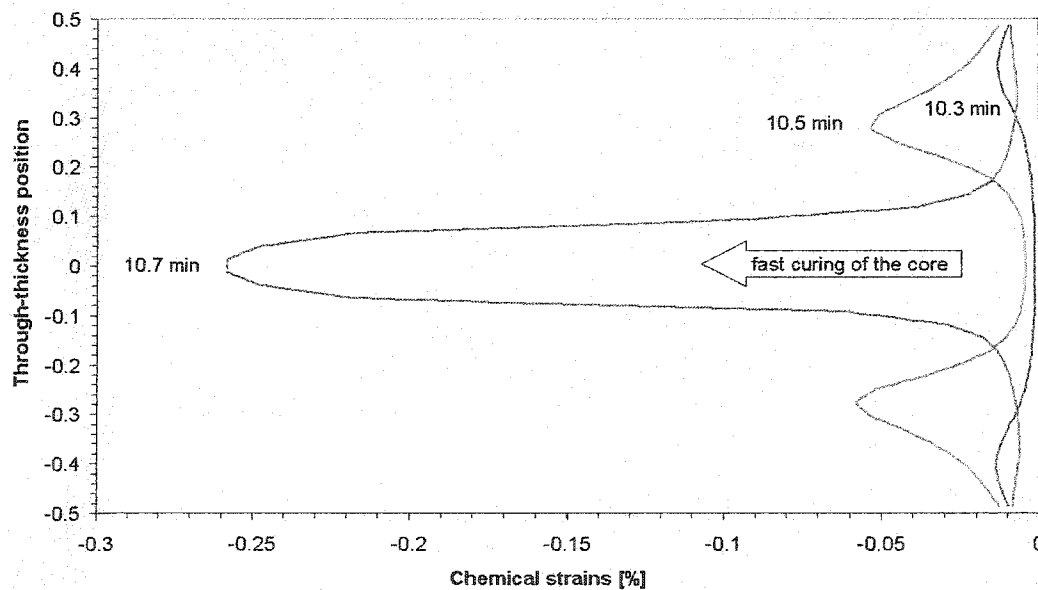


Figure 4.23. Through-thickness chemical strains induced by resin polymerization shrinkage for an *outside-to-inside* cure. At about 10.7 minutes, fast curing of the core generates high chemical strains.

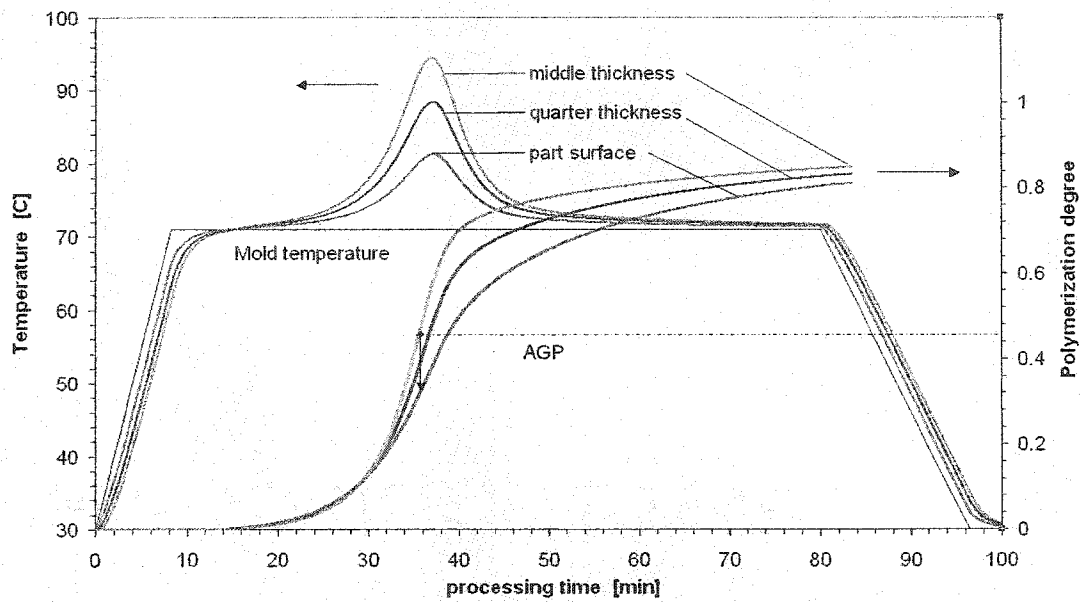


Figure 4.24. Numerical calculation of temperature and through-thickness degree of polymerization for an *inside-to-outside* cure. The thick plate is processed at a temperature of 70 °C.

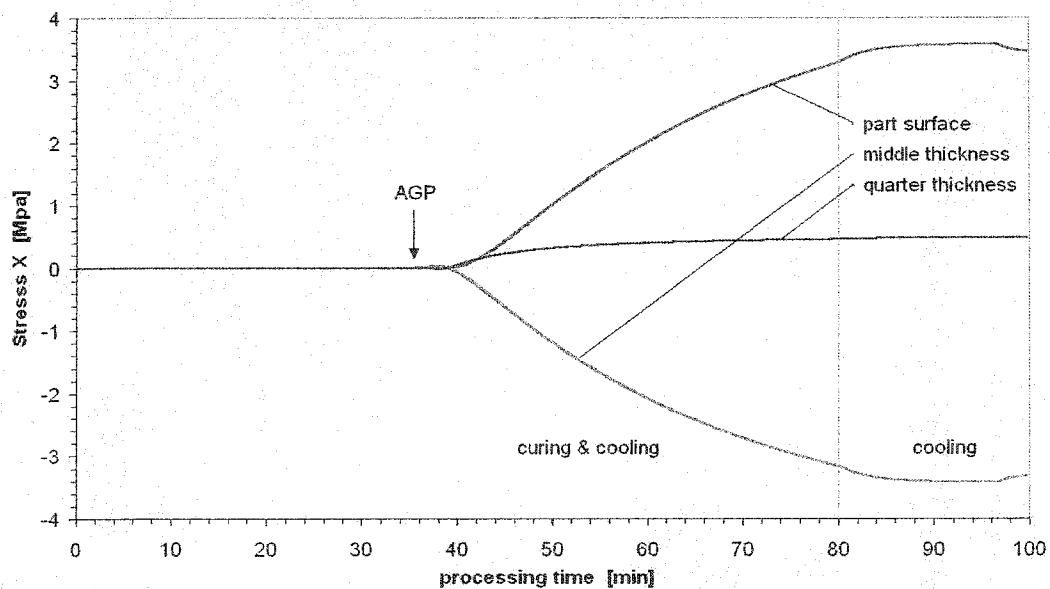


Figure 4.25. Computed internal stresses during *inside-to-outside* cure (plate processed at 70 °C). While no stresses are developed during the cure phase, contraction stresses appear in the core due to thermal variations.

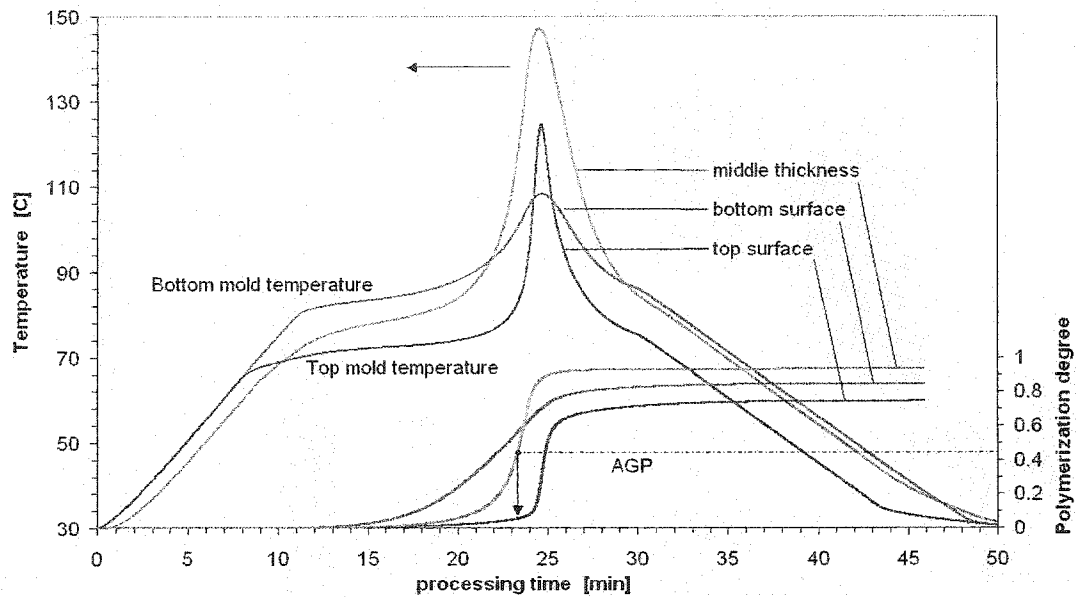


Figure 4.26. Calculated temperature and degree of polymerization during *one-side* cure. Resin polymerization evolves from the hot to cold surface, resulting in a high exothermic peak in the regions close to the cold surface.

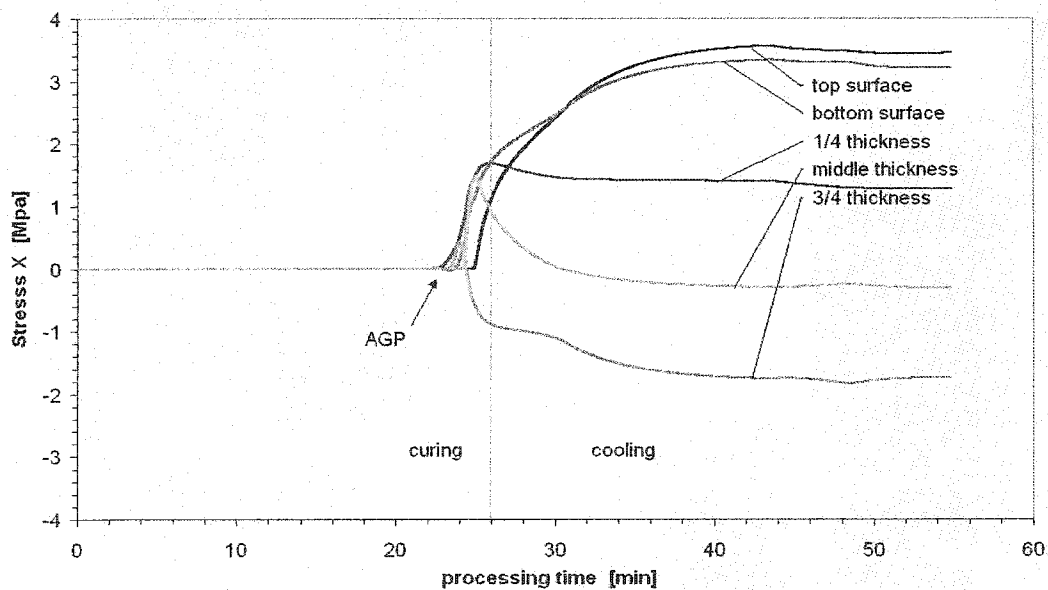


Figure 4.27. Numerical internal stresses during *one-side* cure. Internal stresses grow up in the regions close to the cold surface during resin polymerization (after around 24 minutes).

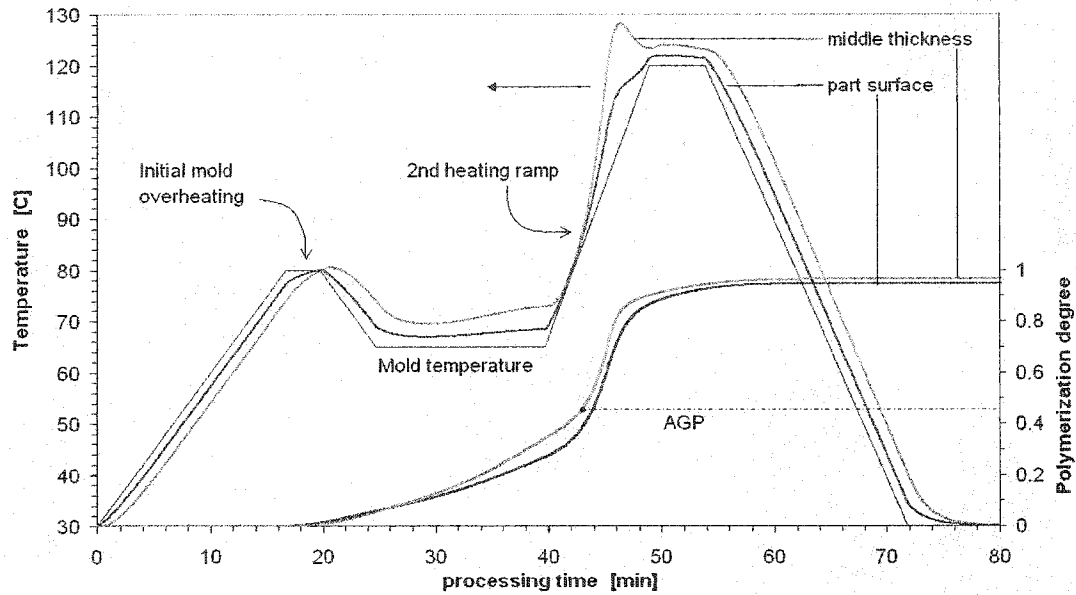


Figure 4.28. Numerical calculation of temperature and degree of cure for an optimized curing cycle. Initial mold overheating and appropriate heating ramps result in a quasi-constant through-thickness progression of polymerization and minimization of temperature gradients.

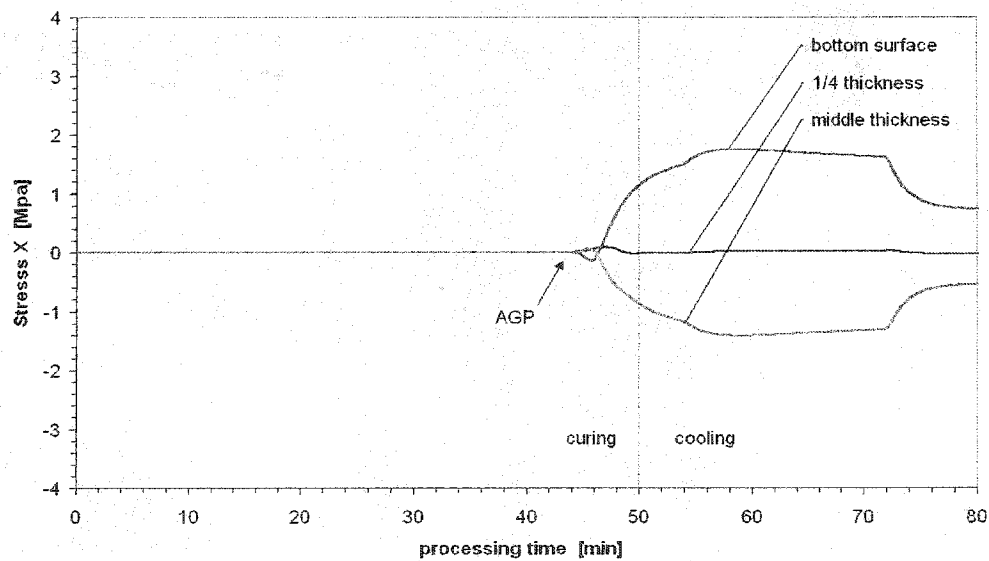


Figure 4.29. Calculation of through-thickness internal stresses during optimized curing cycle. Low residual stresses are found after processing while final polymerization degree is maximized.

Table 4.1. Summary of dimensions and curvatures of eight thin plate samples after demolding. Reported thicknesses are the average of 10 measures along the plates. Curvatures in the X-axis are calculated from 10 measures along this axis.

Test number	NCS 82620 # of plies	U101 # of plies	Length [mm]	Thickness [mm]	X curvature [1/m]
1	2	2	515	2.7	0.314
2	3	2	489	2.7	0.356
3	2	2	493	2.6	0.292
4	4	2	499	2.7	0.496
5	5	2	499	2.8	0.506
6	6	2	504	2.8	0.428
7	4	2	500	2.7	0.375
8	5	2	499	2.8	0.404

Table 4.2. Comparison of ultimate plate deflection during cooling after re-heating at 150 °C. Numerical and measured deflections are taken at room temperature.

Test number	Measured deflection [mm]	Numerical deflection [mm]	Error [%]
2	12.8	13.0	1.79
5	15.0	14.8	1.27
6	12.7	12.9	1.09
7	14.4	14.4	0.13
8	12.6	12.7	0.37

CHAPITRE 5

COUPLED NON-CONFORMING FINITE ELEMENT AND FINITE DIFFERENCE APPROXIMATION BASED ON LAMINATE EXTRAPOLATION TO SIMULATE LIQUID COMPOSITE MOLDING PROCESSES. PART I: ISOTHERMAL FLOW

Présentation du chapitre

Les travaux précédents ont porté sur l'étude des phénomènes thermiques et rhéologiques développés au cours de la cuisson de la résine dans le cas idéal où la température et la polymérisation sont uniformes partout dans la pièce. Tel que souligné dans la revue bibliographique du chapitre 1, l'histoire thermique et rhéologique pendant la phase de remplissage de la cavité du moule a une influence décisive sur l'uniformité du degré de polymérisation et des propriétés mécaniques de la pièce. Dans les chapitres 5 et 6, un article en deux parties s'intéresse à la modélisation numérique du remplissage non isotherme et de la cuisson de pièces tridimensionnelles.

La première partie de ce travail est consacrée au développement d'une méthode d'extrapolation de maillage selon la stratification des couches de renfort. Partant d'un maillage d'éléments finis bidimensionnel, un maillage stratifié tridimensionnel est créé pour représenter la cavité du moule. Pour améliorer la rapidité et la qualité du calcul du flux de résine dans un milieu poreux, un nouvel élément fini discontinu tridimensionnel est présenté. L'élément de forme prismatique contient des fonctions de forme non conformes pour assurer la conservation de la matière dans le plan de la pièce. Diverses comparaisons entre les simulations numériques, des solutions analytiques et les résultats expérimentaux sont décrits, qui ont permis de vérifier la

qualité du nouvel élément fini. Enfin, pour illustrer la souplesse des méthodes d'extrapolation de maillage et de calcul avec des éléments prismatiques stratifiés, une pièce industrielle est traitée dans le cas d'un remplissage isotherme.

Coupled Non-Conforming Finite Element and Finite Difference
Approximation Based on Laminate Extrapolation to Simulate Liquid
Composite Molding Processes. Part I: Isothermal Flow

Edu Ruiz, Vincent Achim and François Trochu

Centre de Recherches Appliquées Sur les Polymères (CRASP)

Département de Génie Mécanique,

École Polytechnique de l'Université de Montréal,

e-mails: eduardo.ruiz@polymtl.ca, francois.trochu@polymtl.ca

Keywords: Transfer Molding (RTM), thermal analysis, residual stress, weaving.

Article soumis à la revue

International Journal for Numerical Methods in Engineering

Novembre 2003

5.1 Abstract

In composite manufacturing by resin injection through a fibrous reinforcement, several phenomena occur involving the flow of resin and heat exchanges by the resin with the fiber bed and the mold. During processing, through-thickness flows commonly appear when the fibrous preform is made out of a stack of plies of different permeabilities. In many situations, simulation of the mold filling in Liquid Composite Molding (LCM) requires to perform a full three-dimensional analysis. In the pre-processing stage, the

construction of three-dimensional finite element meshes of complex parts made out of components of small thickness with respect to their length is very tedious. These parts are typically composed of an assembly of shell and flat panels. In such parts, a good aspect ratio of the finite elements must be respected to ensure appropriate simulation results. These conditions result in meshes with a very large number of degrees of freedom, which translates into a too high computational burden. For these reasons, a new numerical approach is presented in this paper for accurate and faster simulation of the filling phase in LCM. Based on the fabric reinforcement layup, a new non-conforming finite element is developed to quickly evaluate the through-thickness flow. Starting with a spatial triangular mesh as input geometry and based on the stacking sequence of the preform, an extrapolation algorithm is used to extrude the mesh in the thickness direction and generate the 3D non-conforming finite elements. To further evaluate the validity of the three-dimensional model, an experimental verification was performed for a typical through-thickness flow. Then, a comparative study is conducted to demonstrate the advantages of the proposed methodology in terms of accuracy. The results are compared with 2D (triangles) and 3D (tetrahedrons) finite element solutions. Finally, the performance of the model is assessed in terms of computer time.

5.2 Introduction

Polymer composites are presently the focus of much interest for the engineering design of structural and semi-structural parts. Diverse composite processing techniques have been investigated in recent years to improve part quality and reduce manufacturing costs. In the processing of thermosetting polymer matrices, Liquid Composite Molding (LCM) techniques such as Resin Transfer Molding (RTM) or Resin Film Infusion (RFI) have demonstrated potential advantages over traditional methods. In the aerospace field, the RTM process has now become mature technology to manufacture high performance composites by resin injection. In the automobile sector, these

technologies are still expensive and present research aims mainly at reducing cycle time. Several automotive companies have recently launched investigations or collaborate in research networks such as Auto 21 [1] to acquire advanced knowledge on these new manufacturing techniques and improve the design of production tools. Appropriate tooling is actually crucial to ensure proper mold filling and curing of composite parts. Air bubbles, dry spots or resin rich areas are common problems that must be avoided during the filling stage. Residual stresses, warpage and spring-in are another category of problems that occur during processing. In these comprehensive investigations, numerical simulation is critical to successfully design the mold and optimize the production cycle.

The advantage of computational techniques to prevent filling problems and get better molding results was established by several authors [2-6]. Analysis of mold deformation during filling [3], comparison of various injection strategies and optimization of the injection flow rate [6] illustrate the potential advantages brought by numerical simulation. Even if these advantages have been well defined, filling simulations are mainly carried out in thin shell geometries for the following reasons: (1) composite parts have usually a small thickness compared to their surfaces so that usually the through-thickness flow can be neglected; (2) the generation of a 3D mesh for a part of small thickness is a complex operation. The setup of boundary conditions is not an easy task for complex 3D parts; (3) the number of solid finite elements required to obtain accurate solutions makes three-dimensional simulation tedious in terms of computer time.

In this paper, a new methodology is proposed to compute complex flows in LCM. The method is based on the concept of non-conforming finite element and mesh extrusion. Starting with a mid-surface mesh, a three-dimensional mesh is constructed by extrusion from the two-dimensional finite element mesh. The extrusion is defined by the preform stacking sequence. Different fabric permeabilities and fiber volume fractions can be

used in each laminate ply. After starting the computations that govern fluid flows through porous media, the discretized finite element (FE) formulation is developed with the non-conforming shape functions defined on prismatic elements. To evaluate the validity of the calculations, the results of two experiments are compared to the numerical solution: (1) unidirectional flow through a multi-layer preform; (2) pointwise injection in a thick part. Finally, test case of a truck fender is studied to assess the quality of the proposed methodology and compare the results of three-dimensional flow simulations with two-dimensional calculations.

5.3 Governing equations

A typical mold filling process to manufacture composite parts involves the injection of a liquid resin into the mold cavity. As illustrated in Figure 5.1, the central issue in the analysis of mold filling consists of tracking the free surface between the filling material (i.e., liquid resin) and the escaping gas (usually air) present in the mold cavity before the injection. The flow of fluid through a fibrous network has been analyzed either at the microscopic or macroscopic levels. In the microscopic analysis, the flow through the fibrous reinforcement is governed by Navier-Stokes equation. However, this approach may be misleading because of the complex architecture of the reinforcement and the difficulty to find appropriate boundary conditions. In macroscopic investigations, the flow of resin through a fiber bed is modeled by Darcy's law, which governs incompressible flows through porous media. Therefore the filling stage in LCM must respect resin mass conservation and following Darcy's law, the resin flow rate is proportional to the pressure drop.

A porous medium may be defined as a solid containing holes or voids, connected or not, regularly or randomly dispersed. Porosity is the fraction of the bulk volume of the

material occupied by voids. Permeability is the property that characterizes the facility of a fluid submitted to a pressure field to permeate through a porous medium. In order to simulate the filling process, several assumptions must be made to simplify the problem. In general, the fabric reinforcement placed in the mold cavity is assumed to be rigid during filling and inertia effects are neglected because of the low Reynolds number. Furthermore, at the pressure level usually created in LCM molds to drive the flow, surface tension may be neglected compared to the dominant viscous force. The equation of mass conservation for the fluid phase can then be written as:

$$\text{div}(\rho \cdot \bar{v}) = 0 \quad (5.1)$$

where ρ is the density of the resin injected and \bar{v} is the superficial fluid velocity, i.e., the velocity at which the fluid actually travels, rather than the observed macroscopic velocity. Note that we consider here that the flow takes place in rigid molds. Otherwise the equation of mass conservation (5.1) should consider also deformation of the fabric structure. Darcy's law is as the equation that drives the flow of an incompressible fluid through a porous medium. It is expressed as follows:

$$\bar{v} = -\frac{1}{\mu} [K] \cdot \nabla p \quad (5.2)$$

where $[K]$ is a 3x3 permeability tensor, μ is the resin viscosity and ∇p is the pressure gradient. Equation (5.2) relates the three components of the superficial fluid velocity vector to the pressure and gravity gradient. This relationship is only valid for Newtonian fluids and ignores gravity effects and mold deformation. Note that these effects can also be considered using a more elaborate equation [7]. Combining equations (5.1) and (5.2), the partial differential equation that governs the fluid flow is:

$$\operatorname{div}\left(-\frac{1}{\mu}[K]\nabla p\right)=-\rho \quad (5.3)$$

where p is the scalar potential on Ω (see Figure 5.1). The term $[K]/\mu$ represents the dual scalar field and ρ is a volume source term.

5.4 Potential formulation

To solve equations (5.1) and (5.2), a weak formulation can be written in terms of weighted residuals [8]. Defining a test function equal to the scalar potential p and introducing a space $F(\Omega)$ of shape functions w , the elliptic partial differential equation (5.3) is replaced by an equivalent variational or weak formulation obtained as the integral of the scalar potential p on Ω multiplied by w . The weak formulation can be expressed as follows:

$$\int_{\Omega} \nabla w \cdot \operatorname{div}\left(-\frac{1}{\mu}[K]\nabla p\right) \partial\Omega + \int_{\Omega} (w \cdot \rho) \partial\Omega = 0 \quad (5.4)$$

for any *test function* w belonging to the space $F(\Omega)$. If Green theorem is applied for a Newtonian and incompressible fluid without any source term, the integration by parts gives:

$$\int_{\Omega} \nabla w \cdot \left(-\frac{1}{\mu}[K]\nabla p\right) \partial\Omega - \int_{\Gamma_d} (w \cdot (\hat{n} \cdot \bar{v})) \partial\Gamma_d = 0, \quad \forall w \in F(\Omega) \quad (5.5)$$

5.5 Finite elements discretization

The discrete finite element method (FEM) consists of finding a set of shape functions w that properly approximate the scalar potential p on the whole domain Ω . The scalar potential is unknown in Ω , but defined on the boundaries Γ_q, Γ_p and on the flow front. The domain Ω is decomposed into small elements of simple geometrical shape, where p is approximated by a linear combination of *shape functions* defined on a specific finite element of the mesh. For a general *shape function* s_n and *test function* s_j associated to the group of nodes in the finite volume V_e , the Galerkin formulation is:

$$\sum_{n=1}^{N_e} \left[p_n \int_{V_e} \nabla s_j \cdot \left(\frac{[K]}{\mu} \nabla s_n \right) \partial V_e \right] = \int_{\Gamma_e} (s_j \cdot (\hat{n} \cdot \bar{v})) \partial \Gamma_e, \quad \forall s_j \in V_e \quad (5.6)$$

where N_e are the element nodes and Γ_e the boundary of the finite volume V_e . The scalar potential field p is computed as

$$p(x) = \sum_{n=1}^N p_n s_n(x) \quad (5.7)$$

where $s_n(x)$ is a piecewise linear shape function and x the position vector in the domain Ω . In matrix notation, equation (5.6) can be rewritten as follows:

$$[M]\{p\} = \{R\} \quad (5.8)$$

where $[M]$ represents the $N \times N$ stiffness matrix of the scalar potential field. An element of matrix M is defined as:

$$a_{jn} = \int_{V_e} \nabla s_j \cdot \left(\frac{[K]}{\mu} \nabla s_n \right) \partial V_e, \quad \text{for } j, n = 1, \dots, N \quad (5.9)$$

and $\{R\}$ is a vector $\{r_j\}$ containing the boundary conditions:

$$r_j = \int_{\Gamma_e} (s_j \cdot (\hat{n} \cdot \bar{v})) \partial \Gamma_e, \quad j = 1, \dots, N \quad (5.10)$$

The approximate solution of the scalar potential p is then obtained by solving the linear system (5.8) of N equations with N unknowns.

5.5.1 Mass conservation and div-conform approximation

In the finite elements discretization of incompressible flows through porous media, the fluid mass is typically assumed to be constant within a defined control volume (CV). In our case, instead of the traditional nodal control volume technique, the geometry of the finite element is considered to represent the control volume where the mass balance equation is solved [2]. The fluid mass transported between adjacent elements is the scalar product of the normal vector at the interface by the mass velocity $\rho \cdot \bar{v}$ (see Figure 5.2a). The conservation of the fluid mass at the interface between two adjacent elements is not ensured with *conforming* finite element approximations. As matter of fact, the continuous shape function obtained by Lagrange interpolation at the element nodes (see Figure 5.2b) results in a piecewise linear scalar approximation of the pressure field on each finite element of the mesh. The gradient of the scalar potential, i.e., the dual scalar field \bar{v} , is constant on each element, but the normal fluid velocity is not continuous across the element interface (edge E in Figure 5.2b). As a result of this discontinuous normal velocity across the interfaces between neighboring elements, the approximate solution of the flow equation (5.2) does not satisfy exactly the mass balance equation (5.1).

A discontinuous shape function may be obtained by interpolating the pressure field on the element edges as depicted in Figure 5.2c in the 2D case. In the 3D case, the interpolation is performed on the faces of each solid element. This non-conforming interpolation leads to a functional space of shape functions that ensures a continuous mass flow, i.e., $\hat{n} \cdot \rho \bar{v}$ is constant across the interfaces between neighboring elements. On the other hand, equation (5.3) with source term implies that the integral of the divergence in an element is equal to the balance of resin mass flowing across its boundary BC:

$$\int_{CV} \text{div}(\rho \bar{v}) dV = \int_{BC} \hat{n} \cdot \rho \bar{v} dA \quad (5.11)$$

In numerical analysis, this kind of approximation is called div-conform. So, the fluid mass is conserved in the flow and across the interfaces between elements. As demonstrated in [9], the use of non-conforming finite elements is essential to ensure mass conservation and obtain accurate numerical results in the simulation of injection molding.

5.5.2 Finite elements for LCM simulation

In the particular case of pure Darcy's flow, the discontinuous interpolating polynomial may be chosen as piecewise linear [9]. For the triangular non-conforming finite element of Figure 5.3, the three degrees of freedom are assigned at the middle points of the element edges. Considering a classical reference triangle with a local linear approximation space of dimension 3, the element shape functions s_e write as follows:

$$s_e = \begin{cases} s_1 = 1 - 2\eta \\ s_2 = 2(\zeta + \eta) - 1 \\ s_3 = 1 - 2\zeta \end{cases} \quad 0 \leq \zeta, \eta \leq 1 \quad (5.12)$$

where ζ , η and τ are the local coordinates in a local reference system. The gradients of these shape functions can be written as a 3×3 matrix of the form:

$$\dot{s}_e = \begin{bmatrix} 0 & -2 & 0 \\ 2 & 2 & 0 \\ -2 & 0 & 0 \end{bmatrix} \quad (5.13)$$

Parts manufactured by LCM have usually a surface dimension much larger than their thickness. For this reason, most composite parts are commonly considered as thin shells and simulated using two-dimensional finite element shell approximation with through-thickness averaging. In many cases, three dimensional simulations are required to predict accurately the injection time and detect local filling problems. Because composite parts are made out of thin laminates, parallel layers of three-dimensional finite elements can easily be generated automatically to model the properties of each ply. As will be shown later, prismatic elements constructed from triangular mesh present the advantage of simplifying considerably the mesh generation for composite analysis by allowing parallel processing of layers stacked elements. In this work, a new non-conforming prismatic element is introduced for the three-dimensional analysis of mold filling in LCM. This prismatic element contains 6 nodes and is the result of an extrapolation of a triangular shell element (see Figure 5.3). The degrees of freedom are also extended on the edges of the two triangular faces. The linear function space will have now 6 degrees of freedom. The element shape functions s_e of the *Prism6* element are:

$$s_e = \begin{cases} s_1 = (1-2\eta) \cdot (1-\tau) \\ s_2 = (2\zeta + 2\eta - 1) \cdot (1-\tau) \\ s_3 = (1-2\zeta) \cdot (1-\tau) \\ s_4 = (1-2\eta) \cdot (1+\tau) \\ s_5 = (2\zeta + 2\eta - 1) \cdot (1+\tau) \\ s_6 = (1-2\zeta) \cdot (1+\tau) \end{cases} \quad \begin{matrix} 0 \leq \zeta, \eta \leq 1 \\ -0,5 \leq \tau \leq 0,5 \end{matrix} \quad (5.14)$$

where the third dimension τ is referenced from the element midplane. The gradient of the shape function is the following 6x3 matrix:

$$\dot{s}_e = \begin{bmatrix} 0 & -(1-\tau) & -(1-2\eta) \cdot 0.5 \\ (1-\tau) & (1-\tau) & -(2\zeta + 2\eta - 1) \cdot 0.5 \\ -(1-\tau) & 0 & -(1-2\zeta) \cdot 0.5 \\ 0 & -(1+\tau) & (1-2\eta) \cdot 0.5 \\ (1+\tau) & (1+\tau) & (2\zeta + 2\eta - 1) \cdot 0.5 \\ -(1+\tau) & 0 & (1-2\zeta) \cdot 0.5 \end{bmatrix} \quad (5.15)$$

Note that the *Prism6* element is non-conforming with *div-conformity* in the bottom and top planes of the triangular faces, but it is *div-non conform* through the element thickness. In other words, the resin mass will be conserved in the element plane, but mass may be lost through the element height (or thickness). Because the element thickness in our application is small compared to the part surface, the accuracy of through-thickness flow calculations remained acceptable.

5.6 Flow front advancement

The unsteady flow can be solved by considering a succession of quasi steady-state approximations, dividing the problem into a sequence of spatial and transient analyses. At each computed time step, the free surface Γ_d is moving inside the mold cavity Ω . The new location of the free surface is defined by its location at the previous time step and the actual velocity field. The methodology used to track the displacement of the free surface is defined in [9]. A scalar field $S(x,t)$, called the *saturation coefficient* (or fill factor), is defined in Ω . In a fully saturated porous medium (fully impregnated preform) S is equal to one, while in the unsaturated region (dry fabric) it is zero. In the partially saturated medium (in the vicinity of the flow front position), $S(x,t)$ lies between these two values. The fill factor is transported in the partially and fully saturated regions until it finally reaches the value of full saturation ($S=1$) everywhere in the cavity. The pure transport equation for a scalar field S is:

$$\frac{\partial S}{\partial t} + \bar{v} \cdot \nabla S = 0 \quad (5.16)$$

Due that the control volumes used in this approximation are in fact the finite elements of the mesh. The flow front is advanced by transporting the fill factor across the inter-element boundaries (the element edges in 2D or the faces in 3D).

5.7 Application to 3-dimensional flows in LCM

Typical composite parts manufactured by LCM are very often thin shells consisting of planar facets of uniform thickness. The fabric preform is made of homogeneous layers of constant thickness. This implies that the permeability tensor is assumed to have everywhere a symmetry plane parallel to the part midsurface, the in-plane tensor of the

component layers is assured not to differ by more than one order of magnitude. This approach allows the isothermal fluid flow to be calculated in two dimensions, in fact in the midplane of the part. The pressure and velocity fields are evaluated by solving the two-dimensional Darcy's equation using a weighted average permeability. The fluid flow is then advanced considering the thickness variations of the part to verify exactly the mass balance in the filling algorithm.

When important variations in the permeability tensor appear between preform layers (or when thickness of the part changes), the fluid will flow with a different velocity in each ply. If the planar velocity strongly differs from one layer to the other, a through-thickness flow is generated across the plies. In this case, the three-dimensional flow solution does not match anymore with the averaged flow, and the approach of a midplane surface is no longer acceptable. In addition, through-thickness phenomena such as dry spots may appear in the low permeability layers, which remain hidden in the averaged flow analysis. In the above cases, three-dimensional solutions must be implemented for accurate prediction of the filling process.

From the experience gained in the simulation of composite processing by LCM, three-dimensional finite element modeling was found to be a complex task that requires advanced knowledge on mesh generation and process parameters. A refined mesh is not always accessible for calculation, and coarse meshes do not provide adequate information on the flow front. Although the midplane surface and 2D mesh can be constructed relatively quickly, the construction of a solid mesh requires a patient work of verification of the lines and surface patches that define the geometry of the part. Once the mesh has been generated, a careful time-consuming check of possible degenerated elements must be performed. In addition, three-dimensional mesh refinement in regions close to flow or thermal boundary conditions is not always evident to achieve, (such as remeshing along the edges of a mold cavity to model race-tracking).

5.8 Mesh generation for through-thickness flow analysis

A potential benefit was found in the concept of mesh extrusion to improve the geometric modeling of 3D parts for LCM simulations. A midplane mesh usually constructed for thin shell simulations, can be extrapolated in a certain number of layers Nl (see Figure 5.4) to create automatically a three-dimensional mesh with a multi-layer structure well suited for composite analysis. Boundary conditions can be easily imposed on any surface of the final mesh. Moreover, the in-plane and through-thickness properties of the fibrous reinforcement can also be set for each extrapolated layer. To extrude the midsurface elements, mesh nodes need first to be extrapolated. To do so, the direction of extrapolation must be defined. As depicted in Figure 5.5, the node N_i is connected to a group of k two-dimensional elements. The normal vector to the discrete geometry at point N_i can be evaluated from the normals to the adjacent elements and their aspect ratios. For a typical adjacent element e_j , the normal is interpolated from the vertex normal ($Edge_1$ and $Edge_2$) as follows:

$$\hat{n}_{e_j} = \frac{Edge_1 \times Edge_2}{\|Edge_1 \times Edge_2\|} \quad (5.17)$$

The extrusion considers also the angles between any two edges of coincident elements that at the node considered, i.e.; the angle defined by:

$$\cos \varphi_{e_j} = \left(\frac{Edge_1 \cdot Edge_2}{\|Edge_1\| \cdot \|Edge_2\|} \right) \quad (5.18)$$

Let $\hat{n}_{e_j}^\varphi$ denote the normal weighted by the base angle φ_{e_j} and $\hat{n}_{e_j}^A$ the normal weighted by the area A_{e_j} of element e_j :

$$\hat{n}_{e_1}^\varphi = \hat{n}_{e_1} \cdot \varphi_{e_1} \quad (5.19)$$

$$\hat{n}_{e_1}^A = \frac{\hat{n}_{e_1} \cdot \varphi_{e_1}}{A_{e_1}} \quad (5.20)$$

For a node N_i , its normal vector is computed by summation for all the elements containing the node. Denoting by Nb the number of neighboring elements containing the same node, the generalized angle-based and area-weighted normals at node N_i can be write as follows:

$$\hat{n}_i^\varphi = \text{norm} \left(\sum_{j=1}^{Nb} \hat{n}_{e_j}^\varphi \right) = \left\| \sum_{j=1}^{Nb} \hat{n}_{e_j} \cdot \varphi_{e_j} \right\| \quad (5.21)$$

$$\hat{n}_i^A = \sum_{j=1}^{Nb} \hat{n}_{e_j}^A = \sum_{j=1}^{Nb} \left(\frac{\hat{n}_{e_j} \cdot \varphi_{e_j}}{A_{e_j}} \right) \quad (5.22)$$

Pillai et al. [17] proposed an approach to calculate the normal at a node based on the minimization of the net deviation of the projected thickness. A small radius commonly appears in meshes of thin shell parts where the area of the elements strongly varies from the rest of the part. Based on the Pillai et al. approach, to account for the influence of the element dimension on the averaged node normal, the extrapolation direction can be computed as follows:

$$\hat{n}_i = \frac{(\hat{n}_i^\varphi)^2 \cdot \hat{n}_i^A}{\sum_{j=1}^{Nb} \left((\hat{n}_j \cdot \hat{n}_i^\varphi)^2 \cdot \frac{\varphi_j}{A_j} \right)} \quad (5.23)$$

This solution is appropriate to extrude complex curved surfaces, although it may be limited by the interference between extruded elements. A practical limitation is then

imposed between the curvature of the geometry and the thickness to avoid mesh interference during extrusion.

Once the normal at a node has been defined, a group of new nodes must be extrapolated in the normal direction. If the extrapolated node must be extruded by a thickness of ply_th , the new node position can be found by a vector summation of the original nodal coordinates \bar{N}_i (coordinates of the node in the 2D mesh) and the normal vector \hat{n}_i :

$$\bar{N}_i^p = \bar{N}_i + \hat{n}_i \cdot ply_th \quad (5.24)$$

where \bar{N}_i^p denotes the extruded nodal coordinates and p is the extrapolation index (or ply number). In general, equation (5.24) can be transformed to consider the total extrusion thickness $total_th$ of the part. For the ply position ply_ps defined in percent of total thickness, the new nodal coordinates can be obtained from:

$$\begin{aligned} \bar{N}_i^p &= \bar{N}_i + \hat{n}_i \cdot total_th \cdot node_ps \\ node_ps &= (\chi \cdot ply_ps + \gamma), \text{ with } 0 \leq ply_ps \leq 1 \end{aligned} \quad (5.25)$$

Here, χ and γ are two unitary coefficients. As shown in Figure 5.6, different extrusion scenarios are possible by combining χ and γ values. These coefficients allow the node extrapolation to be carried out from midplane position in the normal direction (a) or in the opposite normal direction (c). Nodes can also be generated from a position at +/- half thickness (b), or from any position in between. Finally, the use of χ and γ permits to introduce the ply thickness as a spatial function that varies along the part geometry (d).

After the new nodes have been created, the three-dimensional finite element must be generated following the connectivity of the 2D mesh. Note that material properties and boundary conditions are not necessarily identical for each extrapolated layer, and then cannot be copied from the initial 2D mesh. Next, a data structure will be presented to allow the setup of different materials through the thickness of the part.

5.8.1 Structure of the laminate

A class structure is proposed to define the properties of the layers to be extruded according to the laminate structure. In composite manufacturing, consecutive fabric plies are stacked on the mold surface forming a material lay-up usually called *laminate* or *stacked preform*. As shown in Figure 5.7, the plies can be of different materials or exhibit different planar orientations, resulting for example in a non-uniform permeability tensor through the thickness. Moreover, ply thickness may vary as they are made out of materials with different compaction behaviours. The laminate data structure must contain, for each ply in the stack, the required information to reconstruct the layer geometry with the associated material properties.

Based on the concept used in PamRTMTM [11] to divide the part geometry into zones (see Figure 5.8), a laminate definition is connected to each mesh zone. The laminate structure contains useful information on ply properties, stacking sequence and direction of extrusion. The subclass *ply* contains a link to the specific fabric material and encapsulates a series of variables including ply thickness, porosity and fabric orientation. If two plies are made out of the same material, but differ in their planar orientation, during extrusion the permeability tensor associated to the two-dimensional finite element is rotated according to the ply orientation. For complex geometries that require draped directions of the fabric preform, a draping analysis may be performed with QuickFormTM [12] or PamFormTM [13]. Fiber orientations can then be linked to the laminate following the instructions of reference [12].

This data structure stores the ply information for each zone of the mesh and contains the properties of the finite element for each extruded layer. The division into zones with different laminate structures allows the construction of complex three-dimensional geometries as illustrated in Figure 5.9. Parts containing out-of-plane ribs can be generated by setting a different number of plies between zones. Thick parts with impermeable foam cores can also be constructed from the 2D mesh and proper laminate definition. In order to demonstrate the capabilities and accuracy of the proposed methodology, laboratory injections inducing through-thickness flow are compared to numerical predictions in two cases: (1) unidirectional flow through multi-layer preform; (2) pointwise injection in a thick composite.

5.9 Experimental validation – Case I

The experiment performed by Diallo et al. [14] involves the injection of pressurized oil into a rectangular cavity filled with a stack of fibrous reinforcements. Figure 5.10 shows a schematic of the experimental set-up used to record the flow front position in time. The mold assembly is made of two tempered glass plates of $930 \times 130 \times 19 \text{ mm}$. The mold cavity thickness was set with a 12 mm thick spacer. A silicone sealant was used to prevent edge effects along the mold edges. A constant injection flow rate was performed with a hydraulic cylinder mounted on a tensile testing machine. The reinforcement was a thermo-formable glass fabric EB-315-E01-120 from Brochier, which has an anisotropic permeability and surface density of 315 g/m^2 . For this fabric with a fiber volume fraction of 45%, the measured permeability in the weft direction is $K_{\text{weft}} = 6.5 \times 10^{-10} \text{ m}^2$, in the warp direction $K_{\text{warp}} = 5.5 \times 10^{-11} \text{ m}^2$ and through-thickness $K_z = 2.0 \times 10^{-11} \text{ m}^2$. The oil viscosity measured at room temperature was 0.103 Pa.s . As illustrated in Figure 5.10, 20 small wires of 0.1005 circular inches ($\sim 0.35 \text{ mm}$ diameter) were inserted between the reinforcement plies to measure the shape of the through-

thickness flow front. One wire was placed at the injection port and used as ground. As the oil impregnates the wires, an electrical contact is established and the position of the flow front can be recorded in time.

In order to create a through-thickness flow, the preform was constructed from the superposition of 20 plies of fabric materials aligned in the weft direction, and 20 plies aligned in the warp direction. The upper plies form a high permeability layer that speeds up the flow, while the low permeability of the lower plies delays the flow. In this experiment, the injection flow rate was maintained constant at 3.04 cc/s. To simulate this laboratory injection, the three-dimensional mesh of Figure 5.11 was generated using prismatic (6 nodes) finite elements. As shown in Figure 5.11, the 3D model is a brick of size 500 mm \times 12 mm \times 20 mm with 4 *prism6* elements per layer (a total of 8 finite elements through the thickness). The injection boundary condition is set on the faces of the finite elements on the left side of the plate.

A comparison of the experimental flow with the results of the simulation can be seen in Figure 5.12. At the start of filling, a distortion in the flow front develops quickly (for injection times less than 20 sec.). Afterwards the two in-plane flows reach an equilibrium state and the distortion is stabilized. The progression of the flow front on the bottom and top mold surfaces is in good agreement with experimental results. The caption of Figure 5.12 shows the through-thickness profile of the flow at 88 seconds, which corresponds very well to the measures of the electrical wires.

Since the *prism6* element does not ensure continuity of the resin mass following through the thickness of the composite as it does for the in-plane flow, the fluid mass lost may affect the flow front geometry. To quantify the error in the solution arising from this, a series of five simulations were carried out. As listed in Table 5.1, the permeability ratio between the upper and lower layers changes from 1 (no transverse flow) to 6 (high transverse flow). The approximate solution obtained with the new

finite element is compared with the experimentally validated two-dimensional solution of PAM-RTM calculated with triangular non-conforming finite elements. A simulation with tetrahedral elements is taken as reference of the performance of the three-dimensional solution. The triangular mesh contains 5,700 elements divided into 16 layers through the thickness (see Table 5.2). The *prism6* mesh was decomposed into 17,000 elements and 16 layers, while the tetrahedron mesh has 65,500 elements and 24 layers. Note that tetrahedrons must not be degenerated to ensure convergence of the solution. This implies an aspect ratio close to one, i.e., height and planar dimensions are of the same order of magnitude. If the thickness of the part is small compared to its area, the number of tetrahedrons required for a proper solution is extremely high. The numerical simulations were carried out on an IBM IntelliStation M-Pro PC with a Pentium III (1.0 GHz) processor.

For the five cases tested, the progression of the flow front at the interface between the two zones of different permeability (at half thickness) is displayed in Figure 5.13 for different anisotropy ratios. The flow front progression in the mid-plane is representative of the averaged flow and is expected to fit between meshes if no mass is lost during filling. The calculation for the highest anisotropy ratio required less than 25 minutes to run with the triangular mesh of 5,700 elements. The same case took around 36 hours to compute with the 65,500 tetrahedrons of the 3D mesh, while the *prism6* model needed nearly 5 hours. The strong cpu time reduction is due to differences in the number of degree of freedoms of the models. A comparison of mass lost at the end of filling is shown on Figure 5.14. The mass loss is calculated as the difference between the injected flow rate along the inlet channel and the flow rate at the flow front location. After filling, the total injected mass must equal the free volume in the mold cavity. The error on the mass loss remains in all cases smaller than 3%. It is maximum for tetrahedrons, and minimum for triangles. The cause of the mass loss with the non-conforming tetrahedrons is connected with the aspect ratio which was no longer equal

to 1, but decreased to around 0.6. Note that the mass loss in the *prism6* solution is of the same order of magnitude as that of the triangular mesh.

The *prism6* elements are expected to conserve the fluid mass across their rectangular faces, but not across the thickness (triangular faces). Since the thickness is small compared to the longitudinal extension of the part, the mass lost through the thickness is a small quantity of the total injected mass. This means that even if the total mass seems to be conserved, the flow front geometry may disagree with the 2D solution (triangular mesh). To quantify this error, an estimator was used based on the difference in the through-thickness flow profile between the prismatic or tetrahedron meshes and the triangular model (see Figure 5.15). The values presented in that figure are the sum of the two differences in the positions of the flow front at the upper and lower mold surfaces. It is remarkable to note that the mass loss induces a distortion of the flow profile. The *prism6* elements give a less accurate solution than tetrahedrons. Although the error seems more important for the prismatic elements, note that the number of degrees of freedom in the tetrahedron mesh is much larger than in the *prism6* model. When the number of degrees of freedom in the *prism6* mesh was increased to 27,000 elements, the flow front error was reduced to similar values as that of the tetrahedron solution and even to a lower value for higher anisotropy ratios.

5.10 Experimental validation – Case II

As a further validation exercise, the proposed numerical method was compared with experiments in the case of a spherical 3-dimensional flow. Bréard [15], has performed central injections in a thick mold containing an anisotropic reinforcing material. This result was used in Bréard and Trochu [18] in a comparison with the numerical solution of LCMFlot software. The position of the spherical 3D flow front was detected by X-Ray radiography. As drawn in Figure 5.16, in this example the rectangular mold is an

internal cavity volume of $300 \times 300 \times 20 \text{ mm}^3$. Silicon oil was injected through the cylindrical inlet (5 mm diameter) from the centre of the mold. The injection pressure was $1.89 \times 10^5 \text{ Pa}$, and the silicon oil viscosity 0.1 Pa.s . The in-plane permeability of the porous material used was $K_X = K_Y = 3.95 \times 10^{-10} \text{ m}^2$, and the transverse permeability $K_Z = 9.3 \times 10^{-11} \text{ m}^2$. The anisotropy ratio between the in-plane and transverse permeabilities is $K_X/K_Z = 4.25$.

A three-dimensional mesh was constructed to discretize a quarter of the rectangular mold with *Prism6* elements extruded in the thickness direction. The model contains around 30 elements along x and y axes, and 50 elements in the transverse direction (z axis). Elements are refined around the injection gate to ensure a good reproduction of the boundary condition. Figure 5.17 shows a comparison between experimental flow front locations and numerical calculations. Predicted positions of the resin flow front in both directions (planar and through-thickness) correlate very well with measures, although a small divergence is observed at the beginning of the injection (prior to 2 sec). The reason of these differences may be explained by the preform compaction at the beginning of the injection in the surroundings of the injection gate.

To quantify the error on the flow front prediction, a comparison with an elliptic three-dimensional flow was carried out. Consider a cavity similar to the previous experimental case, but filled with an isotropic material. The flow front position at time t_{fill} can be obtained by solving Darcy's equation for an elliptic flow:

$$t_{fill} = \frac{\phi\mu}{6K} \left(R_f^2 \left(2 \left(\frac{R_f}{R_0} \right) - 3 \right) + R_0^2 \right) \quad (5.26)$$

where K is the isotropic permeability and R_0 , R_f denote respectively the injection gate radius and the position of the flow front. The properties considered here are a

permeability $K = 1 \times 10^{-10} \text{ m}^2$, a porosity of 0.5, a fluid viscosity of 0.1 Pa.s and an injection radius of 1.12 mm , while the injection pressure was set to $1 \times 10^5 \text{ Pa}$. Meshes were constructed with different numbers of elements in the radius direction. *Prism6* and tetrahedron elements were used to run a series of filling simulations. Figure 5.18 shows a comparison of the numerical results with the three different meshes. Note that the mesh with 30 *prism6* elements in the radius direction shows a better agreement with theoretical values than the mesh with 50 tetrahedrons. The error on the flow front prediction at the end of filling can be seen in Figure 5.19. The convergence of the *prism6* mesh is higher than for tetrahedron elements. For the same number of elements along the radius, the *prism6* mesh gives a smaller error on the flow front estimation than tetrahedrons. Remark that, in this analysis, the fluid flow occurs in a three-dimensional space. The pressure gradient in the x , y and z directions will be of the same order of magnitude. Although this comparison is very convincing about the ability of the proposed model to predict three-dimensional flows, a loss of fluid mass appears due to the *div-non conformity* in the through-thickness direction. Therefore, even if the flow front is well predicted, some fluid mass may be lost during the filling simulation.

5.11 Case study – Truck fender

In order to demonstrate the practical validity of the proposed solution, the three-dimensional mesh extrusion and mold filling analysis are carried now for a typical LCM automotive part. The objective of this test is to demonstrate the advantage in terms of user time of a quick methodology to simulate irregular flows in a complex geometry. The truck fender of Figure 5.20 has a complex three-dimensional shape of variable thickness, and contains different fibrous materials and stacking sequences. The finite element mesh generated from the CAD geometric model 17,000 triangular elements and 8,500 nodes. The part is decomposed into 13 zones with different laminate structures.

In LCM, because of the cutting of the fibers and the free space created along the mold edges, the fluid (resin) may flow through a preferential path along the edges of the part. This phenomenon called *edge effect* or *race tracking* can be numerically modeled using an enhanced permeability in the elements located along the edges [16]. During mold closure, preform interference often appears in surfaces with double curvature, in straight chamfers or in fillets with different internal and external radius. These draping problems create fiber or void rich zones that strongly influence the flow during mold filling. In some cases, the fluid flow is faster in these regions (resin rich zone) than in the adjacent preform. In other cases, the flow slows down in regions of high fiber volume content and surrounds the low permeability zones. In the fender model, diverse draping problems are considered, which translate into zones of higher or lower permeability and porosity.

The injection strategy consists of four inlet gates and two vents placed all around the part. The two inlet gates at the upper corners (1 and 2 in Figures 5.20 and 5.21) are connected to an open channel free of any reinforcement. This channel allows a quick evolution along the part length (x -axis) and then distributes the resin vertically. This filling strategy is usually called a peripheral injection. Inlet 3 is also connected to an open channel at the end of the stiffener. This strategy is used to ensure a proper impregnation of the longitudinal rib. Injection gate 4 is positioned at the interior of the light support, where the laminate is made out of different materials. This central injection gate permits to fill up the low permeability zone containing the above mentioned laminate. For all injection gates, the injection pressure is maintained constant at $3.0 \times 10^5 \text{ Pa}$. An isothermal resin viscosity of 0.1 Pa.s was used for this analysis. To expel the air from the mold, two vent points are set: one at the center of the elliptic shape (vent 1), and the other one in the fender lower corner (vent 2). The vent in the elliptic shape of the part is closed when the resin arrives to it.

The laminates associated to each zone of the part are defined in Table 5.3. A maximum of six layers were used in the stiffener and in the light support. In zone 10, an impermeable foam core is wrapped by two fabric skins. The layer on the surface of the part has a lower permeability than the hidden ply; this can be explained by a non-uniform compaction of the double curvature foam core. Race tracking effects are modeled around the foam core (zone 7) to reproduce the resin rich zone along the foam edges. At the intersection between planar surfaces where straight angled chamfers appear, a lower permeability is considered locally (zones 2, 3, 6 and 8). Figure 5.22 shows the final three-dimensional model after the triangular mesh extrapolation is carried out based on the laminate structure. The open channels in the upper edge of the part, as well as the foam core, are meshed in detail. The whole model contains 60,000 prismatic elements and 40,000 nodes.

The performance of the proposed methodology and numerical extrapolation scheme is compared with the solution of the shell model. To compute both cases, the same mesh and laminate definition are entered in the input data of the program. If no extrapolation is required, the program automatically computes the gapwise average permeability of the laminate according to the classical weighted average:

$$\bar{K} = \frac{\sum_{i=0}^{NI} h_i \cdot K_i}{\sum_{i=0}^{NI} h_i} \quad (5.27)$$

with,

NI : number plies in the laminate

h_i : thickness of the i -ply.

K_i : permeability of the i -ply.

Predicted filling times for the shell model with averaged permeabilities are given in Figure 5.23. This calculation required 44.5 minutes to run on a IBM IntelliStation M-Pro PC with a Pentium III (1.0 GHz) processor. An injection time of 24.5 *sec* was obtained when the resin arrived to the second vent. The flow front profiles clearly show that resin runs along the upper open channel (between gates 1 and 2) and through the vertical right panel (below gate 2). Resin also flows horizontally in the stiffener zone from gates 3 and 4. Possible dry spots have been detected at the interference between the upper descending and the central ascending flows (denoted as “D” in Figure 5.23). The calculated flow front distribution in the light support is uniform and does not show any impregnation problem. About 8 seconds after the beginning of injection, the resin fronts merge and enclose an air bubble trapped in the center of the part. The air in the bubble exits through the vent gate 1. Approximately at 20 seconds, the resin arrives to vent 1, which is automatically closed. This generates a dry spot. At the end of filling (after 21 *sec.*), the resin flow in the foam takes the shape a bubble, although no dry spots were numerically detected.

For the extrapolated three-dimensional mesh, the resulting flow front progression is shown in Figure 5.24. This solution took 9.5 hours to run on the same computer. A total filling time of 30.6 *sec* was obtained with this model (25% more than previous solution). Although the shapes of the flow front profiles are in general similar in all the simulations carried out, important differences can be noted. In the 2D model, the resin runs faster in the open channels principally along the rib stiffener. In the 3D solution, the modeling of the rib with an open channel results in a transverse flow that differs from the 2D prediction (see details in Figure 5.24). As a consequence of this three-dimensional flow, the dry spots in the part center were not detected in the 3D model. At around 17 *sec.*, the upper descending and the central ascending flows meet without air trapped between them. In the zone with a foam core, the flow predictions vary for the top and bottom skins, while the 2D model gives the average flow location. This difference in the flow between layers creates an air bubble in the top foam skin

close to vent 2. This entrapped air is not detected in the 2D solution, even if the permeability of the foam zone is changed. The results of the 2D model with different permeabilities are illustrated in Figures 5.25 and 5.26. The zone with a foam core was assumed to have the permeability of the top or bottom skins, respectively. In none of the two cases, the entrapped air bubble could be detected numerically.

5.12 Summary

In this paper, a new methodology is proposed to compute three-dimensional flows in LCM. The method is based on a new *non-conforming* finite element approximation and on a mesh extrusion algorithm to generate three-dimensional multi-layer finite element mesh well suited for composite analysis. Beginning with a thin shell mesh, a solid mesh is constructed by extrusion from the 2D finite element shell mesh. The extrusion is defined by the preform stacking sequence of the reinforcement. This allows considering different fabric permeabilities and fiber volume fractions in each laminate ply. Boundary conditions may also be extruded through the thickness or set on the top or bottom part surfaces. The development of a new prismatic non-conforming finite element approximation provides accurate through-thickness solutions that minimize the number of elements. This methodology presents several advantages in addition to being user friendly and to facilitate the mesh generation for LCM application. Numerical extrusion gives also the possibility of saving computer time before and after processing. It also minimizes considerably the number of 3D finite elements required to calculate accurate solutions of the flow problem, and hence reduces the computer time as well.

The proposed method has demonstrated a good performance to calculate with a good accuracy complex three-dimensional flows without having to create a 3D mesh. Although the required computer time is higher than for the 2D solution, the methodology remains simple thanks to the automatic generation of the 3D mesh by

extrusion. The quality of the numerical results is equivalent to that of a full 3D solution with tetrahedrons, but with a great reduction in computer time. This approach will now be applied in Part II to non-isothermal flows in thin and thick LCM parts.

5.13 Acknowledgements

The authors thank the *National Science and Engineering Research Council of Canada* (NSERC) and *Fonds Québécois pour la Recherche sur la Nature et la Technologie* (FQRNT) for their financial support. The contribution of *ESI_Group* and their numerical support is also gratefully acknowledged, as well as the program of *Bourses d'Excellence du Ministère de l'Éducation du Québec* that made this research possible.

5.14 References

1. <http://www.auto21.ca/> *Network of Centers of Excellence on the Automobile of the 21st Century*. Page web consulted 2003 Nov 09.
2. Trochu F., Gauvin R., Gao D. M. Numerical Analysis of the Resin Transfer Molding Process by The Finite Element Method. *Advances in Polymer Technology*. 1993; 12(4):329-342.
3. Ruiz E., Demaria C., *Diseño, Análisis y Procesos de Fabricación de la puerta de un vehículo eléctrico ciudadano en RTM*. Eng. repport, Instituto Universitario Aeronáutico, Univ. Católica de Córdoba, Argentine, 1998; 320 pgs.
4. Voller V., Peng S. An Algorithm for the Analysis of Polymer Filling Molds. *Polymer Eng. and Sci*. 1995; 35(22):1758-1765.
5. Maier R., Rohaly T., Advani S. G., Fickie K. A Fast Numerical Method for Isothermal Resin Transfer Molding Filling. *Int. Journal for Numerical Methods in Eng.* 1996; 39:1405-1417.

6. Achim V., Ruiz E., Soukane S., Trochu F. Optimization of Flow Rate in Resin Transfer Molding (RTM). *8th Japan International SAMPE Symposium and Exhibition (JISSE-8)* Tokyo, Nov. 18-21 2003.
7. Trochu F., Boudreault J. F., Gao D. M., Gauvin R. Three-Dimensional Flow Simulations for the Resin Transfer Molding Process. *Materials and Manufacturing Processes*. 1995; 10(1):21-26.
8. Remacle J.-F., Bréard J., Trochu F. A Natural Way to Simulate Flow Driven Injections in Liquid Composite Molding. *Proc. CADCOMP 98, Computer Methods in Composite Materials*. 1998; 6:97-107.
9. Trochu F., Gauvin R., Gao D. M. Numerical Analysis of the Resin Transfer Molding Process by the Finite Element Method. *Advances in Polymer Technology*. 1993; 12(4):329-342.
10. Bohr E. *Etude des Échanges Thermiques dans la Fabrication des Composites par les Procédés d'Injection sur Renfort*. Mémoire de Maîtrise en Sciences Appliquées. Dep. Génie Mécanique. École Polytechnique de Montréal. 2000; 267 pgs.
11. PAM-RTM™ *User's Documentation*. ESI_Group Software manual. 2002.
12. QUICK-FORM™ *User's Documentation*. ESI_Group Software manual. 2002.
13. PAM-FORM™ *User's Documentation*. ESI_Group Software manual. 2002.
14. Diallo M. L., Gauvin R., Trochu F. Experimental Analysis and Simulation of Flow Through Multi-layer Fiber Reinforcements in Liquid Composite Molding. *Polymer Composites*. 1998; 19(3):246-256.
15. Bréard J., *Matériaux Composites à Matrice Polymère*. Phd. Thesis, Université du Havre, France, 1997; 195 pgs.
16. Hammami A., Gauvin R., Trochu F., Touret O., Ferland P. Analysis of the Edge Effect on Flow Patterns in Liquid Composite Molding. *Applied Composite Materials*. 1998; 5:161-173.
17. Pillai K. M., Tucker C. L., Phelan F. R. Numerical simulation of injection/compression liquid composite molding. Part 1. Mesh generation. *Composites: Part A*. 2000; 31:87-94.

18. Bréard J., Trochu F. *Modélisation de la Dynamique des Écoulements d'un Fluid Réactif à Travers un Milieu Poreux Déformable en Condition Anisotherme. Application : procédés LCM*. Internal report, Ecole Polytechnique de Montréal, 1999.

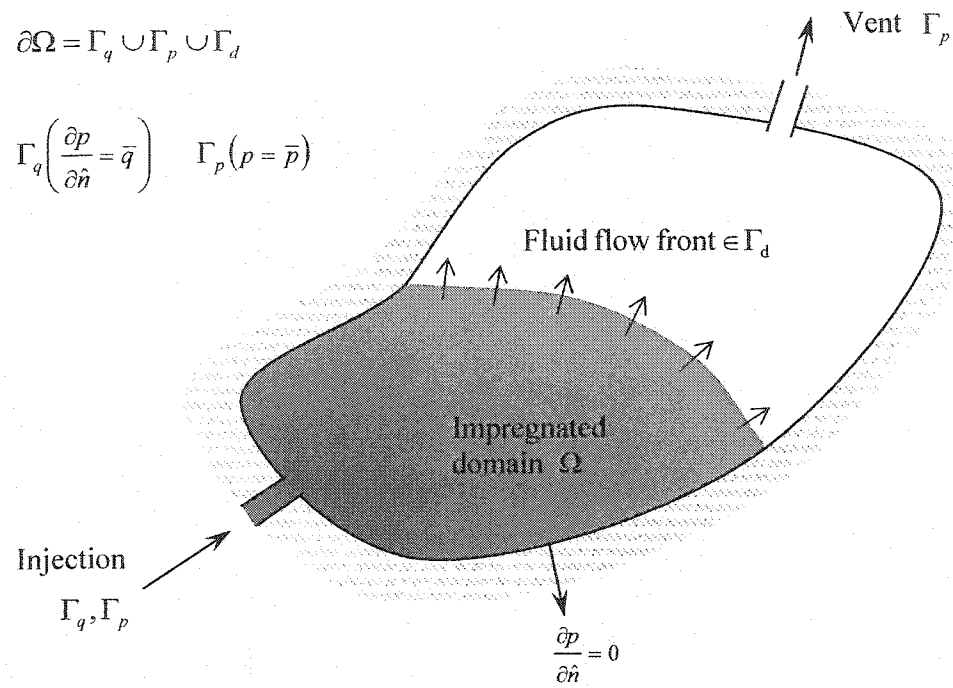


Figure 5.1. Schematic representation of the domain Ω representing the mold cavity. The boundary is defined by $\partial\Omega = \Gamma_q \cup \Gamma_p \cup \Gamma_d$. (Note that Γ_d was deliberately removed for clarity.)

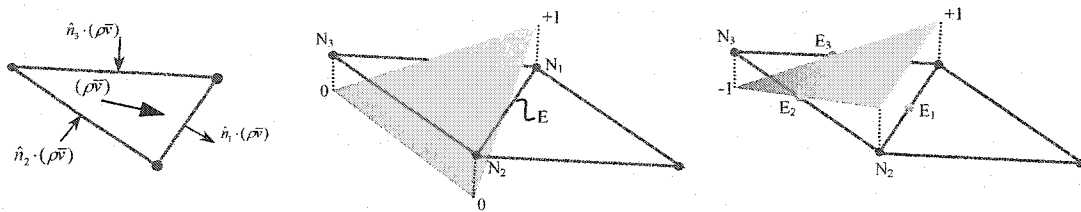
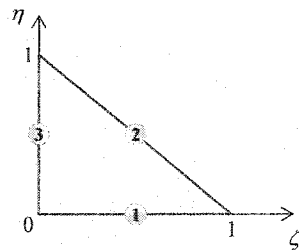
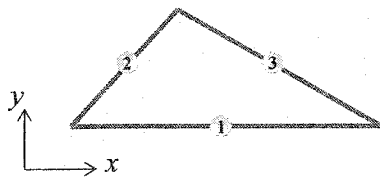
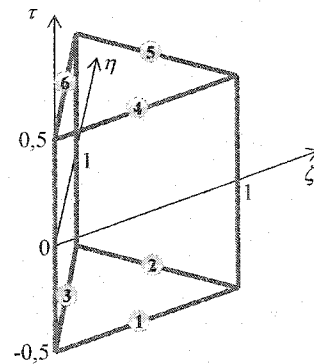


Figure 5.2. Triangular finite element: (a) incoming and out-coming flows in the FE; (b) conforming shape function at node N_1 ; (c) non-conforming shape function associated to edge E_1 .

Triangular non-conforming finite element



Reference triangular non-conforming finite element



Reference prismatic finite element (6 nodes)

Figure 5.3. Triangular and prismatic (6 nodes) non-conforming finite elements. The degrees of freedom are assigned at the middle edges; ζ , η and τ denote the local coordinates in the reference element.

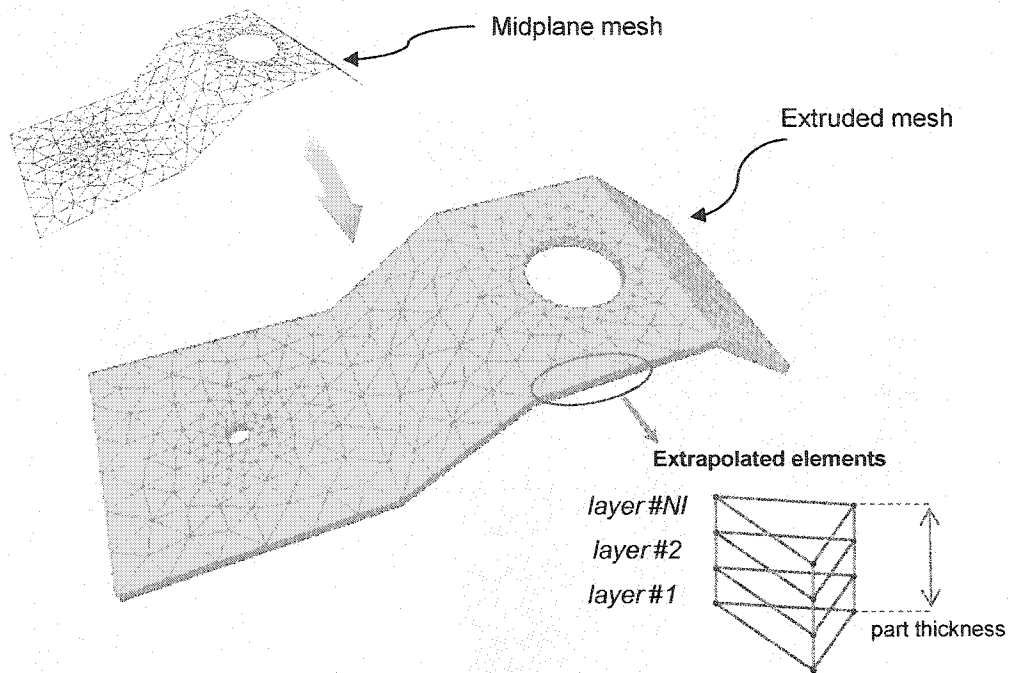


Figure 5.4. Extrusion of a midplane mesh through the thickness of the composite. From 2D finite elements, a solid mesh consisting of N layers may be constructed to calculate 3D flows.

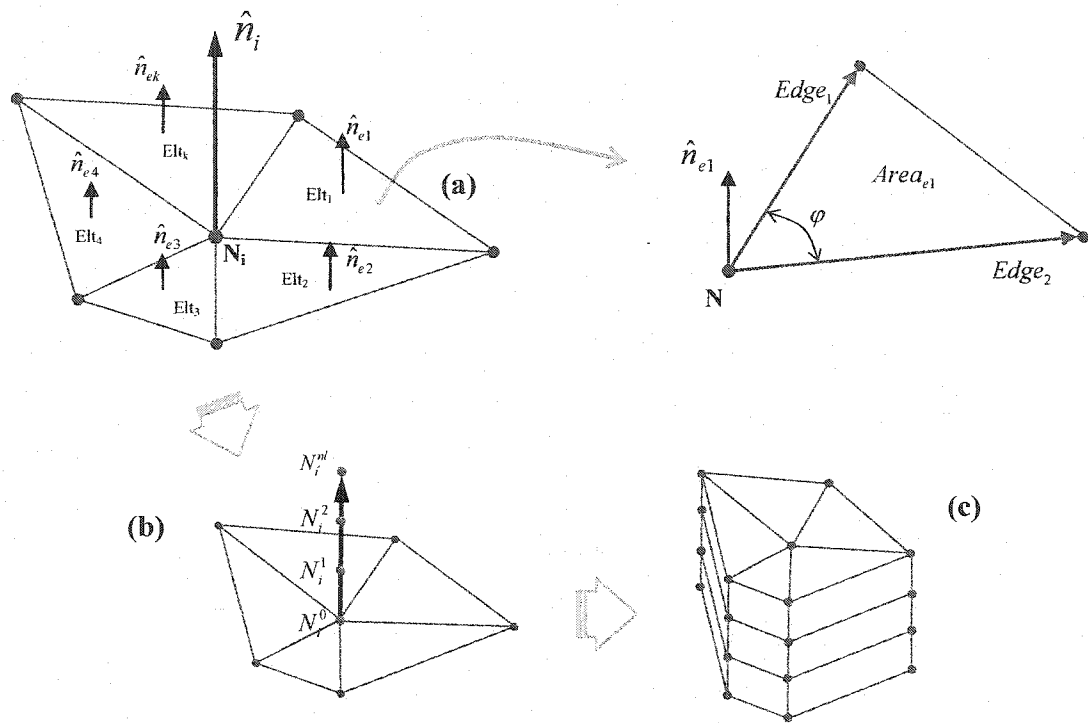


Figure 5.5. Procedure for mesh extrusion: (a) the nodes normal are computed from the normals in adjacent elements, (b) new nodes are created along the calculated normal, (c) finally adjacent elements are extruded.

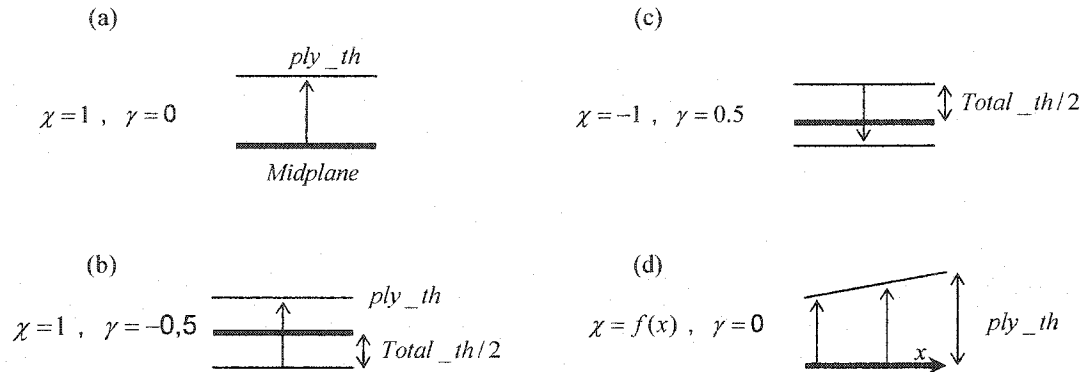


Figure 5.6. Selection of the extrusion direction using the χ and γ coefficients of equation (21). (a) the position of the new nodes can be computed from the midplane position; (b) from the half thickness; (c) or in the opposite normal direction; (d) ply thickness can also be set as a spatial function.

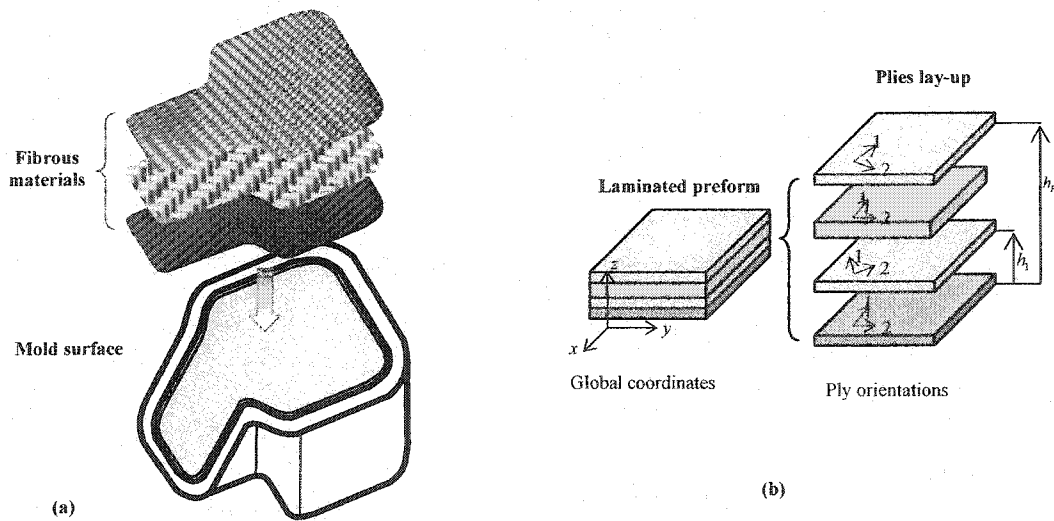


Figure 5.7. (a) In composite manufacturing, layers of fibrous materials are stacked to form a compact preform. (b) The plies of the laminate can have a different thickness and fiber orientation.

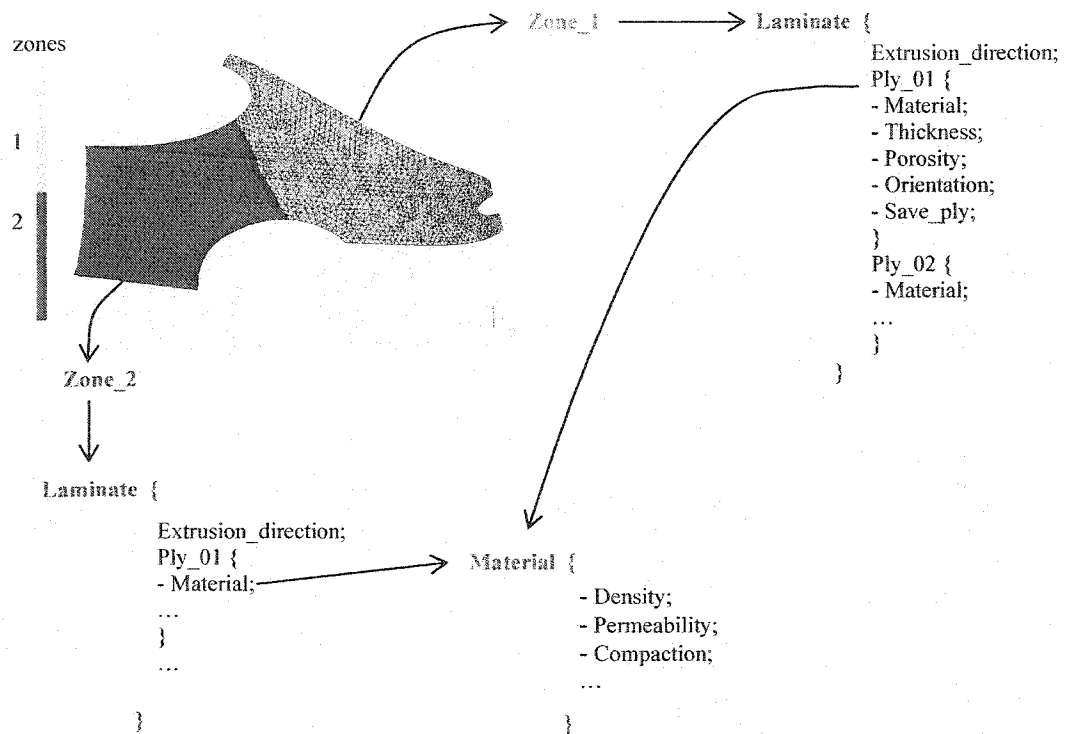


Figure 5.8. Data structure used to relate zones of PamRTM [11] with the structure of the laminate. Each ply of the laminate is related to a fabric material. Multiple zones can be connected to the same laminate and different plies can point to the same material.

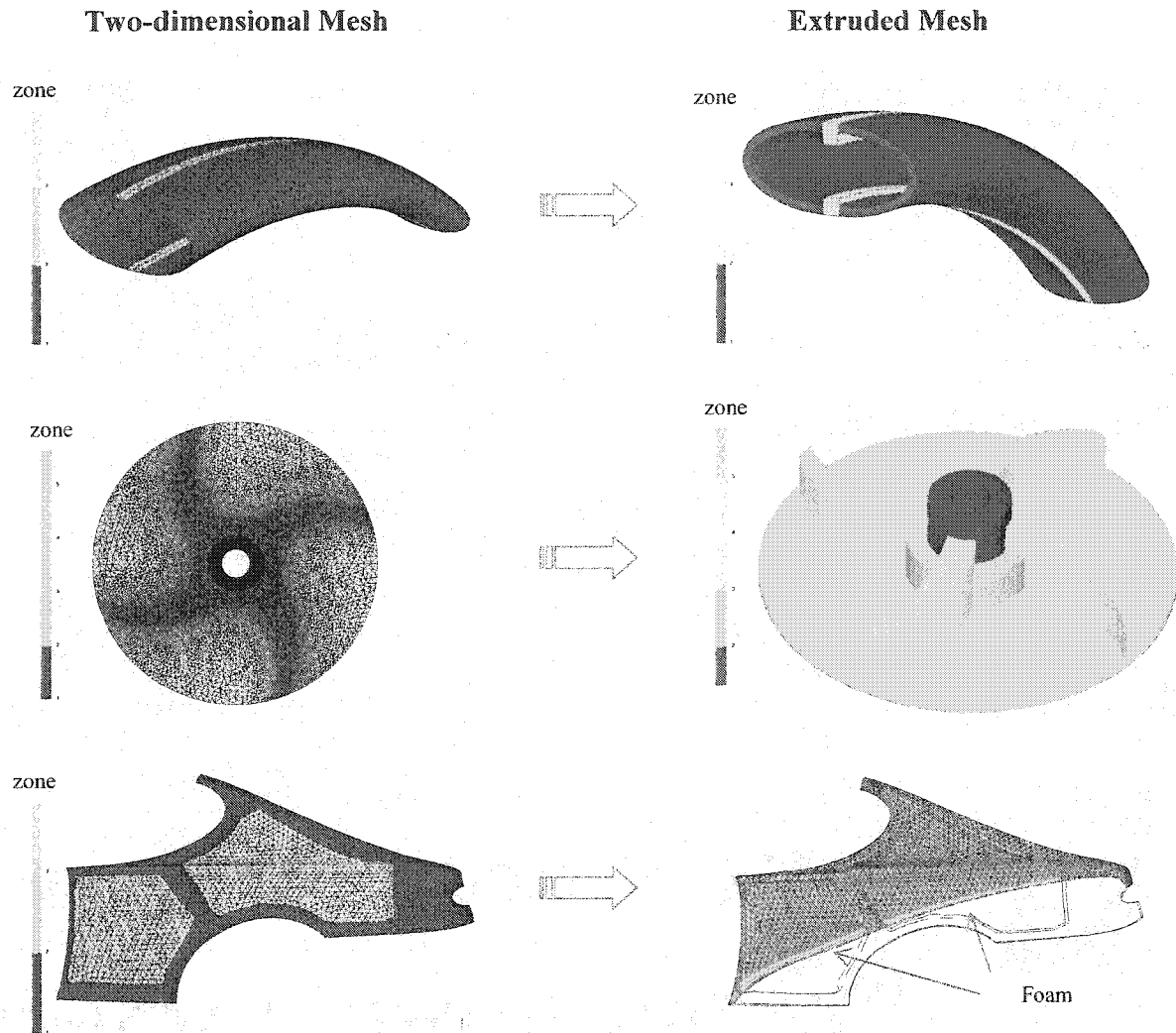


Figure 5.9. Typical applications of the extrusion algorithm. Examples of three-dimensional meshes for various stacked materials may be constructed from the midsurface mesh and structure of the laminate. The first example shows an irregular surface of revolution. The second example is a ribbed part. The third example shows that an impermeable foam core can also be considered as part of the laminate structure.

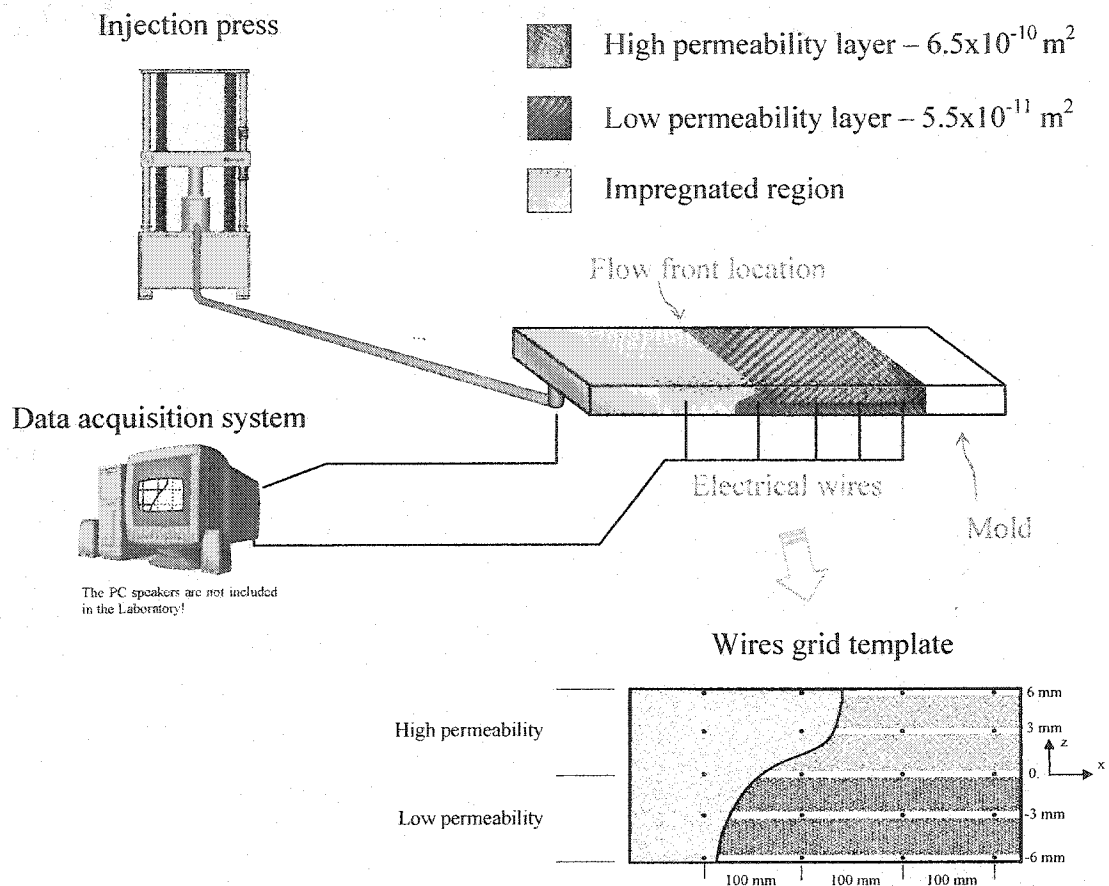


Figure 5.10. Schematic diagram of the through-thickness flow front shape measurement system used by Diallo et al. [14].

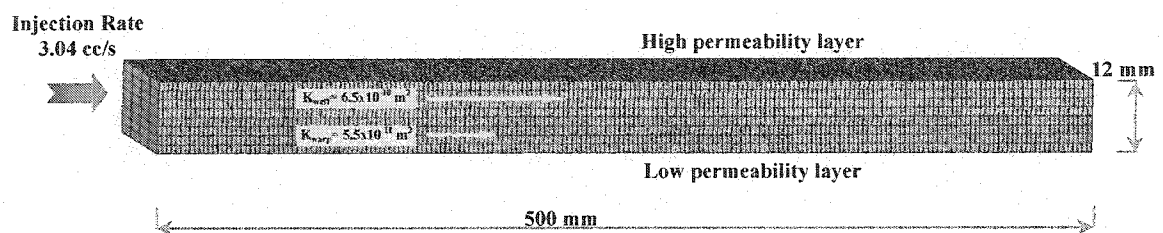


Figure 5.11. Three-dimensional model used to simulate the experiments of Diallo et al. [14]. In each layer of the laminate, the mesh contains 4 *prism6* finite elements in the through-thickness direction.

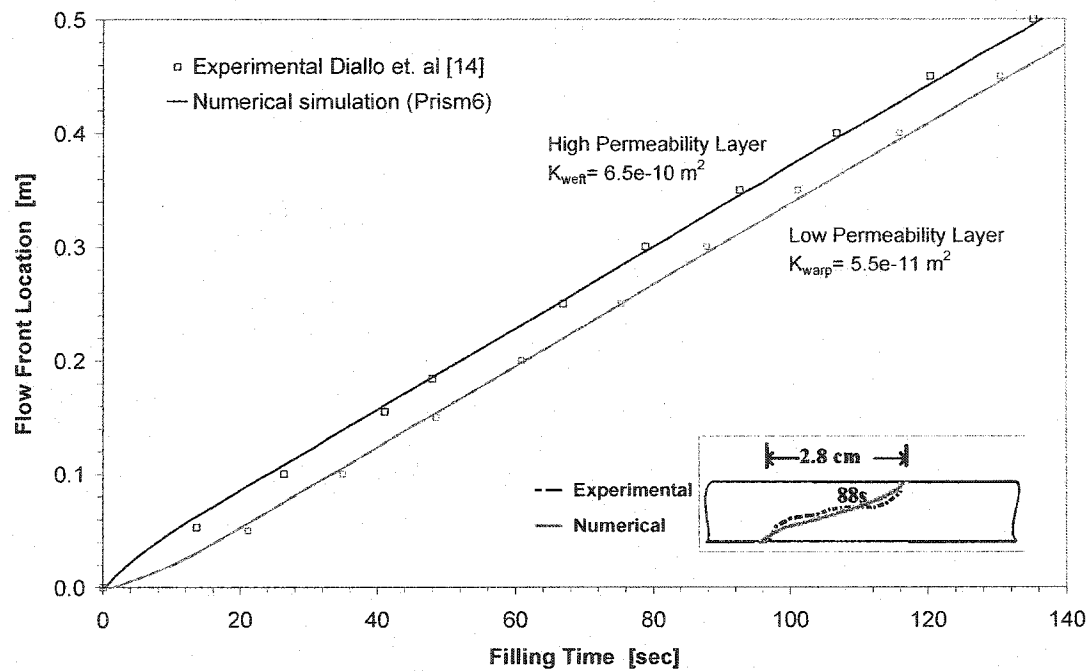


Figure 5.12. Flow front progression in the top and bottom mold surfaces. Numerical results are compared to experimental values. The flow front distortion is stabilized after 20 sec. The numerical through-thickness front at 88 seconds is shown in the bottom right caption and is very close to the experimental profile.

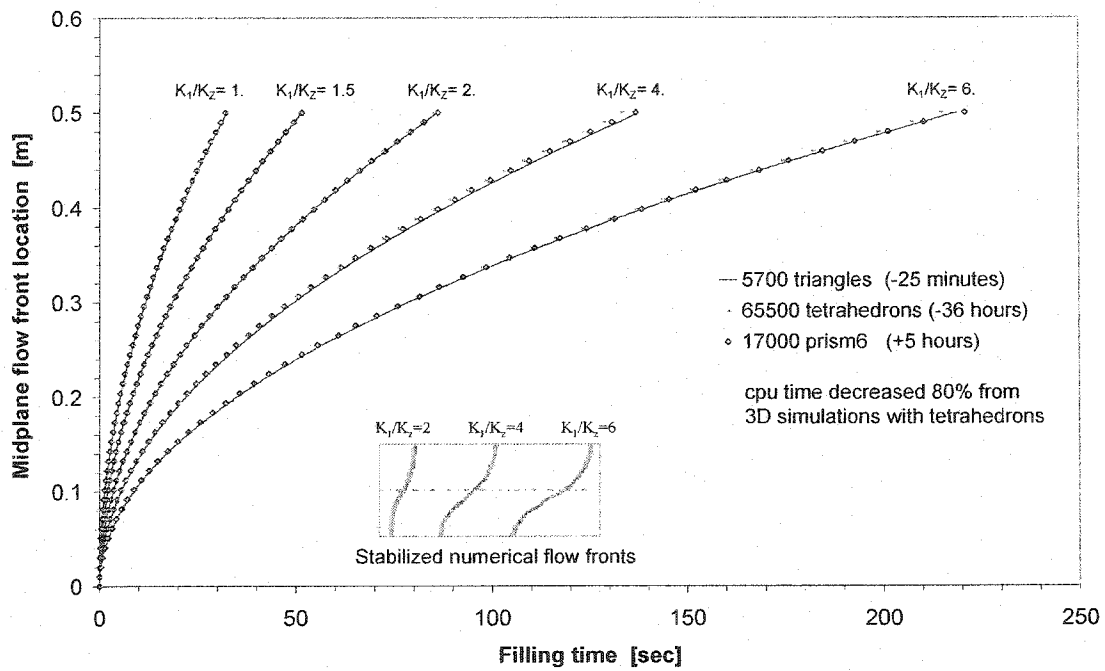


Figure 5.13. Progression of the flow front in the midplane for different anisotropy ratios. Compared to the two-dimensional (triangles) solution, the tetrahedron and prism6 solutions predict well the filling at the interface.

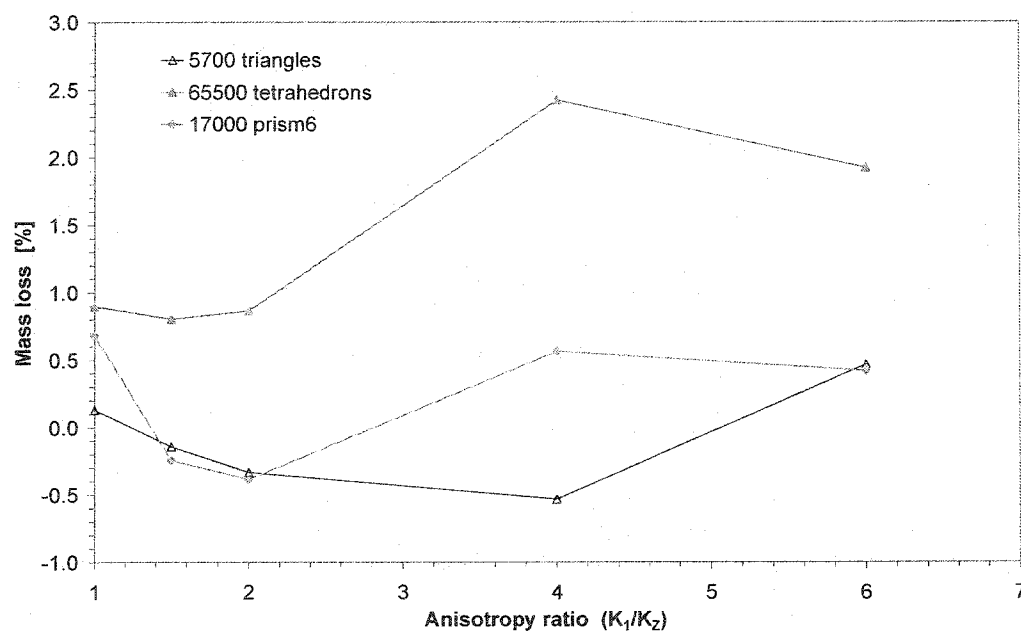


Figure 5.14. Comparison of mass loss for simulations with triangles, tetrahedrons and *prism6* elements. In all cases, the mass loss is less than 3%. The *prism6* solution is systematically more conservative than tetrahedrons and never worse than the triangle solution.

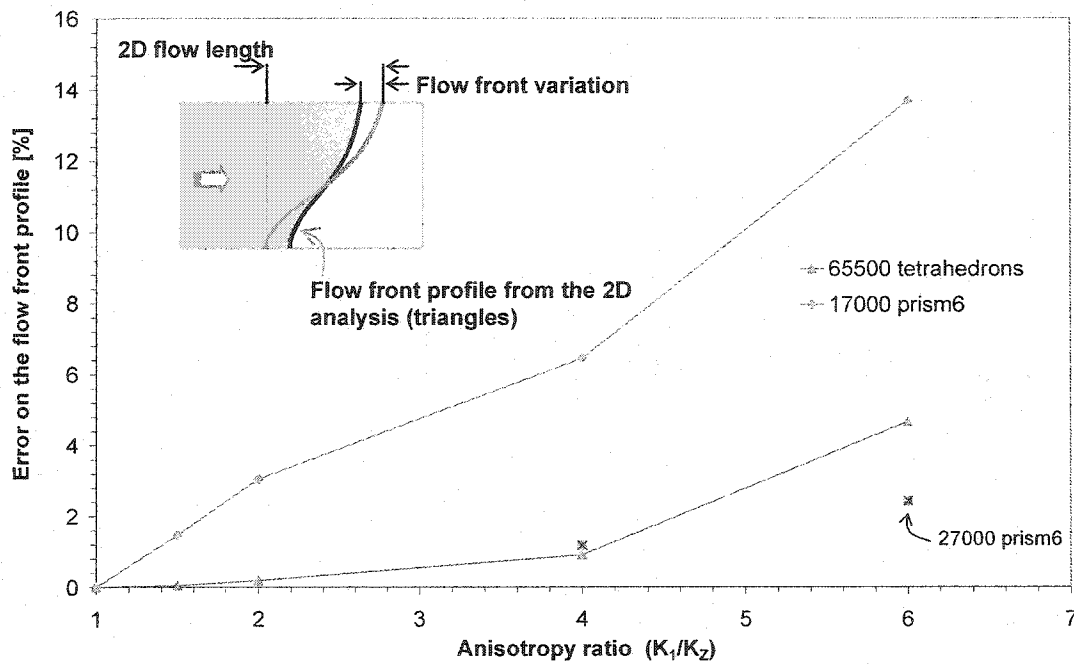


Figure 5.15. The distortion of the through-thickness flow front profile for *prism6* and tetrahedrons is compared to a 2D reference simulation (triangles). Tetrahedrons are able to represent correctly the front geometry for high anisotropy ratios. When the size of the *prism6* mesh is increased to a half of the elements of the tetrahedron mesh, the flow front error is even improved compared to the tetrahedron solution.

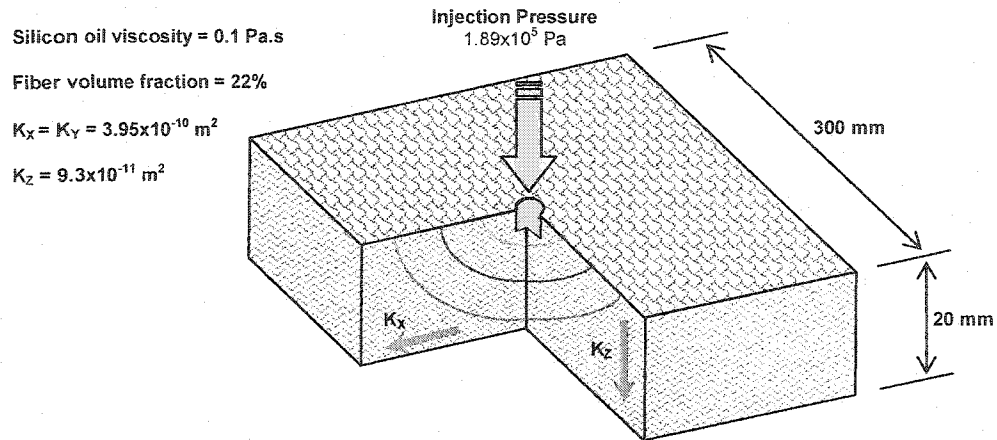


Figure 5.16. Schematic drawing of a spherical central injection. The experiment of Bréard et al. [15] was carried out in a thick rectangular mold. The fibrous preform had an anisotropy ratio of 4.25 between the planar and transverse permeabilities. X-Ray radioscopy was implemented to detect the progression of the three-dimensional fluid flow.

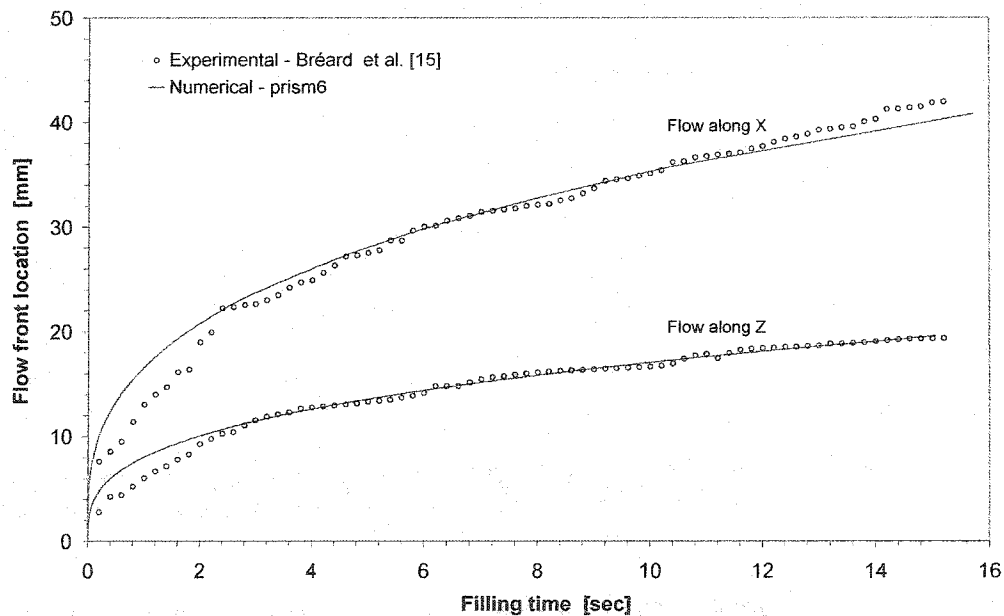


Figure 5.17. Comparison of predicted and measured flow fronts in the spherical injection. Numerical results are in good agreement with experimental values. At the beginning of the injection (before 2 sec), preform compaction may be the cause of the observed divergence with the numerical predictions.

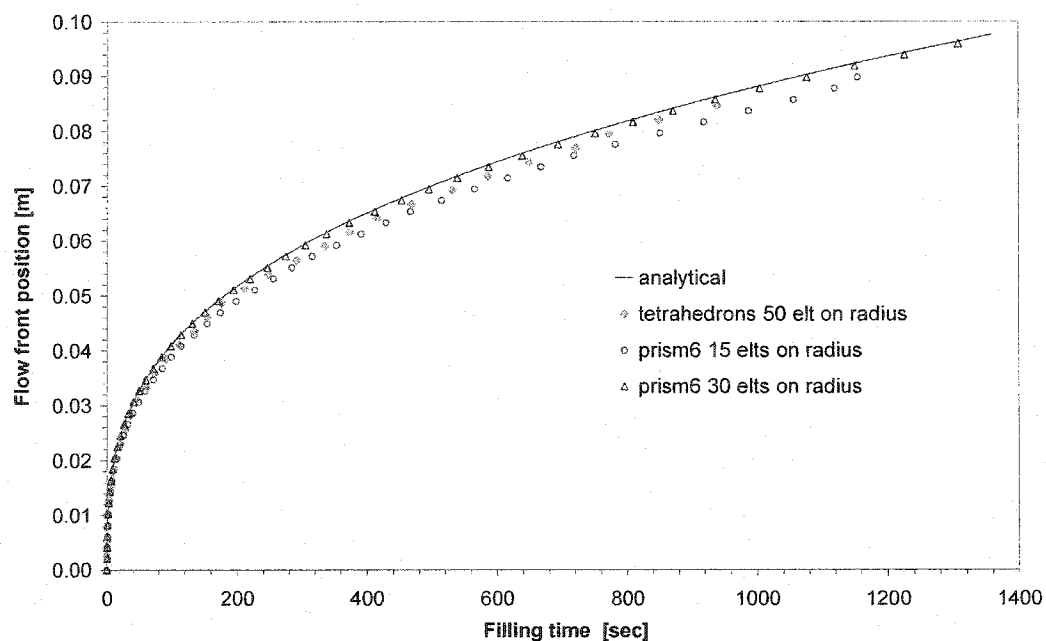


Figure 5.18. Comparison of flow front positions calculated for different mesh sizes with the theoretical solution of an elliptic flow through an isotropic material.

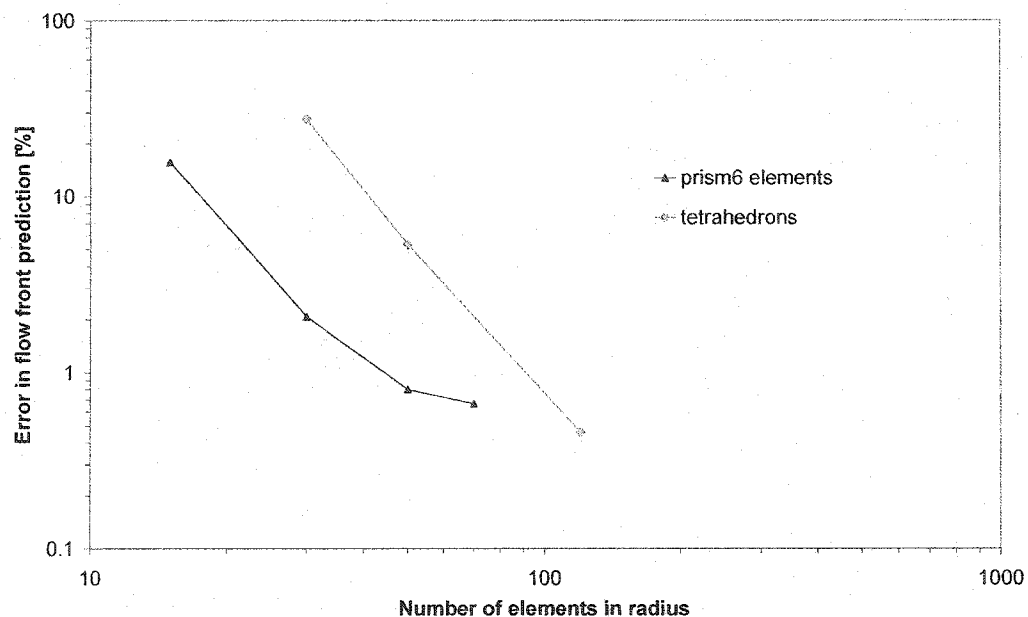


Figure 5.19. Convergence of mesh refinement for the elliptic flow through an isotropic material. For the same number of elements on radius, the *prism6* solution yields better results than the tetrahedron one.

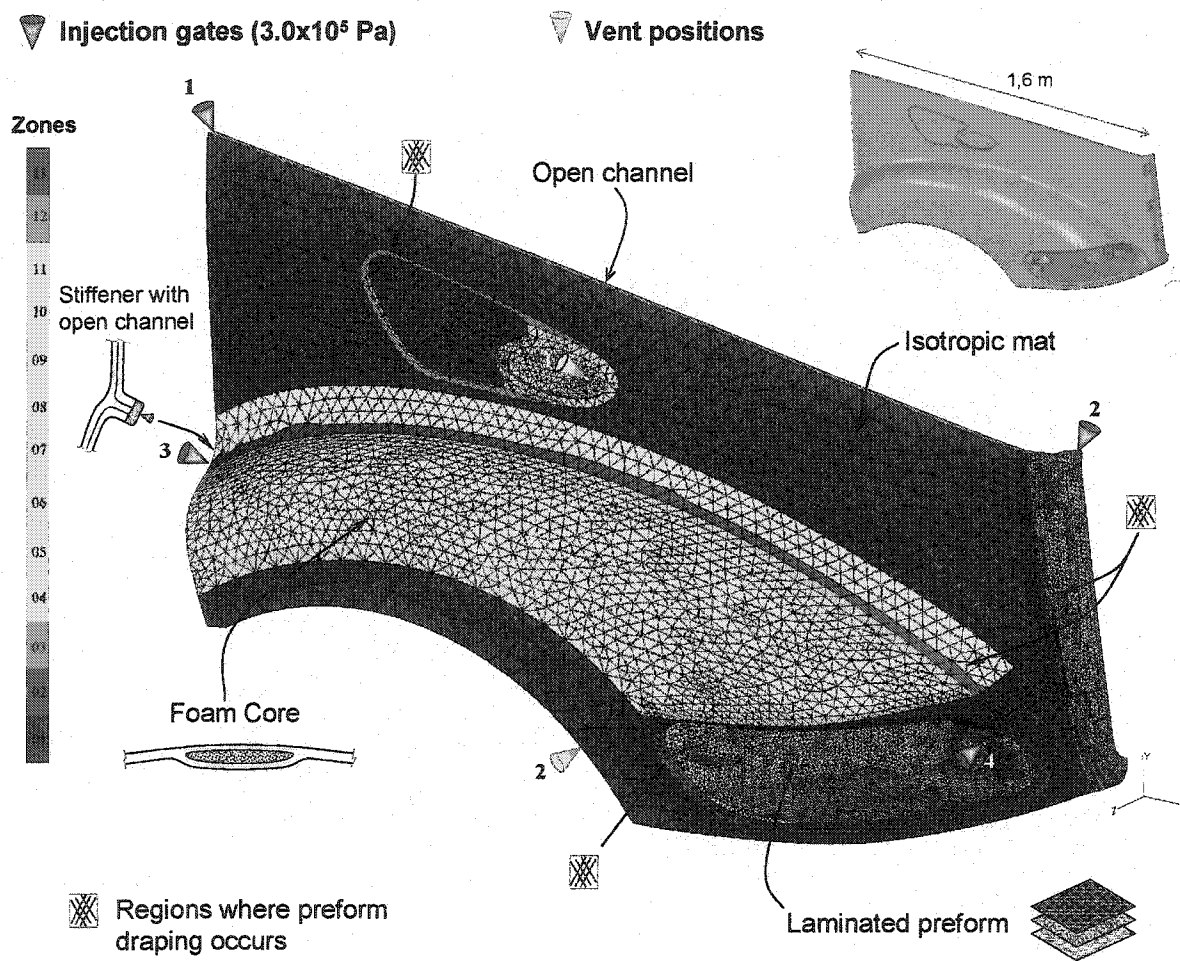


Figure 5.20. a Typical LCM part used to demonstrate the capabilities of the model. The mesh contains 17,000 triangles and 8,500 nodes. The injection strategy consists of four inlet gates at the upper part corners, at the stiffener ends, and in the laminated zone. An impermeable foam core is wrapped by fabric skins in zone 10. Draping effects are represented as regions with high or low permeabilities.

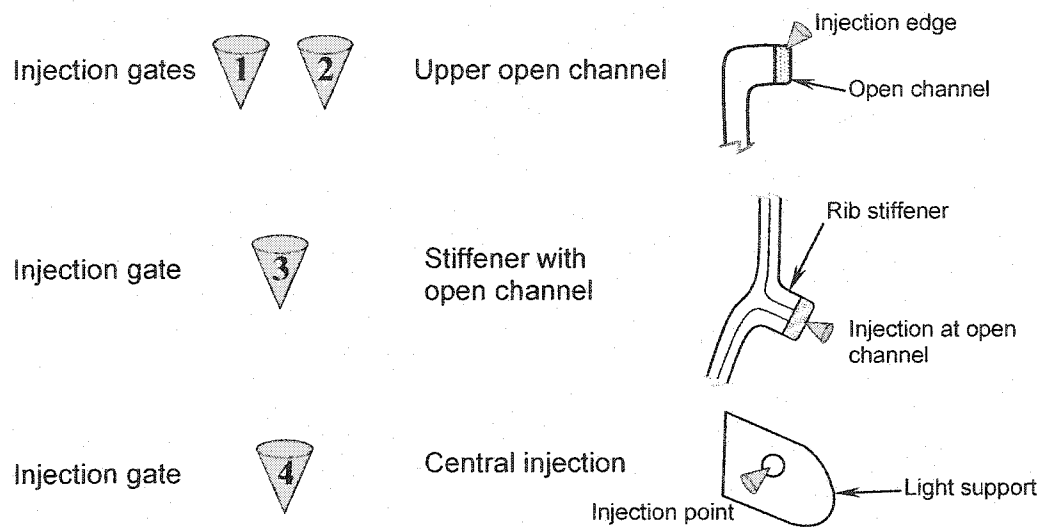


Figure 5.21. Injection strategy used for the truck fender. Four injection gates are set in the mold. Open channels are used for a better distribution of the resin flow. To ensure filling of the stiffener, an open channel is created at the extremity of the rib.

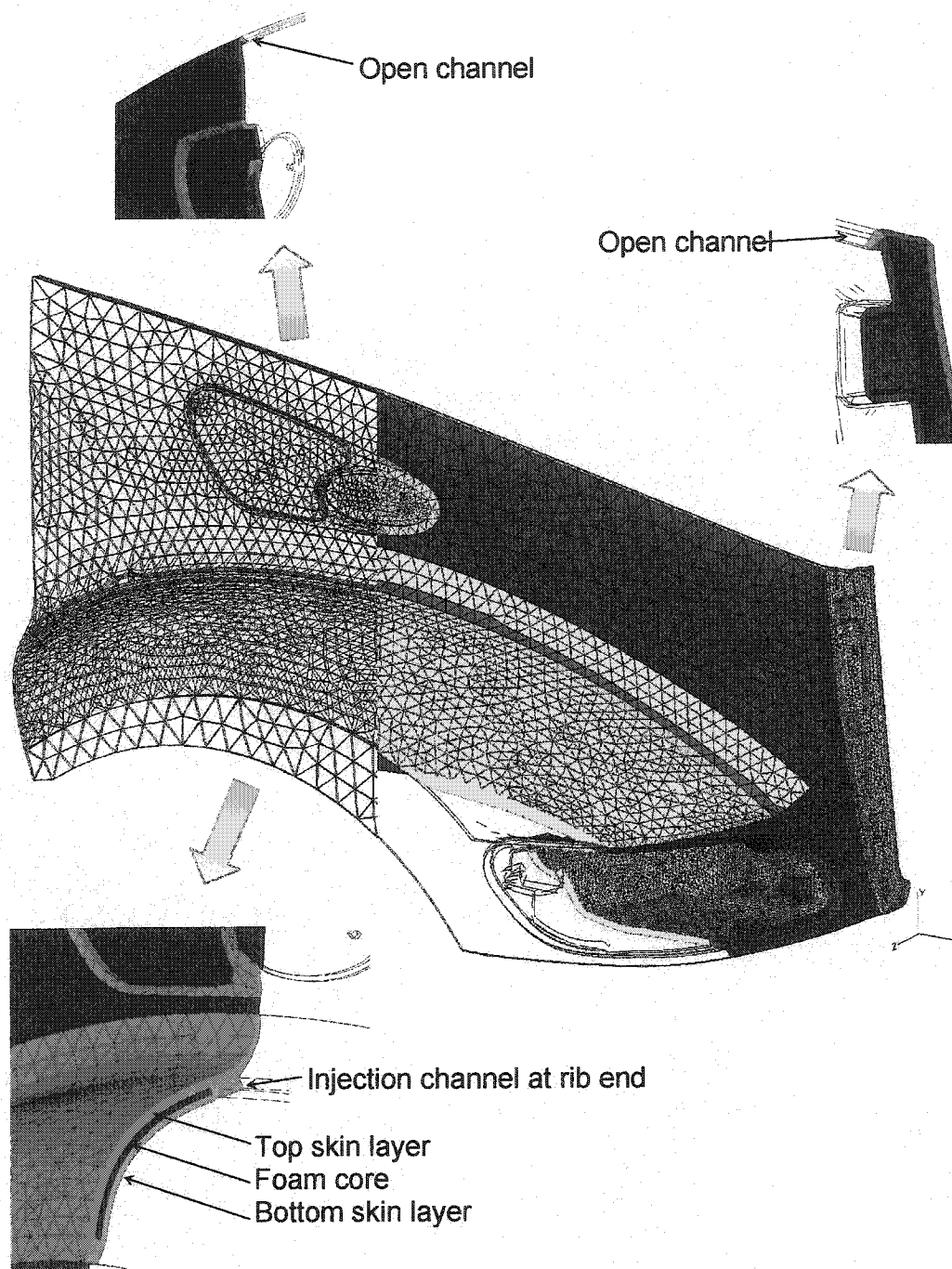


Figure 5.22. Three-dimensional model obtained after mesh extrusion. The mesh contains 60,000 *prism6* elements and 40,000 nodes.

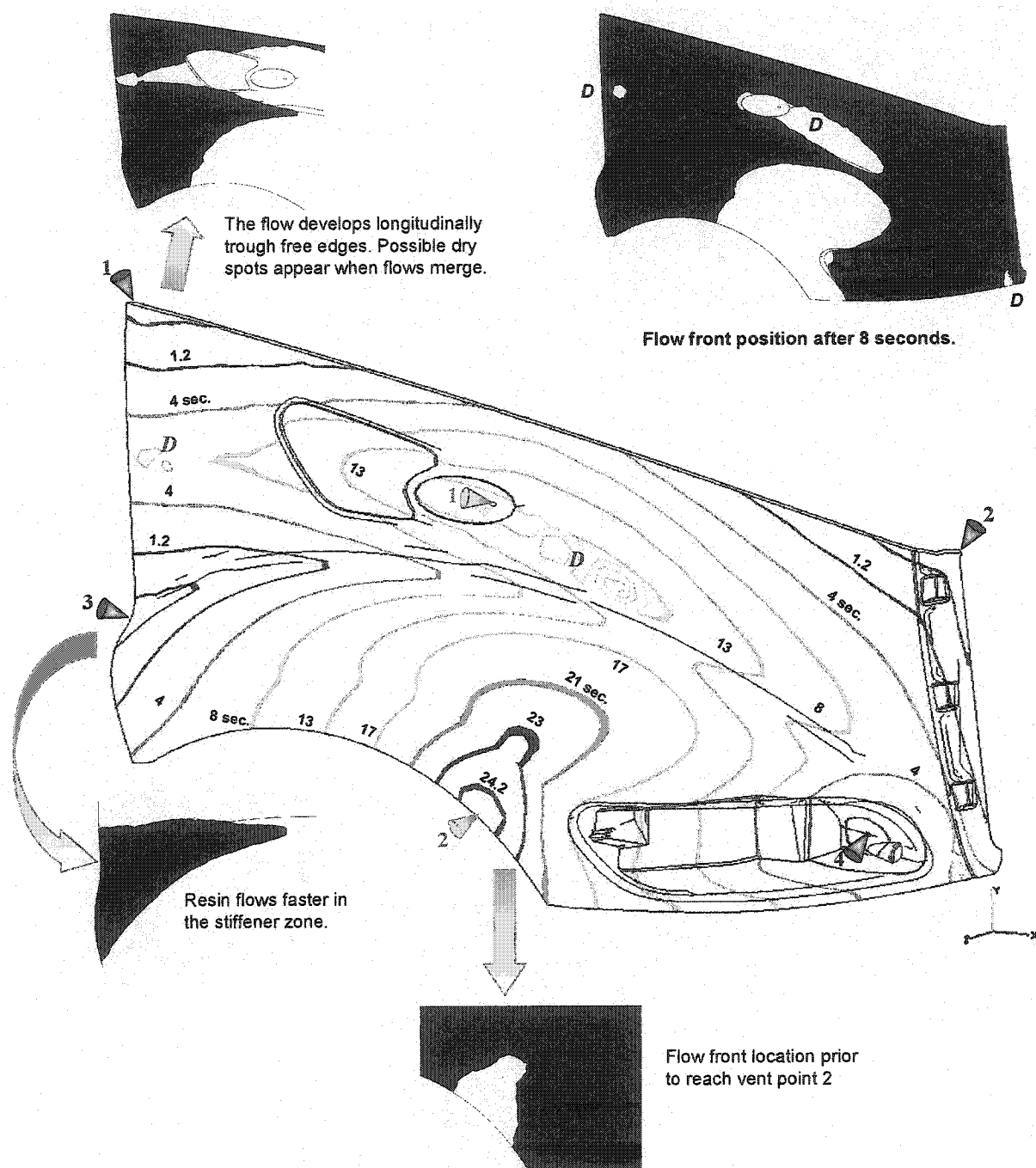


Figure 5.23. Predicted filling times with the triangular mesh for through-thickness averaged permeabilities. A total filling time of 24.6 sec was calculated. "D" indicates possible dry spots.

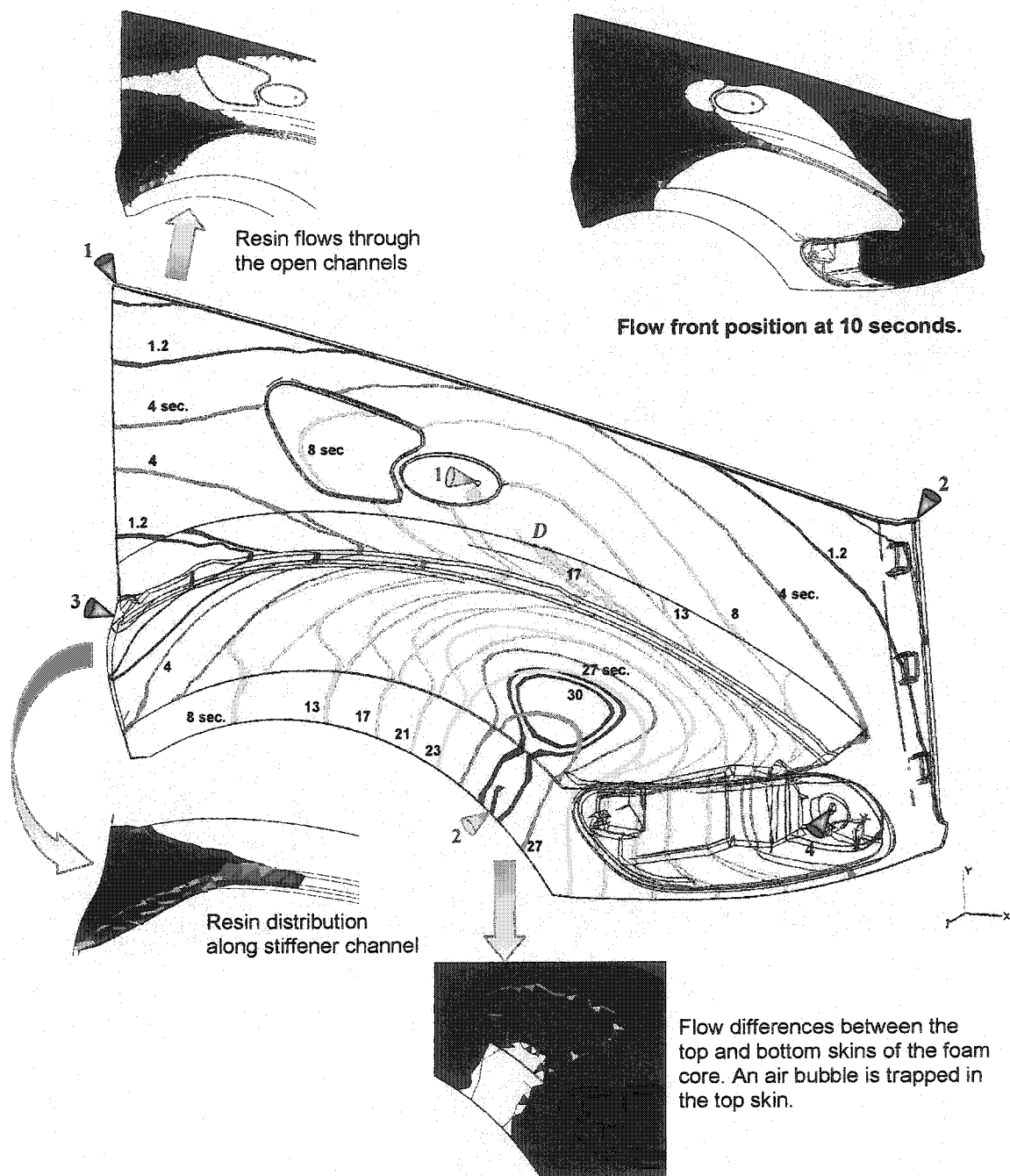


Figure 5.24. Predicted flow front locations with the prismatic mesh with multi-layer extrapolation. A total filling time of 30.6 sec was calculated. An air bubble was trapped in the upper foam skin.

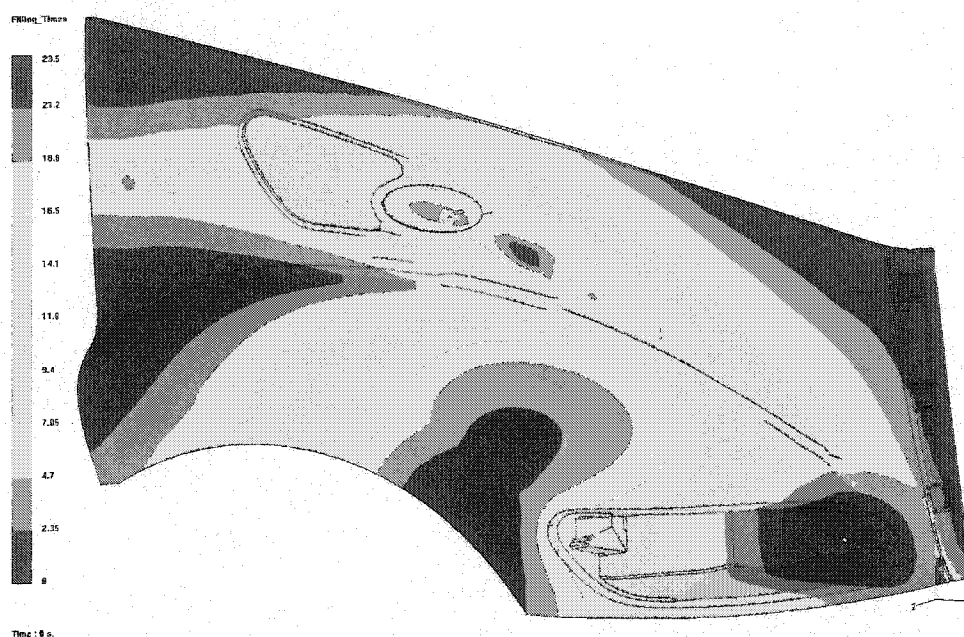


Figure 5.25. Predicted flow front positions with the triangular mesh with the *bottom* foam skin permeability. A filling time of 23.5 sec was obtained.

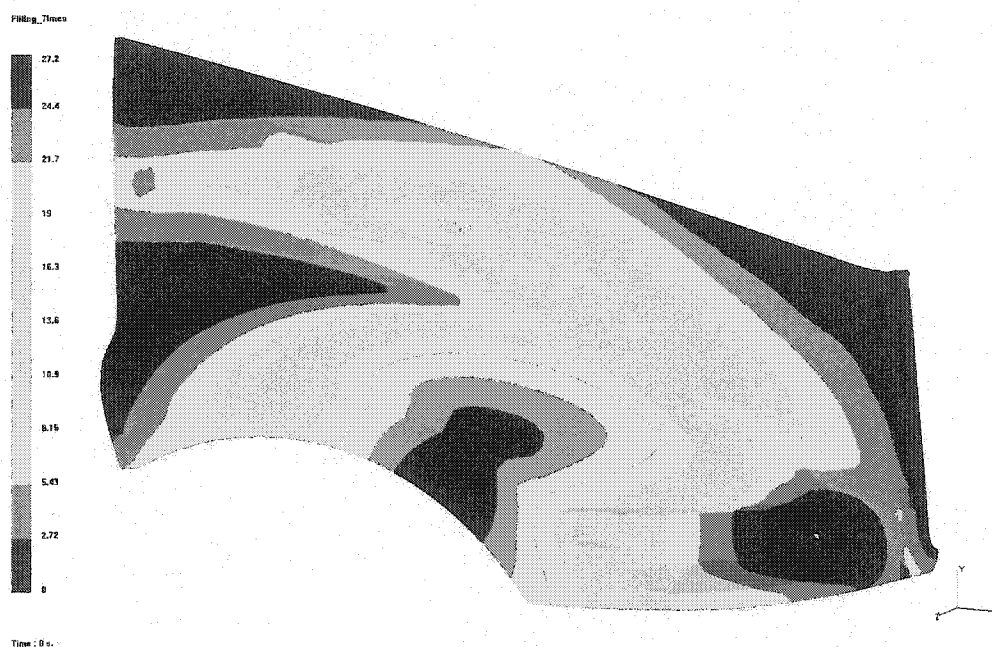


Figure 5.26. Predicted flow front positions with the triangular mesh with the *top* foam skin permeability. A filling time of 27.2 sec was calculated.

Table 5.1. Series of test carried out to quantify the resin mass loss when using *prism6* finite elements.

Permeability ($\times 10^{-9} \text{ m}^2$)			
Test #	K_1	$K_2 = K_Z$	K_1/K_Z
1	2	2	1
2	1.5	1	1.5
3	1	0.5	2
4	0.75	0.1875	4
5	0.5	0.0833	6

Table 5.2. Description of the 2D and 3D meshes used to compare the error on the mass loss.




Geometry of the FE's	Number of Finite Elements		
	Thickness	Length	Total
Triangles 	16	710	5700
Prism6 	16	330	17000
Tetrahedrons 	24	270	65500
Part dimensions : 500x12x12 mm			

Table 5.3. Permeability and porosity for each zone of the truck fender model.

Zone Id	Ply # →	1	2	3	4	5	6			
1	porosity	0.8								
	thickness [mm]	5								
	permeability 10 ⁻⁹ [m ²]	2								
2	porosity	0.8	0.8	0.8	0.8					
	thickness [mm]	5	5	5	3					
	permeability 10 ⁻⁹ [m ²]	0.3	0.3	0.3	0.3					
3	porosity	0.6								
	thickness [mm]	5								
	permeability 10 ⁻⁹ [m ²]	0.3								
4	porosity	0.8	0.8	0.8	0.8	0.8	0.8			
	thickness [mm]	5	3	3	5	2	2			
	permeability 10 ⁻⁹ [m ²]	3.5	3.5	3.5	0.7	0.7	0.7			
5	porosity	0.8								
	thickness [mm]	5								
	permeability 10 ⁻⁹ [m ²]	0.8								
6	porosity	0.6								
	thickness [mm]	5								
	permeability 10 ⁻⁹ [m ²]	0.3								
7	porosity	0.8	0.8	0.8						
	thickness [mm]	5	6	6						
	permeability 10 ⁻⁹ [m ²]	3.5	3.5	3.5						
8	porosity	0.6								
	thickness [mm]	5								
	permeability 10 ⁻⁹ [m ²]	0.3								
9	porosity	0.8								
	thickness [mm]	5								
	permeability 10 ⁻⁹ [m ²]	2								
10	porosity	0.8	0.8	0.8						
	thickness [mm]	5	10	7						
	permeability 10 ⁻⁹ [m ²]	0.8	Foam	2						
11	porosity	0.75	0.75							
	thickness [mm]	3	3							
	permeability 10 ⁻⁹ [m ²]	1.5	1.5							
12	porosity	0.99	0.99	0.99						
	thickness [mm]	4	3	3						
	permeability 10 ⁻⁹ [m ²]	100	100	100						
13	porosity	0.8	0.8	0.8	0.8	0.8	8			
	thickness [mm]	5	6	6	3	3	3			
	permeability 10 ⁻⁹ [m ²]	1.5	1.5	1.5	1.5	100	100			

CHAPITRE 6

COUPLED NON-CONFORMING FINITE ELEMENT AND FINITE DIFFERENCE APPROXIMATION BASED ON LAMINATE EXTRAPOLATION TO SIMULATE LIQUID COMPOSITE MOLDING PROCESSES. PART II: NON-ISOTHERMAL FLOW

Présentation du chapitre

Dans le chapitre 5, une méthodologie d'extrapolation de maillage a été développée sur le concept d'un composite stratifié. Un nouvel élément fini discontinu tridimensionnel a été développé pour améliorer la rapidité et la qualité des calculs du remplissage isotherme. Dans le chapitre 6, cette méthodologie est étendue au cas du remplissage non isotherme et de la cuisson de pièces tridimensionnelles. Pour l'évolution des flux thermiques dans la cavité du moule, une approche mixte couplant éléments finis et différences finies est proposée. La méthode développée consiste à calculer les variations de température par conduction et convection dans le plan de la pièce par la méthode des éléments finis, tandis que le flux de la chaleur à travers l'épaisseur du composite est évalué au moyen d'une approximation par différences finies unidimensionnelles. Cette formulation hybride a pour objectif d'améliorer la qualité et la vitesse des calculs thermiques et du changement d'état de la matière. La combinaison de la méthode d'extrapolation de maillage 3D en couches parallèles avec la formulation thermique hybride donne la possibilité de définir différents niveaux de couplage entre le flux de résine et les échanges thermiques. La méthodologie proposée dans cette approche permet à l'utilisateur du code de définir, à partir du même maillage 2D initial le niveau de complexité du modèle numérique. Les résultats obtenus pour chacun des

niveaux de couplage sont validés par comparaison avec diverses solutions analytiques. À la fin, les phases de remplissage non isotherme et de cuisson d'une pièce réelle 3D sont traités. Les résultats des anciens et des nouveaux modèles sont comparés, et la performance de la simulation numérique est établie.

Coupled Non-Conforming Finite Element and Finite Difference
Approximation Based on Laminate Extrapolation to Simulate Liquid
Composite Molding Processes. Part II: Non-Isothermal Flow

Edu Ruiz and François Trochu

Centre de Recherches Appliquées Sur les Polymères (CRASP)

Département de Génie Mécanique,

École Polytechnique de l'Université de Montréal,

e-mails: eduardo.ruiz@polymtl.ca, francois.trochu@polymtl.ca

Keywords: Transfer Molding (RTM), thermal analysis, residual stress, weaving.

Article soumis à la revue

International Journal for Numerical Methods in Engineering

Novembre 2003

6.1 Abstract

A numerical methodology is presented for the accurate simulation of non-isothermal mold filling in Liquid Composite Molding. Starting with a mid-surface mesh and based on the structure of the fabric reinforcement, the extrapolation algorithm described in Part I is used to generate 3D finite elements or parallel layers of 2D elements. To solve the coupled flow/energy/chemical species equations, two methodologies are used. The finite element formulation presented in Part I is first coupled with a 3D finite element formulation for heat and curing analyses. In the second approach, a hybrid finite element and finite difference model is proposed. As the heat conduction and convection is evaluated in the

plane of the elements by the finite element formulation, the through-thickness heat flow is computed by a one-dimensional finite difference approximation. The combination of the three-dimensional mesh extrapolated in parallel layers with the thermal formulations allows investigating diverse degrees of coupling between the fluid and heat flows. With the same initial 2D mesh and material data, the user can easily define the level of complexity to be used in the numerical model. The results of the thermal formulations are validated with analytical tests. The performance of the model as well as the gain in cpu time are summarized. Finally a test case is presented to illustrate the advantages of the coupled model in terms of accuracy

6.2 Introduction

Liquid Composite Molding (LCM) refers to a group of related and widely used manufacturing processes for composite materials. These processes consist in general of injecting a thermosetting resin in a closed mold where a dry-fibrous reinforcement has been placed. During the process, a catalyzed resin is injected under pressure into the pre-heated mold cavity. In case of thermosets, the resin reacts and solidifies during the curing phase. Once the resin has cured, the mold is opened and the composite part is demolded. The flow front locations in time, the pressure distribution and the temperature field are the main parameters that govern the molding process and the final properties of the part. These parameters can be predicted by numerical simulations during the filling and curing stages, to assist in designing the mold and improve the manufacturing process. During last decade, several computational studies have demonstrated that modeling and process simulation can help in tool design by providing preliminary information of fluid and heat flow evolutions. However, due to the complexity of the physical phenomena involved in LCM and their intrinsic coupling, a series of non-linear differential equations must be solved iteratively. For large scale models, a significant computational effort is required to run a complete

simulation of the manufacturing process. This renders the optimization of the full process a complex numerical challenge.

The control of heat transfer and chemical reaction in LCM is complex because a hard number of factors interact. As schematically indicated in Figure 6.1, four categories of phenomena occur during composite processing: rheological, thermal, chemical and viscoelastic. The resin flowing across the mold cavity absorbs heat by conduction from the mold walls and from the heated preform; temperature is also transported by convective forces. The rheological phenomena depend on the temperature and degree of conversion of the resin via the resin viscosity. In turn, the velocity field characterizing the fluid flow transports the chemical species and influences the thermal field. It also determines how the mold is going to be filled up by the resin and the quantity of heat that will be generated by viscous dissipation. On one hand, the chemical reactivity of the resin increases with temperature, on the other hand the exothermy of the polymerization reaction is usually sufficient to increase the temperature notably. Resin thermal and mechanical properties such as specific heat, thermal conductivity or elastic modulus depend on temperature and resin degree of conversion. The strain-stress relationship depends on temperature through the thermal expansion/contraction of the resin; it is also related to the degree of cure via the chemical shrinkage produced during the cross-linking polymerization. Finally, viscoelastic behaviour of the polymer depends on temperature, degree of cure and time (stress relaxation is observed during cure). The multiple interactions between these phenomena make the numerical modeling of the full process a complex, and sometimes unfeasible, task.

Researchers have resolved this complexity by building mathematical models of flow, heat transfer, chemical reaction and strain-stress relationship. Finite element software has been developed to implement some of these mathematical models for complex three-dimensional parts [1-10]. The energy equation was solved both by finite element

and finite difference. Guyonvarch et al. [1] presented a heat transfer analysis integrated with a non-isothermal 3D filling model. They used a Taylor-Galerkin method in a finite element model that guarantees a reasonable stability and accuracy of the temperature calculation even when convection becomes dominant. The calculated transient temperature response in a preheated mold showed a good agreement with experiments. The temperature calculated in mold filling simulations allows reproducing the high temperature gradients observed experimentally across the thickness of the part and in the mold during fiber impregnation. However, the scheme is not unconditionally stable, which creates numerical difficulties. The simulation predicts the temperature distribution in a three-dimensional cavity and in the heating mold, but at a considerably high computational cost.

Lebrun et al. [2] conducted an experimental investigation of heat transfer during the filling stage by measuring temperatures through the thickness of the part at four different locations in the flow direction. The authors presented a finite difference program used to calculate the temperature distribution through the thickness of the steel wall. They showed that it is possible to evaluate the effective thermal conductivity of a resin saturated fibrous preform by recording the temperatures inside the mold wall and in the mold cavity during the filling stage. This analysis has shown also that the thermal properties of the composite obtained by the rule of mixtures provide reliable information. Large discrepancies were obtained between the Nusselt numbers found in the literature and experimental results. In fact, all models underestimate the heat transfer at the surface of the mold, except the one accounting for thermal dispersion, which overestimated it. Experimental Nusselt numbers have been shown to be dependent on the molding conditions. An increase of the injection pressure increased the experimental Nusselt number, in a consistent way with the corresponding augmentation of resin velocity. However, an increase of the mold temperature caused a drop in the Nusselt number due to the competing effect between the temperature gradient at the mold surface and the difference between the surface temperature and the

inlet resin temperature. Finally, the authors presented a model for the Nusselt number, which takes into account the effects of thermal dispersion, variable resin viscosity, fiber volume content and mold temperature. This model gave better results than the previous ones documented in the literature.

In order to incorporate these considerations in non-isothermal filling simulations, Audet [18] implemented a Taylor-Galerkin method to solve the energy equation. Even if Taylor series approximation leads to both explicit and implicit numerical scheme, for stability considerations the implicit one was used. To minimize the numerical oscillations that tend to perturb the temperature distribution in transport problems coupled with diffusion, a second order Taylor series was considered. Although numerical stability is guaranteed, when convective terms become dominant in the heat flow, temperature oscillations appear at the boundaries. In extension of the model of Audet, Bohr [3] used a standard Galerkin formulation with an artificial diffusion term. In this approach, the thermal instabilities of the numerical scheme were solved by coupling the Galerkin formulation with the piecewise discontinuous finite element approximation of Lesaint-Raviart for transport problems. The resulting coupled formulation with a time Gear interpolation for the transient solution is unconditionally stable and does not require smaller time step iterations.

Tucker [4] presented a comprehensive analysis of the issues in the modeling of heat transfer and chemical reaction in resin transfer molding and structural reaction injection molding. The discussion was organized in four stages: incorporating the physical phenomena into a model, gathering material data, analyzing the model to provide physical understanding, and solving the model for a series of relevant cases. A rigorous derivation of the governing equations by the local volume averaging method has cleared up ambiguities about how some terms should be handled, and has clearly shown the need of adding dispersion terms in the energy balance and cure equations.

The author has also introduced a useful set of dimensionless parameters for the flow, heat transfer and cure models, and provides analytical solutions in some specific cases.

Gauvin and Trochu [5] analyzed non-isothermal fluid flows through multilayer preforms. Experimental results showed the influence of the mold temperature on the distribution of the resin temperature through the thickness of a composite. Since resin viscosity is highly sensitive to temperature, they suggested that a reliable simulation should take this dependence into account. Although the three-dimensional solution of the filling stage is robust and accurate, it still requires a large amount of computational time. Since the thickness of the cavity is usually small compared to the characteristic length of the part, it defines the size of the mesh used in numerical simulations. A minimum number of finite elements through the thickness of the part is necessary in order to obtain an acceptable solution. Moreover, the aspect ratio of these elements can not be too small to avoid numerical inconsistencies. These limitations result in a very dense mesh, which makes the three-dimensional finite element implementation of the solver highly computer intensive. The large number of degrees of freedom needed to model complex three-dimensional composite parts results in time consuming calculations that makes process optimization extremely difficult, if not impossible.

Extensive efforts have been made by researchers to decrease the computer time required to solve the coupled flow and thermal formulations. In a thin mold cavity, the flow may be simplified to a two-dimensional problem, but the three-dimensional heat transfer problem must be considered as such because of the important heat convection in the planar direction and heat conduction through the thickness of the part. When LCM parts are considered as thin shells, the permeability, diffusion and dispersion tensors are homogeneous through the thickness. In addition, thermal and chemical species diffusion due to mechanical dispersion is assumed to be of purely kinematic origin, and thus proportional to the velocity norm. Since the velocity can be neglected in the thickness direction, the chemical species dispersion may be evaluated in the

planar direction only, so that two-dimensional flow analysis can be carried out with three-dimensional heat transfer calculation.

To solve this simplified problem, different approximations have been suggested. Bruschke and Advani [8] proposed a mixed model based on in-plane flow solution (by 2D finite elements and element control volume) while the heat conduction/convection is solved by finite differences (FD) in 3D. The through-thickness heat convection is neglected and only in-plane heat transport is introduced into the FD thermal formulation. The convection term is added to the FD model using a thickness averaged velocity. In a similar way, Ngo and Tamma [9] have used a 2D FE formulation for the in-plane flow and a 3D FE formulation for the heat conduction/convection. The fluid flow calculation was based on the nodal control volume approach with conforming finite element approximation. To improve the numerical stability of the thermal formulation, the Streamline Upwind Petrov-Galerkin (SUPG) weighting functions were employed. The algorithm presented accounts for the three-dimensional mesh generation used to solve the heat transport problem and sub-time stepping of the filling time step to ensure the stability of the thermal solution. These methods are faster than full three-dimensional analysis but only consider a thickness-averaged permeability and resin viscosity. In fact, an averaged flow front is calculated in the midplane of the mold cavity. Moreover, finite difference formulations are not unconditionally stable when implemented to solve heat conduction and convection problems. For accurate solutions, the FD grid or the time step must be refined as a function of Fourier's and Nusselt's numbers. In practice, when the heat flow is dominated by convection, which is usually the case in Resin Transfer Molding (RTM), the number of time steps required to properly solve the FD model for each iteration of the flow solution turns out to make the calculations very computer intensive.

Based on physical considerations and on the combined implementation of several numerical algorithms, a new methodology is proposed to solve the non-isothermal

filling and curing phases in LCM. It consists of combining different FE and FD formulations depending on the degree of coupling needed between the thermal and flow phenomena to simulate accurately the manufacturing process. Starting with a midplane mesh, different options are possible. In the simplest case, no significant coupling is assumed to exist between the fluid flow and the heat transfer in the through-thickness direction. A numerical in-plane solution of the two-dimensional fluid flow and heat transfer is sufficient if it is coupled with a one-dimensional heat transfer analysis. When a full coupling has to be considered, a pure three-dimensional flow and thermal analysis can be carried out. Between these two solutions, various levels of coupling can be implemented on the same 2D mesh. The proposed algorithm permits the user to specify the level of complexity of the analysis without any additional meshing effort. A series of tests are carried out to validate by comparison with analytical results the different models proposed. Finally, a typical part will be analyzed to demonstrate the capabilities of the numerical algorithms implemented in this investigation.

6.3 Governing equations

6.3.1 Momentum equation

In Part I, a system of non-linear partial differential equations has been formulated in order to evaluate the flow of Newtonian fluids through a porous medium. The model accounts for isothermal flows in undeformable media and considers pressure of flow rate boundary conditions. In this part of the work, non-isothermal viscous flows in porous media will be modelled in presence of heat sources. Recalling Part I, the equation of mass conservation for the fluid phase can be written as:

$$\text{div}(\rho_f \cdot \vec{v}) = 0 \quad (6.1)$$

where ρ_r is the density of the injected resin and \bar{v} is the superficial fluid velocity. Darcy's law for Newtonian fluid flow through porous media was used as momentum equation and is expressed as follows:

$$\bar{v} = -\frac{1}{\mu}[K].\nabla p \quad (6.2)$$

in which $[K]$ is the permeability tensor, taking the form of a 3x3 matrix, μ is the resin viscosity and ∇P the pressure gradient. Polymer viscosity depends on temperature and on chemical changes during polymerization. The rheological characterization of reactive materials is complex because of the large number of variables that come into play. Polymer rheology is influenced by the chemical formulation and filler concentration (in general calcium carbonate). The viscosity of a reactive resin system is a function of pressure, temperature, shear rate and time. The time dependence is due to the growing size of the polymer molecules as polymerization progresses. Therefore, viscosity can be defined as:

$$\mu = f(P, T, \dot{\gamma}, \alpha, \varphi) \quad (6.3)$$

where T , $\dot{\gamma}$, α and φ denote respectively temperature, shear rate, resin degree of cure and filler concentration. In LCM, the reactive system is injected at low viscosity. Viscosity increases with conversion and reaches an infinite value when the material solidifies either by chemical cross-linking or as result of physical changes such as phase separation or crystallization. During processing, mold filling must be completed before resin viscosity reaches too high a value. The upward limit of resin viscosity is attained at the gel point. As demonstrated by Han and Lem [11], non-Newtonian effects appear to be small for polymer built up from breached monomers, except near the gel point.

Most viscosity models for reactive resins neglect the non-Newtonian effects because temperature and network formation tend to dominate the rheological changes.

Although it is usually valid to consider flow and cure independently, high speed processing may imply that some conversion occurs during resin impregnation. Conversion-based viscosity models have been extensively applied to polymers. The most widely used rheological model that accounts for the effect of polymer conversion on viscosity is the Castro-Macosko model [12]:

$$\mu(T, \alpha) = \mu(T) \cdot \left(\frac{\alpha_{gel}}{\alpha_{gel} - \alpha} \right)^{C_1 + C_2 \cdot \alpha} \quad (6.4)$$

$$\mu(T) = C_T \cdot \exp\left(\frac{T_g}{T}\right) \quad (6.5)$$

where α and α_{gel} are the instantaneous and gelation chemical conversions respectively, C_1 , C_2 , and C_T are empirical constants, and T_g is the polymer glass transition temperature.

6.3.2 Energy and chemical species

In order to model the influence of heat transfer on the temperature of the resin, mold and fibrous reinforcement, it is necessary to carry out an energy balance between each of the constituents. In general, two approaches may be followed to find the temperature field [13-15]. In the first one, the resin and the fibers are considered as separate constituents (two phase model) used their temperatures may differ at any point of the mold. In the second approach, the resin and fibers are assumed to be at the same temperature (the so-called *lumped* system). In general, the equilibrium model, i.e., the second approach, is considered reasonably accurate for RTM [13, 15], in which fluid

flow is relatively slow. Considering the lumped system, the energy and chemical species balance equations for the resin-fiber mix leads to a transient temperature T solution of the following equation:

$$\tilde{\rho} \tilde{Cp} \frac{\partial T}{\partial t} + \phi \rho_r Cp_r \nabla(\bar{v} \cdot T) + \nabla(\bar{v} \cdot P) = \left\{ \nabla([k] + [k_D]) \nabla T \right\} + \phi \rho_r H_{Tot} \dot{H} \quad (6.6)$$

where the density $\tilde{\rho}$, heat capacity \tilde{Cp} and conductivity \tilde{k} of the composite are the effective properties defined as:

a) for non-impregnated fibers

$$\begin{aligned} \tilde{Cp} &= Cp_a w_a + Cp_f w_f, & \tilde{\rho} &= (\rho_a \rho_f) / (\rho_a w_a + \rho_f w_f) \\ \tilde{k} &= (k_a k_f) / (k_a w_a + \bar{k}_f w_f), & w_a &= (\phi / \rho_f) / (\phi / \rho_f + (1 - \phi / \rho_a)) \\ w_f &= 1 - w_a \end{aligned} \quad (6.7a)$$

b) for impregnated fibers

$$\begin{aligned} \tilde{Cp} &= Cp_r w_r + Cp_f w_f, & \tilde{\rho} &= (\rho_r \rho_f) / (\rho_r w_r + \rho_f w_f) \\ \tilde{k} &= (k_r k_f) / (k_r w_r + \bar{k}_f w_f), & w_r &= (\phi / \rho_f) / (\phi / \rho_f + (1 - \phi / \rho_r)) \\ w_f &= 1 - w_r \end{aligned} \quad (6.7b)$$

In the above equations ϕ is the porosity and w_r , w_f and w_a denote the weight fractions of resin fibers and air, respectively. Note that the conductivity tensor $[k]$ of the composite is averaged in each direction. The subscript r stands for the resin, f for the fibers and a for the air. The coefficient $[k_D]$ represents the thermal dispersion tensor arising from

hydrodynamic dispersion. It can be evaluated as a function of Peclet number or characterized experimentally as a function of the fluid velocity [2, 18].

The following initial and boundary conditions are required to solve the energy equation (6.6):

$$\begin{aligned} T &= T_r^{inj} && \text{at the injection gates} \\ T &= T_f \quad \text{or} \quad q = (1 - \phi) \rho_f C p_f (\hat{n} \cdot \bar{v}) (T_f - T) && \text{at the flow front} \\ q &= h_{eff} A \cdot (T_{wall} - T) && \text{at mold walls} \end{aligned}$$

where T_r^{inj} and T_f denote the resin temperature at the injection gate and the temperature of the dry fibrous reinforcement, respectively, T_{wall} is the mold temperature at the surface (i.e., at the interface between mold and the fluid flow), h_{eff} denotes the effective heat transfer coefficient between the mold wall and the fluid, and q represents the heat flow through the surface area A .

The source term on the right side of equation (6.6) accounts for the internal heat generated by the exothermic chemical reaction in thermoset resin systems. The value $H_{Tot} \dot{H}$ denotes the instantaneous heat generated by the cross-linking polymerization reaction and H_{Tot} is the total or ultimate heat of reaction during cure. This source term is usually assumed to be proportional to the reaction rate $d\alpha/dt$.

Conservation of chemical species can be expressed through the continuity equation:

$$\phi \frac{\partial \alpha}{\partial t} + \bar{v} \cdot \nabla \alpha = \phi \dot{H} \quad (6.9)$$

To compute the energy equation (6.6), the dependence of the reaction rate must be modeled as a function of temperature and degree of polymerization α . The empirical

autocatalytic model of Kamal-Sourour [16] that describes free-radical polymerization reaction is used in this study and can be formulated as follows:

$$\frac{d\alpha}{dt} = \left(A_1 \cdot \exp\left(\frac{-E_1}{R \cdot T}\right) + A_2 \cdot \exp\left(\frac{-E_2}{R \cdot T}\right) \cdot \alpha^{m_1} \right) \cdot (1 - \alpha)^{n_1} \quad (6.10)$$

where coefficients A_1 and A_2 are Arrhenius constants, E_1 and E_2 are activation energies, R is the ideal gas constant and, n_1 and m_1 are the catalytic constants.

6.4 Finite elements formulation

Following the procedure described in Part I for the flow model, the energy balance equation (6.6) can be integrated over a control volume as:

$$\begin{aligned} \frac{\partial}{\partial t} \int_{\Omega} \tilde{\rho} \tilde{C}_p T \, d\Omega + \int_{\Omega} \phi \rho_r C_{p_r} \cdot (\hat{n} \cdot \bar{v}) \nabla T \, d\Omega + \int_{\Omega} (\hat{n} \cdot \bar{v}) \nabla P \, d\Omega \\ + \int_{\Omega} \nabla(\hat{n} \cdot ([\tilde{k}] + [K_D]) \nabla T) \, d\Omega = \int_{\Omega} \phi \rho_r \dot{H} \, d\Omega \end{aligned} \quad (6.12)$$

where Ω is the integration domain (in this case the volume of the element). The numerical solution of the integral energy equation is based on the standard Galerkin implemented by Bohr [3]. A Lesaint-Raviart formulation that avoids artificial oscillations is used to solve the transport problem. This method is based on the separation of the coupled convection/diffusion problem into a convective and a diffusive solution. The heat diffusion is initially solved by a standard Galerkin formulation; then temperature is transported using the Lesaint-Raviart approximation

with discontinuous finite elements. In the presence of thermal convection, the transport equation can be written in the following form:

$$\begin{aligned} \frac{\partial T}{\partial t} + \bar{v} \cdot \nabla T &= f, \quad \text{on } \Omega \\ T &= T(t), \quad \text{on } \Gamma_q \end{aligned} \quad (6.13)$$

where T is the temperature transported at velocity \bar{v} on the domain Ω , and $T(t)$ is an imposed temperature at the domain boundary Γ_q (usually the resin injection temperature). Function f represents a source term that can be a function of time and position. Using a variational formulation, the weak form of equation (6.13) is expressed as:

$$\int_{\Omega} w \left(\frac{\partial T}{\partial t} + \bar{v} \cdot \nabla T \right) d\Omega = \int_{\Omega} w f d\Omega + \int_{\Gamma_d} |T^+ - T^-| (\hat{n} \cdot \bar{v}) d\Gamma_d \quad (6.14)$$

for a test function w belonging to the space $F(\Omega)$, where T^+ and T^- are the temperature values on the two sides of the boundary Γ_d . The finite element solution of equation (6.14) is an iterative process that consists of building a sequence of elements in the fluid flow domain. Beginning with the elements adjacent to the injection gate, the temperature is transferred using an upwind scheme based on to the mesh connectivity. The heat convection is finally solved using a Gear implicit scheme for the time derivative:

$$\int_{\Omega} w \left(\frac{1.5T^n - 2T^{n-1} + 0.5T^{n-2}}{\Delta t} + \bar{v} \cdot \nabla T^n \right) d\Omega = \int_{\Omega} w f d\Omega + \int_{\Gamma_d} |T^{n+} - T^{n-}| (\hat{n} \cdot \bar{v}) d\Gamma_d \quad (6.15)$$

where indices n , $n-1$ and $n-2$ account for the actual and previous time steps. To evaluate the temperature field, a classical predictor-corrector method is used. The temperature is predicted by the diffusion equation and corrected by the convection solution. The iterative procedure consists of advancing half a time step in conduction and the other half in convection. The approximation of the energy equation by a sequence of conductive and convective solutions requires the continuity of the scalar field (i.e., the temperature field) at the nodes of the Galerkin formulation. For this reason, conforming shape functions are used in the 2D and 3D finite element approximations of the conduction/diffusion equation (6.6).

In a similar way to the energy equation, the balance of chemical species is solved separately for convection and for the polymerization reaction. The convective term of equation (6.9) can then be written as follows:

$$\int_{\Omega} w \left(\frac{\partial \alpha}{\partial t} + \bar{v} \cdot \nabla \alpha \right) d\Omega = \int_{\Gamma_d} [\alpha^+ - \alpha^-] (\hat{n} \cdot \bar{v}) d\Gamma_d \quad (6.16)$$

$$\alpha = \alpha_0 \quad , \quad \text{on } \Gamma_q$$

where α_0 is the initial degree of cure at the boundary Γ_q (generally the injection gate). The diffusion of chemical species is governed by a partial differential equation that requires proper time integration. Bohr [3] proposed to use fourth and fifth orders Runge-Kutta methods to solve the differential equation (6.10) of resin polymerization. In this paper, the fourth order Runge-Kutta method is used to evaluate the polymerization reaction. The degree of cure obtained is then transported with the Lesaint-Raviart integral formulation (6.16).

6.5 Solution of shell-like geometries

Finite element analysis is widely recognized as an accurate approximation method to solve coupled flow and thermal problems. One of the main advantages of this technique lies in its ability to minimize the temperature oscillations induced by convection terms. Even if complex solutions of non-isothermal flows are unconditionally stable, one main disadvantage is the computational cost. In three-dimensional modeling, the large number of elements required for proper spatial discretization leads to time consuming simulations. In many cases, a compromise has to be sought between accuracy and computer time. Since in LCM applications the thickness is usually much smaller than the other dimensions of the part, a very large number elements is required to model through-thickness variations of permeability or of viscosity in the case of non-isothermal injections. As a result the resin flows with a different velocity in each layer of the composite. If these velocity changes are important, a three-dimensional analysis becomes unavoidable.

Note that a non-uniform viscosity appears through the thickness of a composite shell when the mold walls are heated at a higher temperature than the fibers and the resin injected (see Figure 6.2). The temperature dependence of viscosity will induce velocity variations and a through-thickness resin flow. When a gap-wise averaged velocity is acceptable, the flow equation (6.2) can be reduced to the following two-dimensional form:

$$\begin{bmatrix} v_{\xi} \\ v_{\gamma} \end{bmatrix} = - \begin{bmatrix} S_{\xi\xi} & S_{\xi\gamma} \\ S_{\gamma\xi} & S_{\gamma\gamma} \end{bmatrix} \cdot \begin{bmatrix} \frac{\partial P}{\partial \xi} \\ \frac{\partial P}{\partial \gamma} \end{bmatrix} \quad (6.17)$$

$$\begin{bmatrix} S_{\xi\xi} & S_{\xi\gamma} \\ S_{\gamma\xi} & S_{\gamma\gamma} \end{bmatrix} = \frac{1}{h_\tau} \int_{-\frac{h_\tau}{2}}^{\frac{h_\tau}{2}} \frac{1}{\mu(\xi, \gamma, \tau, T, \alpha)} \cdot \begin{bmatrix} K_{\xi\xi} & K_{\xi\gamma} \\ K_{\gamma\xi} & K_{\gamma\gamma} \end{bmatrix} \cdot d\tau$$

where ξ and γ are the local coordinates of the planar geometry, τ denotes the gapwise coordinate and h_τ is the thickness of the gap. The velocity components v_ξ and v_γ are the gapwise averaged values in the planar directions, and $[K_{ij}]$ is the in-plane permeability tensor.

The mold walls in LCM have a strong influence on the energy balance. This implies that the heat transfer must be analyzed not only in the cavity but also in the mold. When three-dimensional FE formulations are used, the sparse matrix requires a large cpu time to be solved. If pure 3D finite differences (FD) solutions are implemented, undesirable temperature oscillations appear in convection dominated flows. In this work, a hybrid scheme is proposed to evaluate the three-dimensional energy equation, so as to obtain a stable and efficient numerical methodology to calculate non-isothermal flows and curing phases in shell composite parts. Based on the concept of separation of the conduction and convection phenomena, the approach consists of solving the 3D heat conduction by coupling the two-dimensional in-plane solution of the convective heat transfer with a one-dimensional through-thickness heat conduction analysis. First, the in-plane thermal conduction is calculated by the standard Galerkin formulation. Then, with the gapwise averaged velocity the planar convection is computed by the Lesaint-Raviart transport approximation. Once temperature is corrected, the through-thickness conduction and curing are evaluated by a finite difference approximation. Using successive half time stepping, the three formulations are solved for a single flow time step. Note that in this procedure, the connectivity of the finite element mesh exists only the two-dimensional space while finite difference nodes are coupled only in the thickness direction. The matrices of the FD formulation are tridiagonal (or quasi

tridiagonal), so the numerical solution is highly efficient in terms of computer time. The stability of this numerical scheme is guaranteed because each of the formulations is unconditionally stable. In addition, any temperature oscillation induced by the FD approximation is diffused during the same time step by the FE solution.

6.6 Finite difference formulation

The solution of the through-thickness energy balance involves a subdivision of the in-plane control volumes (defined by the finite element edges) into a certain number of layers. The Galerkin finite element approximation of the heat conduction problem is calculated with conforming shape functions. This implies that the temperature scalar field is evaluated at the element nodes. In the hybrid FE/FD scheme, the connection between two-dimensional FE and one-dimensional FD formulations must then be done through the element nodes. As depicted in Figure 6.3, the finite difference nodes are extrapolated from the mesh nodes by the extrapolation algorithm described in Part I. Every FD node is associated to a control volume bound by the centroids and the mid-edges of the connected elements. The energy balance equation (6.6) becomes Fourier's heat conduction equation in one dimension. The volume averaged 1D Fourier's equation is written as:

$$V \tilde{\rho} \tilde{C}_p \frac{\partial T}{\partial t} = A \tilde{k}_\tau \frac{\partial^2 T}{\partial \tau^2} + V \phi \rho_r H_{tot} \dot{H} \quad (6.18)$$

where $T(t, \tau)$ is the transient absolute temperature at position τ through the total part thickness $part_thickness$ ($0 \leq \tau \leq part_thickness$), A and V denote respectively the interface area between control volumes and volume of the control volume depicted in Figure 6.4. The discretization of the partial differential equation (6.18) is done with an implicit finite difference scheme. Crank-Nicolson formulation is used because it gives

the smallest accumulated truncation error and an unconditionally stable linear system. In adimensional form, the energy balance for node j at position i and time step $t+1$ results in the following expression:

$$T_j^{i,t+1} - T_j^{i,t} = Fo_j^{i,t+1/2} \cdot \left[(T_j^{i+1,t} - 2T_j^{i,t} + T_j^{i-1,t}) + (T_j^{i+1,t+1} - 2T_j^{i,t+1} + T_j^{i-1,t+1}) \right] + \Omega_j^{i,t+1/2} \quad (6.19)$$

Here Fo represents Fourier's number defined by:

$$Fo_j^{i,t+1/2} = \left(\frac{\tilde{k}_t}{\tilde{\rho} \cdot \tilde{C}_p} \right)_j^{i,t+1/2} \cdot \frac{\Delta t}{(\Delta h_j)^2} \quad (6.20)$$

where Δt is the time step increment and Δh_j the distance between two adjacent nodes. For a better adimensional modeling, a constant grid spacing is assumed for the through-thickness finite difference nodes. The term Ω_j^i in equation (6.19) is the heat generated by the resin exothermy in the control volume; it is expressed by:

$$\Omega_j^{i,t+1/2} = \left(\frac{\partial \alpha}{\partial t} \cdot \frac{\phi \rho_r}{\tilde{\rho} \tilde{C}_p} \right)_j^{i,t+1/2} \Delta t H_{Tot} \quad (6.21)$$

The calculation of $Fo_j^{i,t+1/2}$ and $\Omega_j^{i,t+1/2}$ require the knowledge of the spatial and temporal averaged properties in the control volume. If thermal properties do not strongly vary between two time steps, equation (6.19) reduces to:

$$\begin{aligned} & T_j^{i,t+1} (1 + 2Fo_j^{i,t}) - T_j^{i+1,t+1} Fo_j^{i+1,t} - T_j^{i-1,t+1} Fo_j^{i-1,t} \\ & = T_j^{i,t} (1 - 2Fo_j^{i,t}) + T_j^{i+1,t} Fo_j^{i+1,t} + T_j^{i-1,t} Fo_j^{i-1,t} + \Omega_j^{i,t} \end{aligned} \quad (6.22)$$

For a group of finite difference nodes connected through the thickness, the solution is expanded into the following matrix notation:

$$\begin{aligned}
 & \begin{bmatrix} 1 & 0 & 0 & 0 & \cdot & \cdot & 0 \\ -Fo^1 & 1+2Fo^2 & -Fo^3 & 0 & \cdot & \cdot & \cdot \\ 0 & \cdot & \cdot & \cdot & \cdot & \cdot & 0 \\ \cdot & \cdot & \cdot & \cdot & \cdot & \cdot & \cdot \\ \cdot & \cdot & \cdot & \cdot & \cdot & \cdot & \cdot \\ \cdot & \cdot & \cdot & 0 & -Fo^{Nf-2} & 1+2Fo^{Nf-1} & -Fo^{Nf} \\ 0 & \cdot & \cdot & 0 & 0 & 0 & 1 \end{bmatrix}_j^t \cdot \begin{Bmatrix} T^1 \\ T^2 \\ \cdot \\ \cdot \\ \cdot \\ T^{Nf-1} \\ T^{Nf} \end{Bmatrix}_j^{t+1} = \\
 (6.23) \quad & = \begin{Bmatrix} T^{wall_top,t+1} \\ T^{2,t}(1-2Fo^{2,t}) + T^{3,t}Fo^{3,t} + T^{1,t}Fo^{1,t} + \Omega^{2,t} \\ \cdot \\ \cdot \\ \cdot \\ T^{Nf-1,t}(1-2Fo^{Nf-1,t}) + T^{Nf,t}Fo^{Nf,t} + T^{Nf-2,t}Fo^{Nf-2,t} + \Omega^{Nf-1,t} \\ T^{wall_bot,t+1} \end{Bmatrix}_j
 \end{aligned}$$

where j denotes the in-plane mesh node where finite differences are extrapolated, and Nf is the total number of finite difference nodes. To avoid confusion between FE and FD entities, the finite difference nodes are renamed *pseudo nodes* because they do not necessary represent the part geometry. In fact, the 1D Fourier's equation is adimensionally represented as a percent of the part thickness at the mesh node position. The vector $\{T^i\}_j^{t+1}$ represents the unknown temperatures of the *pseudo nodes* at time step $t+1$. The boundary conditions $T^{wall_top,t+1}$ and $T^{wall_bot,t+1}$ are imposed at time step

$t+1$, i.e., imposed as the reference temperature of the top and bottom mold walls respectively.

Experimental studies of LCM processing have shown that significant temperature fluctuations appear at the mold walls during the filling and curing phases [2]. This implies that the assumption of a constant mold wall temperature is not always verified. To account for appropriate thermal boundary representation, different types of boundary conditions are considered. As shown in Figure 6.5, the mold wall can include a heating/cooling duct pipe at a distance d from the mold surface. The following general thermal boundary condition may then be applied:

$$k_{eff} \frac{\partial T^{wall}}{\partial \tau} + h_{eff} [T^{wall} - T_{ref}(t)] = 0 \quad \text{for } \tau = 0, h_j \quad (6.24)$$

where T^{wall} is the temperature of the mold wall, and T_{ref} is a reference temperature of the fluid in the duct pipe. The coefficients k_{eff} and h_{eff} represent respectively the effective mold thermal conductivity and the convective heat transfer coefficient between the fluid and the pipe. The approximation of a constant mold wall temperature can be derived from equation (6.24) by setting:

$$T^{wall} = T_{ref}^t \quad (6.25)$$

where T^{wall} represents the temperature of the top or bottom mold surfaces, and T_{ref}^t is the mold platen reference temperature which varies in time. In this case, both temperatures are identical. A second boundary condition can be derived from the quasi-steady-state analysis of the mold heating/cooling system of Figure 6.5. This configuration results in the following equation:

$$\frac{T^{wall} - T_j^t}{d} + \left(\frac{h_{eff}}{k_{eff}} \right) \cdot [T^{wall} - T_{ref}^t] = 0 \quad \text{for } i = 2, Nf-1 \quad (6.26)$$

Regrouping terms, the expression of T_{wall} for a given time step $t+1$ will be:

$$T^{wall, t+1} = (T_{ref}^{t+1} \cdot (h_{eff} / k_{eff}) + T_j^t / d) / (d + h_{eff} / k_{eff}) \quad \text{for } i = 2, Nf-1 \quad (6.27)$$

This approach represents fairly well the interactions between the mold walls and the surface of the part, although it is limited to the quasi-steady-state solution. This means that the temperature variations of the mold platens in time must be slow enough to allow a steady heat flow through the mold walls. In a more general case, it is necessary to solve a non-steady-state temperature evolution between the mold wall and the heating/cooling pipes. This problem can be solved by adding a finite difference grid into the mold walls and using an experimental value of the convection coefficient h_{eff} .

The accuracy of the solution of equation (6.23) depends on the choice of Fourier's number Fo (or Δt). Even if the Crank-Nicolson scheme is unconditionally stable, a choice of Fo close to unity tends to minimize the accumulated truncation error. In this work, an adaptative time step algorithm was implemented to provide a Fourier's number close to one. This algorithm calculates the time step Δt required to obtain a value of Fo close to unity. Because the thermal properties of the composite depend on both the temperature and the resin degree of cure, Fourier's number is expected to vary through the thickness of the part. From all the values of Fo calculated for a stack of finite difference volumes, the adaptative time step algorithm selects the one that results in the minimum value of Δt required for convergence.

During composite processing, the exothermic chemical reaction of resin polymerization causes a quick temperature increase in the core of the part. The temperature rate $\partial T / \partial t$ between two time steps may become high enough to generate numerical oscillations

and alter the calculated temperature profile through the thickness. Therefore, it is necessary to decrease the time step in order to keep the desired accuracy of the numerical solution. In the particular case of LCM, this can be achieved by setting Δt as a function of temperature and the cure rate $\partial\alpha/\partial t$ with the following empirical condition:

$$\frac{\partial\alpha}{\partial t}T \leq 1 \quad (6.28)$$

6.7 Numerical implementation of the hybrid FE/FD model

In Part I, a methodology was presented to solve the inconvenience of multi-material definition of the laminated preform. Isothermal three-dimensional flows were calculated by constructing automatically with an extrapolation algorithm, non-conforming finite elements from the two-dimensional mesh. Beginning with a thin shell mesh, a solid mesh is generated by extruding the 2D finite element mesh. The extrusion is defined by the preform stacking sequence that allows the use of different material properties for each laminate ply. This methodology can also be applied to generate parallel layers of two-dimensional elements not coupled with the through-thickness direction. As depicted in Figure 6.6, different levels of inter-layer coupling are possible when the mesh extrapolation is combined with the one-dimensional finite difference grid. As already mentioned, the simulation of LCM processes involves in complex coupling between pressure, temperature and degree of cure. Two or three-dimensional solutions are required depending on to the level of coupling between the different physical phenomena that came into play in LCM process. It is common practice in computer simulation to begin with simple models so as to understand the global flow evolution and verify the geometrical model. Then, model refinement is carried out and more elaborated mathematical formulations are progressively implemented. Finally,

complex mathematical and geometrical models are resolved to predict accurately the filling and curing stages. In this iterative process, the remeshing of 3D geometries is a complex task especially when thermal boundary conditions have to be specified on a three-dimensional mesh.

In this investigation, an integrated methodology is proposed to analyze the level of complexity of the numerical and geometrical models. As shown in the schematic representation of Figure 6.7, various levels of coupling may be obtained by combining the finite element mesh with the finite difference grid. The numerical formulations presented in this paper stand for the following solutions:

- Flow analysis (Darcy and filling):
 - 2D and 3D finite elements
- Heat conduction (energy balance):
 - 2D and 3D finite elements
 - 2D finite elements + 1D finite differences
- Transport equation (balance of chemical species):
 - 2D and 3D finite elements
- Resin cure:
 - 2D and 3D finite elements
 - 2D finite elements + 1D finite differences

The possible combinations between these approximations are listed in Table 6.1. Different levels of integration of the flow, thermal and curing formulations are possible. In the simplest coupling, the flow is evaluated on the 2D mesh and the energy balance is studied with the 2D finite element space and 1D finite difference approximation. In a higher level of coupling, flow and transport are calculated on 2D parallel meshes, but pressure is not considered uniform in the through-thickness direction. Heat conduction

and resin cure is solved on the parallel FE meshes and coupled across the thickness via the FD grid. The most complex formulation is the pure three-dimensional FE solution based on *prism6* extrapolated elements or tetrahedrons.

An algorithm was developed to perform compatible calculations on a series of parallel meshes. The pressure, temperature, degree of cure and viscosity are averaged and transferred between the FE and FD control volumes. The aim of this integrated methodology is to help in process design. Beginning with the same 2D mesh, global flows can be rapidly computed. More complex solutions may be performed without much user effort. It is well known that in numerical process optimization, the successive evaluations of complex geometrical models results in extremely high cpu times. The multiple coupling method has the ability to initially evaluate the global problem in a simple solution and progressively increase the model complexity according to the optimization convergence. The method is promising and may turn full process optimization feasible. Figure 6.8 shows the flow chart used to solve the coupled equations of the non-isothermal filling/curing simulation.

6.8 Analytical validations

6.8.1 Case I: 3D heat conduction - steady-state

To validate the numerical solution of the heat equation, an analytical comparison is carried out in the three dimensional space. In this test case, a cubic geometry was selected to evaluate the steady-state heat conduction. As shown in Figure 6.9, the upper surface of the cube is maintained at a constant non null temperature while the bottom surface and two sides are assumed to have a zero constant temperature. Considering

that thermal properties are all unity, the analytical solution of the stationary temperature profile is:

$$T(x, y, z) = \frac{16}{\pi^2} \sum_{n=0}^{\infty} \sum_{m=0}^{\infty} \frac{\sin \frac{(2n+1)\pi x}{L} \sin \frac{(2m+1)\pi y}{W} \sinh \pi z \sqrt{\frac{(2n+1)^2}{L^2} + \frac{(2m+1)^2}{W^2}}}{(2n+1)(2m+1) \sinh \pi H \sqrt{\frac{(2n+1)^2}{L^2} + \frac{(2m+1)^2}{W^2}}} \quad (6.29)$$

where L , W and H are the cube dimensions. Two formulations were tested in the steady state: full 3D finite elements and hybrid 2D FE/1D FD. The geometrical support used for each formulation is depicted in Figure 6.10. To ensure a good aspect ratio of the *prism6* finite elements, the number of nodes in the transverse direction H is double that of the in-plane nodes. Note that non-connected layers of the hybrid FE/FD model are extrapolated at the midplane of the connected layers. Figure 6.11 shows the temperature distribution along the z -axis for $x = y = 1$. The theoretical temperature profiles are compared with the numerical simulations for both formulations. The 3D mesh consists of 5×5 nodes in the xy plane and 10 extrapolated layers. The hybrid mesh has only 5 FE layers, while the number of FD nodes in the z -direction was varied between 7 and 21. A good approximation of the analytical values was found for the pure FE solution. The hybrid formulation increases in accuracy with the number of finite difference nodes. The maximum relative error for different mesh sizes is shown in Figure 6.12. Due to the 3D behavior of heat conduction, the three spatial dimensions must be increased proportionally to compare the error between meshes. For the pure FE solution, the error decreases logarithmically when the number of mesh nodes is duplicated. The results of the hybrid FE/FD formulation are in good agreement with analytical values even for a coarse mesh. For the same mesh, an important gain in accuracy is observed when the FD nodes are duplicated.

6.8.2 Case II: 3D heat diffusion - un-steady-state

A two-dimensional heat diffusion analysis has been used to test the proposed thermal formulations. As depicts Figure 6.13, a rectangular domain is considered to be at initial temperature $T_0=0$. A constant temperature is imposed at two sides of the rectangle $T(t)=1$. Also, the meshes generated to test the FE and hybrid FE/FD formulations are depicted in the same figure. The analytical solution can be found by the method of separation-of-variables [19]. The dimensionless temperature distribution may be expressed as the product of the solutions in each direction:

$$\left(\frac{T - T_\infty}{T_0 - T_\infty} \right)_{X,Y} = \left(\frac{T - T_\infty}{T_0 - T_\infty} \right)_X \cdot \left(\frac{T - T_\infty}{T_0 - T_\infty} \right)_Y \quad (6.30)$$

where T_0 is the initial temperature, and T_∞ the boundary condition outside the domain. A square is considered in this test with $L=H=1$ and a constant boundary condition on two sides. The one-dimensional solution is applicable here to the X and Y axes, and may be written with a Fourier sine expansion as follows:

$$\left(\frac{T - T_\infty}{T_0 - T_\infty} \right)_{X \text{ or } Y} = \frac{4}{\pi} \sum_{i=0}^{\infty} \frac{\sin(\psi_i \cdot x)}{\psi_i} \cdot \exp(-\psi_i^2 \cdot \alpha \cdot t) \quad (6.31)$$

$$\psi_i = \frac{2n+1}{L} \pi$$

where α is the thermal diffusivity of the material (in this case $\alpha=1$). Finally, the theoretical solution is finally the combination of equations (6.30) and (6.31). The numerical simulation was performed using different mesh sizes and number of extrapolated layers. The number of elements in the gapwise direction was kept at one, while the ratio of the in-plane number of elements along the X and Y directions of the

3D mesh was maintained constant. Figure 6.14 depicts the temperature evolution at a control point $X=Y=1$. Theoretical values are compared to the results of the pure FE and hybrid FE/FD solutions for two mesh sizes. The pure FE formulation shows a good agreement with analytical values even for a coarse mesh (5x5 nodes). The hybrid formulation for 5 extrapolated layers gives also a good approximation. When only one extrapolated layer is used, the solution seems to diverge from exact values.

The L_n -norm of the error between the temperature calculated at a given position ε and the theoretical solution is defined as:

$$L_n(\varepsilon) = \left(\sum_{t=1}^I |T_\varepsilon^{cal}(t) - T_\varepsilon^{exact}(t)|^n / I \right)^{1/n} \quad (6.32)$$

where $T_\varepsilon^{exact}(t)$ and $T_\varepsilon^{cal}(t)$ are the exact and calculated temperatures at position ε and time t , and I denote the number of time steps. A mesh refinement study has been performed to evaluate the influence of the mesh on the rate of convergence. Figure 6.15 shows the L_2 -norm of the error for each mesh size. An error of less than 2% was found for the pure FE formulation when using a mesh of 5x5 nodes. The error decreased to around 1% for a 30x30 mesh. In the hybrid formulation, the error with one mesh layer of 5 nodes and finite differences in the transverse direction was 4.5%. Increasing the number of extrapolated layers, the number of transverse FD nodes was duplicated resulting in higher convergence rates. The accuracy of the hybrid solution for a mesh of 10 nodes along the X -axis, 10 extrapolated layers and 20 FD nodes was 0.15%. These results show that both formulations converge to the theoretical values even for coarse meshes. The hybrid formulation gave increased convergence rates than the three-dimensional FE solution.

6.8.3 Case III: heat diffusion with source term - curing analysis

One of the most important analyses in LCM concerns the prediction of the chemical conversion during the exothermic polymerization. To test the quality of the numerical formulations, a curing test was carried out in a rectangular cavity similar to test case II. The cavity has dimensions 0.1 m length, 0.05 m thickness and 0.005 m width. A mix of 50 % resin and fibers is considered to be initially at 300°K. In the top and bottom surfaces, a mold temperature of 400°K was fixed. On one side of the cavity, a temperature of 350°K was set to induce an in-plane heat flow. The kinetic modeling of the resin and the thermal properties of the fibers and resin are presented in Table 6.2. In a typical LCM curing of thick composite parts, in-plane heat flow plays an important role in the evolution of resin polymerization. This heat flow induces a non-uniform conversion rate in the part that results in residual stresses and geometrical distortions. In the cavity tested, a control point located at the centre is used to compare the differences in the exothermic temperature and degree of cure between numerical formulations. Figure 6.16 shows the pure FE and hybrid FE/FD solutions of temperature and degree of cure at the control point. A two-dimensional finite elements solution is also drawn as a reference. For the same number of mesh and FD nodes, the hybrid formulation seems to better approximate the two-dimensional solution. This is mainly because the control volumes are defined coincident with the elements and the curing formulation uses an averaged element temperature to evaluate the resin kinetics. The FD formulation considers the control volumes associated to each node, and uses the nodal temperatures for kinetic calculations. To compare these results, an error estimator of the computed curing time (R_c) may be defined as follows:

$$R_c = \frac{|t_c^{ref} - t_c|}{\Delta t^{ref}} \quad (6.33)$$

where t_c is the calculated time to fully cure the cavity, t_c^{ref} is a reference time considered to be the curing time calculated by the two-dimensional solution. Δt^{ref} is a reference time variation ($\Delta t^{ref} = 60 \text{ sec.}$). The resulting error on the curing time for different mesh sizes is given in Figure 6.17. For the same number of layers and FD nodes, the hybrid FE/FD formulation shows a smaller error than the pure FE formulation. The error decreases logarithmically for both formulations when the number of through-thickness layers increases. To estimate the performance of the solutions, the computer time is combined with the error on curing time in the following form:

$$R_p = (1 - R_c) \cdot (1 - R_{cpu}) \quad (6.34)$$

where

$$R_{cpu} = t_{cpu} / t_{cpu}^{ref} \quad (6.35)$$

Here t_{cpu}^{ref} and t_{cpu} denote respectively a reference cpu time and the cpu time to calculate a given solution. Figure 6.18 shows the performance index R_p for different solutions of both models. For coarse meshes, the gain in cpu time is compensated by the important error of the solution, resulting in a worse performance. When the number of through-thickness layers or finite difference nodes is increased, the performance shows a peak for around 15 layers. In all cases the hybrid formulation gives an improved performance with respect to the pure FE solution. This is due to the quality of the FD calculations and the fast solution of the tri-diagonal linear systems of the hybrid formulation. After the peak, the mesh or grid refinement results in a decrease of performance. The decay of the FE solution is more pronounced than for the hybrid formulation due to time consuming inversion of sparse FE matrices. In conclusion, the hybrid formulation presents strong advantages in terms of performance compared to pure FE techniques.

6.8.4 Case IV: heat convection test

In order to analyze the effects of the heat convection during filling, a linear injection in a heated cavity is considered. As depicted in Figure 6.19, the 0.5 m length rectangular cavity has a constant thickness of 5 mm. Temperature is fixed at the top and bottom surfaces of the mold at 350 °K and 330 °K respectively. A fiber reinforcement with an isotropic permeability of $1\text{e-}10\text{ m}^2$ is considered to fulfill the cavity with a fiber bed of volume content 50%. The thermal properties of the fibers and resin are the same as in the previous cases (see Table 6.2). The initial temperature of the fibers is 310 °K while the resin is injected into the cavity at 300 °K with a constant pressure of $1\text{e}5\text{ Pa}$. To evaluate the pure heat transport, the resin viscosity is considered to be constant with temperature at a value of 1 Pa.s . As a result of the linear flow in the rectangular cavity and the transverse heat conduction, a non-uniform heat convection will appear across the cavity thickness. In order to solve this heat transport problem, different models were generated combining FE and FD formulations supported by 2D and 3D finite elements. As shown in Table 6.3, six models are presented to account for various FE/FD combinations. Models #1 and #2 are the standard solutions used in the previous LCM simulation code for 2D and 3D analyses respectively. Model #3 is the new proposed 3D pure FE solution based on *prism6* elements, while models #4 to #6 are the new simplified solutions combining FE with FD formulations.

Figure 6.20 shows the temperature evolution on a fixed position along the longitudinal axis ($x = 30\text{ mm}$) for the six models tested. At the beginning, the temperature evolves due to through-thickness conduction. At around 20 seconds, the flow front arrives to the fixed position inducing a temperature increment due to the heat transport. While during the conduction period the models are reasonably close to each other, in the heat convection regime a maximum variation of 2 °K appears between the 2D solution of model #1 and the FE/FD models #5 and #6. The simplest solution of one layer of 2D

finite elements and through-thickness finite differences (model #4) shows a small overheating at the flow front arrival, and then converges to the stabilized value of models #5 and #6. Figure 6.21 depicts the temperature distribution in the cavity midplane at the end of filling for the six models tested. Nearly the injection side, where the heat flow is convection dominated, variations were found between models. Combined FE/FD formulations on a coarse mesh show a delay in the temperature evolution with respect to the 2D solution of model #1 obtained on a refined mesh. The 3D pure finite element solutions of models #2 and #3 are more accurate than the 2D heat transport of models #4 to #6. For the same number of layers, the new *prism6* element gives a better solution than the tetrahedrons model. Note that in the stabilized regime, a temperature oscillation appears in the tetrahedron solution because the velocity vector is outside the plane of the elements. This effect disappears in the *prism6* solution because the velocity is aligned with the element plane.

Table 6.4 gives the computer times required to run each model on an IBM IntelliStation Z-Pro PC with a Pentium IV (2.8 GHz) processor. While the standard tetrahedrons solution took more than 4300 seconds to run, the new *prism6* model required only 1700 seconds for an improved solution. The 2D FE/1D FD models #4 and #5 show an important advantage in terms of cpu times (simulations in 24 and 280 seconds respectively). This analysis shows that even if the quality of the 2D FE/1D FD is not as precise as the pure 3D finite element solution, the gains in computer time make the simplified model reliable for a first approximation of the flow solution. Depending on the complexity of the flow, the model quality can be progressively increased to approach the solution. The simplified model can initially be used to evaluate the global problem in order to optimize the filling and/or curing stages. As the numerical optimization algorithm progresses, model complexity can be increased to improve the accuracy of the local optimum.

6.9 Case study – Automotive front hood

To illustrate the advantages of the proposed models and of the extrusion methodology, a non-isothermal filling and curing simulations of an automotive front hood have been conducted. As depicted in Figure 6.22, the mid-plane geometry of the front hood is discretized with a 2D finite element mesh containing 3000 triangular elements and 1600 nodes. The dimensions of the part are approximately 1.56 m length by 1.15 m width with 5 mm thickness. During the non-isothermal filling, the resin is injected at a constant pressure of 3×10^5 Pa at 330 °K. The mold cavity contains an isotropic fiber mat with a permeability of 1×10^{-9} m² ($V_f = 50\%$). The fibers are considered to be preheated at 350 °K while a fixed temperature 370 °K is set on the top and bottom mold walls. To account for the resin polymerization during the filling flow, the resin viscosity was modeled as dependent of the temperature and the degree of conversion (see Table 6.5). The thermo-kinetic parameters used in the simulation are listed in Table 6.2. As presented in Table 6.6, five models were selected to run the non-isothermal filling followed by a curing phase. Pure FE solutions are calculated with a tetrahedron mesh (model #1) and a *prism6* mesh (model #2). Three combined FE/FD formulations are proposed. The first two (models #3 and #4) are the simplest solution consisting of one layer of 2D finite elements (triangles) to evaluate the in-plane fluid flow and heat transport, coupled with 1D through-thickness finite differences to account for the transverse conduction. Model #5 combines the 2D FE and 1D FD heat conduction (triangles) with 3D heat and flow transport in *prism6* elements.

Figure 6.23 shows the flow front locations in time for the non-isothermal filling simulation of models #1, #2, #4 and #5. A good agreement was found between the models. A maximum predicted filling time of 590 seconds was obtained for the hybrid 3D FE/FD formulation of model #5 versus 540 seconds of the pure 3D FE solution with *prism6* elements (model #2). Figure 6.24 depicts the degree of resin conversion calculated at the midplane of the cavity at the end of filling. As expected, the resin at

the flow front has the longest residence time and has received the highest amount of heat. As a result of this progressive heating, the maximum degree of polymerization at the end of filling will be found in the latest filled regions and at the periphery of the part. While a degree of cure of about $5e-3$ was calculated for the pure 3D formulations (models #1 and #2), a value close to $2e-2$ was obtained for the hybrid FE/FD formulations (models #4 and #5). Note that the transport of the degree of cure in the pure 3D solutions shows a diffusion near the flow front. The maximum degree of cure is not exactly at the flow front location as expected. This numerical diffusion is not observed in the hybrid formulations. Table 6.7 summarizes the results obtained with the five models tested for the filling and curing simulations. The theoretical degree of cure was obtained by solving the kinetic equation at the mold wall temperature (assumed to be the temperature of the resin particles on the flow front near the mold wall). The comparison indicates that 2D heat transport models provide the best predictions of the ultimate degree of polymerization at the end of filling.

Once the mold is filled-up, the simulation continues with a curing analysis until the part is fully cured. Figure 6.25 shows the degree of resin conversion at 1500 seconds after the beginning of the injection. A curing front from the perimeters of the part towards the centre is induced by thermal effects during filling. Numerical diffusion in the 3D FE formulation still appears as a consequence of the diffused cure transport during filling. Table 6.7 resumes the curing times and exothermic temperatures for the five models tested. The theoretical values were calculated in a 1D solution for the cavity thickness at the averaged boundary condition between injection resin temperature and initial fibers temperature (considering that injection gate is the latest region to cure). The comparison demonstrates that the 1D FD model in the through-thickness direction is well appropriate to solve this complex thermal problem. Figure 6.26 compares the computer times required to run each model. While the tetrahedron solution took more than 44 hours, the model with the new *prism6* element required only 1 hour 40 minutes, and the hybrid 2D FE/1D FD models around 5 minutes. This study demonstrates the

many advantages of the proposed hybrid formulation. The methodology presented here to increase the level of coupling between the physical phenomena that govern the solution is remarkably interesting because of the important time savings it brings.

6.10 Summary

In this study, a new hybrid finite element/finite difference approximation has been developed to describe the chemorheological behaviors of non-isothermal resin flows and the curing phase in LCM. The fluid flow was computed through the FE/CV method described in Part I, two numerical methods were implemented to solve the energy balance and curing equations. A pure finite element formulation has been initially used to calculate the heat exchanges and resin cure in three-dimensional parts. The method consists of a mixed Galerkin/Lessaint-Raviart schema for heat conduction/diffusion and transport respectively evaluated in a new prismatic *prism6* element. The second approach presented is the hybrid FE/FD scheme. In this case, a finite element formulation used to evaluate the in-plane heat exchange in the part is coupled with a one-dimensional finite difference approximation to calculate the through-thickness heat flow. The latter numerical method is stable and showed much improvement in performance in terms of precision and computational efforts, mainly for large parts.

Comparisons with analytical 2D and 3D heat flows have demonstrated the accuracy of the numerical solutions. Based on the mesh extrusion concept, connected prismatic elements (*prism6*) or non-connected parallel layers of triangles are generated automatically by an extrapolation algorithm from a mid-surface mesh. The combination of the extrusion methodology with the two thermal formulations results in different levels of user defined through-thickness coupling. This allows the selection of increasing levels of complexity to compute the coupled equations. Analysis of a case test was conducted to illustrate the capabilities of the extrusion methodology and of the

hybrid FE/FD formulation. A quick evaluation of the virtual process can be first carried out by a simple FE/FD coupling. To obtain more accurate results, the level of coupling can then be progressively increased with the same input mesh and process data. This methodology is promising especially for numerical optimization when a large number of evaluations are required. The optimization algorithm can begin with a simulation model looking for a global optimum and then increase the quality of the model as convergence progresses towards a refined optimum. Future research efforts will aim to implement this possibility.

6.11 Acknowledgements

The authors thank the *National Science and Engineering Research Council of Canada* (NSERC) and *Fonds Québécois pour la Recherche sur la Nature et la Technologie* (FQRNT) for their financial support. The contribution of *ESI_Group* and their numerical support is also gratefully acknowledged, as well as the program of *Bourses d'Excellence du Ministère de l'Éducation du Québec* that made this research possible.

6.12 References

1. Guyonvarch G., Audet M., Qian Y. Y., Trochu F., Delaunay D. Validation of Non-Isothermal Resin Transfer Molding Simulations. *Joint European Conference JEC*. Paris, April 24-26 1996.
2. Lebrun G., Gauvin R. Heat Transfer Analysis in a Heated Mold during the Impregnation Phase of the Resin Transfer Molding Process. *Journal of Material Processing and Manufacturing Sci.* 1995; 4:81-104.

3. Bohr E. *Etude des Échanges Thermiques dans la Fabrication des Composites par les Procédés d'Injection sur Renfort*. Mémoire de Maîtrise en Sciences Appliquées. Dep. Génie Mécanique. École Polytechnique de Montréal. 2000; 267 pgs.
4. Tucker C. Heat Transfer and Reaction Issues in Liquid Composite Molding. *Polymer Composites* 1996; 17(1):60-72.
5. Gauvin R., Trochu F. Key Issues in Numerical Simulation for Liquid Composite Molding Processes. *Polymer Composites*. 1998; 19:233-240.
6. Ferland P., Trochu F., Gauvin R., Guittard D., Boime B. Rate of Conversion, Temperature Variation and Flow Simulation of Reactive Liquid during RTM and SRIM Mold Filling. *ENERCOMP 95 conf.* Montreal, Quebec, May 1995.
7. Young W.-B. Three-Dimensional Non-Isothermal Mold Filling Simulations in Resin Transfer Molding. *Polymer Composites*. 1994; 15(2):118-127.
8. Bruschke M. V., Advani S. G. A Numerical Approach to Model Non-Isothermal Viscous Flow Through Fibrous Media with Free Surfaces *International Journal for Numerical Methods in Fluids*. 1994; 19:575-603.
9. Ngo N. D., Tamma K. K. Non-Isothermal 2D Flow/3D Thermal Developments Encompassing Process Modelling of Composites: Flow/Thermal/Cure Formulations and Validations. *International Journal for Numerical Methods in Engineering*. 2001; 50:1559-1585.
10. Chang A., Hwang S., Modeling Nonisothermal Impregnation of Fibrous Media with Reactive Polymer Resin. *Polymer Eng. and Sci.* 1992; 32(5):310-318.
11. Han C., Lem K. Chemorheology of Thermosetting Resins I. The Chemorheology and Curing Kinetics of Unsaturated Polyester Resin. *Journal of Applied Polymer Sci.* 1983; 28:3155-3183.
12. Castro J. M., Macosko C. W., Perry S. J. *Polymer Commun.* 1984; 25:82.
13. Lin R. J., Lee L. J., Llou M. L. Mold Filling and Curing Modeling of RTM and SRIM Processes. *Advanced Composite Materials, Conf. Proceedings, Detroit USA, Sept. 30–Oct. 3 1991*; 165-174.

14. Advani S. G. editor, *Flow and Rheology in Polymer Composites Manufacturing*. Elsevier Sci., 1994; ISBN: 0444893474.
15. Rudd C., Long, A., Kendall K., Mangin C. *Liquid Moulding Technologies*. SAE International, 1997; ISBN: 0768000165.
16. Kamal M., Sourour S. Kinetics and Thermal Characterization of Thermoset Cure. *Polymer Eng. Sci.* 1973; 13(1):59-64.
17. Ruiz E., Trochu F. Numerical Analysis of Cure Temperature and Internal Stresses in Thin and Thick RTM Parts. Submitted to *Composites Part A*. (Nov. 2003) 38 pgs.
18. Audet M. *Simulation Numérique Tridimensionnelle du Transfert de Chaleur dans les Moules d'Injection pour Matériaux Composites*. Mémoire de Maîtrise en Sciences Appliquées. Dep. Génie Mécanique. École Polytechnique de Montréal. 1996 ; 305 pgs.
19. Holman J. P. *Heat Transfer*. McGraw Hill, 9th Edition 2002; ISBN: 0072406550.

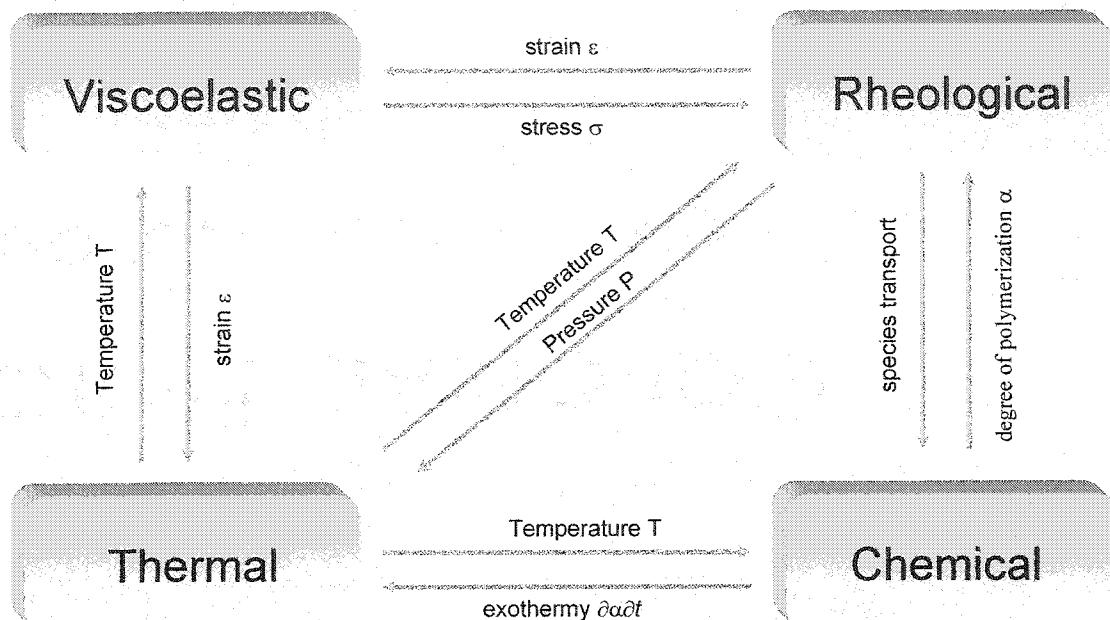


Figure 6.1. Coupling of physical phenomena in Liquid Composite Molding (LCM).

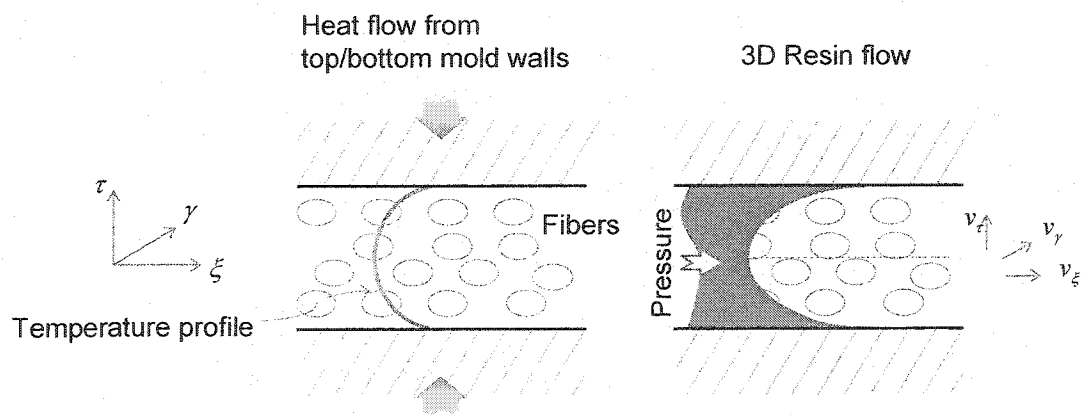


Figure 6.2. Cross-section of the mold cavity showing the three-dimensional heat and fluid flows. The trough-thickness temperature profile results in variable resin viscosity and transverse fluid flow.

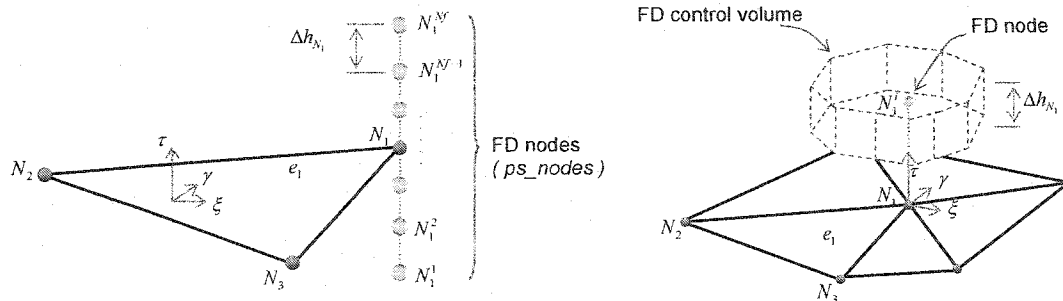


Figure 6.3. Because conforming finite elements are used in the heat transfer formulation, the coupling between 2D in-plane and 1D gapwise solutions is done via the control volume of the FD nodes defined by the centroids and mid-edges of connected elements.

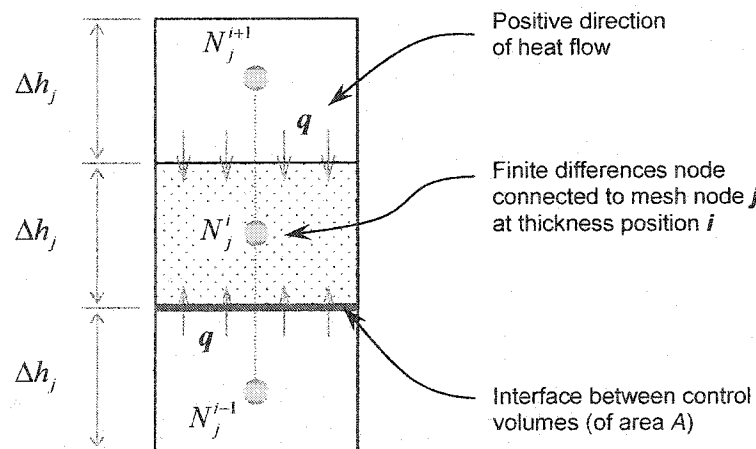


Figure 6.4. Control volume of the one-dimensional finite difference approximation.

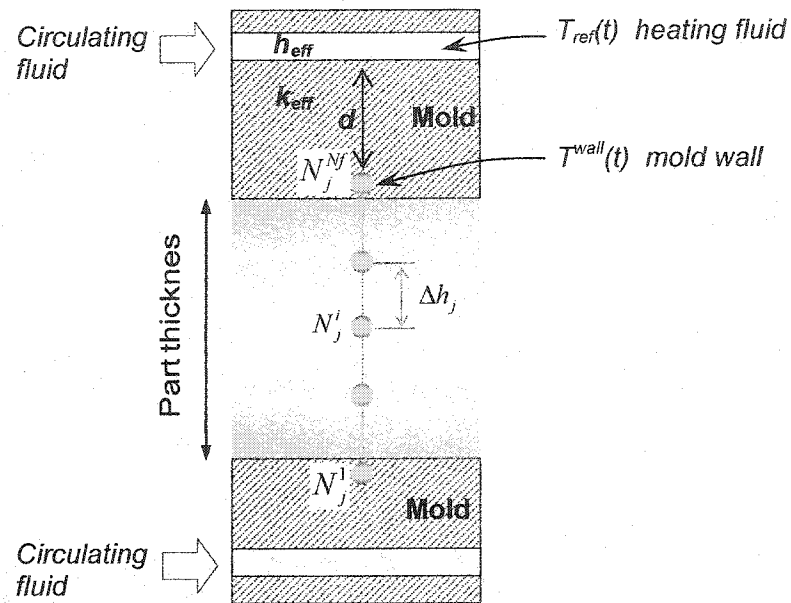


Figure 6.5. One-dimensional finite difference grid through the part thickness. The mold walls are heated or cooled by duct pipes maintained at a known reference temperature T_{ref} .

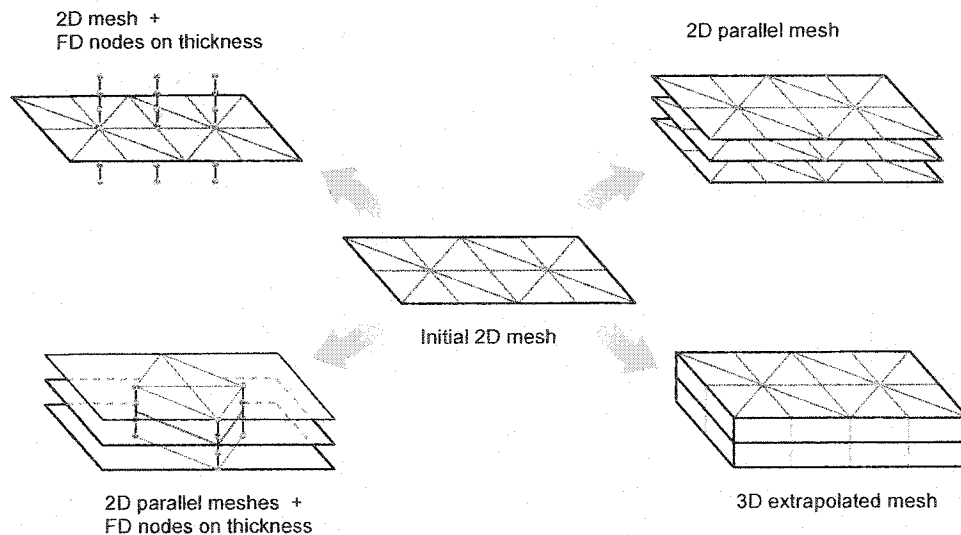


Figure 6.6. Different levels of inter-layer coupling with the mesh extrapolation algorithm and the 1D finite difference grid.

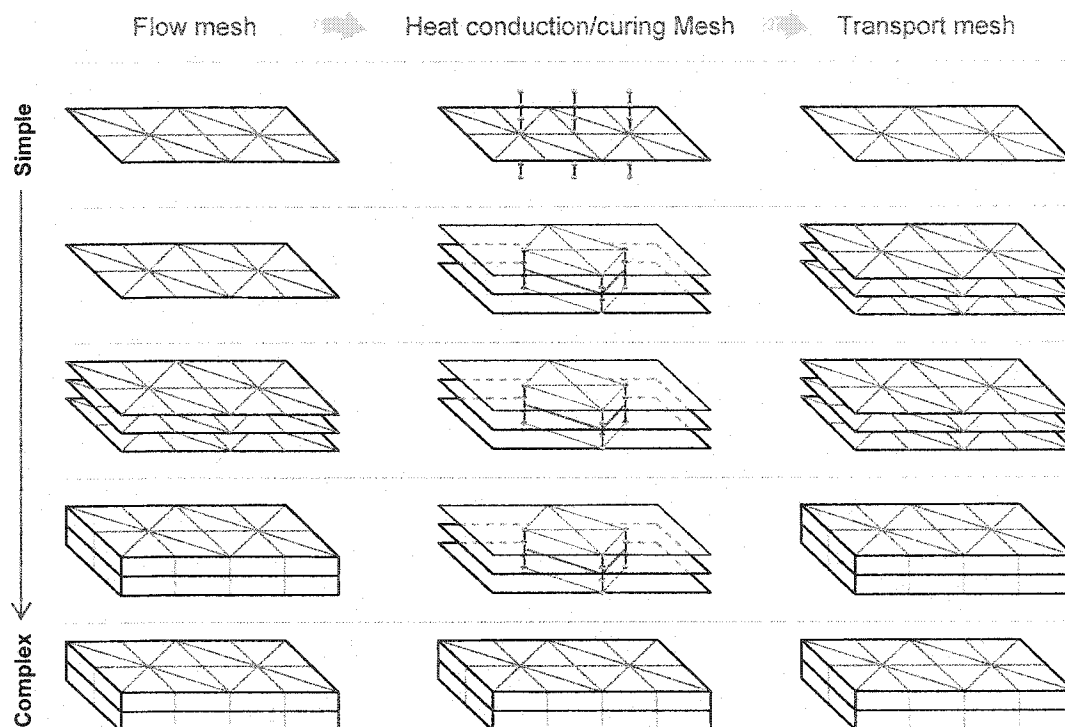


Figure 6.7. Schematic representation showing increasingly complex integration of flow, conduction and transport solutions. Different levels degrees of coupling are obtained by combining FE meshes and FD grids.

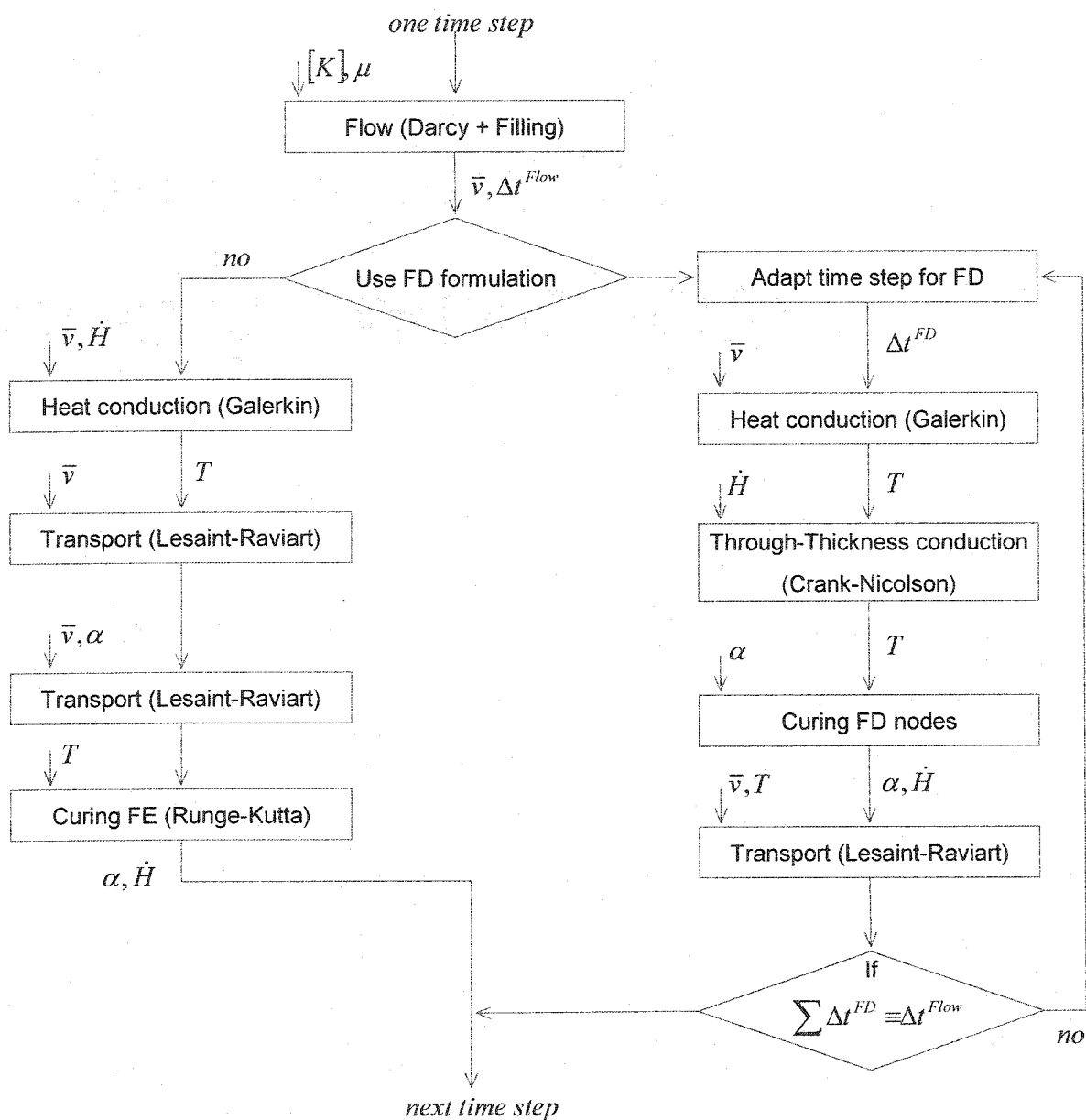


Figure 6.8. Flow chart of the numerical algorithm for the non-isothermal analysis.

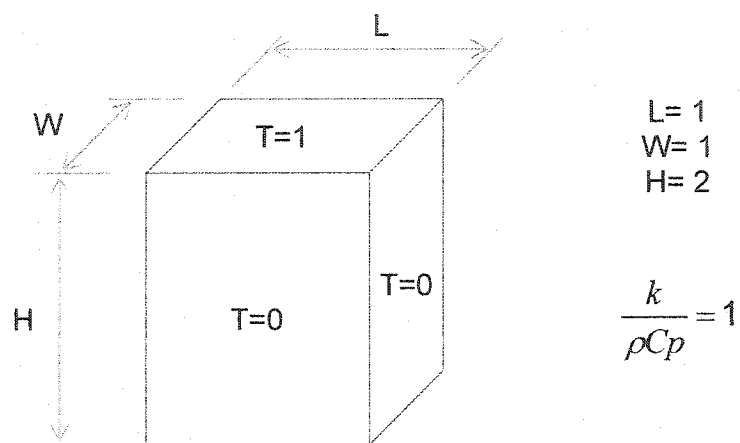


Figure 6.9. Domain used for the validation test I.

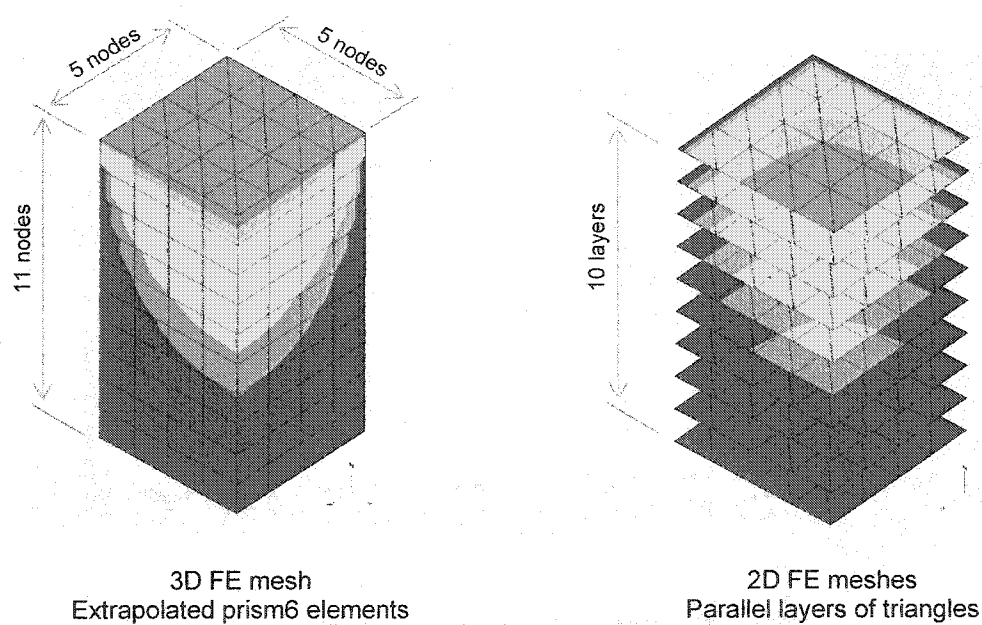


Figure 6.10. Two meshes used for test case I: extrapolated parallel layers coincide with the midplanes of each connected layer.

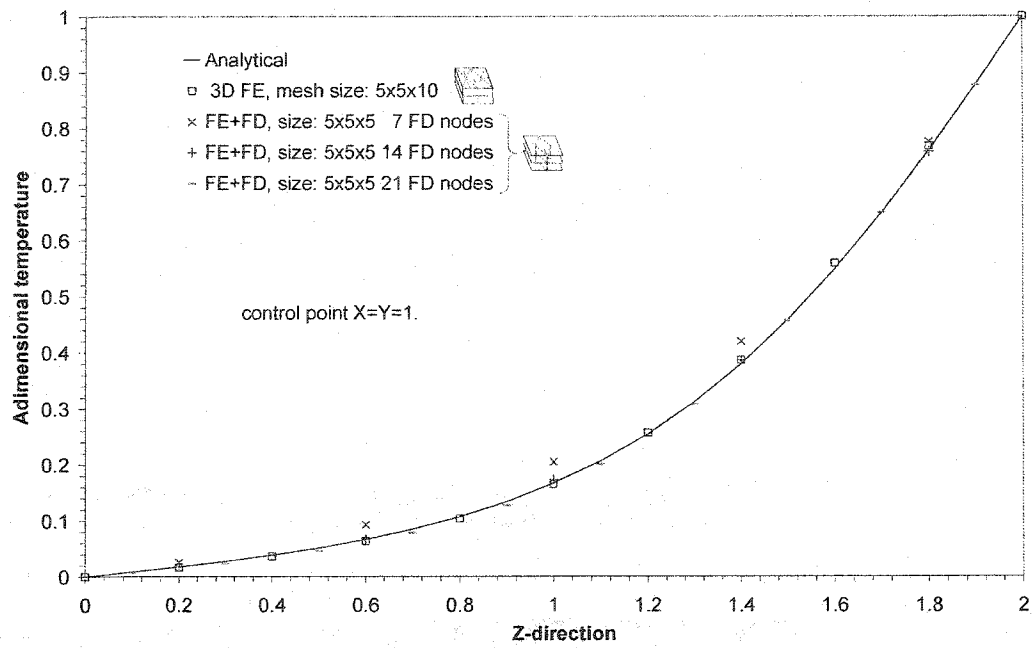


Figure 6.11. Comparison of pure FE and hybrid FE/FD solutions with theoretical values for test case I.

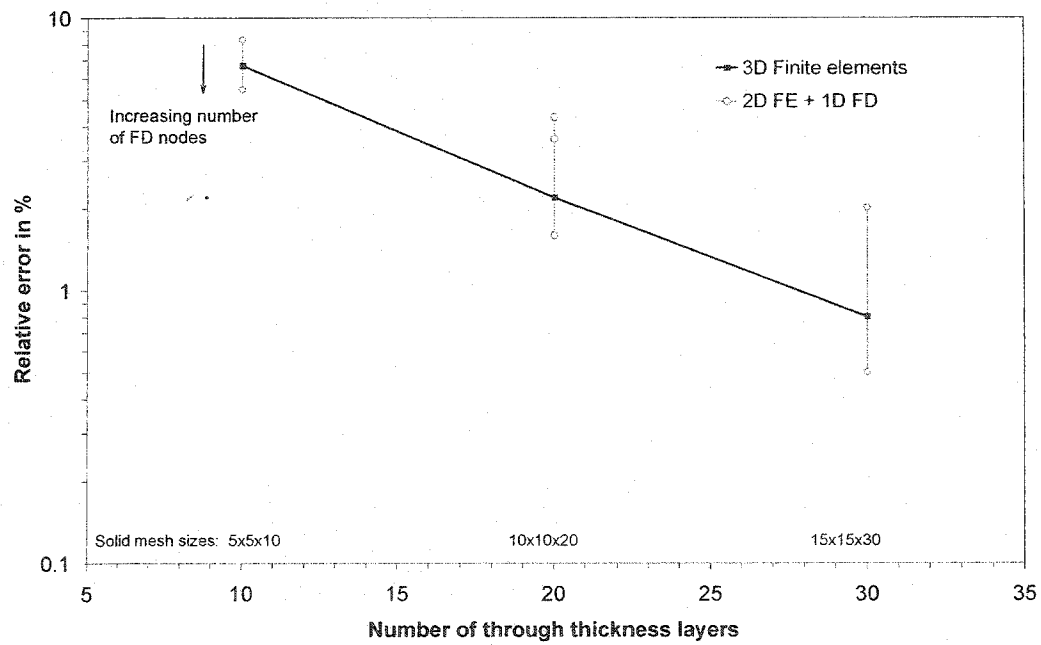


Figure 6.12. Maximum error of both formulations obtained for different mesh and grid sizes in test case I.

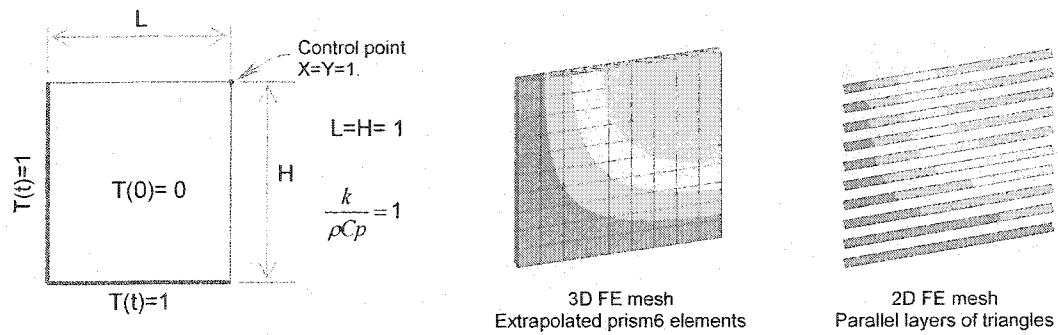


Figure 6.13. Rectangular domain used for validation test II and display of the 3D and parallel layers meshes.

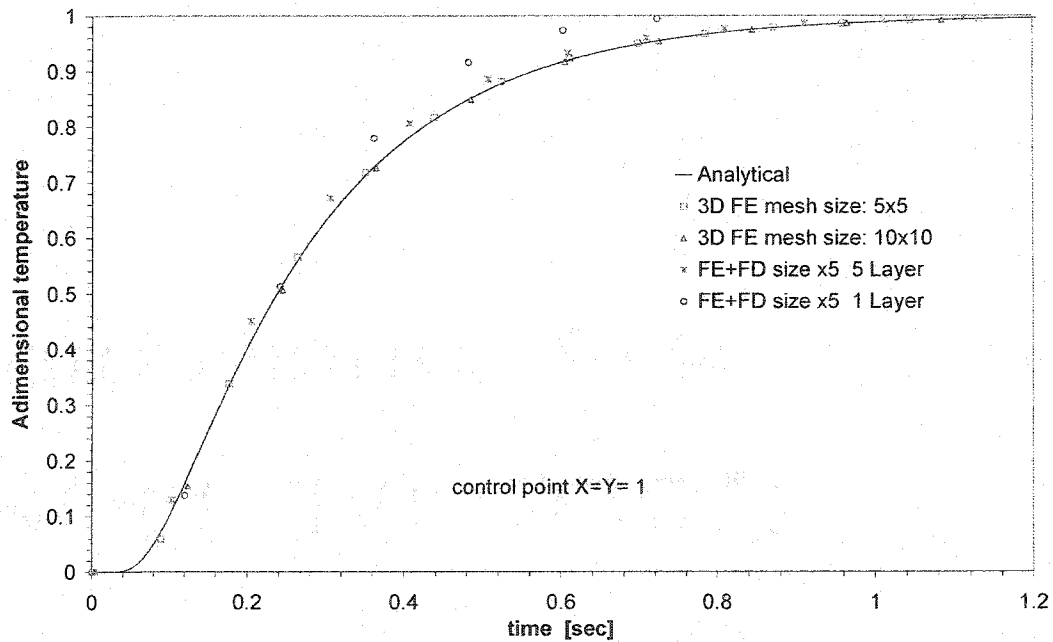


Figure 6.14. Comparison with analytical values of adimensional temperature at point $X=Y=1$ for pure FE and hybrid FE/FD solutions (test case II.).

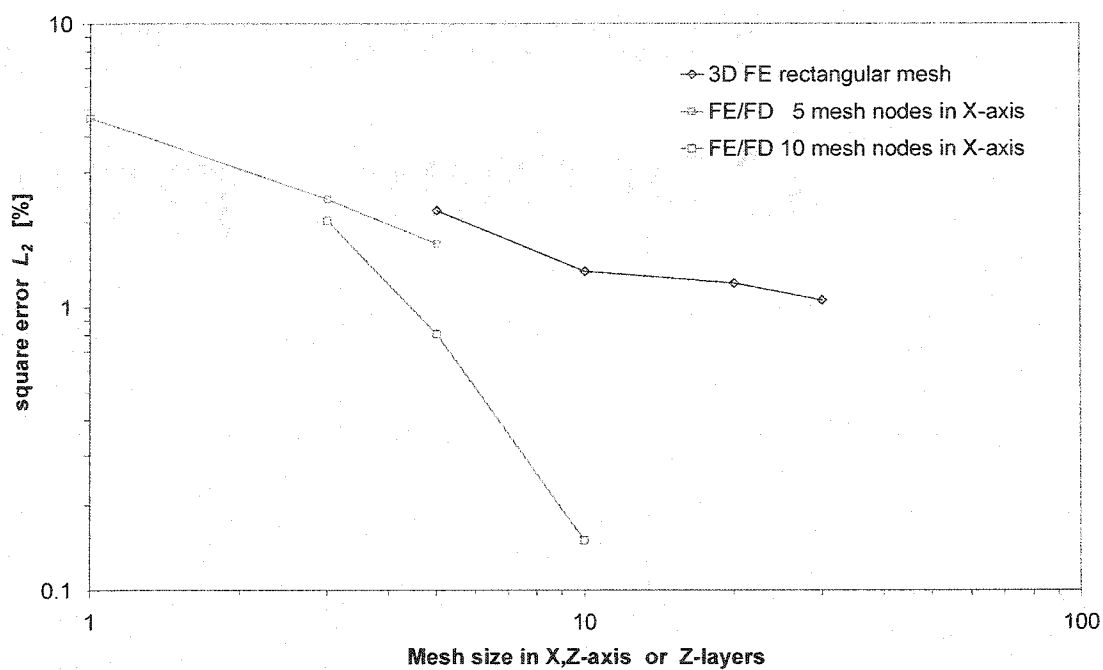


Figure 6.15. Convergence for 3D mesh refinement and parallel layers increment. The rate of convergence increases more with the number of layers (FE/FD solution) than with the number of nodes (FE solution). Note that the number of finite difference nodes is twice the number of layers.

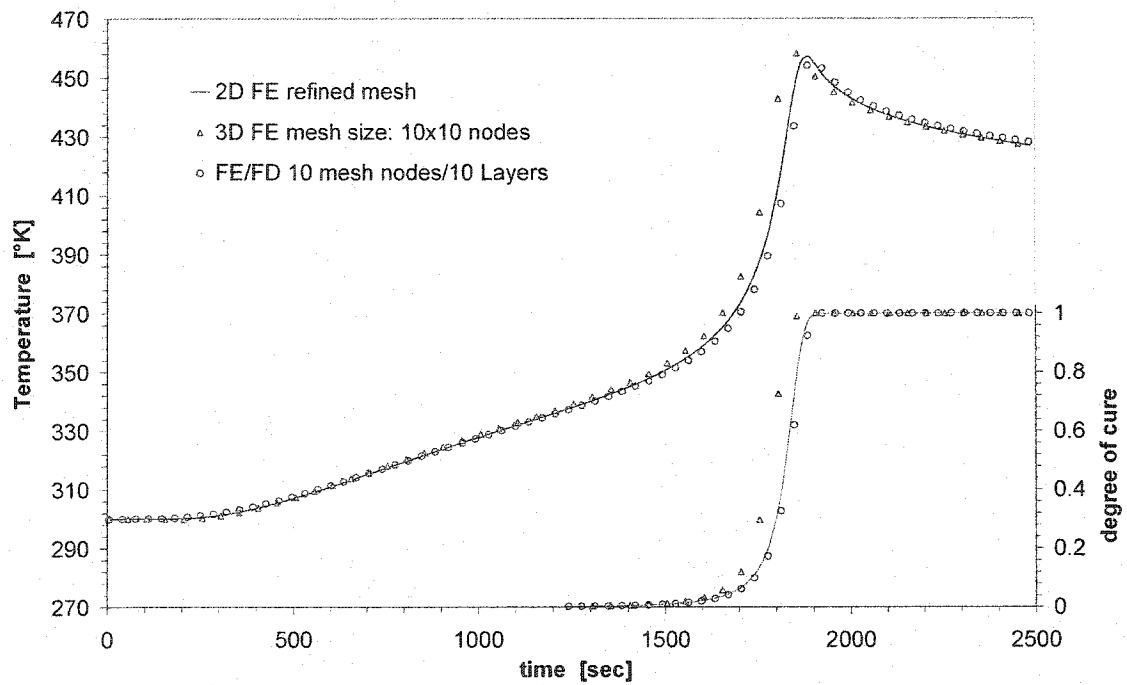


Figure 6.16. Evolution of temperature and cure profiles at the cavity centre is depicted for pure finite elements and hybrid FE/FD solutions. The 2D FE solution is used as reference.

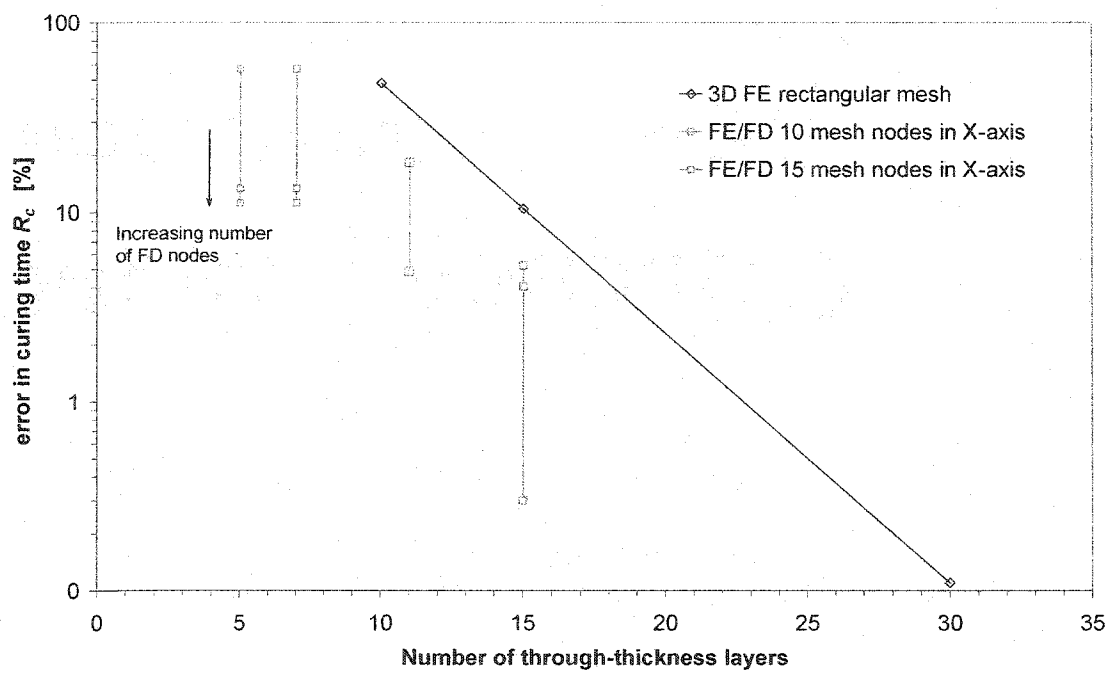


Figure 6.17. Comparison of error in the estimation of curing time for different mesh sizes. The hybrid formulation gives a better approximation than pure finite elements for the same number of through-thickness layers.

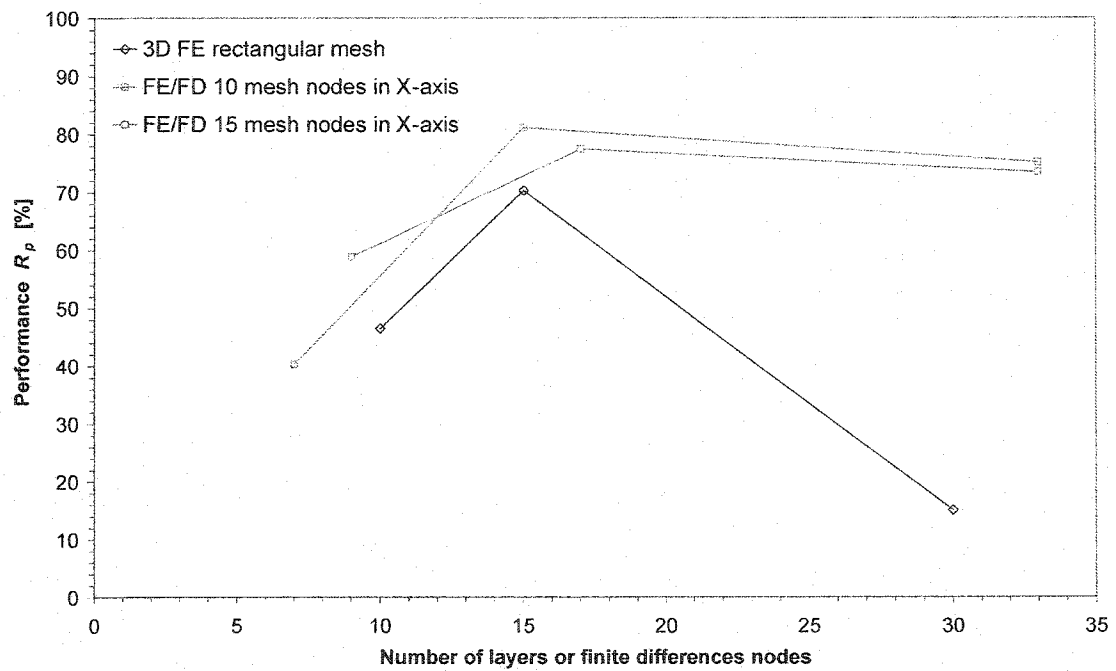


Figure 6.18. The performance of diver solutions is compared for various meshes with increased number of through-thickness layers of finite differences nodes. The hybrid formulations seem to give a better performance for curing analyses.

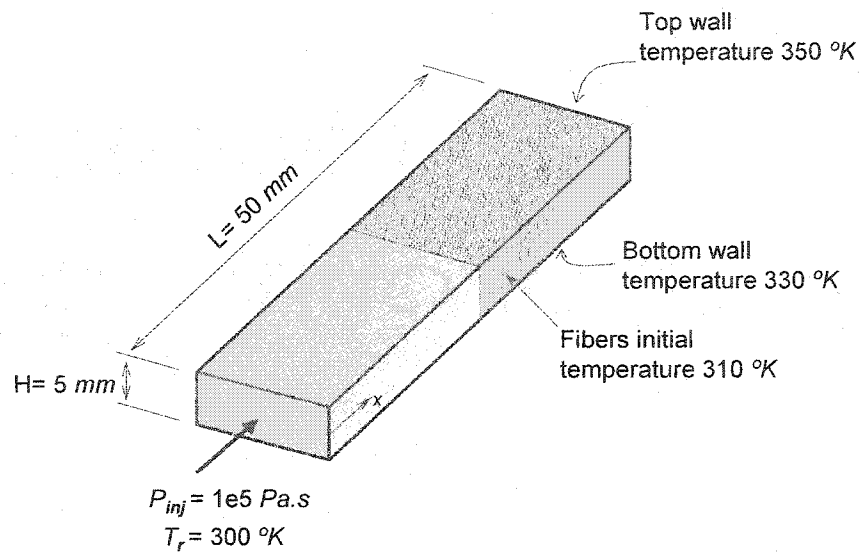


Figure 6.19. Rectangular cavity used for the 2D convection test with different top and bottom mold wall temperatures.

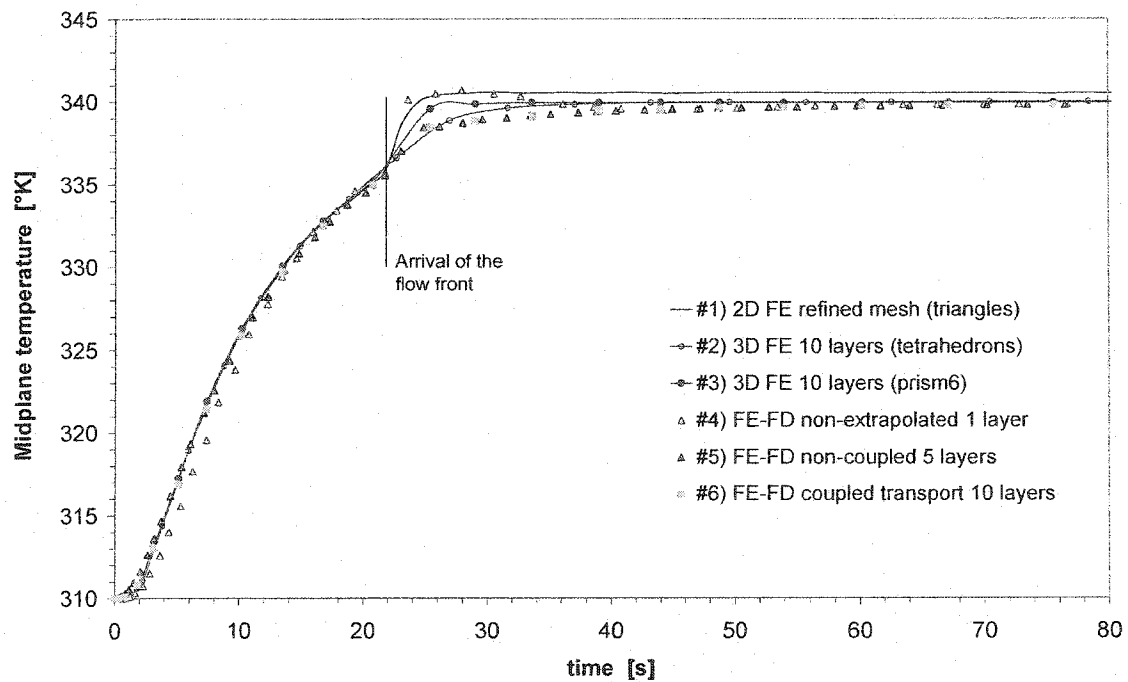


Figure 6.20. Temperature evolution at the control point for the six solutions tested.

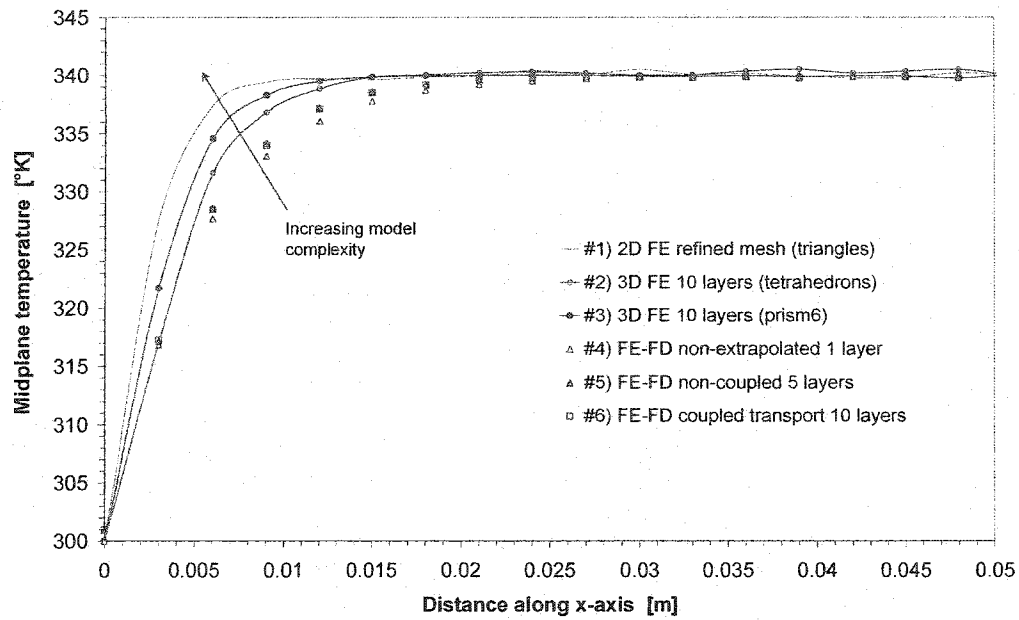


Figure 6.21. Temperature distribution at the end of filling along the cavity midplane for the six solutions tested.

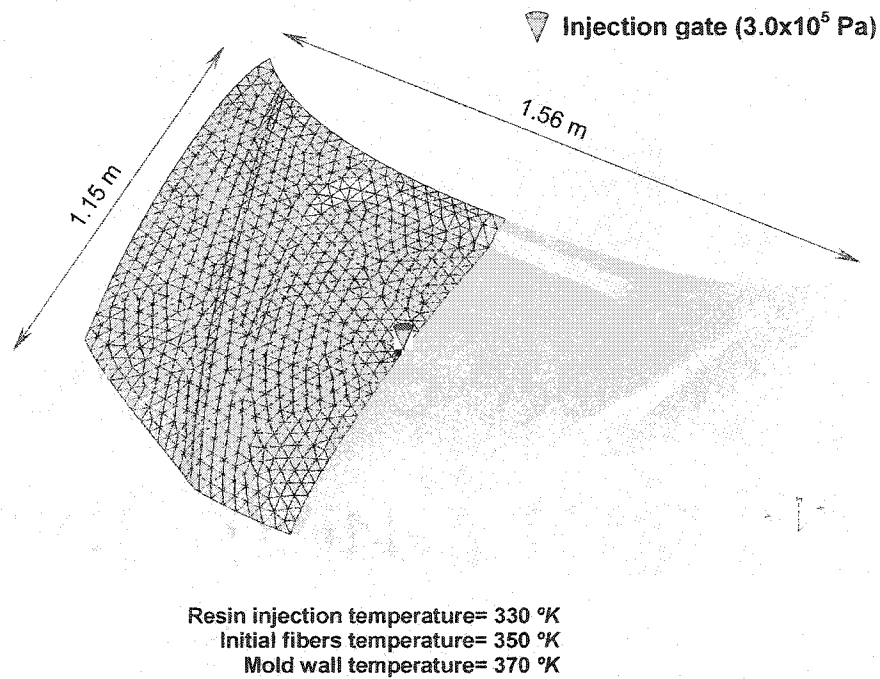


Figure 6.22. Midplane geometry and finite element discretization of the automotive hood used for the case study.

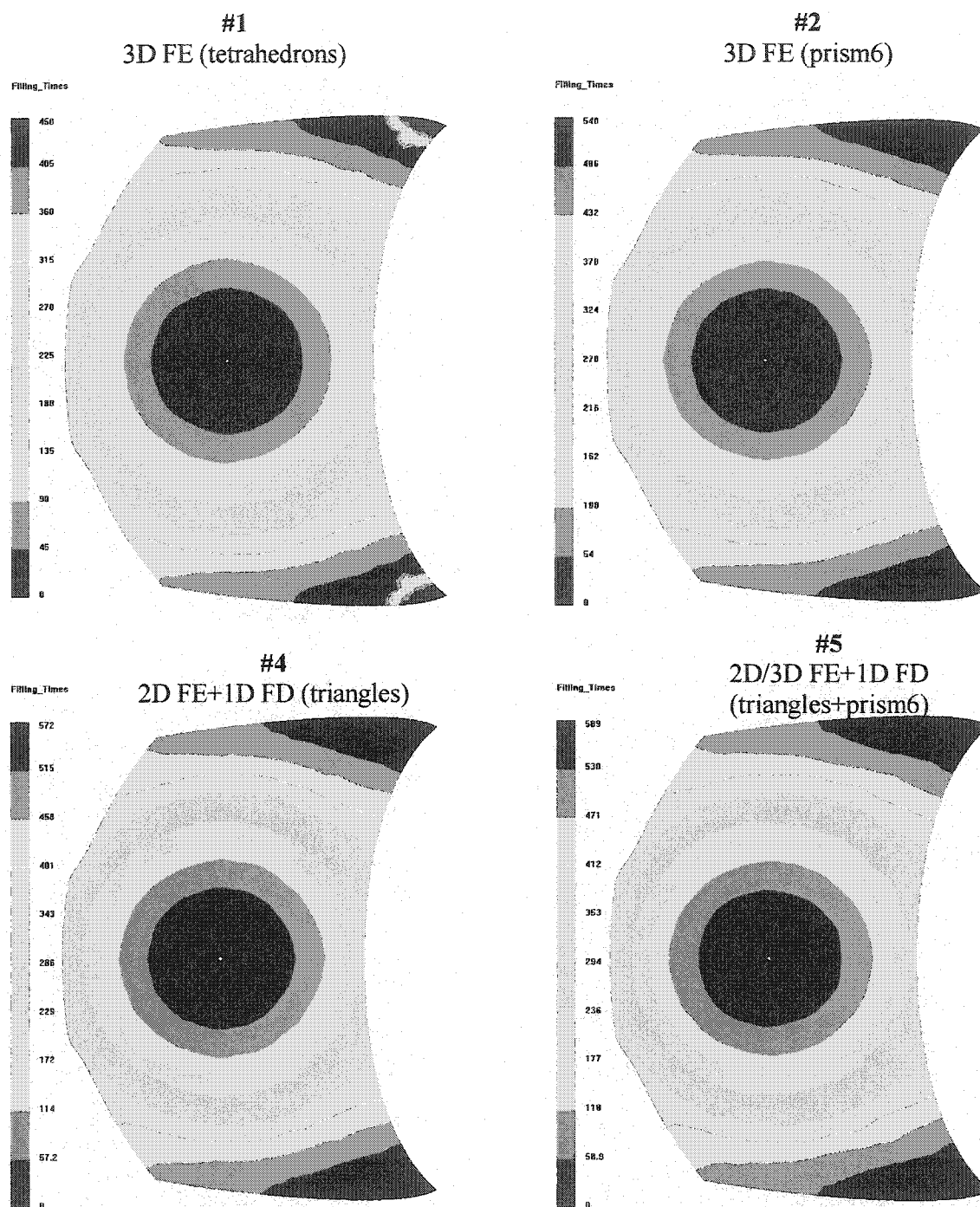


Figure 6.23. Flow front position in time for the non-isothermal mold filling of an automotive front hood. The solutions of four solution tested are depicted.

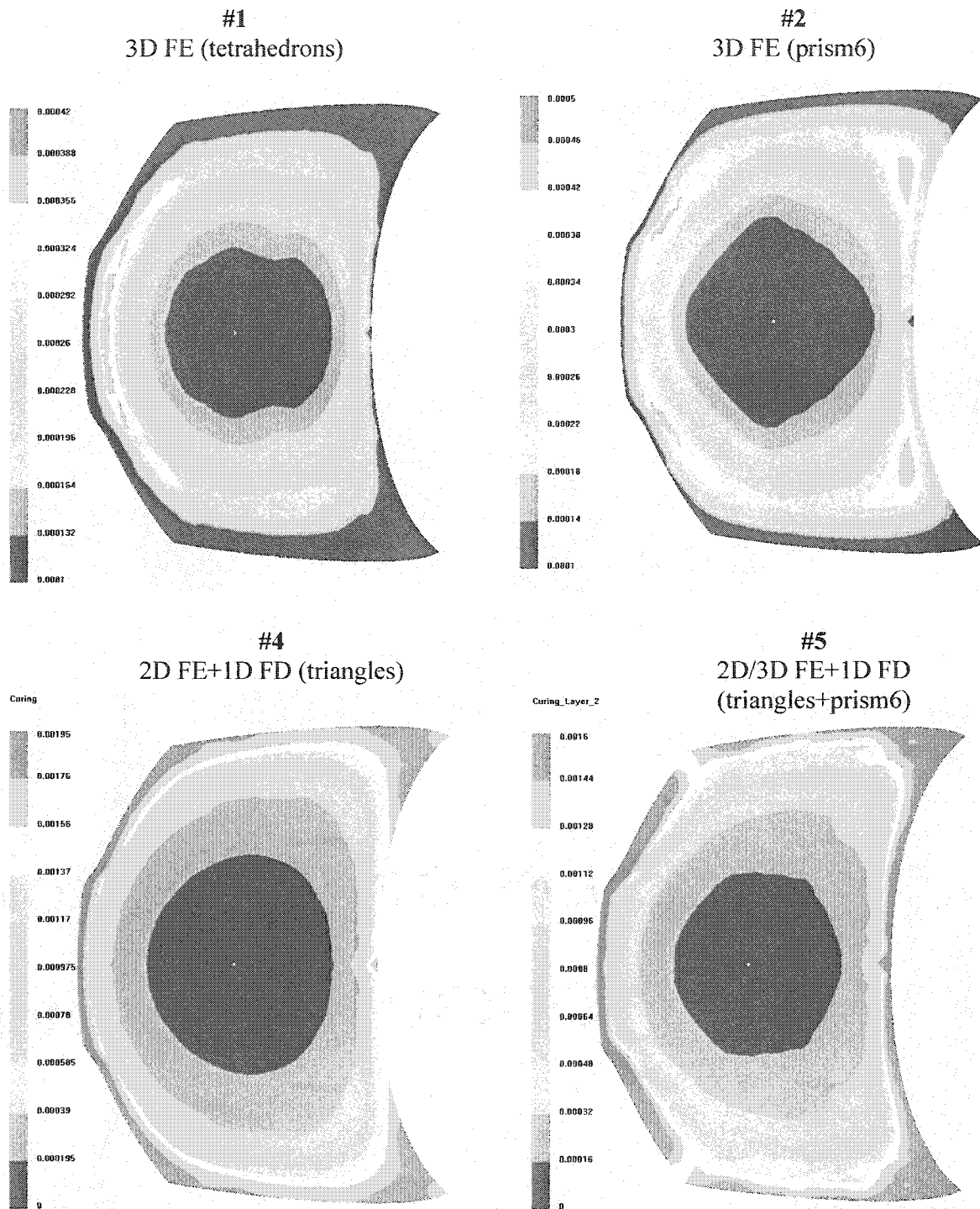


Figure 6.24. Degree of conversion at the end of filling in the automotive front hood. The two dimensional solutions seems to better account for cure transport at flow front.

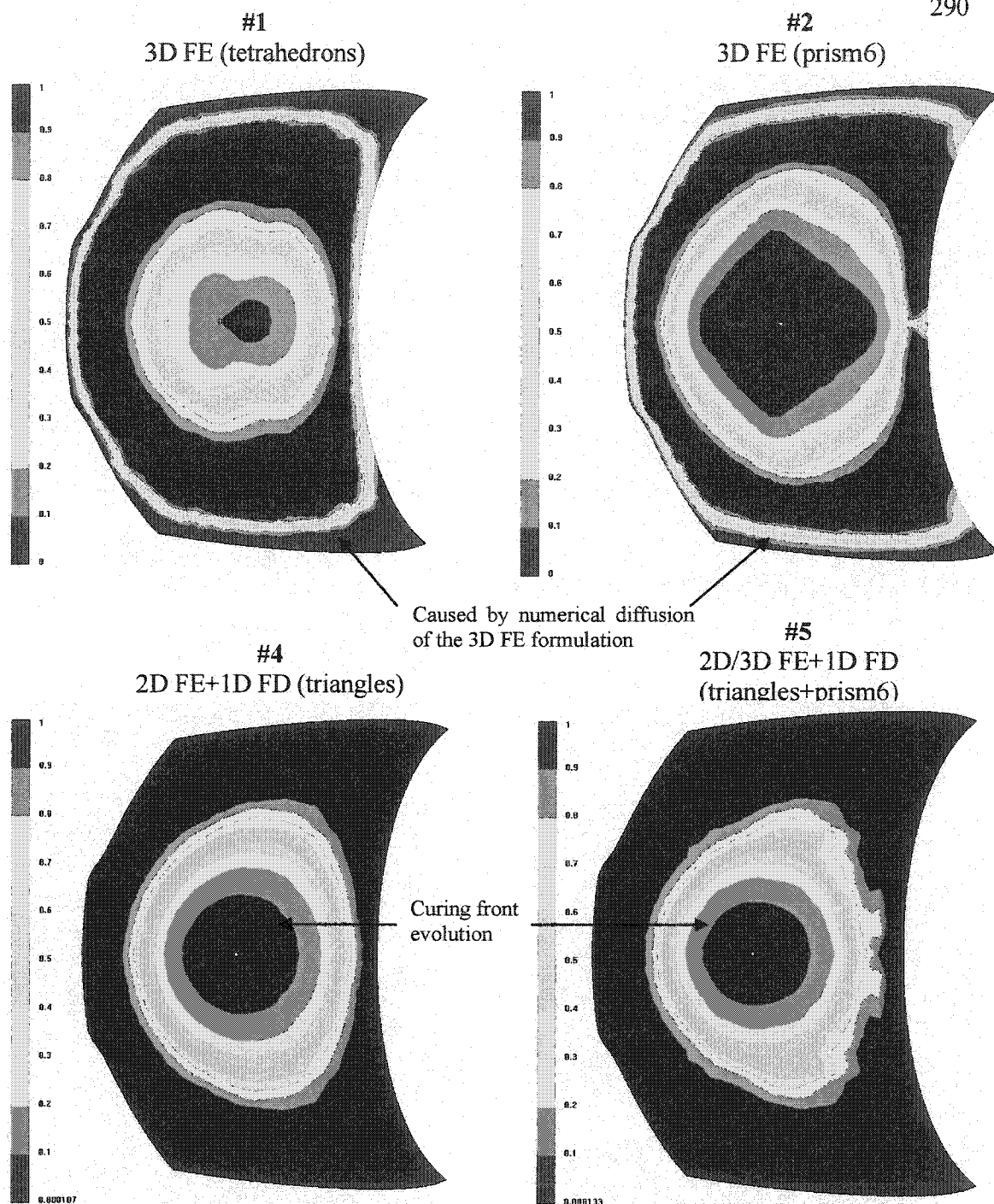


Figure 6.25. Evolution of the degree of conversion after filling for a curing time of 1500 sec. A curing front from the part perimeter to the center is induced by the non-isothermal filling.

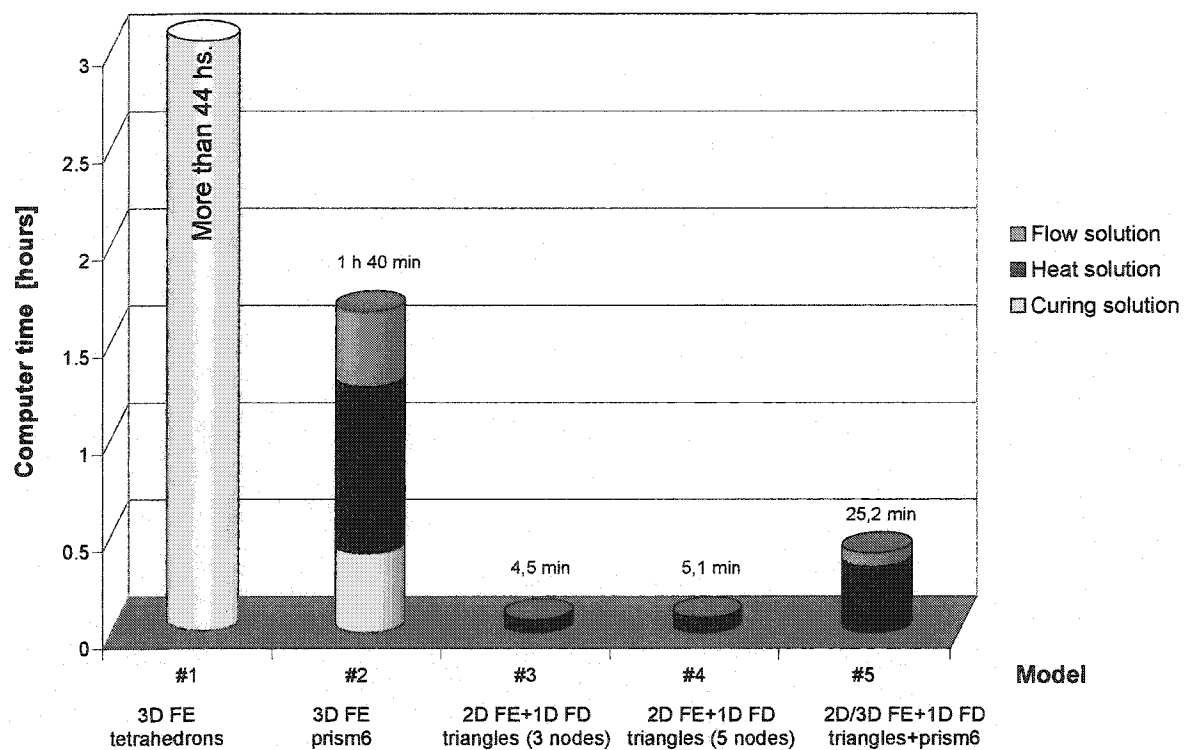


Figure 6.26. Comparison of computer times required for each model tested. While previous 3D solutions with tetrahedrons required more than 44 hours, the new *prism6* runs in 1 hour 40 min and the hybrid FE/FD solutions in 5 minutes.

Table 6.1. Different levels of integration of flow/thermal/curing formulations depending on the level of mesh coupling.

Model	Simple \longrightarrow Complex					
Darcy Pressure	NE FE	C FE	NE FE	C FE	C FE	C FE
Fluid Transport	NE FE	NE FE	NE FE	C FE	C FE	C FE
Heat Conduction	NE FE + FDT	NE FE + FDT	C FE	NE FE + FDT	NC FE + FDT	C FE
Viscosity	Averaged Thickness	Averaged Thickness	Averaged Thickness	Averaged Element	Averaged Element	Averaged Element
Kinetic reaction	FDT	FDT	C FE	FDT	FDT	C FE

NE FE : No mesh Extrapolation – Finite Element solution

NC FE : Non Coupled extrapolated mesh – Finite Element solution

C FE : Coupled extrapolated mesh – Finite Element solution

FDT : Through-Thickness Finite Differences solution

Table 6.2. Kinetic model and thermal properties used in test case III.

Kinetic Model $\frac{d\alpha}{dt} = \left(A_1 \cdot \exp\left(\frac{-E_1}{T}\right) \alpha^m \right) \cdot (1-\alpha)^p$			
Property	Units	Resin	Fibers
Density	Kg/m ³	1000	2500
Specific Heat	J/Kg °K	1500	800
Heat conductivity	W/m °K	0.25	0.25
Heat of reaction	KJ	250	-
A ₁	1/sec	1.0	-
E ₁	°K	1400	-
m	-	1.2	-
p	-	0.8	-

Table 6.3. Combination of different formulations and elements used for test case IV.

Model	#1	#2	#3	#4	#5	#6
Formulation	FE	FE	FE	FE+FD	FE+FD	FE+FD
Finite Element	triangles	tetrahedrons	prism6	triangles	triangles	triangles+prism6
Heat solution	2D	3D	3D	2D+1D	2D+1D	2D+1D
Transport	2D	3D	3D	2D	2D	3D
Nbr. of layers	20	10	10	1	5	10
Nbr. of FD nodes	-	-	-	10	10	12
Status in the code	in use	in use	new	new	new	new

Table 6.4. Computer times required to calculate for each solution of test case IV (times are in seconds).

Model	#1	#2	#3	#4	#5	#6
Finite Element	triangles	tetrahedrons	prism6	triangles	triangles	triangles+prism6
Flow cpu time	167.6	1135.1	1474.4	14.9	51	1184
Heat cpu time	668.1	3211.4	223.5	5.8	211.2	221.2
In/output time	2.9	1.1	3.4	1.2	9.2	6.8
Tolat cpu time	853.8	4378.2	1712	24.1	283.6	1439.3

Table 6.5. Rheological model used in the non-isothermal simulation of the automotive front hood.

Rheological Model $\mu(T, \alpha) = A_{\mu} \cdot \exp\left(\frac{E_{\mu}}{T} + B_{\mu} \alpha\right)$		
Coefficient	Units	Value
A_{μ}	Pa.s	0.0001
E_{μ}	°K	2500
B_{μ}	-	2.8

Table 6.6. Description of the five models used to compute the non-isothermal filling and curing of the automotive front hood.

Model	#1	#2	#3	#4	#5
Formulation	FE	FE	FE+FD	FE+FD	FE+FD
Finite Element	tetrahedrons	prism6	triangles	triangles	triangles+prism6
Heat solution	3D	3D	2D+1D	2D+1D	2D+1D
Transport	3D	3D	2D	2D	3D
Nbr. of layers	5	5	1	1	3
Nbr. of FD nodes	-	-	3	5	7

Table 6.7. Comparison of results obtained with the five models tested for the non-isothermal filling and curing of the automotive front hood.

Model	theoretical	#1	#2	#3	#4	#5
Finite Element	-	tetrahedrons	prism6	triangles	triangles	triangles+prism6
Filling time [sec]	-	450	540.15	502.96	569	589
Cure at end of filling	0.001356	0.00045	0.00047	0.00114	0.00195	0.00167
Mass loss [%]	-	14.6	-0.62	0.12	0.13	-0.63
Total curing time [sec]	1898	2091	1940	1806.3	1903	1845.53
Exothermic temperature [K]	377.35	380	380	375	377	378

CHAPITRE 7

COMPREHENSIVE THERMAL OPTIMIZATION OF LIQUID COMPOSITE MOLDING TO REDUCE CYCLE TIME AND PROCESSING STRESSES

Présentation du chapitre

Dans les chapitres précédents, les propriétés thermomécaniques et la cinétique de polymérisation de la résine ont été caractérisées et, des modèles numériques ont été présentés pour évaluer les flux thermiques, le changement d'état du matériau et les contraintes internes dans le composite générés pendant la cuisson et le refroidissement. Il fut démontré que l'utilisation d'une température de moulage appropriée est un facteur clé pour éviter des défauts dans le laminé ou des distorsions géométriques dans la pièce. Ce dernier chapitre est consacré à l'optimisation numérique des cycles de chauffage, cuisson et refroidissement dans la fabrication des pièces composites par injection sur renfort. L'approche proposée concerne la minimisation du temps du cycle, l'amélioration des propriétés mécaniques et la réduction des contraintes résiduelles dans le composite. La minimisation des gradients thermiques et de cuisson à travers l'épaisseur est fondée sur sept sous-fonctions objective. La fonction objective finale est une combinaison linéaire de ces sous-fonctions. Un algorithme d'évolution fondé sur les algorithmes génétiques, et appelé LeCoq (« Logical Evolutionary Curing Optimization and Quenching »), est développé pour minimiser la fonction objective en fonction de plusieurs paramètres. Pour évaluer la fonction objective à chaque itération de l'algorithme génétique, l'analyse unidimensionnelle de la cuisson et des contraintes résiduelles est incluse à l'intérieur du code LeCoq. Pour augmenter la vitesse de convergence de l'algorithme d'évolution, les sept sous-fonctions objective sont définies sous la forme de sigmoïdes unitaires. Pour démontrer les capacités de la méthode

proposée des études d'optimisation du cycle de cuisson pour des pièces minces et épaisses sont présentées et discutées.

Comprehensive Thermal Optimization of Liquid Composite Molding to Reduce Cycle Time and Processing Stresses

Edu Ruiz and François Trochu

Centre de Recherches Appliquées Sur les Polymères (CRASP)

Département de Génie Mécanique,

École Polytechnique de l'Université de Montréal,

e-mails: eduardo.ruiz@polymtl.ca, francois.trochu@polymtl.ca

Keywords: Transfer Molding (RTM), thermal analysis, residual stress, weaving,
optimization.

Article soumis à la revue *Polymer Composites*

Décembre 2003

7.1 Abstract

Liquid Composite Molding (LCM) is a well established and flexible composite manufacturing technology capable of producing large parts at a relatively low cost. In this family of related injection processes, a large number of design variables have strong impact on manufacturing performance. The determination of adequate process parameters is key to yield successful molding conditions, and reduce cycle time. In addition, properties and durability of composite parts are strongly affected by internal stresses. Excessive stress levels may lead to important defects in the part at the curing stage and after processing, when the part is cooled to room temperature. In this

investigation, a comprehensive curing optimization algorithm is proposed to reduce internal stresses during composite processing. This study focuses on the minimization of the macroscopic residual stresses that appear during cure and cooling in thermoset composite laminates as a result of temperature and degree of cure gradients. The proposed fitness function to be minimized is based on the physics of the matrix material transformation and on the mechanical behaviour of the composite material. An evolutionary strategy based on Genetic Algorithms (GA) is implemented for the minimization of the fitness function. Optimization is carried out for thin and thick glass/polyester laminated composites. Different optimization schemes with thermo-elastic and viscoelastic models of the composite mechanical properties are studied. The advantages and drawbacks of each model are stated and discussed.

7.2 Introduction

Liquid Composite Molding (LCM) regroups a number of increasingly used manufacturing techniques of fibre reinforced composite parts. This family of related processes offer a great flexibility in terms of part dimension together with lower production costs. The basic process consists of injecting under pressure a pre-catalyzed thermoset resin into a mold cavity containing a fibrous preform. Once the cavity is filled up and the preform has been completely saturated, the liquid resin system reacts following an exothermic process. The polymerization reaction results on a three-dimensional cross-linked polymer network that gives the solid shape of the part.

In liquid composite molding, a large number of design variables impact on process performance. As depicted in Figure 7.1, the mold temperature and inlet pressure must be appropriate to allow a proper fiber impregnation and avoid resin gel prior to fill up. The determination of adequate process parameters is key to ensure successful molding conditions. In addition, proper process parameters can reduce cycle time, heating

sources, mold deformation, and the requirements on the injection apparatus and mold clamping systems. Minimization of the mold filling and curing times is equivalent to reduce energy consumption during the molding cycle. Finally, and maybe this is the most important point to consider in the processing of thick composites, an optimum choice of process variables will result in minimum part defects, such as micro-cracks, delamination, warpage, spring-in, etc. In composite manufacturing, the existence of a sophisticated relationship between process parameters and measurable process issues complicates the optimization problem (see Figure 7.1). Due to the complexity of the interactions, most process engineers depend more often on their experience or knowledge rather than on a systematic optimization based on virtual prototyping. However, recent advances in LCM simulation and process optimization software are beginning to change that situation.

It is well understood that the final mechanical properties of the composite are affected by the processing of the part. Researchers have studied these relationships and presented experimental investigations on the sensitivity of mechanical properties to process parameters [1-4]. Most investigations agree that preheating of the mold helps to wet out the preform, and consequently improves product quality. Preheating of the resin at the injection gate has also lead to improved results in the mechanical analysis of fully cured parts [5]. It is also reasonable that injection pressure and temperatures of the fiber bed and mold during filling play a decisive role in processes for which the gel time is close to the filling time.

Historically, autoclave cure cycles have been developed by trial-and-error methods, but this procedure is evidently inefficient as it depends on the knowledge acquired by a limited number of experts. Many investigators have attempted to obtain optimal cure cycles. The results of these trial-and-error methods have lead to the development of various rule-based heuristic expert systems to guide process development. Xiao et al. [6] developed an expert heuristic system for Resin Transfer Molding (RTM),

comparing mechanical properties after cure with different curing conditions. Two variables, injection pressure and mold temperature were studied. Rudd et al. [7] used an expert heuristic system to optimize the injection temperature of the resin in RTM. However, the applicability of heuristic approaches is often limited by specific material, geometric and practical restrictions. These approaches cannot obtain an optimal design, especially when a large number of process parameters and constraints that are not always measurable came into play.

Spoerre et al. [8] proposed to use Genetic Algorithms (GA) in conjunction with a cascade correlation neural networks architecture (CCA-NN) to establish a model that predicts and optimizes part performance and quality in RTM. In this approach, the authors did not use numerical simulation to construct the objective function to be optimized, but preferred to rely on an experimental database. They concluded that although the process optimization algorithm showed convergence to the estimated optimum values, the use of this technique is restrained by the need to develop a resin transfer molding database. Chen et al. [9] analyzed the effects of moisture upon the optimal cooling temperature profile after post curing of a symmetric composite laminate. They constructed a based gradient algorithm to found the optimum cooldown temperature path that minimizes thickness-averaged residual stresses after post cure. This technique is well adapted to the small number of parameters used on the one-dimensional simulation, but it may be hard to implement for complex combination of process parameters and evaluation functions.

Recently, Li et al. [10] used a methodology based on design sensitivity analysis to optimize the autoclave temperature for a graphite/epoxy composite. Design sensitivity information is extracted by an analytical and direct differentiation approach. The sensitivities are then used with a gradient optimization technique to systematically improve the curing process. In this work, the cure cycle is constrained to a maximum temperature within the composite and a minimum degree of cure. To obtain the

minimum cycle time, one, two and three dwell temperatures were proposed. Finally, the optimization algorithm finds smooth cure and temperature profiles through the thickness. The authors conclude that the method is most useful to improve designs that are generated by less precise methods, such as design rules, expert system, and heuristics approaches.

Ruiz [11] developed a one-dimensional optimization of non-isothermal filling in RTM, and a temperature optimization of the cure cycle. In the one-dimensional filling optimization, intersections between curves interpolated by kriging were used to obtain adequate results between numerical evaluations. For the cure cycle optimization, the heating ramp and dwell temperature were found by intersecting parametric kriging surfaces. Although the method showed a high convergence rate, it can only be applied to a small group of process parameters.

Young [12] used the GA method to search for the optimal gate locations and constant injection pressure that minimize the filling time. The GA method converged to near optimal global solutions in a large search space with many local maximums, but a poor rate of convergence was found. A comparison with random search and hill climbing shows that this latter yields the faster convergence, but because there are many local solutions in the search space, this method usually converges to a local solution. On the other hand, random search showed a lower rate of convergence than GA. In the last year, Lin et al. [13] presented a RTM filling process optimization with an interesting discussion over two different search methodologies to find optimum values. The authors have tested and compared the convergence of gradient-based versus genetic algorithms. Objective functions were based at the locations of the injection gates and a simple design variable, the filling time, was used to determine the optimization. The conclusion indicated that genetic algorithms are strong enough to find a near optimal solution, although a poor rate of convergence was observed. Note that the authors used a pure GA optimization without any method to accelerate convergence.

Michaud et al. [14] developed a robust simulation-based optimization procedure to identify the optimal curing conditions for a thick RTM part. In that work, two design parameters were used to account for the part quality and processing time. The first one is a direct function of the extent of cure cross-over (i.e., the point where extent of cure at the surface and in the core of the part have the same magnitude). The second design parameter is a linear function of the curing time and ultimate extent of cure. Improved average part quality was experimentally observed when this thermal optimization methodology is applied to the cure of a 2.54 *cm* thick composite laminate. In this investigation, the authors considered that the development of internal stresses depends only on the extent of cure. This assumption does not consider the processing stresses that result of the thermal gradients created across the composite laminate at the exothermic peak and during cooling.

Up to now, the work on thermal optimization during cure for liquid composite molding reported in the literature can be divided as follows:

- Reduction of cycle time.
- Reduction of cure gradients.
- Reduction of thermal gradients.
- Reduction of cooling stresses.

Although these optimizations were independently applied, no coupled optimizations were found in the literature. This investigation aims at the development of a comprehensive optimization methodology that considers each of these effects based on a physical background. The study focuses on the minimization of the internal stresses that appear during cure and cooling in thermoset composite laminates as a result of temperature and cure gradients. The objective function (called fitness function) to be minimized is constructed with physical considerations of the cure and temperature gradients, the cure and cooling stresses, the cycle time and the maximum allowed

exothermic temperature. An evolutionary strategy based on Genetic Algorithms (GA) is implemented for the minimization of the fitness function. Optimization studies are carried out for thin and thick glass/polyester laminated composites with thermo-elastic and viscoelastic models of the mechanical properties.

7.3 Governing equations

In a non-isothermal LCM injection, the mold is typically at a higher temperature than the resin and fibers. The heat exchanged between the preform, the resin and the mold walls during resin injection produces temperature variations in the part. Sometimes, curing is affected by the heat transfer in the cavity during the filling stage. However, when thermal effects during filling have little influence on the initial polymerization degree of the resin, it is possible to decouple filling and curing as two distinct stages of the manufacturing process. In order to verify if the chemical reaction can be neglected during mold filling, the adimensional number called the gelling ratio (Ge) is used. This number relates the time required to fill up the mold (injection time) with the time needed to cure the part (reaction time). For a small gelling ratio, it is possible to decouple the curing process from the filling stage. In the case of polyester based resin systems, the free radicals generated are initially deactivated by reacting with an inhibitor, so the gelling number can be defined as the ratio of the filling time (t_f) over the inhibition time (t_m) at mold temperature. From this definition, a gelling ratio smaller than unity means that the curing process can be decoupled from mold filling, which is the case assumed in this investigation:

$$Ge = \frac{\text{injection time}}{\text{reaction time}} \quad (7.1)$$

$$Ge = \frac{\text{filling time}}{\text{inhibition time}} = \frac{t_f}{t_m} < 1 \quad (7.2)$$

7.3.1 Energy balance equation

In the present work the curing of the composite laminate is analyzed through the thickness of the part. If the lumped temperature approach is considered [15], the transient absolute temperature $T(z,t)$ at position z and time t , through the total part thickness H can be obtained by the one-dimensional Fourier's heat conduction equation:

$$\tilde{\rho} \tilde{C}_p \frac{\partial T}{\partial t} = \tilde{k} \frac{\partial^2 T}{\partial z^2} + Q \quad 0 \leq z \leq H \quad (7.3)$$

where the density $\tilde{\rho}$, heat capacity \tilde{C}_p and conductivity \tilde{k} of the composite are defined as the effective properties obtained by the rule of mixture. The source term Q represents the instantaneous heat generated by the cross-linking polymerization of the resin, and it is assumed to be proportional to the reaction rate. The Crank-Nicolson finite differences formulation described in [16] was used to solve the one-dimensional energy equation (7.3). The numerical methodology has an adaptative time step control based on Fourier's number and in the reaction rate to avoid computational inconsistencies. On this approach, different thermal boundary conditions can be set at the mold surface or at the position of the heating/cooling system inside the mold wall.

To properly simulate the heat exchanges across the mold cavity, thermal and kinetic properties of the composite (and mold) must be appropriately characterized. Thermal parameters in the energy equation may be affected by temperature, such as the thermal conductivity and heat capacity of the resin. This implicates that the numerical solution of the energy equation will be affected by the changes in material properties, thus close loop iteration will be needed to yield adequate numerical results. Similar effects are found in the chemical dependence of the resin properties during cure. The specific heat of the resin varies with the cross-linking polymerization. It is then required, for a proper

thermal analysis during resin cure, to perform a careful characterization of the composite properties as a function of temperature and degree of polymerization. Table 7.1 presents the dependencies of the thermal and kinetic properties used in this investigation. The thermo-chemical characterization and modeling for a glass/polyester composite are taken from [17]. Resin cure kinetics is modeled by an extended autocatalytic equation that describes free-radical polymerization. The kinetic equation accounts for the glass transition temperature effects on the reaction rate. The maximum extent of cure and the inhibitor decomposition are also included in the model.

7.3.2 Strain-stress modeling

It is well known that the general properties and durability of composite parts are strongly affected by internal stresses. Excessive stress levels may lead to important defects in the part during the curing stage or after processing, when the part is cooled to room temperature. A comprehensive cure optimization should then account for the reduction of internal stresses that appear during composite processing. As demonstrated in [15], processing stresses can be calculated with the Classical Laminate Theory (CLT) in a one-dimensional analysis. To compute strain-stress levels through the thickness of the part, the thermal and chemical volume changes of the resin and fibre reinforcement are needed. In the same way, the mechanical properties of the resin must be modeled as a function of temperature and degree of polymerization. Table 7.2 lists the models used in this work to describe the temperature and degree of cure dependence of the composite mechanical properties. More details on experimental characterization can be found in [17]. In that work, two models were presented to evaluate the resin and laminate elastic moduli. The first one is a non linear thermo-chemical elastic modeling that considers fully relaxed material properties above the glass transition temperature. The second one is a viscoelastic model with a time/temperature superposition to describe the relaxation effects during resin polymerization. This investigation aims at

comparing the optimization results obtained with these two models. The advantages and drawbacks of each one will be stated and discussed.

7.4 Evolutionary algorithms

During the last years, Evolutionary Algorithms (EA) have received increasing attention in research and industrial applications. Generally, EA outperform conventional optimization algorithms for problems which are discontinuous, non-differential, multi-modal noisy and not well defined [18]. EA possess the advantage of requiring less expert knowledge of the optimization space and therefore are less case specific. When compared to pure heuristic approaches, EA appear to be computationally more efficient in the optimization of complex manufacturing processes. They use probabilistic transition rules, not deterministic rules, and only require the knowledge of the objective function, but not of their derivatives. EA belong to a category of stochastic search techniques, in which only the fittest will survive during an artificial evolution process based on the mechanics of genetics and natural selection. In an engineering design problem, the surviving design variables represent the optimal solutions. These methods have the potential to find near global optimal solutions in a large search space.

In the application to LCM optimization, EA are often coupled to numerical process simulation. To evaluate the objective function (or fitness function) for a given set of process parameters (called design variables), it is required to run a numerical simulation of the process for these design variables. In the case of curing optimization of composite parts, the energy and kinetic equations must be computed for a set of thermal boundary conditions selected by the optimization algorithm. This can make optimization infeasible if the numerical evaluation of the fitness function requires large computational efforts. The use of one-dimensional process modeling presents the advantage of being not time consuming compared to finite element two or three

dimensional simulations. This permits a large number of evaluations in a relatively short computer time. Despite the fact that in-plane thermal effects are not considered, one-dimensional models can give important information of the process behaviour for different boundary conditions. The finite differences model implemented in this investigation and the application of the CLT for stress analysis have been developed in a C++ code and improved to accelerate the evaluation of the fitness function. The performance of the code was tested to simulate processing of a typical LCM part. Coupled resin cure and composite strain-stress analysis were carried out for a 10 mm thick laminate with 11 fabric layers. The simulation required between 0.5 to 3 seconds (depending on the boundary conditions) to run on a IBM IntelliStation Z-Pro with a Pentium IV (2.8 Gz) processor.

7.4.1 Problem identification

To formulate an optimization problem, one must identify the design variables, the objective function and the constraints. The design variables represent the process parameters that will be adjusted in the optimization procedure. The objective function models quantitatively the goal of the optimization and the constraints represent the physical limitations and practical considerations that must be accounted for in the optimization process. Bogetti and Gillespie [2] presented a simple analysis of the effects of processing history (autoclave temperature) on the evolution of process-induced stress and deformation in thick glass/polyester and graphite/epoxy laminates during cure. The results clearly indicate that the mechanical performance of thick thermoset laminates is strongly dependent on processing history, and that optimization should focus on process efficiency (i.e., consumed energy versus processing time) and part quality (i.e., warpage, micro and macro-cracking). In the present investigation, seven functions have been identified to describe the competing objectives of process

efficiency versus part quality. The final fitness function to be minimized by EA will be a weighted combination of a series of sub-objective functions.

7.4.2 Final extent of cure

The first objective to be studied concerns the ultimate degree of polymerization of the part. To assure appropriate mechanical properties of the composite, the resin extent of cure must reach a minimum value at the end of the curing stage before cooling and demolding the part. A maximum of 100% cure (i.e., complete resin polymerization) is desired after processing, but not always accessible. To account for the final resin conversion, an objective can be stated from the minimum required extent of cure and the last computed resin cure at any position through the thickness:

$$j_{fc} = \frac{\alpha'_{last} - \alpha_{min}}{\alpha_{min}} \quad (7.4)$$

where j_{fc} is the final resin cure objective attained, α_{min} and α'_{last} are respectively the minimum required extent of cure (i.e., 80 % of complete polymerization) and the last extent of cure calculated at position i through the thickness. It is usual in error minimization to use square error functions to increase the convergence rate. Optimization algorithms, particularly evolution algorithms, are well known to be very time consuming in terms of computational resources. Optimization procedures based on EA usually exhibit low convergence rates, requiring sometimes an exorbitant number of evaluations of the fitness function. This situation is problematic when the calculation of the fitness function requires long and complex simulations to be carried out, such as finite element or finite difference simulations. It has been shown that the use of Gauss-Sigmoid fitness functions strongly increases the learning speed of evolutionary

algorithms [19]. The objective function of the final resin cure (J_{fc}) can then be written in the sigmoid form:

$$J_{fc} = \frac{A_{fc}}{B_{fc} + e^{-g_{fg}}} \quad \text{with} \quad g_{fg} = j_{fc} \cdot \frac{C_{fc}}{(\alpha_{ult} - \alpha_{min})} \quad (7.5)$$

where α_{ult} is the ultimate extent of cure for which the resin is considered totally polymerized (i.e., $\alpha_{ult} = 0.95$). Parameters A_{fc} , B_{fc} and C_{fc} are coefficients of the sigmoid function. Note that sub-indexes will be used in the future to identify the function in which the coefficients A , B and C of the sigmoid appear. Figure 7.2 shows a comparison of the square error between α_{last} and α_{min} and the sigmoid function of equation (7.5). Note that the square error decreases from one when $\alpha_{last} = 0$ until it reaches a minimum when $\alpha_{last} = \alpha_{min}$. The sigmoid function assumes that a final extent of cure below α_{min} is not appropriate and then $J_{fc} = 1$. It also considers that a value of $\alpha_{last} = 1$ represents the optimum extent of cure (i.e., $J_{fc} = 0$). Then, this function decreases between $\alpha_{last} = \alpha_{min}$ and $\alpha_{last} = 1$ in a Gaussian form defined by coefficients A , B and C of the sigmoid. In evolutionary algorithms, this sigmoid function returns a low survival probability of the design variables if $\alpha_{last} \leq 0.6$, increasing the convergence rate for values of $\alpha_{last} > \alpha_{min}$.

7.4.3 Maximum exothermic temperature

During the cure of thermoset resins, the exothermic reaction of the matrix increases the temperature in the core of the part. In case of non-uniform curing of thick laminates (i.e., when a curing front appears across the thickness), the maximum exothermic temperature may be high enough to degrade the matrix. In order to improve the

quality of thick composites, the maximum exothermic temperature needs to be controlled to avoid polymer degradation. A temperature constraint may then be expressed as a maximum allowable temperature inside the composite. The degree of resin polymerization is temperature dependent then, a restriction of the maximum curing temperature limits the ultimate extent of cure of the composite. Thus, even if the polymer degradation temperature still constrains the cure process as an upward limit temperature, a maximum curing temperature is desired to decrease processing time and increase resin cure. For these reasons, it would be better to transform the constraint of maximum curing temperature into an objective function. The maximum temperature constraint can be written as an objective function of the maximum allowed exothermic temperature to avoid matrix degradation and the desired temperature at which the resin cure is complete. The objective $J_{T_{\max}}$ can then be written using the following sigmoid function:

$$J_{T_{\max}} = \frac{A_{T_{\max}}}{B_{T_{\max}} + e^{-g_{T_{\max}}}}, \quad \text{with} \quad g_{T_{\max}} = \frac{(T_{\text{exot}} - T_{\text{exot}}^{\min})}{(T_{\text{exot}}^{\max} - T_{\text{exot}}^{\min})} C_{T_{\max}} \quad (7.6)$$

where T^{exot} is the exothermic temperature calculated during processing, and T_{exot}^{\max} and T_{exot}^{\min} are respectively the maximum allowed exothermic temperature (i.e., the degradation temperature of the polymer matrix) and the minimum exothermic temperature desired (i.e., $T_{\text{exot}}^{\min} = 120^\circ\text{C}$ to totally cure composites with unsaturated polyester resins).

7.4.4 Cross-over at After Gel Point objective

The mechanical performance of a composite laminate with a thermoset matrix depends on processing history. It has been demonstrated that the level of internal stresses in the

processing of LCM parts is strongly influenced both, by the resin modulus and the chemical shrinkage [15, 20]. In the elastic and viscoelastic characterization of thermoset resins, it has been found that mechanical properties begin to develop after the resin has reached an important degree of polymerization. For an unsaturated polyester resin, the point at which resin modulus begins to develop (called the After Gel Point AGP) was characterized at around 40 % of the total resin polymerisation [17]. In a previous work [20], it was noted that the AGP point has a significant impact on the magnitude of process-induced residual stresses.

The progression of the curing front through the thickness of the composite was also identified as an important issue related to the development of processing stresses. Progression of resin cure from the part surface towards the core (called *outside-to-inside* cure) must be avoided in the processing of thick composites because of the high level of residual stresses created. An *inside-to-outside* cure (i.e., when the cure front progresses from the core towards the surface) is always preferable to reduce processing stresses. As schematically shown in Figure 7.3, an *inside-to-outside* cure can be achieved for low degrees of polymerization at the cross-over point. For optimization purposes, the initiation delay (see zone I in Figure 7.3) should be minimized while assuring a degree of cure at cross-over ($\alpha_{\text{cross-over}}$) close to the AGP level. This assures that resin mechanical properties begin to develop at once all across the part thickness. Instead of using the $\alpha_{\text{cross-over}}$ definition of Bogetti and Gillespie [2], this objective can be modeled by a sigmoid function of the degree of cure at the part surface and in the core:

$$J_{AGP} = \frac{A_{AGP}}{B_{AGP} + e^{-g_{AGP}}} + D_{AGP} \quad (7.7)$$

$$g_{AGP} = C_{AGP} \left[\frac{\alpha_{\text{surface}}^{AGP-\text{core}} - \alpha_{AGP}}{\alpha_{AGP}} \right]^2$$

where α_{AGP} is the degree of cure at the After Gel Point as defined in [17], and $\alpha_{surface}^{AGP-core}$ is the degree of cure at the part surface when the core reaches the AGP level. Parameters A , B , C and D are the coefficients of the J_{AGP} sigmoid. Figure 7.4 depicts the shape of the sigmoid of equation (7.7) and the square error of g_{AGP} . Note that the minimization of the J_{AGP} objective results in $\alpha_{cross-over} = \alpha_{AGP}$, but presents the advantage of higher convergence rates than a square error function.

7.4.5 Cure gradients after AGP

Once mechanical properties of the resin begin to develop, the chemical shrinkage promotes the development of internal stresses. The polymerization shrinkage has been characterized as a nearly linear function of the resin degree of cure [17]. Based on this assumption, the variations of chemical shrinkage through the thickness are proportional to the variations of the resin cure after AGP (see region II in Figure 7.4). The apparition of differential chemical shrinkage in the through-thickness direction results in increased internal residual stresses. Then, to reduce internal stresses during cure, the mechanical properties of the resin and the chemical shrinkage should increase uniformly through the thickness. To account for the variations in the cure profile at a given processing time, an analysis of the cure differences between the surface and core of the part can be carried out. As shown in Figure 7.5, successive cure differentials can be evaluated after the AGP level has been reached. The minimization of these cure differences results in a uniform cure profile through the thickness of the part. For a desired degree of cure in the core, the cure difference between the surface and the core of the part can be computed as:

$$\varepsilon_c^i = \left| \frac{\alpha_{surface}^i - \alpha_{core}^i}{\alpha_{AGP}} \right|^{1/2} \quad (7.8)$$

and the sigmoid function of this error will be:

$$g_c^i = \frac{A_c}{B_c + e^{-C_c \epsilon_c^i}} + D_c \quad (7.9)$$

where α_{core}^i denotes a desired degree of cure in the core and $\alpha_{surface}^i$ the cure at the surface of the part at time i . Parameters A , B , C and D are coefficients of the sigmoid. Defining a discrete number of α_{core}^i values, the averaged sigmoid can be obtained in the following form:

$$j_{cure} = \frac{\sum_{i=1}^{Np} g_c^i}{Np} \quad (7.10)$$

where Np is the number of points in the α_{core}^i discretization. Finally, a sigmoid is introduced to describe the averaged error:

$$J_{cure} = \frac{A_c}{B_c + e^{-J_{cure}}} \quad (7.11)$$

where A and B are the same coefficients as in sigmoid (7.9). Figure 7.6 depicts a comparison of the J_{cure} objective function with the sum of the square error ϵ_c^i . While the square error ϵ_c^i has a constant smooth convergence, the sigmoid has the ability to define a small zone of feasibility. In the graph, a maximum of 20% cure difference was allowed for the construction of the minimization curve J_{cure} .

7.4.6 Curing stresses

Residual stresses do not result only of chemical shrinkage, but also of thermal expansion and contraction. During cure, internal stresses (so-called curing stresses) may result from thermal gradients through the thickness of the part. The J_{AGP} and J_{cure} objective functions are not sufficient to ensure minimum curing stresses. To reach that goal, two approaches may be applied: the first one consists of minimizing the thermal gradients in the through-thickness direction. Although the thermal evaluation is computationally improved, it has the disadvantage of producing the slowest curing cycle available (i.e., the smaller is the temperature, the smaller the exothermic reaction and the residual stresses). The second approach consists of analyzing the internal stresses developed during cure. Even if the numerical calculation is time consuming, the evaluation of internal stresses permits to use higher thermal gradients (that reduce processing time) if the composite mechanical properties are not important (such as in the rubbery state of the resin [17]).

As demonstrated by Ruiz and Trochu [20], in the curing phase of thick composite laminates, internal stresses can reach a peak generally related to the fast curing of the core. In this investigation, curing stresses are considered as the maximum internal stresses generated during resin polymerization at any composite layer. In the evaluation of these stresses, the Tsai-Wu safety factor theory for composites was implemented. The objective for curing stresses minimization J_{stress} is written as the following sigmoid function:

$$J_{stress} = \frac{A_{stress}}{B_{stress} + e^{C_{stress} S_{T-W}^2}} \quad (7.12)$$

where S_{T-W}^L is the minimum Tsai-Wu safety factor at layer L , and A , B and C are the coefficients of the sigmoid.

7.4.7 Cooling stresses

Composites processing does not stop at the end of the curing phase. The part also needs to be cooled to room temperature. If this process is not thermally balanced through the thickness, differential material contractions will create internal stresses resulting in part warpage or poor geometrical stability. If the cooling is balanced such that the same transient temperature profile is applied to each composite layer simultaneously, then internal cooling stresses will be negligible. For the minimization of the cooling stresses, two conditions are required: a low curing temperature, and a small cooling ramp. These conditions may be in conflict with the objective of final extent of cure (J_{fc}) and the minimum curing time requirement (as in the case of thick composites processing by LCM). The competition between these factors will depend upon the used desirable objective to be reached (i.e., minimum curing time, minimum residual stresses, maximum final extent of cure, etc.). The role of the cooling path in the development of residual stresses may be taken into account through the Tsai-Wu safety factors along the path. Following equation (7.12), the objective function can now be stated as:

$$J_{cooling} = \frac{A_{cooling}}{B_{cooling} + e^{C_{cooling} S_{T-W}^L}} \quad (7.13)$$

where S_{T-W}^L is the minimum Tsai-Wu safety factor at layer L , and A , B and C are the coefficients of the sigmoid.

7.4.8 Processing time

In the optimization of medium to high production cycles such as in the automotive industry, the first goal is always to minimize the processing time. In the case of composite manufacturing by liquid molding, the cycle-time required from the beginning of the injection until the part is demolded is key for process optimization and reduction of energy consumption. Although there is no ideal processing time (if no other process parameters are taken into account), expert knowledge can be considered to identify the characteristic cycle-time for a given part. The assumption of an expert desired processing time is used in this investigation to define the time objective function J_{time} in the following quadratic form:

$$J_{time} = \left[\frac{t_{cycle}}{t_{cycle}^{exp}} \right]^2 \quad (7.14)$$

where t_{cycle}^{exp} is the expert desired cycle time and t_{cycle} is the calculated cycle time for a given set of design variables.

7.4.9 Design parameters

In most LCM applications, the mold is maintained at constant temperature without heating/cooling control. Because the resin exothermic reaction increases the mold temperature, the curing process becomes self-accelerated. A minimum quality of molded parts is more often obtained by experimental trial and error than by using numerical optimization procedures. In autoclave processing, the autoclave is heated according to predetermined cure cycles. Usually this temperature profile is set by a series of constant temperature levels (called dwell temperatures) connected by periods of constant heating ramps. The autoclave allows a certain level of temperature control

that permits to improve the quality of the part. One important difference between these methods is related to the processing time. The goal of thermal optimization in LCM is to minimize the cycle-time and increase mechanical properties and part quality.

As shown in Figure 7.7, the mold temperature profile containing heating and cooling ramps is described by a series of design variables. In this assumption, at the beginning of the cure process the part and mold are considered to be at the equilibrium temperature. This temperature can be obtained from a non-isothermal filling optimization [11]. Beginning with this equilibrium temperature T_{init} , the transient temperature profile can be divided into a discrete sequence of heating ramps Q_i and dwell times dt_i . The design parameters of the optimization are then the sum of the (Q_i, dt_i) pairs that describe the mold temperature profile. These parameters are subject to the technical limitations of the heating/cooling system. The constraint can now be set as the maximum permitted heating ramp Q_{max}^+ and the maximum cooling ramp allowed by the mold Q_{max}^- , always subject to the initial mold temperature T_{init} and the room temperature T_{room} at the end of the process. The design variables can be regrouped to form the design vector Vd written in the following way:

$$Vd = [Q_1, dt_1, Q_2, dt_2, \dots, Q_n, dt_n] \quad (7.15)$$

subject to the constraints vector (Cs):

$$Cs = [T_{init}, T_{room}, Q_{max}^+, Q_{max}^-] \quad (7.16)$$

The advantage of evolutionary algorithms is that the number of design parameters used for the optimization (i.e., the number of points of the discrete temperature profile) can be more elevated than with other techniques, although slow convergence rates should

be attained. In this work, seven pairs of parameters (Q_i, dt_i) were selected to describe the temperature profile, resulting in a design vector containing 14 design parameters.

7.5 Fitness function

As it was discussed in the previous sections, the quality of molded composite parts depends upon a number of different factors such as resin mechanical properties, maximum exothermic temperature, curing stresses, etc. In this investigation seven objective functions were identified as directly related to part quality and process cycle-time. The degree of success of a set of design parameters can be quantified by a weighted function of these objectives. The cure-cycle optimization in LCM can thus be stated as:

$$\text{minimize:} \quad F_f(Vd) = \frac{A_f}{B_f + e^{-F_\omega C_f}} + D_f \quad (7.17)$$

$$F_\omega = \omega_{fc} J_{fc} + \omega_{T_{\max}} J_{T_{\max}} + \omega_{AGP} J_{AGP} + \omega_{cure} J_{cure} + \omega_{stress} J_{stress} + \omega_{cooling} J_{cooling} + \omega_{time} J_{time}$$

$$\text{subject to:} \quad Vd \in Cs \quad (7.18)$$

where $F_f(Vd)$ is the fitness function to be optimized, and parameters ω are the weighting coefficients for each sub-objective function. Note that the use of sigmoid functions scaled between 0 and 1 avoids the complex setting of weighting coefficients. In this case, the coefficients are implemented to allow the user to define their particular interest regarding the optimization procedure. In fact, the default value of the weighting coefficients is 1, indicating that the minimization of the fitness function considers proportionally the effects of each one of the sub-objective functions. In the processing

of thin composite laminates, the exothermic reaction is small and the heat generated is quickly dissipated through the thickness. The temperature and degree of cure profiles are wide uniform and no important thermal or curing gradients appear in the through-thickness direction. If it is desired for this part to obtain a maximum degree of cure in the minimum cycle-time while reducing cooling stresses, then the weighting coefficients ω_{fc} , $\omega_{cooling}$ and ω_{time} can be set to 1 and the others to a value of 0.5 or less.

In the processing of a thick composite part in a very low production volume, the cure and cooling times are not important issues related to the process optimization. If the aim is the minimization of the curing stresses while increasing the mechanical properties, the ω_{fc} and ω_{stress} coefficients can be set to 1, $\omega_{cooling}$ and ω_{time} to 0 and the rest to a value between 0.5 and 1. The proposed fitness functions $F_f(Vd)$ accounts for a variety of different LCM process optimizations based on the physics of the matrix material transformation and on the mechanical behaviour of the composite material.

7.6 Results and discussion

In this section, the proposed methodology is used for the cure cycle optimization of liquid composite molding in the cases of thin and thick parts. The numerical implementation is based on a Genetic Algorithm with real-valued genomes (instead of typical binary representation). The fitness function F_f for a given set of design variables is calculated by running a curing cycle simulation coupled with a CLT stress analysis [15, 20] and extracting the resulting sub-objective functions. The optimization code called LeCoq (Logical Evolutionary Curing Optimization and Quenching) was developed in C++ language with two libraries for the cure-cycle and stress analysis simulation. This allows the information between the EA and the simulation libraries to be transferred via flush memory avoiding time consuming file input/output tasks.

In the next topics, three typical LCM curing optimizations will be studied. The first one is a simple two heating ramps cure cycle of a thick bi-directional laminate. The second one consists of optimizing the fast processing of a thin composite, and comparing the effects of using elastic or viscolastic material characterization. Finally, the curing optimization of a thick non-balanced composite is presented. In all cases, the parameters used for the evaluation of the sub-objective functions were maintained constants. A list of the sigmoid constants for each sub-objective function is presented in Table 7.3. The variations between the cases are based on the proper selection of the weighting coefficients (ω) of the fitness function (F_f) to account for each sub-objective function. The thermo-kinetic and thermo-mechanical characterizations of the materials used in this analysis are those presented in a previous work [17].

7.6.1 Two ramps curing-cycle

The widely used two heating ramps curing cycle is now studied for a thick composite plate. The composite is a bi-directional glass/polyester laminate made of NCS-82620 fabric from J. B. Martin and T580-63 unsaturated polyester resin from AOC Inc. [17]. The plate is 20 mm thick with 43% of fiber volume fraction. A fixed mold wall temperature is considered as the thermal boundary condition. The two heating ramps cycle is schematically shown in Figure 7.8. The curing cycle has two variables (the design variables to be tested), the first heating ramp Q_1 and the first dwell time dt_2 while the other parameters of the temperature profile are fixed. By changing Q_1 and dt_2 , a bi-dimensional search space can be defined. The interest of this optimization is centered on the minimization of the curing stresses avoiding excessive processing times. Because the curing temperature (i.e., the higher temperature of the profile) is a fixed parameter, the final extent of cure sub-objective function is neglected. The process is ended after the second dwell temperature (T_3) and for instance the cooling stresses sub-objective function can also be neglected. In the first case, it is assumed that residual stresses can be minimized by the minimization of the curing gradients. This

means that only J_{AGP} and J_{cure} sub-objective functions can be used to reduce curing stresses. To account for excessive processing times and to avoid matrix degradation, the J_{time} and J_{Tmax} sub-objective functions are included. The weighting coefficients of the fitness function in this case will be:

$$\begin{aligned} \omega_{AGP} &= 1 & \omega_{cure} &= 1 \\ \omega_{time} &= 0.75 & \omega_{Tmax} &= 0.75 \\ \omega_{stress} &= 0 & \omega_{cooling} &= 0 & \omega_{fc} &= 0 \end{aligned} \quad (7.19)$$

while the design variables Q_1 and dt_2 will be subject to the following constraints:

$$\begin{aligned} 0 < Q_1 &< 1.5 \text{ } ^\circ\text{C/min} \\ 0 < dt_2 &< 85 \text{ min} \end{aligned} \quad (7.20)$$

A study is initially carried out to define the behaviour of the fitness function in the search space. To do so, the design variables were progressively increased in a step of 1/100 times of their maximum limit. A total of 10,000 curing cycles were analyzed in a period of 20 minutes of cpu time (at a rate of 0.12 seconds per simulation) on a IBM IntelliStation Z-Pro with a Pentium IV (2.8 Gz) processor. The resulting fitness function is drawn in the contour plot of Figure 7.9. A ditch of near optimum values vertically divides the fitness representation into two zones. At low values of the initial heating ramp (zone 1), excessive processing times dominate the fitness function (i.e., $J_{time} = 1$). Increasing the value of Q_1 , the processing time decreases, but an *outside-to-inside* cure appears resulting in high cure restrictions of the fitness function (i.e., $J_{AGP} = J_{cure} = 1$). For higher values of the initial heating ramp, the cure front is transformed into an *inside-to-outside* curing (zone 2). In this zone, the J_{time} , J_{AGP} and J_{cure} objective functions are all smaller than one (i.e., the contour plot of the fitness function is lighter in zone 2 than in zone 1). Between these two regions of the search space, the minimum of the fitness function can be found at the limit where the *outside-to-inside* cure

changes into an *inside-to-outside* cure profile (the dark vertical dish). A large number of combinations of the two design variables will return a near optimal solution (i.e., the nearest minimum of the fitness function). The two ramps temperature profile was then optimized using the LeCoq code. Note that the optimization algorithm does not analyze the discrete functional space of the contour plot. Instead of reading the output files of a series of simulations, the fitness function is evaluated for a set of design variables by a numerical simulation of the cure cycle. As depicted in Figure 7.9, an optimum value of the first heating ramp and first dwell time was obtained at $Q_1 = 0.9 \text{ } ^\circ\text{C}/\text{min}$ and $dt_2 = 26 \text{ min}$, a point that graphically corresponds to the minimum of the fitness function (darkness contour plot).

In the second approximation, the internal stresses developed during resin cure are considered in addition to the optimization of the cure profile. Because the objective of the optimization is the reduction of these processing stresses, the J_{stress} function should have a higher weighting factor than the rest of the objectives. In this case, the weighting coefficients of the sub-objective functions can be expressed as follows:

$$\begin{aligned} \omega_{stress} &= 1 & \omega_{AGP} &= 0.75 & \omega_{cure} &= 0.75 \\ \omega_{time} &= 0.5 & \omega_{T_{max}} &= 0.75 & & \\ \omega_{cooling} &= 0 & \omega_{fc} &= 0 & & \end{aligned} \quad (7.21)$$

A new set of design variables was run for coupled curing and stress analysis. The 10,000 curing/stress cycles simulated required 25 cpu minutes (a rate of 0.15 seconds per simulation) on the same computer. Figure 7.10 shows the contour plot of the evaluated fitness function. Important differences were found between the two solutions. In this case, the time constrained region (zone 1) has a smaller fitness value than the cure constrained zone 2 (seen as the lighter color of the contour plot). The main difference with the previous non-stress fitness function resides in the higher fitness

values of zone 2. It was before stated that increasing the first heating ramp makes the cure front to develop as an *inside-to-outside* curing. Even if the cure profile uniformly evolves through the thickness (i.e., $J_{AGP} < 1$ and $J_{cure} < 1$), important thermal gradients may be generated due to the high exothermic reaction of the resin. In a thick composite laminate, the through-thickness thermal gradients induce internal stresses during cure that should not be neglected. As a result of these thermal gradients, the fast *inside-to-outside* curing produces high curing stresses. The right zone of the search space is then constrained by the stress objective function (i.e., $J_{stress} = 1$), and near optimum solutions are reduced to lie in the lighter *knife-shaped* region.

The temperature profile was then optimized for the set of weighting coefficients given by equation (7.21). The minimum value of the fitness function was found to be at $Q_1 = 0.82\text{ }^{\circ}\text{C}/\text{min}$ and $dt_2 = 46\text{ min}$ (see detail in Figure 7.10). Note that the optimum value of these two design variables has considerably changed from the previous solution (i.e., fitness function without stress analysis). While the first heating ramp was decreased around $0.1\text{ }^{\circ}\text{C}/\text{min}$, the first dwell time increased almost 20 min . In other words, the cure cycle was retarded to prevent the apparition of internal curing stresses. Figure 7.11 shows the result of the optimized cure cycle with stress analysis. The cross-over point at 90 min is located at the AGP degree of cure (i.e., $J_{AGP} \approx 0$). After that, the cure profiles at the surface and in the core of the part uniformly increase until the resin is fully cured (i.e., $J_{cure} \approx 0$). From this cure cycle, maximum internal stresses of around 0.1 Mpa were calculated while in the previous optimization without stress analysis, a value of 5.4 Mpa was obtained. This analysis clearly demonstrates that stress analysis is key for the optimization of composites processing. If internal stresses are not considered, the optimized parameters may even produce parts of low quality in terms of mechanical properties and geometrical stability.

A comparison of the convergence of the LeCoq optimization for the two sets of weighting coefficients tested is shown in Figure 7.12. In the case without stress

analysis, the fitness function decreases progressively, jumping between local minimums. Around 100 EA iterations were required prior convergence to the assumed near optimal solution (a minimum of 0.035). In the second solution (that considers curing stresses), a higher convergence rate is observed. This is mainly because the search space consists of a plateau with a fall in the centre. The minimum of the fitness function was found to be 0.045, and almost 50 iterations were required to converge. In both cases, around 1100 cure cycle simulations were accomplished at the end of the 200 EA iterations with a total computer time of 106 seconds.

7.6.2 Thin part optimization

A thin composite laminate is now considered for the cure cycle optimization. The 2 mm thick plate studied is made of 6 layers of NCS 82620 bi-directional glass fabric and T-580-63 polyester resin with a fiber volume fraction of 43% [17]. When curing thin composites in closed molds, the transient temperature profile through the laminate thickness is nearly constant. This implies that the heat flow from the mold walls uniformly increases the temperature across the thickness, and as a consequence the cure profile remains constant through the thickness. In this case, it is not necessary to use a two heating ramps curing cycle. Only a heating ramp followed by a constant dwell temperature is enough to cure the thin laminate without the presence of cure gradients through the thickness. As shown in the temperature profile of Figure 7.13, in this case, the following five design variables are considered:

$$\begin{aligned}
 \text{Heating:} \quad & 0 < Q_1 < 30 \text{ } ^\circ\text{C/min} \\
 \text{Cooling:} \quad & 0 > Q_3 > -30 \text{ } ^\circ\text{C/min} \\
 \text{Dwell times:} \quad & 0 < dt_1, dt_2, dt_3 < 10 \text{ min}
 \end{aligned} \tag{7.22}$$

The processing optimization of thin composites is focusing on the minimization of the cycle time, while ensuring an appropriate degree of cure and a minimization of residual

stresses. Because no cure gradients appear through the thickness of the laminate, the sub-objective functions J_{AGP} and J_{cure} may not be included into the objective vector. The weighting coefficients of the fitness function for thin parts will be:

$$\begin{aligned} \omega_{stress} &= 1 & \omega_{cooling} &= 1 & \omega_{fc} &= 1 \\ \omega_{time} &= 1 & \omega_{T_{max}} &= 0.75 & & \\ \omega_{AGP} &= 0 & \omega_{cure} &= 0 & & \end{aligned} \quad (7.23)$$

In a previous work [17], two models were presented for the prediction of the composite mechanical properties during processing. The first one is a thermo-elastic modeling based on relaxed/unrelaxed elastic properties, while the second one is a viscoelastic modeling that depends on relaxation time. The two models are tested in this case to assess the differences on the optimized temperature profile. Figure 7.14 shows the resulting temperature and cure profiles for the elastic and viscoelastic models of composite mechanical properties. Note that in both cases, no relevant cure gradients appeared between the surface and middle-thickness of the part, and that small thermal gradients through the thickness are generated during the exothermic reaction. Thermo-elastic and viscoelastic optimizations resulted in similar processing times and final degree of cure. While the curing temperature is very close between models, the main difference is related to the heating and cooling ramps. The thermo-elastic model of mechanical properties considers a full stress relaxation for temperatures above the glass transition temperature. The viscoelastic model extends this concept to the progressive relaxation when the material is in a rubbery state. As a consequence of this viscoelastic behaviour, the first heating ramp can be increased without creating more internal stresses. In a similar but inversed way, after cure the viscoelastic model resulted in a smaller cooling ramp compared to the thermo-elastic model.

Table 7.4 lists the optimized parameters obtained with the thermo-elastic and viscoelastic models, and compares the results of two cure cycles commonly used for thin parts. These typical cure cycles were chosen for fast or slow processing and both were run with the viscoelastic model. The fast cure is carried out with the maximum heating and cooling ramps, and a curing temperature of 130 °C. With this curing cycle, a final degree of cure of 0.92 and a plate curvature along the x-axis of 4.51 m^{-1} were obtained after more than 11 minutes of processing time. The slow curing has smaller heating and cooling ramps and a processing time of 23 minutes. The result is a degree of cure of 0.88 and an x-curvature of 3.13 m^{-1} . Process optimization with the thermo-elastic and viscoelastic models resulted in a processing time of around 15 minutes and a final degree of cure of 0.91. The optimized cycle with viscoelastic modeling has an x-curvature of 3.32 m^{-1} , which is close to the curvature obtained for the slow processing. This indicates that even in the simple case of a thin laminate, optimized heating and cooling ramps exist so that processing time as well as residual stresses can be minimized. The optimization with the thermo-elastic model resulted in a similar optimum temperature profile although the x-curvature was 4.14 m^{-1} . In conclusion, the thermo-elastic model gives enough information on the evolution of mechanical properties for the cure cycle optimization of thin parts. Even if the resulting level of internal stresses is not quantitatively appropriate, the quality of the optimization is comparable to that of the viscoelastic model.

7.6.3 Thick part optimization

The proposed optimization methodology is now applied to the reduction of thermal and cure gradients in a thick composite plate. The 25 mm thick laminate is made of NCS 82620 glass fabric and T580-63 polyester resin with a 43 % of fiber volume fraction. To cure this thick part, the temperature profile of figure 7.7 is used with two heating and two cooling ramps. The constraints on the design variables that define this temperature profile are:

$$\begin{aligned}
0 < Q_1, Q_5 < 8 \text{ } ^\circ\text{C/min} \\
0 > Q_3, Q_7 > -3 \text{ } ^\circ\text{C/min} \\
0 < dt_1, dt_2, dt_3, dt_4, dt_5, dt_6 < 80 \text{ min}
\end{aligned} \tag{7.24}$$

Two optimization criteria were selected to assess the differences between a simple cure gradient minimization and the complex cure/stress minimization proposed in this work. The first criterion intends to minimize the cure gradients and processing time while assuring a desirable final degree of cure. In this curing cycle optimization, the minimization of the cure gradients is assumed to be equivalent to the reduction of internal stresses developed during processing. Indeed, processing stresses are not considered in this optimization. The weighting coefficients of the fitness function for this case will be:

$$\begin{aligned}
\omega_{AGP} &= 1 & \omega_{cure} &= 1 & \omega_{fc} &= 1 \\
\omega_{time} &= 1 & \omega_{T_{max}} &= 1 & & \\
\omega_{stress} &= 0 & \omega_{cooling} &= 0 & &
\end{aligned} \tag{7.25}$$

The second criterion is the full optimization stated in this investigation, which considers the inclusion of the processing stresses in the fitness function. For this cure and stress minimization, two optimization are carried out with the thermo-elastic and the viscoelastic model of mechanical properties. The weighting coefficients in this case are written as follows:

$$\begin{aligned}
\omega_{AGP} &= 1 & \omega_{cure} &= 1 & \omega_{fc} &= 1 \\
\omega_{time} &= 1 & \omega_{T_{max}} &= 1 & & \\
\omega_{stress} &= 1 & \omega_{cooling} &= 1 & &
\end{aligned} \tag{7.26}$$

Figure 7.15 depicts the optimized temperature profiles for the three analyses presented above and denoted as follows: cure gradients minimization (no stress), cure/stress minimization with thermo-elastic modeling (elastic) and cure/stress minimization with viscoelastic modeling (viscoelastic). Table 7.5 lists the optimized design parameters for the three temperature profiles. These three optimized profiles have practically the same curing temperature (close to 116 °C) and a similar final degree of cure (between 0.97 and 0.99). Although the final mechanical properties of the part seem to be optimized in the three cases, some important differences must be noticed. The first difference is related to the cycle time. If processing stresses are not considered in the fitness function, the resulting cure cycle lasts around 150 minutes. The cure/stress minimization with thermo-elastic model required an increased cycle time (around 205 minutes) to avoid the development of internal stress. The optimization with the viscoelastic modeling needed even longer processing time (a cycle time close to 250 minutes was obtained). Note that the cooling ramp to room temperature (Q_7) decreases with the complexity of the model of mechanical properties, from -3 °C/min for the no stress optimization to -1.2 °C/min for the thermo-elastic model and -0.8 °C/min for the viscoelastic model. This decrement between the last two optimizations is directly related to the time required for stress relaxation. The thermo-elastic model is based on relaxed/unrelaxed properties that depend on glass transition temperature, while the viscoelastic model is based on time/temperature relaxation.

A proper second heating ramp (Q_5) called curing ramp is essential for the minimization of the cure gradients, and it is clearly understood that its value is mainly defined by the J_{cure} sub-objective function. When attained, the optimized curing ramp is nearly the same for the three criteria analyzed (an averaged value of 4.26 °C/min with a variation of ± 25 °C/min was found).

Figures 7.16 to 7.18 show the temperature and cure profiles for the three optimizations studied. In all cases, the exothermic peak temperature was maintained below 125 °C, avoiding possible matrix degradation and excessive cooling from high temperatures. As can be seen in the three optimized cycles, the first overheating composed by heating and cooling ramps (i.e., until t_4 in Figure 7.7) is needed to initiate resin polymerization in the core of the part. Because of the low thermal conductivity of the composite and the exothermic reaction of the resin, the surface of the part must be heated and maintained above 60 °C until the core begins to react. At this time (i.e., at t_2 in Figure 7.7), the mold is cooled to release the exothermic heat from the core and slow down the polymerization reaction at the part surface. When the resin reaches to a degree of cure close to the AGP at any position through the thickness, the mold is heated by the curing ramp.

In the three optimizations, the cross-over point was obtained at the AGP (i.e., $J_{AGP} \approx 0$) at the beginning of the curing ramp. The cure gradients developed during this heating are also minimized in all cases (i.e., $J_{cure} \approx 0$). An important difference can be noted between the optimized cure cycle with no stress analysis and those optimized with internal stress reduction. In the first case, an important curing reaction is allowed prior to the cross-over at AGP (see Figure 7.16 at 60 to 90 minutes). In the optimization with stress minimization, the degree of cure at the core is not developed prior to the AGP as in the previous case (see Figures 7.17 and 7.18 between 50 and 110 minutes). This increment in the mechanical properties of the composite prior to the AGP has relevant consequences on the evolution of the internal stresses.

Figure 7.19 depicts the evolution of the processing stresses when the optimized temperature profile with minimization of cure gradients is applied (i.e., the temperature profile of Figure 7.16). The viscoelastic modeling was implemented to calculate the processing stresses generated in this curing cycle. Once the resin reaches the AGP, the mechanical properties begin to grow and internal stresses develop. Internal stresses

developed during cure (called curing stresses) show a peak prior to 100 minutes. This peak coincide with the thermal gradients generated during the curing ramp, and these thermal gradients are a consequence of the low reactivity remaining in the core after the cross-over at AGP. The peak on the curing stresses has a maximum value of -10 Mpa at around 98 minutes at the middle thickness and then decreases because the thermal gradients are inversed prior to 100 minutes (see Figure 7.16). The inversion of the thermal gradients induces an inversion of the internal stresses, which is noticed by the stress evolution at the part surface. At the curing temperature between 100 and 115 minutes, the internal stresses are slightly relaxed. Finally, the processing stresses increase up to 6 Mpa due to the cooling ramp until the composite reaches the room temperature.

Figure 7.20 shows the evolution of the laminate stresses when the optimized temperature profile is applied with the thermo-elastic model. Because this model considers fully relaxed properties above the glass transition temperature, no stresses are developed during the curing ramp (prior to 110 minutes). Stresses begin to grow due to the inversion of the thermal gradients at around 111 minutes, with a maximum below 1.3 Mpa . Then, internal stresses are inversed during cooling to room temperature. Figure 7.21 depicts the processing stresses for the optimized temperature profile with viscoelastic modeling. The behaviour of internal stresses is similar to the previous case, although with significant differences in value. In this analysis, stresses are not fully relaxed during cure showing a peak of -5.3 Mpa in the core before 102 minutes. Then, stresses decrease due to the inversion of the thermal gradients. Finally, internal stresses develop during cooling. A maximum of -3 Mpa was obtained at the end of cooling. Note that these values are about half of the values obtained with the optimized cure cycle without stress analysis.

From the above results, it can be concluded that the minimization of the cure gradients is not enough to optimize the cure cycle. The evolution of processing stresses must

necessarily be considered for a proper minimization of residual stresses. Moreover, to avoid the risk of delamination, the analysis of curing stresses is fundamental. Minimization of the internal stresses developed during the inversion of thermal gradients is key to avoid matrix degradation and composite delamination. After curing, the cooling ramp needs also to be optimized to reduce cooling stresses. Even if the thermo-elastic model gives smaller internal stresses than those obtained with the viscoelastic one, the optimized temperature profile showed a good agreement with that of the viscoelastic model. This indicates that the consideration of relaxed/unrelaxed behaviour of composite properties gives enough information for process optimization. When processing stresses are not included into the optimization criteria, the resulting cure cycle is shorter than the cycle optimized with the elastic or viscoelastic analyses. The longer cycle times are directly related to the initial heating ramp and the final cooling ramp required for internal stress reduction.

7.7 Summary

In this investigation, a methodology is proposed for the optimization of the curing cycle in LCM manufacturing. Seven optimization criteria are presented for the minimization of the thermal and cure gradients and for the reduction of the processing stresses. These criteria are considered as sub-objective functions that each take into account the cycle time, the final degree of cure, the maximum exothermic temperature, the degree of cure at cross-over, the cure gradients after gel point (AGP) and the curing and cooling stresses. To increase the convergence rate of the search algorithm, the sub-objectives are constructed with sigmoid functions. The fitness function to be minimized is a weighted combination of the seven sigmoid functions. The temperature profile to be optimized is discretized in a series of heating/cooling ramps and dwell times that are called the design vector.

The search algorithm is an evolutionary strategy based on genetic algorithms implemented in C++ code denominated Logical Evolutionary Curing Optimization and Quenching (LeCoq). For the evaluation of the fitness function, a one dimensional curing simulation with stress analysis is included in LeCoq. The calculation of internal stresses is carried out with the classical laminated plate theory. Because of the high number of iterations required for convergence of the evolutionary strategies, the curing/stress analysis was optimized to decrease the computer time of the simulation (i.e., computer time for an evaluation of the fitness function). For a typical thick composite part, 10,000 curing cycles were evaluated in 20 minutes of computer time (at a rate of 0.12 seconds per simulation).

The proposed methodology was used to minimize the processing time and residual stresses in a thin composite laminate. It was found that even in the simple case without cure gradients through the thickness of the laminate, an optimized temperature profile can improve curing while reducing processing stresses. In thin laminates, the reduction of internal stresses developed during cure and cooling is directly related to the geometrical stability of the molded part (i.e., curvature of a flat plate).

Finally, a 25 mm thick part was studied to demonstrate the capability of the proposed algorithm to optimize the processing of thick composites. Three optimizations were carried out. The first one is a minimization of cure gradients without stress analysis. The second optimization is a cure/stress minimization with a thermo-elastic model of mechanical properties, and the last one is a curing/stress minimization with a viscoelastic model. The thermo-elastic model is a non linear thermo-chemical elastic model that considers fully relaxed material properties above the glass transition temperature. The viscoelastic model is based on time/temperature superposition and describes the relaxation effects during resin polymerization. These analyses showed that the minimization of cure gradients only is not enough for thermal optimization of the cure cycle. The evolution of processing stresses must necessarily be considered for

a proper minimization of internal stresses. In the comparison between the thermoelastic and viscoelastic models, the consideration of relaxed/unrelaxed material properties provides enough information for process optimization. The optimized temperature profile obtained with both models was nearly the same, although the viscoelastic model gave longer cycle times.

7.8 Acknowledgements

The authors thank the *National Science and Engineering Research Council of Canada* (NSERC) and *Fonds Québécois pour la Recherche sur la Nature et la Technologie* (FQRNT) for their financial support. The contribution of *ESI_Group* and their numerical support is also gratefully acknowledged, as well as the program of *Bourses d'Excellence du Ministère de l'Éducation du Québec* that made this research possible. The LeCoq code used the *Galib* genetic algorithm package, written by *Matthew Wall* at the *Massachusetts Institute of Technology*.

7.9 References

1. S. R. White, and H. T. Hahn, *Polymer Eng. and Sci.*, 30, 1465 (1990).
2. T. A. Bogetti, and J. W. Gillespie, *J. of Composite Materials*, 26, 626 (1992).
3. V. Kostopoulos, and D. Th. Korontzis, *Composites Sci. and Technology*, 63, 1441 (2003).
4. H. H. Hilton, and S. Yi, *J. of Sandwich Structures and Materials*, 1, 111 (1999).
5. M. S. Johnson, C. D. Rudd, and D. J. Hill, "Effects of Microwave Resin Preheating on the Quality of RTM Laminates," *Proceedings of ICCM-11, Gold Coast, Australia, July 14th-18th (1997).*

6. X. Xiao, V. Astakhov, and T. Su, "A Study of Resin Transfer Molding Process Using Experimental Design Method," Proceedings of ICCM-12, Paris, France (1999).
7. M. S. Johnson, C. D. Rudd, and D. J. Hill, *Composites Part A*, 29, 71 (1998).
8. J. Spoerre, C. Zhang, B. Wang, and R. Parnas, *J. of Composite Materials*, 32, 1244 (1998).
9. R. Chen, C. Tu, and H. Tsai, *J. of Composite Materials*, 27, 1578 (1993).
10. M. Li, Q. Zhu, P. H. Geubelle, and C. Trucker, *Polymer Composites*, 22, 118 (2001).
11. Edu Ruiz, "Thermal Optimization of the RTM process", Ecole Polytechnique de Montreal, internal report, 115 pgs. (1999).
12. W.-B. Young, *J. of Composite Materials*, 28, 12 (1994).
13. M. Lin, M. Murphy, and T. H. Hahn, *Composites Part A*, 31, 361 (2000).
14. D. J. Michaud, A. N. Beris, and P. S. Dhurjati, *J. of Composite Materials*, 36, 1201 (2002).
15. Edu Ruiz, F. Trochu, and R. Gauvin, "Internal Stresses and Warpage of Thin Composite Parts Manufactured by RTM", accepted for publication in *Advanced Composite Letters*, Sept. 2003.
16. Edu Ruiz, and F. Trochu, "Coupled Non-Conforming Finite Element and Finite Difference Approximation Based on Laminate Extrapolation to Simulate Liquid Composite Molding Processes Part II: Non-Isothermal Filling and Curing", submitted to *Int. J. of Numerical Methods in Eng.*, Oct. 2003.
17. Edu Ruiz, and F. Trochu, "Thermo-Mechanical Properties during Cure of Glass-Polyester RTM Composites: Elastic and Viscoelastic Modeling", submitted to *J. Composite Materials*, Oct. 2003.
18. H.P. Schwefel, *Evolution and Optimum Seeking*. Wiley ed. (1995).
19. K. Shibata, and K. Ito, "Gauss-Sigmoid Neural Network", Proceedings of Int. Joint Conference on Neural Networks IJCNN'99, Washington, DC, USA (1999).
20. Edu Ruiz, and F. Trochu, "Numerical Analysis of Cure Temperature and Internal Stresses in Thin and Thick RTM parts", submitted to *Composites Part A*, Oct. 2003.

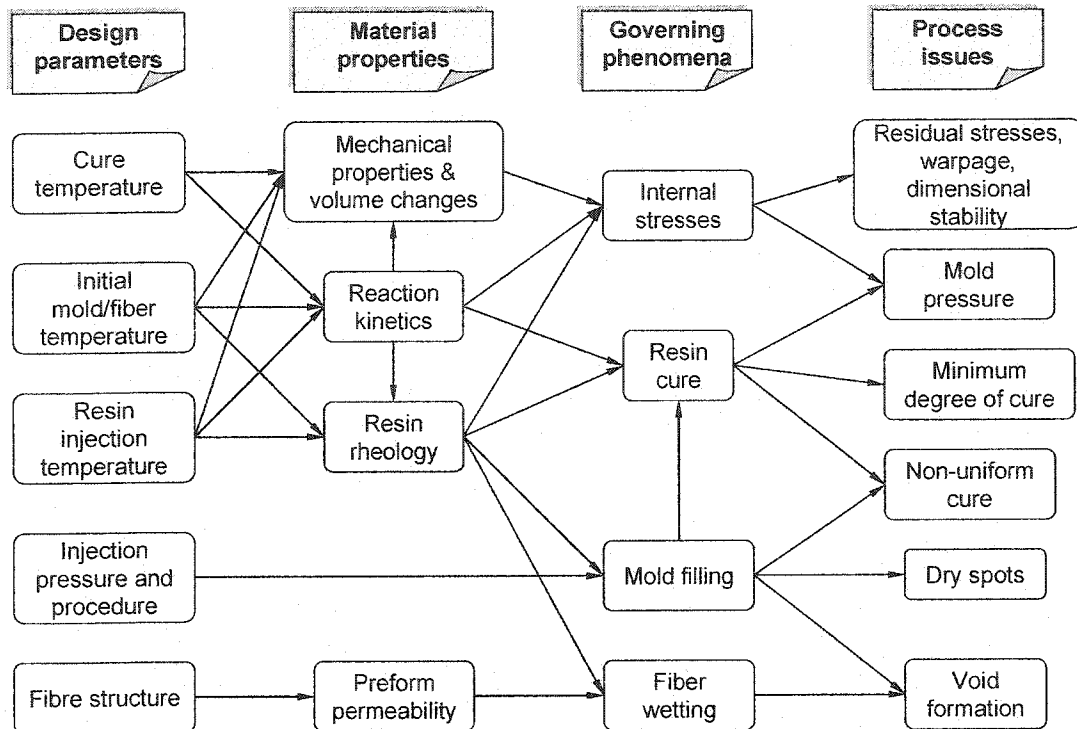


Figure 7.1. Process parameters and issues in LCM optimization.

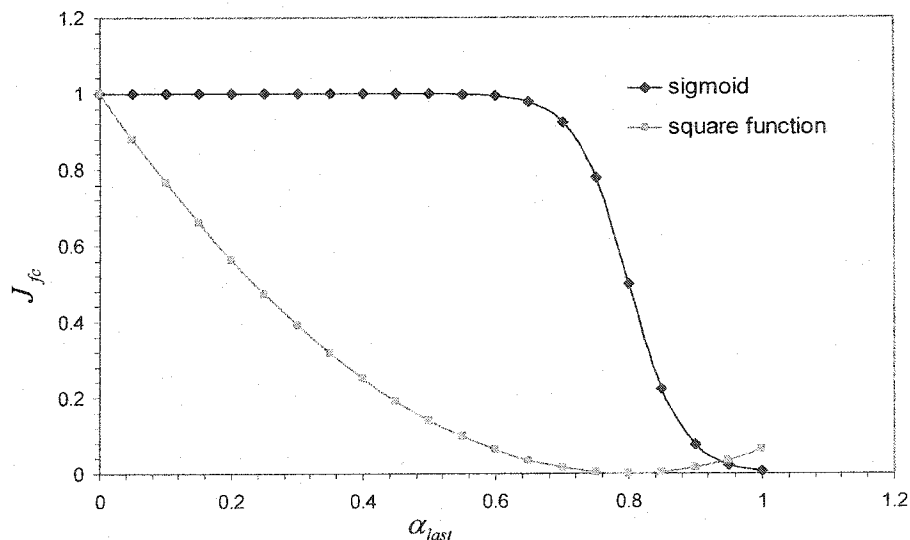


Figure 7.2. Square error versus sigmoid function for the final extent of cure sub-objective function. The sigmoid permits to increase the learning speed of the evolutionary algorithm (EA) near the desired optimization space.

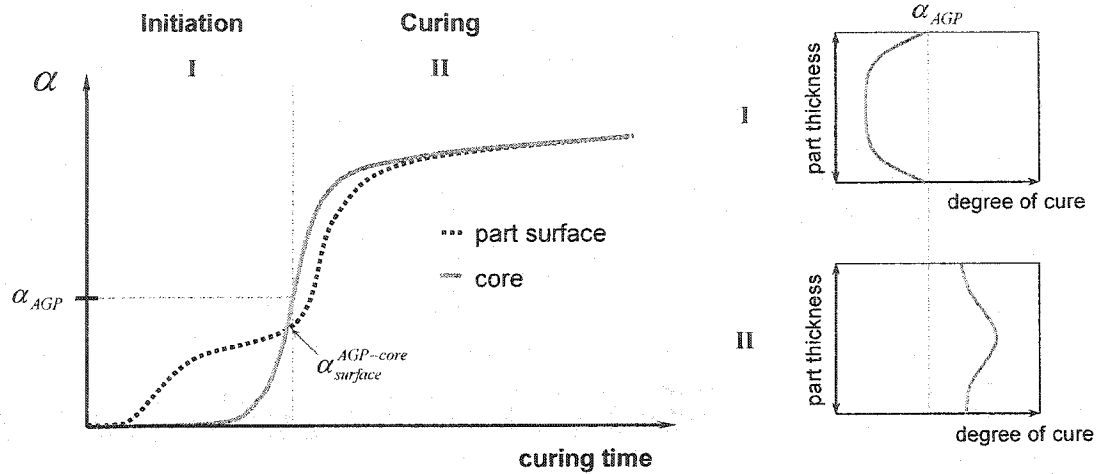


Figure 7.3. Schematic of the through-thickness curing front in a typical thick composite laminate. The cross-over point $\alpha_{cross-over}$ must approach the α_{AGP} level to decrease the initiation delay.

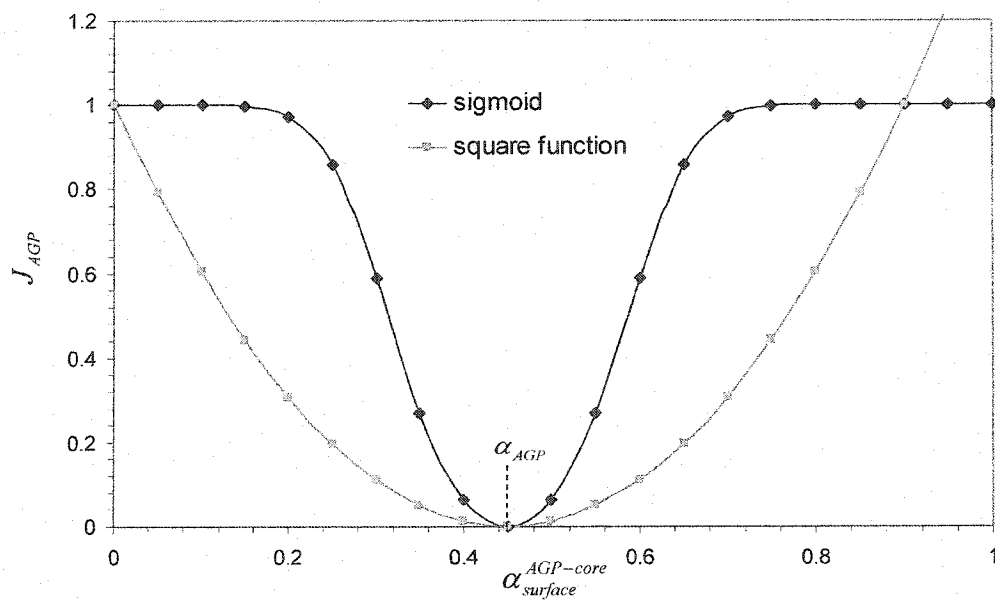


Figure 7.4. Comparison between the square error of g_{AGP} and the sigmoid objective J_{AGP} of equation (7.7).

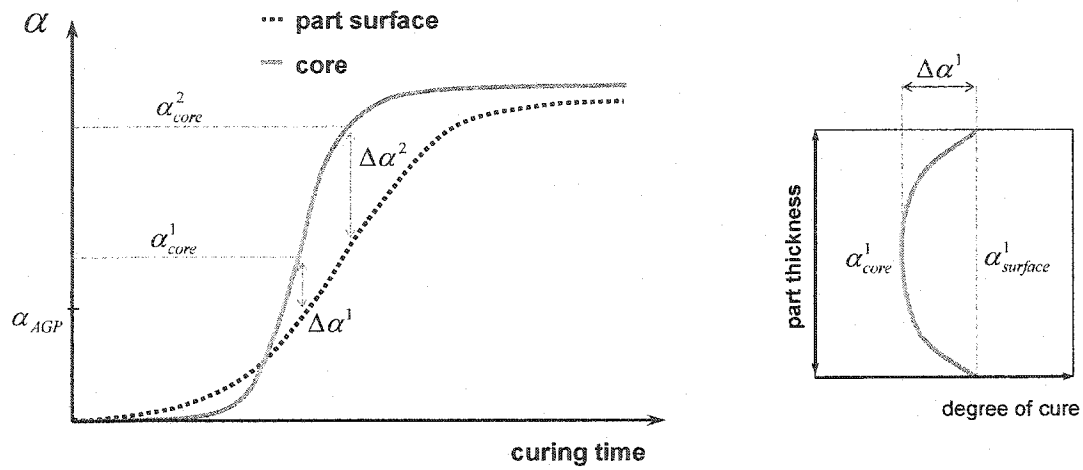


Figure 7.5. Schematic representation of the cure differentials between the part surface and the core. The sum of differentials is used to construct the objective sigmoid J_{cure} .

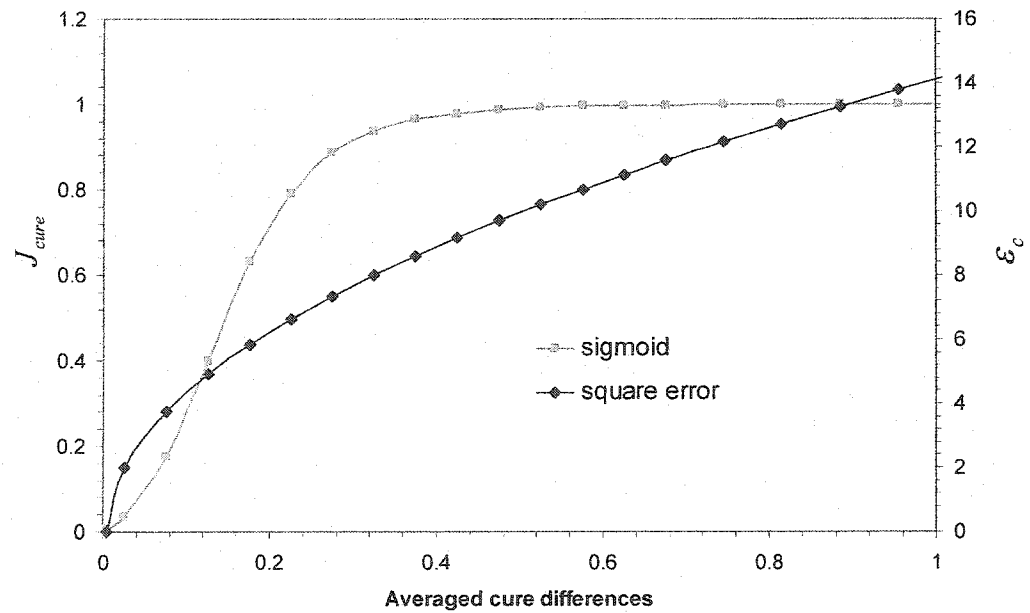


Figure 7.6. Comparison between the square error of ε_c and the sigmoid objective J_{cure} of equation (7.11).

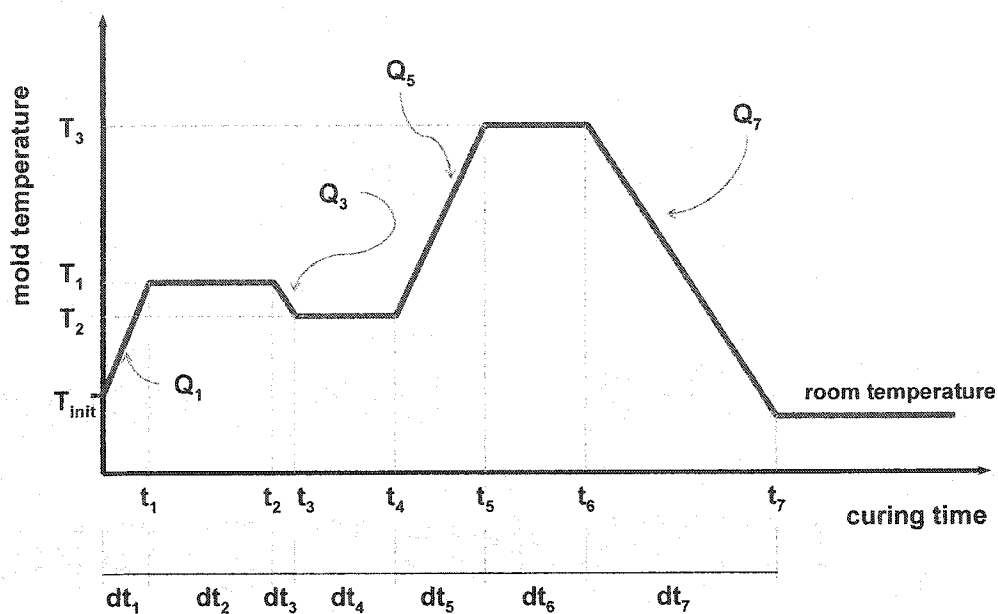


Figure 7.7. Discretization of the temperature profile into a series of dwell times and heating/cooling ramps.

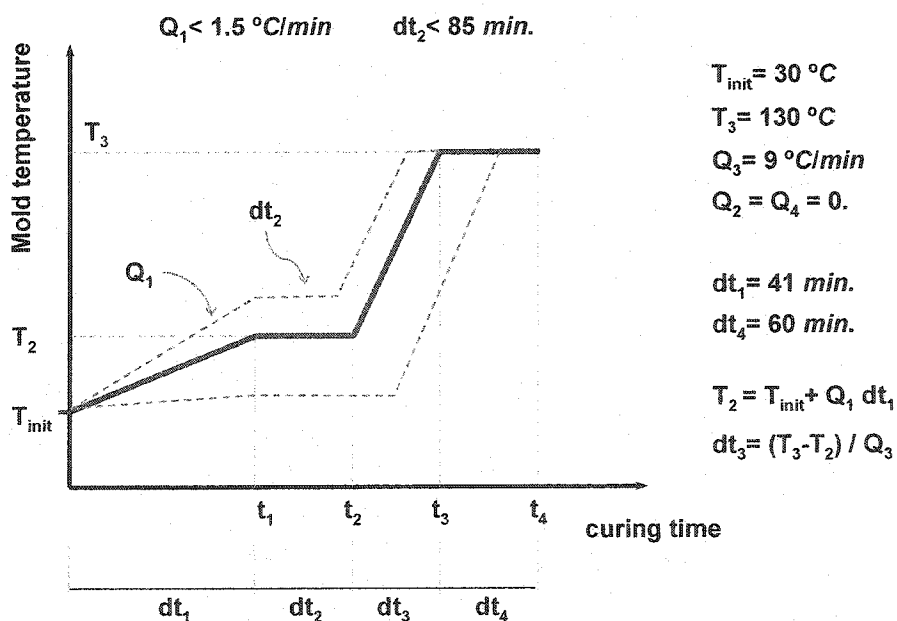


Figure 7.8. Two step curing cycle used for the evaluation of the fitness function.

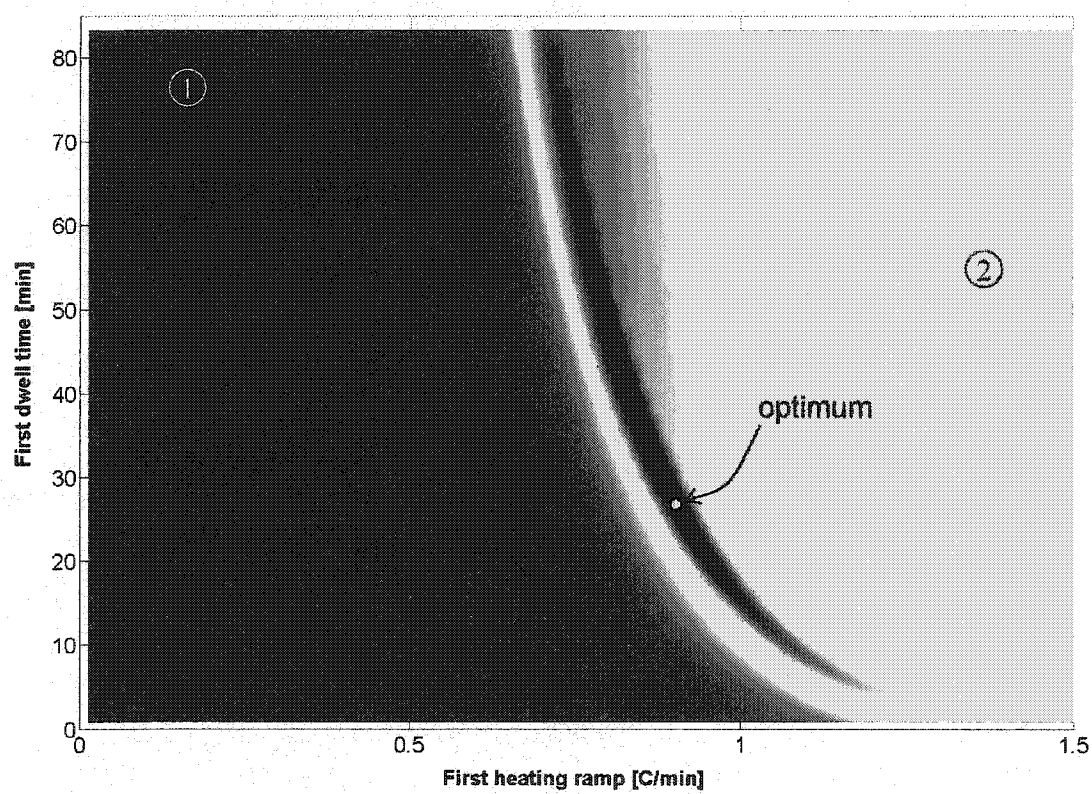


Figure 7.9. Contour plot of the fitness function F_f for the curing cycle with two heating ramps (without considering internal stresses).

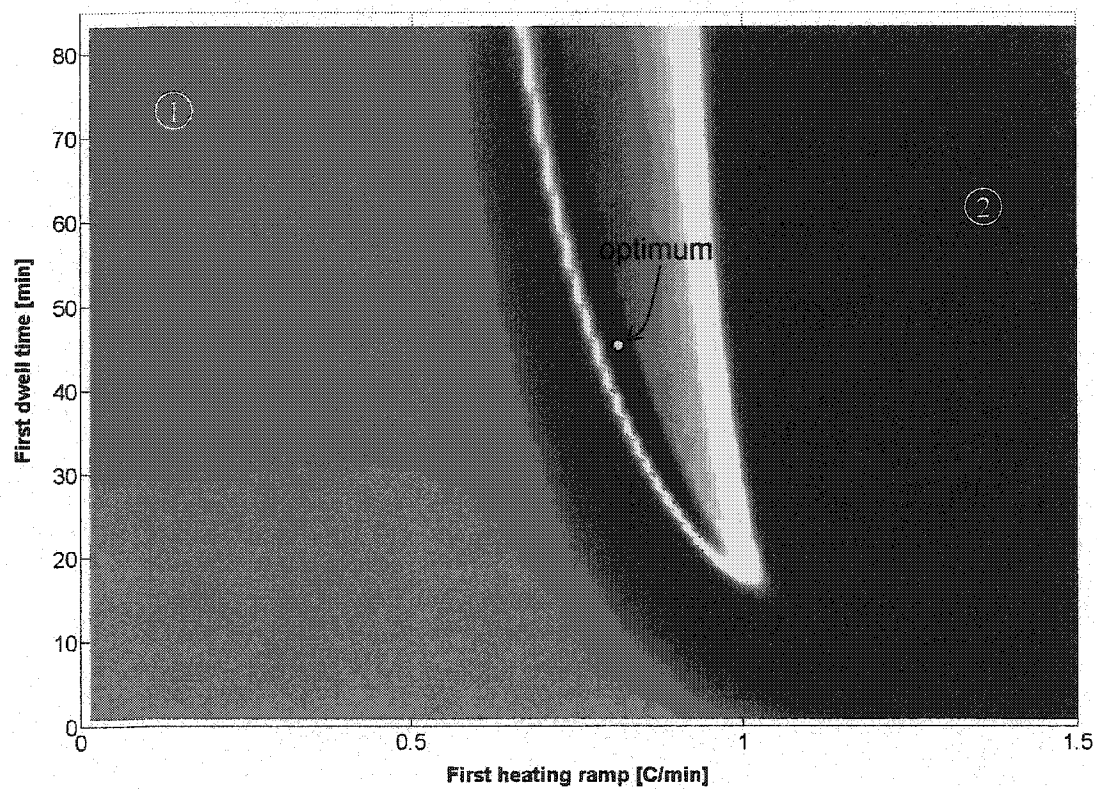


Figure 7.10. Contour plot of the fitness function F_f for the curing cycle with two heating ramps (considering the effects of internal stresses).

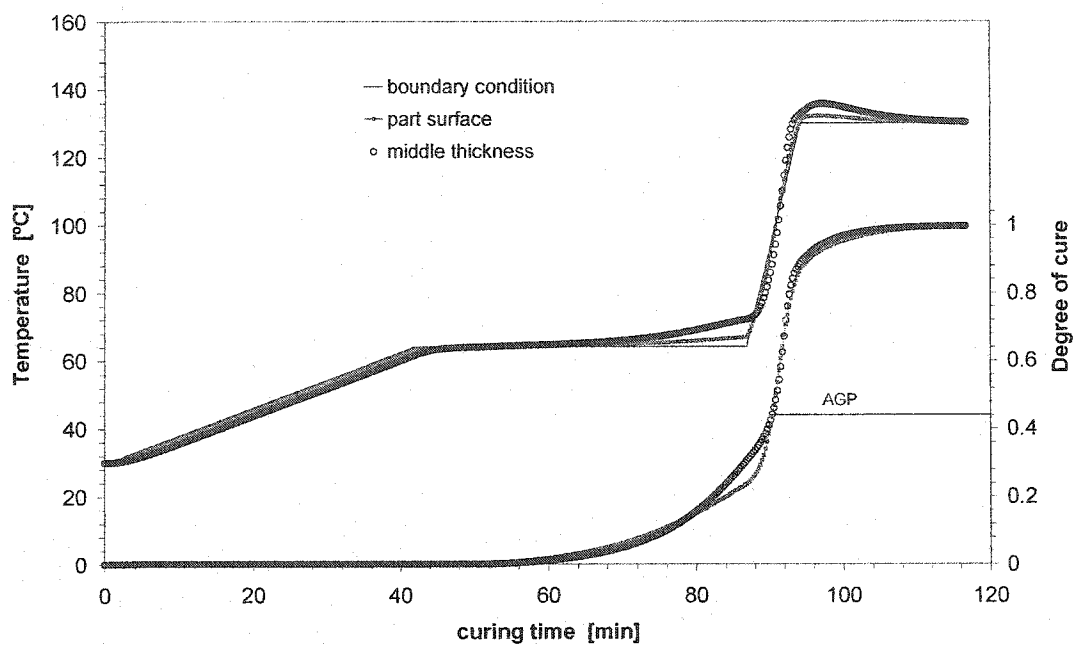


Figure 7.11. Cure cycle of the optimized temperature profile (with stress analysis) for the two heating ramps: $Q_1 = 0.82 \text{ } ^\circ\text{C/min}$ and $dt_2 = 46 \text{ min}$.

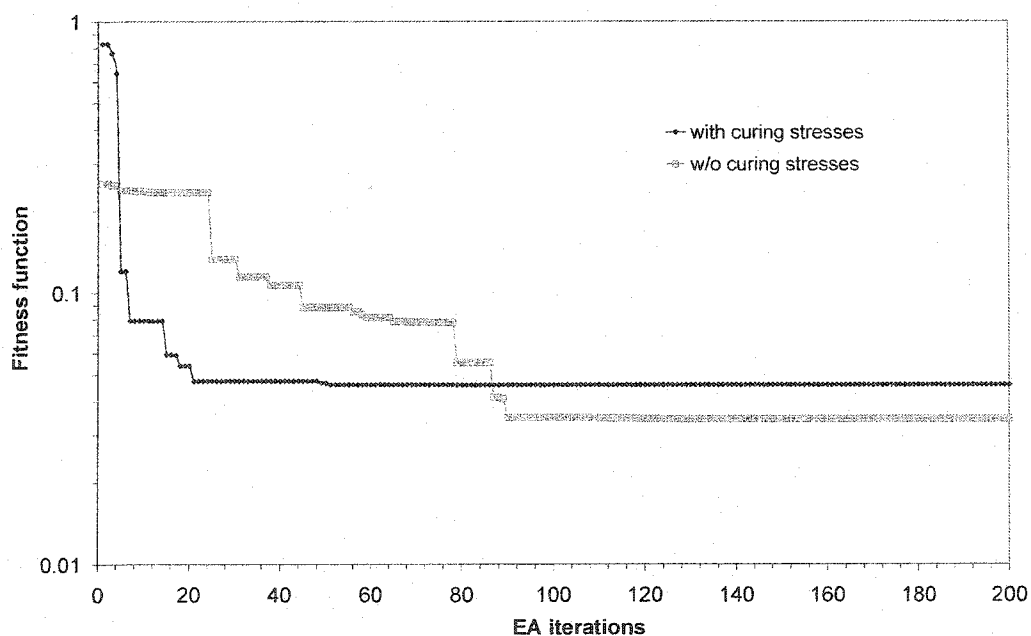


Figure 7.12. Convergence of the fitness function for LeCoq optimization for the two heating ramps with and without curing stresses.

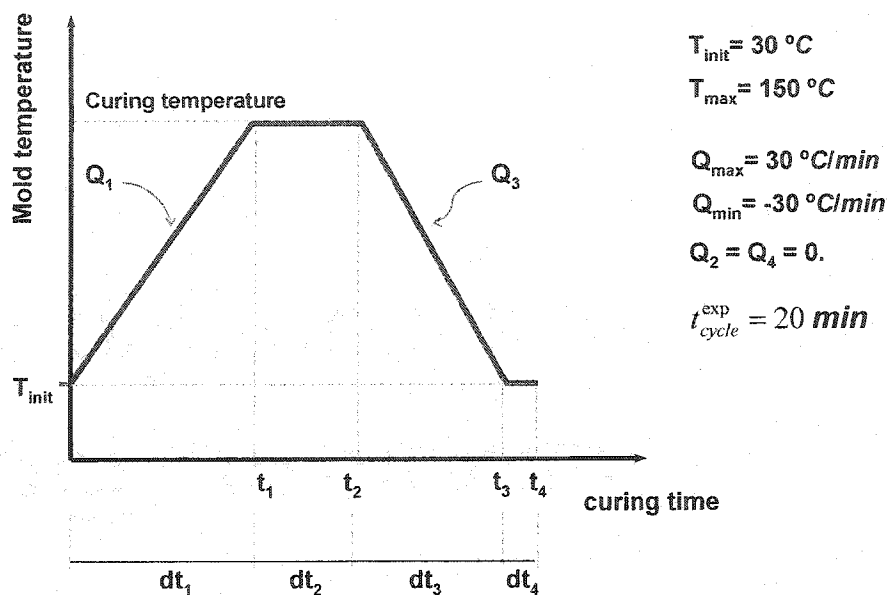


Figure 7.13. Typically temperature profile used for the curing optimization of thin composite laminates.

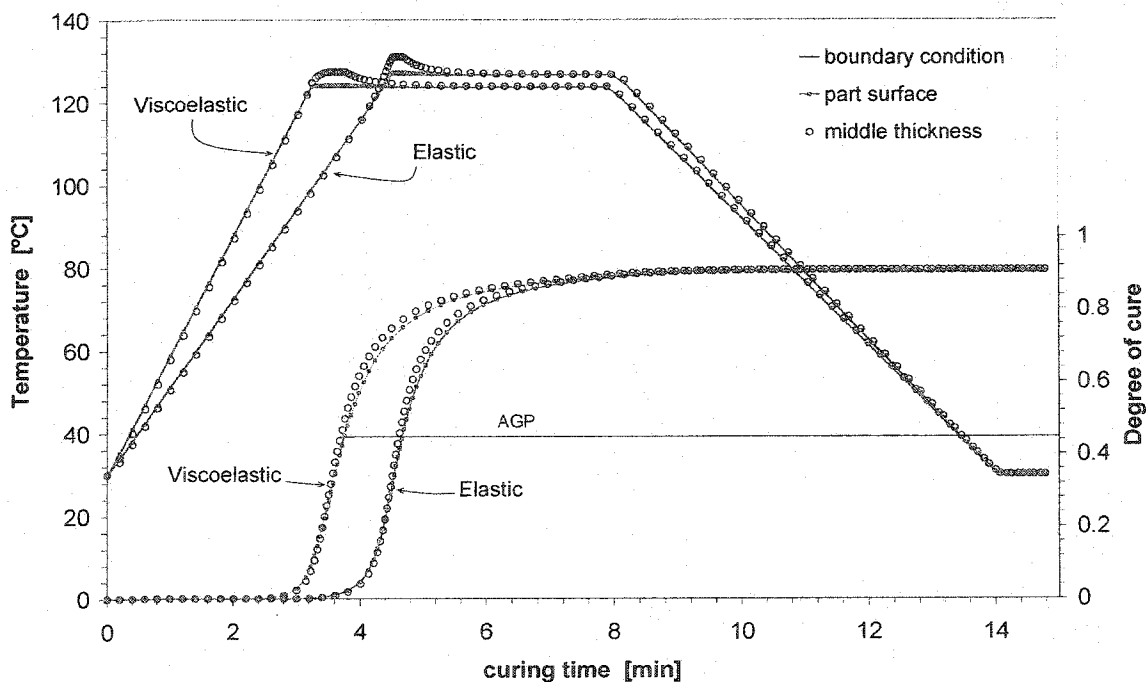


Figure 7.14. Optimized temperature and cure profiles for the elastic and viscoelastic modeling of mechanical properties.

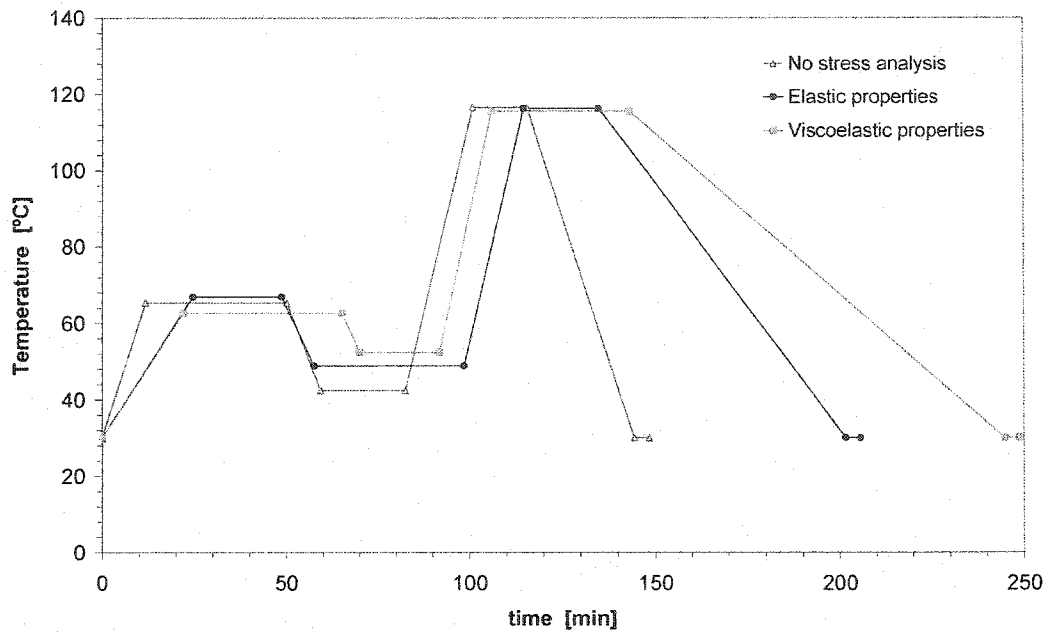


Figure 7.15. Temperature profile used for the curing optimization of thick composite laminates.

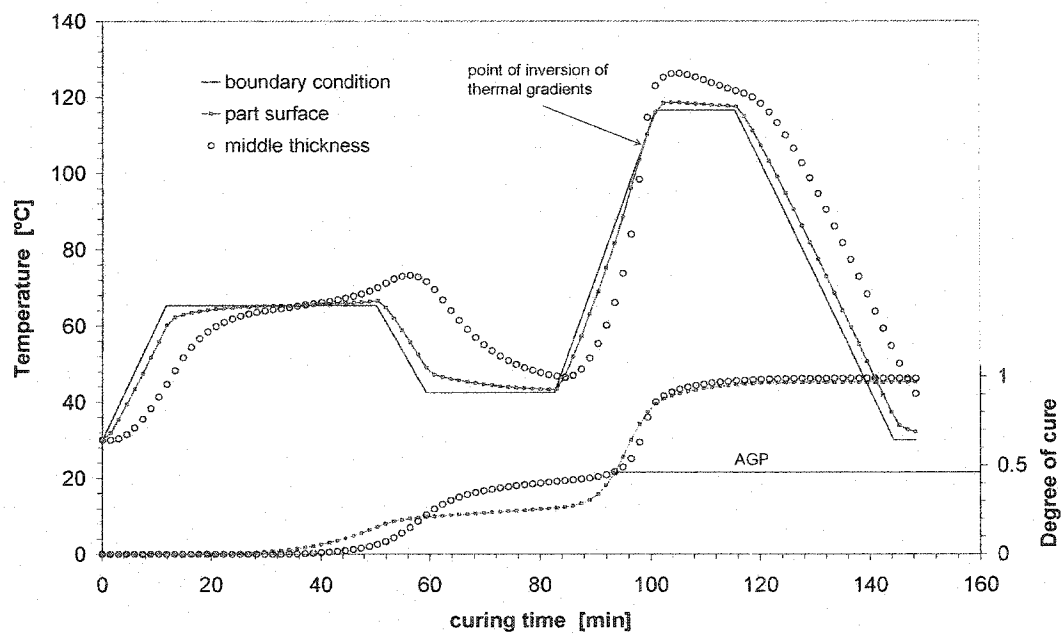


Figure 7.16. Optimized temperature and cure profiles for the 25 mm thick laminate with cure gradients minimization (i.e., no stress analysis).

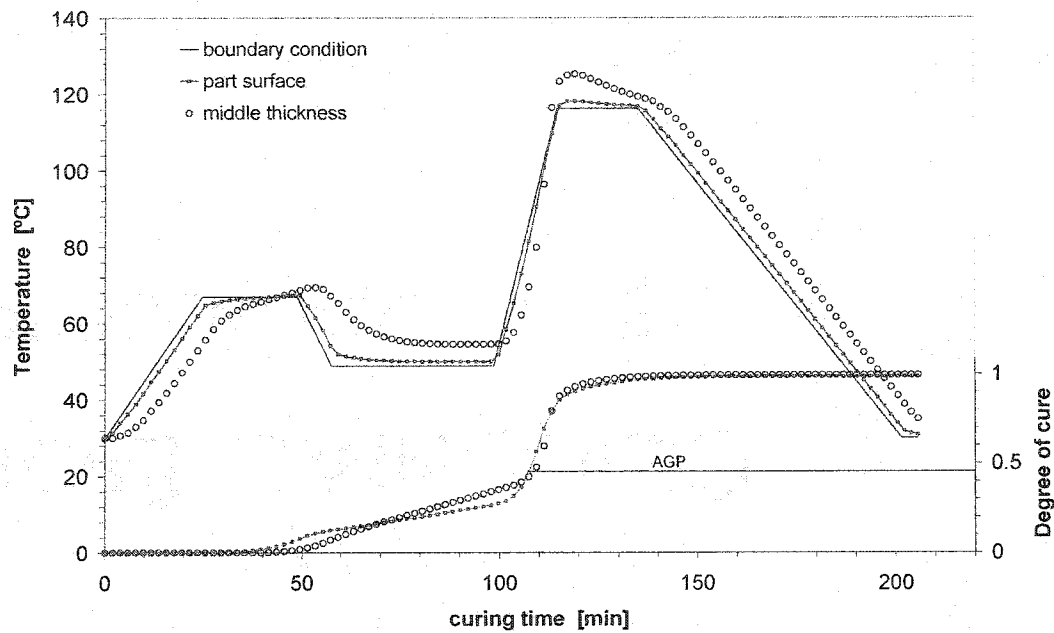


Figure 7.17. Optimized temperature and cure profiles for the 25 *mm* thick laminate with elastic modeling of mechanical properties.

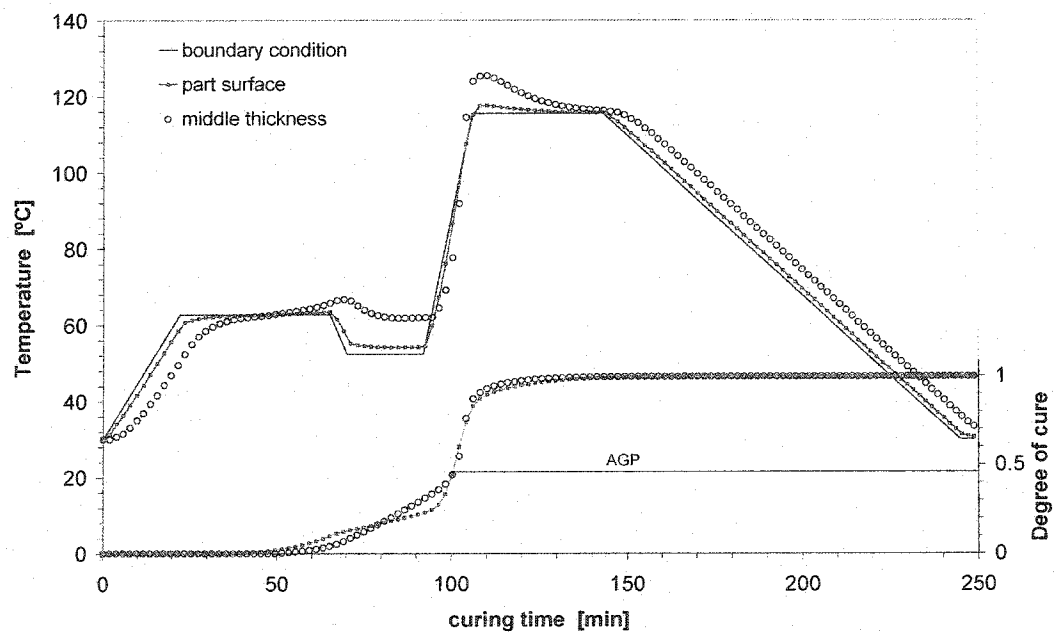


Figure 7.18. Optimized temperature and cure profiles for the 25 *mm* thick laminate with viscoelastic modeling of mechanical properties.

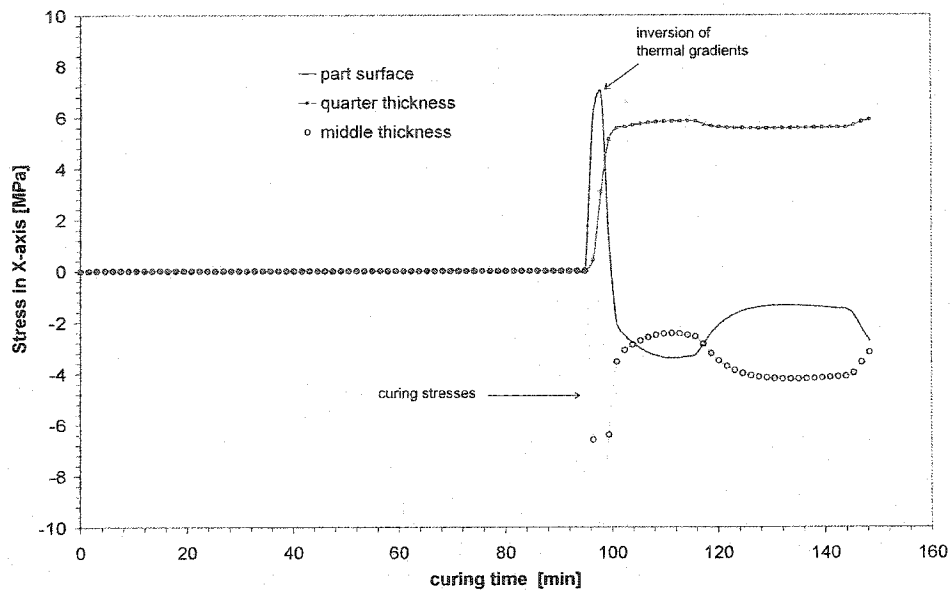


Figure 7.19. Processing stresses for the 25 mm thick laminate applying the optimized temperature profile with minimization of cure gradients (i.e., no stress analysis). The viscoelastic modeling was used for the stress calculation.

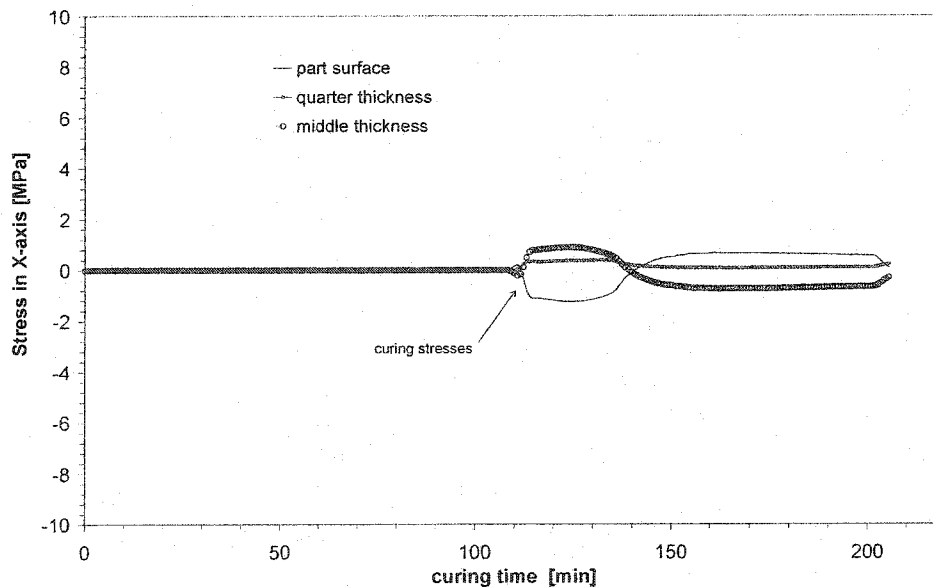


Figure 7.20. Processing stresses for the 25 mm thick laminate with the optimized temperature profile and elastic modeling of mechanical properties.

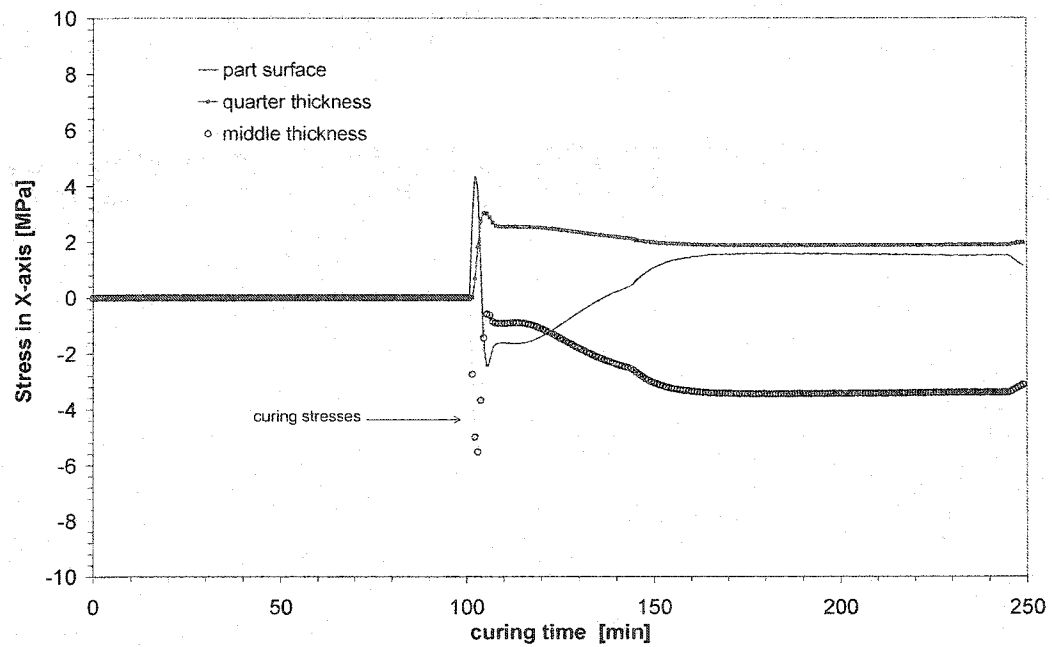


Figure 7.21. Processing stresses for the 25 *mm* thick laminate with the optimized temperature profile and viscoelastic modeling of mechanical properties.

Table 7.1. Characterized material properties to evaluate the energy and species balances during processing. Models are described in [A2].

	Temperature dependence	Chemical dependence	Model	Measurement method
Resin kinetics	✓	✓	Complex	DSC
Initiator decomposition	✓		Complex	DSC
Resin thermal conductivity	✓	✓	Lineal	Thermal measure
Resin specific heat	✓	✓	Lineal	DSC
Fiber preform thermal conductivity & specific heat			Constant	Data
Mold thermal conductivity & specific heat			Constant	Data
Heating/Cooling system effective convection	✓		Lineal	Thermal measure

Table 7.2. Characterized mechanical properties for the analysis of internal processing stresses. Models are described in [A2].

	Temperature dependence	Chemical dependence	Model	Measurement method
Resin thermal expansion/contraction	✓	✓	Lineal	Dilatometer & TMA
Resin shrinkage		✓	Lineal	Ultrasound-dilatometer & TMA
Resin mechanical properties	✓	✓	Complex	DMTA
Fiber preform thermal expansion/contraction			Constant	Data
Fiber preform mechanical properties			Constant	Data

Table 7.3. Coefficients used in for the construction of the sigmoid of sub-objective functions and fitness function.

	<i>A</i>	<i>B</i>	<i>C</i>	<i>D</i>		
J_{fc}	1	1	100	0	$\alpha_{ult} = 0.95$	$\alpha_{min} = 0.80$
$J_{T_{max}}$	1	1	2000	0	$T_{exot}^{max} = 450^{\circ}K$	$T_{exot}^{min} = 430^{\circ}K$
J_{AGP}	0.75	0.5	15	0.5	$\alpha_{AGP} = 0.45$	
J_{cure}	0.005	0.005	1	0	$Np = 50$	
J_{stress}	1	1	3	0		
$J_{cooling}$	1	1	3	0		
J_{time}					$t_{cycle}^{exp} = 5000$	
F_f	0.75	0.5	1	0.5		

Table 7.4. Comparison of standard cure cycles with optimized cycles for the thin composite laminate.

	Processing time [min]	Heating ramp [°C/min]	Cooling ramp [°C/min]	Curing Temperature [°C]	Final degree of cure	X-curvature [1/m]
Fast processing Viscoelastic	11.6	30	-30	130	0.92	4.51
Slow processing Viscoelastic	23.5	15	-5	120	0.88	3.13
Optimized Elastic	15.0	21.5	-16.2	127	0.91	4.14
Optimized Viscoelastic	14.8	29.3	-15.3	124	0.91	3.32

Table 7.5. Summary of the optimized cure cycles for a 25 *mm* thick composite laminate.

	Processing time [min]	Q_1 [°C/min]	Q_5 [°C/min]	Q_7 [°C/min]	Curing Temperature [°C]	Final degree of cure
Optimized without stress	149	3.02	4.07	-3	117	0.968
Optimized Elastic	206	1.50	4.20	-1.29	116	0.985
Optimized Viscoelastic	249	1.48	4.51	-0.81	116	0.996

CHAPITRE 8

DISCUSSION GÉNÉRALE ET PERSPECTIVES

8.1 Discussion générale

L'objectif de cette thèse était de développer des équations caractérisant le comportement thermomécanique et le changement de phase des matériaux composites thermodurcissables, des modèles numériques pour simuler la mise en forme et optimiser le cycle de cuisson et le refroidissement des composites fabriqués par injection sur renfort (LCM). Dans ces procédés, le renfort fibreux est progressivement saturé par la résine à l'état liquide. Une fois la cavité du moule rempli, la résine thermodurcissable réagit en chaîne selon un phénomène appelé polymérisation (« cross-linking polymerization reaction »). Pendant la réaction de polymérisation, habituellement nommée « cuisson », la résine se solidifie et donne sa forme finale à la pièce. Du point de vue de la simulation numérique, le procédé de moulage liquide des composites peut être divisé en trois étapes : (1) le remplissage, (2) la cuisson et (3) le refroidissement et démoulage. La caractérisation, la simulation et finalement l'optimisation de ces étapes font partie des contributions nouvelles présentées dans cette thèse.

La première partie de l'étude a fait le point sur la caractérisation de la cinétique de polymérisation et du comportement viscoélastique d'un composite verre/polyester. La cinétique de polymérisation d'une résine polyester insaturée commerciale a été étudiée à l'aide d'un calorimètre différentiel DSC (« Differential Scanning Calorimeter »). Un modèle semi-empirique a été développé pour tenir compte des effets de l'inhibiteur et

de la transition vitreuse du matériau dans la cinétique de polymérisation. Le modèle permet aussi de calculer le degré de polymérisation maximum atteint pour une température de cuisson donnée. L'évolution des propriétés mécaniques de deux composites verre/polyester a été étudiée par la suite au moyen d'une analyse mécanique dynamique avec un appareil DMTA (« Dynamical Mechanical Thermal Analyzer ») et une analyse thermomécanique dans un appareil TMA (« Thermo-Mechanical Analyzer »). Deux modèles différents ont été proposés pour décrire les effets thermiques et chimiques sur les propriétés mécaniques du matériau. Le premier est un modèle thermochimique élastique non linéaire qui considère la relaxation totale du matériau à l'état caoutchoutique, en haut de la température de transition vitreuse. Le deuxième est un modèle viscoélastique complexe fondé sur une mesure de la relaxation des contraintes et sur le principe de superposition temps/température. La caractérisation viscoélastique de la résine polyester étudiée, a montré que le module de relaxation est brusquement affecté par le degré de polymérisation. La comparaison des essais mécaniques et calorimétriques, a permis de démontrer l'existence d'un degré de polymérisation en bas duquel les propriétés mécaniques sont négligeables. Ce degré de polymérisation, nommé « After Gel Point » (AGP), est beaucoup plus important que le degré de polymérisation à l'état de gel. Le concept d'AGP est fondamental pour la suite des études présentées dans cette thèse. Les analyses thermomécaniques menées avec la TMA ont permis de générer un modèle simple de l'expansion thermique du composite en fonction de la température, du degré de polymérisation et du contenu en volume des fibres. A la fin de l'étape de caractérisation, le retrait de polymérisation de la résine a été mesuré et modélisé en fonction du degré de polymérisation. Les modèles de comportement thermochimique viscoélastique ont permis d'approfondir les connaissances des phénomènes mécaniques et volumiques reliés à la réaction de polymérisation d'une résine polyester insaturée.

L'étape suivante de l'étude a été orientée sur la mise au point de la solution numérique par une nouvelle approche de l'équation de l'énergie couplée à une analyse des

contraintes à travers l'épaisseur du composite. Ce travail a permis de simuler les effets thermiques, chimiques et mécaniques pendant la phase de cuisson des matériaux composites fabriqués par injection sur renfort. Une formulation de différences finies de type Crank Nicolson avec terme source (et adimensionalisée avec le nombre de Fourier) a été développée pour évaluer les variations de température et du degré de polymérisation à travers l'épaisseur de la pièce. La théorie classique des laminés a été utilisée pour calculer les contraintes internes dans le stratifié. Pour valider les caractérisations physiques et les modèles numériques, une série d'échantillons de verre/polyester ont été fabriqués. Pour forcer une déformation hors du plan, les échantillons ont été laminés asymétriquement. Après la mise en forme, les plaques minces ont été chauffées en haut de la température de transition vitreuse. Par la suite, la déformation des plaques pendant le refroidissement a été mesurée à l'aide d'un LVDT (« Linear Variable Displacement Transducer »). Les prédictions du modèle thermomécanique ont pu être vérifiées avec une erreur de moins de 2%.

L'analyse de contraintes résiduelles a été poursuivie dans le cas de la mise en forme de plaques épaisses. L'étude a porté sur l'évaluation des contraintes internes pendant les cycles de cuisson et de refroidissement de plaques de 15 mm d'épaisseur. Les résultats ont été comparés pour différents profils de température du moule typiquement utilisés dans l'industrie. De cette étude numérique, on a conclu que le degré de polymérisation au point de croisement entre le profil de polymérisation à la surface et au coeur du laminé est fondamental pour la génération des contraintes internes. Également, des contraintes internes importantes apparaissent en présence de gradients thermiques ou de cuisson. Différentes sources des contraintes internes peuvent être identifiées dans les phases de cuisson et de refroidissement respectivement. Autant dans la première phase les gradients thermiques et de cuisson sont importants, dans la dernière, l'effet de la transition vitreuse du matériau est primordial. Un profil de température du moule optimisé a été appliqué dans le cas d'une plaque épaisse pour démontrer l'intérêt d'une telle optimisation. On peut conclure que l'utilisation d'un profil de

chauffage/refroidissement optimal permet de réduire les contraintes internes, et donc les défauts de fabrication, dans le moulage de pièces composites par injection sur renfort.

Les études thermiques, rhéologiques et mécaniques précédentes ont été développées au cours de la cuisson de la résine dans le cas idéal d'uniformité de la température et du degré de polymérisation partout dans la pièce. L'expérience a révélé que l'histoire thermique et rhéologique pendant la phase de remplissage de la cavité du moule a une influence décisive sur l'uniformité du degré de polymérisation et des propriétés mécaniques de la pièce. Pour étudier ces variations, une modélisation numérique du remplissage non isotherme et de la cuisson des pièces tridimensionnelles a été présentée. La première partie de ce travail numérique est consacrée au développement d'une méthode d'extrapolation de maillage selon la stratification des couches de renfort. Partant d'un maillage d'éléments finis bidimensionnels, un maillage 3D stratifié est créé pour représenter la cavité du moule. La méthode d'extrapolation est fondée sur la définition du laminé et la connaissance des directions transverses dans les éléments. Des propriétés ou directions différentes peuvent être définies dans chacun des plis, et les conditions limites extrapolées sur les surfaces supérieure ou inférieure de la pièce pour représenter les effets du moule. La méthode a démontré son efficacité et son utilité dans la génération de divers types de maillages tridimensionnels.

Pendant le remplissage, les fibres sont progressivement saturées par la résine. La loi qui gouverne l'imprégnation d'un milieu poreux est la loi de Darcy. Dans ce travail, une formulation d'éléments finis qui résout le problème de Darcy pour chaque pas de temps a été utilisée pour évaluer l'avancement de la résine pendant la phase de remplissage. Dans la fabrication des composites par injection sur renfort, les pièces ont généralement une épaisseur faible comparée aux autres dimensions. Par conséquent, le flux de résine pendant le remplissage de la cavité du moule se produit principalement dans le plan de la pièce. Pour améliorer la rapidité et la qualité du calcul du flux de résine pendant le remplissage, un nouvel élément fini tridimensionnel discontinu a été développé. Cet

élément de forme prismatique contient des fonctions de forme non conformes pour assurer la conservation de la matière dans le plan de la pièce. Diverses comparaisons entre les simulations numériques, des solutions analytiques et des résultats expérimentaux ont été présentées pour valider l'intérêt d'utiliser ce nouvel élément fini. Cet élément prismatique a été comparé à un élément tétraédrique non conforme actuellement utilisé dans le programme commercial Pam-RTM de la compagnie ESI_Group. Dans tous les cas testés, le nouvel élément fini a produit de meilleurs résultats avec des temps de calcul très inférieurs à ceux de l'ancien élément. Pour démontrer la souplesse de cette méthode d'extrapolation de maillage et la génération des éléments prismatiques stratifiés, une pièce industrielle a été traitée dans le cas d'un remplissage isotherme.

L'intérêt de cette méthode d'extrapolation et du nouvel élément fini 3D concerne aussi le calcul du remplissage non isotherme et les variations du degré de polymérisation à la fin de l'injection de résine. Pour évaluer les flux thermiques dans la cavité du moule, une approche mixte couplant éléments finis et différences finies a été proposée. Cette approche consiste à calculer les variations de température par conduction et convection dans le plan de la pièce avec la formulation des éléments finis, tandis que le flux de la chaleur à travers l'épaisseur du composite est évalué par une approximation par différences finies. La combinaison de la méthode d'extrapolation de maillage 3D en couches parallèles avec cette formulation thermique hybride donne la possibilité de définir différents niveaux de couplage entre l'écoulement et l'analyse thermique. La méthodologie proposée dans ce travail permet à l'utilisateur du code de définir, à partir du même maillage 2D initial, le niveau de complexité qui doit être utilisé par le modèle numérique. Une série de comparaisons analytiques a eu pour objectif d'estimer les erreurs de calcul de la formulation hybride et d'évaluer la performance numérique de chacun des niveaux de couplage. On arrive à la conclusion que l'approximation mixte donne de meilleurs résultats que les éléments finis tridimensionnels et ce pour des

temps de calculs très inférieurs. La performance numérique de la nouvelle approche a été toujours supérieure à celle de la méthode des éléments finis pur.

Une pièce industrielle tridimensionnelle a été traitée pour démontrer les capacités réelles des différents couplages proposés. La phase de remplissage non isotherme de la pièce avec transport du degré de polymérisation a été simulée suivie par la phase de cuisson. De la comparaison des résultats avec l'ancienne approche, on en déduit que la qualité des calculs a été améliorée en raison de l'utilisation des éléments prismatiques et que le temps de calcul était devenu environ 4% du temps requis précédemment. Les solutions obtenues avec des niveaux de couplage simples entre les formulations ont été très satisfaisantes, puisque le temps de calcul a été divisé par 500 par rapport au temps de l'ancienne formulation par éléments finis tridimensionnels. Les études présentées ont permis aussi d'identifier le niveau de non uniformité de la température et du degré de polymérisation dans la pièce qui affectera l'évolution des propriétés mécaniques et entraînera la génération de contraintes résiduelles.

A la fin de la thèse, la recherche a porté sur le développement d'une méthode d'optimisation de la mise en forme des pièces composites. Il s'agit d'une optimisation complète des cycles de chauffage, cuisson et refroidissement dans la fabrication des pièces composites par injection sur renfort. L'approche développée concerne la minimisation du temps du cycle, l'amélioration des propriétés mécaniques et la réduction des contraintes résiduelles dans le composite. La minimisation des gradients thermiques et de cuisson à travers l'épaisseur a été formulée au moyen de sept sous-fonctions objective. Ces fonctions sont fondées sur la compréhension des phénomènes de polymérisation et de génération des contraintes internes dans un composite laminé. Les critères étudiés, tel que le point après gel (AGP), le degré final de polymérisation ou la relation entre le retrait et les contraintes internes, ont été, dans cette étape du travail, fondamentales pour la création des fonctions objectives relatives à la minimisation désirée. La fonction objective finale a été obtenue comme une

combinaison linéaire des sous-fonctions. Un algorithme d'évolution fondé sur les algorithmes génétiques, et appelé LeCoq (« Logical Evolutionary Curing Optimization and Quenching »), a été développé pour minimiser la fonction objective à plusieurs paramètres. Pour évaluer la fonction objective à chaque itération de l'algorithme génétique, l'analyse unidimensionnelle de la cuisson et des contraintes résiduelles a été incluse à l'intérieur du code LeCoq. Pour augmenter la vitesse de convergence de l'algorithme d'évolution, les sept sous-fonctions objective ont été définies sous la forme de sigmoïdes unitaires. En raison du grand nombre d'itérations requises pour la convergence des algorithmes génétiques, la vitesse de calcul du code thermomécanique unidimensionnel a dû être optimisée. Pour une simulation de cuisson et refroidissement d'une pièce composite de 15 mm d'épaisseur, 10,000 cycles de cuisson ont été évalués en 20 minutes (soit environ 0.12 secondes par simulation) avec un ordinateur IBM IntelliStation Z-Pro munie un processeur Pentium IV à 2.8 Gz.

La méthodologie développée par la suite a été utilisée pour optimiser le cycle de cuisson de pièces composites minces. Même dans le cas simple de la mise en forme d'une telle pièce, sans gradients de cuisson à travers l'épaisseur, un profil de température du moule optimisé peut améliorer les propriétés mécaniques de la pièce tout en minimisant les contraintes résiduelles. Dans les composites minces, ces contraintes sont directement reliées à une distorsion géométrique de la pièce. Donc, la minimisation des contraintes internes dans la pièce indique une réduction de ces instabilités géométriques.

L'étude finale a été orientée vers l'optimisation numérique du cycle de cuisson de pièces composites épaisses. La cuisson d'un composite verre/polyester de 15 mm d'épaisseur a été optimisée avec l'algorithme LeCoq. Les modèles thermochimique élastique et viscoélastique développés dans ce travail pour une résine polyester insaturée, ont été utilisés pour comparer les résultats d'optimisation. Les résultats ont démontré que la minimisation des gradients de cuisson n'est pas suffisante pour assurer

l'absence de contraintes résiduelles. L'évolution des contraintes internes doit nécessairement être incluse dans l'optimisation pour obtenir une minimisation appropriée des contraintes et des défauts possibles dans la pièce. On a constaté que le modèle thermoélastique simple donne suffisamment d'informations pour l'optimisation du procédé. Donc, une caractérisation simple du comportement élastique relaxé/nonrelaxé du matériau peut être utilisée pour optimiser les cycles de cuisson et refroidissement dans les procédés d'injection sur renfort. Le profil de température du moule optimisé a été similaire pour les deux modèles utilisés.

Cette dernière étude met en valeur tous les travaux réalisés dans le cadre de cette thèse. La caractérisation des matériaux est nécessaire pour la compréhension des phénomènes reliés à la réaction de polymérisation de la résine et pour la validation expérimentale des simulations. La modélisation numérique des transferts thermiques, de la réaction de polymérisation et des contraintes internes est fondamentale pour évaluer les effets des paramètres de moulage (tel que la température) sur la mise en forme d'une pièce composite. Toutes les connaissances acquises dans le domaine du comportement du matériau ont permis de formuler les fonctions objectifs qui définissent les critères d'optimisation. Finalement, l'utilisation d'un algorithme d'évolution pour la minimisation de la fonction objectif a permis d'appliquer la méthode d'optimisation en fonction d'un grand nombre de paramètres de design.

8.2 Perspectives

Le travail présenté dans cette thèse constitue le début d'une méthodologie originale sur la caractérisation, d'une modélisation numérique et l'optimisation des cycles de cuisson et de refroidissement de pièces composites fabriqués par injection sur renfort (LCM). Les trois domaines mentionnés, sont des champs de recherche encore fertiles. La caractérisation des propriétés viscoélastiques peut être étendue en ajoutant aux

modèles proposés les effets du taux de cisaillement. Pour des analyses plus fines, le modèle linéaire de retrait de la résine peut être amélioré, quoique ceci implique la fabrication d'un moule spécial.

Bien que la théorie classique de laminés utilisée dans cette recherche donne une bonne idée du niveau des contraintes internes, cette analyse est limitée pour l'instant à une dimension d'espace à travers l'épaisseur du composite. De plus, les contraintes transverses (dans la direction de l'épaisseur du laminé) ne sont pas prises en compte dans cette approche. Dans l'analyse unidimensionnelle, il est recommandé d'étendre la théorie classique des laminés pour considérer les contraintes transverses. Aussi, un modèle tridimensionnel des contraintes servira à observer les déformations mécaniques dans la pièce due à la non uniformité du degré de polymérisation à la fin du remplissage. Les conséquences sur la géométrie de la pièce d'un profil de température du moule optimisé peuvent être aussi calculés par un tel modèle.

Maintenant que les temps de calcul des simulations de remplissage non isotherme ont été fortement diminués grâce à la formulation hybride présentée, et que un algorithme d'évolution a déjà été implémenté, il est opportun d'étudier l'optimisation du cycle de remplissage. Diverses optimisations ont été rapportées dans la littérature pour cette phase du procédé, dont l'objectif principal était de minimiser le temps d'injection de la résine. Une optimisation de grand intérêt concerne la réduction des gradients thermiques et de cuisson dans le plan de la pièce pour minimiser les variations géométriques dues à la non uniformité du degré de polymérisation à la fin du remplissage de la cavité du moule. Une optimisation simplifiée est possible à partir de la modélisation numérique du remplissage non isotherme en une dimension. Inévitablement, l'optimisation thermique du remplissage aura une influence sur la phase de cuisson de la résine. Une optimisation globale du procédé peut être envisagée pour réduire les effets couplés de l'optimisation de ces deux phases. Le graphique

suisant donne une vision schématique de la démarche d'optimisation qui peut être développée à partir de cette thèse.

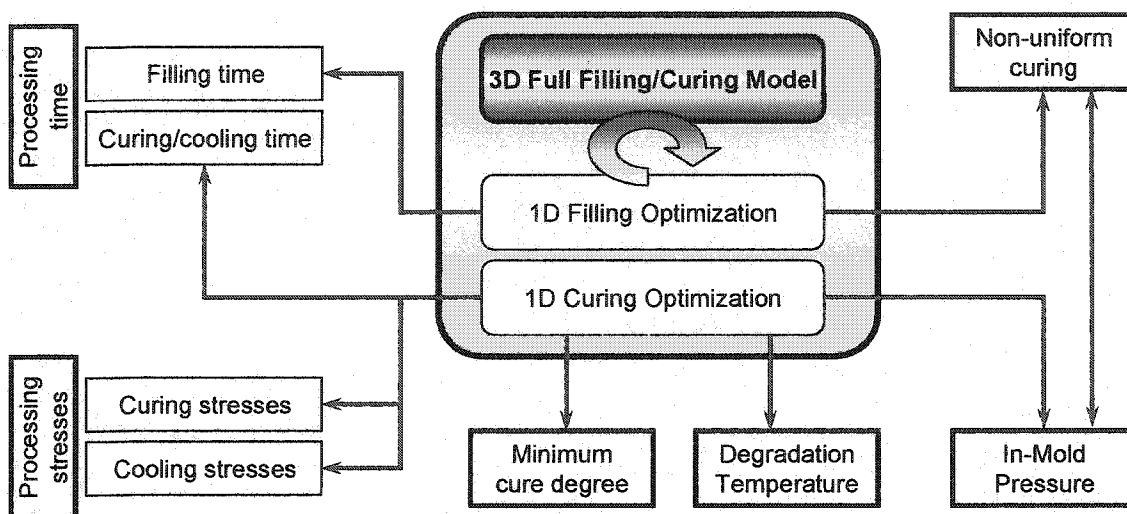


Figure 8.1. Couplage possible des optimisations unidimensionnelles

Comme cette approche utilise deux simulations numériques unidimensionnelles pour obtenir les profils de température optimaux, des variations importantes peuvent apparaître dans la pièce tridimensionnelle. Une manière de tenir compte de ces variations est de choisir le point de la pièce le plus représentatif pour créer les modèles 1D. De cette façon, un cycle complet d'optimisation tridimensionnelle peut être développé si une boucle est effectuée pour chercher le point le plus représentatif dans le maillage tridimensionnel. Des itérations entre les optimisations unidimensionnelles et la sélection du nouveau point représentatif seront suffisantes pour converger vers un optimum. Le graphique suivant schématise le diagramme possible d'une optimisation complète des procédés d'injection sur renfort.

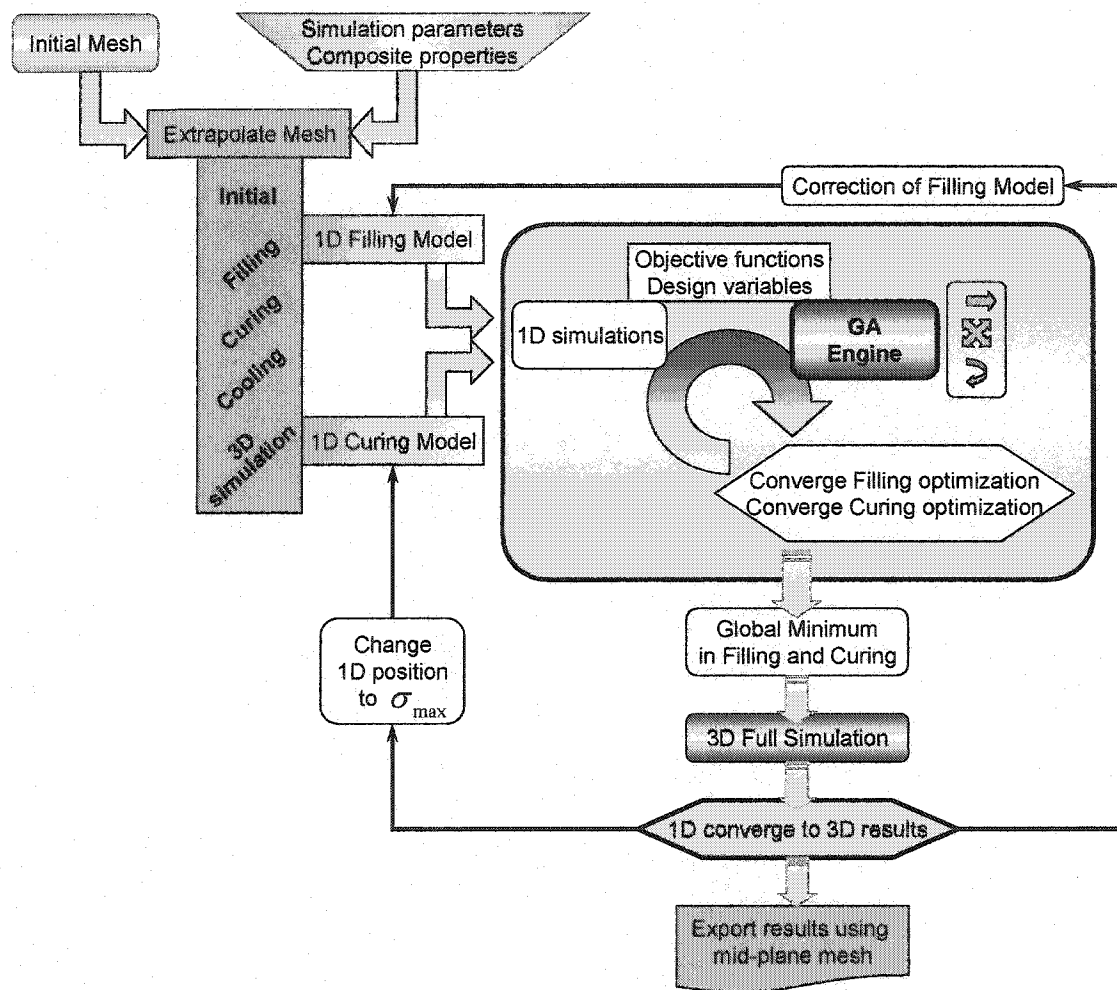


Figure 8.2. Algorithme d'optimisation globale des procédés d'injection sur renfort.

8.3 Importance des travaux pour l'industrie canadienne

La qualité et la reproductibilité des pièces composites exigées par les différentes normes de fabrication demandent de plus en plus aux compagnies, de maîtriser des technologies de fabrication avancées. Le RTM à moule rigide commence à être utilisé au Canada dans le domaine aérospatial (Bombardier, Bell Hélicoptère, Composites Atlantic) et automobile (SLP Automotive, Locus Speech, etc.). Les nouvelles variantes légères du RTM sont déjà employées par nombreuses petits et moyennes entreprises canadiennes comme Fibres Design, Fibre CNC ou Vézina Composites entre autres. Autant que les technologies de fabrication avancent, les demandes sur les modèles numériques de simulation sont aussi croissantes. Divers entreprises multinationales comme General Motors, Ford, Honda, Toyota et plusieurs autres, intéressées par la conception de nouveaux véhicules de transport routier (voitures, camions) se sont récemment lancées dans le développement d'un réseau scientifique au Canada. Ce réseau, appelé Auto 21 pour l'automobile du 21^{ème} siècle s'intéresse particulièrement aux applications industrielles des méthodes de simulation numérique afin de disposer dans un futur proche des outils indispensables pour réduire les coûts de fabrication. Les développements réalisés dans le cadre de cette thèse ont un impact direct au niveau de la simulation et de l'optimisation numérique des procédés LCM. Ce projet est donc important afin de répondre à court terme à ces besoins, et de faciliter de façon indirecte le transfert de connaissances scientifiques dans le domaine de la fabrication des composites par injection vers l'industrie locale.

8.4 Matériaux utilisés

Cette thèse a porté sur l'étude et optimisation du moulage des pièces composites à matrice thermodurcissable. Les propriétés thermomécaniques et la cinétique de polymérisation de la résine ont été caractérisées et modélisées selon la méthodologie

décrite dans l'article du chapitre 2. Cette partie présente les matériaux utilisés dans le cadre de cette étude.

8.4.1 Résine

La matrice a été choisie afin d'étudier les résines les plus couramment utilisées par l'industrie dans notre domaine d'intérêt (principalement le transport). Une résine polyester insaturée orthophtalique de faible viscosité a été finalement choisie. La résine T-580-63 est fabriquée par la compagnie AOC Canada Inc. (au prix de 18\$ CAD par Kg). Cette résine possède une viscosité de 181 cPo à température ambiante, ce qui est idéal pour la production de pièces par le procédé RTM à haute température afin de réduire la viscosité et accélérer le remplissage des moules. L'inhibiteur inclus dans la résine possède une vie moyenne de six mois avant sa décomposition, afin de permettre le stockage du produit. Le catalyseur utilisé est le Norox Pulcat A, fabriqué par Norac, un peroxyde organique à base de Méthyl Isobutyle Cétone Peroxyde (MIBKP). Ce catalyseur à basse réactivité possède une demi-vie de 10 heures à 70 °C. Il est principalement conçu pour la production des pièces à haute température (car il permet de démarrer la réaction en chaîne à partir de 75 °C). Un pourcentage de 1.5% en poids de Norox Pulcat A a été fixé pour la formulation de la résine. Les fiches techniques de ces matériaux sont données à l'annexe IV.

8.4.2 Renforts

Pour la fabrication des plaques composites, deux renforts fibreux ont été sélectionnés. Le premier est l'Unifilo U101 de la compagnie Vetrotex, un mat en fibres de verre continues de type E de structure aléatoire avec une densité surfacique de 600 grammes par mètre carré. Il est communément utilisé dans la fabrication de panneaux sandwichs pour véhicules ou comme renfort de peau. Il permet une très bonne imprégnation des fibres, qui donne un bon niveau de transparence des pièces fabriquées. La fiche

technique de ce matériau peut être trouvée à l'annexe IV. Le deuxième renfort choisi dans ce travail est le NCS-82620-A, de la compagnie J.B. Martin, un renfort bidirectionnel en fibres de verre de type E. Les fibres non tissées sont cousues par un fil de polyéthylène. Le renfort possède une densité superficielle de 300 gr/m^2 .

8.5 Instruments de caractérisation

Pour caractériser la cinétique de polymérisation d'une résine thermodurcissable, une mesure calorimétrique peut être réalisée. Les variations du flux de chaleur d'un échantillon pendant la réaction peuvent être reliées au nombre des chaînes de polymère créées. Pour réaliser ces essais, un calorimètre différentiel DSC (« Dynamic Scanning Calorimeter ») est essentiel. Le modèle DSC 910 de la compagnie DuPont a été utilisé (voir figure ci-dessous).

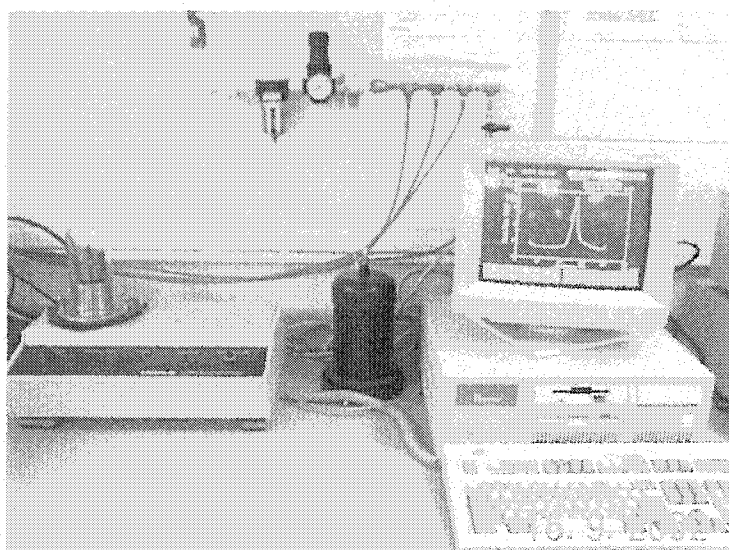
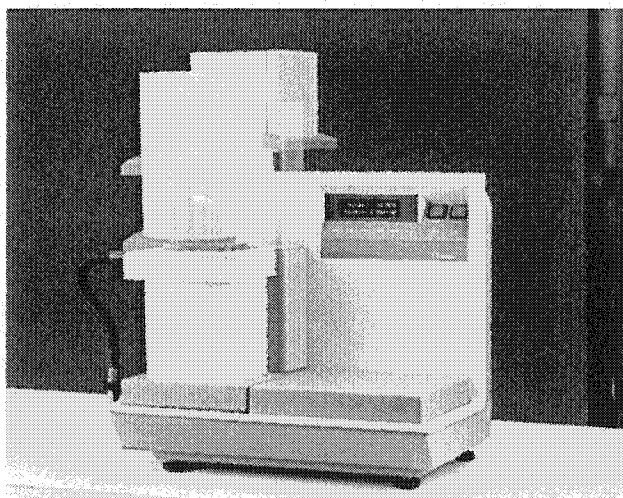


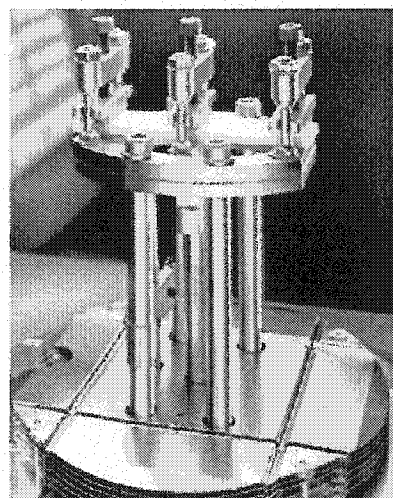
Figure 8.3. Calorimètre DSC 910 et ordinateur de traitement des données.

Cet instrument travaille dans une gamme de température entre $-170\text{ }^{\circ}\text{C}$ et $725\text{ }^{\circ}\text{C}$, avec des échantillons entre 0.5 mgr et 200 mgr . Pour contrôler l'environnement de la chambre d'essai, l'appareil est connecté à une bouteille de gaz neutre (azote) pour permettre l'évacuation des gaz qui pourraient éventuellement s'échapper de l'échantillon. Le refroidissement est contrôlé par injection d'air pressurisé autour de la chambre d'essai.

La caractérisation des propriétés viscoélastiques a été réalisée avec une DTMA (Dynamic Mechanical Thermal Analyzer). L'instrument DMTA 2980 de la compagnie TA Instrument a été utilisé. Cet appareil (voir image dessous) contient une chambre fermée pour assurer l'isolation de l'échantillon dans un environnement contrôlé (l'azote peut être utilisé). Un contrôle de température permet de chauffer les échantillons jusqu'à $600\text{ }^{\circ}\text{C}$ à une vitesse de $20\text{ }^{\circ}\text{C}/\text{min}$.



(a)

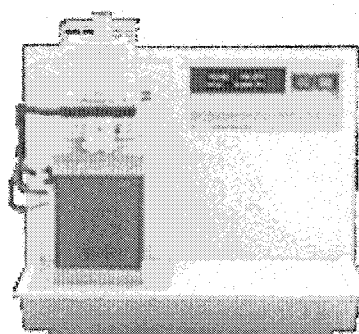


(b)

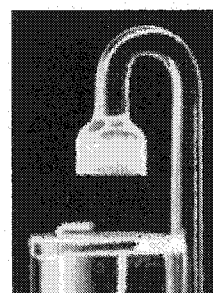
Figure 8.4. Instrument d'essais mécaniques dynamiques : a) DMTA 2980 de TA Instrument, b) montage typique d'un échantillon en flexion double cantilever.

Diverses méthodes de mesure sont possibles avec cet appareil, comme la compaction, traction, flexion en trois points, flexion de barres fixées, etc. Dans cette étude, le montage de flexion en trois points a été utilisé pour des échantillons de 50 *mm* de longueur, 15 *mm* de largeur et 3 *mm* d'épaisseur. L'instrument est capable de varier la fréquence d'excitation de 0.01 Hz à 200 Hz pour une force maximale de 18 Newtons.

La caractérisation thermomécanique des matériaux utilisés dans cette thèse a été effectuée à l'aide d'une machine TMA 2940 de la compagnie TA Instrument (voir la figure suivante). Cet instrument mesure les changements dimensionnels dans l'échantillon en fonction de la température ou du temps. Il permet la détermination précise des variations de longueur, d'épaisseur ou de volume d'un matériau. Les coefficients d'expansion thermique des composites ont été mesurés avec cet instrument.



(a)



(b)

Figure 8.5. Instrument d'essais thermomécaniques : a) TMA 2940 de TA Instrument, b) montage d'expansion thermique.

L'appareil est constitué d'une chambre fermée de similaires caractéristiques à la DMTA. L'azote est utilisé pour contrôler l'environnement de la chambre et l'air pressurisé utilisé pour la refroidir. La fixation employée dans ce travail est un montage d'expansion thermique qui nous a permis de mesurer les variations d'épaisseur d'échantillons de 5 *mm* de diamètre et 3 *mm* d'épaisseur.

8.6 Statistiques du travail

Les recherches entreprises dans le cadre de cette thèse avaient une durée d'approximativement quatre ans, considérant un passage direct de la maîtrise au doctorat au début de l'année 2001. Un échéancier des développements réalisés pendant cette période est présenté à la figure 8.6. Une division de ces travaux devient pertinente pour mieux exprimer les statistiques du projet. On pourra donc regrouper les tâches comme suit: le travail numérique pour le volet simulation, et le travail expérimental pour le volet validation. Par la suite, les statistiques seront données pour chacun des volets.

Pour les travaux numériques, un ordinateur de haute performance est requis en raison du temps de compilation et d'exécution des codes d'éléments finis complexes. Dans l'étape de simulation d'une pièce réelle, la minimisation du temps de calcul devient aussi importante afin d'être capable de tester le code d'optimisation dans un délai acceptable. Pendant les quatre années du projet, trois ordinateurs ont été progressivement utilisés. Ils sont listés ci-dessous :

- PC IBM compatible. Processeur Intel Pentium II à 500 *MHz*.
- IBM IntelliStation M-Pro. Biprocesseur Intel Pentium III à 1.0 *GHz*.
- IBM IntelliStation Z-Pro. Biprocesseur Intel Pentium IV à 2.8 *GHz*.

Tous les codes présentés ont été développés dans le langage C++, et le compilateur utilisé a été Visual C++ v5.0 et v6.0 de la compagnie Microsoft. Le tableau de la figure 8.7 donne des statistiques sur les codes développés. Douze programmes ont été produits pour l'analyse des données provenant des instruments de caractérisation, la génération des modèles mathématiques, la simulation et l'optimisation numérique. De l'addition de ces douze programmes, un total de 27800 lignes de code ont été écrites pendant les

quatre ans de ce travail. Trois bibliothèques générées en code C++ sont reliées à ces programmes. La bibliothèque de krigeage appelé *LibKrig* est un utilitaire d'accès publique généralement utilisé dans le cours MEC 6310 *Krigeage en CAO et FAO*, donné par le professeur F. Trochu à l'École Polytechnique de Montréal. La bibliothèque de algorithmes génétiques implémentée dans les codes d'optimisation et de génération des modèles, appartenant au domaine publique *GALib* écrite par Matthew Wall au MIT (Massachusetts Institute of Technology). Finalement, la bibliothèque *Proflot* d'ESI-Group a été utilisée pour les calculs des flux de fluide et de chaleur dans les calculs par éléments finis.

Dans le volet validation expérimental, la résine et les fibres sont requises pour la fabrication des plaques. La résine T-580-63 de la compagnie AOC Canada a été commandée en conteneurs de 5 gallons (20 Kg) au prix de 18\$ CAD par Kg. Le catalyseur Norox Pulcat A et l'agent démoulant étaient déjà disponibles dans le laboratoire du CRASP (des faibles quantités ont été utilisées). Les deux renforts de verre utilisés étaient aussi disponibles au CRASP. Des quantités de moins de 5 mètres carrés de chacun des matériaux ont été requis.

Pendant la recherche, des anciennes thèses, des rapports internes et des publications ont été indispensables pour amener des conclusions valables dans divers sujets. Dans les quatre ans d'investigation, un total de 690 (± 20) articles scientifiques ont été collectés et classifiés par sujet. Les revues de la bibliothèque de l'école et ses ressources électroniques ont été fondamentales pour la recherche, acquisition et organisation de ces documents.

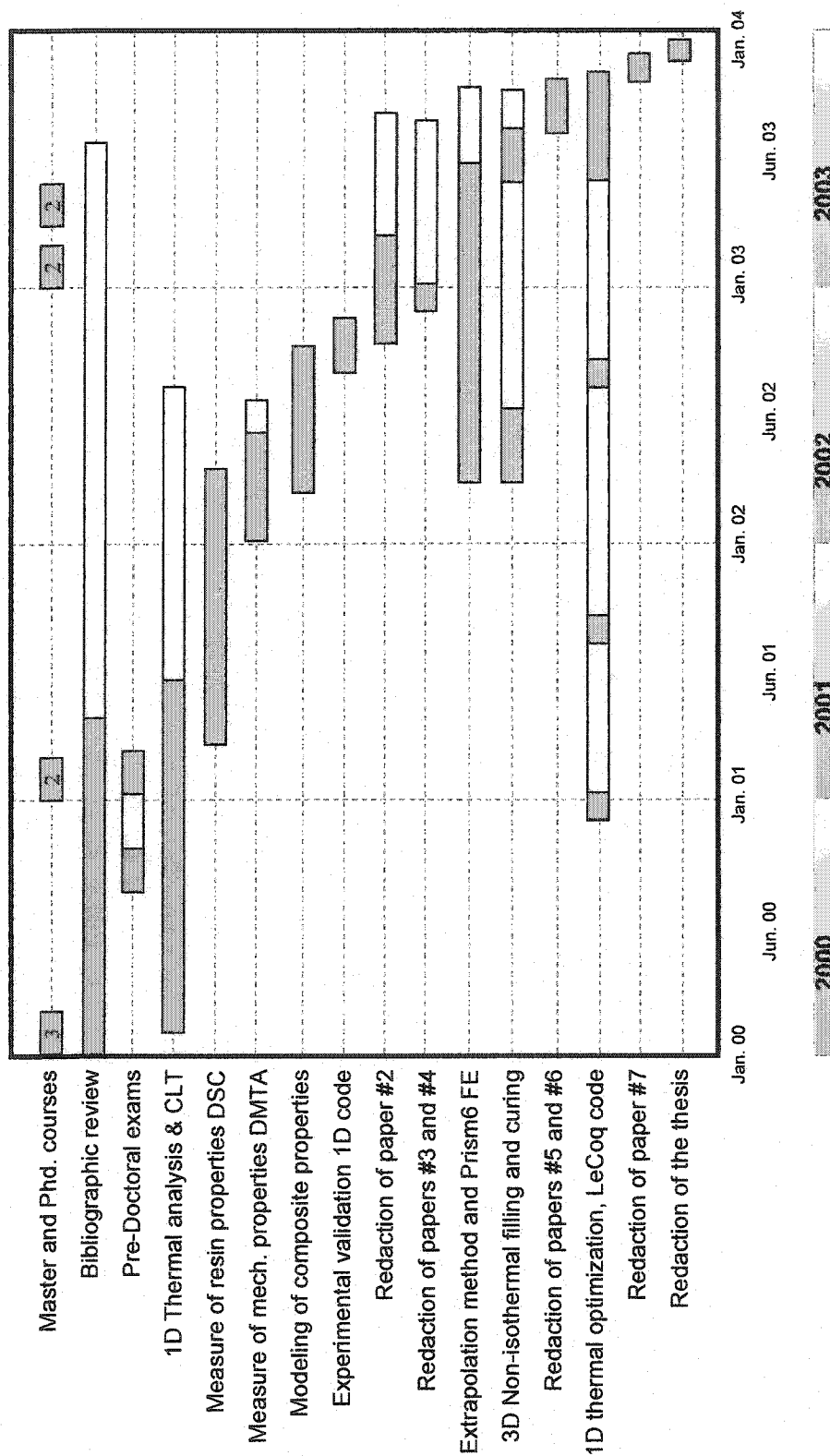


Figure 8.6 Échéancier des travaux réalisés dans le cadre de cette thèse.

Program Name	Code lines	Head files	Code files	Classes	Uses Kriging library	Uses Genetic Algorithms	Uses Proflot library
Kinetic modeling	5815	0	1	0	✓	✓	
DTMA data analysis	200	0	1	0	✓		
TMA data analysis	197	0	1	0	✓		
Viscoelastic modeling	1454	0	1	0	✓	✓	
Classical laminate plate theory	2003	3	4	3	✓		✓
1D finite differences/stress	5398	8	9	10	✓		✓
Convection 2D analytical	123	0	1	0			
Diffusion 1D analytical	112	0	1	0			
Diffusion 2D analytical	131	0	1	0			
Diffusion 3D analytical	108	0	1	0			
1D thermal optimization	7203	9	10	11	✓	✓	✓
3D non-isothermal filling	7656	7	8	10	✓		✓

Figure 8.7 Statistique des codes en C++ développés dans cette travail.

CONCLUSION

Cette thèse a démontré l'utilité des modèles appropriés des propriétés thermomécaniques et des méthodes numériques appliquées à la simulation et à l'optimisation de la mise en forme des matériaux composites à matrice thermodurcissable. Des modèles semi-empiriques ont été développés pour caractériser la cinétique de polymérisation et le comportement viscoélastique d'un composite verre/polyester. Afin de caractériser les propriétés de la résine et du composite, des mesures calorimétriques avec un appareil de calorimétrie différentielle DSC (« *Differential Scanning Calorimeter* ») et des mesures thermomécaniques avec appareils DMTA (« *Dynamical Mechanical Thermal Analyzer* ») et TMA (« *Thermo-Mechanical Analyzer* ») ont été réalisées. Un code de calcul de la cuisson et de la déformation des plaques composites a été développé et validé expérimentalement. En fin, une étude préliminaire sur les évolutions des contraintes internes pendant la polymérisation de la résine et le refroidissement de pièces composites épaisses a été présentée et la possibilité d'optimiser la cuisson au moyen de l'analyse numérique démontrée travers divers exemples.

Pour améliorer la rapidité et la qualité du calcul du flux de résine pendant le remplissage des pièces tridimensionnelles, une méthode d'extrapolation de maillage et un nouvel élément fini discontinu ont été développés. Pour évaluer les flux thermiques dans la cavité du moule, une approche originale couplant éléments finis et différences finies a également été proposée. Au niveau du remplissage non isotherme, on a pu constater que la performance de cette nouvelle approche mixte a été toujours supérieure à celle de la méthode des éléments finis tridimensionnels. La comparaison des résultats

obtenus avec le nouvel élément fini montre que la qualité des calculs est améliorée et que la durée du calcul devient environ 4% du temps requis par la version précédente.

Pour terminer, un code de calcul fondé sur les algorithmes génétiques a été développé pour optimiser le cycle de cuisson des pièces composites fabriquées par injection sur renfort. Une étude de la cuisson des pièces minces a démontré l'importance de l'optimisation multicritères proposée par rapport à la minimisation des gradients thermiques qui est couramment utilisée. Les analyses d'optimisation ont mis en valeur l'ensemble des travaux réalisés dans le cadre de cette thèse : la caractérisation des matériaux qui est indispensable pour comprendre les phénomènes reliés à la polymérisation de la résine, la modélisation numérique de la cuisson et des contraintes résiduelles, qui est fondamentale pour évaluer les effets des paramètres de moulage sur la mise en forme des pièces. En fin, toutes les connaissances acquises dans la simulation et validation expérimentale ont permis de formuler les critères d'optimisation utilisés dans cette étude.

Les travaux futurs qui découlent naturellement de cette thèse portent essentiellement sur l'optimisation du procédé : optimisation de la position des points d'injection et des événements, optimisation de la pression ou du débit d'injection, minimisation du temps de remplissage et optimisation des contraintes résiduelles dans toute la pièce.

BIBLIOGRAPHIE

ADVANI S. G. (1994). Flow and Rheology in Polymer Composites Manufacturing. Elsevier Sci. Series. ISBN: 0444893474.

ALEXANDROU A. et AHMED A. (1993). Injection Molding Using Generalized Eulerian Lagrangian Formulations. Polymer Eng. and Sci., vol. 33, No. 16, pp. 1055-1064.

ATARSIA A. et BOUKHILI R. (2000). Relationship Between Isothermal and Dynamic Cure of Thermosets Via the Isoconversion Representation. Polymer Eng. Sci., vol. 40, No. 3, pp. 607-620.

BECHET E., RUIZ E., TROCHU F. et CUILIERE J.-C. (2001). Re-Meshing Algorithms Applied to Resin Transfer Molding Simulations. International Canada Composites Conference CANCOM'01, Montreal, Canada, August 7-14.

BOCCARD A., LEE W. et SPRINGER G. (1995). Model for Determining the Vent Locations and the Fill Time of Resin Transfer Molds. Journal of Composite Materials, vol. 29, No. 3, pp. 306-333.

BOGETTI T. et GILLESPIE J. (1992). Process-Induced Stress and Deformation in Thick-Sectioned Thermoset Composite Laminates. Journal of Composite Materials, vol. 26, No 5, pp. 626-660.

CARMAN P. (1937). Fluid Flow Through Granular Beds. Trans. Int. Chem. Eng., vol. 15, pp. 150-166.

CHANG A. et HWANG S. (1992). Modeling Nonisothermal Impregnation of Fibrous Media with Reactive Polymer Resin. Polymer Eng. and Sci., vol. 32, No. 5, pp. 310-318.

CHEN B. et LIU W. (1989). Numerical Simulation and Experimental Investigation of Injection Mold Filling with Melt Solidification. Polymer Eng. and Sci., vol. 29, No. 15, pp. 1039-1050.

CHEN R., TU C. et TSAI H. (1993). The Effects of Moisture upon the optimal Temperature Path of the Viscoelastic Symmetric Composite Laminates after Post Cure. Journal of Composite Materials, vol. 27, No.16, pp. 1578-1597.

CORDEN T.J., JONES I. A., JONES D.T. et MIDDLETON V. (1998). The Mechanisms of Interlaminar Cracking in Thick Resin Transfer Moulded Composite Cylinders. Composites Part A, vol. 29A, pp. 455-464.

COULTER J. et GUCERI S. (1988). Resin Impregnation During the Manufacturing of Composite Materials Subject to Prescribed Injection Rate. Journal of Reinforced Plastics and Composites, vol. 7, pp. 201-219.

COULTER J. et GUCERI S. (1989). Resin Impregantion During Composites Manufacturing: Theory and Experimentation. Composites Sci. and Technology, vol. 35, pp. 317-330.

DARCY H. (1856). Les Fontaines Publiques de la Ville de Dijon, Paris, Dalmont.

EOM Y., BOUGH L., MICHAUD V., SUNDERLAND P. et MANSON, J. (2000). Time-Cure-Temperature Superposition for the Prediction of Instantaneous Viscoelastic Properties During Cure. Polymer Eng. and Sci., vol. 40, No. 6, pp. 1281-1292.

ERHUN M. et ADVANI S. G. (1992). BEM Approach to Model Heat Flow During Crystallization. Int. Journal for Numerical Methods in Eng., vol. 35, pp. 351-368.

GAUVIN R. et TROCHU F. (1998). Key Issues in Numerical Simulation for Liquid Composite Molding Processes. Polymer Composites, vol. 19, pp. 233-240.

GOLESTANIAN H. et, EL-GIZAWY S. (1997). Cure Dependent Lamina Stiffness Matrices of Resin Transfer Molded Composite Parts. Journal of Composite Materials, vol. 31, No. 23, pp. 2402-2423.

GUTOWSKI T. (1997) Advanced Composites Manufacturing. Edited by John Wiley & Sons, Inc. ISBN: 047115301X.

GUYONVARCH G., AUDET M., QIAN Y., TROCHU F. et DELAUNAY D. (1996). Validation of Non Isothermal Resin Transfer Molding Simulations. Joint European Conference JEC, Paris, France, April 24-26.

HAN C. et LEE D. (1987). Analysis of the Curing Behavior of Unsaturated Polyester Resins Using the Approach of Free Radical Polymerization. Journal of Applied Polymer Sci., vol. 336, pp. 2859-2876.

HAN C. et LEM K. (1983). Chemorheology of Thermosetting Resins I. The Chemorheology and Curing Kinetics of Unsaturated Polyester Resin. Journal of Applied Polymer Sci., vol. 28, pp. 3155-3183.

HAN C. et LEM K.-W. (1984). Chemorheology of Thermosetting Resins. IV. The Chemorheology and Curing Kinetics of Vinyl Ester Resin. Journal of Applied Polymer Sci., vol. 29, pp. 1879-1902.

HUANG Y.-J. et SU C.-C. (1995). Effects of Poly(vinyl acetate) and Poly(methyl methacrylate) Low-Profile Additives on the Curing of Unsaturated Polyester Resins. I. Curing Kinetics by DSC and FTIR. Journal of Applied Polymer Sci., vol. 55, pp. 305-322.

JAYARAMAN K. et REIFSNIDER K. (1992). Residual Stresses in a Composite with Continuously Varying Young's Modulus in the Fiber/Matrix Interphase. Journal of Composite Materials, vol. 26, No. 6, pp. 770-791.

KAMAL M. et SOUROUR S. (1973). Kinetics and Thermal Characterization of Thermoset Cure. Polymer Eng. & Sci., vol. 13, No. 1, pp. 59-64.

KANG M., JUNG J. et LEE W. (2000). Analysis of Resin Transfer Moulding Process with Controlled Multiple Gates Resin Injection. Composites Part A, vol. 31, pp. 407-422.

KINKELAAR M. et LEE L. (1992). Development of a Dilatometer and Its Application to Low-Shrink Unsaturated Polyester Resins. Journal of Applied Polymer Sci., vol. 45, pp. 37-50.

KINKELAAR M., MUZUMDAR S. et LEE L. (1995). Dilatometric Study of Low-Profile Unsaturated Polyester Resins. Polymer Eng. and Sci., vol. 35, No. 10, pp. 823-836.

LEBRUN G. et GAUVIN, R. (1995). Heat Transfer Analysis in a Heated Mold during the Impregnation Phase of the Resin Transfer Molding Process. Journal of Material Processing and Manufacturing Sci., vol. 4, pp. 81-104.

LEBRUN G., GAUVIN R. et KENDALL K. (1996). Experimental Investigation of Resin Temperature and Pressure during Filling and Curing in a flat steel RTM mould. Composites Part A, vol. 27(A), pp. 347-355.

LEBRUN G., RUDD C. et GAUVIN R. (1995). Laminate Temperature Distributions and Filling Time Prediction During Non-Isothermal Impregnation of Fiber Preforms. Journal of Reinforced Plastics and Composites, vol. 14, pp. 1069-1080.

LI M., ZHU Q., GEUBELLE H. et TRUCKER C. (2001). Optimal Curing for Thermoset Matrix Composites: Thermochemical Considerations. Polymer Composites, vol. 2, No. 1, pp. 118-132.

LIN M., MURPHY M. et HAHN, T. H. (2000). Resin Transfer Molding Process Optimization. Composites Part A, vol. 31, pp. 361-371.

LIN R., LEE L. et LIOU M. (1991). Mold Filling and Curing Modeling of RTM and SRIM Processes. Advanced Composite Materials Conf., Detroit, Michigan, USA, Sept. 30–Oct. 3, pp. 165-174.

LIU C., KIASAT M., NIJHOF A., BLOKLAND H. et MARISSEN R. (1999). The Effect of the Addition of a Low Profile Additive on the Curing Shrinkage of an Unsaturated Polyester Resin. Polymer Eng. and Sci., vol. 39, No. 1, pp. 18-25.

LUO J., LIANG Z., ZHANG C. et WANG, B. (2001). Optimum Tooling Design for Resin Transfer Molding with Virtual Manufacturing and Artificial Intelligence. Composites Part A, vol. 32, pp. 877-888.

MANSON J.-A. et SEFERIS J. (1992). Process Simulated Laminate (PSL): A Metodology to Internal Stress Characterization in Advanced Composite Materials. Journal of Composite Materials, vol. 26, No. 3, pp. 405-431.

MICHAUD D., BERIS A. et DHURJATI P. (1998). Curing Behavior of Thick-Sectioned RTM Composites. Journal of Composite Materials, vol. 32, No. 14, pp. 1273-1295.

Owen M., Rudd C. et Kendall K. (1991). Modeling the Resin Transfer Molding (RTM) Process. Advanced Composite Materials Conf., Detroit, Michigan, USA, Sept. 30–Oct. 3, pp. 187-202.

PEARCE N., GUILD F. et SUMMERSCALES J. (1998). A Study of the Effects of Convergent Flow Fronts on the Properties of Fiber Reinforced Composites Produced by RTM. Composites Part A, vol 29(A), pp. 141-152.

RUDD C., LONG A., KENDALL K. et MANGIN C. (1997) Liquid Moulding Technologies. SAE International book. ISBN: 0768000165.

RUIZ E. et DEMARIA C. (1998). Diseño, Análisis y Procesos de Fabricación de la puerta de un vehículo eléctrico ciudadano en RTM. Eng. thesis, Instituto Universitario Aeronáutico, Universidad Católica de Córdoba, Argentine, 360 pages.

SALLA J. et RAMIS X. (1996). Comparative Study of the Cure Kinetics of an Unsaturated Polyester Resin Using Different Procedures. Polymer Eng. Sci., vol. 36, No. 6, pp. 835-851.

SPOERRE J., ZHANG C., WANG B. et PARNAS R. (1998). Integrated Product and Process Design for Resin Transfer molded Parts. Journal of Composite Materials, vol. 32, No. 13, pp. 1244-1273.

TROCHU F. et GAUVIN R. (1992). Limitations of a Boundary-Fitted Finite Difference Method for the Simulation of the Resin Transfer Molding Process. Journal of Reinforced Plastics and Composites, vol. 11, pp. 772-786.

TROCHU F., GAUVIN R. et GAO D. (1993). Numerical Analysis of the Resin Transfer Molding Process by the Finite Element Method. Advances in Polymer Technology, vol. 12, No. 4, pp. 329-342.

TUCKER C. (1996). Heat Transfer and Reaction Issues in Liquid Composite Molding. Polymer Composites, vol. 17, No. 1, pp. 60-72.

UM M.-K. et LEE W.-I. (1991). A Study on the Mold Filling Process in Resin Transfer Molding. Polymer Eng. and Sci., vol. 31, No. 11, pp. 765-771.

VOLLER V. et PENG S. (1995). An Algorithm for the Analysis of Polymer Filling Molds. Polymer Eng. and Sci., vol. 35, No. 22, pp. 1758-1767.

WHITE S. et HAHN H. (1992). Process Modeling of Composite Materials: Residual Stress Development during Cure. Part I Model Formulation. Journal of Composite Materials, vol. 26, No. 16, pp. 2402-2422.

WHITE S. et HAHN H. (1992). Process Modeling of Composite Materials: Residual Stress Development during Cure. Part II Experimental Validation. Journal of Composite Materials, vol. 26, No. 16, pp. 2423-2453.

WHITE S. et HAHN H. (1993). Cure Cycle Optimization for the Reduction of Processing-Induced Residual Stresses in Composite Materials. Journal of Composite Materials, vol. 27, No. 14, pp. 1353-1378.

YOUSEFI-MOSHIRABAD A. (1996). Cure Analysis of Promoted Polyester and Vinylester Reinforced Composites and Heat Transfer in RTM Molds. Thèse de Philosophie Doctor, Département de Génie Mécanique, École Polytechnique de Montreal.

YU H.-W. et YOUNG W.-B. (1997). Optimal Design of Process Parameters for Resin Transfer Molding. Journal of Composite Materials, vol. 31, No.11, pp. 1113-1140.

ANNEXE I

CODES C++

Cette annexe présente, les codes développés pour la solution analytique des exemples décrits dans ce travail. Les codes sont écrites en langage C++ et compilés en Microsoft VisualC++ v6.0.

One dimensional diffusion problem

```
/* ===== */
```

Analytical solution of transient heat conduction equation

Program by Edu Ruiz - July 2001

Copyright Ecole Polytechnique de Montreal

All rights reserved.

$$T(x,t) = T(0,t) + 2/L * (-T(0,t) * \sum_{n=1, \infty} \exp(-L_d^2 * t * \sin(L_d * x) / L_d))$$

where:

L = length of the domain (=1)

$T(0,t)$ = thermal boundary condition (=1)

$L_d = (2 * n - 1) * \pi / (2 * L)$

n = sum number

x = any position in the length

the better comparison is to fix a position x and calculate $T(x,t)$

```
/* ===== */
```

```
#include <stdio.h>
```

```
#include <math.h>
```

```
int main() {
```

```
{
```

```
    /* first solution:
```

```
        - fix a position x and calculate T(x,t)
```

```
        - boundary condition T(0,t)=1
```

```
        - L=4
```

```

        - x= 0.5
    */

float L=4;
float x=4;
int n=500;
double pi= 3.1415926535897932384626433832795;
float T_0_t= 1;
int time_steps=120;

// loop in time
for (int i=0; i<=time_steps; i++)
{
    double time=i/4;
    double suma=0;

    // loop in n
    for (int j=1; j<=n; j++)
    {
        double Ld= (2*j-1)*pi/2/L;
        suma += exp(-pow(Ld,2)*time)*sin(Ld*x)/Ld;
    }

    double T_x_t= T_0_t + 2/L*(-T_0_t)*suma;

    { // save datas
        printf(" step : %4d,  time : %6.0f,  T(x,t) : %8.4f\n",i, time, T_x_t );

        FILE *fp = NULL;
        if ( i == 0)
        {
            fp = fopen("otput.sal", "wt");
        } else {
            fp = fopen("otput.sal", "at");
        }
    }
}

```

```

    }

    if (fp)
    {
        if (i == 0)
        {
            fprintf(fp, " Analytical solution of transient heat
conduction equation\n");

            fprintf(fp, "\n");
            fprintf(fp, " Program by Edu Ruiz - 08-2001\n");
            fprintf(fp, "\n");
            fprintf(fp, " values are: iteration id, time ,
temperature \n");

            fprintf(fp, "\n");
        }
        fprintf(fp, " %4d %6.2f %8.4f\n", i, time, T_x_t);
        fclose(fp);
    }
}

} // end of time loop
} // end first solution

{
    /* second solution:
        - fix a position x and calculate T(x,t)
        - boundary condition T(0,t)=1
        - L=4
    */

    float L=4;
    float x=0;
    int n=500;
    double pi= 3.1415926535897932384626433832795;
    float T_0_t= 1;

```

```

int time_steps=60;

// loop in time
for (int i=0; i<=time_steps; i++)
{
    double time=(float)i/2;

    // loop in thickness
    for (int k=0; k<=8; k++)
    {
        x= k*L/8;
        double suma=0;

        // loop in n
        for (int j=1; j<=n; j++)
        {
            double Ld= (2*j-1)*pi/2/L;
            suma += exp(-pow(Ld,2)*time)*sin(Ld*x)/Ld;
        }
        double T_x_t= T_0_t + 2/L*(-T_0_t)*suma;

        { // save datas

            FILE *fp = NULL;
            if ( (i == 0) & (k==0) )
            {
                fp = fopen("otput2.sal", "wt");
            } else {
                fp = fopen("otput2.sal", "at");
            }

            if (fp)
            {
                if ( (i == 0) & (k==0) )

```

```

{
    fprintf(fp," Analytical solution of transient heat
conduction equation\n");

    fprintf(fp,"\n");
    fprintf(fp," Program by Edu Ruiz - 08-2001\n");
    fprintf(fp,"\n");
    fprintf(fp," values are: iteration id, time ,
temperatures in thickness \n");

    fprintf(fp,"\n");

    // save x position
    fprintf(fp,"\n x positions:");
    for (int kk=0; kk<=8; kk++)
    {
        float xx= kk*L/8;
        fprintf(fp," %6.4f ",xx );
    }

}

if ( k==0) {
    fprintf(fp,"\n %4d %6.3f ",i, time );
}
fprintf(fp," %8.4f ", T_x_t );
fclose(fp);
}
}

} // loop in thickness

printf(" step : %4d, time : %6.2f\n",i, time);

} // end of time loop
}
return 1; };

```

Two dimensional diffusion problem on a rectangle

/* ===== *

Analytical solution of transient heat conduction equation

For a bidimensional space, a rectangle of $X=Y=1$ is considered here

Program by Edu Ruiz - 10-2003

Copyright Ecole Polytechnique de Montreal

All rights reserved.

The analytical solution for 2D is the combination of the 1D solutions

$$(T-T_{bc})/(T_0-T_{bc})=(T_x-T_{bc})/(T_0-T_{bc})*(T_y-T_{bc})/(T_0-T_{bc})$$

where T_x and T_y are the 1D solutions

T_0 is the initial temperature $T_0=0$

T_{bc} is the boundary condition temperature $T_{bc}=1$ for two sides of the rectangle

for 1-D solution it is:

$$T(x,t)=T(0,t)+2/L*(-T(0,t)*\sum_{n=1,\infty} \exp(-L_d^2*t*\sin(L_d*x)/L_d))$$

where:

L = length of the domain (=1)

$T(0,t)$ = thermal boundary condition (=1)

$L_d=(2*n-1)*\pi/(2*L)$

n = sum number

x = any position in the length

the better comparison is to fix a position x and calculate $T(x,t)$

* ===== */

```

#include <stdio.h>
#include <math.h>

int main() {

    /* solution:
        - fix a position x,y and calculate T(x,y,t)
        - boundary condition T(0,t)=1
        - L=W= 1
        - x=y= 1
    */

    float L=1.;
    float x=1.;
    int n=1000;
    double pi= 3.1415926535897932384626433832795;
    float T_0_t= 1.;
    float time_tot= 2.;
    int time_steps= 1000;

    // loop in time
    for (int i=0; i<=time_steps; i++)
    {
        double time= time_tot*i/time_steps;
        double suma=0;

        // loop in n
        for (int j=1; j<=n; j++)
        {
            double Ld= (2.*j-1.)*pi/2./L;
            suma += exp(-pow(Ld,2)*time)*sin(Ld*x)/Ld;
        }
        double T_x_t= T_0_t + 2./L*(-T_0_t)*suma;
    }
}

```

```

{ // save datas
    printf(" step : %4d, time : %6.0f, T(x,t) : %8.4f\n",i, time, T_x_t);

    FILE *fp = NULL;
    if ( i == 0)
    {
        fp = fopen("otput.sal", "wt");
    } else {
        fp = fopen("otput.sal", "at");
    }

    if (fp)
    {
        if ( i == 0)
        {
            fprintf(fp, " Analytical solution of transient heat
conduction equation in a rectangle\n");

            fprintf(fp, "\n");
            fprintf(fp, " Program by Edu Ruiz - 10-2003\n");
            fprintf(fp, "\n");
            fprintf(fp, " values are: iteration id, time ,
temperature \n");

            fprintf(fp, "\n");
        }
        fprintf(fp, " %4d %12e %12e\n",i, time, -((T_x_t-1.)/-
1.)*(T_x_t-1.)/-1.+1.);

        fclose(fp);
    }
}

} // end of time loop

return 1;
};

```


Three dimensional diffusion problem on a cube

```
/* ===== */
```

Analytical solution of transient heat conduction equation

Program by Edu Ruiz - July 2001

Copyright Ecole Polytechnique de Montreal

All rights reserved.

Heat diffusion on a cube $T(x,y,z)$

$T(x,y,z)$ = equation on Annex D of E. Bohr (2000)

```
/* ===== */
```

```
#include <stdio.h>
```

```
#include <stdlib.h>
```

```
#include <math.h>
```

```
const double pi= 3.14159265358979323846;
```

```
void main(void) {
```

```
    int i,j,k,n,m,N;
```

```
    double x,y,z,sol[5][5][21],L,W,H;
```

```
    N=80;
```

```
    L= 1.;
```

```
    W= 1.;
```

```
    H= 1.;
```

```
    x=y=z=0.;
```

```

for (i=0; i<4; i++)
{
    x= L*((i+1)/6.);

    for (j=0; j<4; j++)
    {
        y= W*((j+1)/6.);

        for (k=0; k<21; k++)
        {
            z= H*(k/20.);
            sol[i][j][k]= 0.0;

            for (n=0; n<=N; n++)
            {
                for (m=0; m<=N; m++)
                {
                    double a= sinl((2*n+1)*pi*x/L);
                    double b= sinl((2*m+1)*pi*y/W);
                    double c= sqrt( (2*n+1)*(2*n+1)/L/L +
(2*m+1)*(2*m+1)/W/W );

                    sol[i][j][k] += 16./pi*pi*a*b*sinhl(pi*z*c)/(
(2*n+1)*(2*m+1)*sinhl(pi*H*c));

                }
            }
        }
    }
}

```

```

H *= 2.;

// print out
FILE *out= fopen("cube.sal","w");

fprintf(out,"Heat diffusion on a cube T(x,y,z)= equation on Annex D of E. Bohr (2000)\n\n\n");
fprintf(out,"For Y= W/2 :\n");
fprintf(out,"  Z  X1  X2  X3\n");
fprintf(out,"%f, %f, %f, %f\n\n",0.,L*(1./6.),L*(2./6.),L*(3./6.));

for (k=0; k<21; k++)
{
    z= H*(k/20.);
    fprintf(out,"%12.5E %12.5E %12.5E %12.5E\n",
        z,sol[0][2][k],sol[1][2][k],sol[2][2][k]);
}

fprintf(out,"\n\n\nFor X= L/2 :\n");
fprintf(out,"  Z  Y1  Y2  Y3  Y4\n");
fprintf(out,"%f, %f, %f, %f\n\n",0.,W*(1./6.),W*(2./6.),W*(3./6.));

for (k=0; k<21; k++)
{
    z= H*(k/20.);

    fprintf(out,"%12.5E %12.5E %12.5E %12.5E\n",
        z,sol[2][0][k],sol[2][1][k],sol[2][2][k]);
}

fclose(out);
};

```

ANNEXE II

ALGORITHME UNIDIMENSIONNEL DE CONTRAINTES RESIDUELLES

Cette annexe présente l'organigramme de l'algorithme de calcul de contraintes résiduelles unidimensionnelles pendant la cuisson et refroidissement du composite. L'organigramme correspond aux codes de différences finies de Crank-Nicolson et contraintes du composite par la théorie classique des laminés.

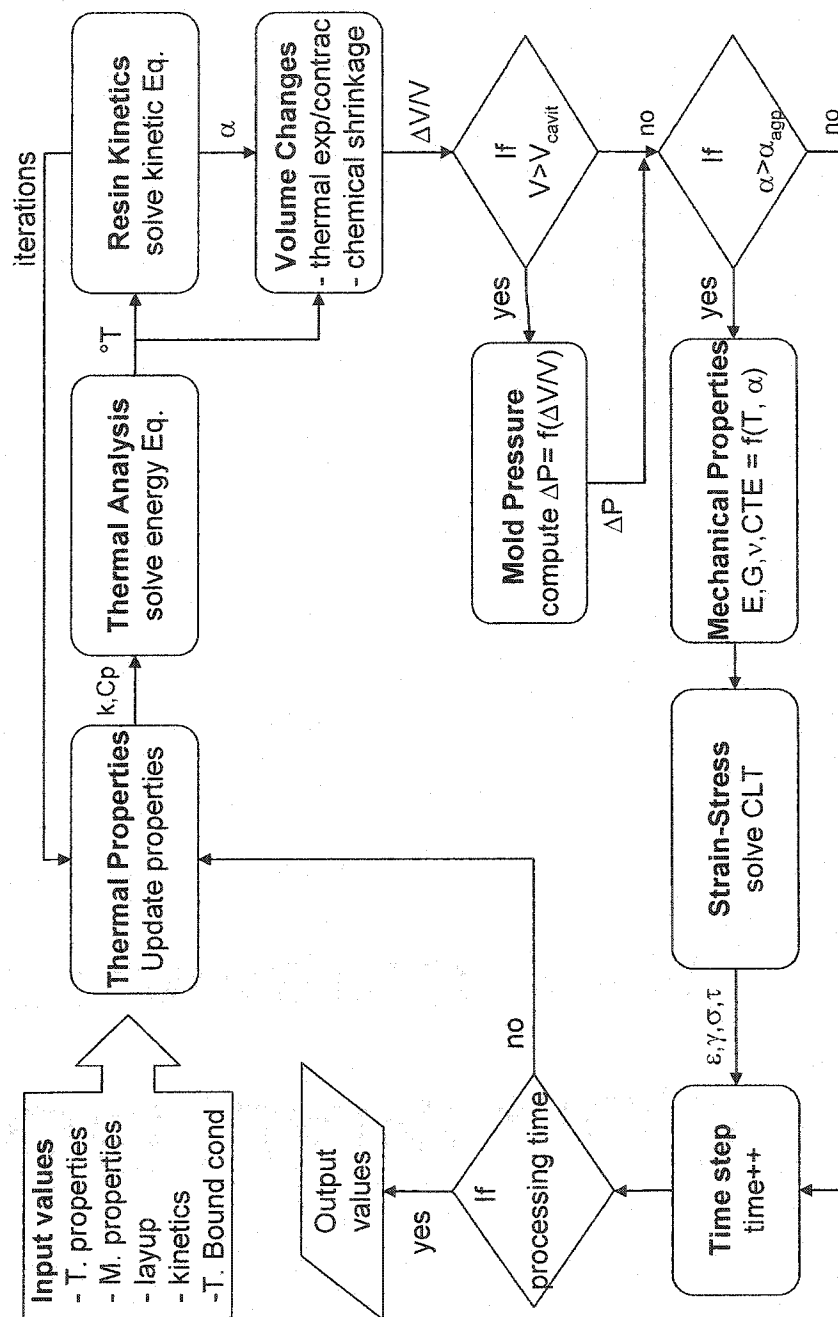


Figure A-II.1. Organigramme de calcul de contraintes résiduelles.

ANNEXE III

COURBES DE CARACTÉRISATION DE LA CINÉTIQUE DE CUISSON

Dans cette annexe pourront être trouvés les courbes détaillées de la caractérisation cinétique de la résine, les résultats de la méthode d'isoconversion de temps/température et les comparaisons après la modélisation.

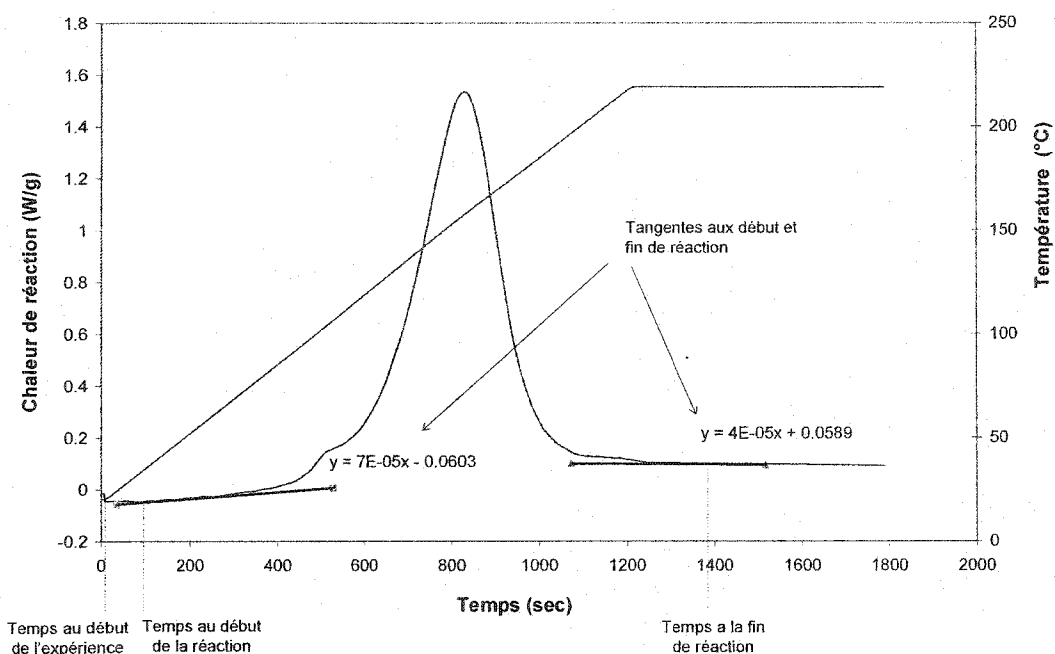


Figure A-III.1. Dynamic DSC measure showing beginning and end of reaction.

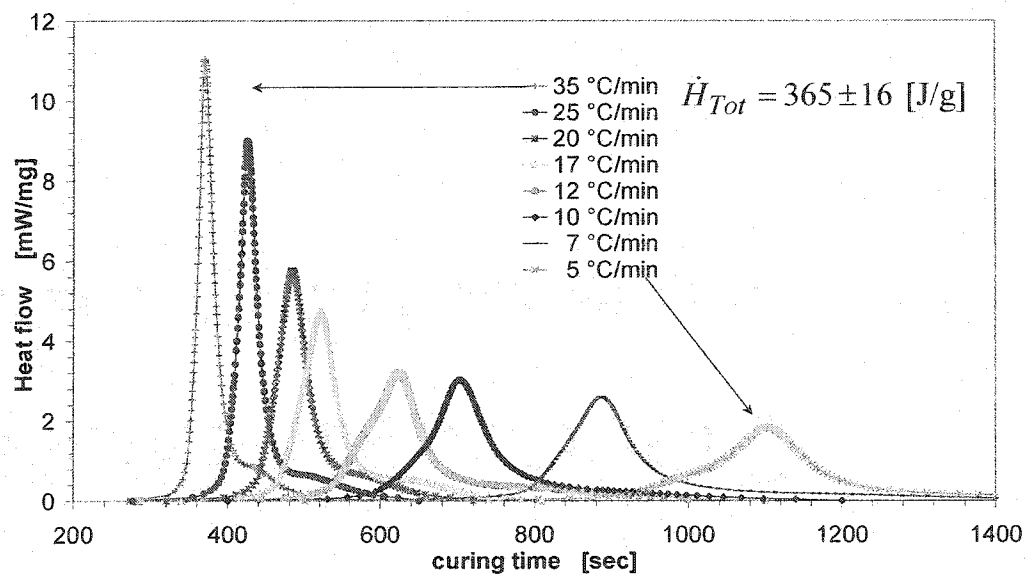


Figure A-III.2. Dynamic resin reactions at different heating rates after treatment of DSC data.

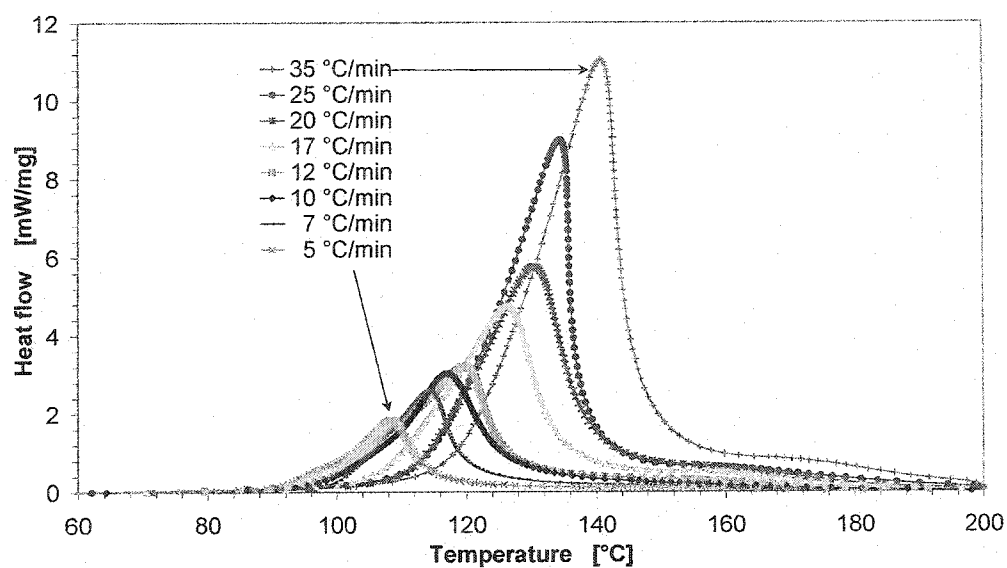


Figure A-III.3. Dynamic resin reactions at different heating rates as a function of DSC temperature.

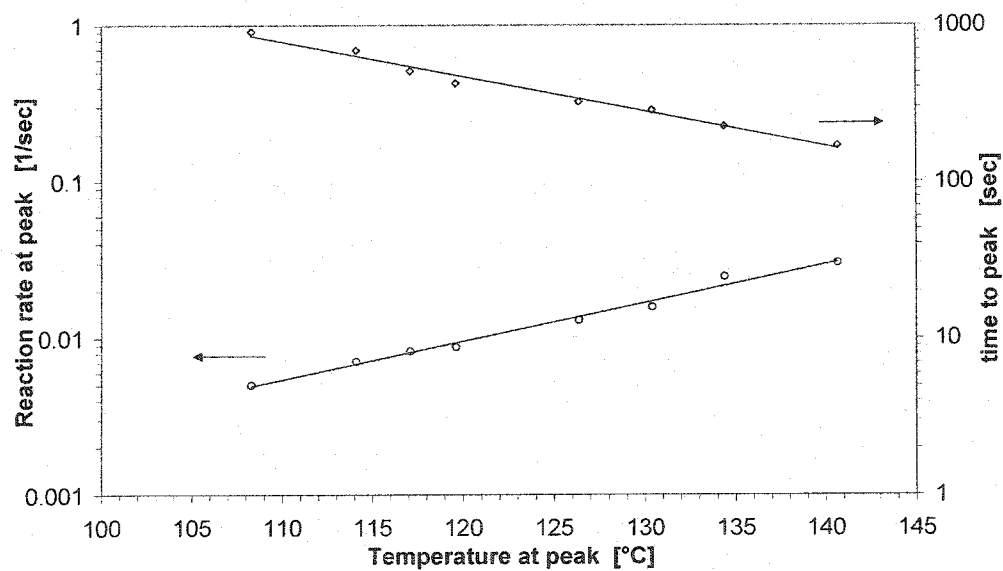


Figure A-III.4. Extraction of reaction rates at peak and times to peak from dynamic measurements.

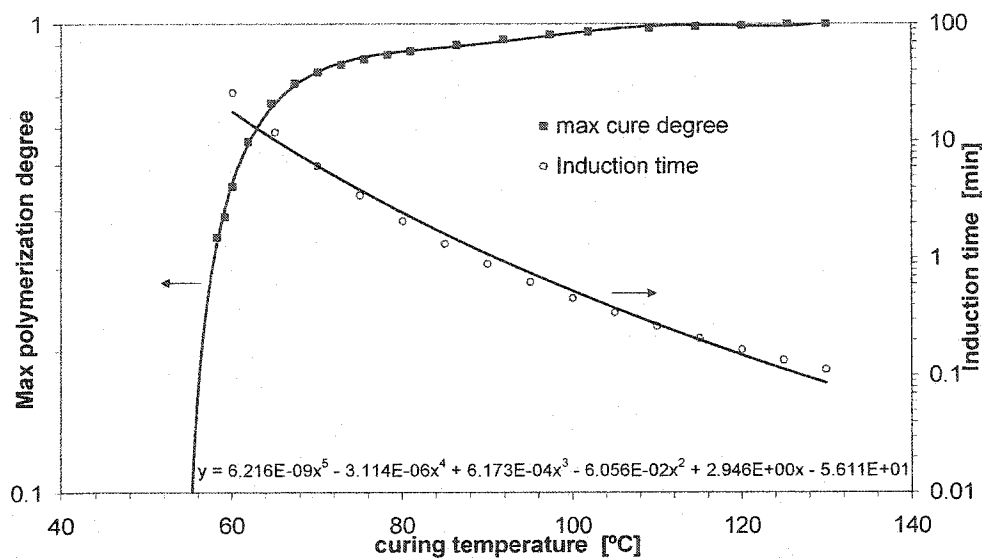


Figure A-III.5. Extraction of maximum degree of cure after isoconversion and induction times for isothermal cures.

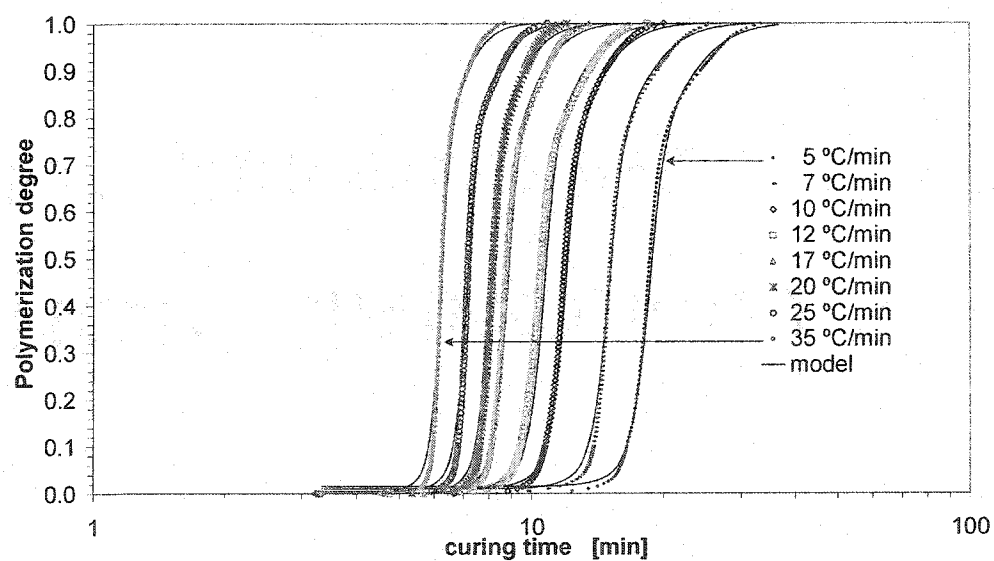
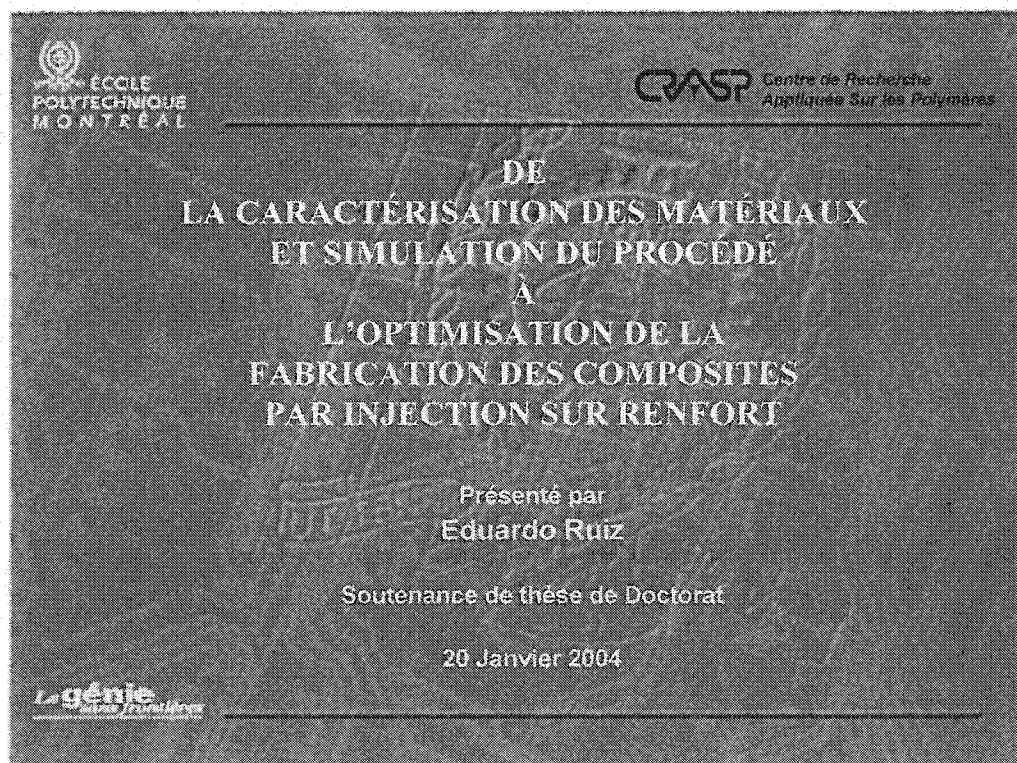


Figure A-III.6. Dynamic curing profiles after DSC data treatment, also RUIZ kinetic modeling is compared.

ANNEXE IV
DIAPPOSITIVES DE LA PRÉSENTATION DE SOUTENANCE
(20 Janvier 2004)



Plan

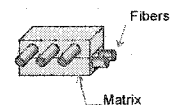
1. Introduction
2. Objectifs
3. Caractérisation des matériaux
4. Analyse unidimensionnelle de la cuisson
5. Simulation du remplissage non isotherme
6. Optimisation de la cuisson
7. Conclusions

Introduction – Matériaux composites

USA TODAY - 02/06/2002

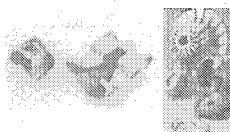
Man's evolution has been tied to his progress in materials. Yesterday it was the Stone, Bronze and Iron Ages. Today it is the **Age of Composites**. However, even in these earlier ages man experimented with and learned to use composite materials....

Composite (ASTM) : A multiphase material formed from a combination of materials which differ in composition or form, remain bonded together, and retain their identities and properties. The combination results in a material that maximizes specific performance properties.



Aujourd'hui, les composites synthétiques les plus communs peuvent être divisés dans trois groupes principaux:

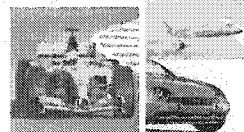
Metal Matrix Composites



Ceramic Matrix Composites



Polymer Matrix Composites



Composites thermodurcissables?

Reinforced plastics demand in US is projected to grow 2.5% annually for 2007, while for **thermosetting composites**, a growth of 7% per year is expected, mainly in the transport and construction industries (*New Materials International 2000*)

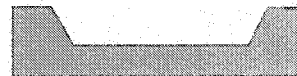
Introduction aux procédés d'injection sur renfort

Liquid Composite Molding (LCM): RTM, VARTM, VARI, SCRIMP, etc.

Description du procédé RTM typique

- Le renfort est placé dans le moule.
- Le moule est fermé et serré.
- La résine est injectée dans la cavité du moule sous pression.
- La résine polymérise.
- La pièce est démoulée.

RTM Process



Plan

1. Introduction
2. Objectifs
3. Caractérisation des matériaux
4. Analyse unidimensionnelle de la cuisson
5. Simulation du remplissage non isotherme
6. Optimisation de la cuisson
7. Conclusion

Objectif global

**Création
Matrice**

Hysté-résis

Optimisation thermique du procédé

Gauchissement

Ondulaton

Objectifs spécifiques de cette thèse

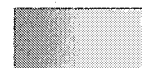
- 1) **Caractérisation** thermique et mécanique des matériaux.

Polymérisation
Module élastique
Dilatation et retrait

- 2) **Modélisation** unidimensionnelle de la cuisson et des contraintes résiduelles à travers l'épaisseur.



- 3) **Simulation** numérique d'un écoulement stratifié dans une pièce composite.



- 4) **Optimisation** thermique du cycle de cuisson et refroidissement à travers l'épaisseur.



Nécessité d'étudier les phénomènes thermiques à travers l'épaisseur du composite afin d'optimiser le cycle de fabrication et les propriétés mécaniques des pièces

Organisation de la thèse

Sept articles scientifiques

1. State of the art review of numerical simulation in LCM processes. *Recent Research Developments in Material Sci. & Eng.*, soumis Déc. 2003
2. Thermo-mechanical properties during cure of glass/polyester RTM composites. *J. of Composite Materials*, soumis Nov. 2003
3. Internal stresses and warpage of thin composite parts manufactured by RTM. *Advanced Composites Letters*, accepté Sept 2003
4. Numerical analysis of cure temperature and internal stresses in thin and thick RTM parts. *Composites Part A*, soumis Déc. 2003
5. Coupled non-conforming finite element and finite difference approximation based on laminate extrapolation to simulate liquid composite molding processes Part I: isothermal flow. *Int. J. for Numerical Methods in Eng.*, soumis Nov. 2003
6. Coupled non-conforming finite element and finite difference approximation based on laminate extrapolation to simulate liquid composite molding processes Part II: non-isothermal flow. *Int. J. for Numerical Methods in Eng.*, soumis Nov. 2003
7. Comprehensive thermal optimization of liquid composite molding to reduce cycle time and processing stresses. *Polymer Composites*, soumis Déc. 2003

Caractérisation
Modélisation
cuisson/contraînes
Simulation 3D
remplissage
Optimisation
thermique

Plan

1. Introduction
2. Objectifs
3. Caractérisation des matériaux
4. Analyse unidimensionnelle de la cuisson
5. Simulation du remplissage non isotherme
6. Optimisation de la cuisson
7. Conclusion

Objectifs de la caractérisation

Optimisation thermique de la cuisson

Simulation numérique du procédé

Equation de l'énergie
 $T \Rightarrow K, C_p, Q$

Equation de contraintes
 $\sigma, \epsilon \Rightarrow E, \nu, \Delta \text{Volume}$

Cinétique de cuisson
 $d\alpha/dt \Rightarrow dH/dt$

Module élastique
 $E' = f(T, \alpha, t, \epsilon)$

Dilatation / retrait
 $dV/dt f(T, \alpha, t) \Rightarrow \text{CTE, retrait}$

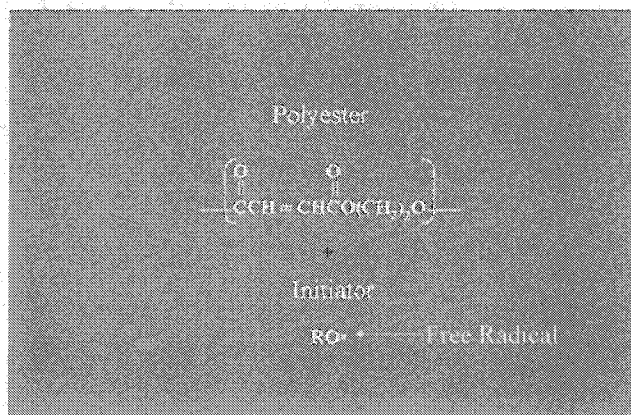
Mécanisme de polymérisation

Résine Polyester = Monomère polyester + Monomère styrène + Peroxyde
(agent de croisement) (initiateur)

Réaction exothermique



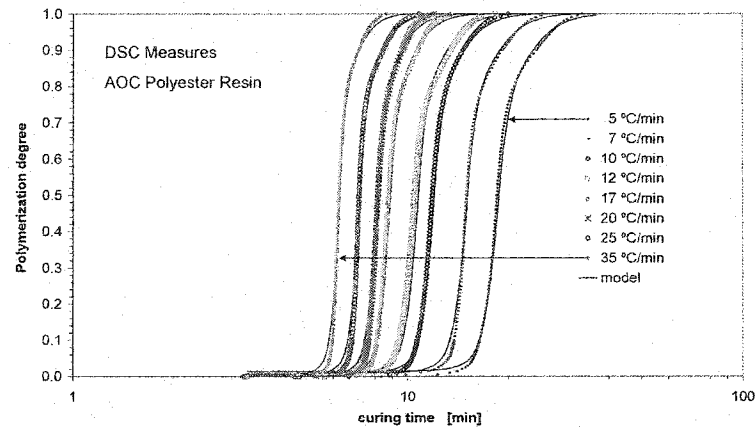
Calorimètre différentiel
DSC



Modèle de la cinétique de cuisson

Nouvelle modèle cinétique

$$\frac{d\alpha}{dt} = K_1(T) \cdot K_2(\alpha) \cdot K_3(T, \alpha) \cdot K_4(I_d)$$



CRASP Centre de Recherche Appliquée sur les Polymères Edu Ruiz

Article/Chapitre 2, Caractérisation des matériaux : cinétique de polymérisation

Caractérisation des propriétés mécaniques

Module élastique du composite = $E'(t, T, \alpha, \dots)$

Deux modèles proposés:

1.- Modèle relaxé/non relaxé $E'(T, \alpha, T_g)$

simple (sans intégration temporelle)

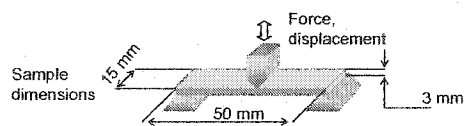
2.- Modèle viscoélastique $E'(t, T, \alpha)$

complexe (requiert intégration temporelle)

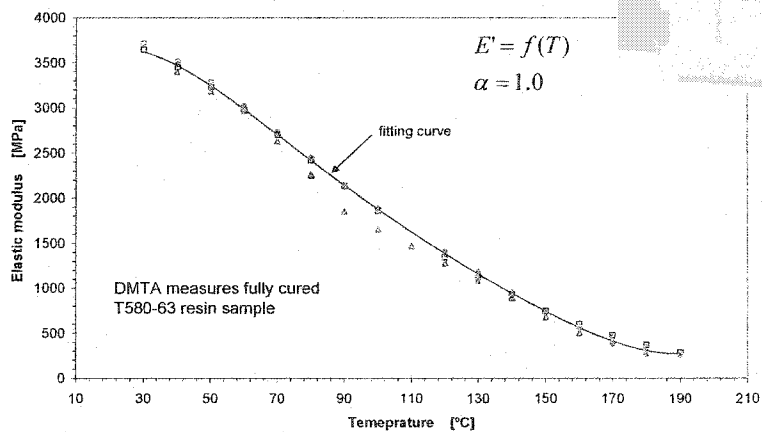
CRASP Centre de Recherche Appliquée sur les Polymères Edu Ruiz

Article/Chapitre 2, Caractérisation des matériaux : propriétés mécaniques

Modèle relaxé/non relaxé $E(T, \alpha, T_g)$



DMTA 2960 TA Instruments



CRASP

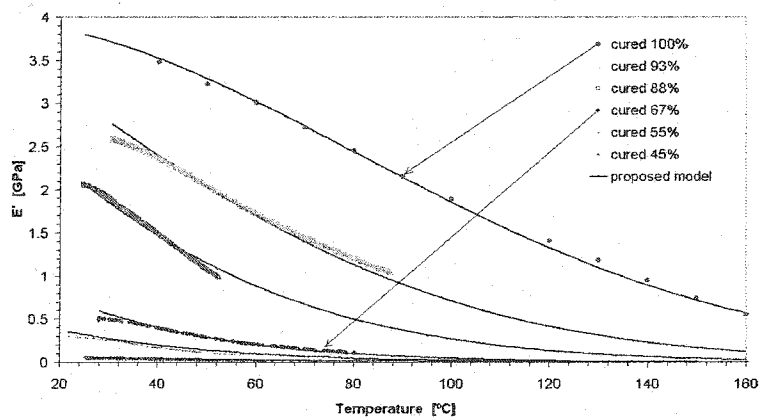
Centre de Recherche Appliquée sur les Polymères
Edu Ruiz

Article/Chapitre 2, Caractérisation des matériaux : modèle thermo-élastique

Modèle relaxé/non relaxé $E(T, \alpha, T_g)$

Vérification du modèle

$$\frac{E_r - E_{app}(T)}{E_r(T) - E_{app}(T)} = F_r(\alpha) \cdot W_r(T_g)$$



CRASP

Centre de Recherche Appliquée sur les Polymères
Edu Ruiz

Article/Chapitre 2, Caractérisation des matériaux : modèle thermo-élastique

Modèle relaxé/non relaxé $E(T, \alpha, T_g)$

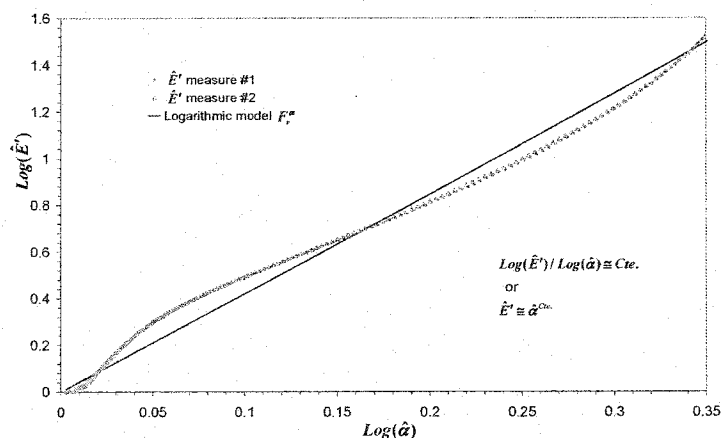
Evolution des propriétés mécaniques pendant la polymérisation

Mesures de DSC vs. DMTA

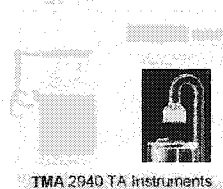
AGP Point

$\alpha \approx 0.4$

$E' \leq 200 E'(\alpha=1)$



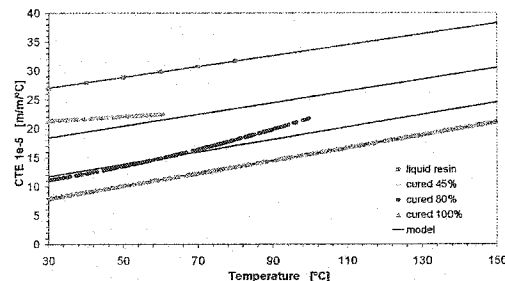
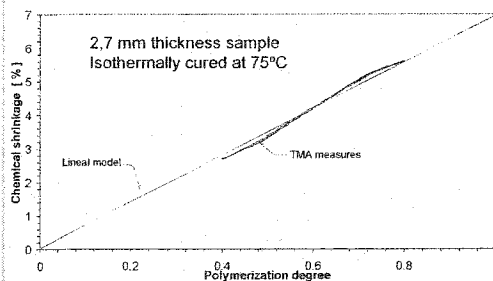
Equation des changements de volume



$$\left(\frac{1}{V_0} \frac{dV}{dt} \right)_{\text{Overall}} = \left(\frac{1}{V_0} \frac{dV}{dt} \right)_{\text{Thermal Contribution}} - \left(\frac{1}{V_0} \frac{dV}{dt} \right)_{\text{Polymerization Shrinkage}}$$

$$\left(\frac{1}{V_0} \frac{dV}{dt} \right)_{\text{Polymerization Shrinkage}} = \lambda_{\text{chem}} \frac{d\alpha}{dt}$$

$$\left(\frac{1}{V_0} \frac{dV}{dt} \right)_{\text{Thermal Contribution}} = \text{CTE}_{\text{gel}} \cdot \frac{dT}{dt} + [(\text{CTE}_{\text{cured}} - \text{CTE}_{\text{gel}})] \cdot \alpha \cdot \frac{dT}{dt}$$



Résumé des caractérisations

1.- Cinétique de polymérisation

$$\frac{d\alpha}{dt} = K_1(T) \cdot K_2(\alpha) \cdot K_3(T, \alpha) \cdot K_4(I_d)$$

2.- Modèle relaxé/non relaxé $E'(T, \alpha, T_g, V_f)$

$$E_r(T, \alpha) = E_{\text{exp}}(T) + [E_r(T) - E_{\text{exp}}(T)] \cdot F_r(\alpha) \cdot W_r(T_g)$$

3.- Modèle viscoélastique $E'(t, T, \alpha, V_f)$

$$E(\xi) = E_u \cdot \exp\left[-\Omega_1 \cdot (\xi + \tau_0)^{\Omega_2}\right] \cdot (\xi + \tau_0)^{-\Omega_3} \quad \xi = \int_0^t \frac{1}{a_T} dt$$

4.- Equation des changements de volume

$$\left(\frac{1}{V_o} \frac{dV}{dt}\right)_{\text{Overall}} = \left(\frac{1}{V_o} \frac{dV}{dt}\right)_{\text{Thermal Contraction}} - \left(\frac{1}{V_o} \frac{dV}{dt}\right)_{\text{Polymerization Swelling}}$$

Plan

1. Introduction
2. Objectifs
3. Caractérisation des matériaux
4. Analyse unidimensionnelle de la cuisson
5. Simulation du remplissage non isotherme
6. Optimisation de la cuisson
7. Conclusion

Objectifs de la simulation numérique

Optimisation thermique de la cuisson

Simulation numérique du procédé

Équation de l'énergie

$$\partial T / \partial t = \alpha \nabla^2 T + Q$$



Équation de contraintes

$$\{\Delta \sigma\} = [C] \cdot \{\Delta \varepsilon\}$$

Cinétique de cuisson

$$d\alpha/dt \Rightarrow dH/dt$$

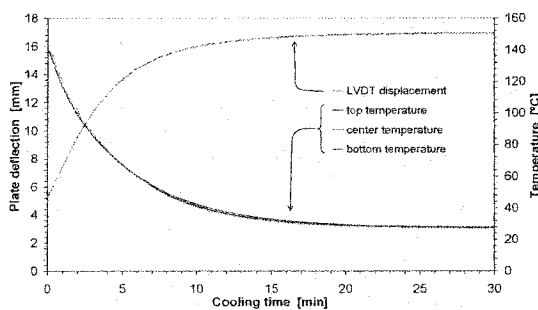
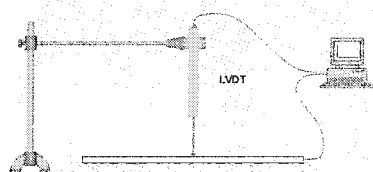
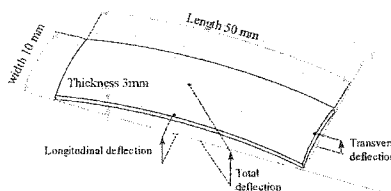
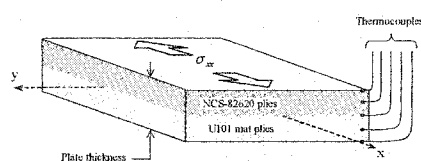
Module élastique

$$E = f(T, \alpha, t, v)$$

Dilatation / retrait

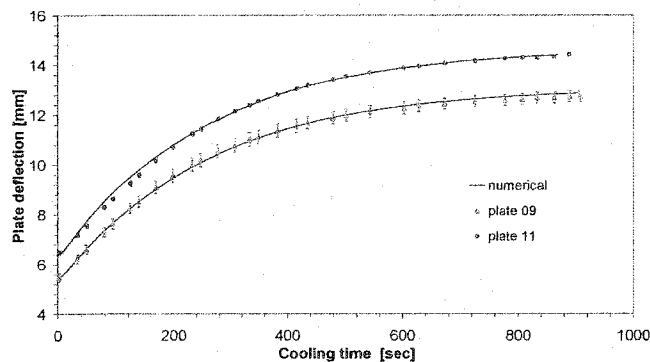
$$dV/dt f(T, \alpha, t) \Rightarrow \text{CTE, retrait}$$

Validation - plaques minces



Validation - plaques minces

Comparaison des mesures de déflexion (LVDT) avec le modèle numérique des contraintes résiduelles.

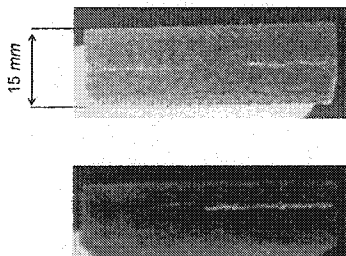


Test number	measured deflection [mm]	numerical deflection [mm]	Error [%]
2	12.8	13.0	1.79
5	15.0	14.8	1.27
6	12.7	12.9	1.09
7	14.4	14.4	0.13
8	12.6	12.7	0.37

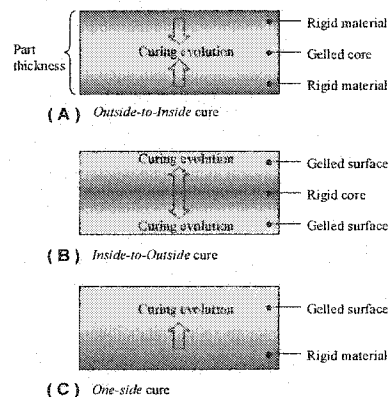
Analyse de plaques épaisses

Problème de cuisson de plaques épaisses

Fissure de la matrice et délamination du composite apparaissant généralement dans pièces composites épaisses traitées à haute température de cuisson.



Stratégies de cuisson



Plan

1. Introduction
2. Objectifs
3. Caractérisation des matériaux
4. Analyse unidimensionnelle de la cuisson
5. **Simulation du remplissage non isotherme**
6. Optimisation de la cuisson
7. Conclusion

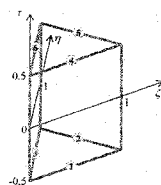
Simulation du remplissage 3D

Cuisson 1D

Uniformité de température
dans le plan de la pièce

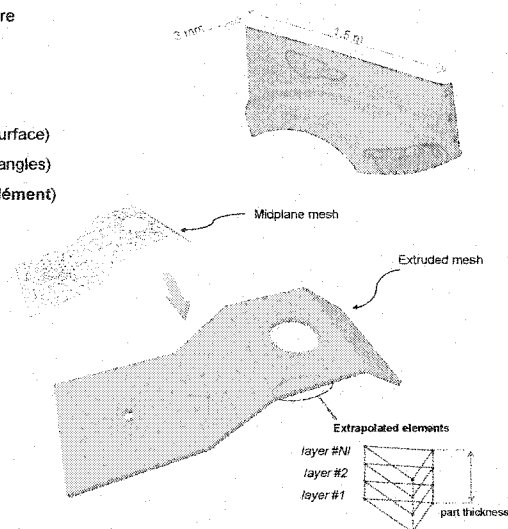
Simulation de remplissage:

- 1.- Pièces minces (épaisseur \ll surface)
- 2.- Maillage du plan moyen 2D (triangles)
- 3.- Maillage extrudé 3D (nouvel élément)

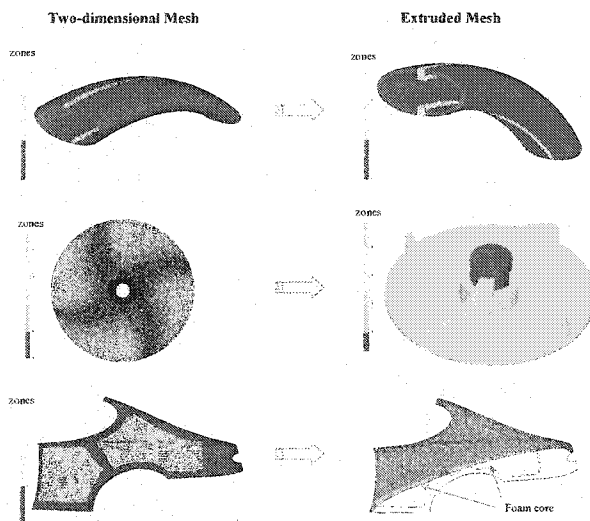


Reference prismatic finite element
(6 nodes)

Prism6

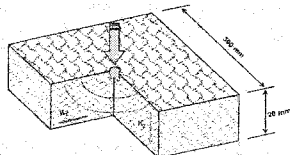


Résultats du code d'extrusion



Vérification expérimental du *Prism6*

Injection pressure 1.89×10^5 Pa



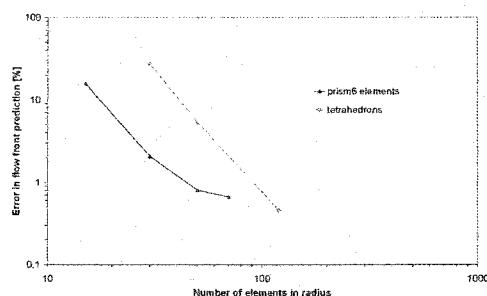
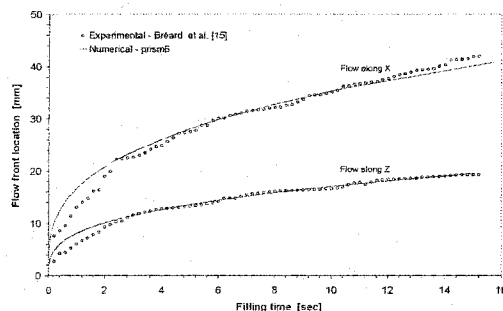
Injection centrale dans une préforme anisotrope
Flux elliptique 3D (cas isotherme)

Silicon oil viscosity = 0.1 Pa.s

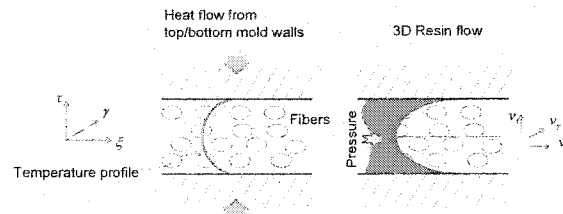
Fiber volume fraction = 22%

$K_x = K_y = 3.95 \times 10^{-10} \text{ m}^2$

$K_z = 9.3 \times 10^{-11} \text{ m}^2$



Effets thermiques pendant le remplissage



Energy equation

$$\rho C_p \frac{\partial T}{\partial t} + \nabla \cdot (\mathbf{q}) = k \nabla^2 T + Q$$

Equation

$$\frac{1}{u} [K] \nabla T$$

$$\frac{d\alpha}{dt} = (k_1 + k_2 \cdot \alpha^m) (1 - \alpha)^n$$

Extrusion et remplissage non-isotherme
~7500 lignes de code.

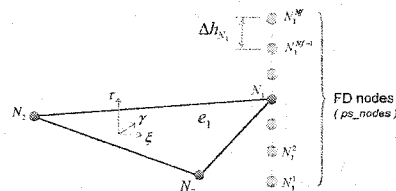
Approximation des effets thermiques travers l'épaisseur

1.- Maillage tridimensionnel
maillage 3D de *Prism6*



Éléments prismatiques extrudés

2.- Maillage bidimensionnel
maillage 2D (triangles)
+ différences finies 1D



Niveaux de couplage des EF et DF

Flow mesh



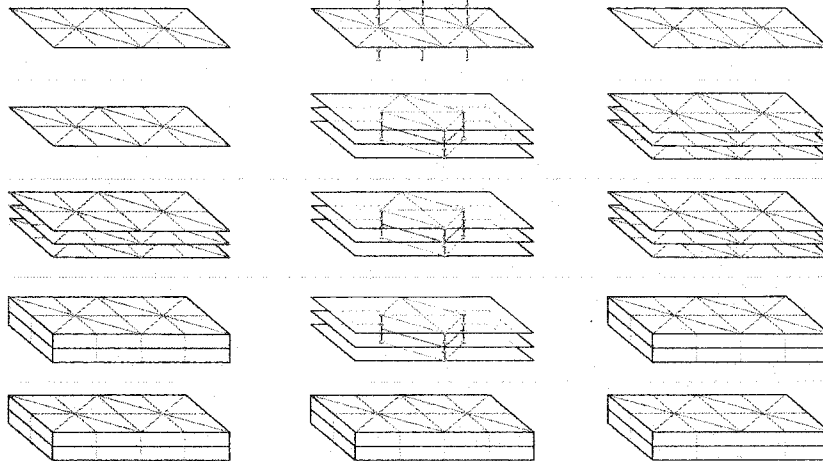
Heat conduction/curing Mesh



Transport mesh

Simple

Complex



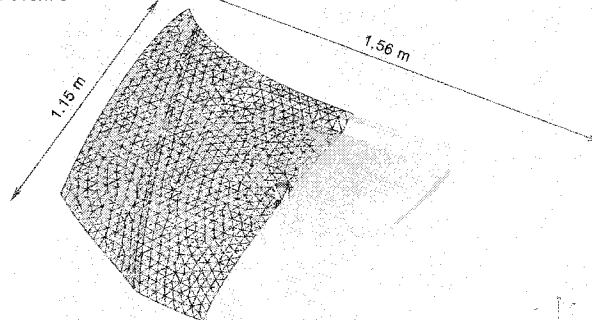
CRASP

Centre de Recherche Appliquée sur les Polymères
Edu Ruiz

Article/Chapitre 6, Simulation du remplissage non-isotherme

Solution d'un cas typique

Capot de voiture

Injection gate (3.0×10^5 Pa)

Resin injection temperature= 330 °K

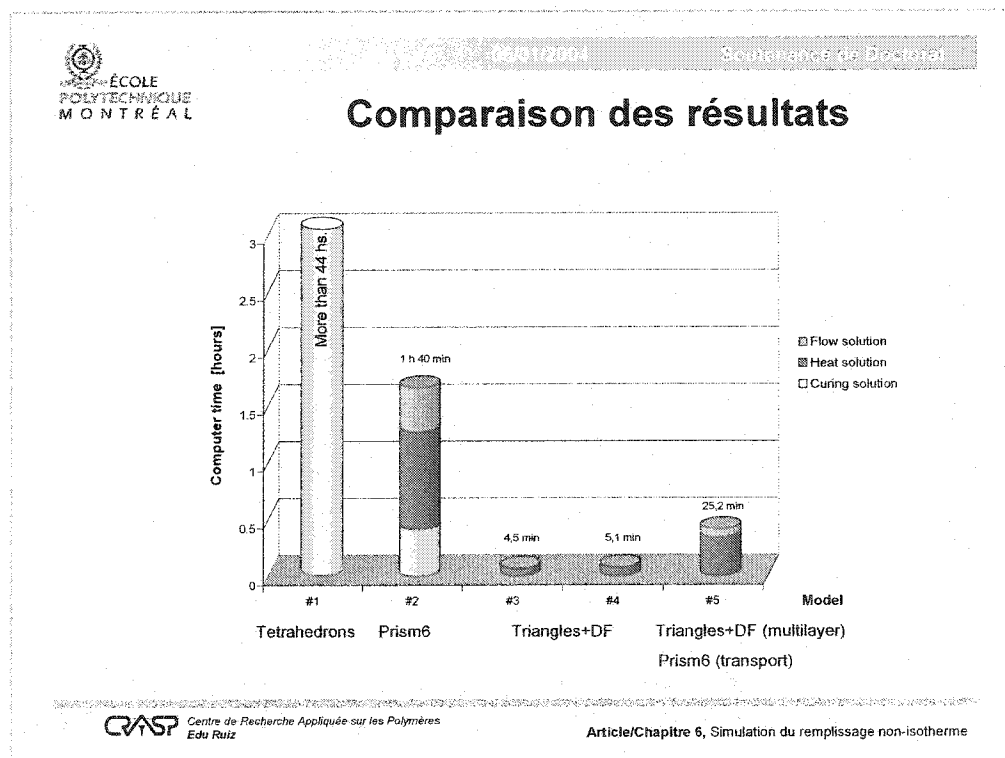
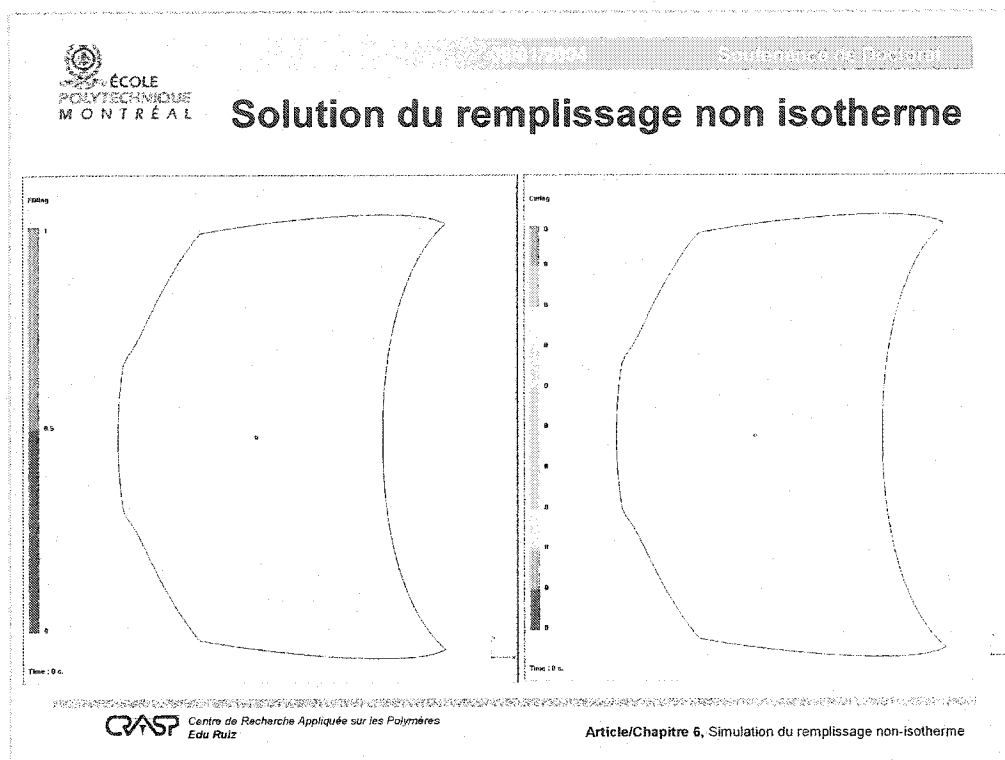
Initial fibers temperature= 350 °K

Mold wall temperature= 370 °K

CRASP

Centre de Recherche Appliquée sur les Polymères
Edu Ruiz

Article/Chapitre 6, Simulation du remplissage non-isotherme



Plan

1. Introduction
2. Objectifs
3. Caractérisation des matériaux
4. Analyse unidimensionnelle de la cuisson
5. Simulation de remplissage non isotherme
6. Optimisation de la cuisson
7. Conclusion

Objectifs de l'optimisation multicritères

Objectifs:

- Maximiser le degré de polymérisation
- Minimiser le temps du cycle
- Minimiser les contraintes de cuisson
- Minimiser les contraintes de refroidissement
- Minimiser la température exothermique

7 fonctions sous-objectifs
du type sigmoïde

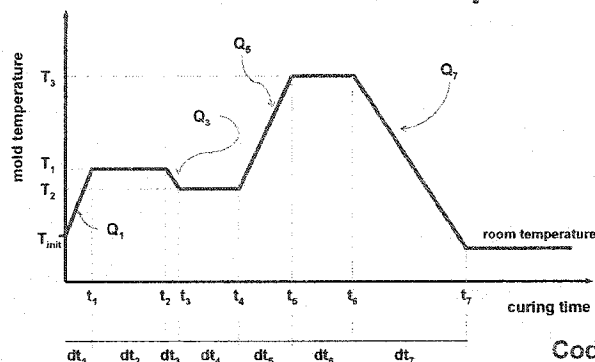
Autres chercheurs :

- Minimisation des gradients thermiques
- ou minimisation des contraintes
- ou minimisation du temps du cycle

Fonction objectif multicritères
avec des poids pour tenir
compte de plusieurs critères

Fonction à évaluer pour un
cycle de cuisson donné

Paramètres du procédé

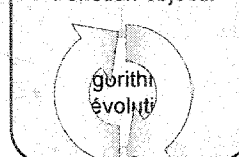


Variables de conception $Vd = [Q_1, dt_1, Q_2, dt_2, \dots, Q_n, dt_n]$
(design vector)

Contraintes $Cs = [T_{init}, T_{room}, Q_{max}^+, Q_{max}^-]$

Code « LeCoq »

Fonction objectif



CRAST

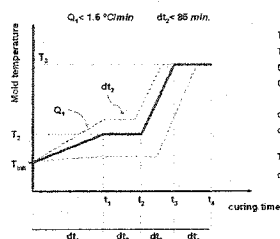
Centre de Recherche Appliquée sur les Polymères
Edu Ruiz

Article/Chapitre 7, Optimisation de la cuisson

Optimisation de la cuisson de pièces minces – deux rampes de chauffage

Comparaison des optimisations :

- A) sans contraintes résiduelles
- B) avec contraintes résiduelles
(multicritères)

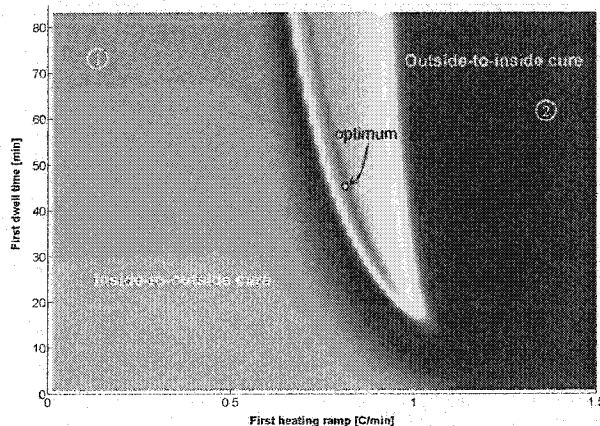


$T_{max} = 30^\circ\text{C}$
 $T_2 = 130^\circ\text{C}$
 $Q_2 = 9^\circ\text{C/min}$
 $Q_3 = Q_4 = 0$

$dt_2 = 41 \text{ min.}$
 $dt_3 = 60 \text{ min.}$

$T_3 = T_{max} + Q_3 \cdot d$
 $dt_4 = (T_3 - T_2) / C$

Avec contraintes résiduelles



CRAST

Centre de Recherche Appliquée sur les Polymères
Edu Ruiz

Article/Chapitre 7, Optimisation de la cuisson

Plan

1. Introduction
2. Objectifs
3. Caractérisation des matériaux
4. Analyse unidimensionnelle de la cuisson
5. Simulation du remplissage non isotherme
6. Optimisation de la cuisson
7. Conclusion

Conclusions

L'objectif de cette thèse était de développer les points suivants :

- Équations caractéristiques du comportement thermomécanique et le changement de phase des matériaux composites thermodurcissables.
- Modèles numériques pour simuler la mise en forme du procédé d'injection sur renfort (LCM).
- L'optimisation du cycle de cuisson et de refroidissement des composites fabriqués par LCM.

Contributions scientifiques

	Articles	Conférences
1) Connaissances sur la caractérisation des matériaux :		
- nouveau modèle de la cinétique de cuisson incluant la transition vitreuse	1	1
- concept d'AGP et de l'évolution des propriétés mécaniques pendant la polymérisation		
- modèle élastique relaxé/non relaxé		
- modèle viscoélastique		
- modèle de dilatation et retrait de polymérisation		
2) Modèle numérique pour résoudre le couplage cuisson/contraintes résiduelles	2	1
3) Modèle numérique pour simuler le remplissage multicouches non-isotherme	2	
4) Optimisation complète du cycle de cuisson et refroidissement	2	1
Total :	7	3

- Une partie des développements numériques réalisés sous contrat industriel.
- Ce travail a débouché sur deux maîtrises en cours au CRASP.
- Participation à 4 articles, 5 rapports techniques et 2 conférences non incluses.

Recommandations

- 1) Vérifier expérimentalement la procédure d'optimisation multicritère.
- 2) Obtenir une méthodologie pratique pour la **détermination d'AGP**.
- 3) Développer une **Théorie Classique de Laminés** avec contrainte transverse et un modèle de contraintes tridimensionnelles.
- 4) Améliorer les **modèles mécaniques** en ajoutant l'effet du taux de cisaillement.
- 5) Travailler avec une méthode d'**optimisation multicritère**.
- 6) Développer une méthodologie d'**optimisation globale** à partir des optimisation unidimensionnelle à travers l'épaisseur.

Optimisation des points d'injection

Code d'optimisation

Solution inverse
(algorithme one-shot)
par Vincent Achim

$$v = -\frac{[K]}{\mu} \bar{v}_D \text{ Darcy}$$

Temps de remplissage

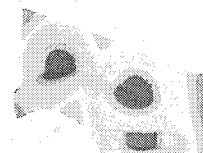
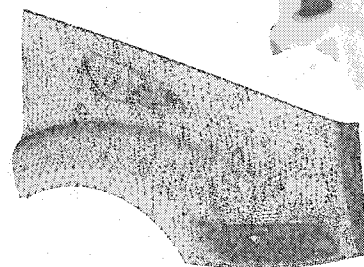
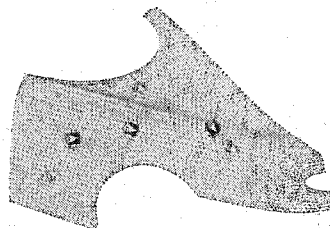
Position des
points d'injection

Algorithme
d'évolution

1 point d'injection

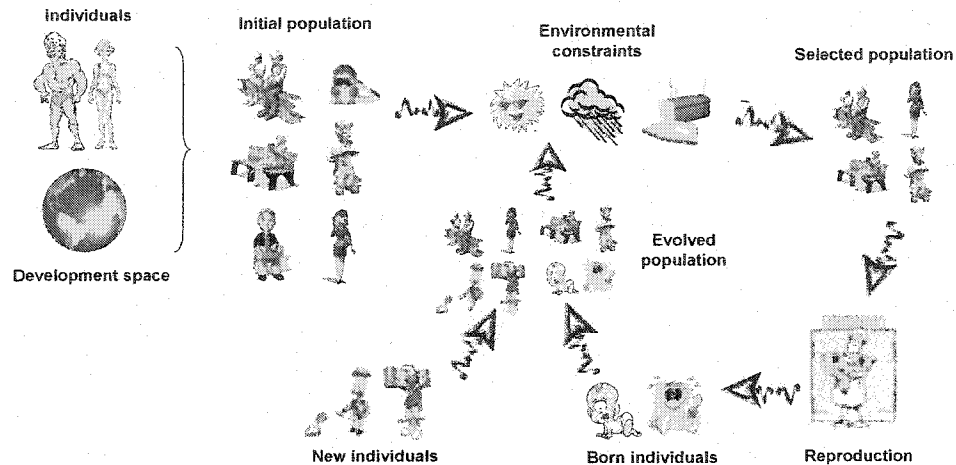
2 points d'injection

3 points d'injection



Algorithme génétique

Genetic Algorithms are adaptive heuristic search algorithm premised on the evolutionary ideas of natural selection and genetic. First pioneered by John Holland in the 60s.



Formulation d'éléments finis

Convergence d'un ensemble d'éléments (patch test)

Solution de l'équation de Darcy

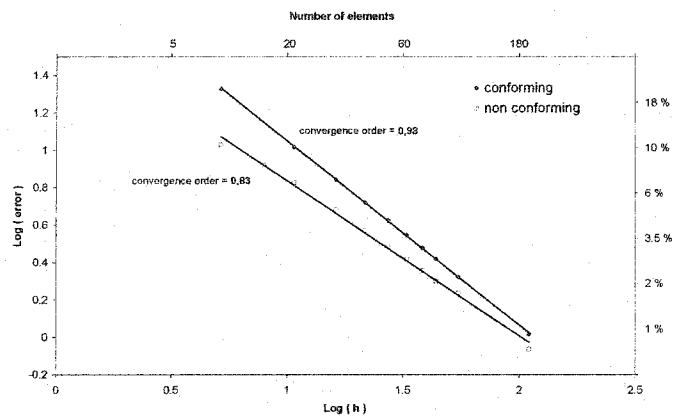
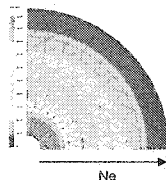
$$\nabla \left(-\frac{1}{\mu} [K] \nabla p \right) = 0$$

Géométrie radial divergente

Cavité remplie

Élément prismatique

Erreur sur la variable secondaire



ANNEXE V : FICHES TECHNIQUES DES MATÉRIAUX

Cette annexe contient les fiches techniques de des matériaux utilisés pour la caractérisation et validation expérimentale.

Reinforcements Europe

Unifilo* continuous filament mat

*Registered trademark

Unifilo is an E-glass continuous strand mat of random orientation in multiple layers and held together by a binder.

U101

- for translucent sheets
- for the manufacture of flat sandwich panels for vehicle bodies by continuous impregnation process
- as a surface layer in preforms made with the U700 series of preformable Unifilo mats : RTM moulding

U164

- for the production of self-supporting panels
- for the production by continuous impregnation of flat panels for vehicle bodies.

(U100 series : compatibles with UP and EP resins)

Identification

Example : U101 450-138
 U : Continuous strand mat (Unifilo)
 101 : Vetrotex product classification code
 450 : Nominal weight per unit area (g/m²)
 138 : Roll width (cm)

Technical characteristics (nominal values)

Ref	Basic size	Solubility in styrene	Linear weight of basic strands (tex)	Loss on ignition (%)	Moisture (%)
			ISO 1889	ISO 1887	ISO 3944
U101	Silane	High	25	4.5	< 0.15
U164	Silane	Low	50/100	4.0	< 0.15

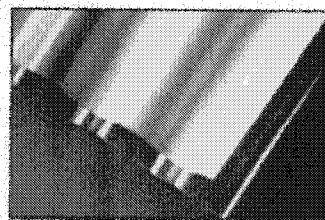
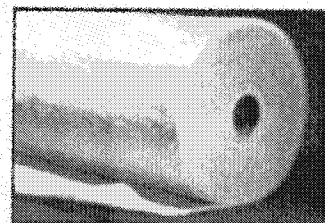
Refer to the Standard Product Specification for more precise information on the characteristics of the product.

U101 U164

Technical data sheet

Properties

- **U101 :**
 - very good impregnation
 - high level of translucency (very good surface finish when moulded by RTM)
- **U164 :**
 - can be used with highly filled resins (50%) thanks to its 50/100 tex strand construction and to a low solubility in styrene.



Translucent sheets

SAINT-GOBAIN
VETROTEx

Products available

Roll width (cm)	Standard weights (g/m ²)	Approximate dimensions of full* roll, 138 cm wide					
		Diameter (cm)		nominal length (m)		nominal weight (kg)	
		U101	U164	U101	U164	U101	U164
60/300	300	55	55	311		129	
	450	55	55	207	175	129	109
	600	55	55	157		130	

* by a full roll, is understood a roll having a guaranteed length of at least 90% of the value indicated above.

Individual and bulk packaging

- Each roll of Uniflo is wound onto a cardboard tube of 8.7 kg/m and internal diameter 103 mm, then individually wrapped with a transparent stretch film.
- Pallet type:
 - For rolls with a width \leq 205 cm, a standard pallet is used (vertical rolls).
 - For rolls with a width $>$ 205 cm, a wooden crate is used (horizontal rolls).
- Protection type:
 - Standard pallet = cardboard base and cover, fully wrapped in stretch film.
 - Wooden crate = each roll packaged in a polyethylene bag.

Roll diameter (cm)	Roll width H (cm)	Number of rolls per pallet	Pallet dimensions length x width x height	Pallet net* weight (kg)	
				U101	U164
55	60 to 65	12	114 x 114 (H = 16)	538	436
	66 to 105	8	114 x 114 (H = 18)	491	390
	106 to 205	4	114 x 114 (H = 18)	394	302
52 35	206 to 300	9	H x 109 x 216	-	-
		9	H x 109 x 124	741	570

* for rolls of 450 g/m² weight and for:

- height 106 cm when packed in 4 on a standard pallet,
- height 66 cm when packed in 8 on a standard pallet,
- height 60 cm when packed in 12 on a standard pallet,
- height 206 cm when packed in wooden crate.

Storage

Uniflo mat must be stored in its original packaging in a place avoiding humidity and heat. The best conditions are temperature between 15 and 35°C and a relative humidity level between 35 and 85%.

If the product is stored at low temperature (below 15°C), it is advisable to condition the mat in the workshop for at least 24 hours before use, to prevent condensation.

Edited by:



Saint-Gobain
Vetroflex International SA
 787, rue des Alouettes
 F-73009 Chambéry
 France
 Tel: +33 (0)4 79 75 54 87
 Fax: +33 (0)4 79 75 62 99

Vetroflex Reinforcement S.A.
 136, avenue des Eclairés - 59100
 59100 Châtellain (France)
 France
 Tel: +33 (0)4 79 75 54 87
 Fax: +33 (0)4 79 75 62 99

Vetroflex Reinforcement S.A.
 Carrière de la Chapelle - 13000
 13000 Aix-en-Provence (France)
 France
 Tel: +33 (0)4 79 75 54 87
 Fax: +33 (0)4 79 75 62 99

Vetroflex Reinforcement S.A.
 136, avenue des Eclairés - 59100
 59100 Châtellain (France)
 France
 Tel: +33 (0)4 79 75 54 87
 Fax: +33 (0)4 79 75 62 99

Vetroflex S.A.
 136, avenue des Eclairés - 59100
 59100 Châtellain (France)
 France
 Tel: +33 (0)4 79 75 54 87
 Fax: +33 (0)4 79 75 62 99

Saint-Gobain Vetroflex S.A.
 136, avenue des Eclairés - 59100
 59100 Châtellain (France)
 France
 Tel: +33 (0)4 79 75 54 87
 Fax: +33 (0)4 79 75 62 99

Saint-Gobain Vetroflex S.A.
 136, avenue des Eclairés - 59100
 59100 Châtellain (France)
 France
 Tel: +33 (0)4 79 75 54 87
 Fax: +33 (0)4 79 75 62 99

Vetroflex Reinforcement S.A.
 136, avenue des Eclairés - 59100
 59100 Châtellain (France)
 France
 Tel: +33 (0)4 79 75 54 87
 Fax: +33 (0)4 79 75 62 99

Vetroflex Reinforcement S.A.
 136, avenue des Eclairés - 59100
 59100 Châtellain (France)
 France
 Tel: +33 (0)4 79 75 54 87
 Fax: +33 (0)4 79 75 62 99

Saint-Gobain Vetroflex S.A. 136, avenue des Eclairés - 59100 Châtellain (France) France

(12/1/99)



MATERIAL SAFETY DATA SHEET

NOROX[®] PULCAT[™] A



SECTION 1 - IDENTIFICATION OF THE PRODUCT AND THE COMPANY

PRODUCT NAME	NOROX [®] PULCAT [™] AW	TELEPHONE	(626) 334-2908
MANUFACTURER	Norac, Inc.	CHEMTREC (24hr)	1-800-424-9300
ADDRESS	405 S. Motor Ave., Azusa, CA 91702	CAS NO.	See Section II
CHEMICAL NAME	Methyl Isobutyl Ketone Peroxide (MIBKP)	CHEMICAL FORMULA	Mixture
CHEMICAL FAMILY	Organic Peroxide - Ketone Peroxide		

SECTION 2 - COMPOSITION/INFORMATION ON INGREDIENTS

COMPONENTS	CAS NO.	%
Methyl Isobutyl Ketone Peroxide	37206-20-5	45
Diisobutyl Phthalate	84-69-5	36
Methyl Isobutyl Ketone	108-10-1	14
2,2,4-Trimethyl-1,3-pentanediol diisobutyrate	6846-50-0	5

SECTION 3 - HAZARD IDENTIFICATION OF THE PREPARATION

PHYSICAL HAZARDS	Organic Peroxide. Decomposition
HEALTH HAZARDS	Severe Irritant
EXPOSURE LIMITS	TLV: 50 PPM for MIBK
ROUTES OF EXPOSURE	
Skin Contact	Severe skin irritant, causes redness, blistering, and edema.
Eye Contact	Eye contact causes severe corrosion and may cause blindness.
Ingestion	Human systemic effects by ingestion: changes in structure or function of esophagus, nausea, or vomiting, and other gastrointestinal effects.
Inhalation	Moderately toxic by inhalation.
EFFECTS OF OVER-EXPOSURE	Prolonged inhalation of vapors may cause mucous membrane irritation and vertigo. There are no known medical conditions, which are recognized as being aggravated by exposure.

SECTION 4 - FIRST-AID MEASURES

Skin	Immediately remove any contaminated clothing. Wash contaminated area thoroughly with soap and copious amounts of water for at least 15 minutes. If irritation or adverse symptoms develop seek medical attention.
Eyes	Remove any contact lenses at once. Flush eyes with water for at least 15 minutes. Ensure adequate flushing by separating the eyelids with fingers. If irritation or adverse symptoms develop seek medical attention.
Ingestion	Do Not induce vomiting. Drink plenty of water. Immediately call a physician. For aid to physician, suggest local Poison Control Center.
Inhalation	Remove to fresh air, if coughing, breathing becomes labored, irritation develops or other symptoms develop, seek medical attention at once, even if symptoms develop several hours after the exposure.

SECTION 5 - FIRE-FIGHTING MEASURES

FLASH POINT	> 140°F (60°C) C.O.C
FLAMMABLE LIMITS	Unknown
AUTOIGNITION POINT	Unknown
EXTINGUISHING MEDIA	Water from a safe distance - preferably with a fog nozzle. In case of very small fires, other means such as carbon dioxide, foam or dry chemical extinguishers may be effective. Dry chemical combined with MIBKP may re-ignite. Light water additives may be particularly effective at extinguishing MIBKP fires.

MATERIAL SAFETY DATA SHEET

NOROX® PULCAT™ A**SPECIAL FIRE FIGHTING PROCEDURES**

Firemen should be equipped with protective clothing and SCBA's. In case of fire near storage area, cool the containers with water spray. If dry chemical is used to extinguish an MIBKP fire, the extinguished area must be thoroughly wetted down with water to prevent re-ignition.

UNUSUAL FIRE AND EXPLOSION HAZARDS

The heat of decomposition of the peroxides adds to the heat of the fire. Dry chemical fire extinguishing agent may catalyze the decomposition.

SECTION 6 - ACCIDENTAL RELEASE MEASURES**STEPS TO BE TAKEN IN EVENT OF SPILL OR RELEASE**

Dike spill to prevent runoff from entering drains, sewers, streams, etc. Wet spilled material with water and absorb with an inert absorbent material such as perlite, vermiculite, or sand. Sweep up using non-sparking tools and place in a clean polyethylene drum or a polyethylene pail. **DO NOT** place into a steel container, lined or unlined, as a decomposition may occur. Treat any contaminated cardboard packaging as hazardous waste. Wet container contents with additional water prior to sealing.

SECTION 7 - HANDLING AND STORAGE**HANDLING**

Keep containers closed to prevent contamination. Rotate stock using the oldest material first. The activity and stability of MIBKP is directly related to the shipping and storage temperature history. Cool storage at 80°F or below is recommended for longer shelf life and stability. Prolonged storage at elevated temperatures of 100°F and higher will cause product degradation, gassing and potential container rupture which can result in a fire and/or explosion.

STORAGE

MIBKP should never be added to hot solvents or monomers as a violent decomposition and/or reaction may result. When using spray equipment, never spray raw MIBKP onto curing or into raw resin or flues. Keep MIBKP in its original container. **DO NOT STORE WITH FOOD OR DRINK. DO NOT USE NEAR FOOD OR DRINK.**

OTHER PRECAUTIONS

Unmixed, uncontaminated material, remaining at the end of the day, shall be returned to a proper organic peroxide storage area¹. Under no circumstances should material be returned to the original container.²

SECTION 8 - EXPOSURE CONTROL/PERSONAL PROTECTION**VENTILATION**

Mechanical, general.

RESPIRATORY PROTECTION

If airborne concentrations are expected to exceed acceptable levels wear a NIOSH/MSHA approved air-purifying respirator with an organic vapor cartridge or canister. When using respirators refer to OSHA's 29CFR 1910.134.

EYE PROTECTION

Safety goggles recommended. Permanent eyewash is highly recommended.

HAND PROTECTION

Protective gloves recommended, solvent resistant, such as butyl rubber, nitrile or neoprene.

OTHER

A safety shower and eyewash is recommended when the risk of a significant exposure exists.

SECTION 9 - PHYSICAL AND CHEMICAL PROPERTIES**APPEARANCE AND ODOR:**

Water white liquid with a slight odor.

BOILING POINT:

Unknown

SPECIFIC GRAVITY: 1.0

VAPOR PRESSURE:

Unknown

FLASH POINT: >140°F (60°C) C.O.C

VAPOR DENSITY:

> 1

FLAMMABLE LIMITS: Unknown

EVAPORATION RATE:

Unknown

SADT: >60°C (140°F)

% VOLATILE BY VOLUME:

Unknown

pH: Not applicable

SOLUBILITY IN WATER:

Slightly soluble in water.

¹ See CCR Title 8 Section 5461, NFPA 432, and UFC (91) Sec. 80.307.

² See NFPA 14-3

NOROX® PULCAT™ A**SECTION 10 - STABILITY AND REACTIVITY**

STABILITY	Stable when kept in original, closed container, out of direct sunlight at temperatures below 80°F (27°C).
CONDITIONS TO AVOID	Contamination. Direct sunlight. Open flames. Prolonged storage above 100°F (38°C). Storage above SADT. Storage near flammable or combustible materials.
MATERIALS TO AVOID	Dimethylaniline, cobalt napthenate and other promoters, promoted resins, accelerators, oxidizing and reducing agents, strong acids, bases, metals, metal alloys and salts, sulfur compounds, amines or any hot material.
HAZARDOUS DECOMPOSITION PRODUCTS	Decomposition products are flammable. Acrid smoke and irritating fumes.
HAZARDOUS POLYMERIZATION	Will not occur.

SECTION 11 - TOXICOLOGICAL INFORMATION**Methyl Isobutyl Ketone Peroxide****Hazard Data:**Inhalation: Rat--LC₅₀: 1.5 mg/l-4hr;Oral: Rat--LD₅₀: 1700 mg/kg;**Diisobutyl Phthalate****Hazard Data:**Oral: Rat--LD₅₀: 15 g/kg.**Methyl Isobutyl Ketone****Hazard Data:**Dermal: Rabbit--LD₅₀: >20,000 mg/kg;Inhalation: Mouse--LC₅₀: 23,000 mg/;Oral: Rat--LD₅₀: 2080 mg/kg.**2,2,4-Trimethyl-1,3-pentanediol diisobutyrate****Hazard Data:**Oral: Rat--LD₅₀: >3200 mg/kg**SECTION 12 - ECOLOGICAL INFORMATION**

No data is available on the preparation itself. The product should be prevented from entering drains, sewers, streams, etc.

SECTION 13 - DISPOSAL CONSIDERATIONS

Prevent material from entering drains, sewers, streams, etc.

Immediately dispose of waste material at a RCRA approved hazardous waste management facility in accordance with federal, state and local regulations.

SECTION 14 - TRANSPORT INFORMATION

DOT Shipping Name:	ORGANIC PEROXIDE TYPE D, LIQUID, (METHYL ISOBUTYL KETONE PEROXIDE, ≤45%)
DOT Hazard Class:	5.2
UN/NA ID No.:	UN3105
DOT Packing Group:	PG II
Labels:	5.2 (Organic Peroxide)
2000 ERG GUIDE NO.:	145

SECTION 15 - REGULATORY INFORMATION

The following chemicals are subject to the reporting requirements of Section 313 of Title III of the Superfund Amendments and Reauthorization Act of 1986 and 40 CFR Part 372.

<u>Chemical Name</u>	<u>CAS Number</u>	<u>Percent</u>
Dimethyl Phthalate	84-69-5	38
Methyl Isobutyl Ketone	108-10-1	14

NOROX® PULCAT™ A

MATERIAL SAFETY DATA SHEET

TSCA Status

The ingredients in this product are listed in the US Toxic Substances Control Act (TSCA) Inventory.

Status of Carcinogenicity

Not recognized as a carcinogen by the IARC, NTP or OSHA.

SECTION 16 - OTHER INFORMATION**VOC Information**

Using ASTM Test Method D-2369-87, but at 40°C (since MIBKP decomposes rapidly above 100°C and is not a VOC), PULCAT™ A contains 13.8% VOC, by weight, or 134 grams per liter. For more information call Norac.

NFPA 432 Organic Peroxide Classification

Class III

NFPA 704 Rating

<u>Health</u>	<u>Flammability</u>	<u>Reactivity</u>
3	2	2

HMIS Rating

<u>Health</u>	<u>Flammability</u>	<u>Reactivity</u>
3	2	2

MSDS Reference: Pulcat A 0201.1

DISCLAIMER OF LIABILITY

The information in this MSDS was obtained from sources, which we believe are reliable. However, the information is provided without any warranty, express or implied, regarding its correctness.

The conditions or methods of handling, storage, use and disposal of the product are beyond our control and may be beyond our knowledge. For this and other reasons, we do not assume responsibility and expressly disclaim liability for loss, damage or expense arising out of or in any way connected with the handling, storage, use, or disposal of the product.

This MSDS was prepared and is to be used only for this product. If the product is used as a component in another product, this MSDS information may not be applicable.